

SOLID SURFACES

and the Gas-Solid Interface

Papers presented at the
Kendall Award Symposium honoring Stephen Brunauer
Division of Colloid and Surface Chemistry
139th Meeting of the American Chemical Society
St. Louis, Mo., March 1961

EDITORIAL CONSULTANTS: Lewellyn E. Copeland, *symposium chairman*
Ralph A. Beebe
Donald P. Graham
Albert C. Zettlemoyer
William A. Zisman



Number 33

ADVANCES IN CHEMISTRY SERIES

American Chemical Society

Washington, D. C.

1961

Copyright © 1961
AMERICAN CHEMICAL SOCIETY
All Rights Reserved

Library of Congress Catalog Card No. 61-18397

PRINTED IN THE UNITED STATES OF AMERICA

**American Chemical Society
Library**

**1155 16th St., N.W.
Washington, D.C. 20036**

In SOLID SURFACES; Copeland, L., et al.;

Advances in Chemistry; American Chemical Society: Washington, DC, 1961.

ADVANCES IN CHEMISTRY SERIES

Robert F. Gould, Editor

AMERICAN CHEMICAL SOCIETY APPLIED PUBLICATIONS

ADVISORY BOARD

Allen L. Alexander

Walter C. McCrone, Jr.

Wyndham D. Miles

William J. Sparks

Calvin L. Stevens

Glenn E. Ulliyot

Calvin A. VanderWerf

George W. Watt

Albert C. Zettlemoyer

FOREWORD

The announcement that Stephen Brunauer was the recipient of the Kendall Award in Colloid Chemistry for 1961 was made at the meeting of the American Chemical Society in New York in September 1960. Donald Graham, who was then Chairman of the Division of Colloid and Surface Chemistry, asked Dr. Brunauer to choose someone to organize the symposium that is held traditionally to honor the recipient of the award, and he chose me. I considered it a great honor to be so chosen, but it was not without trepidation that I accepted the assignment. However, my worries soon proved to be baseless. Dr. Brunauer's many friends responded enthusiastically, and in ever-increasing numbers. We soon saw that we could plan on three sessions, then four, and finally five full sessions. The symposium was held during the 139th National Meeting of the American Chemical Society in St. Louis on March 27 to 29, 1961. I held the chair during the first session, and the chairmen of the four subsequent sessions were A. C. Zettlemoyer, W. A. Zisman, R. A. Beebe, and Donald Graham. The quality of the papers and the excellence of the presentations made the symposium highly successful.

W. A. Zisman suggested that the papers presented at the symposium be published as a volume in the *ADVANCES IN CHEMISTRY SERIES*. Robert Gould welcomed the idea, and the contributors willingly consented. The chairmen of the five sessions assumed the responsibility of reviewing the papers presented at their sessions for technical content, and Gould and his staff performed the editorial reviewing.

The order of the papers in the book is the same as the order of their presentation at the symposium. That order was chosen for the symposium partly on the basis of subject matter, and partly to prevent the presentation of too many theoretical papers in any one session. An attempt to classify the papers in a more logical arrangement for the book proved fruitless, because so many of the papers could not logically be placed in any single class.

With deep gratitude I acknowledge the wonderful cooperation of each contributor, and the invaluable aid and advice I received from the four chairmen and Mr. Gould. Without their help, the publication of this book would have been impossible.

L. E. COPELAND

Honoring the B in BET

An Address in Presentation of Dr. Stephen Brunauer for the Kendall Award

HUGH S. TAYLOR

Woodrow Wilson National Fellowship Foundation, Princeton, N. J.

A former recipient of the Kendall Award, Paul Hugh Emmett, is flanked on each side of the initial of his surname, E, by the initials of the surnames of two Hungarians, two of many who have enriched the scientific life and increased the stature of American science in the present century. The three initials, BET, have circumnavigated the globe in every research institute wherever it is necessary to define the surface area of solid bodies, whether they be fine but compact particles or porous solid structures. BET has become a shorthand notation for a measurement which has been of inestimable benefit to a wide spectrum of scientific workers in the last 25 years. Their appreciation of this new tool for surface area measurement can never be as whole-hearted as that of those of us who, in the 25 years preceding the BET equation, had literally to "grope in outer darkness." Indeed, such people occasionally are given to admiration, at the quality of their own intuitions, their leaps of faith, in the absence of the equation to which these three initials were given. To give a personal illustration, how could one dare to talk about "active centers on catalyst surfaces" in 1925, when there was no available definition of the totality of centers in the surfaces?

von Neumann, Wigner, Szilard, Teller, and others came to the United States by a primrose path. With already established reputations in science, they were hospitably welcomed to these shores by one or another of the great universities. Their obvious talents guaranteed to the country of their adoption a rich and precious reward.

This was not the case with the one we honor today. Born in Budapest, Hungary, on February 12, 1903, he graduated from the gymnasium in June 1921, a little over 18 years of age. Graduation in Hungary is labeled "matura," maturity. In his case, however, the designation was *praeclarus maturus*, outstandingly mature, the nearest American equivalent of which would be "valedictorian" of his class in high school.

By October of the same year he had emigrated to this country and the next seven years are a heroic illustration of trials and tribulations, and also the heart-warming achievement of a university education in spite of all the difficulties. Six days after arrival in New York he was at work in a factory by day, and attending evening school for immigrants to learn English by night. Eight months later, he started to attend the City College of New York in the evenings and kept on working during the day. He passed through college in four years, because Columbia University granted two years of college credit on the strength of the *praeclarus maturus*. He earned his living in these years in three factories, in a grocery store, in a laundry, in several restaurants as bus boy. He recalls, with

modest pride, that he never washed dishes. When he had saved enough money to pay for his tuition, he attended Columbia University as a day student and worked in the evening; when the money ran out, he worked during the day and attended City College at night.

In June 1925, he received an A.B. from Columbia University, majoring in chemistry and English. He learned from the *Spectator*, the university newspaper, that he was one of seven elected to Phi Beta Kappa. He had no idea at the time what that meant and was equally certain that he had no money to join a Greek letter fraternity. So he went to the library and read up on Phi Beta Kappa. How many members of this honor society have put forth such effort to be admitted to the select circle? It must have been, at many times, a painful discipline, but the richest rewards are so often those that are purchased dearly in toil and effort.

He preferred physics and chemistry to biology. But relatives wanted him to enter medical school. Fortunately for us, he had no money to pay his tuition fees at New York University, where he had been admitted. So he went back to City College and chemical engineering. In the last semester of his chemical engineer's training program he was offered a position as junior chemist in the Department of Agriculture, which he accepted. It was March 1928, the work was in the Fixed Nitrogen Research Laboratory. It was at this time that B joined E to make the BE or EB combination which adorns the pages of the *Journal of the American Chemical Society* from 1930 to 1937.

Many of us can remember the years of the Great Depression. One consequence was that he remained a junior chemist for eight years, but rose three steps in the next six years, leaving as a chemist to join the Navy as a lieutenant in October 1942. He married Esther Caukin in 1931. There were two children, Kathryn in 1938 and Betty in 1942. There was an M.S. at George Washington University in 1929, and a Ph.D. degree at Johns Hopkins in 1933. A year's leave of absence from the department served to meet the residence and language requirements, the preliminary and oral examinations, a joint paper with Joseph and Maria Mayer, and election to Sigma Xi. The dissertation was performed, by permission, at the Fixed Nitrogen Research Laboratory.

It has always seemed appropriate to this writer that the elbow in the adsorption isotherms of nitrogen on finely divided materials at liquid air temperatures should have been called Point B, because it was the outcome of a brilliant series of experimental measurements of such isotherms by the man we honor today. It was correctly identified as the approximate position of the completion of a monolayer of adsorption on the surface of the material and the beginning of multilayer adsorption. It is now common knowledge to students of even elementary physical chemistry that, in 1938, a theory of adsorption of gases in multimolecular layers was published. Point B was merged into the BET equation. The Washington Section of the American Chemical Society made him the Hillebrand prize winner in 1945 for this work.

It is in the record that the application for a commission in the United States Navy soon after the war broke out was rejected, with the statement that there was no need for a man of his qualifications. Fortunately for them, the Navy changed its mind and the call to active duty came in October 1942. The delay permitted the completion of the manuscript on "Adsorption of Gases and Vapors." I am happy to relate that it was started, at my persuasion, 21 months previously; I was instrumental in having it published at Princeton University Press in this country and at Oxford University Press in England. The manuscript was sent to Princeton on the day that the commission in the Navy was received. For that

reason, we can be thankful that the commission was delayed, more thankful because, though now nearly 20 years old, it has never been supplanted by a worthier successor. One casualty of the war was a second volume which was to deal with "Chemisorption" by the same author. His publication with Emmett in 1940 displays the quality which such a volume would have revealed.

High explosives research and development in which the next eight and a half years were spent, four in uniform and the remainder as a civilian, recall the Phi Beta Kappa episode. At the outset, the sum total of his background was that he knew the terms TNT and dynamite. By the end of the war, he was supervising the work of 45 persons and many more indirectly. Among his list of consultants, listed in alphabetical order, were Richard Courant, Albert Einstein, Henry Eyring, George Gamov, Jack Kirkwood, and John von Neumann. He rose from lieutenant to lieutenant commander, commander, then received the Commendation Ribbon of the Navy and, like myself, was made an Officer in the Order of the British Empire for services rendered to the United States, one of Britain's allies in World War II.

We should perhaps draw a discreet veil over the years immediately preceding September 1951, or stand for a silent moment in tribute to one who not only served his country well and faithfully but was also persecuted by his country.

Catalysis, adsorption, explosives, and like activities lost, simultaneously, a gifted scientist, but the Portland Cement Association was the gainer in its senior research chemist, its principal research chemist, and, since July 1958, its manager of the Basic Research Section. Esther Caukin, who shared the bitter years, died in June 1959, but we welcome his new wife and wish for them both long years of happiness together.

We could continue indefinitely, comparing and contrasting the pre-1940 and the post-1951 stages. We would come up always with the same answer. It would be of a man who could attain Phi Beta Kappa as an A.B. majoring in chemistry and English, one who might have enriched medical science but went through chemical engineering to illuminate physical chemical research in ways undreamed and unanticipated by him. This symposium by friends who have gathered to do him honor is vivid testimony to the quality of man who came to this country, unheralded and unsung, in the summer of 1921, and 40 years later receives from his peers in the science of chemistry one of their most distinguished awards. He has spoken to me often of the friendship and inspiration that has been his from his friends in the ups and downs of his life. I am proud that he asked me to be your spokesman in the conferring of the Kendall Award, expressing for you and, from the bottom of my heart also, our appreciation of the quality, yes, the nobility of the life of

Stephen Brunauer

Solid Surfaces and the Solid-Gas Interface

THE KENDALL AWARD ADDRESS

STEPHEN BRUNAUER

*Basic Research Section,
Portland Cement Association, Skokie, Ill.*

It is really heart-warming to see so many of my dear friends among you, and it is equally heart-warming to see so many unfamiliar faces, faces of those whom I have not had the privilege of meeting personally as yet. I never thought that the time would come when anyone would make a 20-minute address about me—let alone such an outstanding scientist and human being as Sir Hugh Taylor. I am profoundly grateful to him for honoring me with this wonderful address—it will always be one of the most treasured memories of my life—but I should like to assure him and assure you that I am keenly aware of my unworthiness of the honor bestowed upon me, and that I know full well that I am honored here because of his generosity and your generosity and not because of my own merits.

For all that, I confess that in spite of the knowledge of my inadequacy I am very happy to receive the Kendall Company Award for 1961. So I should like to express my sincere thanks to the Kendall Company for establishing the award and donating the funds for it, to the American Chemical Society for administering the award, to my friends who nominated me for the award, and finally to the Award Committee, whose members are unknown to me, but who selected me for this great honor.

I should like to say at this point also that practically all the contributions I have ever made were made in collaboration with others. So I have only partial share in all these contributions—and part of the honor I am now receiving should go to those with whom I collaborated. Nothing would please me more than to make my acknowledgment to each of them individually, but I am afraid this process would not be very interesting to most of you. I will mention, therefore, only four names now.

The first is the name of my first boss, the first chemist who befriended me, the first man with whom I collaborated, and the first man who made me interested in surface chemistry—Paul Emmett. I owe more to Paul Emmett than I can say here, and I wish to acknowledge it with deep appreciation.

Equal in importance in my scientific growth was Sir Hugh Taylor. Among other things, it was he who persuaded me to write the book, “The Adsorption of Gases and Vapors,” and as I wrote each chapter I sent it to him for his comments. Hugh was a source of guidance for me through much of my scientific life, and a source of inspiration through all of it. For that and for his friendship I want to express my deep gratitude.

The two other names I have picked from the list of my coworkers, one from the first decade and one from the last. The first is Edward Teller, whose name is known to hundreds of millions, and the second is Lew Copeland, to whom I owe

not only thanks for many things but also for organizing this wonderful symposium. To Edward Teller, to Lew Copeland, and to all my past and present coworkers I wish to express my profound gratitude.

Please, forgive me for the long introduction, but I would have felt bad if I had not had the opportunity to say these things. Coming to the subject of my talk, when Mr. Warren asked me last August for a title, I gave him, somewhat hastily, "Solid Surfaces and the Solid-Gas Interface." This may have created the impression in some of you that I intend to give you a bird's-eye view of these two broad fields in a single short lecture, but I do not intend to do that. I doubt that anyone could do that to an audience like this—I certainly could not. The second possibility was to give a bird's-eye view of the contributions that my coworkers and myself have made to these two fields, and that was my original idea. However, on second thought I discarded that, too. If I talk on any given subject for a few minutes, what can anyone get out of that, who does not know the subject, anyhow? So I have ended up by selecting only two topics, one from the field of the solid-gas interface, the other from the field of solid surfaces, and I have decided to discuss these in some detail. The first topic is the BET theory; the second is the surface of a particular solid.

The BET Theory

First, allow me to impart to you some of my present thoughts on the BET theory (3, 4) for whatever they are worth. [Reference (3) is a continuation and extension of the BET theory. Some authors refer to it as the BDDT theory; others call both papers together the BET theory.] Probably there are very few among you who have never made a BET plot, and many of you have made quite a few. I suppose, it will surprise no one among you if I say that I made the first BET plot. I did not know at that time that it was a BET plot, because that name did not exist yet. I tried to give a name to the theory that the three of us had developed, and I called it the multimolecular adsorption theory, which was probably not a very good name, but it was the best I could think of. Fortunately, somewhat later Professor Harkins invented the colorful name "BET theory," and that name has stuck.

The first BET plot was a plot of an adsorption isotherm that Emmett and I obtained a few years before, and it was the adsorption of nitrogen on something at liquid oxygen temperature. I had to make both liquid oxygen and liquid nitrogen myself from liquid air by rather crude means, and since liquid oxygen was easier to make, most of our isotherms were made at liquid oxygen temperature. This isotherm had eight points, ranging from 50- to 750-mm. pressure, a 15-fold range in pressure, and all of the points fell on a straight line—none of them deviated the breadth of a hair. I was astonished, and so was Paul Emmett when I showed him the plot. When I showed it to Edward Teller, he said that this cannot be true. No theory can fit that well. I plotted a lot more isotherms, and they all fitted just about as well. Figure 1 shows a groups of such isotherms. For example, see how accurately the line of curve 4 fits the eight points. Of course, this is because the data were obtained in the relative pressure range in which the BET equation fits, but at that time we did not know this. On one occasion, one of the plots showed a considerable curvature, so I tested the straight-edge I used, and found that it was curved, and not the BET plot. Occasionally, I found a point which fell off the line. Then I went back to the original data, recalculated the point, and found that my old calculation was in error—the point actually did fall on the line.

The fitting of the data with a curve is a necessary condition of the correctness

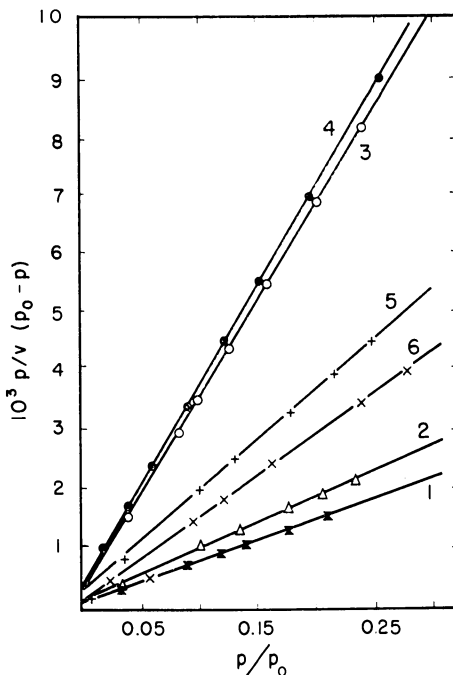


Figure 1. BET plots of nitrogen adsorption isotherms on six adsorbents at -183°C .

of a theory, but not a sufficient condition. This is well known now, but at the time we worked on the BET theory, it was not realized by surface chemists. In all prior theories of adsorption (1), with one exception, this single test of the theory was used to prove or disprove the theory. If the data fell on a straight line, the theory was proved. The one exception was the Polanyi theory, which also used a single criterion for its testing, but a different one. Since it offered no isotherm equation, the sole criterion was the correct prediction of the temperature dependence of the isotherm. We in the BET paper offered not one but four criteria. The first was the fit of the curve, an example of which is shown in Figure 1. The second was the correctness of temperature dependence, the same criterion which was used by Polanyi. Figure 2 shows how well the temperature dependence was reproduced by the theory. The parameters here were evaluated from one isotherm of each pair, and the other isotherm was calculated. If the theory had been wrong, we could have gotten isotherms which fell to the right or left of the experimental isotherms, but they fell on the right spot.

Parameter C. The two other criteria were the reasonableness of the two parameters evaluated from the straight lines, V_m and C . The C parameter includes the heat of adsorption. By assuming that the entropy term is of the order of unity, we calculated an average heat of adsorption for the first layer from C , and found that it was right in the ball park. If the model had been seriously in error, we could have gotten an average heat of adsorption which was ten times as large or one tenth as large as the known average heats of adsorption. Actually, the values were of the right order of magnitude, but they were always smaller than one would expect them to be, sometimes even smaller than 50% of the expected value.

One obvious explanation was pointed out by us at the start. The BET equation is always fitted in the region of monolayer coverage, let us say, in the range of $\theta = 0.5$ to 1.5 monolayers. The points fall off the curve at low coverages, indicating more adsorption and higher heats of adsorption. Thus, the C constant does not evaluate the average heat of adsorption for the entire first layer, but the average heat of adsorption for a part of the first adsorbed layer—that part which takes place on the energetically less active sites of the surface.

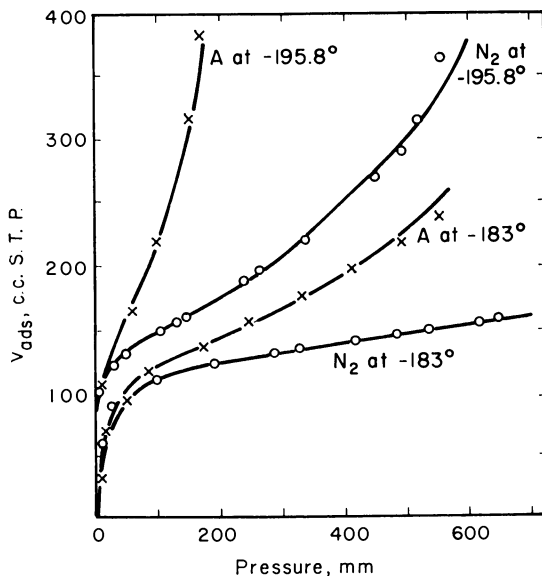


Figure 2. Adsorption isotherms of nitrogen and argon on iron

While this must certainly be a part of the explanation, examination of the heat of adsorption data in the literature indicates that this is not the whole explanation, nor even the most important part. However, a very interesting paper by Clampitt and German (10) goes a long way toward completing the explanation. These investigators have pointed out that the heats of vaporization of thin films of liquid are different from the heat of vaporization of the bulk liquid, and they have developed a theory for calculating the heats of vaporization of these thin films. Figure 3 shows their results for three liquids. The authors then proceeded to rederive the two-parameter BET equation by discarding the assumption that the heat of adsorption was constant for the second and higher adsorbed layers and was equal to E_r , the heat of vaporization of the bulk liquid. They assumed instead that the heat of adsorption for the second, third, etc., adsorbed layers was equal to the heat of vaporization of a film two, three, etc., layers in thickness. The beauty of their treatment was that this assumption did not add an extra parameter to the two, V_m and C ; their final equation was formally identical with the two-parameter BET equation—only the meaning of C changed. The exponential term in C did not contain $E_1 - E_r$ only, but another term as well, which could be calculated from their theory.

Clampitt and German illustrated their results with a reinterpretation of certain data of Harkins and Boyd (16) for the adsorption of benzene on TiO_2 at 25°C .

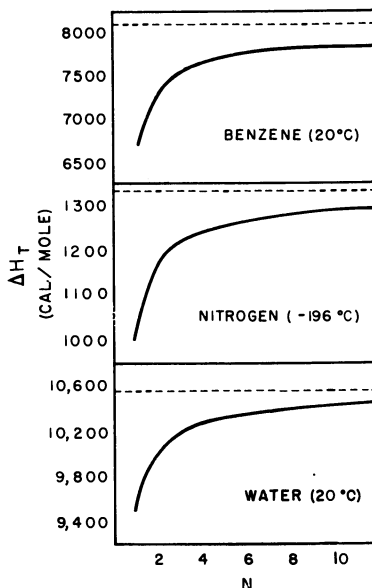


Figure 3. Total heat of vaporization vs. number of adsorbed layers above the first

Harkins and Boyd found by heat of emersion experiments that the value of $E_1 - E_L$ was 5.2 kcal. per mole, whereas the C constant of the BET plot gave a value of only 2.6 kcal. per mole. Clappitt and German calculated the third energy term in C , and showed that with their interpretation of C the value of $E_1 - E_L$ obtained from the BET plot was 4.3 kcal. per mole, which is much closer to the experimental value. If we combine the two explanations I have discussed, the discrepancies between experimental and theoretical values practically disappear.

Parameter V_m . Next I should like to talk about the parameter V_m . The test of the correctness of V_m is, naturally, whether it gives the correct surface area for a given adsorbent or not. When we wrote the BET paper, the best that we could offer in support of the V_m values was their agreement with the Point B values (13). In addition, we pointed out the internal consistency of the results—i.e., different adsorbates gave approximately the same specific surface area for a given adsorbent. For example, for a silica gel sent to us by Lloyd Reyerson we used six different gases (argon, nitrogen, oxygen, carbon monoxide, carbon dioxide, and butane), and none of the surface areas obtained from the V_m values differed from the average by more than 10%. However, internal consistency is only a necessary condition of the correctness of V_m , but not a sufficient one. The question still remained whether the surface obtained from V_m was the true surface or not. By the time I wrote the book (1) a few years later, there was an imposing array of evidence that V_m gave the true surface. I shall recall to you the one I considered the most impressive proof at that time, and still do. For two carbon blacks, electron microscopic average particle size determinations were compared with average particle sizes calculated from BET surfaces. For Micronex, the electron microscope (12) gave an average diameter of 28 $\mu\mu$, nitrogen adsorption gave 28 $\mu\mu$, obtained by Smith, Thornhill, and Bray (25), and 31 $\mu\mu$, obtained by Emmett and DeWitt (14). For acetylene black, the electron microscope gave

51 $\mu\mu$, nitrogen adsorption gave 52 $\mu\mu$, obtained by Emmett and DeWitt, and 53 $\mu\mu$, obtained by Smith, Thornhill, and Bray. This is not merely internal consistency, but true accuracy. In the subsequent two decades, the number of such examples has multiplied.

Let us return now to Lloyd Reyerson's silica gel. Reyerson and Cameron (24), in 1935, published adsorption isotherms of bromine and iodine on silica gel, and obtained some beautiful and quaint isotherms of the kind that are now called Type III isotherms. The bromine isotherms are shown in Figure 4. Five years later, in the BDDT paper we showed that the simple, two-parameter BET equation can describe Reyerson's Type III isotherms even better than it can describe Type II isotherms. By making a single assumption that the value of the C parameter for bromine was 1, the four isotherms of Reyerson at four temperatures were accurately calculated. Thus, not only the course of the isotherms was described, but also their temperature dependence came out almost perfectly, as seen in Figure 4. The curves are theoretical; the points are experimental. I said that there was a single assumption, $C = 1$, but even this can hardly be called an assumption, because the isosteric heats of absorption calculated by Reyerson and Cameron strongly indicated that E_1 was very close to E_L . Now comes the thing that gave me one of the greatest thrills of my entire research career—and it still does quite a bit—the V_m value evaluated from the bromine data gave a specific surface for the silica gel that agreed within 5 or 6% with the surface obtained from Type II isotherms of the six other gases about which I talked before. As you see, these Type III isotherms do not have a Point B—there is nothing in the isotherm that indicates the completion of a monolayer. When $C = 1$, V is equal to V_m at the relative pressure of 0.5, but this point is an indiscriminate point on a continuously rising isotherm.

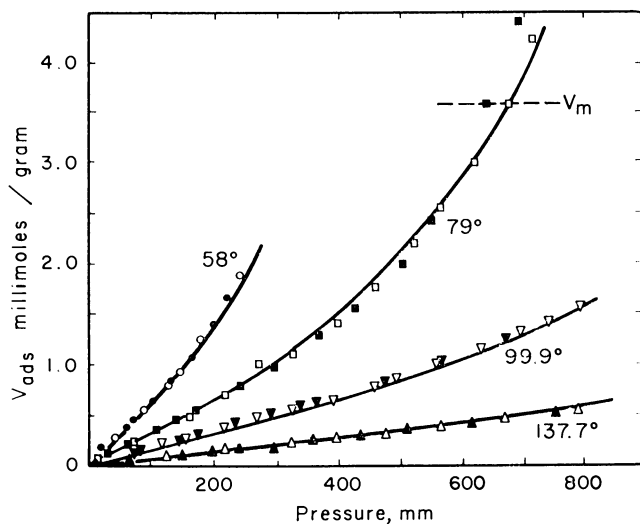


Figure 4. Adsorption isotherms of bromine on silica gel

By assuming a value of C which was considerably less than 1, the four Type III iodine isotherms of Reyerson and Cameron were very well fitted. Because the value of C was 1 for bromine and only a fraction of 1 for iodine, it was easy to see that it should be well over 1 for chlorine; so we predicted that chlorine would

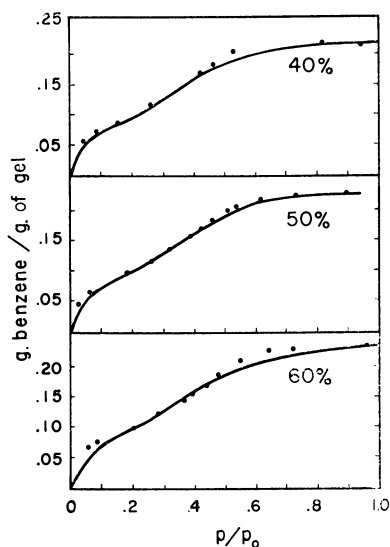


Figure 5. Adsorption isotherms of benzene on ferric oxide gel

give Type II and not Type III isotherms on silica gel. Whereupon Reyerson and Bemmels (23) went ahead and investigated the adsorption of chlorine on this same silica gel and did obtain Type II isotherms—and the isotherms agreed well with the BET theory.

Type IV Isotherms. I wish to say a few words now about the Type IV isotherms for which we advanced a theoretical explanation in the BDDT paper (3). Edward Teller and I independently derived the isotherm equations for this case, and he dictated his equation to me into the phone. It was a long one, as some of you know, and I got a different one, which was even longer. Because I could not get together with him for some time, I showed my derivation to Ed Deming, and he concluded that my derivation was correct. I am not saying this to boast that there was an occasion when I was right and Edward Teller was wrong, because I am quite sure that if one of us had been wrong, it would have been I. What happened was that we were both right. In the derivation, there is a parameter n , which represents the maximum number of layers that can fit into a capillary. Edward assumed that the n layers fitted the capillary exactly, whereas I assumed that the n layers did not fit the capillary exactly. In the paper you can find both equations.

These are four-parameter equations, and Lola Deming spent weeks at her desk calculating machine to fit the curves that Lambert and Clark obtained for the adsorption of benzene on ferric oxide gel (21). These isotherms are shown in Figure 5. I do not blame anyone for not using these equations, and actually very few have used them to date. Joyner and Emmett (20) were among the hardy souls who did. Clampitt and German published another paper very recently (11), which is well worth reading for all those who deal with Type IV isotherms.

Criticism of BET Theory

I should like to tell you only one more thing about the BET theory. Many years ago Cassie (9), and somewhat later Terrell Hill (18), derived the BET

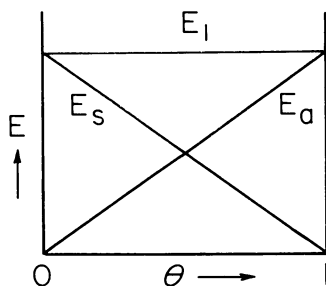


Figure 6. Idealized variation of heat of adsorption, E , with coverage, θ

E_s . Surface condition
 E_a . Adsorbate interaction contribution

equation by statistical mechanics. In these derivations, the assumptions were made that adsorption takes place on a uniform surface and that there is no lateral interaction between the adsorbate molecules. Ever since that time—or perhaps even before that time—practically all writers of books and papers have repeated that the BET theory assumes a uniform surface and no interactions between the adsorbate molecules. Back in 1952, there was a conference on solid surfaces, the proceedings of which appeared in a book, edited by Gomer and Smith (15). In this book, there is a paper by Hill (19), to which a discussion of mine is attached (2), in which I pointed out that neither the BET theory nor the Langmuir theory, on which it is based, makes such assumptions. Not many people have read this discussion, so even last year at the Gordon Conference on Chemistry at Interfaces I had to argue with several of our leading surface chemists on this point, but I think I succeeded in convincing them.

For simplicity, we will talk about the Langmuir theory. This theory assumes that the heat of adsorption is constant over the entire surface—and so does the BET theory. Naturally, if one has a uniform surface and there is no interaction between the adsorbate molecules, one gets a constant heat of adsorption—this is a sufficient condition, but not a necessary one. One can get a constant heat of adsorption in other ways, as well. This is illustrated in Figure 6, taken from the Gomer-Smith book. Of course, this is an extremely idealized example, but it will make the point clear. Most adsorbents have nonuniform surfaces, and if you plot the differential heat of adsorption against fraction of the surface covered, you get a diminishing function like E_s , because adsorption at low coverages takes place on the energetically more active sites. Let us consider next lateral interaction on a uniform surface. If you plot the energy of interaction against the fraction of the surface covered, you get an increasing function like E_a , because the more adsorbate you have on the surface, the more interaction energy you will have. So these two effects are in the opposite directions, and if and when they balance each other, you have a constant heat of adsorption. My good friend Prof. Shereshefsky asked me how frequently I would expect such a balancing. My answer is that mathematically never or hardly ever, physicochemically possibly quite frequently. If the sum of the two effects is a slightly decreasing function, or a slightly increasing function, or if it goes up and down—but not too strongly—about a mean, you have an approximately constant heat of adsorption, and, physicochemically, that is all you need.

What I have been trying to do in this discussion is to show that the BET theory, and its continuation, the BDDT theory, can do a good deal more than merely give the specific surface areas of finely divided solids. It can give a description of the process of physical adsorption, and it can account for five different isotherm types—the account being, at worst, semiquantitative, at best, quantitative. I have also meant to imply not that all criticism of the theory is wrong, but that some of the criticism is wrong. I am well aware of the shortcomings of the theory and I not only hope but I am certain that the time will come when it will be superseded by a more complete and more accurate theory of physical adsorption. Right now we have a number of theories which can describe some of the aspects of physical adsorption more accurately than the BET theory.

Surface of Tobermorite

The second part of my talk deals with the surface of a particular solid, a calcium silicate hydrate, called tobermorite. The two main constituents of portland cements are two calcium silicates, which make up about 75% or more of a portland cement by weight, and both of these silicates produce tobermorite in their reaction with water. This tobermorite is the most important constituent of hydrated portland cement, concrete, and mortar. That is not the reason, however, for my talking about it—the reason is that it is a fascinating substance for a colloid chemist. I will discuss only two properties of the tobermorite surface: the surface area and the surface energy.

The tobermorite obtained in the hydration of tricalcium silicate (Ca_3SiO_2), β -dicalcium silicate ($\beta\text{-Ca}_2\text{SiO}_4$), portland cement, and concrete is a colloid, with a specific surface area of the order of 300 sq. meters per gram. To give an idea of how the elementary particles of tobermorite look, Figure 7 is an electron micrograph of a few particles (obtained by L. E. Copeland and Edith G. Schulz at the Portland Cement Association Research and Development Laboratories). These particles look like fibers, but if you watch them closely, you see that they are very thin sheets, rolled up as one would roll up a sheet of paper. At the lower end the sheets are partly unrolled. When one prepares tobermorite by the reaction of lime and silica, one usually obtains crumpled sheets, which are not rolled up. The electron microscopists tell us that the sheets are very thin, of the order of a single unit cell in thickness.

Tobermorite is a layer crystal, like many clay minerals—e.g., montmorillite and vermiculite. The unit cell of tobermorite is orthorhombic—i.e., a , b , and c are perpendicular to each other. The dimensions of the unit cell were determined by Heller and Taylor (17). Dimensions a and b lie within the layer, and c is perpendicular to the layer—it is the distance between two layers.

Let us calculate now the specific surface area of tobermorite, with the assumption that the sheets are one unit cell in thickness (5). Because the length and breadth of the sheet are very large compared to its thickness, just as for a piece of paper, it can be assumed that all the surface is on the two sides of the sheet, and the areas along the edges can be neglected. The surface contributed by a unit cell is $2ab$, and if there are N unit cells in the sheet, the surface area is $2abN$. If there are n molecules in the unit cell, and the weight of a molecule is m , the weight of a unit cell is nm , and the weight of the sheet is nmN . The specific surface area then is $2ab/nm$, and these are all known quantities. The result is 755 sq. meters per gram.

Let us assume next that the sheet is two unit cells thick. We can still neglect the edge areas, so the surface remains unchanged, but now the weight is doubled.

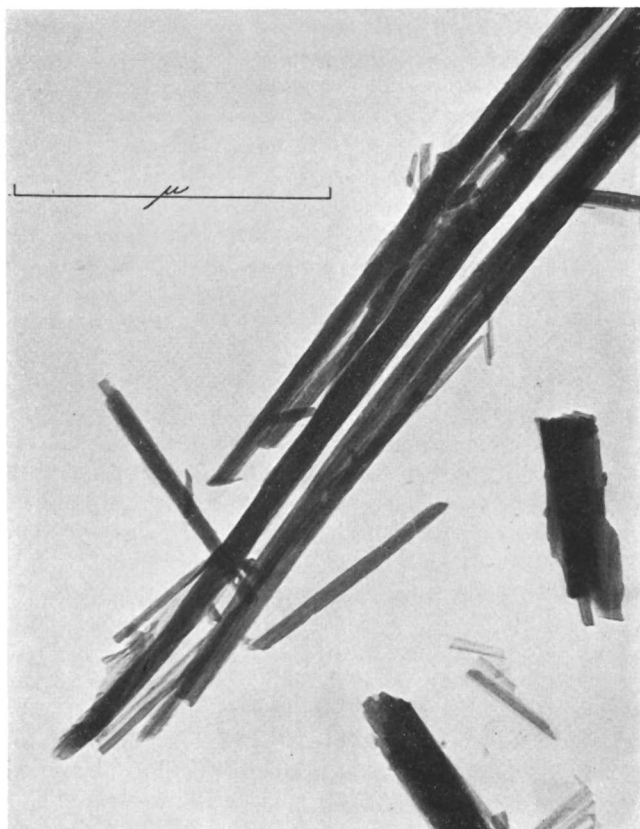


Figure 7. *Electron micrograph of tobermorite obtained from hydration of β -dicalcium silicate*

So we have a specific surface of 377 sq. meters per gram. Finally, let us assume that the sheet is three unit cells thick. Then the specific surface is 252 sq. meters per gram.

In a series of experiments (8), we determined the specific surface areas of 14 tobermorite preparations, made from different starting materials (Ca_3SiO_5 and $\beta\text{-Ca}_2\text{SiO}_4$), with different water to solid ratios (0.7 and 9.0), and using different methods of preparation. The BET method was used, with water vapor as the adsorbate. We use nitrogen, too, but it did not measure the total surface, as I will show. The largest specific surface we measured was 376 sq. meters per gram, the smallest was 245, and all the others fell between these limits. We concluded, therefore, that in one preparation practically all of the tobermorite sheets were two unit cells thick, in another practically all of them were three unit cells thick, and in all the rest the particles were either two or three unit cells thick.

I believe that this is a fine confirmation of the correctness of the V_m values obtained by water vapor adsorption. On the other hand, nitrogen adsorption gave surface areas that ranged from 20 to 100% of the surface areas obtained by water vapor adsorption. I said that nitrogen did not measure the total surface, and I give one evidence for it now and one later. Dr. Copeland determined the specific surface of a hydrated portland cement by small-angle x-ray scattering. The value he obtained checked the water adsorption value within 2 or 3%. On the other

hand, nitrogen adsorption gave a surface about half as large. The other evidence will be given after I discuss the surface energy of tobermorite.

Surface energy is an abbreviation for surface total energy, and it can be defined as the difference between the total energy of a molecule of a given substance in the surface layer and the total energy of the same molecule inside the body of that substance. It is customary to express it in ergs per square centimeter. In the best determinations to date, the heat of solution method of Lipsett, Johnson, and Maass (22) has been used. A substance in different states of subdivision is dissolved in a suitable solvent, and the heat of solution is plotted as a function of the specific surface area. The slope of the curve is the surface energy. To be sure, what one obtains in this way is really the surface enthalpy, but the pv term in the surface region is small, so beginning with Gibbs and continuing with Harkins most investigators have made no distinction between surface total energies and surface enthalpies.

Some years ago, Kantro, Weise, and I set out to determine the surface energy of tobermorite. We came to grief, because the practice is usually not as simple as the principle. We decided, therefore, to work on some simpler but closely related substances, and we determined the surface energies of calcium oxide, calcium hydroxide, amorphous silica, and hydrous amorphous silica. Even these determinations did not turn out to be simple. We published these in two papers in the *Canadian Journal of Chemistry* in 1956 (6, 7). After this work, we felt strong enough to tackle tobermorite, and we published the surface energy of tobermorite in the same journal three years later (8).

I told you about the variability of the tobermorite specific surface, and in Figure 8 I show you the variation of the heat of solution with specific surface. The 14 preparations I mentioned before are represented by the 14 points on this curve, and the points randomly scatter around the least squares straight line. They do

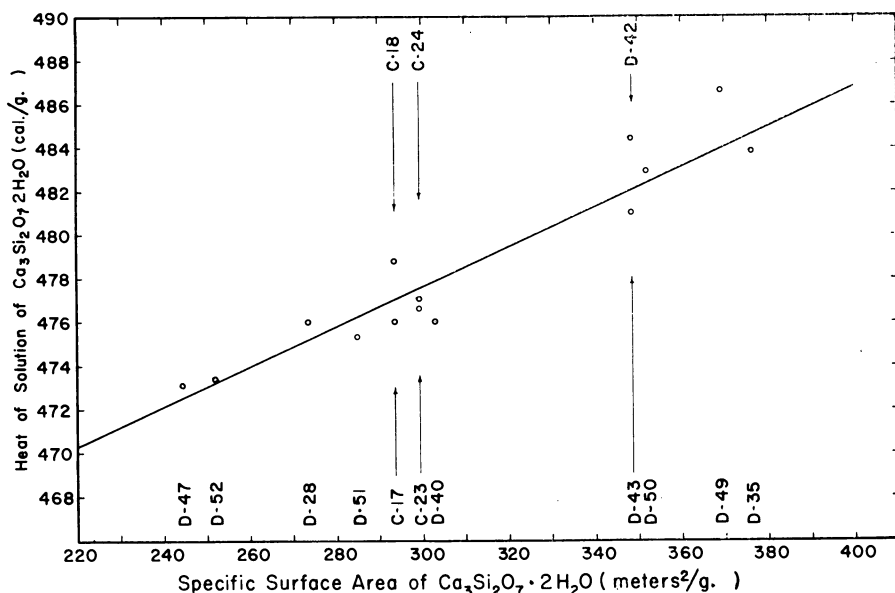


Figure 8. Variation of heat solution of $\text{Ca}_3\text{Si}_2\text{O}_7 \cdot 2\text{H}_2\text{O}$ with specific surface area for 1.0-gram samples

not fall beautifully on a straight line, but if you knew the difficulties encountered in this system, you would not be the least bit surprised. The slope of this line gives a surface energy of 386 ± 20 ergs per sq. cm.

If I had been asked before we started to determine the surface energy of tobermorite, to make an educated guess of what the result would be, I would have argued this way. Speaking with some license, the surface of this calcium silicate hydrate is a sort of "chemical mixture" between the surface of calcium hydroxide and that of hydrous silica. Add to this the fact that the calcium hydroxide we used in the surface energy determination contained almost perfect crystals, the hydrous silica was amorphous, and the calcium silicate hydrate, tobermorite, was intermediate between these extremes, it was poorly crystallized. The surface energy of calcium hydroxide was 1180 ergs per sq. cm., that of hydrous silica 129 ergs per sq. cm., so I would have guessed that the surface energy of tobermorite would be the geometric mean of these two. It has turned out to be almost exactly that.

The surface areas of calcium hydroxide and hydrous amorphous silica were determined by means of nitrogen adsorption. The surface areas of tobermorite were determined by water vapor adsorption, and as you see, the three surface energies thus determined show a remarkable consistency. I said also that nitrogen adsorption did not give the entire surface area for tobermorite, and let me tell you now what I meant. Please look at the point D-28 in Figure 8. This preparation gave one of the smallest heats of solution, but it gave the largest area by nitrogen adsorption. On the other hand, preparation D-42, which gave a heat of solution more than 8 cal. per gram larger than D-28, had a nitrogen surface that was less than 40% of the nitrogen surface of D-28. If we would calculate the surface energy from these two preparations, we would get a large negative value, which is absurd. Actually, there was no correlation between heat of solution and nitrogen surface.

The probable explanation, I believe, is the following. The sheets of tobermorite roll into fibers, as in the electron micrograph (Figure 7). This rolling of the sheets plus the aggregation of the fibers create spaces into which nitrogen cannot penetrate but water can. This is not merely because of the difference between the sizes of the molecules, but also because the tobermorite surface is strongly hydrophylic.

I will say only two more things about this slide, and that will conclude my talk. I mentioned that we used a variety of ways to prepare the samples of Figure 8. The four points in the middle (C-17, 18, 23, and 24) were obtained by paste hydration. The calcium silicates were mixed with water for a few minutes, then the mixture was allowed to stand for about a year and a half. This type of hydration is very slow. The four points at the left end (D-47, 52, 28, and 51) were obtained by hydration in a small steel ball mill. This produces a much faster hydration—complete hydration was obtained in 6 weeks. My knowledge of solid state physics is negligible within experimental error, but I would think that the preparations that were banged around by steel balls for 6 weeks or longer should have more defects than the preparations that were allowed to stand peacefully. This would lead to higher energies for the ball-mill preparations, and higher heats of solution, but, as you see, the reverse is true. I do not mean to imply that there are no defects in our tobermorites, but I believe that these defects do not play a decisive role in these experiments.

The last remark is this. Please look at point D-49. This is the point that falls farthest away from the straight line—it is 2.6 cal. per gram too high. I am con-

vinced that this is random error, but let us assume that it is not. Let us assume first that all of this difference is caused by some variation in the body structure, such as differences in defects, for example. The 2.6 cal. per gram amounts to only 0.58% of the heat of solution. Let us assume next that none of this difference is caused by variation in the body structure, but all is caused by variation in the surface structure. This amounts to only 7.6% of the surface energy of tobermorite. Please note that I am giving these figures for the preparation which showed the maximum deviation. If I made the same calculations for the average deviation, which is only 1.1 cal. per gram, the results would be less than half of the values I gave before.

The conclusion is that both the body structure and the surface structure of tobermorite are highly reproducible. Whether we use tricalcium silicate or β -dicalcium silicate as starting solids, whether we use a water to solid ratio of 0.7 or 9.0, whether we use paste hydration or ball-mill hydration or a third type which I have not discussed (which gave the six other points on the curve), we wind up with a tobermorite having very nearly the same body structure and surface structure.

Literature Cited

- (1) Brunauer, S., "Adsorption of Gases and Vapors," Vol. I, "Physical Adsorption," pp. 53-149, Princeton University Press, Princeton, N. J., 1943.
- (2) Brunauer, S., "Structure and Properties of Solid Surfaces," R. Gomer, C. S. Smith, eds., p. 395, University of Chicago Press, Chicago, 1953.
- (3) Brunauer, S., Deming, L. S., Deming, W. E., Teller, E., *J. Am. Chem. Soc.* **62**, 1723 (1940).
- (4) Brunauer, S., Emmett, P. H., Teller, E., *Ibid.*, **60**, 309 (1938).
- (5) Brunauer, S., Kantro, D. L., Copeland, L. E., *Ibid.*, **80**, 761 (1958).
- (6) Brunauer, S., Kantro, D. L., Weise, C. H., *Can. J. Chem.* **34**, 729 (1956).
- (7) *Ibid.*, p. 1483.
- (8) *Ibid.*, **37**, 714 (1959).
- (9) Cassie, A. B. D., *Trans. Faraday Soc.* **41**, 450 (1945).
- (10) Clampitt, B. H., German, D. E., *J. Phys. Chem.* **62**, 438 (1957).
- (11) *Ibid.*, **64**, 284 (1960).
- (12) Columbian Carbon Co., *Ind. Eng. Chem., News Ed.* **18**, 492 (1940).
- (13) Emmett, P. H., Brunauer, S., *J. Am. Chem. Soc.* **59**, 1553 (1937).
- (14) Emmett, P. H., DeWitt, T., *Ind. Eng. Chem., Anal. Ed.* **13**, 28 (1941).
- (15) Gomer, R., Smith, C. S., eds., "Structure and Properties of Solid Surfaces," University of Chicago Press, Chicago, 1953.
- (16) Harkins, W. D., Boyd, G. E., *J. Am. Chem. Soc.* **64**, 1195 (1942).
- (17) Heller, L., Taylor, H. F. W., *J. Chem. Soc.* **1951**, 2397.
- (18) Hill, T. L., *J. Chem. Phys.* **14**, 263 (1946).
- (19) Hill T. L., "Structure and Properties of Solid Surfaces," R. Gomer, C. S. Smith, eds., p. 384, University of Chicago Press, Chicago, 1953.
- (20) Joyner, L. G., Emmett, P. H., *J. Am. Chem. Soc.* **70**, 2359 (1948).
- (21) Lambert, B., Clark, A. M., *Proc. Roy. Soc. (London)* **A122**, 497 (1929).
- (22) Lipsett, S. G., Johnson, F. M. G., Maass, O., *J. Am. Chem. Soc.* **49**, 925 (1940).
- (23) Reyerson, L. H., Bemmels, C., *J. Phys. Chem.* **46**, 31 (1942).
- (24) Reyerson, L. H., Cameron, A. E., *Ibid.*, **39**, 181 (1935).
- (25) Smith, W. R., Thornhill, F. S., Bray, R. I., *Ind. Eng. Chem.* **33**, 1303 (1941).

RECEIVED May 9, 1961.

Sintering of Refractory Materials at Room Temperature by High Pressures

PETER W. MONTGOMERY, HAROLD STROMBERG, and GEORGE JURA

*Department of Chemistry and Lawrence Radiation Laboratory,
University of California, Berkeley, Calif.*

The process of sintering refractory solids at room temperature by high pressures was studied, including the effect of purity, particle size, and calcining temperature. A possible mechanism for the sintering is discussed. Two applications are presented: first, the determination of spectra of solids which in general cannot be obtained because they are available only as powders; and second, squeezing out the pores of a catalyst support, which permitted determination of the rate of growth of platinum particles on an alumina support as a function of temperature.

The primary objective of our high pressure program is the study of the electrical and magnetic properties of solids. With our present apparatus we can reach pressures as high as 500,000 atm. In pursuing the main objective we have stumbled on a phenomenon described in this paper—namely, the compaction of finely divided solids into transparent disks which must have densities very close to the theoretical density of the solid. For want of a better term we have called this pressure sintering. In the ordinary sintering process the material is subjected to a pressure of several hundred atmospheres at an elevated temperature. In the present process, a similar result is obtained at room temperature but at very high pressures, the pressure required being a function of the material. This process is only partially understood at the present time; however, a reasonable explanation can be given for the results obtained.

The compression of a solid to transparency is really not new. A standard technique in infrared spectroscopy is the use of mulls made of the heavier alkali halides. These materials are squeezed transparent at relatively low pressures. However, when these low pressures are used, evacuation of the sample is essential. In our work, evacuation is not necessary. A reasonable review of the alkali halide work is given by Ford, Wilkinson, and Price (4).

Our attention was first called to the possibility of sintering at room temperature some five or six years ago, when we found that lithium aluminum hydride was as transparent as glass after having been subjected to a pressure of 100,000 atm.

With the passage of time we also have been able to squeeze many oxides to the transparent state. The disks remained transparent even after several years of aging. Some of the disks developed cracks, but this was not unexpected because of the strain that was introduced by subjecting the materials to stresses beyond their elastic limits.

Optical Transparency

The criterion that we use for the approach to theoretical density is that of optical transparency. This criterion limits the work at the present time to materials that are transparent in the visible or have absorption bands that do not extend over the entire visible region. In general, and for mechanical reasons alone, the size of the sample is about 10 mg. We are not equipped to measure directly the densities of such small samples with high precision. However, if we start with particles that are as small as 100 Å. on edge, and the final sample is transparent, it is reasonable to suppose that the number of scattering centers is very small. The very small number of scattering interfaces indicates that the particles have come into intimate contact with each other—i.e., the large number of solid-air interfaces have been replaced by solid-solid interfaces. On this basis we assume that the samples have approached theoretical density. For example, after application of 60,000-atm. pressure, a sample of magnesium oxide 0.02 cm. thick showed 85% light transmittance.

In order to understand the pressure-sintering process, first consider the behavior of a single crystal placed in a pressure chamber whose volume is greater than that of the crystal. In this case, the course of events as pressure is applied to and incurred on the sample can be easily predicted. At the lowest applied pressure, the crystal would deform elastically. At a pressure above the strength of the material, the crystal would flow until the pressure chamber is entirely filled by the crystal. Further application of pressure would merely compress the materials.

In our studies, we start with finely divided powder. This complicates the analysis to the point where it is not possible to present more than a simple qualitative explanation of the pressure-sintering process. In general, the apparent density of a powder is about 50% of that of a single crystal. Furthermore, the particles are randomly oriented. When pressure is applied to this conglomeration, particles certainly can move with respect to each other to fill the space more completely. Also, it appears reasonable that a certain number of particles are oriented so that they can undergo plastic flow. What is certain is that, at some pressure, the total force will be sufficiently great so that plastic flow will occur in all particles. When this pressure is reached, in the absence of any gases, the particles will flow until they come into contact and the flow will continue until no void space remains within the sample.

Bridgman (1) has found in his studies of the compression of nitrogen and argon that these gases diffused through steel containers so rapidly at pressures above 30,000 atm. that equation of state work could not be extended above this pressure at room temperature. It is reasonable to assume that ordinary air would behave in a similar manner. Thus, one would expect that at a pressure of about 30,000 atm. the air surrounding the powder particles would start diffusing out of the sample, and the flow of the material would not be restricted by the gas originally present. In short, at pressures above 30,000 atm., one would not expect the atmosphere to impede the flow of the individual particles by the formation of an

air pocket. For this reason, if the compaction is done at the very high pressures we use, it is not necessary to evacuate the sample before sintering.

One further condition is necessary that has not been discussed. In the foregoing discussion it was tacitly assumed that the deformation and flow of the container were small compared to those of the sample. If the material in the pressure cavity is harder or stronger than the apparatus, the flow will occur in the apparatus and not in the sample. However, when we attempted to pressure-sinter diamond dust, it was the apparatus that flowed and not the diamond particles. Besides the high pressure, it is essential that the sample be softer than the material of the apparatus. This last limitation precludes very few materials from study, since the parts of the apparatus in contact with the sample are compacted tungsten carbides, such as G. E. Carboloy 999, which is extremely hard.

The pressure vessel used in these experiments was a set of anvils similar to that described by Bridgman (2). The necessary thrust was developed with a hydraulic press of 100-, 200-, or 500-ton capacity, depending on the total force needed. The total force required depends on the nature and diameter of the sample.

Before the actual sintering, the powder was pelleted in a small die. The pellets varied from $7/16$ to $3/16$ inch in diameter and were about 0.006 inch thick. After pelletization, the sample was placed between the faces of the anvils. A ferric oxide-coated pyrophyllite ring was used to contain the sample. Pressure was increased in 10,000-atm. increments. About 2 minutes were allowed for the dissipation of the heat generated by each compression. The sample was maintained at the maximum pressure for about 10 minutes, after which pressure was reduced continuously until the press rams opened, permitting withdrawal of anvils.

Three general observations have been made which seem to influence the pressure at which transparency for a given solid was obtained. In general, higher pressure was required when the particle size increased, the purity of the sample lowered, and the calcining temperature of the solid before application of pressure was raised. The first two factors are in accord with temperature sintering. The latter seems to have no counterpart, and it seems difficult to account for this behavior. However, this behavior has been observed repeatedly. For example, eta-aluminum oxide calcined to 600° C. became transparent at a pressure of 100,000 atm. If the same sample was calcined to 800° C., a pressure of 400,000 atm. was necessary before sintering was accomplished. This observation gives rise to a great deal of speculation, but no one argument leads to a reasonable explanation at the present time.

Earlier it was stated that the transparency of the sample was maintained at room temperature for several years. If the sample of an oxide was annealed at a sufficiently low temperature, no change in transparency or structure of the sample was apparent to the human senses. However, as the annealing temperature was increased, opaqueness and mechanical weakness set in at a temperature characteristic of the solid. At about 100° to 200° C. after this degeneration set in, the sample crumbled and appeared to revert to its initial condition.

A plausible explanation for this behavior is based on the existence of hydroxide on the surface of the individual particles. It is known that the surfaces of most oxides are hydroxide rather than oxide. In some oxides this is true of the surface alone, while for others, the complete sample can be converted to hydroxide on prolonged contact with the atmosphere. When the temperature is raised sufficiently, the hydroxide decomposes to water and oxide. Gaseous water is certainly formed at the grain boundary. At a sufficiently high temperature the pressure of

the water vapor probably becomes great enough to separate the particles from each other.

X-Ray Study of Magnesium Oxide

A partial x-ray study of magnesium oxide gave some insight into the details of the internal changes. The specific area as measured by nitrogen adsorption was such that if the particles were in the shape of cubes, the cubes would be 100 Å. on edge. This sample showed transparency when pressed at 30,000 atm. or higher. Figure 1 exhibits the half width of the 200 line as a function of the pressure to which the oxide had been subjected. Because of the very large line width, this was the only line that could be studied. The half width increases by nearly two between 30,000 and 200,000 atm.

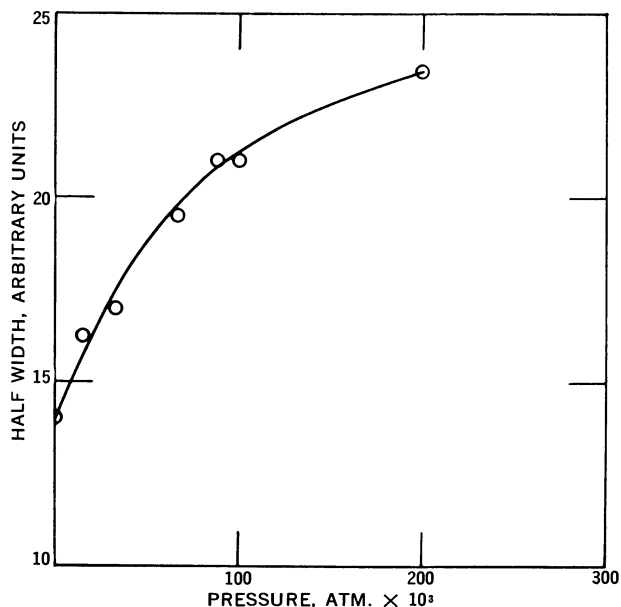


Figure 1. Effect of pressure on the half width of the 200 line of MgO

Figure 2 shows the effect of annealing on the half width of the 200 line for a sample that had been originally compacted at 60,000 atm. The disk was heated to 350° C. for 15 minutes, and its half width measured. The same sample was then annealed for the same length of time, increasing the temperature at 50° intervals until the sample crumbled. For reference, the same treatment and measurement were made on the original powder.

The initial anneal to 350° showed a very marked narrowing of the half width of the line. Further heat treatment to 550° C. showed a small decrease in half width. Above this temperature, where crystal growth sets in, the two became indistinguishable, indicating that crystal growth was the most important factor in the determination of the x-ray line width when heated above this temperature.

The x-ray experiment is not conclusive, because only a single line could be

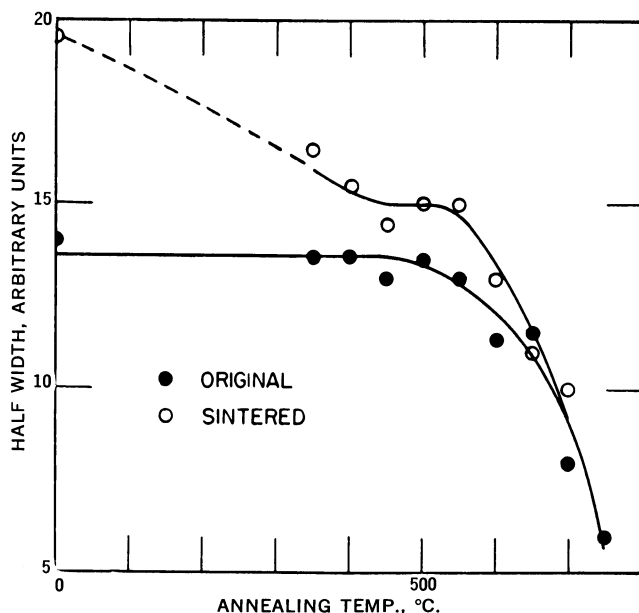


Figure 2. Effect of annealing on the half width of the 200 line of MgO

Original powder and sample sintered at 65,000 atm.

studied. The increase in line width could have been due to a decrease in the particle size or to the introduction of strain. If the increase in line width was caused by the diminution of the size of the particles, then the half width could have been proportional to $\tan^2 \theta$ if the increase in width was due to the introduction of strain in the sample. The rapid decrease in line width at temperatures below that at which crystal growth normally occurs indicates that a large part of the line width increase was due to strain. The remaining increase in line width indicated that there also has been a decrease in the size of the particles. Considering the manner in which the compaction occurs, this appears to be a foregone conclusion without the x-ray evidence.

Apart from the intrinsic interest in the process, there are a number of applications of pressure sintering. We mention two. First, this compaction permits the determination of the spectra of solids which cannot be obtained when the sample is in its usual form. For example, Conway (3) has determined the adsorption spectrum of gadolinium oxide down to 2000 Å. A similar study is being made on europium oxide by Nathans (5).

The second application has a direct bearing on catalysis. Powell, Somerjai, and Montgomery (6) have used this pressure-sintering process to determine the rate of growth of platinum particles on a catalyst support.

Growth of Platinum Particles

The basic experimental problem was the determination of the rate of growth of platinum particles on an eta-alumina support. The method that these authors wished to use to detect the growth was low-angle x-ray scattering. The difficulty in this experiment is the scattering from the alumina-air interface, which is large.

When the metal is introduced, the scattering is changed, but the observed scattering is now due to alumina-air, platinum-air, and alumina-platinum. There is no way in which the scattering can be correlated directly to the platinum size, since no way can be found to correct the background scattering.

A possible solution is to fill the pores with a material that is volumetrically isoelectronic with alumina. These authors, however, found it more convenient to squeeze the pores out of the alumina. The scattering of the alumina could be reduced to the point where it was negligible. Figure 3 shows the low-angle x-ray scattering through pressed alumina as a function of the pressure to which the sample had been subjected. At 100,000 atm., the difference between air and

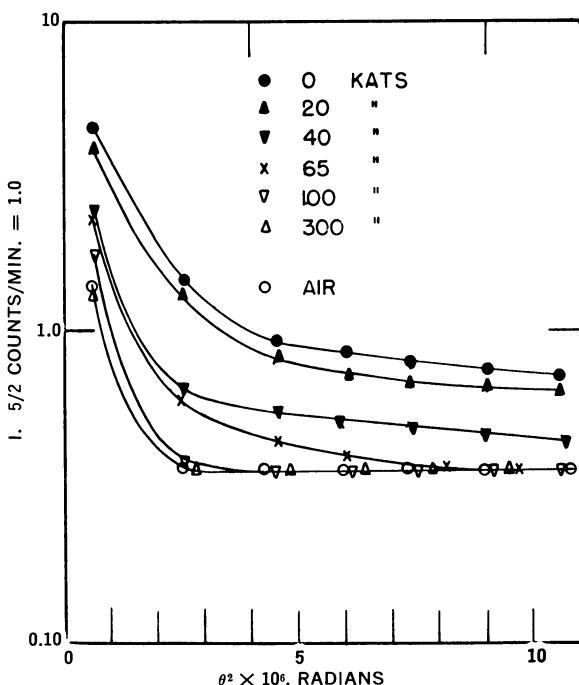


Figure 3. Effect of pressure on the low angle x-ray scattering of eta-alumina

alumina scattering is negligibly small and measurable only at the lowest angles. At a pressure of 300,000 atm., the presence of the alumina in the beam is undetectable at any angle measured by these investigators. By using this technique, it thus becomes possible to look at the platinum scattering completely uncomplicated by any other scattering process.

Figure 4 shows the effect of platinum concentration on the scattering. From data such as these the authors were able to study the growth rate of platinum as a function of temperature and atmosphere and to obtain sufficient data to formulate a theory for the growth rate. Their forthcoming paper should be consulted for the details of their experiments. Obviously this technique is not restricted to platinum and alumina, but should be applicable to the study of the growth of any metal on any support as long as the scattering from the metal is different from that of the support.

Finally, Figure 5 exhibits some of the results obtained by Powell and co-

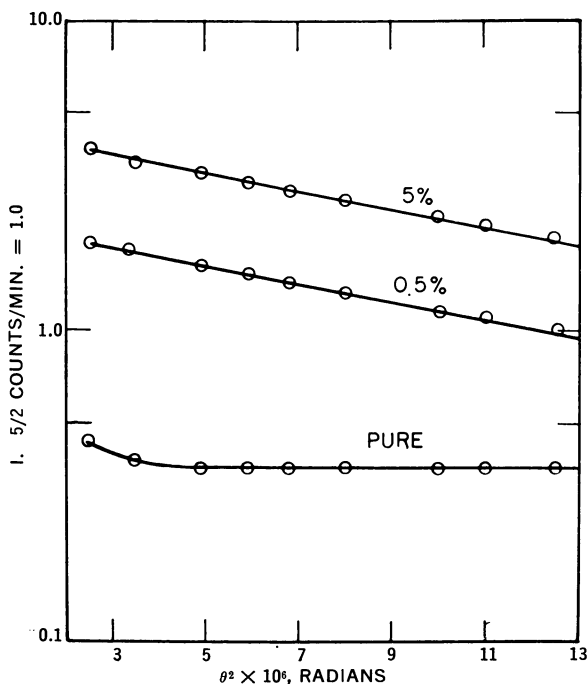


Figure 4. Low-angle x-ray scattering of platinum particles on an alumina support

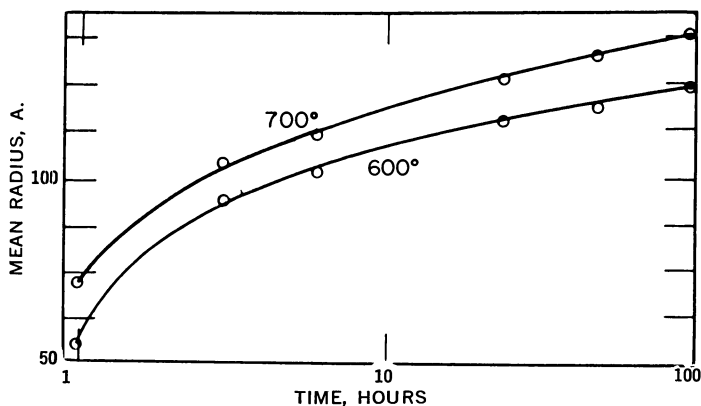


Figure 5. Effect of time at temperature in a reducing atmosphere on the mean radius of platinum particles

Values obtained from data as shown in Figure 4

workers on the change in the mean size of the platinum particles as a function of time at temperature. These results were obtained in a reducing atmosphere. The authors found that different results were obtained with a change in atmosphere.

Conclusions

Our experiments, which are truly only preliminary, indicate that much is yet to be learned concerning the manner in which the compaction occurs. It appears

that much information can be obtained from this approach that cannot be conveniently obtained by more standard methods.

Acknowledgment

The measurements in the x-ray study of magnesium oxide were made by L. Grossman. The magnesium oxide was obtained from Norman Phillips, University of California.

Literature Cited

- (1) Bridgman, P. W., *Phys. Rev.* **46**, 930 (1934).
- (2) Bridgman, P. W., *Proc. Am. Acad. Arts Sci.* **81**, 165 (1952).
- (3) Conway, J., Lawrence Radiation Laboratory, Berkeley, Calif., private communication.
- (4) Ford, M. A., Wilkinson, G. R., Price, W. C., "Molecular Spectroscopy," Institute of Petroleum, London, 1955.
- (5) Nathans, M., Lawrence Radiation Laboratory, Livermore, Calif., private communication.
- (6) Powell, R. E., Somerjai, G., Montgomery, P. W., private communication.

RECEIVED July 20, 1961.

Calculation of the Distortion in the Surface Region of an Alkali Halide Crystal Bounded by a $\{100\}$ Face

G. C. BENSON, P. I. FREEMAN, and EDWARD DEMPSEY¹

Division of Pure Chemistry, National Research Council, Ottawa, Canada

The model described allows the ions of the first n layers at the free $\{100\}$ face of a hemicrystal with sodium chloride structure to relax in a direction normal to the face and to be polarized by the electric field in the surface region. The equilibrium configuration is determined by minimizing the energy of the system. Numerical results for sodium chloride are presented for the five cases $1 \leq n \leq 5$. A value of -107.4 erg cm.^{-2} is estimated for the total correction to the surface energy of this material due to surface distortion.

A knowledge of the structure in the boundary region of a crystal is of considerable importance to the understanding of surface phenomena in chemistry. It has been recognized for a long time that the relative configuration of the atoms or ions near the surface of a crystal will differ from that in the bulk of the material. Unfortunately, there is as yet no reliable experimental method for determining in detail what perturbations of the regular lattice structure occur and recourse must be made to the predictions of reasonable theoretical models.

With few exceptions most theoretical investigations of surface distortion have been limited to the consideration of the outer layer and leave unanswered the question of how far significant distortion extends into the crystal. Recently Alder, Vaisnys, and Jura (1) have given a careful analysis of the depth of penetration of surface effects in inert gas crystals. It was found that the expansion between adjacent layers falls off as the inverse cube of the distance from the surface and that the deeper lying perturbations make relatively small contributions to the surface energy.

In the case of ionic crystals, the presence of different ionic species and the possibility of polarization effects inherently complicate the estimation of surface distortion. Previous considerations of the depth of penetration of surface effects in these materials (7, 10) have used oversimplified interaction potential functions or have imposed rather severe constraints on the form of relaxation permitted. A fairly detailed treatment of the distortion in the outermost layer of a free $\{100\}$

¹ Present address, Union Carbide Corp. Research Institute, P. O. Box 278, Tarrytown, N. Y.

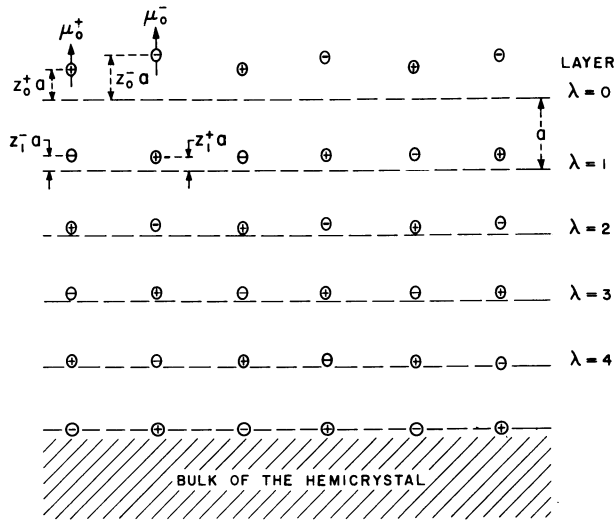


Figure 1. Variables used to describe configuration in surface region of crystal with sodium chloride structure and bounded by {100} face

face of a semi-infinite alkali halide crystal has been given by Benson, Balk, and White (2); the present paper is a preliminary report of the extension of these calculations to a consideration of the distortion in the first five layers at the surface of a sodium chloride crystal. Further details of the calculations will be presented later, when results have been obtained for other alkali halides.

Model and Method of Computation

A section normal to the {100} face of a semi-infinite crystal having a sodium chloride type structure is shown schematically in Figure 1. The nearest neighbor separation in the regular lattice is denoted by a . Layers parallel to the {100} face are indicated by an index λ , which for increasing depth takes on values 0, 1, 2, . . . , etc. The distortion is restricted to a surface region for which $0 \leq \lambda \leq n - 1$; in the present work $1 \leq n \leq 5$. Positive and negative ions of layer λ are assumed to be displaced from the regular lattice sites, in the direction of the outward normal to the surface, by distances $z_\lambda^+ a$ and $z_\lambda^- a$, respectively, and to have dipole moments μ_λ^+ and μ_λ^- in this direction. Thus the values of four variables (z_λ^+ , z_λ^- , μ_λ^+ , and μ_λ^-) are needed to specify the configuration of each layer in the surface region.

The interaction energy of two ions, i and j , is taken to be

$$u_{ij} = u_{ij}^0 - e_i(\mathbf{r}_{ij} \cdot \boldsymbol{\mu}_j)r_{ij}^{-3} + e_j(\mathbf{r}_{ij} \cdot \boldsymbol{\mu}_i)r_{ij}^{-3} - 3(\mathbf{r}_{ij} \cdot \boldsymbol{\mu}_i)(\mathbf{r}_{ij} \cdot \boldsymbol{\mu}_j)r_{ij}^{-5} + (\boldsymbol{\mu}_i \cdot \boldsymbol{\mu}_j)r_{ij}^{-7} \quad (1)$$

where e and $\boldsymbol{\mu}$ denote charge and dipole moment and \mathbf{r}_{ij} is the position vector of ion j relative to ion i ,

$$u_{ij}^0 = e_i e_j r_{ij}^{-1} - c_{ij} r_{ij}^{-6} - d_{ij} r_{ij}^{-8} + b_{ij} \exp(-r_{ij}/\rho) \quad (2)$$

is the usual Born-Mayer form of potential function and represents a sum of coulombic, van der Waals, and repulsive contributions. The other terms in Equation 1 are energies of charge-dipole and dipole-dipole interactions arising from the polarization of the ions.

For any configuration, the energy of the hemicrystal is obtained by summing the expression for u_{ij} over all pairs of ions and adding for each ion in the surface region a term corresponding to the quasielastic energy. The latter is given by $(\mu_i^2/2\alpha_i)$, where α_i is the electronic polarizability of the ion. The distortion energy, $\Delta U[z_0^+, z_0^-, \mu_0^+, \mu_0^-, z_1^+ \dots \mu_{(n-1)}^-]$, is a function of $4n$ variables. It is defined as the amount by which the energy of the hemicrystal in a given configuration $(z_0^+ \dots \mu_{(n-1)}^-)$ exceeds the energy in the undistorted state (for which all displacements and dipole moments are equal to zero) and is stated per ion pair in the surface. Since the area occupied by an ion pair is $2a^2$, the correction to the surface energy of the crystal is given by the equation

$$\Delta\sigma_{\{100\}} = [\Delta U]_{\min}/2a^2 \quad (3)$$

where $[\Delta U]_{\min}$ is the value of the distortion energy corresponding to the equilibrium configuration of the surface region.

In calculating ΔU it is convenient to group together terms from the interactions between ions located in two different layers (λ and μ) of the surface region and to denote these collectively by $\Delta U^{\lambda\mu}$. The remaining terms of ΔU arise either from pairs of ions in the same layer λ of the surface region, or from the interactions of ions in layer λ with those in the undistorted part of the crystal; they may thus be written in groups ΔU^λ associated with each layer. The distortion energy then can be expressed in the form

$$\Delta U = \sum_{\lambda}^{(n-1)} \Delta U^\lambda + \sum_{\lambda}^{(n-2)} \sum_{\mu}^{(n-1)} \Delta U^{\lambda\mu} \quad (4)$$

Evaluation of ΔU^λ and $\Delta U^{\lambda\mu}$ follows the same pattern as the previous single layer treatment (2) in which two simplifications are introduced to make the calculation more tractable.

1. Repulsive interactions between ions farther apart than the next nearest neighbor distance are neglected. This is the usual assumption in calculating the cohesive energies of alkali halide crystals (4, 5, 9) and is based on the fact that the exponential forms representing these interactions die away rapidly.

2. All energy terms are expanded as Taylor series in the displacement variables and terms of order higher than the fourth are discarded. Previous calculations for the distortion of the outer layer (2) have shown that this is a reasonable approximation, if the displacements are not much larger than 10% of the normal interlayer separation.

Adopting the above approximations, ΔU^λ and $\Delta U^{\lambda\mu}$ can be written formally as

$$\begin{aligned} \Delta U^\lambda = & \sum_p [A_p^\lambda (z_\lambda^+)^p + A_{0p}^\lambda (z_\lambda^-)^p] + \sum_p A_{p01}^\lambda [\mu_\lambda^+ (z_\lambda^+)^p - \mu_\lambda^- (z_\lambda^-)^p] \\ & + \sum_p a_{(2p)} (\delta_\lambda)^{2p} + (\mu_\lambda^+ + \mu_\lambda^-) \sum_p a_{(2p+1)} (\delta_\lambda)^{2p+1} \\ & + \mu^+ \mu^- \sum_p a_{(2p)11} (\delta_\lambda)^{2p} + (\mu_\lambda^+)^2 a_{02} + (\mu_\lambda^-)^2 a_{002} \end{aligned} \quad (5)$$

and

$$\begin{aligned} \Delta U^{\lambda\mu} = & \sum_p \{ [g_p^{(\mu-\lambda)+} + (\mu_\lambda^+ - \mu_\mu^+) g_{p1}^{(\mu-\lambda)} + \mu_\lambda^+ \mu_\mu^+ g_{p11}^{(\mu-\lambda)}] (\delta_{\lambda\mu}^{++})^p \\ & + [u_p^{(\mu-\lambda)} - (\mu_\lambda^+ + \mu_\mu^-) u_{p1}^{(\mu-\lambda)} + \mu_\lambda^+ \mu_\mu^- u_{p11}^{(\mu-\lambda)}] (\delta_{\lambda\mu}^{+-})^p \\ & + [g_p^{(\mu-\lambda)-} - (\mu_\lambda^- - \mu_\mu^-) g_{p1}^{(\mu-\lambda)} + \mu_\lambda^- \mu_\mu^- g_{p11}^{(\mu-\lambda)}] (\delta_{\lambda\mu}^{--})^p \\ & + [u_p^{(\mu-\lambda)} + (\mu_\lambda^- + \mu_\mu^+) u_{p1}^{(\mu-\lambda)} + \mu_\lambda^- \mu_\mu^+ u_{p11}^{(\mu-\lambda)}] (\delta_{\lambda\mu}^{-+})^p \} \end{aligned} \quad (6)$$

In these equations the difference between two position variables z_λ^α and z_μ^β is indicated by

$$\delta_{\lambda\mu}^{\alpha\beta} = z_\lambda^\alpha - z_\mu^\beta \quad (7)$$

where α and β are the signs of the charges of the ions. For the special case $\lambda = \mu$

$$\delta_{\lambda\lambda^+} = z_{\lambda^-} - z_{\lambda^+} = \delta_{\lambda} \tag{8}$$

The various coefficients $A_{\beta}^{\lambda}, A_{0\beta}^{\lambda}, \dots, a_{002}, g_{\beta}^{\mu+}, g_{\beta}^{\mu}, \dots, u_{\beta 11}^{\mu}$ are constants and involve quantities of two types: parameters such as those in Equations 1 and 2, which are characteristic of the ionic species involved and a number of sums associated with the particular lattice structure. Numerical methods for evaluating the latter have been described (14, 15). Formulas for these coefficients are not given in detail here, but those for the coefficients in Equation 5 are similar to expressions given by Benson, Balk, and White (2) for the single layer problem and the forms of the coefficients in Equation 6 follow an analogous pattern.

The equilibrium configuration of the surface region comprising n layers is determined by solving simultaneously the $4n$ equations obtained by equating to zero the partial derivatives of ΔU with respect to each of the variables. The equations so obtained are nonlinear and are solved by an iterative Newton-Raphson procedure (12), which necessitates calculating the second partial derivatives of ΔU with respect to all possible pairs of variables. A Bendix G15D computer was used for all numerical computations—i.e., evaluation of the various lattice sums, calculation of the derivatives of ΔU , and solution of the linearized forms in the Newton-Raphson treatment.

Table I. Equilibrium Configuration of the Surface Region at the {100} Face of Sodium Chloride

(Displacements in units of a ; dipole moments in debye units; energy in erg cm.⁻²)

n	1	2	3	4	5
z_0^-	-0.05176	-0.07518	-0.08543	-0.08712	-0.08708
z_0^+	0.00051	0.01839	0.02526	0.03158	0.03558
μ_0^+	-0.06219	-0.08088	-0.08943	-0.09379	-0.09605
μ_0^-	0.7967	1.2172	1.3874	1.4669	1.5063
z_1^+		0.07820	0.10556	0.12102	0.12945
z_1^-		0.01188	0.01443	0.01865	0.02160
μ_1^+		0.04284	0.05883	0.06661	0.07054
μ_1^-		-0.7169	-0.9861	-1.1109	-1.1724
z_2^+			-0.03225	-0.04749	-0.05502
z_2^-			0.00260	0.00745	0.01098
μ_2^+			-0.02422	-0.03604	-0.04243
μ_2^-			0.4111	0.6306	0.7486
z_3^+				0.03565	0.05409
z_3^-				0.00291	0.00458
μ_3^+				0.01937	0.02942
μ_3^-				-0.3521	-0.5341
z_4^+					-0.02011
z_4^-					0.00106
μ_4^+					-0.01402
μ_4^-					0.2434
$\Delta\sigma$	-52.70	-79.16	-92.53	-99.87	-104.07

Before presenting the results which have been obtained for sodium chloride it is necessary to indicate the sources of the data used for this salt. Van der Waals coefficients were taken from a tabulation by Mayer (11) and electronic polarizabilities of the ions at zero frequency from the work of Tessman, Kahn, and Shockley (13). A value of 4.802×10^{-10} e.s.u. was used for the charge of the electron and the repulsive parameters b_{ij} and ρ were taken from recent publications by Cubicciotti (5, 6). A value of $a = 2.794$ A. was computed for the nearest

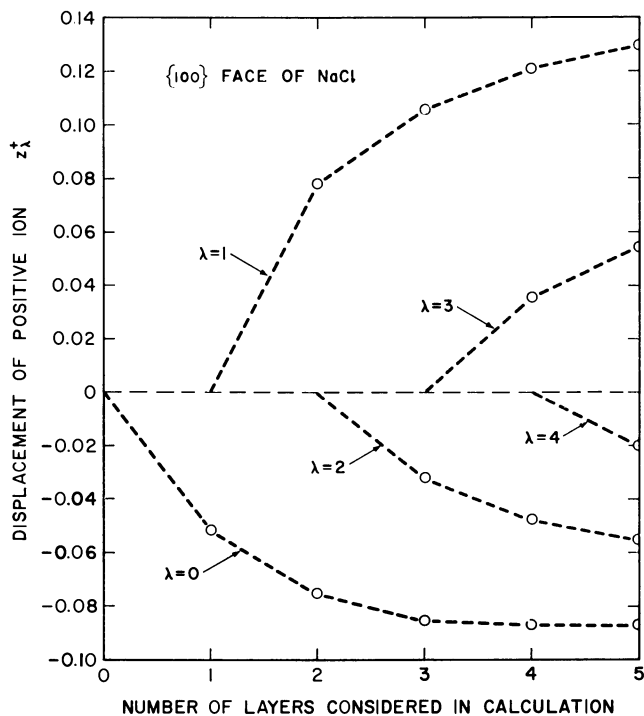


Figure 2. Variation of positive ion displacements (in units of a) with number of layers in model of surface region

Positive values of z_{λ}^{+} correspond to displacements in direction of outward normal to surface

neighbor separation. This result corresponds to the minimum of the cohesive energy for the infinite crystal at 0° K. and is based on the data summarized above.

Results and Discussion

The equilibrium configurations of the surface region and the corresponding corrections to the surface energy are listed in Table I for the $\{100\}$ face of sodium chloride. In interpreting these data it should be remembered that displacements z_{λ}^{+} and z_{λ}^{-} are measured in units of the nearest neighbor distance ($a = 2.794$ A.). The different columns in Table I pertain to models in which the number of layers in the surface region ranges from 1 to 5. In each case the second derivatives of ΔU were examined, to establish that the extremum of the energy located by the Newton-Raphson procedure was really a minimum.

The results for $n = 1$ differ somewhat from those obtained by Benson, Balk, and White (2), because of the different repulsive parameters adopted in the present calculations. The compatibility of the two sets of computations was confirmed by rerunning the original single layer program with the new data inserted. Use of Cubicciotti's repulsive parameters appears to lead to more consistent results in the surface distortion calculations; in particular, it was impossible to find stable equilibrium configurations for models with $n \geq 2$, using the data for sodium chloride employed by Benson, Balk, and White (2).

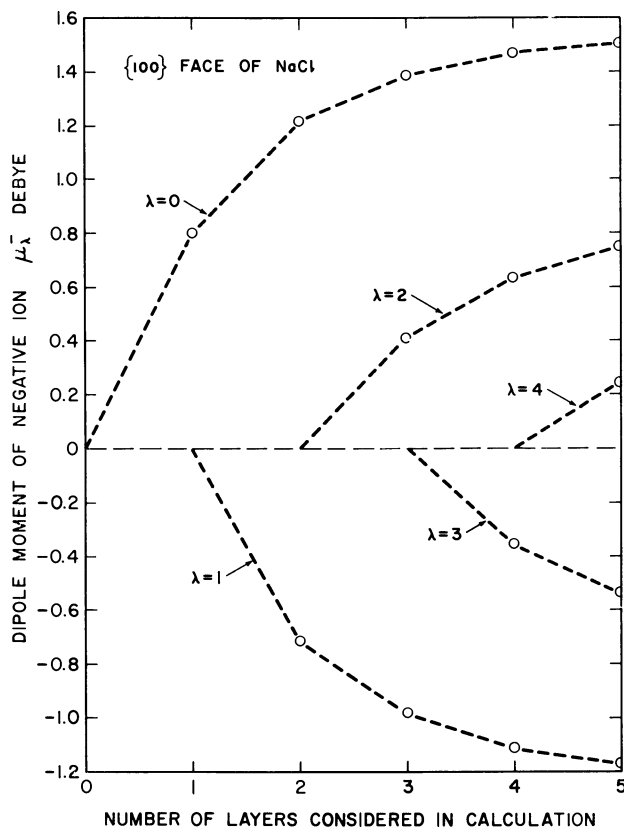


Figure 3. Dependence of dipole moments of negative ions (debye units) on n

In Figure 2 the dependence of the displacements of the sodium ions on the number of layers comprising the surface region is illustrated. Similar plots for the dipole moments of the negative ions are given in Figure 3. It can be seen from these graphs and from Table I that the mutual effects of relaxation extend for about three layers in the crystal. Thus, allowing layer λ to relax makes only a relatively small change in the distortion of layer $(\lambda - 3)$.

Figure 4 is a plot of the surface energy correction $\Delta\sigma(n)$ against n , the number of layers in the surface region. It is evident from this curve that the distortion of further layers—i.e., $\lambda > 4$ —will alter the surface energy only slightly. This is similar to the conclusion of Alder, Vaisnys, and Jura (1) for inert gas crystals. The points for $n \leq 5$ in Figure 4 can be represented to within ± 0.5 erg cm.⁻² by the empirical equation

$$\Delta\sigma(n) = -107.4[1 - \exp(-0.67n)] \quad (9)$$

extrapolation of which, for the case of an unlimited surface region, leads to

$$[\Delta\sigma(\infty)]_{\{100\}} = -107.4 \text{ erg cm.}^{-2}$$

for the asymptotic value of the distortion correction. This is about twice the value obtained from the relaxation of the outer layer alone. Since the surface

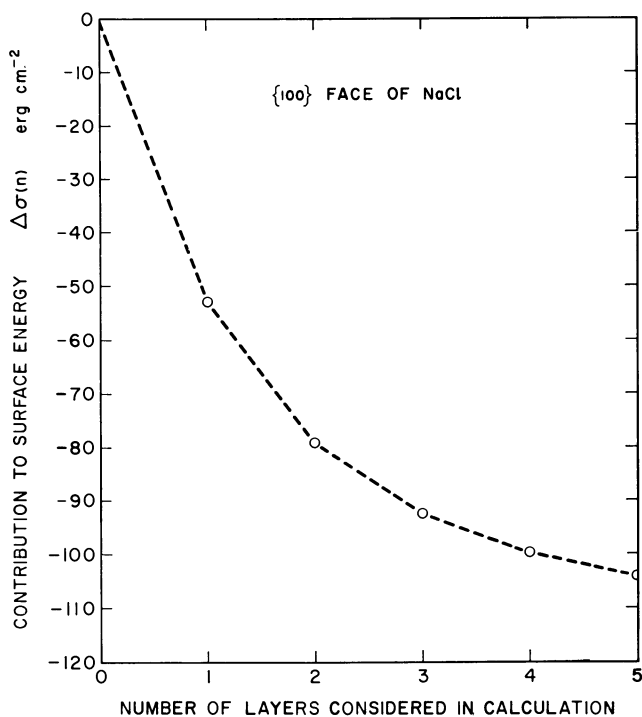


Figure 4. Contribution of distortion to surface energy plotted as a function of n

energy of an undistorted $\{100\}$ face of sodium chloride, based on the data used in the present work, is

$$\sigma^0_{\{100\}} = 210.9 \text{ erg cm.}^{-2}$$

[cf. (15) for the method of calculation] the corrected surface energy value becomes

$$\sigma_{\{100\}} = \sigma^0_{\{100\}} + [\Delta\sigma(\infty)]_{\{100\}} = 103.5 \text{ erg cm.}^{-2}$$

The discrepancy between this result and the value obtained from calorimetric measurements (3) may indicate that the crystals studied experimentally did not have the ideal equilibrium forms considered in the present calculations.

For the model with $n = 5$ the displacements of both positive and negative ions are plotted against the layer number λ in Figure 5. Also represented in the diagram are the directions and magnitudes of the dipole moments. In the case of the negative ions the length of the arrow, interpreted on the ordinate scale, is equal to one tenth of the dipole moment in debye units. Several interesting features appear in these plots. The negative ions are all displaced in the direction of the outward normal to the surface. Since the sodium ions of layer $\lambda = 0$ move inward, the chloride ions occupy relatively exposed positions in the $\{100\}$ face. It has been found experimentally that isotopic exchange between sodium chloride crystals and a gaseous halogen atmosphere occurs with surprising ease (8). The controlling factor for this process must of course lie in the detailed energetics of the situation, but the present calculations indicate that the geometrical location of the surface chloride ions is favorable for such a reaction.

The displacements of the positive ions alternate in sign from layer to layer.

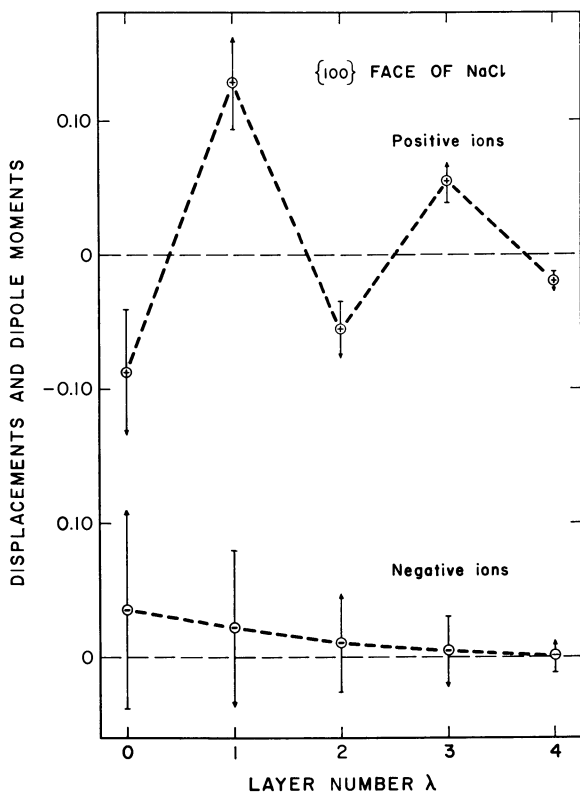


Figure 5. Equilibrium configuration of the first five layers ($\lambda = 0$ to 4) for model with $n = 5$

Displacements in units of a . Positive values indicate movements in direction of outward normal. Direction and magnitude of dipole moments (debye units) indicated by arrows. For negative ions length of arrow corresponds to one tenth of dipole moment

Thus there seems to be a tendency for the layers in the surface region to form pairs. This is even more apparent from an examination of the level of the mass center, \bar{z}_λ , of each layer obtained by weighting the displacements according to the masses of the ions—i.e.,

$$\bar{z}_\lambda = -\lambda + 0.3934 z_\lambda^+ + 0.6066 z_\lambda^- \quad (10)$$

The separation between adjacent levels (in units of a) is

$$\Delta\bar{z}_\lambda = \bar{z}_\lambda - \bar{z}_{\lambda+1} = 1 + 0.3934(z_\lambda^+ - z_{\lambda+1}^+) + 0.6066(z_\lambda^- - z_{\lambda+1}^-) \quad (11)$$

which yields values of 0.92, 1.08, 0.98, and 1.03 for $\lambda = 0$ to 3. The coupling between the displacements of the ions in adjacent layers can also be seen by plotting $\delta_{(\lambda+1)\lambda}^{\alpha\beta}$ against $\delta_{(\lambda+1)\lambda}^{\beta\alpha}$ where (α, β) stands for $(+, -)$ if λ is even and $(-, +)$ if λ is odd. The curve obtained is nearly linear and can be represented approximately by the equation

$$\delta_{(\lambda+1)\lambda}^{\alpha\beta} = -0.0278 + 1.145 \delta_{(\lambda+1)\lambda}^{\beta\alpha} \quad (12)$$

The dipole moments of the positive and negative ions in each layer are opposed and alternate in sign from layer to layer for ions of the same type. This behavior is to be expected from very elementary considerations of the electric field at the lattice sites of the surface region. The net dipole moment of layer λ (per ion pair), defined as

$$\mu_{\lambda} = ae(z_{\lambda}^{+} - z_{\lambda}^{-}) + \mu_{\lambda}^{+} + \mu_{\lambda}^{-} \quad (13)$$

has values of -0.236 , 0.345 , -0.179 , 0.160 , and -0.055 debye for $\lambda = 0$ to 4. Verwey (16) has remarked that in the first layer of the crystal the dipole associated with the displacement of the ions overrides the effects of their polarization and results in a relatively small net moment in the opposite direction. The present calculations show that this is also the case for the other layers in the surface region. It is also evident that the moments of adjacent layers are opposed and that the total effective surface dipole is very small.

Finally, the numerical results obtained with the present model are sensitive to the input data and since these are subject to rather large uncertainties only the over-all pattern of the results is probably of significance. The general applicability of the pattern to other alkali halides cannot be assessed on the basis of calculations for a single crystal. It is hoped that the investigation of other alkali halides will clarify this point.

Acknowledgment

We thank the staff of the Analysis Section, Division of Mechanical Engineering, National Research Council, for allowing us to use their computing facilities.

Literature Cited

- (1) Alder, B. J., Vaisnys, J. R., Jura, G., *J. Phys. Chem. Solids* **11**, 182 (1959).
- (2) Benson, G. C., Balk P., White, P., *J. Chem. Phys.* **31**, 109 (1959).
- (3) Benson, G. C., Schreiber, H. P., van Zeggeren, F., *Can. J. Chem.* **34**, 1553 (1956).
- (4) Born, M., Mayer, J. E., *Z. Physik* **75**, 1 (1932).
- (5) Cubicciotti, D., *J. Chem. Phys.* **31**, 1646 (1959).
- (6) *Ibid.*, **33**, 1579 (1960).
- (7) Glauber, A. E., *Zhur. Fiz. Khim.* **23**, 124 (1949).
- (8) Harrison, L. G., Morrison, J. A., Rose, G. S., "Proceedings of Second International Congress of Surface Activity," p. 287, Butterworths, London, 1957.
- (9) Huggins, M. L., Mayer, J. E., *J. Chem. Phys.* **1**, 643 (1933).
- (10) Madelung, E., *Physik. Z.* **20**, 494 (1919).
- (11) Mayer, J. E., *J. Chem. Phys.* **1**, 270 (1933).
- (12) Scarborough, J. B., "Numerical Mathematical Analysis," 3rd ed., p. 203, Johns Hopkins Press, Baltimore, 1955.
- (13) Tessman, J. R., Kahn, A. H., Shockley, W., *Phys. Rev.* **92**, 890 (1953).
- (14) van der Hoff, B. M. E., Benson, G. C., *Can. J. Phys.* **31**, 1087 (1953).
- (15) van Zeggeren, F., Benson, G. C., *J. Chem. Phys.* **26**, 1077 (1957).
- (16) Verwey, E. J. W., *Rec. trav. chim.* **65**, 521 (1946).

RECEIVED May 9, 1961. N. R. C. No. 6425.

Adsorptive Behavior of Fused Quartz Powders

W. H. WADE, H. D. COLE, D. E. MEYER, and NORMAN HACKERMAN

Department of Chemistry, The University of Texas, Austin, Tex.

The integral heats and entropies of adsorption for water on fused quartz powder have been obtained as a function of particle size. In the light of previous studies, this is indicative of identical surface structure for all samples studied. The results further indicate that many crystalline quartz powders are amorphous in their surface layers.

During the past few years there has been a continued and probably intensified interest in the adsorptive properties of quartz and amorphous silica. This is in a large part attributable to a more detailed knowledge of the surface structure of SiO_2 as obtained from infrared measurements (17, 18, 20). By using these techniques it has been possible to show unequivocally for the first time the existence of surface hydroxyl groups on silica and how their population density varies with outgassing pretreatment. On the basis of this information it has been possible to clarify the variation of immersional heats (ΔH_i) of quartz and silica in water with outgassing temperature.

A number of studies (8, 21, 22, 27) for a wide variety of quartz and silica gel samples with different modes of production show that the ΔH_i 's increase with increasing outgassing temperature, pass through a maximum at 200° to 300° C., and then decrease at higher outgassing temperatures. This is usually interpreted as an initial loss of reversibly adsorbed water, followed by gradual loss of surface hydroxyl groups. This leaves a rather stable siloxane ring structure and provides only a diminished opportunity for hydrogen bonding during the subsequent immersion process; consequently a diminished ΔH_i is observed.

Although the ΔH_i vs. outgassing temperature behavior is fairly well understood, another aspect of the behavior of quartz and amorphous SiO_2 appears to be somewhat anomalous—the remarkable variation of ΔH_i with particle size. A survey of the older literature (1, 2, 4, 14, 15, 19, 28) showed a disparity in ΔH_i 's obtained at various laboratories. The only apparent correlation (21) was that the ΔH_i (per unit area) seemed to decrease with increasing area of the sample under investigation. Several studies initiated in this laboratory to check the validity of this observation (21, 22) show the effect to be real and that ΔH_i can vary from 100 to 900 ergs per sq. cm., depending on the sample and the outgassing temperature chosen. The variation of ΔH_i with specific area of the sample is not restricted to the SiO_2 - H_2O system but is prominent in the Al_2O_3 - H_2O (23), TiO_2 - H_2O (24), and to a lesser extent Al_2O_3 - MeOH (25) and TiO_2 - MeOH (25) sys-

tems. It thus appears to be a general phenomenon, except possibly for nonpolar adsorbates as discussed later.

For the $\text{SiO}_2\text{-H}_2\text{O}$ system the possibility of impurity contents being the determining factor has been eliminated (21). It was also shown (11, 22) that the ΔH_i variation with specific area can be generated from an initially coarse quartz powder by extensive grinding and subsequent fractionation into a series of particle size samples. The various ΔH_a 's obtained from ΔH_i 's (see Equation 1) for SiO_2 samples outgassed at 160°C . and 10^{-6} mm. of Hg are listed in Table I.

Table I. Integral Heats of Adsorption for SiO_2 Samples Outgassed at 160°C .

Sample	Surface Area, Sq. M./G.	ΔH_a , Ergs/Sq. Cm.
Quartz	0.070	729
	0.138	546
Cristobalite	0.541	531
	0.910	388
Quartz	8.12	334
	162.0	-29
Amorphous	162.0	-29
	188.0	43

The adsorption isotherms for many of the samples in Table I have been measured (11), allowing the integral entropies of adsorption to be evaluated according to the prescription of Jura and Hill (16). It was found (11) that the entropy of the adsorbed species relative to that of liquid water decreases regularly with decreasing specific surface area. This would be expected for a gradual decrease in periodicity in the underlying structure and thus in the adsorbed H_2O .

Recent independent measurements from two other laboratories (26, 27) also show the decrease of ΔH_i with increasing specific area. This number of independent studies should confirm the validity of the effect, even in the field of surface chemistry. However, the explanation of this effect remains largely beclouded by the complexities of the system. Our hypotheses are that there is a direct correlation between particle size and the crystalline-amorphous character of the substrate surface. Specifically, quartz powders of low area and large particle size present a crystalline array at the interface, whereas powders of high area and small particle size are amorphous in the surface region. This certainly holds for many quartz powders prepared by grinding processes, which are known to introduce amorphicity in the surface region, and several studies (5, 6, 7, 9, 10, 12) show its existence. Moreover, SiO_2 samples of very high area showed low ΔH_i 's (21, 22) and since these were prepared by flame hydrolysis they are thus, undoubtedly, amorphous.

Once the correlation between ΔH_i and the crystalline-amorphous surface character is accepted, there still remains the need to explain why the interaction energy of a water molecule with the surface Si^{+4} , O^{-2} , and hydroxyl groups should depend on the crystalline character. As was discussed above, experimental results show that the ΔH_i decreases with decreasing surface OH concentration for a given quartz or silica sample. The correlation between ΔH_i and crystalline-amorphous character could be by a diminution of surface OH concentration for higher area samples. Unfortunately, there are no direct measurements of the extent of surface OH coverage as a function of particle size, since infrared measurements are restricted to samples of high specific area (>50 sq. meters per gram) which are probably completely amorphous.

Surface OH concentration can be inferred from weight-loss measurements made on samples with surface areas as low as 1 sq. meter per gram. However, the

results are ambiguous, since the physical adsorption energies for low area powders (as mirrored in the ΔH_i 's) as low coverages do not differ greatly from the hydroxyl group bond energies. Also, it is difficult to separate the weight loss *vs.* outgassing temperature curve into sections corresponding to the loss of physically adsorbed water and the loss of surface hydroxyl groups. This is illustrated by measurements on quartz samples with surface areas of 1.28 (22) and 7.5 sq. meters per gram (26), where the nominal OH surface concentrations were 20 and 9 OH's per 100 sq. A., as calculated from the weight loss from 110° to 450° C. The theoretical upper limit is 8 OH's per 100 sq. A. (15).

Though definite information on OH coverage for low area quartz samples is lacking, it is nevertheless a reasonable guess that any variation in OH coverage cannot explain the major portion of the variation of ΔH_i with particle size for two reasons: First, many high area gels with $\Delta H_i < 200$ ergs per sq. cm. are completely covered with OH groups (15), and, second, the ΔH_i at its maximum for a given sample is at most 150 ergs per sq. cm. higher than at 450° C. where the OH concentration is low (22). Thus, differences of as much of 800 ergs per sq. cm. between low area quartz and high area silica must be explained in another way.

It has been suggested (22) that, qualitatively, the difference can be explained by a detailed consideration of the difference in binding forces of a water molecule in the force field of two limiting types of ionic lattices: (1) The water dipole interacts (vertical to the surface) with alternating layers of O⁻² ions (OH groups in the outer layer) and Si⁺⁴ ions, and (2) the water dipole interacts with layers each of which consists of random Si⁺⁴ and O⁻² ions with the only ordered structure being the SiO⁻⁴ tetrahedra. The latter structure in its bulk is the usual model for fused quartz, whereas the former model is that for several crystal planes of crystalline quartz. The summation of all interaction energies of a water dipole with lattice ions in alternating positive and negative sheets is greater than the summation where positive and negative ions alternate within a given layer (3). In essence the amorphous structure more resembles a covalent structure such as graphite, for which the interaction energies with water are very low (28). Various aspects of the preceding proposal have recently been discussed (27). A pertinent analogy can be drawn to calculated electrostatic field strengths (3) at the surface of NaCl lattices. The field strength (which is a direct measure of interaction energy for polar molecules) over a Cl⁻ ion in a 110 plane surface is three times that over a Cl⁻ ion in a 100 plane surface. For the reason cited above for a dipole adsorbed on a Cl⁻ ion in the 110 plane, there is an excess of Cl⁻ ions in the immediate vicinity and thus less cancellation of ion-dipole contributions to the total interaction energy.

To check on the dependence of ΔH_i on crystallinity, a cristobalite sample was prepared at temperatures high enough to cause a phase transformation (22), and it was assumed that at this temperature any amorphous surface layer would also crystallize. As predicted, the ΔH_i 's increased (approximately 200 ergs per sq. cm.) above the original quartz values. Difficulties of interpretation were not completely obviated, since the surface areas differed by a factor of 2. Also, the ΔH_i 's were for two different crystalline modifications and thus would not be expected to display exactly the same interaction energies with water.

The present study was initiated to eliminate the difficulties inherent in the previous experiments. It consists of measurements of the integral enthalpies (via immersionsal heat measurements) and entropies (via adsorption isotherms) for ground and fractionated powders of fused quartz with a wide spectrum of specific surface areas.

The commonly accepted structure of fused quartz is one of randomly bonded SiO_4 tetrahedra. Relying on the high bond strength within these tetrahedra, grinding of a coarse fused quartz should have little effect on its surface structure. Therefore, it is possible to predict that ΔH_a and ΔS_a for fused quartz should be independent of particle size.

Experimental

The fused quartz was obtained as a single billet from The General Electric Co., Willoughby Quartz Plant, and had a stated purity of 99.97%. The original billet was crushed to a particle size of approximately 100 microns in an iron jaw crusher, washed with HCl, and then ground under water in an agate mortar for approximately 5 days. The resulting material was fractionated by sedimentation in water to give the series of nine samples listed in Table II. The surface areas were obtained by the standard BET analyses of Kr adsorption isotherms taken over a relative pressure range of 0.05 to 0.30 as previously described (22). The heats of immersion were measured at 25.0° C. by techniques already described (21, 22). Samples were run in duplicate, and these agreed to 2 to 3%. Pre-treatment consisted of outgassing at 160° C. and 10^{-6} mm. of Hg for 4 days.

Table II. Adsorption Parameters for Fused Quartz Samples of Various Specific Surface Areas

Sample	Surface Area, Sq. M./G.	ΔH_a , Ergs/Sq. Cm.	π , Ergs/Sq. Cm.	ΔS_a , Ergs/Sq. Cm.- ° C.	ω , Sq. A.
A	0.054	372	128	0.82	17.1
B	0.297	393			
C	0.562	362	143	0.74	19.9
D	1.04	391	159	0.77	14.6
E	1.92	378	126	0.84	19.5
F	3.62	379			
G	7.47	345	163	0.62	14.7
H	13.58	359			
I	25.55	347			

The adsorption isotherms for water with five of the samples were obtained at 25° C. by using a volumetric adsorption apparatus described previously (13). Prior to adsorption measurements these samples were also outgassed at 160° and 10^{-6} mm. Hg. Each adsorption isotherm consisted of 20 to 40 experimental points covering the relative pressure range 0.01 to 0.95.

Results and Discussion

The integral heats of adsorption in Tables I and II were calculated from the heats of immersion by

$$\Delta H_a = \Delta H_i - 118.5 \quad (1)$$

where 118.5 is the surface enthalpy of water. Both ΔH_a and ΔH_i are heats per unit surface area and are referred to the standard states as liquid water. The free energies of adsorption were obtained from the adsorption isotherms by graphical integration of the Gibbs equation

$$\pi = RT \int_0^1 V d \ln P/P^\circ \quad (2)$$

where V is the volume of gas adsorbed per unit area, P/P° is the relative pressure,

and the other symbols have their usual significance. The integral entropies of adsorption per unit area were obtained from

$$\Delta S_a = \frac{\Delta H_a - \pi}{T} \tag{3}$$

which is the Jura and Hill equation (16) modified to unit area for the problem at hand. Table II lists ΔH_a , π , ΔS_a , and ω , which is the area per water molecule obtained from BET analyses of the adsorption isotherms. As is common practice in surface studies, ΔH_a , π , and ΔS_a are opposite in sign when compared with standard thermodynamic conventions. The ΔH_a 's in Table II show no definite trend and have an average value of 370 ergs per sq. cm. with an average deviation of ± 14 ergs per sq. cm. or approximately $\pm 4\%$. This uncertainty would be expected from a combination of uncertainties in measurements of ΔH_i and of surface area.

The adsorption isotherms are shown in Figure 1. There are some differences in shape, although they are all examples of the classic Type II adsorption isotherm.

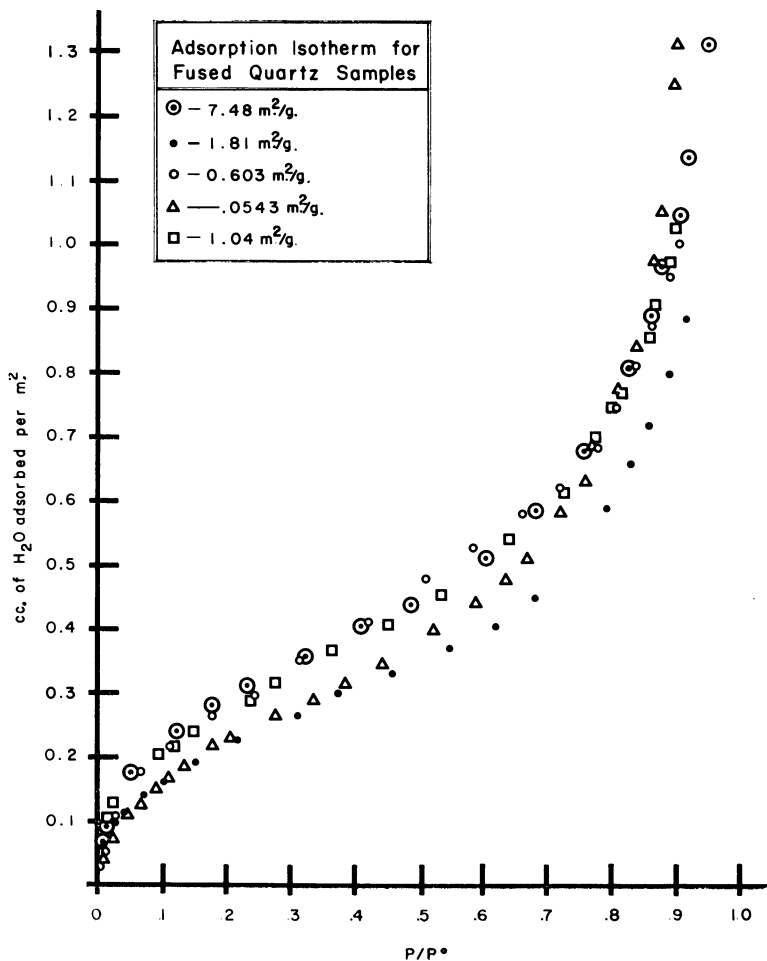


Figure 1. Adsorption isotherm

The integrated free energies of adsorption are listed in Table II. There is no definite trend in these either. The average of all five π values is 140 ergs per sq. cm., with an average deviation of ± 14 ergs per sq. cm. or $\pm 10\%$. The disagreement in π is somewhat greater than in ΔH_i . The entropy values being obtained from both ΔH_a (or ΔH_i) and π show their corresponding uncertainties.

Considering the limitations of the experiment, the ΔH_a , π , and ΔS_a values are independent of particle size over a range in which both the surface areas and ΔH_a 's of crystalline quartz samples varied by a factor of 2 (see Table I).

In comparing Tables I and II, it is observed that the heats of adsorption of the fused quartz are about the same as for the 8 sq. meters per gram "crystalline" quartz and much higher than those for high area amorphous silicas. The entropies of adsorption for the fused quartz samples are between those for 1 and 8 sq. meters per gram crystalline quartz. This indicates that the surface structure of fused quartz and a crystalline quartz of moderate surface area (5 to 10 sq. meters per gram) are probably very similar. In addition, the surfaces of very high area amorphous gels and flame-hydrolyzed silicas must be basically different from fused quartz, since the ΔH_i 's differ so drastically.

An additional bit of information obtained from the experiment indicated that the fused quartz surface is extensively populated with surface OH groups. Sample A (Table II) was inadvertently heated to 400° C. prior to adsorption measurements. The resulting π value was 69 ergs per sq. cm. On repeated soaking in boiling water (2 weeks total) π gradually rose to a final value of 128 ergs per sq. cm. This is consistent with the relatively irreversible loss of surface OH's at 400° C. Also the extent of initial decrease of π indicates an abundant coverage prior to heating to 400° C.

The average entropy decrease on adsorption of approximately 0.75 erg per sq. cm. when converted to a molar basis from the volume adsorbed at saturation vapor pressure is 1.8 ± 0.4 e.u. less than liquid water at 25° C. or about that of liquid water at 0° C. The large uncertainty is due to difficulty in extrapolating to $P/P^\circ = 1$. Since the entropy of adsorbed water molecules in the outermost layer must approximate that of liquid water at 25° C., then the inner layers, to maintain the average of 1.8 e.u., must be icelike with loss of translational modes.

This investigation has offered no firsthand information with regard to the exact mechanism of the crystalline to amorphous conversion in substrates, but it completely supports the previously advanced hypotheses. There yet remains a need for an explanation of the variation of ΔH_i with particle size of Al_2O_3 and TiO_2 (23-25). These samples were exposed to no distortional forces of the type discussed above following their crystallization at elevated temperatures.

Conclusions

The surface structure of fused quartz powders obtained by grinding is independent of specific surface area. The surface structure is similar to a medium area crystalline quartz but differs from that of gels, nonporous silicas of very high area, and coarse crystalline quartz powders.

Acknowledgment

The authors thank the American Petroleum Institute for continued interest and support of this research under API Project 47D.

Literature Cited

- (1) Armstrong, E. J., *Bell System Tech. J.* **25**, 136 (1956).
- (2) Bartell, F. E., Suggitt, R. M., *J. Phys. Chem.* **58**, 36 (1954).
- (3) Boer, J. H. de, *Advances in Colloid Sci.* **3**, 1 (1950).
- (4) Boyd, G. E., Harkins, W. D., *J. Am. Chem. Soc.* **64**, 1190, 1195 (1942).
- (5) Clelland, D. W., Ritchie, P. D., *J. Appl. Chem.* **2**, 31 (1952).
- (6) *Ibid.*, p. 42.
- (7) Dempsted, P. B., Ritchie, P. D., *Ibid.*, **3**, 182 (1953).
- (8) Egorov, M. M., Krasil'nikov, K. G., Syssoev, E. A., *Doklady Akad. Nauk, S.S.S.R.* **108**, 103 (1956).
- (9) D'Eustachio, D., *Phys. Rev.* **70**, 522 (1946).
- (10) D'Eustachio, D., Greenwald, S., *Ibid.*, **69**, 532 (1946).
- (11) Every, R. L., Wade, W. H., Hackerman, N., *J. Phys. Chem.* **65**, 25 (1961).
- (12) Gibb, J. G., Ritchie, P. D., Sharpe, J. W., *J. Appl. Chem.* **3**, 213 (1953).
- (13) Hackerman, N., Hall, A. C., *J. Phys. Chem.* **62**, 1212 (1958).
- (14) Howard, F. L., Culbertson, J. L., *J. Am. Chem. Soc.* **72**, 1185 (1950).
- (15) Iler, R. K., "Colloid Chemistry of Silica and Silicates," pp. 240-2, Cornell Univ. Press, Ithaca, N. Y., 1955.
- (16) Jura, G., Hill, T. L., *J. Am. Chem. Soc.* **74**, 1598 (1952).
- (17) Kiselev, A. V., Lygin, V. I., *Kolloid. Zhur.* **21**, 581 (1959).
- (18) Kiselev, A. V., Lygin, V. I., "Proceedings of Second International Congress on Surface Activity," Vol. II, p. 204, Butterworths Scientific Publications, London, 1957.
- (19) Kiselev, A. V., Mikos, N. N., Romanchuck, M. A., Shcherbakova, K. D., *Zur Fiz. Khim* **21**, 1223 (1947).
- (20) McDonald, R. S., *J. Am. Chem. Soc.* **79**, 850 (1957); *J. Phys. Chem.* **61**, 1168 (1958).
- (21) Makrides, A. C., Hackerman, N., *Ibid.*, **63**, 594 (1959).
- (22) Wade, W. H., Every, R. L., Hackerman, N., *Ibid.*, **64**, 355 (1960).
- (23) Wade, W. H., Hackerman, N., *Ibid.*, **64**, 1196 (1960).
- (24) Wade, W. H., Hackerman, N., National Colloid Symposium Meeting, 1961.
- (25) Wade, W. H., Hackerman, N., unpublished data.
- (26) Whalen, J. W., private communication.
- (27) Young, G. J., Bursh, T. P., *J. Colloid Sci.* **15**, 361 (1960).
- (28) Zettlemoyer, A. C., Young, G. J., Chessick, J. J., Healey, F. H., *J. Phys. Chem.* **57**, 649 (1953).

RECEIVED May 9, 1961.

Adsorption of Cyclohexane and Methanol on Iron Oxide

R. I. RAZOUK, R. SH. MIKHAIL, and B. S. GIRGIS

*Faculty of Science, Ain Shams University, Abbassia,
National Research Centre, Dokki,
Cairo, Egypt, U. A. R.*

The adsorption isotherms of cyclohexane and methanol vapors on synthetic lepidocrocite and goethite, and on their decomposition products prepared by heating at temperatures varying between 150° and 500°C. for different durations, have been determined. The isotherms are in general Type II (Brunauer classification) and not Type IV common to hydrous ferric oxide gels. The adsorption of cyclohexane is physical, whereas that of methanol is partly physical and partly chemical. The surface areas calculated from the total adsorption of methanol agree in most cases with those estimated from cyclohexane adsorption. Surface area-time of heating curves show that at low temperatures the area increases with time, whereas at intermediate temperatures it increases to a maximum value and then decreases; and at higher temperatures the area decreases regularly. The final limiting surface area-temperature of decomposition curve passes in both cases through a maximum at about 200°, above which temperature sintering is appreciable.

The adsorption of gases and vapors on ferric oxide and the hydrous oxide gels of iron has been the subject of numerous investigations (6, 10, 11). The surface properties of active solids prepared by thermal decomposition depend to a great extent on the physical structure of the parent material and how closely the lattice of the latter is related to that of the product (9). Iron oxide provides an interesting case, for it may be prepared from amorphous hydrous gels of indefinite composition or from well-defined crystalline hydroxides—e.g., lepidocrocite and goethite. Almost all the work on the adsorptive properties of ferric oxide has been done on products prepared from hydrous gels containing an indefinite number of water molecules and liable to aging or recrystallization. Recently Goodman and Gregg (8) studied the surface properties of iron oxide prepared from crystalline lepidocrocite.

crocite, but even then their starting material contained a high amount of adsorbed water and only near 250° was there an inflection in their thermogravimetric analysis curve corresponding to the formula $\text{FeO}\cdot\text{OH}$. Furthermore, these measurements were mainly confined to the study of the effect of the temperature of thermal treatment, and the decomposition was carried out in the presence of air. But it is now believed that both the temperature of heating and its duration contribute to the development of the surface area of active solids. Also, the presence of air during decomposition generally gives rise to products possessing lower surface areas (18), resulting from sintering processes operative in air at temperatures lower than is required by the Hüttig mechanism (12).

The object of the present investigation was to study the adsorption of cyclohexane and methanol vapors on ferric hydroxide in the form of synthetic lepidocrocite and goethite, and on the oxides prepared in vacuo by their thermal decomposition at different temperatures and for varying lengths of time.

Experimental

Apparatus. The adsorption of cyclohexane and methanol vapors was measured with the aid of a simple volumetric apparatus similar to that described earlier (19).

Materials. Lepidocrocite was prepared by the method described by Baudisch and Hartung (1) by first forming tetrapyrridiniferrous chloride and then oxidizing it and precipitating the yellow ferric oxide monohydrate. The latter was dried in an evacuated desiccator over calcium chloride and left in an electric oven at 105°C . to constant weight. The structure of lepidocrocite ($\gamma\text{-Fe}_2\text{O}_3\cdot\text{H}_2\text{O}$) was ascertained from the x-ray diffraction patterns obtained with the aid of a Philips x-ray diffraction unit Type PW 1010, using a cobalt target with iron filter. Loss on ignition of the hydroxide was 11.12% (theoretical value 10.14%), and the oxide formed was hematite $\alpha\text{-Fe}_2\text{O}_3$.

Goethite was prepared according to Geith (7) by treating ferrous chloride solution with a solution of ammonium carbonate, oxidizing the ferrous carbonate with hydrogen peroxide, and leaving the gel to age for 12 months. The hydroxide was dried in the manner described above. X-ray diffraction patterns proved that the material was goethite ($\alpha\text{-Fe}_2\text{O}_3\cdot\text{H}_2\text{O}$). Loss on ignition was 12.71%, and the oxide formed was also $\alpha\text{-Fe}_2\text{O}_3$.

The preparation of cyclohexane and methanol has been described (15, 16).

Results and Discussion

Adsorption of Cyclohexane. The adsorption of cyclohexane was determined on synthetic lepidocrocite and its decomposition products prepared by heating it in vacuo for varying intervals of time at 190° , 300° , 400° , and 500° , and also on synthetic goethite and its decomposition products obtained in a similar manner by heating at 150° , 180° , 250° , 300° , and 500° . The adsorption was found to be physical in nature, and the isotherms are Type II of the Brunauer classification (3) in all cases except on iron oxide prepared from goethite at 300° and 500° ; here the isotherms are Type III. This finding is in contrast to the Type IV isotherms common to ferric oxide gels; the difference may be due to the crystalline nature of the parent material.

Typical results are shown in Figures 1 and 2. Thus Figure 1 represents the isotherms of cyclohexane on the two parent materials lepidocrocite and goethite at 35° , while Figure 2 represents the isotherms at the same temperature on iron oxide prepared from lepidocrocite by heating in vacuo at 300° for 0.5, 1, 3, 8, and 18 hours. The results agree with the equation of Brunauer, Emmett, and Teller (4):

$$\frac{p}{s(p_0 - p)} = \frac{1}{s_m c} + \frac{(c - 1) p}{s_m c p_0}$$

as may be judged from the linear plots of $p/s(p_0 - p)$ against p/p_0 shown in the insets of Figures 1 and 2. Here s is the amount adsorbed at equilibrium pressure, p , p_0 is the saturation vapor pressure, s_m is the monolayer capacity, and c is a constant related to the heat of adsorption of the first layer. It was thus possible to calculate the specific surface area of the adsorbent from the slope and the intercept of the linear plot, taking the cross-sectional area of cyclohexane as 39 sq. A. (20).

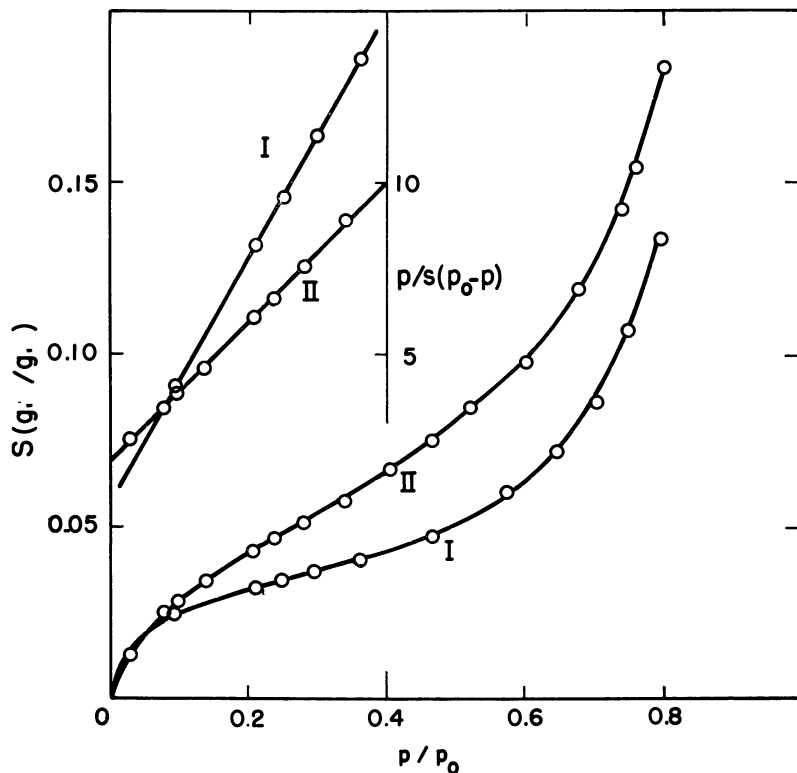


Figure 1. Adsorption isotherms of cyclohexane at 35° C.

- I. *Lepidocrocite*
 II. *Goethite*

The relation between the specific surface area and time of heating at various temperatures is represented in Figures 3 and 4 in the case of goethite and lepidocrocite and their decomposition products, respectively. In general, the surface area of the product increases with the duration of heating at the lower temperatures of preparation as a result of further decomposition. At intermediate temperatures, the specific surface area rises with time of heating up to a maximum and then falls to lower values, while at higher temperatures of decomposition the surface area falls regularly with the duration of heating.

Thus when goethite is decomposed at 150°, the product possesses a surface area very close to that of the parent material. Furthermore, this area does not vary with the duration of heating and subsequently with the amount of water loss;

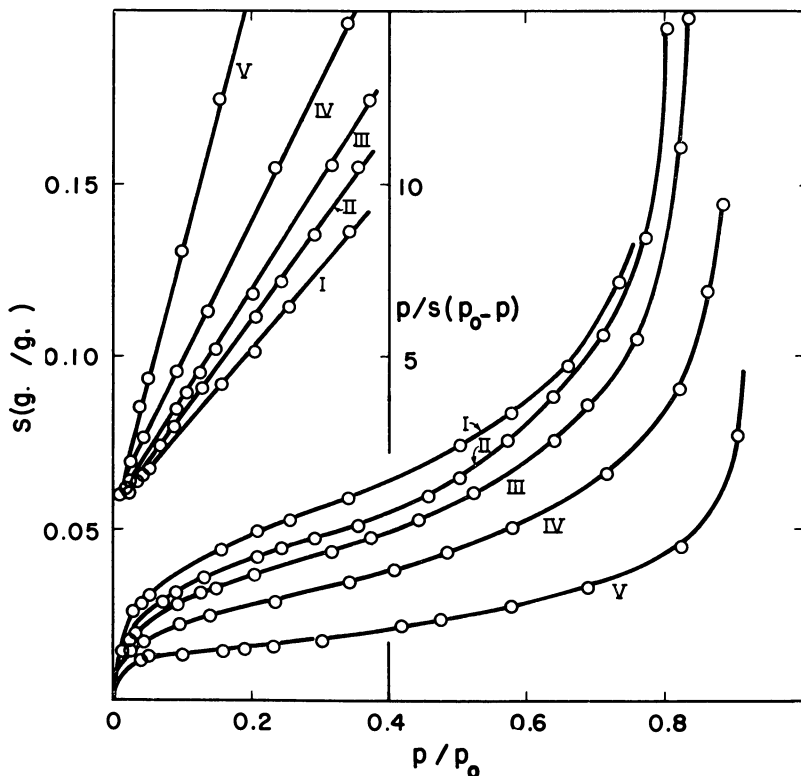


Figure 2. Adsorption isotherms of cyclohexane on ferric oxide prepared from lepidocrocite by decomposition at 300° C.

I, II, III, IV, V. Isotherms at 35° on products obtained by heating for 0.5, 1, 3, 8, and 18 hours

for decomposition at this temperature is slow, and even after heating for 7 hours only 41% of the water content is eliminated. X-ray measurements show that the diffraction patterns of goethite and its product of decomposition in vacuo at 150° are identical, so that the water is driven off from the crystal, leaving a pseudolattice and also a pseudomorph (5) possessing the same surface area. The remaining water may act as a stabilizer for the pseudomorph. Decomposition at 180°, however, produces a product possessing the patterns of hematite ($\alpha\text{-Fe}_2\text{O}_3$) with broadened lines indicating the existence of strain in the lattice which results in the observed increase in the surface area. At 250°, the pattern of the normal lattice of $\alpha\text{-Fe}_2\text{O}_3$ is obtained, and the surface area diminishes regularly as a result of sintering.

The behavior of lepidocrocite on decomposition is slightly different. Heating in vacuo at 190° leads to an increase in surface area with time of heating during the first 2 hours when the water loss amounts to 3.3%, and then the area remains constant, although prolonged heat treatment produces further loss of water, attaining 7.7% after 60 hours and 10.5% after 400 hours. X-ray measurements show that on heating at this temperature, the pattern of lepidocrocite disappears and that of maghemite ($\gamma\text{-Fe}_2\text{O}_3$) makes its appearance, in agreement with the results of Bernal, Dasgupta, and MacKay (2), although the lines are broadened. The independence of the surface area upon the water content at this temperature may

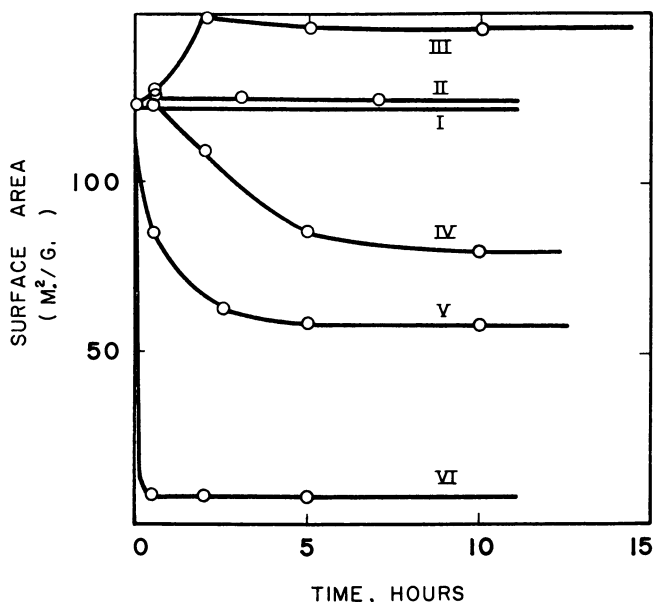


Figure 3. Effect of duration of heating on specific surface area of products prepared from goethite at various temperatures

I. Goethite

II, III, IV, V, VI. Products obtained by heating at 151°, 180°, 250°, 300°, and 500° C.

be explained by assuming that the development of the surface area resulting from decomposition is just counterbalanced by sintering. When decomposition takes place at 300°, activation occurs only at the very early stages of heating, probably as a result of the transformation of maghemite into hematite about this temperature, as was found from x-ray diffraction patterns and also from earlier observations (2). Beyond this stage and above this temperature sintering becomes dominant.

A limiting surface area is always obtained after a sufficiently long heat treatment, and this value is characteristic of each temperature, in agreement with the results obtained with magnesia (17). In Figure 5 the limiting specific surface areas are plotted as a function of the temperature of preparation. The same behavior is encountered in lepidocrocite and goethite. But the area is invariably greater in case of goethite and its products, unless decomposition is carried out at 500°, when the two areas become very small and close to each other. Probably the higher water content in synthetic goethite (12.71%) than in lepidocrocite (11.12%) accounts for the greater activity of the former and its products of decomposition; for the excess of water over the stoichiometric value may be present on either the surface or as a solution in the lattice (21), and in the latter case its presence and removal will induce lattice strains which lead to an increase in the surface area. In both cases, the maximum limiting area is developed at about 200°, and above this temperature sintering becomes appreciable. This temperature is lower than would be expected for ordinary sintering to occur according to the theory of Hüttig (12), but agrees with the results of Goodman and Gregg (8).

During the early stages of the sintering process, and particularly at lower tem-

peratures where there is substantially very little lattice mobility, surface diffusion provides the major contribution to the sintering process. This effect increases rapidly with temperature, as does the depth of the layer over which it operates, and may still persist even at temperatures which permit volume diffusion of the material to take place.

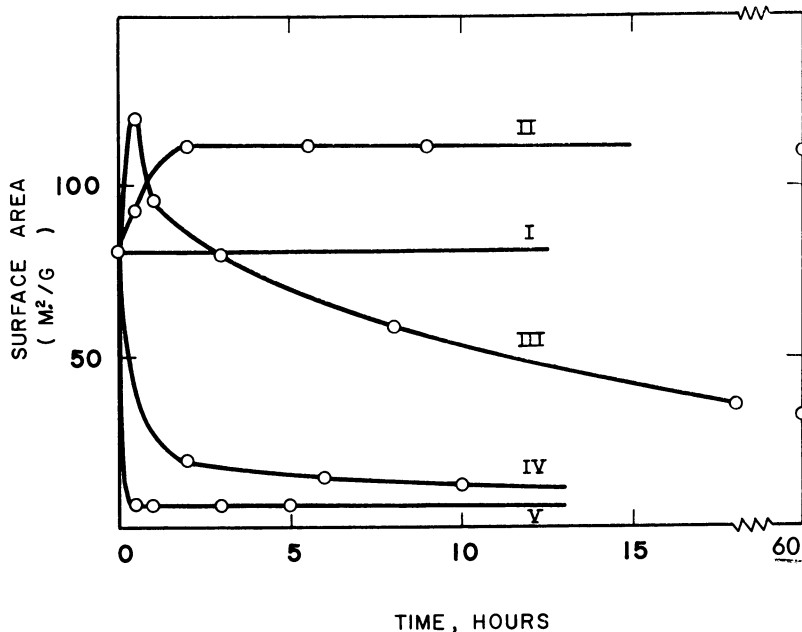


Figure 4. Effect of duration of heating on specific surface area of products prepared from lepidocrocite at various temperatures

I. Lepidocrocite

II, III, IV, V. Products obtained by heating at 190°, 300°, 400°, and 500° C.

Adsorption of Methanol. The adsorption isotherms of methanol on lepidocrocite and goethite and their decomposition products are also sigmoid-shaped Type II. However, with the exception of lepidocrocite itself, there is considerable hysteresis, and outgassing at room temperature does not completely remove the adsorbate. Subsequent isotherms obtained after thorough degassing of the pre-exposed solid at room temperature were reversible and invariably lower than the initial isotherms. In the light of the criteria put forward by Kipling and Peakall (13), the adsorption is regarded as partly physical and partly chemical. The difference between the two isotherms corresponds therefore to the amount of methanol chemisorbed.

The results of typical experiments are shown in Figure 6. The isotherms of methanol also obey the Brunauer, Emmett, and Teller equation, as may be judged from the linear plots in the inset of Figure 6.

The surface areas of the various specimens estimated by applying the Brunauer, Emmett, and Teller equation (4) to the initial adsorption isotherms and using the value of 18 sq. A. (14) are compared with the surface areas calculated from the adsorption of cyclohexane in Table I. The surface areas calculated from the total adsorption of methanol on lepidocrocite as well as its products formed by

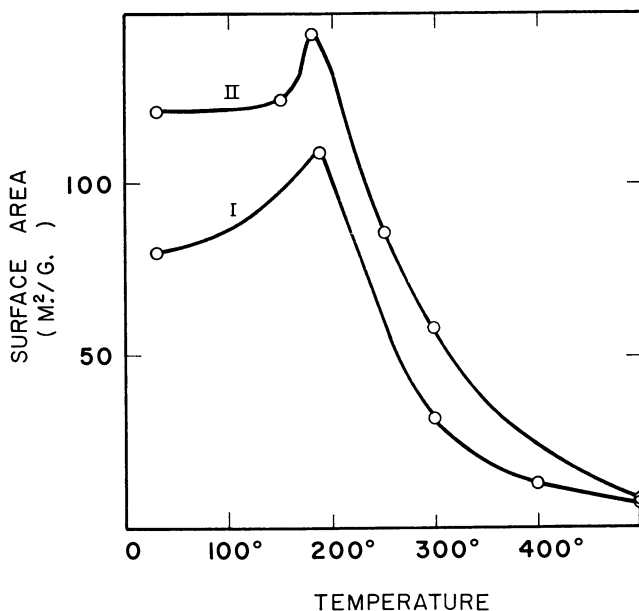


Figure 5. Effect of temperature of preparation on limiting surface areas of products prepared from lepidocrocite (I) and goethite (II)

thermal decomposition at temperatures below 400° are in fair agreement with the areas of the products calculated from the adsorption of cyclohexane. With products formed at 400° and 500°, the surface areas calculated from the adsorption of methanol are appreciably greater than those estimated from the adsorption of cyclohexane. These differences may be attributed to the larger size of the cyclohexane molecule in comparison with that of methanol. At the higher temperatures where sintering is liable to take place readily, most of the pores will have sizes accessible to the molecules of methanol and not to those of cyclohexane.

Table I. Surface Areas Calculated from the Adsorption of Cyclohexane and of Methanol

Material	Thermal Treatment		Water Content, %	Surface Area, Sq. M./G.		
	Temp., °C.	Duration, hours		Cyclohexane	Methanol	
Lepidocrocite	35	—	11.12	81	80	
	190	60	3.4	110	117	
	300	0.5	3	0	120	125
			8	0	81	76
			8	0	59	49
	400	0.5	0	20	34	
	500	0.5	1	0	7	23
			3	0	7	17
			3	0	7	10
			3	0	7	10
Goethite	35	—	12.7	122	71	
	150	0.5	7	9.8	125	71
			7	7.5	125	71
			7	7.5	125	71
	250	0.5	2.1	122	109	
			5	1.4	85	70
	300	0.5	0.1	85	84	
			2.5	0.1	63	69
			10	0.1	58	65

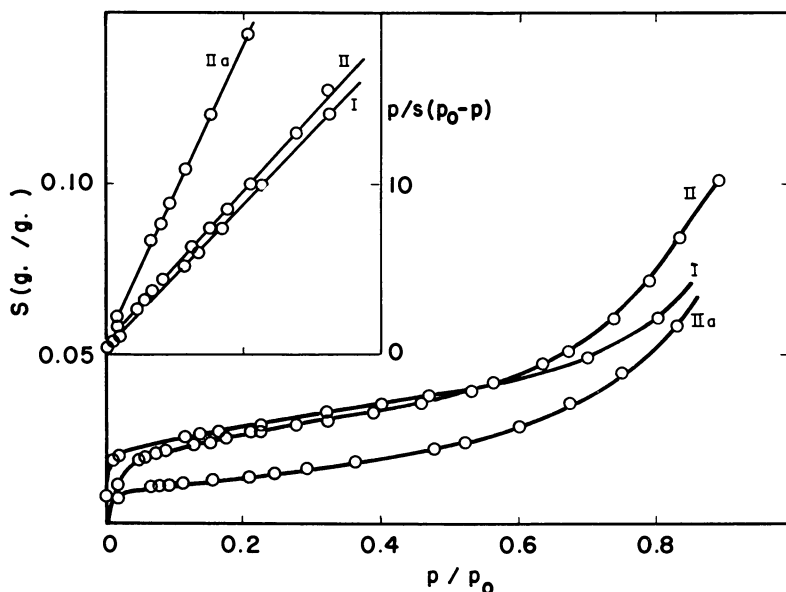


Figure 6. Adsorption-resorption isotherms of methanol at 35° C.

I. *Lepidocrocite*
 II. *Goethite, adsorption*
 IIa. *Goethite, resorption*

However, in the case of goethite and its products of decomposition formed at 150°, the surface area calculated from the total adsorption of methanol is appreciably less than that calculated from the adsorption of cyclohexane, whereas with products formed at the higher temperatures the two values are in fair agreement. It is not possible at present to give a satisfactory explanation for this peculiar behavior of goethite and of the products of decomposition formed at 150°. Probably the excess of water above the stoichiometric content for goethite (which is eventually greater by 1.6% than for lepidocrocite), as well as the high water content of the partly decomposed products obtained at 150° accounts for the lower adsorption of methanol. The assumption is made that some water molecules already occupy sites which otherwise would be occupied by methanol molecules.

In all cases, except with lepidocrocite where the adsorption is physical in nature, the fraction of the surface covered by physically adsorbed methanol is approximately 40 to 60% of the total surface, and both types of adsorption take place side by side, presumably on different sites.

Literature Cited

- (1) Baudisch, O., Hartung, W. H., "Inorganic Syntheses," H. S. Booth, ed., p. 185, McGraw-Hill, New York, 1939.
- (2) Bernal, J. D., Dasgupta, D.R., MacKay, A. L., *Nature* **180**, 645 (1957).
- (3) Brunauer, S., "Adsorption of Gases and Vapors," p. 150, Oxford University Press, 1944.
- (4) Brunauer, S., Emmett, P. H., Teller, E., *J. Am. Chem. Soc.* **60**, 309 (1938).
- (5) "Dana's System of Mineralogy," 7th ed., p. 683, Wiley, New York, 1958.
- (6) Foster, A. G., et al., *Proc. Roy. Soc. (London)* **A136**, 363 (1932); **A147**, 128 (1934); *J. Chem. Soc.* **1946**, 446; **1952**, 1139.
- (7) Geith, M. A., *Am. J. Sci.* **250**, 677 (1952).
- (8) Goodman, J. F., Gregg, S. J., *J. Chem. Soc.* **1956**, 3612.

- (9) Gregg, S. J., *Ibid.*, 1953, 3940.
- (10) Gregg, S. J., *et al.*, *Ibid.*, 1953, 3945.
- (11) Harkins, W. D., *et al.*, *J. Chem. Phys.* **14**, 117 (1946); *J. Am. Chem. Soc.* **72**, 3427 (1950).
- (12) Hüttig, G. F., *Kolloid-Z.* **98**, 63 (1942); **99**, 362 (1942).
- (13) Kipling, J. J., Peakall, D. B., *J. Chem. Soc.* 1957, 834.
- (14) Razouk, R. I., ElGobeily, M. A., *J. Phys. Colloid Chem.* **54**, 1087 (1950).
- (15) Razouk, R. I., Mikhail, R. Sh., *Ain Shams Sci. Bull.* **4**, 147 (1959).
- (16) Razouk, R. I., Mikhail, R. Sh., *J. Phys. Chem.* **61**, 886 (1957).
- (17) *Ibid.*, **63**, 1050 (1959).
- (18) Razouk, R. I., Mikhail, R. Sh., 2nd Intern. Congr. on Catalysis, Paris, July 1960.
- (19) Razouk, R. I., Salem, A. S., *J. Phys. Colloid Chem.* **52**, 1208 (1948).
- (20) Smith, N., Pierce, C., Cordes, N., *J. Am. Chem. Soc.* **72**, 5595 (1950).
- (21) Weiser, H. B., "Inorganic Colloid Chemistry," Vol. II, p. 29, Wiley, New York, 1935.

RECEIVED May 9, 1961.

Effect of Radiation on the Surfaces of Solids

I. Analysis of Adsorption Isotherms to Obtain Site Energy Distributions

ARTHUR W. ADAMSON and IRENE LING

Department of Chemistry, University of Southern California, Los Angeles 7, Calif.

A method is described whereby the site energy distribution function, $f(Q)$, may be obtained from an experimental adsorption isotherm, $\theta(P,T)$ and an arbitrarily assumed local isotherm function, $\theta(Q,P,T)$. As the method is graphical, it is not necessary to represent either θ or θ analytically, and successive approximations are used. The method is first applied to a synthetic isotherm calculated from an assumed site energy distribution with θ taken to be the Langmuir function, to show that the original distribution is indeed regenerated. On treating various systems for which literature data are available, very similar site energy distributions result if θ is taken to be either the simple Langmuir equation or one with lateral interaction included. The distributions are temperature-independent, and are consistent with isosteric and differential heats of adsorption.

The treatment of adsorption on a heterogeneous surface has constituted a topic of perennial interest, and this paper provides an extension, to the point of practical usefulness, of an approach for which the groundwork has been in existence for some time. Our interest in this matter developed out of work in this laboratory on the effects of radiation on the surfaces of solids, where changes in the nature of surface heterogeneities were obviously taking place. The results of these studies are given by Adamson, Ling, and Datta (2).

The problem of obtaining site energy distributions from adsorption isotherms may be defined as follows:

Let $\theta(P,T)$ be the observed adsorption function, usually obtained as $\theta(P)$ —i.e., as an adsorption isotherm. It is assumed that the adsorbent surface can be treated as consisting of noninteracting regions, each of which can be considered as homogeneous in nature and obeying a local adsorption isotherm, $\theta(P)$, or, in general, an adsorption function, $\theta(P,T,Q)$, where Q denotes the adsorbent adsorbate interaction energy. Also, let $\bar{F}(Q)$ denote the integral site energy

distribution—i.e., F is the fraction of surface whose site energy is equal to or greater than Q —and let $f(Q) = dF/dQ$ be the distribution function itself. $F(Q)$ will depend on the nature of both the adsorbent and the adsorbate, and hence is not purely a property of a given adsorbent.

The above quantities are related by the integral equation:

$$\theta = \left[\int_0^{\infty} f(Q)\theta(P,T,Q) dQ \right]_{P,T} = \left[\int_0^1 \theta(P,T,Q)dF \right]_{P,T} \quad (1)$$

Various approaches to the solution of Equation 1 have been considered. An easy one assumes convenient analytical forms for $f(Q)$ and $\theta(P,T,Q)$ which allow integration of Equation 1 to give an explicit expression for θ (containing various adjustable parameters). The usefulness of the function is then tested empirically (1, 18). Unfortunately, experimental adsorption isotherms generally can be fitted by a number of semiempirical equations, and agreement with some particular one provides no assurance that its basic assumptions are correct.

The more desirable approach is to determine $f(Q)$ from an assumed $\theta(P,T,Q)$ and the experimental adsorption isotherm. Sips (16) showed that Equation 1 could be treated by a Stieltjes transform, so that in principle an explicit function could be written for $f(Q)$, provided the experimental isotherm function, θ , could be expressed in analytical form. Subsequently, Honig and coworkers (10, 11, 12) investigated this approach further. The difficulty is that only for certain types of assumed functions θ and θ is the approach practical. As a consequence the procedure has been first to restrict the choice of θ to the Langmuir equation, and second to assume certain simple functions for θ such as the Freundlich and Temkin isotherm equations. The system is thus forced into an arbitrary mold and again it is not certain how much reliance should be placed on the site energy distributions obtained.

No method has so far been advanced for taking the experimental isotherm itself, irrespective of the complexity of its analytical representation, and from it, obtaining the site energy distribution consistent with any arbitrarily chosen local isotherm function, θ , no matter how complex.

The present method meets the above requirement; it consists of a convenient way of making successive graphical approximations to $F(Q)$, using both θ and θ in graphical form. Actually, the method is patterned after the procedure described by Berenyi (3) for obtaining characteristic curves according to the Polanyi potential treatment of adsorption. The procedure is described more specifically below, but may be summarized as follows:

For each pressure, the assumed local adsorption isotherm function allows θ to be determined as a function Q , while from a simple correspondence principle, the experimental adsorption isotherm $\theta(P)$ allows determination of a first approximation of F as a function of Q . From the plots of F vs. Q and θ vs. Q , a subsidiary plot is made for each pressure of θ vs. the corresponding F value. The area under this plot then gives a calculated θ for that pressure. The procedure is then repeated for other assumed pressures. The $\theta_{\text{calcd.}}$ values will in general differ from the experimental ones for the various pressures, and for each, a second approximation to F is made using the relationship:

$$F_2 = F_1\theta_{\text{obsd.}}/\theta_{\text{calcd.}} \quad (2)$$

The procedure is then repeated, using the plot of F_2 vs. Q . In most cases two successive approximations are sufficient, the number increasing the more uniform the surface.

Langmuir Equation as Local Isotherm Function

The procedure is first illustrated in terms of its application to the analysis of an isotherm calculated from an arbitrary assumed site energy distribution, $f(Q)$. For reasons discussed in more detail later, the Langmuir equation—i.e., localized adsorption with no lateral interaction—appears very satisfactory as the form to use for $\theta(P, T, Q)$:

$$\theta = \frac{bP}{1 + bP} \tag{3}$$

The evaluation of constant b is according to the relationship (1):

$$b = N\sigma^0\tau^0(2\pi MRT)^{-1/2}e^{Q/RT} = b_0e^{Q/RT} \tag{4}$$

where σ^0 denotes the actual area per molecule, and τ^0 is Frenkel's characteristic adsorption time (1, 5), here taken to be 10^{-13} second, so that its temperature dependence is neglected. The collection of constants b_0 then becomes approximately $8 \times 10^{-3} T^{-1/2}$ for nitrogen as adsorbate, and pressure in units of atmospheres.

To provide a relatively severe test of the method, an assumed site energy distribution having two peaks was used, as shown in Figure 1. The calculated isotherm, $\theta(P)$, was obtained by summing the occupancy of each site over all sites, for each of a series of pressures to give the plot shown in Figure 1, *b*. This calculated isotherm was then taken as the starting point for obtaining a site energy distribution.

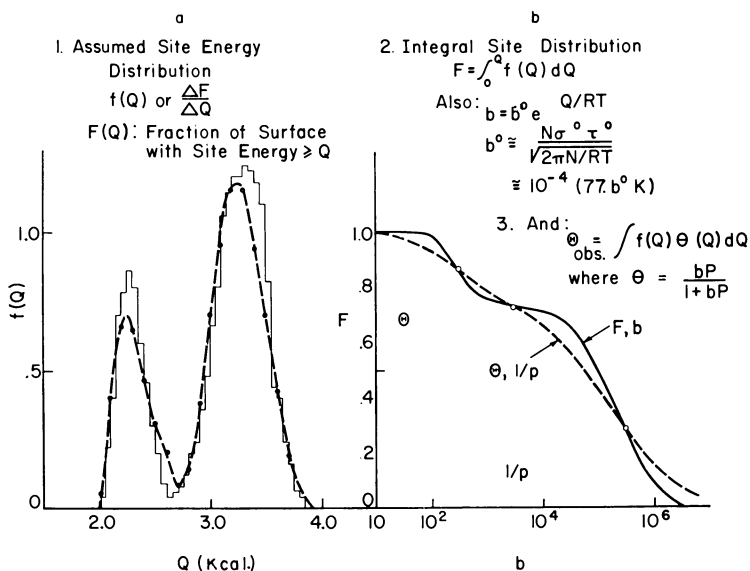


Figure 1. Test of site energy distribution method

- a. — Assumed distribution
- Points and dashed line. Calculated distribution
- b. - - - Calculated isotherm (θ vs. $1/P$)
- Final approximation to site energy distribution (F vs. b)

It was first necessary to obtain some initial approximation to the F vs. Q , or, for convenience in this case, the F vs. b plot. Examination of the form of the

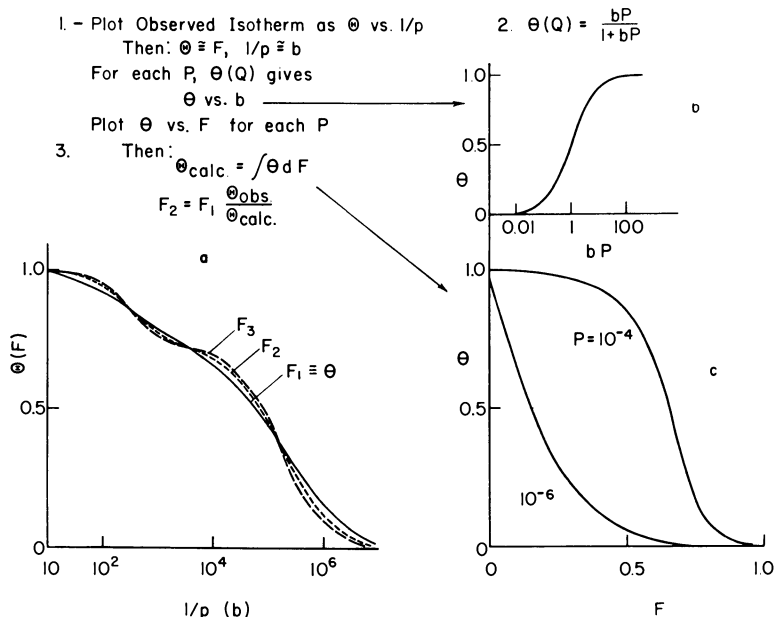


Figure 2. Outline of procedure for obtaining site energy distributions

- a. — Adsorption isotherm plotted as θ vs. $1/P$
 - - - Successive approximations to F vs. b
 b. $\theta(Q)$ (in this case, the Langmuir equation)
 c. θ vs. F plots for two different pressures

Langmuir isotherm (Figure 2,b) shows that 50% occupancy occurs at $P = 1/b$, and a reasonable first approximation is therefore to consider the curve as a step function in which θ jumps from zero to unity at $P = 1/b$. This amounts to assuming that, for a given pressure, sites of b values greater than $1/P$ are completely filled, and the rest are completely empty. In effect, then, a plot of the observed isotherm in the form of θ vs. $1/P$ (as in Figures 1,b and 2,a) becomes the first approximation to the F vs. b function.

The procedure so far is not new. Roginski, who proposed it, did not, however, suggest how to refine the approximate site energy distribution so obtained (17).

To obtain the second approximation to the F vs. b distribution, an auxiliary plot of θ vs. F is now made for each of several pressures. This is done by obtaining the θ value corresponding to a given b value (at the chosen pressure) from the Langmuir isotherm (Figure 2,b), and the F value corresponding to the same b value, using the approximate F vs. b —i.e., the experimental isotherm plotted as θ vs. $1/P$ as in Figures 1,b and 2,a. Two such auxiliary plots are shown in Figure 2,c. The area under each gives a $\theta_{\text{calc.}}$ for that pressure. On insertion into equation 2, a second approximation to F (for the b value corresponding to the pressure) is obtained. In the first round of approximation $F_1 = \theta_{\text{obsd.}}$

The second approximation to the F vs. b plot is shown in Figure 2,a as well as F_3 vs. b , obtained by repeating the above procedure. In the present example F_3 vs. b was taken to be in the terminal approximation (also shown in Figure 1,b) and, by means of Equation 4, the integral site energy distribution $F(Q)$ was obtained. The corresponding differential site energy distribution is shown in

Figure 1,*a*, by the dashed line; the agreement with the originally assumed distribution is reasonably good. The successive approximations converge rapidly, then, even for fairly complex distribution functions.

Turning to actual adsorption data, Brunauer, Love, and Keenan (4) reported on the high temperature adsorption of nitrogen on a synthetic ammonia catalyst. Their isotherms, for two temperatures, are shown in Figure 3,*a*. In order to report their data in terms of v/v_m —i.e., as Θ —the v_m value given by their low temperature nitrogen isotherm is used. An error merely modifies the F and dF/dQ scales in Figure 3,*b* and *c*, by some factor, so there is little effect on the general interpretation of the data.

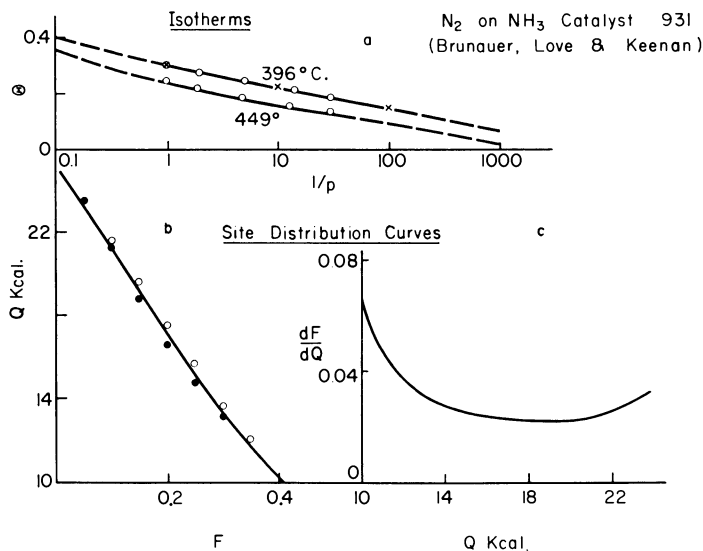


Figure 3. Adsorption of nitrogen on synthetic ammonia catalyst

- a. Adsorption isotherms
- b. Integral site energy distributions
 - 449° C.
 - 396° C.
- c. Differential site energy distribution

These data illustrate one of the requirements for obtaining site energy distributions—namely, that the range of pressure studied must be sufficient to cover either nearly the complete range of v/v_m values, or at least four and preferably five powers of 10 in pressure. In the present case, neither condition is met, with the result that the data do not define any kind of site energy distribution. However, as indicated by the dashed line extensions in Figure 3,*a*, if fairly long (but reasonable) empirical extrapolations of the experimental isotherms are made, an analysis becomes possible. The resulting integral and differential site energy distributions are shown in Figure 3,*b* and *c*; a rather wide spread of site energies is present. The distribution, in fact, approximates the completely uniform one, or horizontal line function, which Sips (16) showed to be implied by the Temkin equation (5) (which the data of Figure 3 fit):

$$\Theta = A \log CP \quad (5)$$

where A and C are constants (1, p. 536).

However, had some more radically curved extensions of the experimental isotherm been assumed in Figure 3,a, a less uniform calculated site energy distribution would have resulted. In other words, the fit to the Temkin equation is in this case over too small a pressure range for the uniform site energy distribution implied by the equation to be considered more than a guess.

The data for 376° and 449° C. give the same site energy distribution (Figure 3,b)—i.e., the calculated distribution is not temperature-dependent. This observation confirms the general consistency of the procedure and assumptions.

A second aspect of our procedure is illustrated in the case of low temperature isotherms, where P/P° values not negligibly small compared to unity are involved. In such cases, some degree of multilayer adsorption is to be expected, and must somehow be corrected for. Where the correction is small, it seems reasonable to make use of the BET treatment (1), from which it may be concluded that the actual fraction of surface covered, Θ , is related to v/v_m by:

$$\Theta = (v/v_m)(1 - P/P^\circ) \quad [= (v/v_m)(1 - x), \text{ where } x = P/P^\circ] \quad (6)$$

Equation 6 will be valid for x values not more than 0.05 to 0.1, if the BET constant, c , is large compared to unity.

As a specific illustration, Honig and Reyerson (12) studied the low temperature adsorption of nitrogen, oxygen, and butane on rutile. Their data are illustrated in Figures 4 and 5; while the important low pressure points are

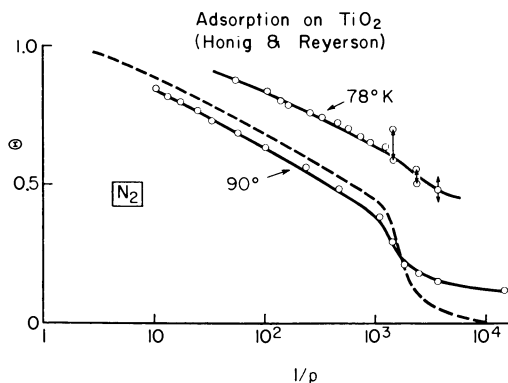


Figure 4. Adsorption of nitrogen on TiO_2
 --- Final F vs. b plot for 90° K

imprecise, qualitative site energy distributions can be constructed from the data. These are shown in Figure 6; similar distributions are obtained for the three vapors, but with maxima shifted towards lower energies in the sequence nitrogen, oxygen, and butane. A similar finding was made by Drain and Morrison (6), who determined site energy distributions from isosteric heats corrected to 0° K by heat capacity corrections. Site energy distributions thus indeed reflect adsorbate as well as adsorbent properties. As in the previous illustration, the distributions are essentially temperature-independent, allowing, in the case of the nitrogen data, for the obviously considerable experimental error in the low pressure region.

A third illustration is provided by the data of Joyner and Emmett (13) for the absorption of nitrogen on Graphon at 78° K. The isotherm is plotted in Figure 7, along with the successive approximations to the F vs. b plot. The

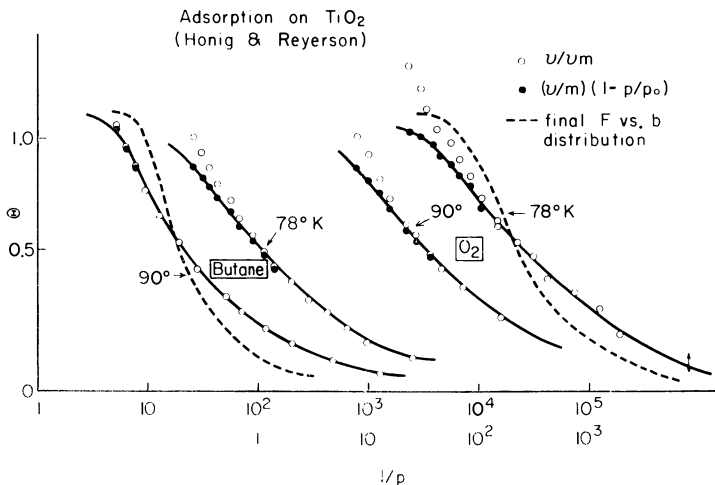


Figure 5. Adsorption of butane and of oxygen on TiO_2

○ v/v_m data
 ● $(v/v_m)(1 - x)$
 - - - Final F vs. b plots for butane at $90^\circ K$ and oxygen at $78^\circ K$

corresponding integral site energy distribution is shown in Figure 8, and is seen to indicate a very nearly uniform surface, with sites of about 2.6-kcal. energy. By way of comparison, the isosteric and calorimetric heats of adsorption are indicated by the dashed line in Figure 8. Here, while the average values agree approximately with that found from the site energy analysis, a maximum and a minimum are present which presumably are real. The difficulty is that an anomalous variation in the entropy of adsorption occurs, whereas, of course, our

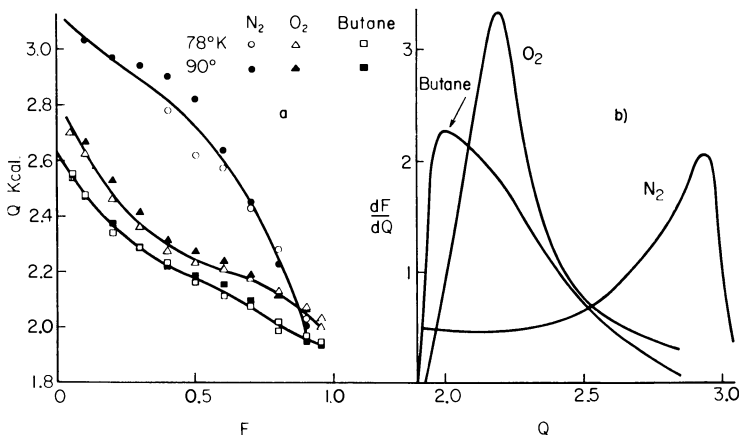


Figure 6. Site energy distributions for nitrogen, oxygen, and butane on TiO_2

a. Integral site energy distributions at 78° and $90^\circ K$ (solid symbols)
 ○ Nitrogen
 △ Oxygen
 □ Butane
 b. Differential site energy distributions

treatment assumed the simple entropy function for localized adsorption. Another point illustrated (in Figure 7) is that the more uniform the surface, the more

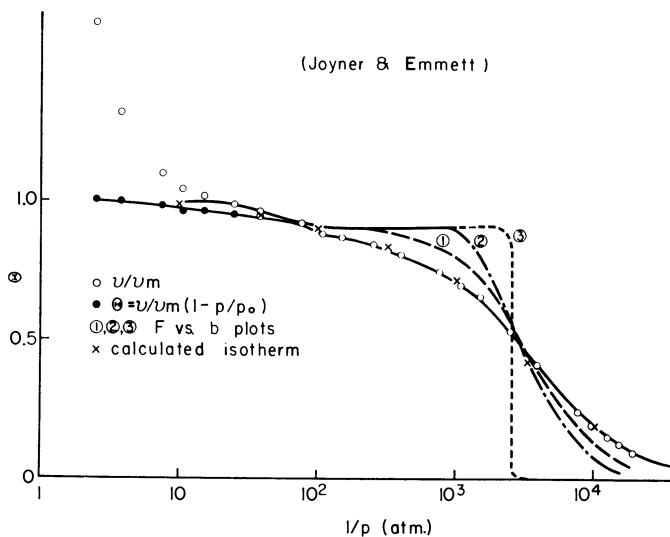


Figure 7. Adsorption of nitrogen on Graphon at 78° K

○ v/v_m
● $(v/v_m)(1 - x)$

Lines 1, 2, and 3 show successive approximations to F vs. b plot

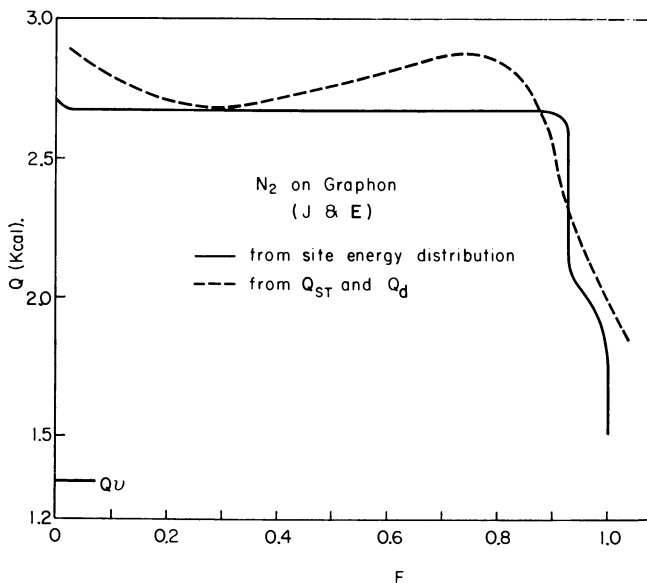


Figure 8. Site energy distribution for nitrogen adsorbed on Graphon

— Calculated from isotherm
- - - From calorimetric and isosteric heats

successive approximations are needed to obtain a self-consistent F vs. b curve—that is, this curve will deviate more from the θ vs. $1/P$ plot of the isotherm data.

Returning to the matter of differential, isosteric, and site energy distributions, it has been shown that if the local isotherm function is taken to be the Langmuir equation, the first two (integral) distributions are identical (9). This may not be true if some other local isotherm function is used. In either case, the site energy distribution will differ in the direction of the differential plot being more sharp, since both the differential and isosteric energy distributions involve an averaging over the range of sites being filled in a given region of the adsorption isotherm. Thus only in the extreme instances of an extremely wide and an extremely narrow site energy distribution is close agreement between all three distributions to be expected. On the other hand, the distinction involved is not a major one, and one does expect qualitative agreement between the various distributions.

Non-Langmuirian Local Isotherm Functions

Our proposed method of site energy distribution analysis can, of course, be applied using any function $\theta(P, T, Q)$ for the local isotherm (or even graphical representations not amenable to analytical replication). Nor need the function be explicit in θ . As an example of this last situation, it has been suggested (7) that lateral interaction be allowed for within the framework of the Langmuir approach by supposing Q to increase linearly with θ :

$$\theta = b'P/(1 + b'P) \quad (7)$$

where

$$b' = b_0 e^{Q_0/RT} e^{\alpha\theta/RT} = b_0 e^{\alpha\theta/RT}$$

and α is taken to be about one fourth of the energy of vaporization of the adsorbate (15).

For the case of nitrogen at 77.6° K, the plot of θ vs. bP now takes the form shown in Figure 9, in which filling occurs more sharply than with the simple Langmuir equation, and is centered at $bP = 1/3$ instead of at $bP = \text{unity}$.

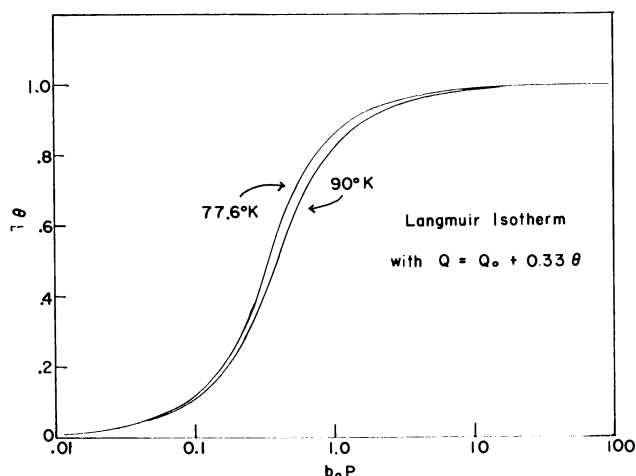


Figure 9. Langmuir-plus-lateral interaction isotherm

Correspondingly, a plot of data in the form of Θ vs. $1/3P$ is now taken to provide the first approximation to the F vs. b distribution. At 90° K, the relation is $b = 0.4/P$.

For cases of nearly uniform site distributions, such as nitrogen on titanium dioxide, the calculated site energy distributions are nearly the same as for the simple Langmuir equation used as the local isotherm function. In the case of nitrogen absorbed on Graphon, however, the distinction between the site energy distributions obtained with Equations 7 and 3 is noticeable; Equation 3 (the simple Langmuir equation) agrees somewhat better with the differential and calorimetric heat data. Graphon is exceptional, however, in having a very uniform surface, and ordinarily the only significant difference to be expected between using Equations 7 and 3 as the local isotherm function is that with the former the entire distribution will be shifted on the energy scale by an amount corresponding to about half of the maximum lateral interaction energy. In other words, the average Q value associated with a given type of site will be about that much greater than the Q_0 value.

It must not be assumed from the above that any local isotherm function will lead to physically acceptable site energy distributions—e.g., ones not involving negative Q values. Thus no isotherm function broader—e.g., whose range of $1/P$ values between say $\theta = 0.1$ and $\theta = 0.9$ is greater—than the experimental isotherm can be made to fit. For example, there is no physically acceptable site energy distribution whereby the Langmuir equation as the local isotherm function could be made to fit data showing a narrower range such as illustrated in Figure 9. Conversely, the very wide range of pressure over which adsorption occurs with local isotherm functions of the Frenkel-Halsey type (1, 8, 14) makes it necessary that experimental data show at least as broad a nature if the equation is not to be ruled out immediately. [As indicated in the discussion on nitrogen adsorption on a synthetic ammonia catalyst, the terms “broad” and “narrow” refer to the range of pressure over which filling of sites takes place. Roughly, if Θ or θ increases from 0.1 to 0.9 over a hundredfold pressure range, the isotherm is considered narrow; if the range is a thousandfold or more, it is considered broad.] If this first criterion is met, it is further necessary that the experimental data cover a very wide range of pressure (10^4 - or 10^5 -fold) in order to determine even a qualitative site energy distribution.

There seem to be no literature data potentially capable of showing definite consistency with Frenkel-Halsey type isotherms, with the exception of the results for nitrogen on titanium dioxide (2). Here we find that no site energy distribution can be constructed using such a local isotherm type which will lead to a fit over the entire range of data. The same appears to be true of local isotherm equations of the polarization theory type:

$$\ln(RT \ln P_0/P) = \ln \epsilon_0 + d\theta \quad (8)$$

Thus, it is concluded that local isotherm functions of a fairly narrow type such as the Langmuir and Langmuir-plus-lateral interaction types are the rule. Conversely, isotherms of the Frenkel-Halsey and polarization types do not seem applicable in the submonolayer region.

Literature Cited

- (1) Adamson, A. W., “The Physical Chemistry of Surfaces,” p. 535, Interscience, New York, 1960.
- (2) Adamson, A. W., Ling, I., Data, S. K., *ADVANCES IN CHEM. SER.*, No. 33, 62 (1961).

- (3) Berenyi, L., *Z. physik. Chem.* **94**, 628 (1920).
- (4) Brunauer, S., Love, K. S., Keenan, R. G., *J. Am. Chem. Soc.* **64**, 751 (1942).
- (5) de Boer, J. H., "The Dynamical Character of Adsorption," Clarendon Press, Oxford, 1953.
- (6) Drain, L. E., Morrison, J. A., *Trans. Faraday Soc.* **49**, 654 (1953).
- (7) Fowler, R. H., Guggenheim, E. A., "Statistical Thermodynamics," p. 431, Cambridge Univ. Press, 1949.
- (8) Halsey, G. D., *J. Chem. Phys.* **16**, 931 (1948).
- (9) Helper, L. G., *Ibid.*, **23**, 2110 (1955).
- (10) Honig, J. M., *Ibid.*, **24**, 510 (1956).
- (11) Honig, J. M., Hill, E., *Ibid.*, **22**, 851 (1954).
- (12) Honig, J. M., Reyerson, L. H., *Ibid.*, **23**, 2179 (1955).
- (13) Joyner, L. G., Emmett, P. H., *J. Am. Chem. Soc.* **70**, 2353 (1948).
- (14) Pierce, C., *J. Phys. Chem.* **64**, 1184 (1960).
- (15) Ross, S., Olivier, J. P., "The Adsorption Isotherm," p. 39f, Rensselaer Polytechnic Inst., Troy, N. Y., 1959.
- (16) Sips, R., *J. Chem. Phys.* **16**, 490 (1948).
- (17) Tolpin, J. G., John, G. S., Field, E., *Advances in Catalysis* **5**, 240 (1953).
- (18) Trapnell, B. M. W., "Chemisorption," Academic Press, New York, 1955.

RECEIVED May 9, 1961. Investigations supported by contract AF 33(616)-5320 between the University of Southern California and the Air Force.

Effect of Radiation on the Surfaces of Solids

II. Changes in Specific Surface Areas and Site Energy Distributions

ARTHUR W. ADAMSON, IRENE LING, and SUNIL K. DATTA

*Department of Chemistry,
University of Southern California, Los Angeles 7, Calif.*

An investigation has been made of the effects of reactor neutrons, fuel rod and Co^{60} γ -rays and copper x-rays on the surface properties of such solids as titanium dioxide (rutile), silica sand, various carbon blacks, and asbestos. The surface properties involved consisted of specific surface area determinations by low temperature nitrogen adsorption, and site energy distributions obtained by low temperature and very low pressure nitrogen adsorption. These solids are fairly insensitive to radiation, with the principal exception of x-irradiation of titanium dioxide which leads to considerable reduction in surface area. The site energy distribution obtained from adsorption in the submonolayer region of the isotherm before and after irradiation showed a considerable migration of sites from high to lower energies. A possible explanation for the special sensitivity of titanium dioxide is discussed.

The present investigations were undertaken to determine how various types of high energy radiation affected such properties as the surface energy and the total surface area of solids, both as such and in relation to changes in bulk properties. On this last point, somewhat opposing arguments can be made, *a priori*. On the one hand, particle radiation is much more effective than electromagnetic radiation in producing atomic displacements within a crystalline solid and surface effects might therefore be expected to appear more readily with the former type of radiation. Furthermore, since the activation energy for displacement of surface atoms is much less than that for internal atoms, it might be expected that surface properties would be more sensitive to radiation than are bulk properties.

By the same token, however, surface changes might be more readily self-annealing, and, moreover, thermal spikes (here, thermal patches) might well assist in reducing high energy and high area regions of a nonequilibrium surface.

Furthermore, multiple ionization, which has been postulated as being able to bring about displacements of interior atoms (30), might be extremely effective in leading to surface migrations and thermal patches, in which case surface properties could be more sensitive to electromagnetic radiation than to particle radiation. It was hoped that the present studies would shed some light on what actually happens.

The literature provides only a general guide to the most profitable systems to study. Spalaris, Bupp, and Gilbert (27) have reported extensive changes in the surface area and heat of nitrogen adsorption on neutron irradiation of synthetic graphite, using *nvt* values up to 10^{20} . The interpretation of their results, however, clearly depends upon and was complicated by the porous nature of the material. Thus the authors concluded that much of the observed effect on surface area was due to progressive blocking of pores as bulk expansion took place. The changes in the adsorption isotherms therefore may not have reflected changes in the intrinsic nature of the solid-gas interface. Leider (20) has reported some changes in the surface structure of sodium chloride crystals, on x-irradiation, as observed by diffraction patterns taken at grazing angles. The changes were attributed to strain relieving and again appear to be more related to bulk effects than to changes in specific surface properties. The *in situ* irradiation of pentane adsorbed on various solids such as silica gels led to increased decomposition rates (7). These, however, were attributed to energy transfer from the bulk to the surface region rather than to permanent changes in the nature of the surface itself. Moreover, in the case of silica gel and alumina, irradiative changes in catalytic ability toward deuterium-hydrogen exchange are at least partly related to changes in the internal pore structure, as evidenced by extreme sensitivity to water content (19). Finally, occasional work has been reported on the effects of radiation on the activity of various catalysts (26, 28), such as copper hydrogenation catalysts.

More pertinent to the present study are reports that irradiation of graphite dust (23) and charcoal (4) by neutrons and by electrons, respectively, did not produce any changes in low temperature adsorption isotherms. Unfortunately, detailed information on the nature of the solids and of the isotherms has not been obtained.

In undertaking the present program, it was felt that:

1. The solids selected should be known to be nonporous—i.e., should not show adsorption of hysteresis characteristic of capillary adsorption. In this way the influence of bulk dimensional changes should be minimized.

2. The solids should be refractory in nature, to reduce effects of heating during irradiation.

3. The use of low temperature adsorption provided the best understood and most accurate means of investigating surface changes.

4. The solids selected should be ones whose properties had been well studied by previous surface chemical investigations.

In view of the above points, the first choice was titanium dioxide powder, and then the various partially graphitized carbon blacks. Titanium dioxide is a nonporous material which can be obtained with a high specific surface area, and has been the object of considerable study (9, 14, 18, 29), so that not only is it known that reproducible and precise surface areas can be obtained by low temperature gas adsorption, but, in addition, the heats and entropies of adsorption by nitrogen and other gases are known. The same may be said of various carbon blacks (9, 11, 17, 21, 25). These are prepared by various types of pyrolytic decomposition of

organic compounds or fuels, followed by varying degrees of heat treatment which induces partial graphitization (31). A particular feature of the heat-treated samples is that they appear to have a very uniform surface. There was thus the possibility of looking for radiation effects not only for such uniform surfaces, but also as a function of degree of uniformity as determined by the amount of heat treatment. Another nonporous, refractory solid selected for some initial study is silica sand; its surface chemistry has been reported by Zettlemoyer (31).

Experimental

Materials. The titanium dioxide powders were rutile in structure (obtained from the Titanium Division, National Lead Co., Amboy, N. J.), with nominal specific surface areas of 10 and of 100 sq. meters per gram. Chemical analysis by the supplier showed negligible impurities except for 0.8% sodium oxide in the TiO_2 -100 and traces of iron in both the TiO_2 -10 and the TiO_2 -100. The presence of iron was confirmed by the nature of the decay of the neutron irradiation-induced radioactivities.

The carbon blacks consisted of Spheron 6 and Sterling FT (fine thermal) black, both non-heat-treated and 2700°C . heat-treated (obtained from the Godfrey L. Cabot Co., Boston, Mass.). Published surface areas for the four carbon blacks are 114, 84.1, 15.5, and 12.5 sq. meters per gram, respectively (31). The silica sand was supplied by the New Jersey Silica Sand Co., Millville, N. J., with the manufacturer's designation of No. 325 flour. Screen analysis by the supplier showed a considerable range in particle size; about 60% was retained on a 90-mesh screen and 90% on a 200-mesh screen. Finally, a sample of asbestos was tested (obtained from the Canadian Johns-Manville Co., Port Credit, Toronto, with the designation 7R). Zettlemoyer (31) has studied this material.

Irradiations. Samples were neutron-irradiated at the Oak Ridge and Chalk River facilities and in the MTR reactor at Arco, Idaho. In the first two cases, powder samples were submitted as such, while for the MTR irradiations both loose samples—i.e., in contact with air—and samples in evacuated quartz ampoules were submitted. Exposures are given as integrated *not* values. No special temperature control was attempted, but irradiation temperatures were probably not over 150°C . at Oak Ridge, and less at the other installations.

A few gamma irradiations were made through the courtesy of Atomic International, using the Co^{60} source, and the rest in the fuel rod assembly at the Argonne National Laboratory. In the last case, the samples were sealed in evacuated glass ampoules.

X-irradiations were made in this laboratory, using first a crystallographic machine and, later, a custom-built unit provided by the H. J. Beets Co., Los Angeles, capable of providing about ten times higher intensities. In both cases a copper target x-ray tube was used. X-irradiations were made using small mica window cells, and the sample was stirred by a slowly turned wire extending into the cell. Since the cells were of about 1 sq. cm. cross section and contained only about 0.2 gram of sample, fairly uniform irradiation probably took place.

Exposures, for both the gamma-irradiated samples at the Argonne facility and the x-irradiated samples, were based on the standard ferrous sulfate dosimeter solution (using a *G* value of 15.6) (12, 15). In the latter case, the mica window sample holder used for sample irradiations was filled with the dosimetric solution for dosage estimations.

Surface Area Determinations. Nitrogen adsorption isotherms were obtained

using a standard-type vacuum line apparatus (1, 5). The temperature was usually that of boiling liquid nitrogen (77.6° K), but was determined in each case by a nitrogen vapor pressure thermometer. Isotherms at 90° K were thermostated by a liquid oxygen bath.

Nitrogen adsorption in the submonolayer region (and hence at very low equilibrium pressures) was determined with the same apparatus but a transistor-type thermal conductivity gage (24) was used for pressure determination. As with the higher pressure runs, equilibrium was checked by taking desorption points; at the very lowest pressures several hours were required to reach equilibrium. Where important, the measured pressure was corrected for the thermal transpiration effect.

Degassing is important in the case of titanium dioxide, and in our case samples pumped for 4 hours while maintained at 150° to 170° C. gave reproducible surface areas. Once degassed, there was little effect of exposure to air (for short periods) or of heating at higher temperatures or for longer periods. While it has been noted (10) that outgassing (with increasing decomposition) continues up to temperatures as high as 1000° C., and Honig and Reyerson (16) have used long pumping at 400° C. as their degassing procedure, we preferred not to subject our samples to more drastic treatment than absolutely necessary. The temperature and pumping time employed here should remove all physically adsorbed gases and actually all gases whose energy of adsorption is below about 6 kcal. The site energy distribution found for our titanium dioxide samples (for nitrogen at low temperatures) showed negligible sites of energy greater than about 3.5 kcal. Our degassing procedure thus should have removed all physically adsorbed impurities (mostly water).

Powder Patterns. Powder patterns on titanium dioxide were obtained using a North American Philips x-ray machine and a standard powder camera. This work was done by A. Caron.

Results and Discussion

The adsorption isotherms were in all cases reversible, in that the desorption points fell on the same curve as the adsorption ones. Although capillary adsorption was therefore presumably not important, some of the carbon samples were porous in the sense that the apparent particle size was much larger than that corresponding to the surface area.

The high pressure isotherms (P/P_0 0.01 to 0.95) could be fitted with normal success to any one of several isotherm equations, and, in fact four procedures were tested. The first was the standard BET method (6), using 16.1 sq. meters per gram as the area of the nitrogen molecule at 77.6°K (14).

The second method, that described by Harkins and Jura (14), applies the semiempirical equation

$$\log P_0/P = B - A/v^2 \quad (1)$$

where P_0 is the saturation pressure, v is the amount adsorbed in cubic centimeters (STP) per gram at pressure P , and A and B are empirical constants. The specific surface area, Σ , was given by the recommended relationship (14):

$$\Sigma = 4.06A^{1/2} \quad (2)$$

in square meters per gram.

The third procedure used an equation based on the Polanyi potential model,

using an inverse cube potential law (1) [see (8, 13) for similar equations]:

$$v = -\alpha + \beta w^{-1/3} \quad (3)$$

Here α and β are empirical constants, and w denotes $\log P_o/P$.

The fourth procedure was based on the observation (1) that it is not actually necessary to use an algebraic representation of the shape of the adsorption isotherm in the multilayer region to obtain relative surface area values. A plot of $\log v$ vs. any convenient function of pressure, here taken to be w , has been found to give the identical shape in the multilayer region for a given adsorbate and temperature, and independent of the nature of the solid. Consequently, different isotherms—i.e., for different solids—differ only in vertical displacement and the relative displacements required for superposition in the multilayer region then give relative values of v_m or of Σ . Such plots are here abbreviated UI for universal isotherm. As with the Harkins-Jura (HJ) and potential (P) plots, numerical specific surface area values are obtained by using an empirical proportionality constant. A less precise approach consists of taking the value of v at some convenient P/P_o value as a means of evaluating Σ :

$$\Sigma = 3.00v \text{ (at } w = 0.5) \quad (4)$$

in square meters per gram—i.e., in terms of the v value for $w = 0.5$ on the smoothed plot.

The use of these various area-determining procedures allows some conclusions as to the best means of obtaining self-consistent relative area values. A few such comparisons are shown in Table I. The best agreement between any pair of

Table I. Comparison of Methods of Surface Area Determination

(TiO₂-100 samples only)

Radiation	Dosage nvt, E.V./G.	Surface Area, Sq. M./G.		
		BET	HJ	UI
None		76.4	(76.7)	(76.4)
		78.2	78.7	79
Neutrons	7.3×10^{19}	77.8	76.7	74.2
	1.0×10^{21}	70.0	76.7	70.3
X-rays	3.4×10^{19}	77.2	75.3	76.4
	9.2×10^{19}	74.9	71.9	73.0
Gammas	1.6×10^{20}	70.0	70.5	71.7
	8.2×10^{22}	75.6	71.0	75.5

methods was between the BET and UI methods, and where extensive data in the multilayer region permit, the latter is preferred, since it uses the adsorption isotherm over a wider region than the BET equation. Since the BET method is the more familiar, however, most of the results are reported in terms of it.

Tables II and III summarize the results of neutron and gamma irradiations (2). Thus, neutron irradiation of TiO₂ produced only slight effects, if any, on the specific surface area. Neither was there any effect of oven heating in air. The x-ray powder patterns for the Arco-irradiated TiO₂-100 showed no detectable change from the $a = 4.599 \pm 0.002$ values for the original powder, in agreement with a similar measurement by Primak (22). Some small changes in specific surface area were found in the various carbons; in the Sterling FT samples, the change is probably within the experimental error. The reduction in the case of the silica sand again is probably within the error of determination, and should be checked using xenon adsorption, which gives more precise low area determinations.

Table II. Effect of Neutron Irradiation on Σ Values

Material	Facility	Integrated nvt, Neutrons/Sq. Cm.	BET Area, Sq. M./G.
TiO ₂ -100		None	77.3
		None; heated in air at 90° C. for 3 weeks	78.8
TiO ₂ -10	Arco	7.3×10^{19}	77.8 ^a
		None	5.1
Spheron 6 (not heat treated)	Oak Ridge	5.6×10^{18}	5.1
		None	107
Spheron 6 (heat treated)	Oak Ridge	5.7×10^{18}	106
	Arco	8.8×10^{19}	110 ^a
Sterling FT (not heat treated)	Oak Ridge	None	86
	Arco	1.4×10^{19}	87
Sterling FT (heat treated)	Oak Ridge	8.9×10^{19}	87 ^a
		None	13.6
SiO ₂ sand	Oak Ridge	1.4×10^{19}	12.1
		None	14.4
Asbestos	Chalk River	6.8×10^{18}	13.4
	Oak Ridge	None	0.99
		7×10^{18}	0.86
			17.8
			16.8

^a Samples irradiated in vacuum.

Table III. Effect of Gamma Irradiation on Σ Values

Material	Facility	Dosage, E.V./G.	BET Area, Sq. M./G.
TiO ₂ -100		None	77.3
	Co ⁶⁰	8.3×10^{21}	79
Spheron 6 (not heat treated)	Argonne	8.2×10^{22}	75 ^a
		None	107
Spheron 6 (heat treated)	Argonne	8.2×10^{22}	107 ^a
		None	86
Sterling FT (heat treated)	Argonne	4.1×10^{22}	87 ^a
		None	14.4
	Argonne	8.2×10^{22}	14.6

^a Samples irradiated in vacuum.

The effect of gamma radiation was again small and, in fact, it is only on x-irradiation of TiO₂ that significant changes were found to occur. It is seen in Table IV that a 4.5×10^{21} e.v. per gram irradiation led to a 13% reduction in surface area; this, moreover, was reproducible. By contrast, similar irradiation of the SiO₂ powder produced no change.

Table IV. Effect of Cu X-Irradiation on Σ Values

Material	Dosage, E.V./G. ^a	BET Area, Sq. M./G.
TiO ₂ -100 ^b	None	77.3
	3.4×10^{19}	77.2 ^c
	9.2×10^{19}	74.9 ^c
	1.6×10^{20}	70.0 ^c
	2.0×10^{21} (10 days)	70 ^b
TiO ₂ -100 ^d	None	97.1
	4.5×10^{21} (1 day)	84.5
SiO ₂	None	0.96 ± 0.04
	1.4×10^{22} (2 days)	0.92 ± 0.04

^a E.v. per gram of H₂O as determined by ferrous sulfate radioactive solution.

^b Here, as with neutron irradiations, TiO₂ was not subjected to prior degassing.

^c Irradiated in vacuum.

^d Samples degassed under vacuum at 150–175° C. for 4 hours prior to use. Note difference in x-ray intensity between ^b and ^d.

Complete degassing of the TiO_2 -100 increased the BET area from 77.3 to 97.1 sq. meters per gram (see Table IV), perhaps because of clearing of cracks or channels. The relative effect of x-irradiation was about the same, however, in that a 10 to 15% decrease occurred with both degassed and nondegassed material.

Site Energy Distribution in TiO_2 . The low pressure portions of the nitrogen isotherms for TiO_2 -100 (using only degassed samples) are shown in Figure 1. Even at the limit of usefulness of the thermistor gage (about 10 microns) there was still about 20% of a monolayer, but even so the region from 20% to complete monolayer coverage is large enough to permit useful analyses of site energy distributions.

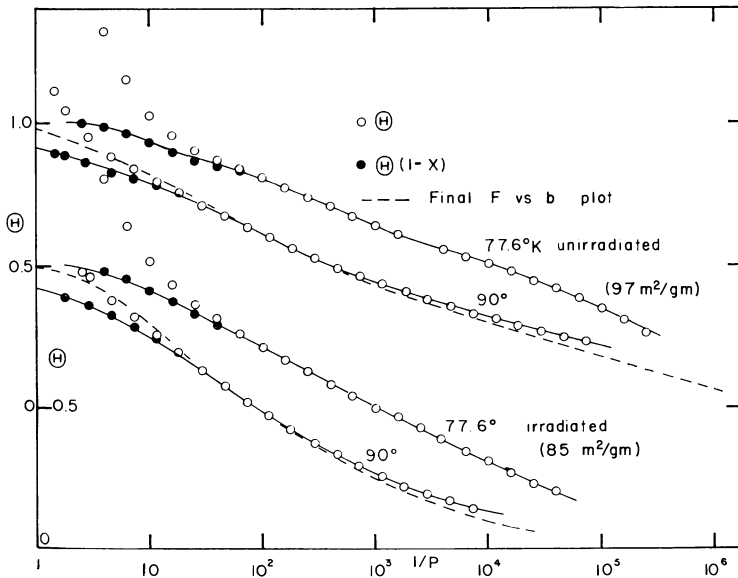


Figure 1. Adsorption of nitrogen on TiO_2 (rutile)

Upper. Unirradiated TiO_2
 Lower. Irradiated at 4.5×10^{21} e.v./g. with Cu x-rays
 ○ v/v_m values (from slightly smoothed isotherms)
 ● $(v/v_m)(1-x)$
 --- F vs. b plots for two 90° K isotherms

The procedure followed is that described by Adamson and Ling (3). In Figure 1 the solid circles represent the multilayer correction. The dashed lines indicate the final F vs. b distributions for two of the isotherms, where b is the constant in the Langmuir equation

$$\theta = bP/(1 + bP)$$

$$b = b_0 e^{Q/RT} \quad (1)$$

and F denotes that fraction of surface having site energies greater than that corresponding to the given b value. The integral site energy distributions are shown in Figure 2; for both the irradiated (copper x-rays and total dose of 4.5×10^{21} e.v. per gram) and unirradiated material, the isotherms at 77.6° and 90° K gave substantially the same distribution. The isosteric heats were less precisely determinable because of their sensitivity to small experimental errors in the isotherms, but, by way of illustration, the values calculated for the irradiated

material are included in Figure 2. As discussed by Adamson and Ling (3) only qualitative correspondence between isosteric heats of adsorption and site energies is to be expected, although the two should be fairly close together in the case of a solid such as TiO_2 which shows a very broad site energy distribution.

The differential site energy distributions, obtained by taking slopes from the integral distributions, are shown in Figure 3. These are necessarily less accurate than the integral distributions, but show more clearly that the essential effect of the x-irradiation has been to decrease the number of sites of energy above 3 kcal., and correspondingly to increase the number with less than 3-kcal. energy. Roughly, 17% of the sites appear to have been decreased in energy and by an average of 1 to 1.5 kcal.

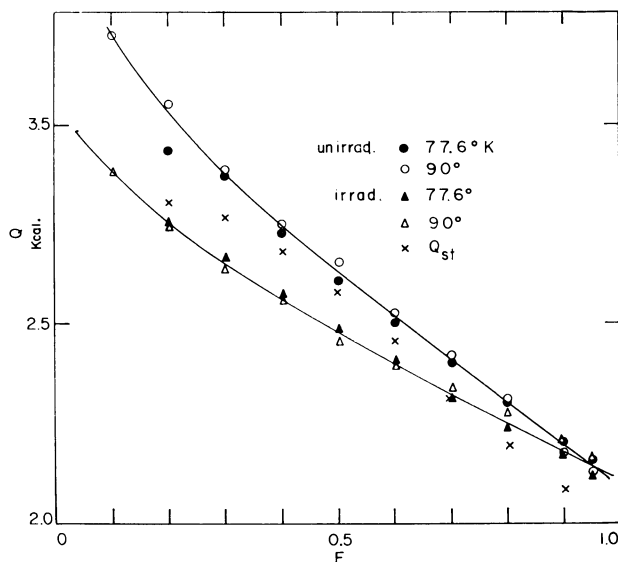


Figure 2. Integral site energy distributions

- Unirradiated TiO_2
- △ Irradiated TiO_2
- Open symbols 77.6° K
- Solid symbols 90° K
- × Q_{st} for irradiated TiO_2

The BET v_m value was used in each case in determining θ , the apparent surface coverage, so that the distributions for the irradiated material refer to a surface having 13% less area than the nonirradiated titania. Thus the effect of the irradiation could be viewed as an elimination of about 15% of the surface, high energy sites being the ones removed. If the higher energy sites were located in pores or cracks, a surface annealing of these defects by irradiation should lead to just this dual result of a simultaneous reduction in area and in proportion of high energy sites.

It is suggestive that TiO_2 appears to be more sensitive to x-irradiation than to gamma radiation, and more sensitive to x-irradiation than is SiO_2 . A possible explanation, advanced earlier (2), is that the photoelectric ejection of K -electrons from titanium should be about ten times more efficient in the case of copper x-rays than the same process in silicon. K -electron ionization would be followed

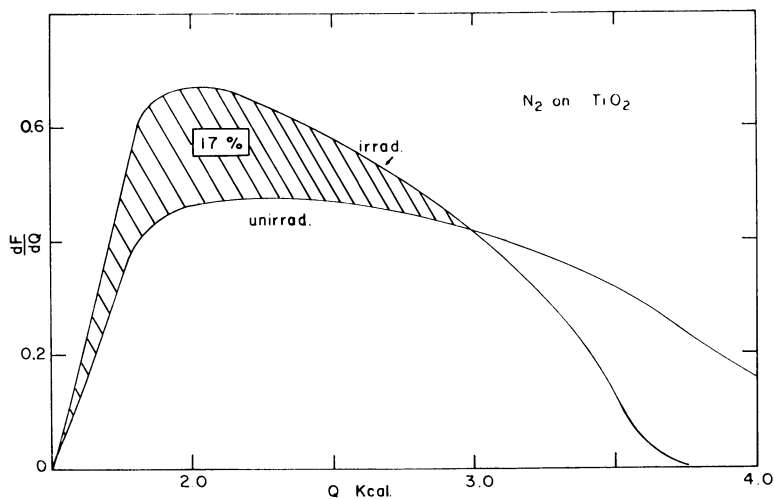


Figure 3. Differential site energy distribution

by internal conversion of the secondary x-rays, and the net Auger ionization should lead to multiply charged ions. This process is known to be much more effective in producing chemical consequences than is simple ionization of outer electrons (12, pp. 429f), and it is therefore to be expected that titanium atoms at or near the surface will receive much higher chemical activation from x-rays than from γ -rays, and that the difference will be much less noticeable in the case of lighter elements such as silicon. Neutralization back to its normal charge of a heavily ionized titanium atom could easily lead to an energy production of 50 to 100 e.v. and a resulting "thermal patch" on the surface (in analogy to thermal spikes in the interior) might well permit annealing of surface cracks or potholes.

Plans are to explore further the possible importance of the Auger effect by varying the energy of the incident x-irradiation and by going to solids, such as metals, containing still heavier atoms than titanium. Among dielectrics, transistor materials such as germanium should be of interest.

Literature Cited

- (1) Adamson, A. W., "Physical Chemistry of Surfaces," Interscience, New York, 1960.
- (2) Adamson, A. W., Datta, S. K., Abstracts, 136th Meeting ACS, Atlantic City, N. J., September 1959, p. 225.
- (3) Adamson, A. W., Ling, I., *ADVANCES IN CHEM. SER.*, No. 33, 51 (1961).
- (4) Amphlett, C. B., Greenfield, B. F., "Krypton and Xenon Adsorption Isotherms on Charcoal Irradiated with 1 Mev Electrons," At. Energy Establishment, Ukaea Research Group, *AERE C/R 2632* (July 1958).
- (5) Brunauer, S., "Adsorption of Gases and Vapors," Vol. 1, Princeton University Press, Princeton, N. J., 1945.
- (6) Brunauer, S., Emmett, P. H., Teller, E., *J. Am. Chem. Soc.* **60**, 309 (1938).
- (7) Caffrey, J. M., Jr., Allen, A. O., *J. Phys. Chem.* **62**, 33 (1958).
- (8) Champion, W. M., Halsey, G. D., *J. Am. Chem. Soc.* **76**, 974 (1954).
- (9) Corrin, M. L., *Ibid.*, **73**, 4062 (1951).
- (10) Czanderna, A. W., Honig, J. M., *J. Phys. Chem.* **63**, 620 (1959).
- (11) Greyson, J., Aston, J. G., *Ibid.*, **61**, 610 (1957).
- (12) Haisinsky, M., "La Chimie Nucleaire et ses Applications," Masson & Co., Paris, 1957; *J. Am. Chem. Soc.* **79**, 1565 (1957).
- (13) Halsey, G. D., *J. Chem. Phys.* **16**, 931 (1948).
- (14) Harkins, W. D., Jura, G., *J. Am. Chem. Soc.* **66**, 921, 1367 (1944).
- (15) Haybittle, J. L., Saunders, R. D., Swallow, A. J., *J. Chem. Phys.* **25**, 1213 (1956).

- (16) Honig, J. M., Reyerson, L. H., *J. Phys. Chem.* **56**, 140 (1952).
- (17) Joyner, L. G., Emmett, P. H., *J. Am. Chem. Soc.* **70**, 2353 (1948).
- (18) Kington, G. L., Beebe, R. A., Polley, M. H., Smith, W. R., *Ibid.*, **72**, 1775 (1950).
- (19) Kohn, H. W., Taylor, E. H., Abstracts, 138th Meeting, ACS, New York, 1960, p. 11-I; *J. Phys. Chem.* **63**, 966 (1959).
- (20) Leider, H. R., *Phys. Rev.* **101**, 56 (1956).
- (21) Pierce, C., *J. Phys. Chem.* **64**, 1184 (1960).
- (22) Primak, W., *Phys. Rev.* **93**, 837 (1954).
- (23) Roberts, L. E. J., "Adsorption on Irradiated Graphite," Ministry of Supply, Harwell, *AERE C/M* (April 15, 1952).
- (24) Rosenberg, A. J., *J. Am. Chem. Soc.* **78**, 2929 (1956).
- (25) Ross, J. W., Good, R. J., *J. Phys. Chem.* **60**, 1167 (1956).
- (26) Saito, Y., Yonoda, Y., Makishima, S., *Nature* **183**, 388 (1959).
- (27) Spalaris, C. N., Bupp, L. P., Gilbert, E. C., *J. Phys. Chem.* **61**, 350 (1957).
- (28) Spilners, A., Smoluchowski, R., Abstracts, 138th Meeting, ACS, New York, N. Y., 1960, p. 11-I.
- (29) Tykodi, R. J., Aston, J. G., Schreiner, G. D. L., *J. Am. Chem. Soc.* **77**, 2168 (1955).
- (30) Varley, J. H. O., *J. Nuclear Energy* **1**, 130 (1954).
- (31) Zettlemoyer, A. C., *J. Phys. Chem.* **57**, 650 (1957).

RECEIVED May 9, 1961. Investigations supported in part by Contract AF 33(616)-5320 between the University of California and the U. S. Air Force.

Effect of the Environment upon the Properties of Solids

W. A. WEYL

*College of Mineral Industries,
The Pennsylvania State University, University Park, Pa.*

The concept of Weyl and Marboe that the melting of most ionic crystals is the result of a disproportionation of all binding forces into stronger and weaker forces is applied to surfaces. Surfaces resemble lattice defects—e.g., vacancies—inasmuch as they represent centers of asymmetry. The degree of asymmetry introduced by a surface depends upon the environment. It is shown how the change of environment can affect rate phenomena even for macroscopic crystals and equilibrium properties of small particles. The thermal vibrations in surface layers are less harmonic than those in the interior of the crystal. The resulting difference in thermal expansivity between surface layer and bulk leads to stresses on cooling which produce dislocations in metals and Griffith flaws in brittle solids.

The melting of a perfect crystal should consist of the overcoming of its binding forces by the thermal energy. Increasing temperature should change a perfect crystal gradually into a viscous liquid. The melting temperature of a perfect crystal can be defined sharply only thermodynamically but not kinetically, because a perfect crystal can be overheated and its melt can be supercooled.

Some substances such as quartz and feldspars melt as perfect crystals. The rigid coordination requirement of the Si^{+4} core does not permit these solids to develop a major concentration of vacant lattice sites. Albite melts at 1118°C ., but such a crystal loses neither its shape nor its birefringence when held for several hours at a temperature 50°C . higher than its melting point (33).

Most substances do not melt as perfect crystals but develop a major concentration of lattice vacancies as the temperature approaches their melting points. Weyl and Marboe (42) showed how a lattice vacancy in a sodium chloride crystal changes the distribution of all binding forces in its vicinity, thus producing ionic clusters in which the ions are bonded together strongly. The fluctuating fissures between these ionic clusters permit easy flow. Fused NaCl has a low viscosity even just above the melting point, so that the latter is sharply defined

both thermodynamically and kinetically. A sodium chloride crystal cannot be overheated and its melt cannot be supercooled to the extent that it will form a glass. Quartz crystals and albite crystals can be overheated and their very viscous melts solidify on cooling without crystallizing.

The fact that most substances accumulate defects on heating, and that each defect causes a disproportionation of the binding forces into weaker and stronger ones which leads to a dynamic structure consisting of ionic clusters separated by fissures, makes it impossible to derive the melting temperature or the mechanical strength of crystals from the thermodynamic data such as the lattice energy.

When Frenkel (16) discussed the relation between the solid and the liquid state of a substance, he commented on the difficulty of explaining the drastic difference between the two states. The distance between the particles increases only 3 to 4% during melting, and the heat of fusion may amount to only a small fraction of the heat of vaporization.

Using the Fajans (9) concept of chemical binding, one can demonstrate how, in spite of the small changes of the average distances and the average binding forces, most crystals change abruptly into a liquid of low viscosity when they are heated above their melting points.

Substances, even those which resemble a perfect crystal because they develop only a low concentration of lattice vacancies on heating, must have surfaces and a surface is the seat of asymmetry because the coordination of surface ions is incomplete. For sodium chloride the change from sixfold coordination of its ions within the crystal to the single vapor molecules causes the Na-Cl distance to decrease from 2.81 to 2.51 Å.

Lennard-Jones and Dent (25) calculated that a slice one atom thick when cleaved from the cube face of an NaCl crystal would contract by 5%. This contraction is the result of the increase of the electron density between the nuclei and is equivalent to a strengthening of the Na-Cl bonds.

Surfaces act like lattice vacancies; they change the binding forces and the distances and lead to a condition which can be called stress if one wants to describe it macroscopically. This condition within a surface film or within the skin of a solid is the result of an asymmetry in the electron density distribution. Hence, everything which affects the symmetry of a surface, even physically adsorbed atoms of the inert gases, must be expected to affect the properties of the solid.

Properties of Solids as Affected by Surfaces

The bulk properties of macroscopic crystals cannot be affected drastically by the difference which exists between the structure of the interior and that of a surface film which is approximately 10,000 atoms deep. However, even for macroscopic crystals, rate phenomena such as modification changes which are initiated within the surface are likely to be influenced by the environment, which would include molecules which are conventionally described as physically adsorbed. Apparently it is not generally understood that even the presence of a noble gas can affect the chemical reactivity of solids. Brunauer (3) explained that in principle physical adsorption of molecules should affect the solid in the same manner as chemisorption. As action and reaction are equal, chemisorption may have a stronger effect on both the solid and the adsorbed molecule.

For small particles or porous systems the environment affects equilibria in addition to rate phenomena, because the disturbed surface film of a small particle

represents a substantial part of its volume. In such a case a measurable difference in the lattice parameters of the crystal might be expected from the change in the binding forces. This difference should be a function of the surface volume ratio and of the environment.

Rymer and Butler (32) found that the lattice parameter of a very thin gold foil parallel to its surface is less than that of macroscopic gold crystals.

Hofmann and Wilm (20) found the same difference in the lattice parameter for graphite.

Boswell (2) demonstrated that the lattice parameters of small particles of alkali halides and metals decrease with decreasing particle size. Nicolson (27) prepared some small crystals of MgO (500 Å.) in vacuo and found their lattice parameter to be smaller than that of a macroscopic crystal. The electron density which represents the bond between the nuclei of Mg and O must be greater in a small crystal than in large ones. The internuclear distances in a small crystal are smaller than in a large one, because the average coordination of its ions has become smaller than that value which characterizes the infinitely extending perfect crystal. The fact that the Mg^{+2} and O^{-2} ions which participate in surfaces, edges, and corners of an MgO crystal have incomplete coordinations (coordination No. < 6) has a noticeable effect upon the electron density distribution within the lattice. Magnesium oxide crystals of the same small size prepared in air have the normal lattice parameter (27). Apparently some of the electron density must have been used for binding molecules of adsorbed gases, a process which might lead to the formation of O^- and $(\text{O}_2)^-$ ions from the ambient oxygen.

A small crystal of MgO prepared in vacuo behaves as if it were under a hydrostatic pressure generated by the changed internuclear distances of its surface film, which would decrease its lattice parameters. As the sum of all stresses in a solid must be zero, the skin must be in a state of tension.

Formation of Dislocations and Griffith Flaws. Fajans (9) defined the chemical bond as follows: "The physical nature of binding forces acting in all states of aggregation of atoms or ions consists in the overcoming of the electrical repulsion between the atomic nuclei almost exclusively by the electrical attraction exerted on them by the electrons." This definition applies equally well to systems which conventionally are described as having ionic, covalent, and metallic bonds. The response of a macroscopic crystal to the change of binding forces and internuclear distance induced by its surface depends upon its ductility. The structural difference can be described as a state of tension parallel to the surface of the crystal which brings the bulk of the crystal into a state of compression. A ductile crystal of a metal can relieve some of these stresses by gliding and formation of dislocations. The types of dislocations, their motion in the lattice, and their importance for crystal growth and the mechanical properties of solids are fairly well understood and much research is being carried out in these directions. The origin of dislocations is not so well understood and they are usually attributed to impurities and thermal stresses. Impurities can become centers of an asymmetry in a lattice and affect the distribution of binding forces. Weyl and Marboe (41) postulated that even under ideal conditions—i.e., in the absence of detrimental temperature gradients—a crystal or glass formed from the melt at high temperature develops stresses because of the change of the binding forces within the surface film and by the greater anharmonicity of thermal vibrations in this film.

The volume of most solids increases with increasing temperature because the oscillations of the atoms around their equilibrium positions are anharmonic. The

degree of anharmonicity increases with increasing amplitude and depends upon the symmetry of the lattice.

Alkali halides which contain ions whose sizes are not too different, can form solid solutions. McKinstry (26) prepared some of these solid solutions in the systems KBr-KCl, KBr-RbBr, RbBr-RbCl, and RbCl-KCl and derived the lattice parameters as functions of the temperature from their x-ray diffraction patterns. In all cases where he found substantial deviations from additivity the solid solutions had the higher expansivities.

I attribute this deviation from additivity to the greater anharmonicity of the thermal vibrations resulting from the lower symmetry of solid solutions as compared with the end members. This phenomenon can be described by saying that in a solid solution the average bond strength has disproportionated into weaker and stronger bonds. The latter description is strongly supported by measurements of the thermal conductivity. Eucken (8) found that the low temperature thermal conductivity of a solid solution of alkali halides is only one tenth of that of the end members. Surface atoms vibrating in a less symmetrical field than corresponding atoms in the interior of a crystal must have a greater anharmonicity in their vibrations than the average atoms. All forms of silica consist of SiO_4 tetrahedra, but their thermal expansions are very different. The thermal expansivity of the anisotropic quartz is more than 20 times that of the isotropic silica glass. Hence, no matter how slowly one cools a crystal or a glass in order to avoid those stresses which result from the temperature gradient, their surface films because of their higher coefficients of expansion will tend to contract more than the bulk in which all thermal vibrations are more harmonic.

Brittle solids—e.g., glasses—cannot lower their stress level by gliding and, consequently, they are likely to develop a crack system in their surfaces which is usually referred to as Griffith's flaws, after Griffith (17) who postulated their existence. These flaws are partly responsible for the drastic difference between the theoretical strength of a brittle solid and its much lower real strength. Some brittle substances can be plastically deformed under conditions which eliminate the formation of Griffith flaws in the surface. The classical experiment which proves that the surface is a seat of inherent weakness is that of Joffe (21). By constantly removing the surface film of a sodium chloride crystal, the crystal could be strengthened to such an extent that it could be plastically deformed by bending it under water. Experiments of the same nature have been performed with other materials and it is generally understood that the surface introduces a weakness.

Phase Transformation. Ever since Mitscherlich's discovery of polymorphism (1822), the reversible change of the red mercuric iodide into its yellow high temperature form, stable above 127°C ., has attracted the attention of physical chemists.

Under the heading "Zur Chemie Fester Körper," Kohlschütter (24) published the extensive work of his father on the polymorphic changes of HgI_2 as affected by the size of the crystals and the ambient atmosphere. The propagation of the transition of the yellow into the red modification of HgI_2 on cooling is time-consuming and was found to follow, as one would expect, some crystallographic directions within the crystal.

This, however, was not true for very thin plates of the yellow HgI_2 and for the surface films of some thicker ones. Kohlschütter observed that in these cases the beginning of the phase transformation at a corner was followed by a radial spreading of the red form which ignored crystallographic directions. Corners, edges, and surfaces are the places where the phase transformation starts and con-

sequently the rate of this process depends strongly upon the environment. The retarding or accelerating effects of gases were also studied by Kohlschütter. Weyl and Enright (40) investigated the influence of adsorbed foreign ions and the nature of the liquid dispersing agents. Embedding the HgI_2 crystals in paraffin, for example, delayed the phase transformation from yellow to red for several days and embedding them in rosin stabilized the high temperature form for years.

The high-low inversion of quartz which takes place at 573°C . can be raised and lowered by introducing foreign atoms into the crystals, as could be demonstrated by Keith and Tuttle (22). The presence of foreign atoms—e.g., Al, Ge, or Li atoms—in quartz introduces local asymmetries and consequently changes the equilibrium temperature between the two modifications. According to Stahl (34), the inversion temperature of small quartz crystals can be changed by adsorbed gases. The equilibrium temperature between the high and the low quartz was found to depend upon both the nature and the quantity of the gas which had been adsorbed at these surfaces.

Forestier and Maurer (15) determined the melting points of metals and salts in different atmospheres. In an atmosphere of helium, for example, the melting point of KNO_3 was 333.8°C . The melting point of KNO_3 in other gases was found to be lower and the degree to which it was lowered increased with the van der Waals forces of the gas. Potassium nitrate melted in hydrogen at 333.5°C ., in argon at 331.8°C ., and in carbon dioxide at 331.0°C .

According to the views of Weyl and Marboe on the kinetics of melting (42), potassium nitrate expands at its melting point because of the formation of ionic clusters separated by the fluctuating fissures. The large internal surface of such a melt, which is responsible for its fluidity, makes it also susceptible to the ambient atmosphere.

Volume Changes of Solids in Different Atmospheres. The fact that small MgO crystals prepared in vacuo and in air have different lattice parameters means that a crystal prepared in vacuo expands when brought into air.

The redistribution of electron densities in surface films can be described as follows: Cations of low polarizabilities will assume positions in which they are screened. The polarizable anions are shifted toward the exterior and all internuclear distances are decreased because of the smaller average coordination number in surface films as compared with the interior. Lowering the coordination leads to a redistribution of the electron density and decreases the internuclear distance from 2.81 Å. in the NaCl crystal to 2.51 Å. in the vapor molecule or from 1.31 Å. in the $(\text{CO}_3)^{-2}$ group to 1.15 Å. in the gaseous CO_2 molecule.

From this description it becomes obvious that a mechanical tension must develop in the surface film, because the atoms will tend to assume a closer packing. Hence any adsorbed molecule or atom which can improve the screening of the solid will decrease their state of tension and cause the surface film to expand and release some of the pressure which it exerted upon the subjacent layers. Adsorption of screeners, even of inert gas atoms such as argon, causes many porous solids to expand.

Volume changes which occur when solids are brought into different environments were studied by Benedicks (1) when he examined the effect of wetting upon the tensile strength of metals. Even the length of a noble metal such as platinum wire depends upon the environment.

Among nonmetallic solids the porous forms of carbon [Haines and McIntosh (18)] and of silica [Yates (44)] have been studied. These solids have surfaces which are rather complex. In contact with air, carbon and silica surfaces contain

O^- and $(O_2)^-$ ions. The quantum state O^{-2} in spite of its octet shell is not stable in the gaseous state. According to Fajans (9), an O^{-2} ion is not stable and will dissociate to form O^- ions.

Yates (44) found that a porous silica glass (Vycor) expands its volume during the adsorption of oxygen, xenon, or argon. If these gases are admitted to the porous silica which has been thoroughly degassed in vacuo, its volume expands in a nearly linear function of the quantity of the adsorbed gas.

For gases which cause a chemical change of the surface of silica—e.g., NH_3 , CO , and SO_2 —the volume expansion was preceded by a contraction. Because of the instability of the O^{-2} ion in surfaces, one finds that the highly degassed surface of SiO_2 contains O^- ions as well as Si^{+2} ions. These quantum states are responsible for some unusual chemical reactions of the fresh surface of silica (38).

Electronic Properties of Solids in Different Environments. When discussing the effect of wetting upon the structures of surface films, the author (39) paid particular attention to the electronic properties of solids, partly because they are directly visible (color, fluorescence), partly because they are easily measured (electrical conductivity) with great accuracy, and partly because they are of considerable technical interest.

The classical observation of Faraday (11) concerning the colors of gold and their reversible changes with changing environment has its modern counterpart in recent studies concerning the colors and conductivities of thin gold films and the effect which the "carrier" has upon these properties. Even if the electronic properties are not of direct interest to chemists, they provide visible and convincing evidence of the profound electronic changes which a carrier can exert upon a catalytically active film.

Barium titanate crystals rank high among those solids on which electronic research has been focused during the last two decades, because this compound and its derivatives belong to a promising group of ferroelectrics. The properties of single crystals of $BaTiO_3$ reveal that the crystals are not uniform; they respond to an electrical field as if they have a skin which covers the bulk of the crystal.

In a recent publication on the performance of single crystals Pulvari (30) wrote: "It is essential, therefore, to distinguish between the skin and bulk properties of a crystal." Thus he explained the discrepancies found by different authors with respect to the lattice parameters for $BaTiO_3$. According to his findings, the lattice parameters change from the skin to the bulk, so that the x-ray diffraction method produces values which are functions of the particle size: The *c*-axis decreases while the *a*-axis increases nearly linearly with crystal thickness. The skin thickness was found to be practically independent of the dimensions of the crystals.

Here we are not interested in the details of his work, which was undertaken for a better understanding and control of the electronic properties of barium titanate single crystals. However, Pulvari was able to control barium titanate with respect to crystal growth and electrical properties by introducing suitable foreign atoms into the lattice. Even for crystals as simple as $NaCl$, a certain concentration of suitable foreign atoms can help toward restoring symmetry in the surface of the forming crystals. Summarizing his experimental work Pulvari wrote: "As a significant result of this work, however, it was found that a small amount of an impurity can cause dramatic changes in skin and bulk properties."

Chemical Reactivity of Solids. The description of the surface film of a solid as containing its ions in a lower than normal coordination and having internuclear distances smaller than those of the bulk of the crystal does not in itself supply the key to a better understanding of surface chemistry. One has to find the relation-

ship between reaction rates and the structure of a surface film under stress.

STATE OF POLARIZATION OF ANIONS AND REACTION RATES. Metallurgists were the first to realize that mechanical stresses can change the chemical property of a homogeneous metal to such an extent that it establishes galvanic potentials in the same fashion as if it were made of two pieces of different metals: stress-corrosion. This phenomenon, however, is not restricted to metals; in a rather general way it modifies the kinetics of solid-state reactions. Changes in density or volume indicate changes in some internuclear distances. Changes in the internuclear distances, in turn, affect the state of polarization of all ions and with it their chemistry.

At ordinary temperature and pressure quartz is the stable modification of silica. Quartz does not noticeably react with water but is readily attacked by HF. A less dense metastable modification of SiO_2 called "silica W" [after Weiss and Weiss (35)] reacts readily with water and forms a yellow silver silicate in contact with an aqueous solution of AgNO_3 . Another newly discovered but dense modification of SiO_2 , called "silica C" [after Coes (6)], which is also metastable under ordinary conditions, is so unreactive that even the smallest crystals are not noticeably attacked by HF. The rates of the reactions of SiO_2 are determined by the polarizability of the O^{-2} ions. The O^{-2} ions are most polarizable in the low density form (silica W) and least polarizable in the high density form (silica C). The reactions of silica with water are initiated by the penetration of protons into the electron clouds of the O^{-2} ions and the rate of proton penetration increases with increasing polarizability of the anions. The phenomena described are strictly rate phenomena, because neither quartz nor the two metastable forms of silica are in equilibrium with HF.

A similar rate phenomenon is used by mineralogists to distinguish calcite from dolomite. The smaller and more polarizing Mg^{+2} ions lower the polarizability of the $(\text{CO}_3)^{-2}$ ions to such an extent that dolomite does not effervesce when brought in contact with dilute HCl. Calcite (CaCO_3) reacts readily with the dilute acid.

The drastic effect of the state of polarization upon the rates of chemical reactions is well known to the analytical chemist. Some metal sulfides—e.g., NiS—cannot be precipitated from an acidified solution but once formed will resist acid attack because the penetration of protons into S^{-2} ions which are polarized by cations such as Ni^{+2} ions is a reaction with a high energy barrier.

The different states of polarization of a film of a given substance deposited upon different carriers cause these films to react very differently. Manganous sulfide, for example, dissolves readily in dilute acetic acid, but, according to Feigl (12), MnS is not soluble when precipitated on HgS. This interaction between the surface film of MnS and the carrier HgS is a mutual one. HgS is readily soluble in alkali sulfides. However, HgS precipitated on MnS loses some of its solubility in alkali sulfides.

We referred to the formation of Griffith flaws or of a crack system in the surface film of a solid which has formed at high temperature because of its paramount importance for the mechanical strength of solids. This phenomenon, however, has some aspects which are of more direct interest to the physical chemist.

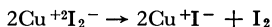
Pryor and Evans (29) found that the apparent solubility of ferric oxide in water depended upon the mass-solvent ratio. Apparently the surface film under tension has a higher solubility than the bulk of the crystal. Only after removal of the more reactive surface film does the solubility become normal—i.e., constant and independent of the mass-solvent ratio. Heating this normal oxide produces again a new dehydrated and stressed surface film which on cooling shows the anomalous high solubility.

Richardson and Waddams (31) found the same behavior for silica. Ground quartz particles agitated with water release some monosilicic acid molecules which form a true solution and, in addition, some very small quartz crystals which form a dispersion in water until a hydrated equilibrium surface is established. Analogous to the ferric oxide, heating the quartz to a temperature above 600° C. regenerates the anomalous solubility behavior.

Oblad, Milliken, and Mills (28) were among the first chemists to be fully aware of the chemical significance of surface stresses in catalysis. They explained the extremely high value for the heat of hydration of a thoroughly degassed alumina-silica catalyst on the basis of stresses. The author prefers to describe a system under tensile stress as acidic because of the incompletely screened cations. Using internuclear distances and the screening demands of cations to describe the difference in surface films carries the macroscopic description of a solid under tension into the atomic dimensions (36).

It is this unpredictable and puzzling chemical reactivity which makes freshly formed silica dust a chemical poison that causes silicosis when it is inhaled. In many processes which deal with mineral products—e.g., the setting of cements, the milling of enamels and of pigments, the slaking of lime, etc.—solids with freshly formed surfaces are brought into contact with water. For understanding these phenomena the kinetics of hydration of incompletely screened surfaces has to be considered.

STATE OF POLARIZATION OF ANIONS AND EQUILIBRIA. The mutual electronic interaction in the cupric halides increases from the fluoride (white) to the chloride (yellow) and reaches a maximum for the bromide (deep red). The nonexistence of the cupric iodide has been explained by Fajans (10) as the result of the change of the continuous polarization into a discontinuous quantum change of the electrons:



Requantization processes of this type are characteristic of compounds which contain both highly polarizable and thermodynamically stable complex anions and highly polarizing cations. The detonation of AgN_3 , $\text{Pb}(\text{N}_3)_2$, $\text{Hg}(\text{N}_3)_2$, etc., as compared with the smooth decomposition of NaN_3 or $\text{Ba}(\text{N}_3)_2$ has been explained by the author (37) on this basis. Thermodynamically there is little difference between $\text{Hg}^{+2}(\text{N}_3)_2^-$ and $\text{Ba}^{+2}(\text{N}_3)_2^-$ because the energy of the two compounds is vested in the labile electronic structure of the $(\text{N}_3)^-$ ions as compared with that of the N_2 molecule. This presents an interesting problem. If the state of mutual polarization is greater in a surface film than in the more symmetrical bulk of the crystal, one could think of a hypothetical solid which would exist if the crystal would not have an asymmetrical surface film. $\text{Cu}^{+2}\text{Br}_2^-$ is stable as a solid, but among the asymmetrical vapor molecules an equilibrium is established among CuBr_2 , CuBr , and Br_2 .

Crystals of mercuric azide can be obtained from an aqueous solution and remain metastable as long as their surfaces are screened by the water. Breaking such a crystal, however, produces an unscreened and less symmetrical surface film in which the mutual polarization is increased to such an extent that the crystal detonates.

Cupric acetylide detonates on heating. However, if the symmetry of its surface film is increased by a partial oxidation of CuC_2 into CuO , the compound decomposes on heating without detonation (23).

Solids are also known which are stable in an ordinary atmosphere only be-

cause their surface films have structures which are sufficiently different from the metastable interior to be in equilibrium with the ambient gas. The first recorded observations go back to Faraday, but many chemists must have noticed that many salts can be obtained from aqueous solutions in a state of hydration which is not in equilibrium with the normal atmosphere. These crystals do not effloresce unless their surfaces are mechanically disturbed—e.g., scratched. Many high hydrates of sulfates, carbonates, and phosphates are metastable in a normal atmosphere at ordinary temperature because these systems can increase their entropies by forming mobile particles. These hydrates can cleave off some of their screening H_2O molecules and change into lower hydrates. Their surface films, however, are in a state of lower symmetry and incomplete coordination which demands more screeners than the interior and, consequently, the surface will not release the screening H_2O molecules.

These examples show that the inherent difference which exists between the structure of the perfect crystal and that of its surface film is of chemical significance. A surface can trigger decompositions—e.g., in some azides—as well as stabilize solids—e.g., the decahydrate of sodium carbonate—which are not in equilibrium with the atmosphere.

The effect which a surface or an interface has upon the stability of solids is of considerable practical significance. The change of one modification of a substance into another one which has a different density can lead to the destruction of solids. The development of ceramic materials with improved electrical properties led to the group of steatite bodies. The calcination of talc and steatite produces a metastable phase called protoenstatite by Buessem, Schusterius, and Stuckardt (4). The change of this modification into the stable one, clinoenstatite, weakens the ceramic body and in extreme cases leads to “dusting,” a process in which the solid completely disintegrates into fine powder which consists of small crystals of the stable modification. Any such change starts at the surface. Hence by choosing firing conditions which coat the individual crystals of the metastable form of magnesium silicate with a glassy phase, the symmetry of its surface is increased, the stress between surface and bulk is decreased, and the transformation into the stable phase is suppressed. It was difficult to discover the presence of protoenstatite in steatite bodies because the normal methods of identifying crystal structures involve powdering the solid or grinding it into thin sections. During these processes the metastable protoenstatite is converted into clinoenstatite.

A very similar reaction was found to occur in certain portland cement clinkers which contain a high concentration of lime and in refractories which are based on calcined lime and dolomite. Here the unstable β -calcium orthosilicate undergoes a phase transformation into the α -form which is stable below 675°C . The volume increase of 10% during this phase change causes dusting. Le Chatelier about 1890 diagnosed the dusting of portland cement clinker as a phase transformation. Ever since that time the phenomenon has been studied and methods were developed for preventing it.

One of the more recent studies by Zerfoss and Davis (46) reveals that the β -orthosilicate of calcium can be stabilized by some foreign atoms which form defective solid solutions and by others which physically protect the crystal boundary from initiating the reaction.

EFFECT OF INERT GASES UPON THE REACTIVITY OF SOLIDS. Many examples of instability of a solid as the result of the asymmetry of its surface—e.g., the detonation of the metastable nitrogen iodide upon removal of its screening film of H_2O and NH_3 in vacuo—can be described in the conventional way by referring to the

breakage of bonds. The screening concept, however, is not limited to chemical forces in the conventional sense.

The high electron density which forms the double bond between two carbon cores in ethylene is a good screener. The screening of cations of the transition elements by the electron density of olefins is analogous to their screening by polarizable anions and leads to those complexes which according to Douglas and Bailar (7) were discovered before the advent of Werner's theory and about which they write: ". . . but the problem of explaining how they are formed and why they are stable is still perplexing."

Argon is a better screener than helium because it has more electrons. It has been pointed out previously that the melting temperature and the phase transitions of solids can be changed by molecules which are screeners and which cannot possibly form chemical bonds except by extending van der Waals forces. This poses the problem of whether even chemically inert gases can affect the reactivity of solids.

Hedvall was probably the first chemist to call attention to the effect of the ambient atmosphere upon chemical reactivity. Hedvall and Runehagen (19) pretreated the different forms of silica with different gases and measured their reaction rates with CaO. Treatment of the silica with SO₃ decreased its reactivity but pretreatment with O₂ increased the reactivities of vitreous silica at 900° C. by 20% and of quartz by 37%.

Using the boiling points as a measure of the van der Waals forces which characterize inert molecules—e.g., N₂, Ar, etc.—Forestier (14) was able to correlate the rates of some solid state reactions with the van der Waals forces of the ambient atmosphere. He postulated that reactions such as the formation of the spinel MgFe₂O₄ from the oxides MgO and Fe₂O₃ would not take place at a measurable rate at a given temperature if the reactants were placed in a perfect vacuum. The greater the van der Waals forces of the physically adsorbed molecules, the more will the surface film resemble the ideal crystal and the greater will be the chemical reactivity of the solid. In strongly asymmetrical surface structures, the binding forces not only may be stronger than in the interior but certain species of ions may not even appear unscreened in a surface. It is very unlikely, for example, that the Si⁺⁴ core can participate in the extreme outer surface of silica.

Effect of Environment on Formation of Solids

Monoatomic gases and those gases which like CH₄ can be treated as spherical particles crystallize as the result of van der Waals forces. Because of their short-range action, the lattice energies and the surface energies of these solids can be calculated for the hexagonal and for the cubic close-packed structures. The lattice energies are nearly the same but the cubic structures have a lower surface energy. For macroscopic crystals the contribution of the surface energy to the free energy is negligible, but this is not the case for nuclei. Hence, all these gases form cubic structures at low temperature.

This influence of the structure of a surface must be felt particularly when a solid crystallizes from a solution. Indeed, the experience of chemists over the centuries may be summarized by the motto of the ancient philosophers, "Natura facit non saltus," meaning that nature does not like abrupt changes. As Zerkow (45) pointed out, if one wants to grow a large perfect crystal from an aqueous solution, one has to select a substance which reveals its affinity for water not only

by its high solubility but also by its ability to take H_2O molecules from the solution into its lattice. One of the alums or cupric sulfate should be used for experiments on crystal growth rather than sodium chloride. There seems to be no abrupt transition between a crystal of $\text{K}_2\text{SO}_4 \cdot \text{Al}_2(\text{SO}_4)_3 \cdot 24 \text{H}_2\text{O}$ and its saturated solution. Lowering the temperature of the system or withdrawing H_2O molecules by evaporation gradually increases the size of the alum crystal. The symmetry of the surface film of this solid must be very much the same as that of a similar layer in the interior.

The crystallization of NaCl from its aqueous solution proceeds very differently. The crystal does not include any H_2O molecules when formed from a saturated solution at ordinary temperature. The absence of cushioning particles makes the transition from saturated solution to crystal surface one of those abrupt changes which nature dislikes. Anhydrous crystals such as NaCl or K_2CrO_4 are not good seeds and even their freshly formed surfaces may remain in contact with a super-saturated solution for measurable times without growing. Crystallization of these substances is not a smooth process; the growth of these crystals is pulsating (5). Layers about 20,000 atoms thick are deposited as a unit from a supersaturated solution at one given moment and the solution becomes saturated. The new surface, however, must have a structure which is sufficiently different from that of the crystal to permit the solution to become supersaturated again. Now the same cycle repeats itself. Experiments of this type are important for two reasons for the understanding of the surface structure of solids. First, a relationship exists between the similarity of a crystal and its ability to act as a seed for a substance to be precipitated from a supersaturated solution. The more the two substances resemble one another, the greater is the efficiency of one acting as a seed for the other. Secondly, these experiments can be carried out so as to eliminate those impurities which only too often are blamed for obscuring surface phenomena which are not understood. There is considerable information accumulated in the literature on crystal growth, so that only two special cases are discussed here.

Nucleation Catalysts. The surface structure of a barium sulfate crystal is very different from that of its aqueous solution. Hence a considerable supersaturation is required for precipitating BaSO_4 from an aqueous solution. If a polarizable cation of a size and charge similar to the Ba^{+2} ion—i.e., the Pb^{+2} ion—is used as a “cushion,” it is possible to make the structural gap from solid to liquid less abrupt and, thus, to precipitate BaSO_4 from solutions which are less supersaturated. PbSO_4 is more soluble in water than BaSO_4 . Nevertheless, a suspension of BaSO_4 in an aqueous solution of $\text{Pb}(\text{ClO}_4)_2$ will exchange its surface cations for Pb^{+2} ions. This process lowers the free energy of the system by decreasing the interfacial energy or by making the gap between solid and liquid less abrupt. Feigl (13) took advantage of this phenomenon for making the tests for Ba^{+2} ion ten times more sensitive. The Pb^{+2} ions because of their $18 + 2$ shell exert a cushioning effect upon the surface and act as nucleation catalysts.

The screening demand of the cations changes the cube face of crystals having NaCl structure from a checkerboard pattern of a positive and negative force field into one which contains predominantly the anions. This structural change represents a barrier which prevents the crystal from growing smoothly and which permits an NaCl solution in contact with an NaCl crystal to develop a finite degree of supersaturation. With increasing degree of supersaturation the probability of new nuclei forming increases very rapidly. Hence, it is practically impossible to grow a single crystal of NaCl from an aqueous solution to a large size without the formation of numerous new crystals.

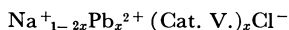
As a rule, increasing the temperature of the system improves the conditions of crystal growth, because at higher temperatures the surface approaches that of the ideal crystal structure. This effect is well known to mineralogists, who found that many crystals which at low temperatures are not suitable for oriented overgrowth (epitaxy) will become suitable hosts when the temperature is raised. At higher temperatures the thermal energy which is available is sufficient to unscreen surface cations and to decrease the constraint in the surface film, so that the difference between bulk and surface structure decreases.

The degree to which a solution can be supersaturated is inversely proportional to the polarizability of its ions. Substances such as CaF_2 require a high degree of supersaturation before nucleation starts, whereas the halides of mercury and lead cannot be kept in a supersaturated solution for any length of time. This difference may be attributed to the closer similarity of a PbBr_2 surface to a checkerboard positive and negative force field than that of a CaF_2 surface. The presence of Pb^{+2} ions in the solution of NaCl has an effect upon the growth of an NaCl crystal similar to that produced by the participation of H_2O molecules in the lattice. From a consideration of polarizability alone the nucleation of calcium sulfate from solution would be expected to be much more difficult than that of the sulfate of the more polarizable barium. The opposite behavior has been found; the reason for this departure is no doubt the fact that calcium sulfate crystallizes as $\text{CaSO}_4 \cdot 2 \text{H}_2\text{O}$, forming surfaces which resemble the solution more than those of the anhydrous BaSO_4 .

The work of Yamamoto (43) with growth-active impurities such as Pb^{+2} , Sn^{+2} , and Mn^{+2} ions reveals that their presence in very small quantities decreases the probability of nucleation, thus extending the metastable region of aqueous solutions of the alkali halides. These ions of the transition elements because of their screening demands withdraw Cl^- ions from solution and form complexes such as $(\text{PbCl}_6)^{-4}$ and $(\text{MnCl}_6)^{-4}$. Without changing the over-all composition of the solution, these ions lower the effective concentration of the Cl^- ions and thus decrease the nucleation rate of NaCl .

According to Yamamoto (43) the addition of Pb^{+2} ions in a concentration which has the most beneficial effect upon growth (1 PbCl_2 : 5400 KCl) increases the supersolubility by 50%.

Perfection of Crystals Grown from Aqueous Solution. Yamamoto (43) discovered that in the presence of non-noble gas-type ions such as Mn^{+2} or Pb^{+2} ions, optically clear crystals are formed from aqueous solutions. These crystals are optically perfect but chemically impure and defective. The formula for NaCl , for example,



indicates that a small concentration of Pb^{+2} ions are included in the structure of the NaCl , which in turn develops a corresponding small concentration of cation vacancies (Cat. V.) in order to balance the higher excess charge of the Pb^{+2} ion. This gives the crystal the flexibility which is necessary in order to form an equilibrium surface that resembles the interior more closely than that of a pure NaCl crystal. The pulsating growth now changes into a smooth growth and the crystal becomes a good seed, so that fewer nuclei form during its growth, because the solution cannot develop the degree of supersaturation in the presence of the crystal which contains Pb^{+2} ions and vacant lattice sites.

When a chemist wants some very pure carbon he might think of using diamonds of gem stone quality. This, however, would be a mistake. The "per-

fect crystals" which nature has produced, whether a diamond or one of the large beautiful quartz crystals from Minas Geraes, Brazil, owe their perfection to "growth-active" impurities.

Summary

The surface of a solid is the seat of an asymmetry which causes a change in the binding forces which affects the solid to a considerable depth. The difference in the electron density distribution brings the interior of the crystal into a state of compression and the surface film into a state of tension. The degree of the disturbance of the solid depends upon the asymmetry which the surface introduces into the system. The latter in turn depends upon the environment of the solid and even physical adsorption of inert gases can influence equilibrium properties of small crystals and their films, such as volume, melting point, phase transformation, color, fluorescence, and electronic conductivities.

As far as macroscopic crystals are concerned, the equilibrium properties will not be noticeably affected by a change in the environment, but the interaction of adsorbed molecules with the surface may trigger a phase change which is initiated in the surface. Hence, even for macroscopic crystals, the environment may influence rate phenomena such as solid-state reactions.

In addition to this disturbance which a surface introduces through a change in the distribution of binding forces as a result of asymmetrical polarization, solids which have formed at high temperature may develop tensions in their surface films because the latter would have a greater thermal expansion than the bulk. The oscillations of all atoms in asymmetrical surface films must be less harmonic than those in the interior and it is the anharmonicity of the thermal vibrations which causes the volume to change on heating and cooling. Hence, we would expect the surface film to have a higher coefficient of expansion than that which is characteristic for the bulk of the crystal. On cooling, the resulting stress leads to dislocations in metals. In brittle glasses, the resulting stress leads to those surface cracks which are generally referred to as Griffith flaws.

From a chemical viewpoint, the interior of a crystal and its surface can be looked upon as if they were different individuals, comparable to two modifications of a substance or to a metal which is under mechanical stresses. The phenomenon of stress corrosion reveals that the part under tension differs in its chemical reactivity from the part under compression. Different modifications of silica can have very different reactivities. Therefore, it must be expected that the surface film can affect the apparent stability of a solid. Indeed, the surface structures of some hydrated salts are in equilibrium with the ambient atmosphere and prevent these crystals from losing water (efflorescing), even if the bulk of the crystal has a higher water vapor pressure than the atmosphere. The formation of a fresh highly asymmetrical surface may also cause substances to detonate.

In these cases we expect that a change of the environment will influence the chemistry of the solid. The isothermal formation of an equilibrium surface—i.e., nucleation and crystal growth—is a process which is strongly affected by the environment—e.g., the nature of the solvent. Good crystals can be grown from aqueous solutions only when the asymmetry, solid-liquid, is a minimum, as is true for those crystals which have a high solubility and whose structures contain water of crystallization (alums but not the alkali halides). Substances such as NaCl can be induced to form better crystals from an aqueous solution by adding growth-active catalysts which temporarily decrease the asymmetry of the crystal-solution

interface. The effects of these impurities upon the structure of the surface of an NaCl crystal are probably responsible for the threefold increase of the tensile strength, as was found by A. Smekal and his school.

Literature Cited

- (1) Benedicks, C., Pittsburgh International Conference on Surface Reactions, 1948.
- (2) Boswell, F. W. C., *Proc. Phys. Soc.* **A64**, 465 (1951).
- (3) Brunauer, S., "Structures and Properties of Solid Surfaces," R. Gomer, C. S. Smith, eds., p. 395, University of Chicago Press, 1952.
- (4) Buessem, W., Schusterius, C., Stuckardt, K., *Wiss. Veröffentl. Siemens Werke* **17**, 1 (1937).
- (5) Bunn, C. W., Emmett, H., *Discussions Faraday Soc.* **5**, 119 (1949).
- (6) Coes, L., *Science* **118**, 131 (1953).
- (7) Douglas, B. E., Bailar, J. C., Jr., "Chemistry of the Coordination Compounds," p. 487, Reinhold, New York, 1956.
- (8) Eucken, A., "Lehrbuch der Chemischen Physik," 3rd ed., Vol. II, p. 754, Akademische Verlagsgesellschaft, Leipzig, 1949.
- (9) Fajans, K., *Chimia* **13**, 349 (1959); *Chem. Eng. News* **27**, 901 (1949); *Ceramic Age* **54**, 288 (1949); *Angew. Chem.* **66**, 608 (1954).
- (10) Fajans, K., *Z. Krist.* **66**, 321 (1928).
- (11) Faraday, M., *Phil. Mag.* **14**, 401, 512 (1857).
- (12) Feigl, F., "Chemistry of Specific, Selective and Sensitive Reactions," pp. 151-2, Academic Press, New York, 1949.
- (13) *Ibid.*, p. 162.
- (14) Forestier, H., "Quelques Problèmes de Chimie Minérale," 10th Conseil de Chimie, p. 505, Institut International de Chimie Solvay, Bruxelles, 1956.
- (15) Forestier, H., Maurer, J., *Compt. rend.* **232**, 1664 (1951).
- (16) Frenkel, J., "Kinetic Theory of Liquids," Clarendon Press, Oxford, 1946.
- (17) Griffith, A. A., *Trans. Roy. Soc. London* **A221**, 162 (1920).
- (18) Haines, R. S., McIntosh, R., *J. Chem. Phys.* **15**, 28 (1947).
- (19) Hedvall, J. A., Runehagen, O., *Naturwissenschaften* **28**, 429 (1940).
- (20) Hofmann, U., Wilm, D., *Z. Elektrochem.* **42**, 504 (1936).
- (21) Joffe, A. F., "The Physics of Crystals," McGraw-Hill, New York, 1928.
- (22) Keith, M. L., Tuttle, O. F., *Am. J. Science*, Bowen Vol. 203 (1952).
- (23) Klement, R., Köddermann, E., *Z. anorg. allgem. Chem.* **254**, 201 (1947).
- (24) Kohlschütter, H. W., *Kolloidchem. Beih.* **24**, 319 (1927).
- (25) Lennard-Jones, J. E., Dent, B. M., *Proc. Roy. Soc. (London)* **A121**, 247 (1928).
- (26) McKinstry, H. A., "Thermal Expansion of Certain Alkali Halides and Their Solid Solutions," Ph.D. thesis, Dept. of Physics, Pennsylvania State University, University Park, August 1960.
- (27) Nicolson, M. M., *Proc. Roy. Soc. (London)* **A228**, 490 (1955).
- (28) Oblad, A. G., Milliken, T. H., Jr., Mills, G. A., *Advances in Catalysis* **3**, 199 (1951).
- (29) Pryor, M. J., Evans, U. R., *J. Chem. Soc.* **1949**, 3330.
- (30) Pulvari, C. F., *J. Am. Ceram. Soc.* **42**, 355 (1959).
- (31) Richardson, E., Waddams, J. A., *Research* **8**, 21 (1955) (correspondence).
- (32) Rymer, T. B., Butler, C. C., *Proc. Phys. Soc.* **59**, 541 (1947).
- (33) Schairer, J. F., "Phase Transformations in Solids," p. 257, Wiley, New York, 1951.
- (34) Stahl, P., *Compt. rend.* **232**, 1669 (1951).
- (35) Weiss, Al., Weiss, Ar., *Z. anorg. allgem. Chem.* **276**, 95 (1954).
- (36) Weyl, W. A., *Glass Ind.* **37**, (5), 264; **37** (6), 325 (1956).
- (37) Weyl, W. A., "New Approach to Surface Chemistry and to Heterogeneous Catalysis," Mineral Industries Experiment Station, Pennsylvania State University, Bull. **57** (1951).
- (38) Weyl, W. A., *Research* **3**, 230 (1950).
- (39) Weyl, W. A., "Structure and Properties of Solid Surfaces," R. Gomer, C. S. Smith, eds., p. 147, University of Chicago Press, 1952.
- (40) Weyl, W. A., Enright, D. P., ONR Tech. Rept. **3** (1949). Contract N6 onr 269, Task Order 8, NR 032-264, 5, College of Mineral Industries, Pennsylvania State University.
- (41) Weyl, W. A., Marboe, E. C., *Glass Ind.* **42** (4), 194 (April 1961).
- (42) Weyl, W. A., Marboe, E. C., *J. Soc. Glass Technol.* **43**, 417 (1959).
- (43) Yamamoto, T., *Sci. Papers Inst. Phys. Chem. Research (Tokyo)* **35**, 228 (1939).
- (44) Yates, D. J. C., *Advances in Catalysis* **9**, 481 (1957).
- (45) Zerfoss, S., *Ceram. Age* **54**, 293 (1949).
- (46) Zerfoss, S., Davis, H. M., *J. Am. Ceram. Soc.* **26**, 302 (1943).

RECEIVED May 9, 1961.

Effect of Hydrogen Adsorption on the Magnetic Susceptibility of Palladium Dispersed on Silica Gel

LLOYD H. REYERSON and AAGE SOLBAKKEN¹

School of Chemistry, University of Minnesota, Minneapolis 14, Minn.

Magnetic susceptibility studies of silica gel-supported palladium indicate that the electronic properties of palladium are strongly dependent on the ratio of surface to bulk. Hydrogen and nitric oxide adsorption indicates surface states different from the bulk state, depending on the same ratio. A nearly monolayer of hydrogen is necessary prior to adsorption by palladium. The increase in lattice parameter during this absorption is believed to be caused by the decrease in the exchange energy between palladium atoms. The results point to the importance of the change in electronic properties of catalyst surfaces as the specific surface area varies.

While studying the sorption of nitric oxide, NO, by finely divided palladium it was found that the magnetic susceptibility of the small palladium crystals, having an average crystallite size of 134 Å and a surface area of 32.7 sq. meters per gram, was more than twice that of the bulk metal (26). The susceptibility diminished as more and more NO was adsorbed. This suggested that the odd electron of NO was pairing with electrons in the palladium. These results raised questions which might be answered, at least in part, by studying the adsorption of hydrogen by silica gel carrying various amounts of palladium dispersed in its pore structure. At each equilibrium point on the isotherm the magnetic susceptibility of the Pd-H sample would be determined.

The ability of palladium to adsorb or absorb large amounts of hydrogen was known before the end of the last century. Much more precise work has been reported in recent years (1, 2, 3, 18). Such studies accurately showed the dependence of the sorption process on pressure and temperature. The isotherms generally indicated a sudden increase in the sorption of hydrogen at a certain pressure, which was very temperature-dependent. This sudden rise in the amounts sorbed at definite pressures suggested a phase shift in the crystalline structure of the palladium from a hydrogen-poor α -phase to a hydrogen-rich β -phase. Such

¹ Present address, Norway University of Technology, Trondheim, Norway.

was found to be the case when x-ray spectra were obtained. Experiments found a change in the lattice parameter of the face-centered cubic palladium crystals from 3.886 Å. for the α -phase to 4.020 Å. in the hydrogen-rich β -phase (7, 8, 9, 13, 14).

The sorption data showed that the change proceeded in an isobaric manner which was strongly temperature-dependent, varying from 4 to 5 mm. at 0° C. to 4000 mm. at 200° C. Sievertz and Brünig (18) constructed a critical zone, similar to those found in gas condensations, under which the amount adsorbed was small and above which the pressure increased sharply. Gillespie and Galstaun (1) found the critical point to be 295.3° C. at 19.87-atm. pressure. Here the H/Pd ratio equalled 0.270. Above this temperature the isotherms showed almost normal character. Sievertz and Brünig (18) found that the $\log P$ at which the transformation took place varied inversely as the absolute temperature.

A number of magnetic studies of the hydrogen-palladium system have been reported. Among the more recent are those of Swensson (23) and Sievertz and Dary (19). These studies showed that the paramagnetic gram susceptibility decreased linearly as hydrogen was sorbed until it reached a zero value at a ratio of about 0.6 H/Pd. Only small amounts of hydrogen were sorbed beyond this value. In fact, Samson and Himmelsturm (15) found that, when the pressure of hydrogen was increased from 1 to 968 atm., the hydrogen-palladium ratio increased only 1%. Such behavior, no doubt, depends upon the extent of the surface of the sample.

The nature of the sorbed hydrogen has led to much speculation and several theories have been advanced in explanation of the observed results. Gillespie and coworkers (1, 2, 3) assumed that metal hydrides formed, while Owens and St. Williams (14) found no evidence for such formation and merely assumed that hydrogen formed a solid solution in the palladium. Smith (20) criticized this point of view and submitted evidence for a single phase boundary which migrated through the bulk palladium. Somewhat earlier Mitchell, Berard, and Chandron (10) believed they had evidence for the formation of a superficial layer of the β -phase on the surface and that the hydrogen diffused through this into the α -phase, saturating it so that it transformed into the β form. NMR measurements by Norberg (12) suggested to him that part of the hydrogen dissociated into protons and electrons. Heat capacity studies by Nace and Aston (11) on this H₂-Pd system led them to conclude that at temperatures below 160° K, the hydride of the form PdH₄-7Pd (4H atoms attached to the corner of the face centered cubic crystal) existed. At higher temperatures they suggested a looser formation with possible dissociation.

In all of this work there was little suggestion that the surface states of the palladium might behave differently from bulk states. Selwood (17) indicated that, from some sorption-magnetic susceptibility data for hydrogen sorbed on palladium which was finely dispersed on alumina gel, the ultimate sorption capacity was approximately at the ratio 2H/Pd. Trzebiatowsky and coworkers (25) deposited palladium on alumina gel in amounts ranging from 0.46 to 9.1% of gel weight. They found the palladium to be present in a normal crystal lattice structure, but its susceptibility was less than for the bulk metal. This suggested to the present authors that the first layer of palladium atoms laid down on the alumina gel underwent an interaction with the alumina, which has some of the properties of a semiconductor. Such behavior was definitely shown in this laboratory (22) in the studies on the sorption of NO by alumina gel. Much of this

recent work strongly suggests that the electronic states of surface atoms of such a metal as palladium differ definitely from bulk states (26).

The investigation here reported was carried out in an attempt to show that such surface states did exist and that sorption and magnetic susceptibility studies of hydrogen-palladium systems might answer some of the questions raised by previous investigators.

Experimental Procedure

The silica gel, used as the support material, was taken from the sample that provided the material for the previous adsorption measurements of NO on the gel (21). The gel had a diamagnetic susceptibility of 0.685×10^{-6} . After the sample had been thoroughly dried, it was dropped into a standard solution containing $\text{Pd}(\text{NH}_3)_4^{+2}$ and let stand for 24 hours with occasional stirring. After filtering and brief washing with deionized water, the sample was dried and then reduced in an atmosphere of hydrogen at 200°C . for 1 hour. Nitrogen then displaced the hydrogen and the sample was cooled in this atmosphere prior to weighing in the spherical borosilicate glass bucket used in the sorption apparatus (21). Once in the system, the sample was desorbed while being heated by infrared lamps. It was again reduced *in situ* by hydrogen and desorbed to a constant pressure of 10^{-6} mm. One such reduction turned out to be sufficient to complete the process and remove any residual oxygen and other impurities. Several such treatments were carried out, however, to provide the constancy of weight and susceptibility.

Upon reaching constant weight, the sample and system were thermostated to the desired temperature and the magnetic susceptibility of the palladized gel was determined. A complete isotherm for the sorption of hydrogen by this gel was then obtained, with magnetic measurements being made on the sample at each sorption point. Upon completion of the measurements on the gel having a minimum amount of palladium on the surface, the sample was taken from the sorption system and once again placed in a solution standardized as to $\text{Pd}(\text{NH}_3)_4^{+2}$. This process was repeated after each isotherm, so that two series of palladized silica gels were prepared and studied.

Series I gels carried palladium on the gel surface varying from 0.43 to 16% of the original weight. Hydrogen isotherms, as well as magnetic measurements, were obtained for each of these samples. Series II gels were prepared to confirm the unusual magnetic values found for Series I as well as to obtain the maximum amounts of hydrogen adsorbed at 0° and 30-mm. pressure, at which point the isotherms had flattened out in the case of the Series I gels. The palladium content of Series II gels varied from 0.78 to 10.86%. Following sorption of hydrogen and the related magnetic measurements on the Series I gel having 16% Pd as well as Series II gel containing 10.86%, complete NO sorptions and magnetic measurements were obtained on these two samples. Standard analytical methods were used to obtain the palladium content of the various treated gels, and these results checked well with the loss of palladium from the solutions following the adsorptions of the complex ion.

The sensitivity of the system permitted the determination of the magnetic values to an accuracy of better than 1%. The amounts of hydrogen absorbed were probably accurate to about 10% on the gels carrying the least palladium and probably better than 1% for the gels carrying the most metal.

Results and Discussion

Magnetic Susceptibility of Palladium Dispersed on Silica Gel. Figure 1 shows the susceptibility values obtained as increasing amounts of palladium were deposited on the gel surface. As ordinates the values of the relative susceptibility, χ_s/χ_o , are plotted against amounts of palladium on the gel. χ_s is the measured susceptibility while χ_o is that of the bulk metal as given in the literature (4, 5).

The two samples show remarkable similarity. The small differences are probably due to slight changes in the handling of the two samples. Silica gel II was more thoroughly dried, before being placed in the solution containing $\text{Pd}(\text{NH}_3)_4^{+2}$, and this shows up in its greater adsorption of this complex ion from the solution than was the case for silica gel I. The gels containing the least palladium had susceptibilities about four times that of the bulk metal. As the amount of palladium increased, the susceptibility fell to a minimum at a palladium content of about 2 to 3% Pd, rose to a maximum at from 7 to 9% Pd, after which it fell, approaching that of the bulk metal at the highest percentages of palladium dispersed on the gel. Changes in other measurable properties appear to follow this behavior closely.

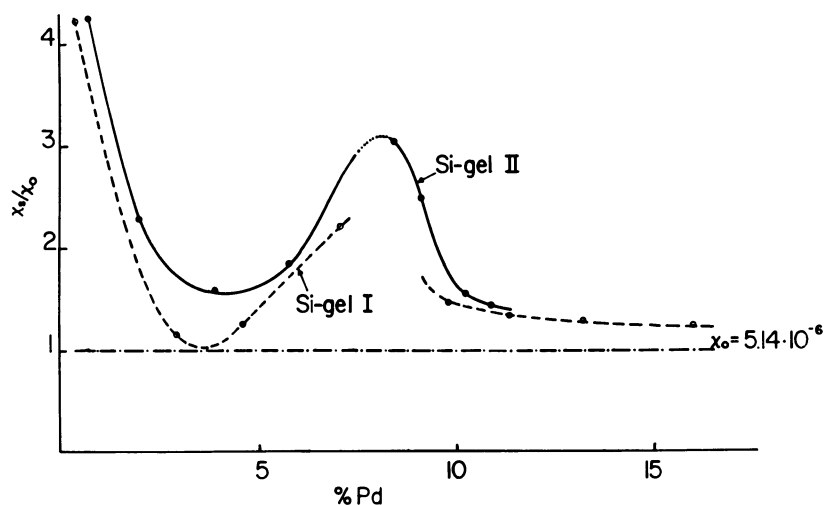


Figure 1. *Relative susceptibility of palladium as function of concentration on two silica gel samples*

These unusual changes in susceptibility, at different degrees of dispersion of the metal on the gel, are at present difficult to explain quantitatively. One may, however, draw some qualitative conclusions from the data. The steep part of the curve at low coverage has a parallel in some work done by Kobozev and co-workers (6), who reported similar increases in the susceptibility of certain salts and metals when dispersed in very small amounts on alumina, silica gel, and charcoal. They also reported exceptionally high susceptibilities in the case of platinum dispersed on charcoal in amounts varying from 0.006 to 0.0001 part per gram. They were unable to explain this "supermagnetic" phenomenon.

As seen from Table I, the adsorptive capacity for hydrogen decreases sharply at the lowest concentrations of palladium. There is reason to believe that a good part of the first palladium atoms reduced on the gel are trapped in narrow cracks and pores. This would largely make them unavailable for hydrogen adsorption, and they will be acted upon by unpredictable and unsymmetric forces, which greatly influence their electronic configuration. In the present work, the measured paramagnetism of $\chi_g = 21$ to 22×10^{-6} indicates that, on the average, there are 2 unpaired electrons in the *d*-band per atom as compared to the accepted value of about 0.6 electron for bulk palladium.

Table I. Data on Two Series of Silica Gels

Sample	% Pd	Dynes/100 Mg. Pd ^a	X_s/X_o ^b	H/Pd ^c	% Para- magnetism ^d Decrease	Ultimate H/Pd ^e	X_s/X_o Calcd. ^f
I ₀	0.43	11.230	4.21	0.420	24.0	1.75	4.20
I ₁	2.80	3.097	1.16	0.580	73.2	0.80	1.43
I ₂	4.55	3.364	1.26	0.717	92.0	0.78	1.38
I ₃	7.08	5.930	2.22	0.722	57.4	1.26	2.62
I ₄	9.80	3.880	1.47	0.751	87.4	0.88	1.62
I ₅	11.36	3.631	1.36	0.795	81.9	0.86	1.57
I ₆	13.20	3.479	1.31	0.691	93.1	0.74	1.30
I ₇	16.00	3.300	1.23	0.663	92.8	0.71	1.23
II ₁	0.78	11.440	4.29	0.280	15.6	1.81	4.42
II ₂	1.97	6.100	2.30	0.581	51.4	1.13	2.26
II ₃	3.54	4.372	1.64	0.737	81.1	0.92	1.72
II ₄	5.98	4.645	1.74	0.673	73.6	0.91	1.69
II ₅	8.44	8.168	3.07	0.722	39.3	1.70	4.03
II ₆	9.10	6.656	2.50	0.711	54.0	1.30	2.74
II ₇	10.16	4.125	1.55	0.708	87.9	0.80	1.43
II ₈	10.86	3.851	1.44	0.693	89.6	0.77	1.36

^a $HdH/ds = 5.18 \times 10^6$.

^b $X_o = 5.14 \times 10^{-6}$.

^c At 30-mm. H₂ pressure.

^d At 30-mm. H₂ pressure.

^e Calculated from remaining paramagnetism.

^f Using ultimate H/Pd in formula for susceptibility.

From the minimum in the susceptibility through the maximum as the amounts of palladium increase, it is clear, from the sorption data, that multilayers of palladium are building up. It is suggested that at least two factors may be involved in the susceptibility changes given in this part of the curves.

1. First-order calculations show that when *s*-bands and *d*-bands in the bulk phase of a metal overlap, the unsymmetric conditions on the surface tend to keep them apart. Such surfaces behave more nearly as single atoms of the metal. Considering the *s*-band, it has been shown by Shockley (16) that the lowest part of this band is the surface "niveau." This so-called Schockley niveau is energetically more stable than the bulk *s*-orbitals, leading to a denser band in the surface than in the bulk state. The opposite effect, the so-called "Tamm state" (24), exists at a somewhat larger distance between the surface atoms. It is believed that the surface part of the *d*-band belongs to the upper part of this state, making the bulk part of the *d*-band more stable with respect to the surface. The net trend of these two states will result in a denser *s*-band in the surface and a poor *d*-band. This leads to higher susceptibility, since the remainder of the electrons, following Hund's rule, tend to occupy different orbitals. As the layers of palladium atoms build up, an increase in the magnetic moment is to be expected up to a certain maximum, where an equilibrium will exist between states. Addition of more palladium will reduce the ratio of surface to bulk atoms, so that properties of the bulk metal will begin to take precedence over those of the surface.

2. The exchange integral, *J*, between two atoms is a function of the distance between the atoms, exhibiting a positive maximum at a definite distance. The stability of a magnetic state is dependent on the sign and magnitude of this exchange integral. In the present study the susceptibility begins to increase before there is sufficient palladium on the gel surface to form a monolayer on the total surface. However, the sorption data strongly suggest that the palladium atoms are building islands or crystallites before reaching complete monolayer coverage. Thicker palladium layers must then exist on the surface, together with single palladium

atoms that may be separated one from the other. Both states will contribute the share of each to the measured susceptibility.

Sorption Data. The sorption data for hydrogen on several palladium gel samples at 0° C. are given in Figure 2. Figure 3 shows the maximum amount of hydrogen adsorbed per palladium atom at 30-mm. pressure of the gas, a pressure at which the isotherms have practically flattened out. The shape of the isotherms in Figure 2 shows that two kinds of sorption exist and that the first is essentially complete before the second begins. At very low pressures the hydrogen is rapidly and strongly sorbed, giving a Langmuir type of isotherm. This sorption is essentially completed by the time the hydrogen pressure reaches 1 mm. No doubt this part of the isotherm represents monolayer adsorption on the available palladium surface. The isotherm remains horizontal for all of the samples until the hydrogen pressure exceeds 2 mm. As can be seen in Figure 2, at a pressure between 2 and 3 mm. the amounts sorbed abruptly increase, reaching a final value at about 30-mm. pressure of hydrogen. The pressure at which the second abrupt increase begins is in excellent agreement with that found by Gillespie and coworkers (1) for bulk palladium at 0° C. Here the rise in the curve was almost vertical, in contrast to the present work where the change is more gradual, indicating that the palladium on the gel consists of small crystallites or less ordered aggregates. The rise in the isotherms is steeper for the samples containing the most palladium, suggesting more nearly bulk state properties in these cases. There is little doubt that the second rise in the isotherms shows the amount of hydrogen that penetrates into the aggregates or crystallites of palladium on the gel surfaces.

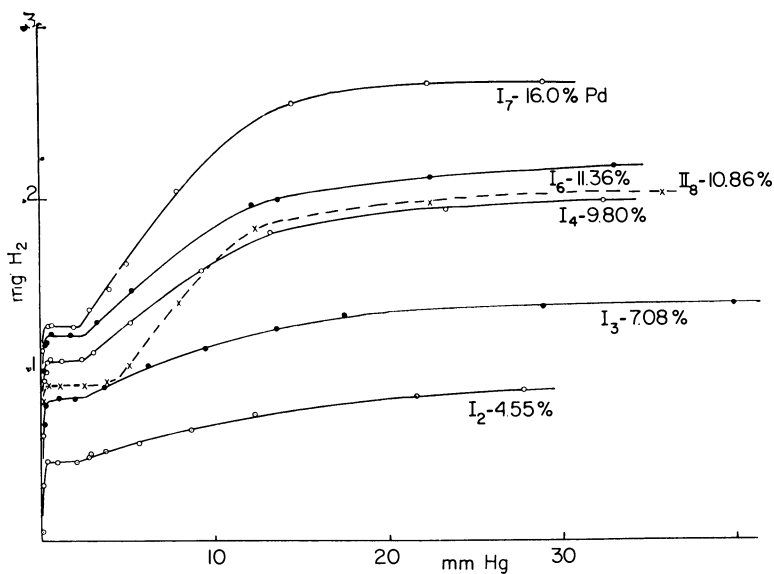


Figure 2. Hydrogen isotherms on dispersed palladium at 0° C.

Except at very low palladium concentrations on the gel surfaces, the amounts of hydrogen sorbed at 30-mm. pressure by the palladium carrying gels appear to be constant at H/Pd ratio of from 0.70 to 0.75. At the low concentrations of palladium on the gel, the nature of the palladium, deposited on the surface or

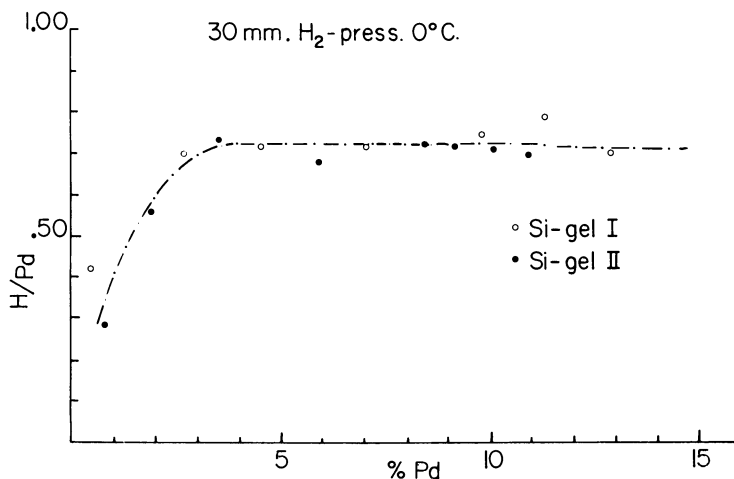


Figure 3. Maximum hydrogen adsorbed at 30-mm. hydrogen pressure as function of palladium concentration on silica gel surface

in the pores and cracks, may limit the sorption of hydrogen. The fairly constant H/Pd ratio at higher palladium concentrations is larger than usually reported for bulk palladium where values of 0.6 to 0.65 are usually reported. Since there is remaining paramagnetism in many of the samples here studied, there must exist a space limit for hydrogen sorption which prevents the H/Pd ratio from exceeding 0.75. What little work was done at 28° C. indicated no sharp upturn in the isotherm at 2- to 3-mm. pressure but a gradual rise followed by a small upturn at 20 to 25 mm. Thus sorptions seem to be temperature dependent, as was earlier found for bulk palladium.

To check surface areas of the palladium, isotherms were measured using NO as the gas. Figure 4 gives the results obtained for two different samples con-

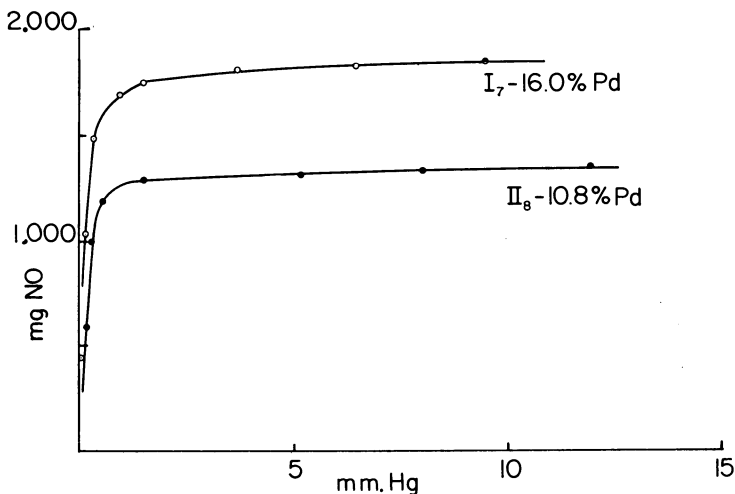


Figure 4. Nitric oxide isotherms on two palladized silica gel samples at 0° C.

taining the largest amounts of palladium on the silica gel. The isotherms are typical Langmuir monolayer adsorptions with no second rise in the curves, showing no penetrations of the metal. Table II gives the amounts of NO adsorbed at the flat part of the isotherms and compares these with the amounts of hydrogen adsorbed on the first horizontal section of the complete hydrogen isotherms. The data clearly show that one NO molecule is equivalent to one hydrogen molecule as far as adsorption on the surface is concerned.

Table II. NO Adsorption on Palladium

<i>Sample</i>	<i>NO/Pd</i>	<i>H₂/Pd (on First Horizontal Section)</i>
I ₇	0.154	0.156
II ₈	0.155	0.152

Effect of Sorbed Hydrogen. To determine the possible effect of sorbed hydrogen on the structure of the palladium aggregates on the silica gel samples, x-ray diffraction patterns were obtained (Figure 5). The upper film strip shows the diffuse band for the pure silica gel, the middle film gives the results for sample II₈ (10.86% Pd on the gel) in a vacuum, and the lower film shows the definite change in the crystal parameter of the same sample under hydrogen pressure. These films establish the crystalline character of the palladium deposited on this gel sample. From these films the lattice parameter of the palladium in a vacuum turns out to be 3.89 ± 0.01 Å., while that of the hydrogen-rich palladium becomes 4.03 ± 0.01 Å. These values are in excellent agreement with those previously reported for the hydrogen-poor α -phase and the hydrogen-rich β -phase of bulk palladium. The evidence presented in the following section indicates that the transformation from the α - to β -phase does not begin until the surface of the palladium is covered by a monolayer of hydrogen.

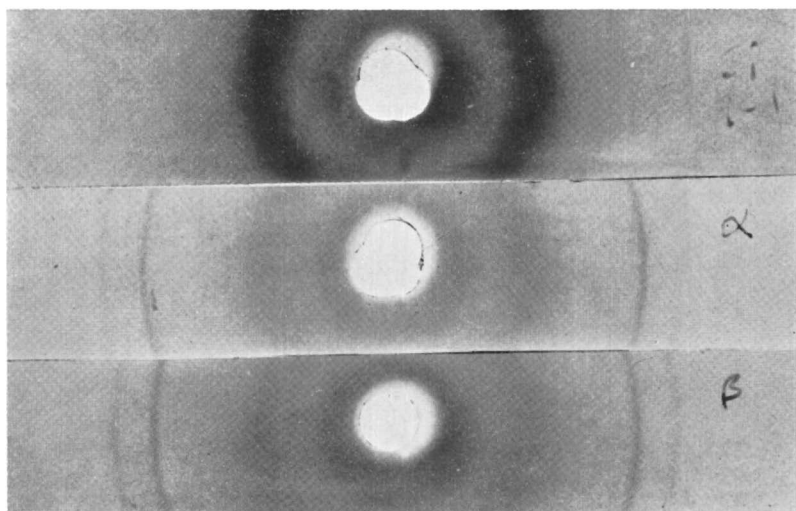


Figure 5. X-ray of pure silica gel (top), 10.86% palladium on silica gel under vacuum (middle), and same sample under 30-mm. hydrogen pressure

a structure on former and β structures in latter
 Calculated lattice dimensions. α . 3.89 ± 0.01 Å.
 β . 4.03 ± 0.01 Å.

These data, coupled with the earlier evidence that the pressure of the gas, at which this transformation takes place, is very temperature-dependent, strongly indicate that the hydrogen forms a definite surface state with the surface atoms of palladium. The data suggest that the β -phase first forms on the surface and then migrates through the metal aggregates. The increase in the lattice parameter of the palladium must be due to hydrogen atoms, the electrons of which occupy levels in the d -band of the metal. These levels are closely related to the intermetallic bonds. The distortion in these bonds influences the energy and consequently the lattice parameter. As the d -band fills, the exchange energy in the crystallites must decrease. Should the d -band be completely filled, then all of the remaining intermetallic bonds would be due to overlapping S and P electrons. In pure bulk palladium, the d levels play an important role in the bonding. The decrease in energy readily explains the larger lattice parameter found for the hydrogen-rich phase. The limit of the uptake of hydrogen by bulk palladium is reached when the d -band is filled, whereas in the case of the palladium dispersed on the gel it appears to be due to actual space limitations.

Magnetic Measurements on Adsorbate-Adsorbent Complex. The magnetic susceptibilities of the palladium as a function of the amounts of hydrogen sorbed are given in Figure 6 for samples I_2 and I_3 at 0° and 28° C.; in Figure 7 for sample I_4 at 0° and 28° C. and for I_6 at 0° C.; and in Figure 8 for samples I_7 and II_8 for H_2 and NO at 0° C. Two striking results, shown in these figures, demand explanation. First, the breaks in all of the magnetic curves for sorbed hydrogen at 0° C. occur in the region of the first horizontal section of the isotherms. At 28° C. there was no such flat portion in the isotherms and there is no break in the magnetic curves at the same temperature. This suggests that, once the surface is

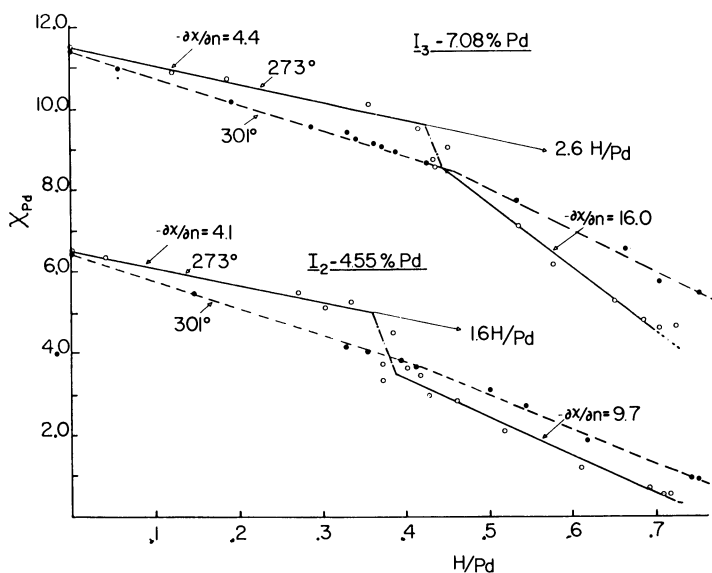


Figure 6. Magnetic susceptibility of palladium on silica gel as function of adsorbed hydrogen

— 0° C. (273° K)
 --- 28° C. (301° K)
 Top. 7.08% Pd
 Bottom. 4.55% Pd

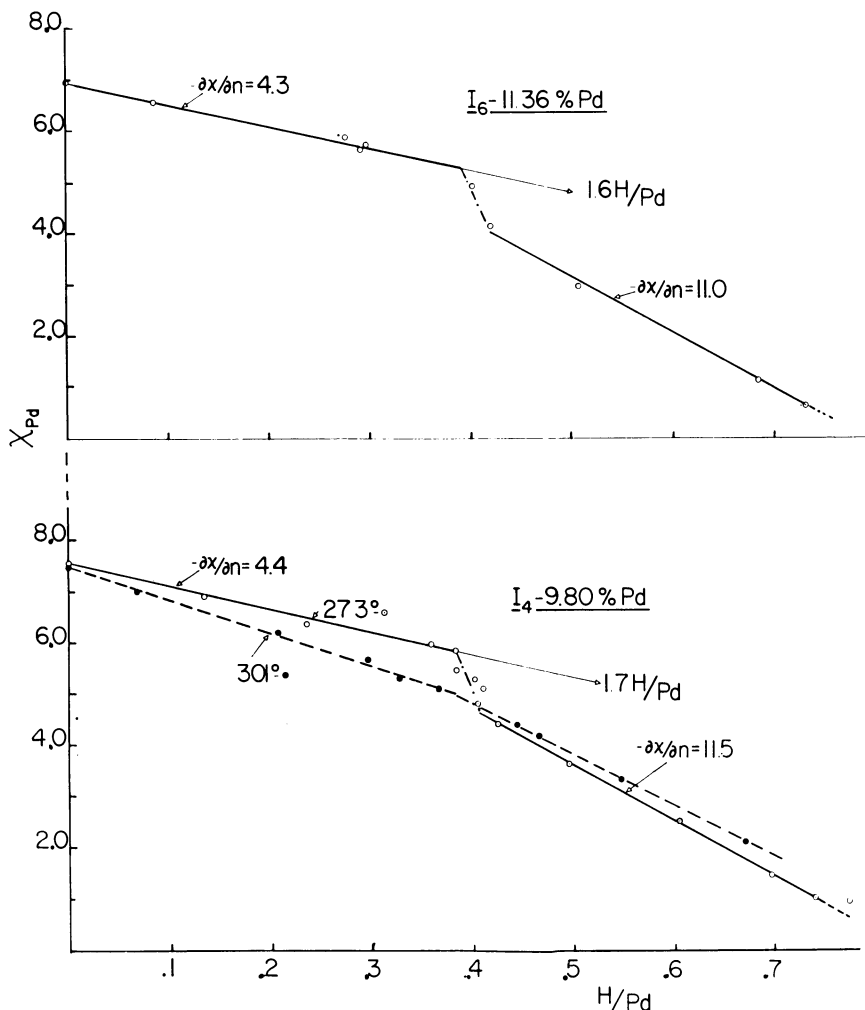


Figure 7. *Magnetic susceptibility of palladium on silica gel as function of adsorbed hydrogen*

— 0° C. (273° K)
 - - - 28° C. (301° K)
 Top. 11.36% Pd
 Bottom. 9.80% Pd

covered at 0° C., a reorganization or dissociation of the adsorbed complex takes place. If the magnetic line, prior to the sudden break, is extrapolated to zero magnetism, the H/Pd ratios vary from 2.6 to 1.3. These values are similar to those reported by Selwood (17). The slope of the curves after the break gives much smaller H/Pd ratios on extrapolation. Secondly, the slope of the magnetic curves, following the break, seems to be a definite function of the original susceptibility of the samples. This can be seen from Figures 1 and 10.

Figure 9 gives the decrease in paramagnetism as calculated by subtracting the magnetism of each sample, at a hydrogen pressure of 30 mm., from the original magnetism and converting to percentages. This shows that physical space is the

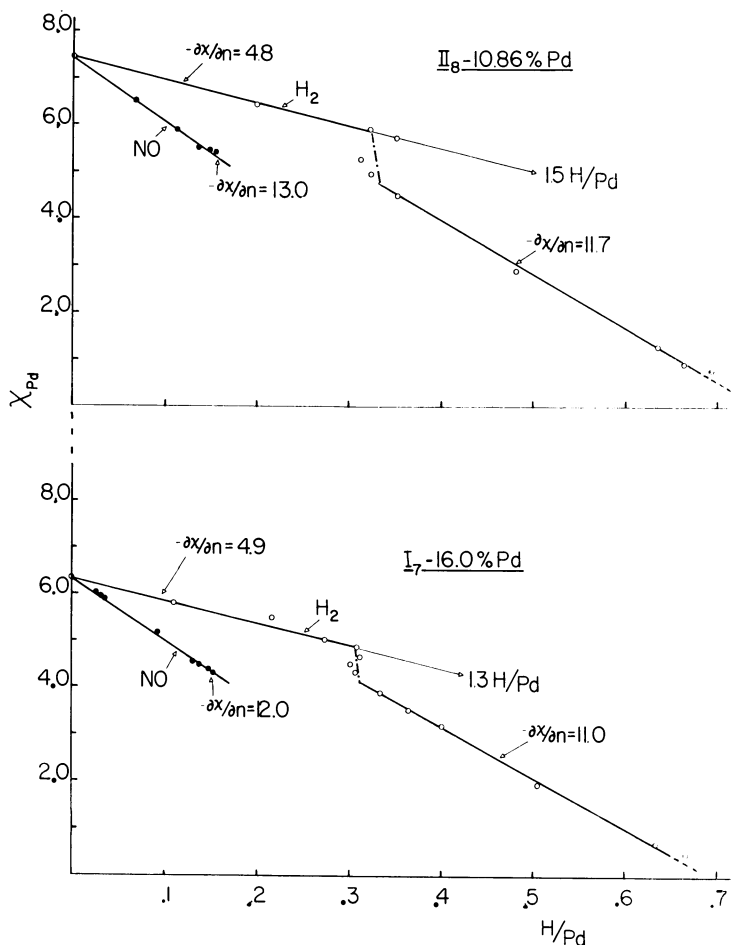


Figure 8. Magnetic susceptibility of palladium on silica gel as function of adsorbed hydrogen and NO at 0° C.

Top. Sample II with 10.86% Pd

Bottom. Sample I with 16.00% Pd

limiting factor in sorption as long as the "holes" in the d -band indicate a greater ultimate capacity than H/Pd of 0.7 to 0.75. Figure 10 shows the ultimate capacity of the dispersed palladium to sorb hydrogen as calculated on the assumptions that all of the hydrogen within the metal is, in the end, sorbed as hydrogen atoms and from the paramagnetism remaining in the sample at a pressure of 30 mm. of hydrogen. These figures are somewhat fictitious as long as there are space limitations to the sorption, but they are of interest in that they confirm the electron structure of palladium. The curves in Figure 10 are almost parallel to those in Figure 1, but when χ_s/χ_o in Table I is compared to Figure 10 it is seen that the susceptibility is proportional to a second-order function of the number of unpaired electrons in the d -band. This agrees with the formula for the susceptibility as derived from magnetic theory

$$\chi = (N\beta^2/3KT)n(n + 2)$$

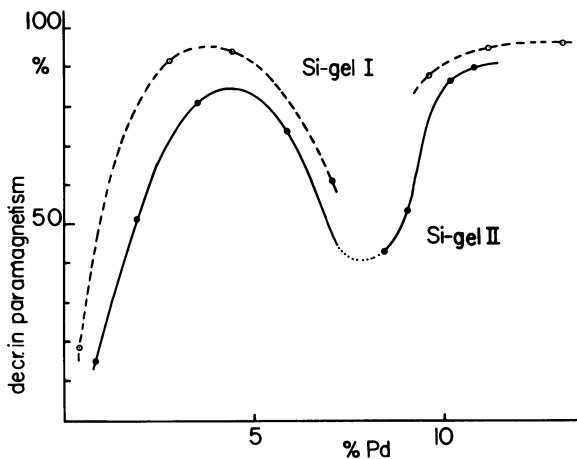


Figure 9. Percentage decrease in paramagnetism of palladium at 30-mm. hydrogen pressure as function of palladium concentration on silica gel

where χ is the susceptibility, β the Bohr magneton, and n the number of unpaired electrons. As a matter of fact this expression was used together with the data from Table I (ultimate H/Pd), as given in Figure 10, to calculate theoretically magnetic susceptibility of pure palladium. These are given under the heading χ_s/χ_o calcd. in Table I and are in very good agreement with the experimental values, when the many approximations are taken into account.

The fact that the susceptibility is proportional to the second order of the number of unpaired electrons explains the steep slope of the NO curves in Figure 8. This shows again that the surface has quite a different electron structure from that of the bulk. The NO is sorbed only on the surface, since there is no evidence that it is able to enter the crystal lattice of palladium. As we have indicated, the

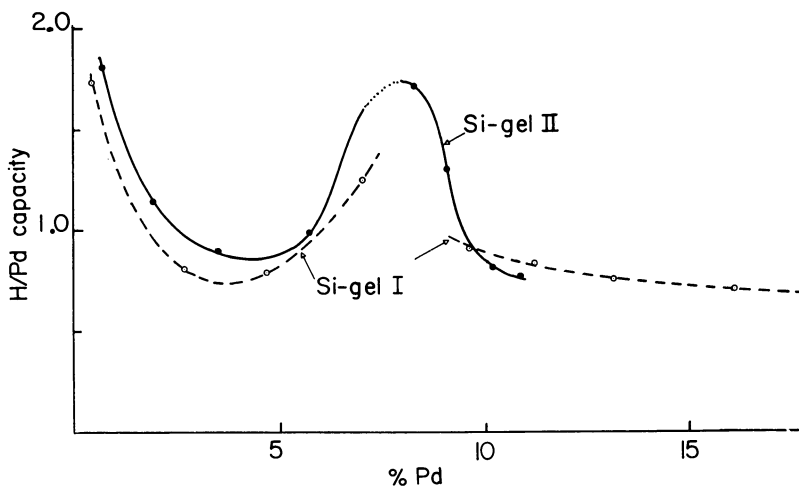


Figure 10. Calculated H/Pd capacity from remaining paramagnetism at 30-mm. hydrogen pressure (0° C.)

Figure with Table I indicates space limitations of H_2 sorption

surface probably has more "holes" in the *d*-band than exist in the bulk state. If now the susceptibility is proportional to a second-order rather than a first-order function of the number of unpaired electrons, the pairing of an electron on the surface will have a greater effect than will be the case for a state having fewer unpaired electrons. Since each NO molecule can provide only one electron for pairing, the data indicate that the palladium atoms in the surface state have more unpaired electrons than the interior atoms.

These suggestions would seem to contradict the results shown in Figures 6, 7, and 8, where the slopes of the magnetic curves for hydrogen sorption before the breaks, at least at 0° C., are less than for NO but are also less for H₂ after the break. It would seem that the hydrogen sorbed on the surfaces at very low pressures must be present as undissociated molecules or possibly as H₂⁺ ions pairing one electron with an electron in the surface *d*-band. At the higher temperature of 28° C. this is much less pronounced, probably because of greater thermal vibration. The sharp break in the susceptibility curves following only slight additions to the amounts of hydrogen sorbed must mean a transformation from H₂ or H₂⁺ to 2 H atoms. From then on, as the pressure increases, the hydrogen atoms formed on the surface will migrate into the palladium lattice until the crystallites are filled. The electrons of these hydrogen atoms must pair with electrons in the *d*-band within the crystallites. It is then possible that the hydrogen atoms may be migrating inside the metal as protons at this temperature.

Conclusion

The measured data give evidence that the susceptibility of palladium deposited on silica gel surfaces is dependent on both the surface to bulk ratio and the lattice constant. They also show definite surface states on the palladium crystallites with more holes in the *d*-band of the surface than in the rest of the metal.

There is reason to believe that this is a general phenomenon, and of great importance to the understanding of catalytic surfaces. The physical structure of the catalyst with regard to the surface area would be of greatest importance to the electronic state of the surface and consequently to the catalytic properties. The significance of a high surface area is not only due to the large area on which the reaction may occur, but also to the influence of the surface on the electronic properties. The latter is probably the more important.

The data also give evidence for a better understanding of the sorption of hydrogen by palladium. The surface-adsorbed hydrogen must apparently reach a certain coverage before entering the lattice, explaining the strong temperature dependence on the transformation point. The transformation in lattice structure is due to the filling up of the *d*-band of the palladium with the electrons in hydrogen. The resulting decrease in exchange energy induces the larger lattice parameter.

Acknowledgment

The authors are indebted to J. Doyle Britton for his assistance in the x-ray determinations.

Literature Cited

- (1) Gillespie, L. J., Galstaum, L. S., *J. Am. Chem. Soc.* **58**, 2565 (1936).
- (2) Gillespie, J. F., Hall, F. P., *Ibid.*, **48**, 1207 (1926).

- (3) Gillespie, L. J., Perry, J. H., *J. Phys. Chem.* **35**, 3367 (1931).
- (4) Hoare, F. E., Mathews, J. C., *Proc. Roy Soc.* **A212**, 137 (1952).
- (5) Hoare, F. E., Walling, F. C., *Proc. phys. Soc. (London)* **64 B**, 337 (1951).
- (6) Kobozev, N. I., Evdomikov, V. B., Zubowich, I. A., Mal'tsev, A. N., *Zhur. Fiz. Chem.* **26**, 1349 (1952).
- (7) Kruger, F., Gehm, G., *Ann. physik.* **16** (5), 174 (1933).
- (8) Linde, J. O., Borelius, G., *Ibid.*, **84** (4), 747 (1927).
- (9) McKeehaan, L. W., *Phys. Rev.* **21**, 334 (1923).
- (10) Mitchell, A., Benard, J., Chandron, G., *Bull. soc. chim.* **12**, 336 (1945).
- (11) Nace, D. M., Aston, J., *J. Am. Chem. Soc.* **79**, 3619, 3623, 3627 (1951).
- (12) Norberg, R. E., *Phys. Rev.* **86**, 745 (1952).
- (13) Owens, E. A., Jones, T. I., *Proc. Phys. Soc. (London)* **49**, 587, 603 (1937).
- (14) Owens, E. A., St. Williams, E., *Ibid.*, **56**, 52 (1944).
- (15) Samson, J., Himmelsturm, D., *Z. anorg. Chem.* **186**, 337 (1930).
- (16) Shockley, W., *Phys. Rev.* **56**, 317 (1939).
- (17) Selwood, P. W., personal communication to H. M. Hulburt, "Catalysis," Vol. II, p. 199.
- (18) Sievertz, A., Brünig, H., *Z. phys. Chem.* **163** (A), 409 (1933).
- (19) Sievertz, A., Dary, W., *Ibid.*, **38** (B), 61 (1937).
- (20) Smith, D. P., *Phil. Mag.* **39**, 477 (1948).
- (21) Solbakken, A., Reyerson, L. H., *J. Phys. Chem.* **63**, 1622 (1959).
- (22) *Ibid.*, **64**, 1903 (1960).
- (23) Swensson, B., *Ann. Physik* **18**, (5), 299 (1933).
- (24) Tamm, I., *J. Phys. U.S.S.R.*, **1**, 733 (1942).
- (25) Trzebiatowsky, W., Kubicka, H., Skiva, A., *Roczniki Chem.* **31**, 497 (1957).
- (26) Zuehlke, Richard, Ph.D. thesis, University of Minnesota, June 1960.

RECEIVED May 29, 1961. Investigation supported in part by a grant from the National Science Foundation.

Low Energy Reference Electrodes for Investigating Adsorption by Contact Potential Measurements

K. W. BEWIG and W. A. ZISMAN

U. S. Naval Research Laboratory, Washington 25, D. C.

Stable reference electrodes of noble metals coated with a thin film of FEP Teflon resin have been developed for the measurement of contact potentials in gases and vapors. Such electrodes exhibit little time-dependent diffusion or surface adsorption by a large class of gaseous compounds because of the density and low critical surface tension of wetting of this coating. They have been used to study the effect of adsorption on surface potentials of bare platinum and other metals in wet and dry nitrogen and oxygen atmospheres and in CO₂, H₂, and He. Also, some of the physical properties of adsorbed polar monolayers of fatty acids, amines, and alcohols have been investigated by means of surface potential measurements using these reference electrodes.

The contact potential difference between two metals in a gaseous atmosphere is greatly altered by an adsorbed film or by mechanical working of the surfaces (18). These are exemplifications of the well-known sensitivity of the electronic work function of a metal to surface-chemical or structural changes. Investigators have had to use the best possible high-vacuum systems, vapor-deposited metal electrodes, and extraordinary care to degas all solids in the system in order to obtain the "intrinsic" contact potentials between metals of basic interest in theories of metal conduction (12).

Efforts have been made by many investigators to use the sensitivity of clean, freshly prepared metallic surfaces to traces of adsorbed compounds as a tool for studying adsorbed films and adsorption. However, any gas or vapor which is able to adsorb on the one metal electrode usually adsorbs to some extent on the other. This difficulty is often decreased by employing as a reference electrode a well-aged gold or platinum surface; unfortunately, this is an unreliable device which is much more limited in application than is commonly realized. The contact potential difference between a noble metal in the air and the surface of water is often used to measure the change with film pressure of the packing and orientation of a mono-

layer of polar molecules adsorbed on the surface of the water (20, 25). Here, maintaining a constant surface state of the reference electrode is especially troublesome because of the proximity of that electrode to the surface of such an adsorptive and volatile polar liquid as water. In short, the literature is replete with investigations showing the need for a method of making one metal behave as a reliable reference electrode for the duration of an experiment on adsorption.

Phillips (19) formed a reference electrode by coating a noble metal with a Langmuir-Blodgett multilayer of calcium palmitate and used it to detect the presence of a polar vapor in dry atmospheres by its adsorption on an uncoated metal electrode. Water vapor and oxygen were carefully excluded from the surrounding atmosphere, since either gas penetrated the multilayer coating on the reference electrode. This report describes the preparation, properties, and several applications of a more general and useful type of reference electrode.

To serve as a reference electrode, a coating for the metal is needed on which gaseous adsorption is either nil in a variable atmosphere or in equilibrium with a constant atmosphere. Usually the vapor of a liquid, which exhibits a large contact angle on a solid surface, will also have a low adsorptivity at temperatures well above the critical temperature.

Studies of the wetting and spreading of liquids on smooth, clean, solid surfaces have revealed that the lower the unit free surface energy (γ_0) of the solid, the lower must be the surface tension (γ_{LV}) of a liquid if it is to be able to spread spontaneously. The concept of the critical surface tension of wetting (γ_C) was developed by Zisman and coworkers (9, 21, 22, 26) to express the fact that on such a solid surface no liquid will spread spontaneously unless γ_{LV} is less than γ_C . Results of many experiments on well-controlled surfaces have revealed that γ_C is determined solely by the nature and packing of the surface atoms in the surface of the solid (22, 26). For example, a surface whose outermost aspect comprises methyl groups in closest packing has a γ_C value of 22 dynes per cm. at 20° C.; it has the lowest surface energy (and the least adsorptivity) of all hydrocarbon surfaces. An approximation to such a surface is made by depositing a Langmuir-Blodgett stearate multilayer on a clean polished metal plate. However, the resulting reference electrode should be limited to measuring the adsorption of vapors of liquids having surface tensions at 20° C. much in excess of 22 dynes per cm. Since the smooth surface of polytetrafluoroethylene (Teflon) has a γ_C value of about 18.5 dynes per cm. at 20° C. (9, 21), and almost all ordinary liquids have surface tensions in excess of that value, the adsorptivity of their vapors on Teflon must be very low at temperatures well above their critical temperatures. Hence, a Teflon-coated metal plate should be one of the best possible reference electrodes.

Bennett and Zisman (1) have reported that copolymers of tetrafluoroethylene (TFE) and hexafluoropropylene (HFP) have γ_C values varying from 18.5 dynes per cm. for polytetrafluoroethylene to about 15 dynes per cm. for polyhexafluoropropylene and have shown that γ_C decreases as the number of $-\text{CF}_3$ side chains increases. Therefore, the poly-HFP resin should be more suitable for coating the reference electrode than the poly-TFE. The solid coating with the lowest surface energy of all would be one whose surface comprises close-packed perfluoromethyl groups; however, suitable materials are not available. A nearly close-packed monolayer of $-\text{CF}_3$ groups results with the adsorption of one of the higher perfluoroalkanoic acids (16, 21), and γ_C for such a surface is between 6 and 8 dynes per cm.; but monolayer coatings of such acids are corrosive, easily damaged, and too speedily penetrated by atmospheric water to be suitable electrode coatings.

Results are reported here of experiments using reference electrodes of several

different metals coated with the TFE-FEP copolymer resin now commercially available as FEP Teflon. The effect on the contact potential difference between these coated reference electrodes and active bare metal surfaces has been studied in atmospheres of oxygen, nitrogen, water vapor, hydrogen, and helium. Electrical properties of several types of adsorbed solid monolayers of aliphatic polar compounds, which were deposited on the surface of the active metal electrode by retraction from solution, were also investigated.

Apparatus and Experimental Methods

The vibrating condenser method (27) was used to measure the contact potential difference. Clean polished steel, aluminum, gold, and platinum electrodes were encapsulated in FEP Teflon resin. Commercial FEP Teflon (17) has about one millionth the melt viscosity of Teflon; hence, it can be successfully applied to the metal electrode by using the "fluidized bed" coating technique (6). Since adhesion of perfluorinated resins to the metal is inherently weak, a circle of small holes was drilled in the face of the electrode to allow columns of the resin to bond the front and back of the coating together. A ring of Duco cement was used to seal the collar around the pin of the electrode. Such coatings of FEP Teflon were even more suitable than Teflon for the purposes of this investigation, not only because of the lower γ_C value but because they are so much less permeable to liquids and vapors. In confirmation of our experience, it has been reported recently (14) that thin films of FEP Teflon backed up by metal surfaces were impermeable to acid and salt solution during immersion tests lasting 30 to 60 days.

Each FEP Teflon-coated reference electrode was cleaned by washing it in Tide detergent solution, scrubbing on a clean Buehler Selvyt polishing cloth under grease-free, flowing, distilled water, rinsing under flowing distilled water, and finally drying in the air at room temperature. Before each experiment unless stated otherwise the reference electrode was mounted in a gas-flow measuring cell adjacent to an uncoated electrode made of identical metal and then both were grounded. The air gap between these two surfaces was exposed next for 5 minutes to the atmospheric ions generated by a nearby Static Master No. 6000A polonium α -particle source; in this way electrostatic charges were removed which may have been formed on the surface of the resin coating of the reference electrode during cleaning and manipulation. Any small contact potential difference between the two identical metals resulted in a minimum residual charge left trapped on the FEP Teflon coating. No mechanical handling of the reference electrode was permitted after the α -particle radiation treatment. This procedure eliminated spurious surface potentials caused by the formation of triboelectric charges on the surface of the resin; such spurious potentials could be as large as 40 volts.

One of the most troublesome experimental problems encountered was elimination of traces of organic polar impurities in the gases studied. Much previous work on contact potentials has been compromised by ignoring this problem. The principal difficulty is the adsorption of such impurities on the active metal electrode to form hydrophobic films which greatly alter the contact potential differences. Each gas was freed from such contaminants by flowing it through a long column packed with Linde 4A adsorbent sieves. It also proved essential to dispense with any plastic tubing such as Tygon tubing, in order to avoid picking up volatile hydrophobic impurities, presumably traces of plasticizers. Therefore, no plastic material was allowed in the entire system, except Teflon and the polyethylene connectors to the glass tubing leading the gases into and out of the system.

A metal surface was considered suitable for this investigation only when it remained hydrophilic during the entire time of the experiment. Clean hydrophilic surfaces can be produced readily on platinum and gold by heating each until dull red in the oxidizing flame of the Bunsen burner; however, more reproducible

surface potentials were obtained on all electrodes by abrading each on No. 600 Carborundum paper under flowing distilled water, polishing at room temperature on a metallographic polishing wheel covered by wet Kittens Ear cloth treated with an aqueous dispersion of Linde A-5175 α -alumina, and then scrubbing on a Buehler Selvyt cloth under flowing distilled water. Where gold or platinum was involved, this treatment was followed by an etch with a 1 to 4 mixture of HNO_3 and H_2SO_4 and a 2-hour cleaning, using C.P. benzene in a Soxhlet extractor.

Comparison of Uncoated with Resin-Coated Electrodes

Early experiments were concerned with the protection against water-vapor adsorption afforded a pair of soft steel electrodes by coating each with FEP Teflon resin. The two coated electrodes were cleaned as before, mounted in the gas cell, and then discharged with gaseous ions while the metal pins were grounded. The resulting contact potential difference was zero. The same result was obtained using a pair of resin-coated aluminum electrodes.

The gas cell was hermetically sealed and 200 ml. per minute of nitrogen gas slightly above atmospheric pressure was passed through a long column of Linde 4A adsorbent sieves and then flowed through the cell containing two FEP-coated electrodes, one of steel and one of aluminum. Each value of the relative humidity was maintained for one hour to be sure that the adsorbed films on the electrodes had attained a steady-state condition. Measurements were made of the potential difference for 96 hours at 23° C., during which time the relative humidity was periodically cycled between 1 and 91% values. No significant effect was observed on the contact potential difference (see lower curve of Figure 1), the maximum variation being no greater than ± 0.005 volt for the entire time. These results prove that water-vapor adsorption on the surface of FEP Teflon is negligible under these extreme conditions. If equal adsorption had occurred on the outer surface of each of the two coated electrodes, their electrical effects could not nullify the different local electric fields of the two different substrate metals; a contact potential change would have resulted.

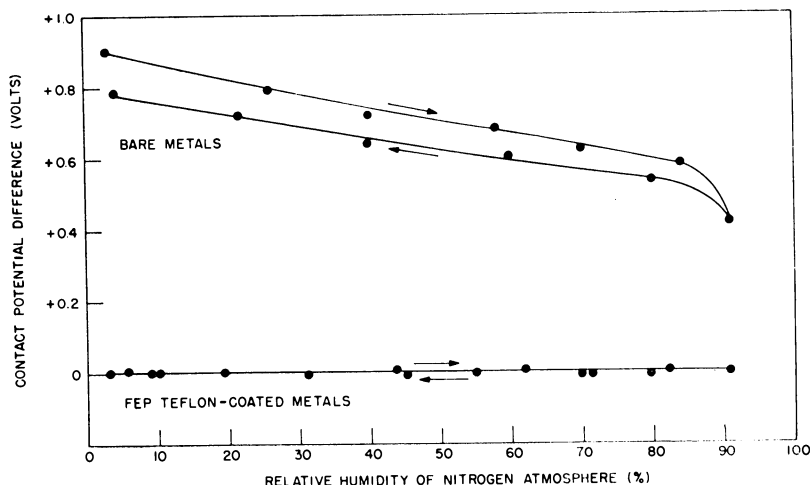


Figure 1. Contact potential difference of aluminum relative to soft steel with and without FEP Teflon resin coating

Comparable data were obtained for the same pair of metals, steel and aluminum, identically prepared and treated but without any protective resin coating. After each electrode was abraded on Carborundum paper, it was polished on a cloth wheel with α -alumina, scrubbed on a cloth under flowing water, rinsed in distilled water, air-dried, and aged for 72 hours in clean dry air. Each measurement plotted in the upper curve of Figure 1 was obtained after holding the system at the relative humidity for one hour, the temperature always remaining 23° C. As in the previous experiment, the atmosphere was nitrogen of controlled humidity. The main effects are: a reversible decrease of 560 mv. in the contact potential difference caused by the physical adsorption of water and a smaller irreversible decrease of 130 mv. Evidently, aging such bare electrodes for 72 hours after polishing and cleaning the surfaces was not sufficient to eliminate irreversible surface aging effects.

Figure 2 shows the change with aging of the contact potential differences between a bare gold electrode and a bare platinum electrode, each against a stable reference electrode of gold coated with FEP Teflon resin. The bare gold and platinum electrodes were prepared as previously described, except that the platinum and gold were finally heated to a dull red in the oxidizing portion of the Bunsen flame to remove any organic contaminants. The reference electrode was cleaned and its surface potential stabilized as explained earlier. Promptly after flaming, each bare metal electrode was introduced into the gas cell, which was then promptly flushed with a stream of nitrogen stabilized at 23° C. and 1% relative humidity. This atmosphere was maintained for 4 days. Initial rates of

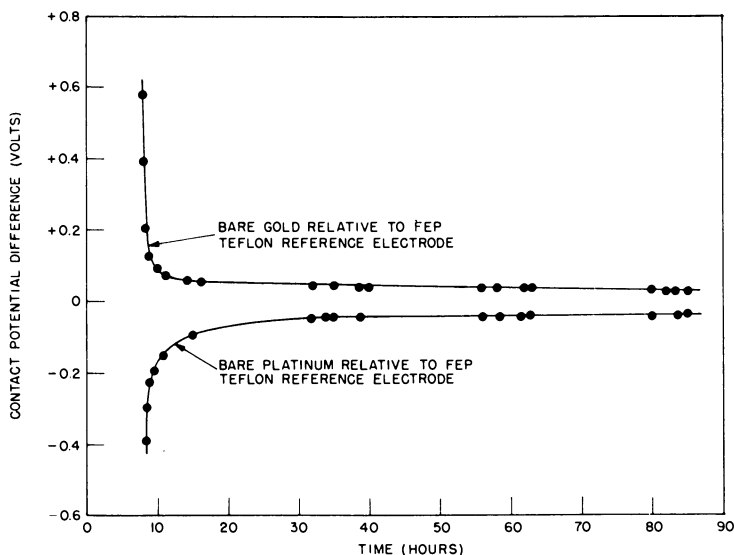


Figure 2. Contact potential difference in dry nitrogen of gold and platinum relative to FEP Teflon-gold reference electrode

1% R.H.

change in the contact potential difference between either bare metal relative to the reference electrode were rapid; but whereas the magnitude of each contact potential difference was initially about 0.4 to 0.6 volt, it had decreased to about 0.2 volt after 3 hours. From these data, an initial potential difference of about

1 volt between bare gold and platinum is calculated. After 32 hours, the potential difference was decreasing at a constant rate of only a few millivolts per 24 hours. After 72 hours of aging either bare noble metal surface, the same cycling of the relative humidity used to produce the data of Figure 1 was employed (Figure 3). An over-all change in contact potential of around 100 mv. had occurred, the effect being reversible within a few millivolts during any one day of measurement. Therefore, the irreversible aging effect for bare steel *vs.* bare aluminum shown in Figure 1 is not peculiar to readily oxidized and corroded metals but also is found with the bare, clean, noble metals. Nevertheless, only 72 hours after polishing and cleaning the noble metal surfaces, the aging effect had decreased to only a few millivolts per day; in contrast, bare steel *vs.* aluminum was still decreasing at a rate of 130 mv. per day. These studies show that aged clean gold or platinum can be used as a reliable reference electrode, only if all conditions are controlled properly.

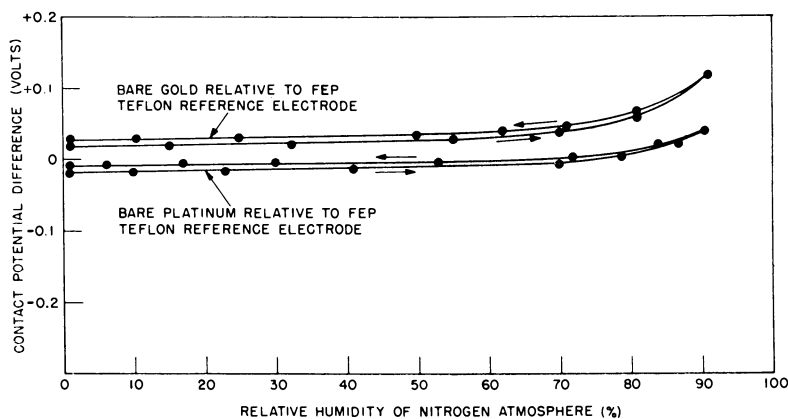


Figure 3. *Effect of varying relative humidity on contact potential difference of gold and platinum*

FEP Teflon-gold reference electrode in nitrogen

Figure 4 shows the effect of cycling the relative humidity on the contact potential difference of either a bare aluminum or a bare steel surface measured against a stabilized reference electrode of gold covered with FEP Teflon. The aluminum electrode was prepared in the same way as other uncoated electrodes, except that no Carborundum abrasive was used. The contact potential difference decreases with the relative humidity rather than increases as in Figure 3 for the cases of bare platinum and bare gold. This difference in behavior could mean that the water molecules had adsorbed on the aged aluminum (or steel), resulting in an effective surface dipole having its negative pole outermost; on either gold or platinum the hydrogen atoms are situated outermost, so that the positive pole of the dipole is outermost. This interpretation is qualitatively in agreement with that of Verwey and de Boer (24) concerning electrical double layers resulting from surface-oxide films on metals and with Suhrmann's explanation (23) of the adsorption of water molecules on platinum.

Gold, platinum, cold-rolled steel, and aluminum electrodes were coated with FEP Teflon and then mounted on a plane circular-rotating stage in the gas chamber in such a way that each in turn could become the stationary electrode of a parallel-plate condenser whose vibrating electrode was an aged, uncoated, aluminum

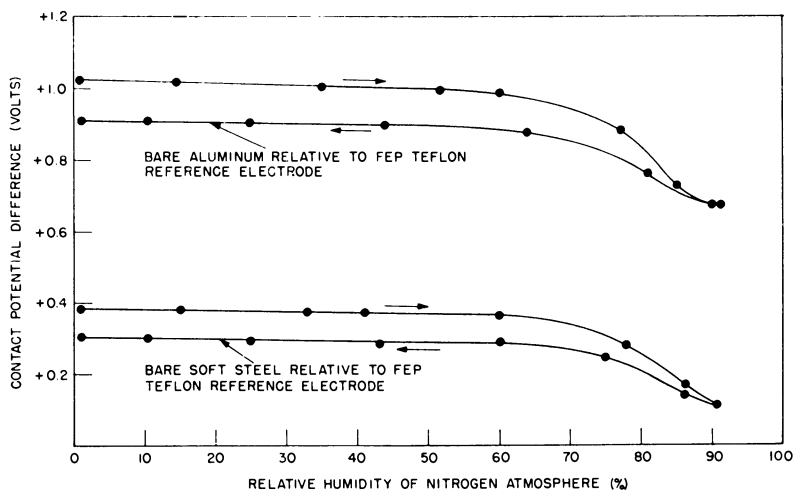


Figure 4. Effect of varying relative humidity on contact potential difference of aluminum and soft steel

FEP Teflon-gold reference electrode in nitrogen

electrode. Thus, surface potential differences between the aluminum surface and each of the four FEP Teflon-coated reference electrodes made from different substrate metals could be compared quickly under the same atmospheric conditions. In comparing the experimental data obtained with the four reference electrodes, the graphs were superimposed by plotting the contact potential differences obtained at relative humidity < 1% as having the value of 1.0 volt. Figure 5 shows the resulting plot of the change in the contact potential difference between the vibrating bare aluminum electrode and each of the four reference electrodes as the relative humidity was increased from 1 to 91% and then returned to 1%. The resulting spread of the data obtained from the different reference electrodes is indicated by the height of the vertical line at each data point. The maximum spread existing between the four reference electrodes varies from 0.010 volt at 1 to 10% R.H. and 0.02 volt at 90% R.H. Within these limits of uncertainty, the results obtained with the different reference electrodes all agreed. Hence, unless one must deal with studies lasting longer than a few days, any of the resin-coated reference electrodes can be used. Where longer runs or more reactive gaseous environments are involved, it would obviously be better to use as the substrate metal of the reference electrode an unreactive metal such as gold.

Effect of Varying Nature of Gas

A bare platinum electrode was cleaned as previously described and then allowed to come to adsorption equilibrium with air in the gas chamber. When dry nitrogen was passed through the chamber, the potential difference between the platinum surface and the FEP resin-coated electrode increased rapidly, reaching an equilibrium value 0.5 volt higher in approximately 2 hours. Dry oxygen was then introduced into the chamber and the surface potential of the platinum decreased to a steady-state value of + 0.2 volt relative to the reference electrode (see Figure 6). This system was allowed to remain in that condition for 24 hours, during which time there was only a 20-mv. increase in the contact

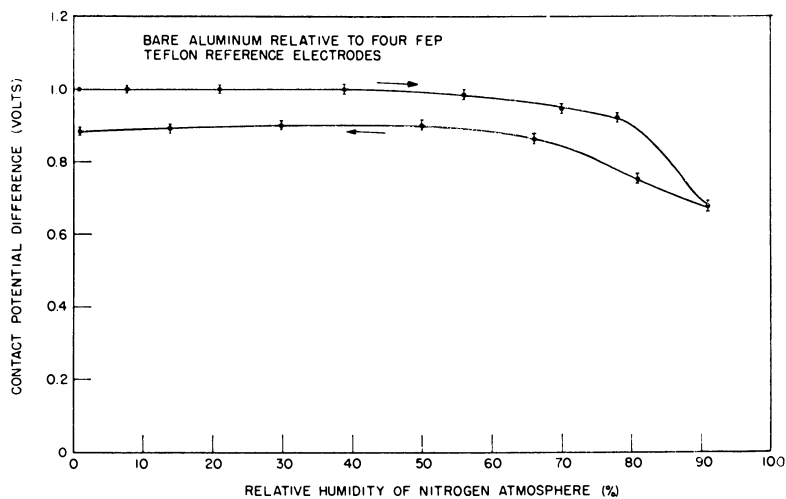


Figure 5. Effect of varying relative humidity on contact potential difference of aluminum relative to gold, platinum, aluminum, and soft steel coated with FEP Teflon resin in nitrogen

potential. Dry nitrogen gas was again introduced, and the potential returned to a value only 20 mv. less than the previous equilibrium value for nitrogen. Additional cycling of the oxygen and nitrogen gas showed a continuing departure from equilibrium values after each cycle, the cause of which could be (1) long-time changes in the aging of the bare platinum electrode, (2) long-time changes in the aging of the reference electrode, and (3) the effect of trace materials in the gases used; in all probability, the first is the main cause.

A bare platinum electrode was coated with a close-packed monolayer of *n*-octadecylamine by retraction from the molten crystal compound (2). The contact angle of methylene iodide with the monolayer was 68° to 70° , which should be true if the film was close packed. This film-coated electrode was used with the FEP resin-covered gold electrode in the experimental sequence described

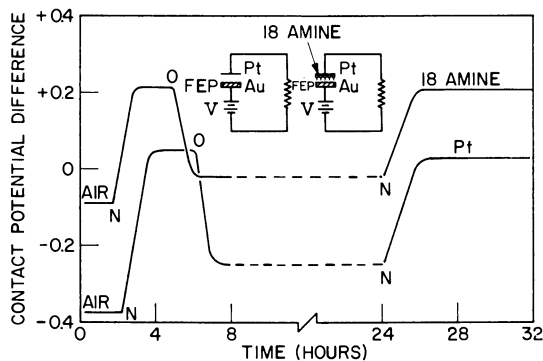


Figure 6. Contact potential difference of platinum and platinum coated with monolayer of octadecylamine

FEP Teflon-gold reference electrode in nitrogen and oxygen gases

above—i. e., the cycling from air to nitrogen to oxygen, etc., was repeated. The results are also given in Figure 6. The behavior is very much like that exhibited by the bare platinum electrode. The only differences were that in this experiment the maximum change in the contact potential was a few hundredths of a volt less than in the former experiment. This shows that the octadecylamine is quickly penetrated by the nitrogen and oxygen gases, and that an adsorbed monolayer of the amine can greatly alter the work function of platinum.

A similar experiment was carried on with the same electrodes in an atmosphere of nitrogen gas whose relative humidity was cycled from an initial value of 75% to less than 1%, back to 75%, back to less than 1%, and finally back to 75%. The entire experiment required 56 hours. Figure 7 shows that for both bare platinum and platinum coated with a condensed monolayer of octadecylamine, the changes in contact potential are almost reversible. But again, as in the case of the behavior of the dry nitrogen and oxygen gases shown in Figure 6, the adsorbed amine monolayer was quickly penetrated by the water vapor, and the maximum potential change observed in the cycling of the relative humidity was greatest with a bare platinum electrode.

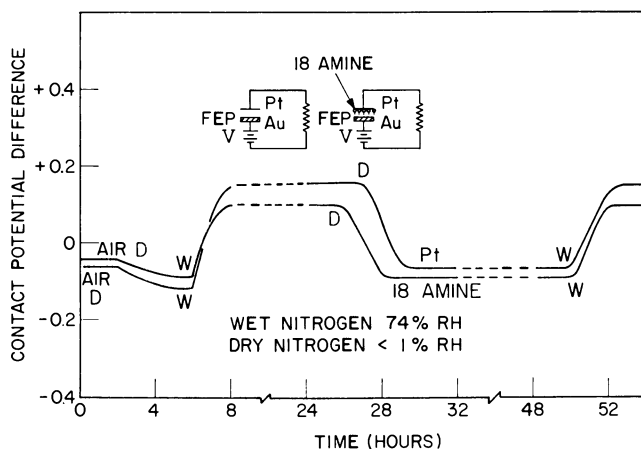


Figure 7. Effect of varying relative humidity on contact potential difference of platinum and platinum coated with monolayer of octadecylamine

FEP Teflon-gold reference electrode in nitrogen

In another experiment the contact potential difference of clean bare platinum was examined against bare gold in an atmosphere varying from nitrogen to hydrogen and then to helium, as indicated in Figure 8. When the hydrogen was introduced into the chamber, the potential difference of platinum relative to gold rose abruptly about 0.8 volt and then decreased somewhat, probably because of a different time rate in the mechanism of adsorption on the two metal surfaces. When helium was introduced into the chamber, there occurred a slight sudden rise followed by a rapid fall. In another similar experiment both electrodes were coated with FEP resin. An essentially similar effect was observed. These experiments prove that hydrogen and helium are able to penetrate the resin coatings rapidly to adsorb on the underlying metals. Furthermore, the almost equal magnitudes of the changes in contact potential reveal that the surface coverage by either the adsorbed hydrogen or helium gas is not very different on resin-coated

metal than on bare metal. The nearly complete reversal of the electrical effect of hydrogen by helium demonstrates that the electrical effect of introducing each gas is *not* an electrostatic charging of the resin such as occurs when a liquid comes in contact with the dielectric surface during cleaning procedures.

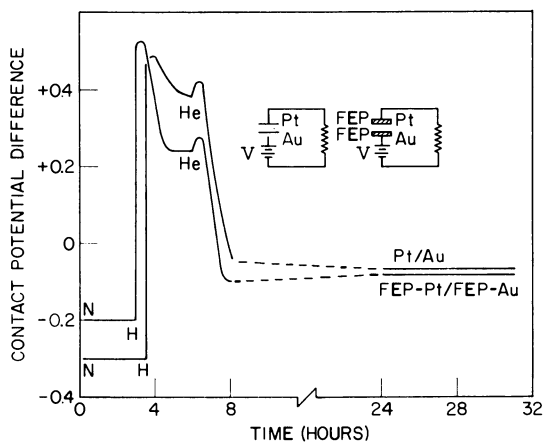


Figure 8. Contact potential difference of platinum relative to gold with and without FEP Teflon resin coating in hydrogen and helium gases

Electrical Study of Durability of a Solid Monolayer

When a drop of pure molten octadecylamine is placed on a polished, horizontal, platinum surface, the excess material spontaneously retracts, leaving a close-packed adsorbed monolayer, the outermost portion of which is comprised of close-packed methyl groups. However, a large flat drop of the molten amine can be deposited on the horizontal surface of the metal, and on cooling an adherent solid layer remains. One can then employ the technique so frequently used by Hardy (11) to prepare a monolayer—i. e., the excess above a monolayer is rubbed off the surface by polishing it vigorously with clean, grease-free, paper tissue. Many investigators questioned whether or not a condensed monolayer is obtained by this procedure. Levine and Zisman (15) have shown that if a fatty acid or amine contains 14 or more carbon atoms per molecule, the film adsorbed by retraction from the melt is solid at 20° C. and possesses such great durability that repeated rubbing under loads much greater than 100,000 p.s.i. may cause no significant film damage. They also concluded that Hardy's method of wiping down an excess deposit on a metal to form a monolayer is reliable only for a polar compound which adsorbs as a solid monolayer.

A series of measurements was made in the air (at about 50% R.H.) of the contact potential difference between a platinum plate coated with molten octadecylamine, which was then allowed to solidify, and an FEP resin-coated gold reference electrode. After each measurement of the contact potential difference, the platinum electrode was wiped vigorously with a clean tissue to remove as much as possible of the octadecylamine. The results of a succession of such measurements and wipings are given in Table I. Whereas the first wipings caused a large decrease in the contact potential difference, no significant change occurred after a succession of six wipings. The entire experiment lasted 30

Table I. Electrical Evidence of Durability of Solid Monolayer

Active electrode. Platinum coated with bulk C_{18} amine
 Reference electrode. Gold with FEP resin coating
 All measurements at 23° C. and 50% R. H.

Wipe No.	Contact Potential Difference, Volts
0	1.031
1	0.899
2	0.878
3	0.893
4	0.897
5	0.884
6	0.892

minutes, during which any long-term drift in the electrodes would be only a few millivolts. The explanation is that the first wiping removed all of the octadecylamine in excess of a solid monolayer. The remaining adsorbed monolayer exhibited a contact angle of 68° with methylene iodide, proving it was a close-packed film, and it resisted further removal by vigorous wiping with a tissue; hence, no change in the surface potential resulted. The electrical measurements give a most convincing verification of the great durability and fully oriented nature of a condensed monolayer of *n*-octadecylamine.

Effect of Varying Polar Terminal Group of Adsorbed Solid Monolayer

Contact potential differences between gold (or platinum) and a reference electrode change greatly by the adsorption of a solid monolayer of octadecylamine and with the nature of the polar terminal group of the paraffinic compound. Clean bare gold (or platinum) was allowed to come to equilibrium in a dry nitrogen atmosphere (R.H. <1%), and the contact potential difference was measured relative to an FEP resin-coated gold electrode. The bare metal electrode was coated by the melt retraction method with a condensed monolayer of one of the following pure compounds: *n*-octadecylamine (m.p. 80° C.), docosyl alcohol (m.p. 58° C.), and stearic acid (m.p. 69.8° C.). That each monolayer so deposited was close packed is attested by the contact angle of methylene iodide of 67° to 68° (22) for each film on gold and 68° to 70° for each film on platinum. Finally, the equilibrium potential difference between the monolayer-coated metal and the reference electrode was measured in the dry nitrogen atmosphere. The change in the contact potential caused by the adsorbed organic monolayer, which is denoted by ΔV_{metal} , is given in the second and third columns of Table II.

Table II. Effect of Varying Polar Terminal Group in Condensed Adsorbed Monolayer

All data taken at 23° C. in nitrogen (1.0% R.H.)

Adsorbate	Caused by Monolayer Adsorption, Volts				Dilute Solution Dipole Moment, Debyes
	ΔV on Pt	ΔV on Au	On water		
			at pH 8.2	at pH 2.5	
$\text{CH}_3(\text{CH}_2)_{17}\text{NH}_2$	0.830	0.790	0.710	0.635	1.2
$\text{CH}_3(\text{CH}_2)_{20}\text{CH}_2\text{OH}$	0.460	0.390	0.430	0.430	1.6
$\text{CH}_3(\text{CH}_2)_{16}\text{COOH}$	0.130	0.049	—	0.355	1.7

Measurements of ΔV_{metal} were reproducible in independent experiments within ± 20 mv. For purposes of comparison, the value of ΔV for a condensed monolayer

adsorbed at the water-air interface at pH 8.2 and pH 2.5 are given in the fourth and fifth columns, respectively (2, 13). In the sixth column will be found the literature value of the dipole moment (μ) of each compound as measured in dilute nonpolar solvents.

Nearly identical contact angles are exhibited by these monolayer coatings, and the results of Chapman and Tabor's electron diffraction studies of retracted monolayers (5) also agree in concluding that the packing of the molecules in these films varies by not over 5% with the nature of the polar group. Therefore, the large changes in ΔV_{metal} in Table II, going from the amine to the alcohol and then to the acid, must be caused by variations in the dipole moments of the fatty molecules or by their interactions with or polarization by any underlying previously adsorbed water molecules. It is obvious that ΔV_{metal} is not proportional to the dipole moment (μ). Differences in dipole orientation do not appear to explain the variations in the second and third columns of Table II, because Brockway and Karle (3) and Chapman and Tabor (5) have shown that these retracted films have nearly perpendicular orientation. It is concluded that there must have been an interaction of the adsorbed dipole with the water, or the oxide coating the metal substrate. In comparing ΔV_{metal} with $\Delta V_{\text{H}_2\text{O}}$ of the same condensed film on bulk water, one would expect that the appropriate pH would be around 9 for the amine and around 2 for the fatty acid, because at these values the adsorbed molecules are not dissociated. The ΔV value for octadecylamine on water of 0.710 volt is not far from that of 0.790 on gold and 0.830 on platinum. The discrepancies may be understood if under these conditions of low relative humidity, gold and platinum adsorb only one or a few monolayers of water; if so, the polarization of such a thin film of adsorbed water would not be quite the same as that of a layer of bulk water.

The consistently lesser value of ΔV_{metal} for gold than platinum, which was observed for each of the three fatty adsorbed compounds, may be due to differences in: (a) the amount of adsorbed water on platinum and gold, (b) the surface oxidation of platinum and gold, or (c) the induced polarization of the terminal group of the monolayer by the electrostatic field of force emanating from each metal. Probably (a) and (b) are somewhat related. However, the differences observed may not be significant in the case of docosyl alcohol, for the ΔV values of 0.460 for platinum and 0.390 volt for gold are in fair agreement with the 0.430 volt reported for the same monolayer adsorbed on bulk water. Since it is not evident why there should not be induced polarization of the alcohol by the local field of the metal, this is good reason for concluding that (a) and (b) are the important factors here. It is presumed that the value of $\Delta V_{\text{H}_2\text{O}}$ for stearic acid on bulk water is zero at alkaline pH because the sodium salt has been formed, and it is 0.355 volt at pH 2.5 because dissociation of the carboxylic acid has been prevented. The much lower values of ΔV_{metal} for the fatty acid film on platinum and gold than on acidified water are evidence that some of the stearic acid molecules have reacted with active portions of the oxidized surface to form a soap, the effect being greater on gold than on platinum.

Discussion

As might have been predicted from the BET theory (4), the shape of the right-hand portions of Figures 1 and 3 is suggestive of the polymolecular condensation of water on the bare metals at R.H. values above 60%. A notable fact is the slight effect of varying the relative humidity when it is in excess of 1% but

less than 60%. The data of Figure 2 demonstrate that during the adsorption of water on a freshly formed metallic surface, there is an extremely rapid change in the contact potential difference. A significant portion of this change must have arisen from the adsorption of water present in the atmosphere used. It can be concluded that the effect of atmospheric humidity on the contact potential is relatively minor over the relative humidity range between 1 and 60%, becomes large because of monomolecular adsorption when the relative humidity is less than 1%, and becomes large again when the relative humidity exceeds about 60% because of the polymolecular condensation of water.

Attention is called to the small positive slope of the graph in Figure 3 and the slight negative slope in Figure 4. These results reveal that it is possible to choose a pair of metals (like gold against iron) such that the net effect of varying the relative humidity is negligible over the range between 1 and 60%.

The irreversible effects exhibited in Figures 1, 3, and 4 are undoubtedly caused by surface changes with the aging of each metal which are not primarily due to water adsorption—i.e., the shift after completion of a hysteresis loop as in Figures 3 and 4 is about that which would be obtained from the change in the contact potential with the aging of the bare metal even in an atmosphere of constant relative humidity. The implication of these results is that the adsorption of water occurring between 1% R.H. and higher values is reversible, and the hysteresis loops found are due to oxidation or other types of change going on at the metal surfaces besides water adsorption.

An explanation is needed as to why the adsorption of water vapor on bare aluminum and soft steel, on the one hand, and on bare gold and platinum, on the other hand, has opposite effects on the contact potential differences. It is concluded that the water molecules adsorbed as dipoles on the first two metals are adsorbed with the negative pole outermost; on the latter two metals the water dipoles adsorb with the positive pole outermost. This behavior is in agreement with the conclusions reported by others.

In a recent investigation by Fowkes (7) the reference electrode used was a plate of gold covered by a layer of a naphthenic, white mineral oil which had been freed of trace polar impurities by treatment with activated silica gel. In effect, the inert electrode coating used was a surface essentially comprised of methyl and methylene groups. Hence it should behave like a reference electrode whose critical surface tension of wetting is between 22 and 32 dynes per cm. The advantage of this coating is its ease of preparation and freedom from surface cracks and imperfections; the disadvantage is the greater adsorptivity of such a surface than that of a stearate multilayer or of the perfluororesins described here. Gottlieb (10) has recently used a reference electrode of platinum covered with the organic solvent being used in the solution adsorption experiments. Such a reference electrode would appear to have few advantages and many disadvantages for most investigations of contact potentials.

The low surface energy of FEP resin coatings makes this substance particularly inert to the adsorption of many gases and vapors, including water vapor. Of course, the physical adsorption of gases or vapors can be forced to occur even on a low-energy surface, if those chosen are studied at a temperature close enough to the critical temperature (or to the boiling point). If one excludes such conditions, the new reference FEP resin-coated electrodes described here make it possible to investigate experimentally the adsorption of compounds on solid and liquid surfaces under a wide variety of conditions.

Literature Cited

- (1) Burnett, M. K., Zisman, W. A., *J. Phys. Chem.* **64**, 1292 (1960).
- (2) Bigelow, W. C., Glass, E., Zisman, W. A., *J. Colloid Chem.* **2**, 563 (1946).
- (3) Brockway, L. O., Karle, J., *J. Colloid Sci.* **2**, 277 (1947).
- (4) Brunauer, S., Deming, L. S., Deming, W. E., Teller, E., *J. Am. Chem. Soc.* **62**, 1723 (1940).
- (5) Chapman, J. A., Tabor, D., *Proc. Roy. Soc. (London)* **A242**, 96 (1957).
- (6) Checkel, R. L., *Modern Plastics* **36** (2), 125 (1958).
- (7) Fowkes, F. M., *J. Phys. Chem.* **64**, 726 (1960).
- (8) Fox, H. W., *Ibid.*, **61**, 1058 (1957).
- (9) Fox, H. W., Zisman, W. A., *J. Colloid Sci.* **5**, 514 (1950).
- (10) Gottlieb, M. H., *J. Phys. Chem.* **64**, 427 (1960).
- (11) Hardy, W. B., "Collected Papers," Cambridge Univ. Press, London, 1936.
- (12) Herring, C., Nichols, M. H., *Revs. Modern Phys.* **21**, 185 (1949).
- (13) Jarvis, N. L., Zisman, W. A., "Properties of the ω -Halogenated Aliphatic Compounds at the Air/Water Interface," to be published.
- (14) *J. Teflon* **1** (4) (April 1960) (Du Pont Co. publication).
- (15) Levine, O., Zisman, W. A., *J. Phys. Chem.* **61**, 1068, 1188 (1957).
- (16) Macfayden, K. A., Holbeche, T. A., *J. Sci. Instr.* **34**, 101 (1957).
- (17) Mallouk, R. S., Thompson, W. B., "Teflon 100X Perfluorocarbon Resin, A New Melt-Extrudable Fluorocarbon Resin," Soc. Plastics Engrs., 14th Annual National Technical Conference, Vol. 4, p. 782, 1958.
- (18) Patai, I. F., Pomerantz, M. A., *J. Franklin Inst.* **252**, 239 (1951).
- (19) Phillips, G., *J. Sci. Instr.* **28**, 342 (1951).
- (20) Schulman, J. H., Rideal, E. K., *Proc. Roy. Soc. (London)* **130**, 259 (1931).
- (21) Schulman, F., Zisman, W. A., *J. Colloid Sci.* **7**, 465 (1962); *J. Am. Chem. Soc.* **74**, 2123 (1952).
- (22) Shafrin, E. G., Zisman, W. A., *J. Phys. Chem.* **64**, 519 (1960).
- (23) Suhrmann, R., *Z. Elektrochem.* **56**, 351 (1952).
- (24) Verwey, E. J. W., de Boer, J. H., *Rec. trav. chim.* **55**, 675 (1936).
- (25) Yamins, H. G., Zisman, W. A., *J. Chem. Phys.* **1**, 656 (1933).
- (26) Zisman, W. A., "Relation of Chemical Constitution to the Wetting and Spreading of Liquids on Solids," NRL Rept. 4932 (May 15, 1957); Decade of Basic and Applied Science in the Navy," Office of Naval Research, Rept. ONR-2, 30 (1957).
- (27) Zisman, W. A., *Rev. Sci. Instr.* **3**, 369 (1932).

RECEIVED May 9, 1961.

The Mechanism of Oxygen Chemisorption on Nickel

H. E. FARNSWORTH and H. H. MADDEN¹

Barus Physics Laboratory, Brown University, Providence, R. I.

Low-energy electron-diffraction and photoelectric work-function instruments are combined in a single experimental tube. An atomically clean (100) surface of a nickel crystal is subjected to controlled exposures of oxygen at 25° and 150° C. Adsorption occurs initially in an amorphous molecular form. Some of the adsorbed molecules diffuse over the surface to lattice-defect sites, where they dissociate. The resulting atoms form in a lattice structure surrounding the defect site. With increased exposure to oxygen, a place exchange between some oxygen and nickel atoms occurs to form a single-spaced, simple structure with a lattice constant slightly greater than that of nickel. This place exchange immediately precedes, in exposure, the formation of the oxide structure with a lattice of the rock salt type.

In recent years, conflicting opinions have been expressed concerning the detailed steps in the chemisorption process. While it is generally agreed that the adsorbed molecule eventually dissociates, there have been questions concerning the steps that precede this dissociation, even though conditions vary greatly with the materials being considered.

During the last three years we have obtained additional information in support of our tentative conclusion that oxygen is initially adsorbed on a (100) nickel surface at room temperature in a molecular form (3). These results indicate that, following adsorption, some of the oxygen molecules diffuse over the surface to lattice-defect sites where they dissociate, and the resulting atoms form in a lattice structure surrounding the defect site. When the adsorbed oxygen reaches a sufficient density, a place exchange between some oxygen and nickel occurs. Further exposure, or in some cases a rearrangement, results in the formation of an oxide structure of the rock salt type.

The observations have been made with a low-energy, electron-diffraction tube which has provision for measuring the photoelectric work function, ϕ , under the same surface and vacuum conditions. Thus, in addition to obtaining the surface

¹ Present address, Department of Physics, Wayne State University, Detroit 2, Mich.

structure by diffraction, observation of φ furnishes a measure of surface polarization and exchange processes. An increase in φ is to be expected when oxygen is chemisorbed on the surface; a decrease, if oxygen penetrates the surface.

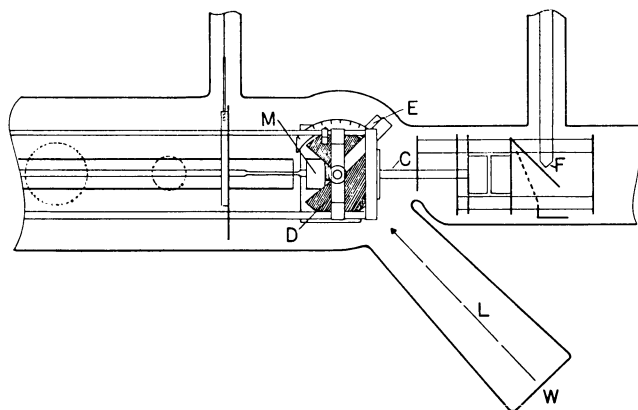


Figure 1. Diagram of experimental tube

- C. Collimator of gun
- D. Shielding drum
- E. Electron collector
- F. Gun filament
- L. Direction of incident ultraviolet light
- M. Crystal mounting
- W. Silica window attached to borosilicate glass envelope with a graded seal

Apparatus and Procedure

The general features of the experimental tube (Figure 1) are similar to others used in this laboratory for low-energy electron diffraction, with added provisions for measuring the photoelectric work function, φ . The diffraction apparatus has been described (2).

A narrow beam of electrons strikes the crystal at normal incidence and the diffraction pattern is determined by measuring the current to an electron collector whose position may be varied by means of an external magnetic control. The crystal may be withdrawn from the diffraction position, to be cleaned by argon ion bombardment and heat treatment. The crystal is held by tungsten springs against the end of molybdenum cylindrical mounting which had been preoutgassed in vacuum. A thermocouple measures the temperature of the molybdenum mounting which is heated by electron bombardment, and the crystal is heated by conduction through a good thermal contact. Optical pyrometer tests show that the temperature of the crystal is less than 30° C. lower than that of the mounting at 750° C.

For measurements of φ , ultraviolet light from a quartz mercury arc passes through a quartz monochromator, silica lens, and window, and is focused onto the crystal at an angle of incidence of about 45°. The saturated photocurrent is collected by the surrounding metal drum to determine φ by the Fowler method (4). A vacuum thermopile measures the light intensity. Photoelectric and diffraction currents are measured by a vibrating reed electrometer. Ultra-high-vacuum techniques are employed, which result in residual pressures of less than 10⁻⁹ mm. of Hg.

Cleaning the crystal surface by a combination of heating at 800° to 900° C., argon ion bombardment, and subsequent annealing results in a close approximation to an atomically clean surface with the exposed surface composed predominantly of (100) planes (2). By varying the amount of annealing subsequent to ion bom-

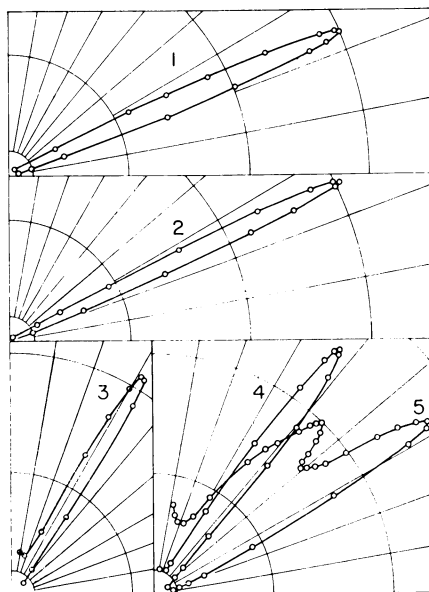
bardment, the number of lattice defects can be altered. The "small" anneal consists of heating the crystal to about 350° C. (thermocouple temperature) in 3 or 4 minutes, then cooling to room temperature by radiation and conduction. The more complete anneal consists of heating the crystal at 750° C. for at least 30 minutes, after which the heating power is gradually reduced to zero during 1 hour.

The control and determination of gas pressure and the method of observation for different gas exposures are similar to those described previously (3).

Results and Discussion

The following observations furnish evidence of molecular adsorption.

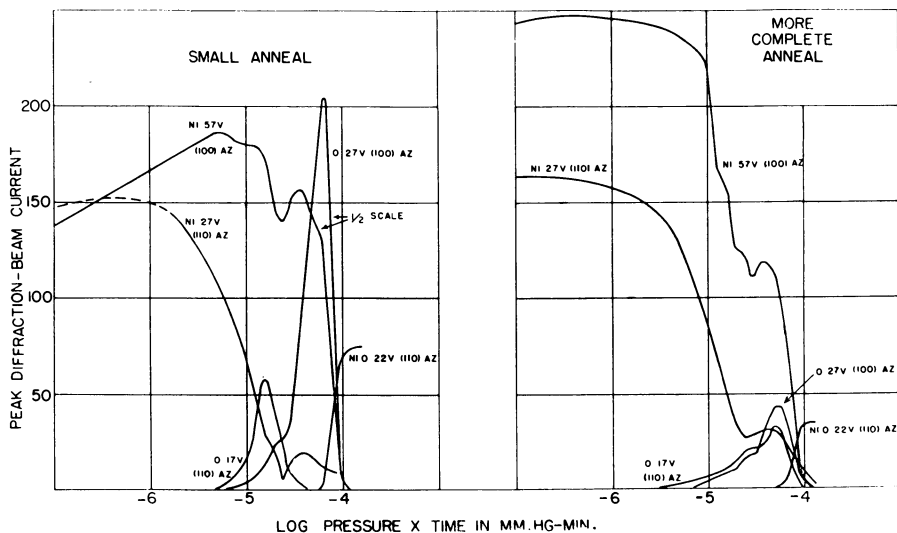
1. As oxygen adsorbs on the nickel surface, the intensity of the diffraction pattern from the nickel lattice decreases, because of the low penetrating power of the electrons and the high scattering power of the adsorbed oxygen. In Figure 2 are shown certain characteristic diffraction beams in the form of colatitude curves.



COURTESY *Journal of Physical and Chemical Solids*

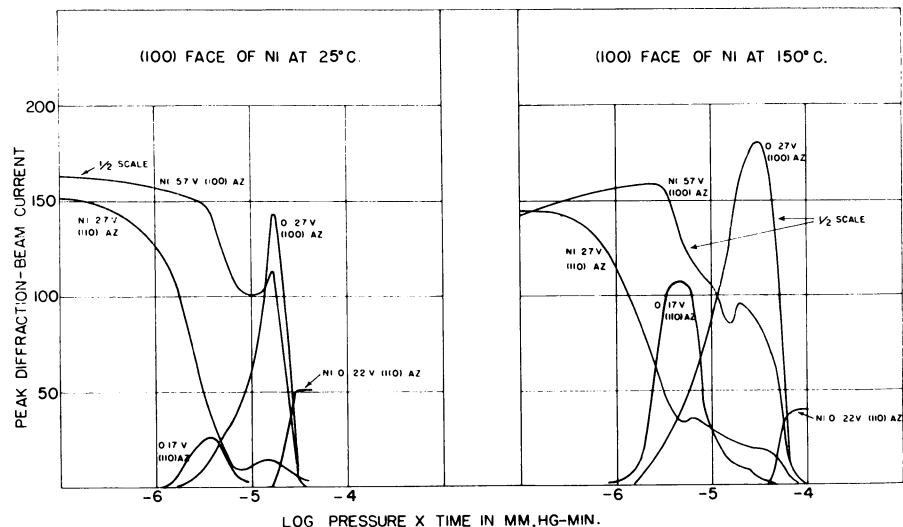
Figure 2. Colatitude curves of diffraction-beam current against colatitude angle for five typical diffraction beams

1. Clean nickel lattice in (110) azimuth at 27 volts. Multiply current scale by 10
 2. Clean nickel lattice in (100) azimuth at 56 volts. Multiply current scale by 20
 3. Double-spaced, face-centered lattice of chemisorbed oxygen in (110) azimuth at 17 volts. Multiply current scale by 6
 4. Single-spaced, simple-square lattice of chemisorbed oxygen in (100) azimuth at 27 volts. Multiply current scale by 10
 5. Nickel oxide lattice on crystal surface in (110) azimuth at 22 volts. Multiply current scale by 5
- 3, 4, 5. Obtained after oxygen exposure at room temperature



COURTESY *Journal of Physical and Chemical Solids*

Figure 3. Peak current vs. \log_{10} (pressure \times time) for five diffraction beams shown in Figure 2, after argon ion bombardment of crystal surface followed by anneals



COURTESY *Journal of Physical and Chemical Solids*

Figure 4. Peak current vs. \log_{10} (pressure \times time) for five diffraction beams shown in Figure 2, after intermediate anneal

Exposures at temperatures indicated

The intensities of these five beams, as represented by the peak maximum corrected for background, are plotted in Figure 3 as a function of exposure to oxygen. The rate of decrease of the beams from nickel with increasing exposure is approximately the same for a surface which has been well annealed as for one which has received a small anneal after ion bombardment cleaning. (The initial increase of the 57-volt

beam for the small anneal is attributed to an annealing effect of the crystal.) In both cases these beams are extinguished by an exposure of about 10^{-4} mm. of Hg \times minutes. However, the diffraction patterns from the gas lattice structures on the surface with the small anneal are much more intense than those from the gas lattice structures on the well annealed surface, because of the different defect densities in the lattices. If the extinction of the pattern from nickel were due to the presence of the gas lattice structures, one would expect a greater rate of extinction for the surface having a small anneal. Since this is not the case, it appears that the major part of the extinction is due to an amorphous structure on the surface, which is independent of the defect density.

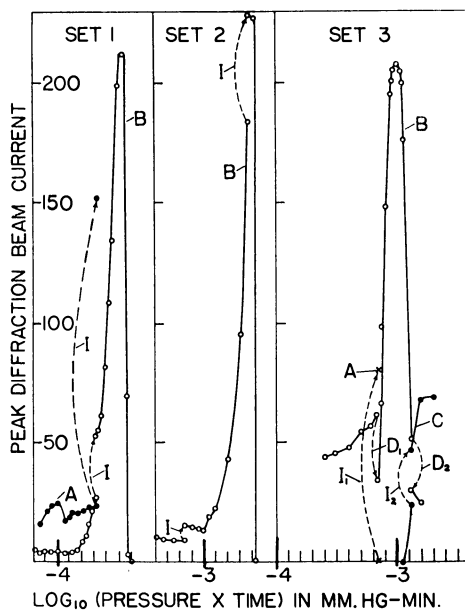


Figure 5. Changes in beam intensity (dashed lines) caused by allowing crystal to remain in vacuum several hours after exposure to oxygen

Multiply ordinate scales by 2 to obtain intensities of curves B

- A. 17-volt diffraction beam in (110) azimuth from double-spaced, face-centered structure
- B. 27-volt diffraction beam in (100) azimuth from single-spaced, simple-square structure
- C. In set 3, 22-volt diffraction beam in (110) azimuth from NiO structure

2. Intensities of the diffraction patterns from gas lattices formed at 150° C. are considerably greater than those formed at 25° C., as shown in Figure 4. However, the rates of extinction of the diffraction patterns from the nickel lattices are approximately the same in the two cases. Thus, these results lead to the same conclusion as in 1.

3. Changes occur in diffracted beam intensity with time of standing in vacuum subsequent to various oxygen exposures. Figure 5 shows several plots of peak diffraction beam current as a function of \log_{10} exposure. The curves in sets 1

and 2 show increases, I , in beam intensities of gas structures which have occurred as a result of conversion of the adsorbed amorphous molecular oxygen into atomic oxygen in a lattice structure. The curves in set 3 show two increases and two decreases in intensity— I_1 , I_2 and D_1 , D_2 , respectively. Decrease D_1 and increase I_1 represent a conversion from one lattice structure to another. Decrease D_2 and increase I_2 represent a conversion from the place exchange structure to the oxide structure. Tests show that these changes are not due to adsorption from the residual ambient. Earlier observations (4) were less detailed and failed to note these changes in intensities with time in vacuum.

Curves 1 and 2 of Figure 6 show that the electron energy, corresponding to the maximum development of the beams from the nickel lattice, changes with the amount of oxygen exposure. However, the diffraction angle also changes in a way such that the plane grating formula is satisfied without a change in the surface lattice spacing. This indicates that the crystal inner potential is altered by the exposure to oxygen, but the surface lattice spacing is unchanged.

Curve 3 in Figure 6 shows how the photoelectric work function, ϕ , of the crystal (after a small anneal) changes with exposure to oxygen over the range of exposures from 0 to that necessary to form an oxide. The initial increase in ϕ due to adsorption is followed by a broad maximum and a subsequent rapid decrease due to oxide formation. Because of the large value of ϕ in the region of the broad maximum, the accuracy is low. Although it is impossible to determine the exact exposure at which ϕ begins to decrease, this decrease occurs at exposures too small for the formation of the oxide.

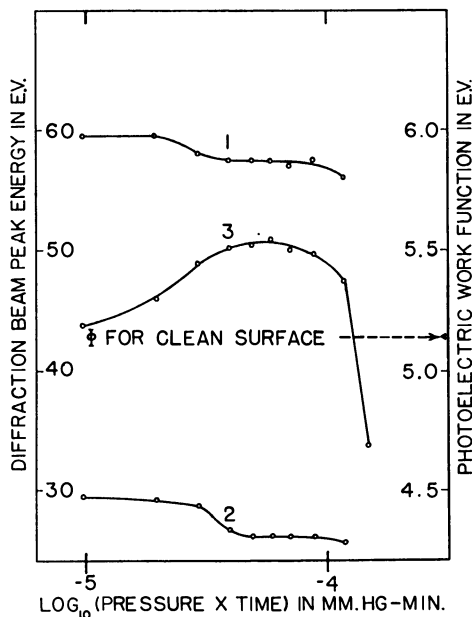


Figure 6. Work function and maximized diffraction beam energy vs. \log_{10} (pressure \times time)

- 1, 2. Peak voltage for beams from nickel lattice vs. \log_{10} exposure (small anneal)
3. Work function vs. \log_{10} exposure (small anneal)

The results of more precise observations over a small range of exposure, in the region just preceding oxide formation, are shown in Figure 7. ϕ is decreasing in the exposure range of the intense single-spaced, simple-square (s-s, s-s) structure which just precedes the formation of the oxide structure. This suggests that a place exchange occurs in the exposure range preceding oxide formation and that the intense s-s, s-s structure is due to this exchange. Additional evidence of this exchange is furnished by the observation that the lattice constant of this structure is 2 to 5% greater than that of clean nickel.

Although the Fowler method of determining the work function does not apply to semiconductors, the experimental data fit the theoretical Fowler curve for all of the surface conditions preceding the oxide formation, indicating that for these observations the surfaces formed by both adsorption and place exchange exhibit the characteristics of a metal. When nickel oxide forms, the data fail to fit the theoretical curve, as would be expected for a semiconductor. The estimated value of ϕ for the oxide was obtained by fitting the experimental points near the high frequency end to the curve, since it has been found in this laboratory (1) that the values of ϕ thus obtained for germanium and silicon are near those obtained by using the contact potential difference method. Although the value of ϕ for the nickel oxide is only approximate, we believe that the trend of the change in ϕ is reliable.

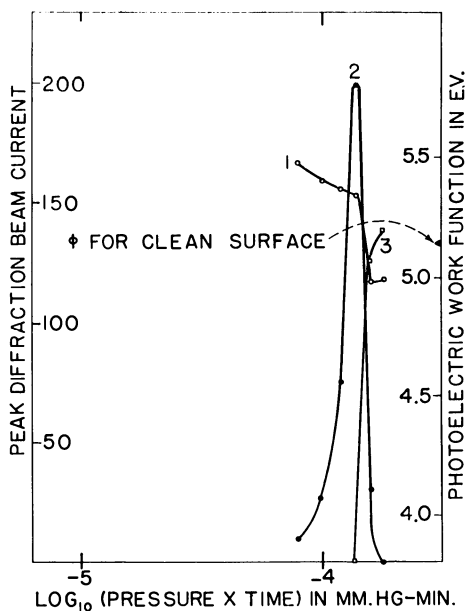


Figure 7. Work function and peak diffraction beam current vs. \log_{10} (pressure \times time)

1. Work function vs. \log_{10} exposure
2. Intensity of 27-volt beam from single-spaced, simple-square structure as function of \log_{10} exposure. Multiply ordinate scale by 4
3. Intensity of 22-volt beam from nickel oxide lattice as function of \log_{10} exposure

Literature Cited

- (1) Dillon, J. A., Jr., Brown University, private communication.
- (2) Farnsworth, H. E., Schlier, R. E., George, T. H., Burger, R. M., *J. Appl. Phys.* **29**, 1150 (1958).
- (3) Farnsworth, H. E., Tuul, Johannes, *J. Phys. Chem. Solids* **9**, 48 (1959).
- (4) Fowler, R. H., *Phys. Rev.* **38**, 45 (1931).

RECEIVED May 9, 1961. Work assisted by the Office of Ordnance Research [now Army Research Office (Durham)], U. S. Army. Figures 2, 3, and 4 taken from a paper by Farnsworth and Tuul. (3).

Some Surface Properties of an Artificial Halozeolite

Examination of the Contributions of Dispersion and Electrostatic Terms to the Heat of Adsorption on Aluminosilicates

PETER CANNON

*General Electric Research Laboratory,
Schenectady, N. Y.*

An artificial halozeolite was prepared by a heterogeneous substitution reaction. The surface behavior of the material was studied, and the molar integral heat of adsorption of argon thereon was determined at $\bar{T} = 83.8^\circ \text{K}$. The results are simple but differ from the usual class of results obtained with zeolites, especially at low coverage. The low early values of the integral heats are accounted for on the basis of pure dispersion (r^{-6}) interactions between the host and the sorbate: The subsequent values correspond to the self-interactions of the argon atoms, as in the case of the unsubstituted material. The salient difference in the low coverage results arises from the nonavailability of Ca^{+2} ions in the halozeolite. The general question of the correlation of observed thermodynamic quantities with the various dispersion and electrostatic forces is discussed.

In physical adsorption involving simple binary elementary systems, the observed interaction energies are properly and simply accounted for by the attractive dispersion forces existing between the particles of the two phases at the interface. Since these forces involve primarily the medium-range (3 to 7Å.) forces between outermost or valence electrons, it is also possible to estimate the forces between species in which the LCAO approximation is valid, or in which one or other of the phases may be treated as a semi-infinite electronic continuum, provided no net charge transfer results from the interaction. It is unfortunate that such approximations fail in some of the most interesting and technically rewarding cases, especially where the adsorbent is a complex aluminosilicate. This complication is due to the presence of cations, necessary to compensate for the electric charge imbalance produced by the presence of tetrahedrally bound aluminum in the lattice.

One approach to the problem is to regard the lattice as equivalent to an incompressible geometric form, and to think of the sorbate as being contained in an equivalent potential box. On this basis, the charge-compensating cations may be neglected, and from this model, one may obtain a fairly accurate idea of the change in heat content of the sorbed phase with respect to concentration. This approach has been used successfully by Barrer and Stuart (2) and by Kington (10) and has been applied by the author (6) to explain the changes in enthalpy of the sorbed phase at high coverage. However, it is not an adequate treatment at low coverage, especially when the sorbate is composed of particles sufficiently small to "resolve" or be severally affected in different ways by the different components of the lattice (9). This type of effect also appears to be responsible for the decomposition of some sorbates by bare aluminosilicate lattices (4, 5).

The question of which lattice components to include in the interpretive analysis reduces to the experimental problem of comparing systems of similar geometry but which contain different species in the lattice—e.g., Ge or Th in substitution for Si (1); S or F in substitution for O or OH, and say 2Na^+ for 1Ca^{+2} . The effect of change of cation is well known. In limiting cases it modifies the Molecular Sieve effect in zeolites. For host substituents, the availability of suitable systems is limited. The present work offers a comparison between a normal aluminosilicate and the same species after subjection to a substitution of halogen for oxygen and hydroxyl.

Experimental

A difficulty in running substitution reactions with these materials is that it is easy to destroy the geometry of the lattice, especially when acid sites are created, even, temporarily, in the lattice. Thus, when CHClF_2 is sorbed by the zeolite Calcium A (4), a marked increase in amorphous background is found when the solid is examined by x-ray diffraction (5). The reaction employed here therefore involved a fully substituted halomethane, CF_2Cl_2 . Zeolite Calcium A sorbs CCl_2F_2

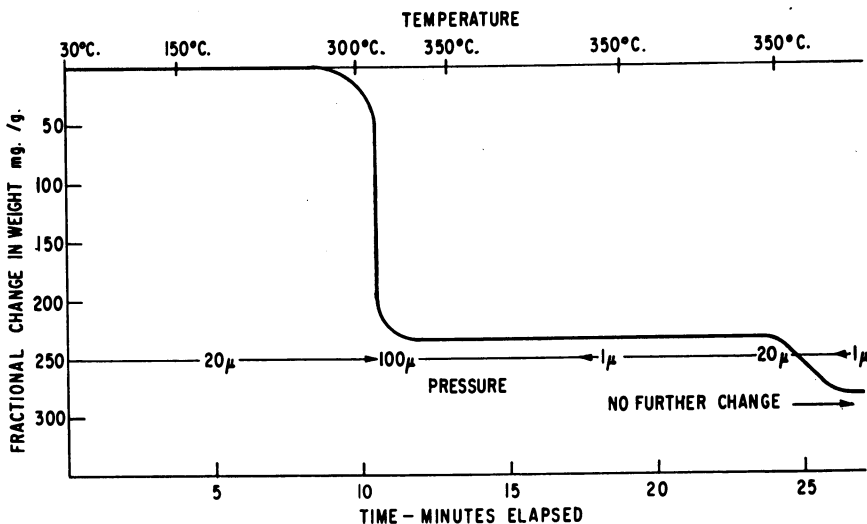


Figure 1. The endotherm for Zeolite A- CCl_2F_2

slowly, equilibrium at any particular initial dose being reached in 12 to 48 hours (5). The equilibrium uptake is similar in terms of liquid volume sorbed to that for many other species, but attempts to remove the sorbate by simply pumping it off are unsuccessful. The effect of raising the temperature [as followed by a continuously recording vacuum balance system (8)] is also negligible, up to a temperature of 290° C. Thereafter, a rapid loss of weight and a considerable gas evolution occur (Figure 1). After the temperature has exceeded 350° C. no further weight change occurs and it is possible to obtain a high vacuum over the specimen. Since the final weight is not the same as the initial weight of bare zeolite, a definite chemical reaction has occurred.

Chemical analysis of the residual material yields the results given in Table I. The notable data are the halogen content and the limited availability of the calcium for base exchange. Infrared absorption peaks found for the clean and reacted material are shown in Table II. The important features are the appearance of a band ascribable to Si-F bonds and a shift in an Si-OH band. X-ray diffraction photographs indicate only a small increase in amorphous background and retention of the greater part of original pattern.

Several samples of this material were prepared, mixed, and sampled. The chemical analysis of that material used in the experiments described below was similar to that given in Table I.

Table I. Typical Analytical Results for a Halozeolite and Its Parent Type Ca-A

	(Per cent)	
	<i>Halozeolite</i>	<i>Ca-A</i>
SiO ₂	41.3	43.19
AlO ₂	37.2	42.40
Total Ca	12.1	14.41
Ca (exchangeable at 25°C. with 1 <i>N</i> NaCl)	0.26	~6
Total F	2.5	
Total Cl	6.3	
Water-soluble F	0.12	} 25°C.
Water-soluble Cl	0.13	
All on ignited samples; weight lost by sample at 25°C. from weight in equilibrium with summer moist air (RH 85%), 17.8%		22.2%

Table II. Principal Features of Infrared Spectra of Halozeolite and Parent Ca-A Frequency^a

	(Cm. ⁻¹)			
<i>Halozeolite</i>	<i>Structure</i>	<i>Ca-A</i>	<i>Structure</i>	
3600 (s)	OH	3640 (s) 2670 (s)	OH	
1640 (m)	H ₂ O	1630 (m) 1125 (m)	H ₂ O	
1010 (s)	SiO	1010 (vs) 920 (vs)	SiO	
700 (w)	Si-F			

^a Spectra of the summer air-equilibrated halozeolite were obtained from KBr pelletized samples containing 0.2 to 2% (w./w.) of sample. The absorption bands were very broad, making it difficult to define the maxima. Data for the parent substance are from Breck *et al.* (3).

Adsorption Experiments

The apparatus, techniques, and primary data corrections used in this laboratory have been fully described (7).

In general, adsorption isotherms obtained with this and other zeolitic substrates are of Brunauer's Type I, the simple hyperbolic form also known as the Langmuir isotherm. Consequently, the asymptotic limit of adsorption is used instead of the value of V_m normally derived from the BET evaluation of specific surface area. It is, of course, not possible to define exact monolayer or multi-layer adsorption in these three-dimensional interconnected pore systems.

The adsorption of rigorously dried CO_2 at 29.6°C . on this halozeolite gave a Type I isotherm and a saturation uptake corresponding to a specific surface area of 546 sq. meters per gram. This may be compared with $\Sigma = 592$ for CO_2 on clean Calcium A. A similar experiment with CHClF_2 vapor gave an inflected isotherm (Figure 2), which appears to consist of an early portion which is a simple Type I, followed by another portion which corresponds in magnitude to adsorption of the vapor on the outside of the zeolite particles. The second portion is not well developed below ~ 3000 mm., and this type of secondary development may be more general than is normally thought, since adsorption measurements are rarely made at supra-atmospheric pressures. In this system no decomposition of the CHClF_2 was seen, in marked contrast with the CHClF_2 -Calcium A reaction.

In the CO_2 case, the adsorption potential (approximately $RT \ln p/p_0$) was lower at any particular value of coverage fraction than in the case involving the

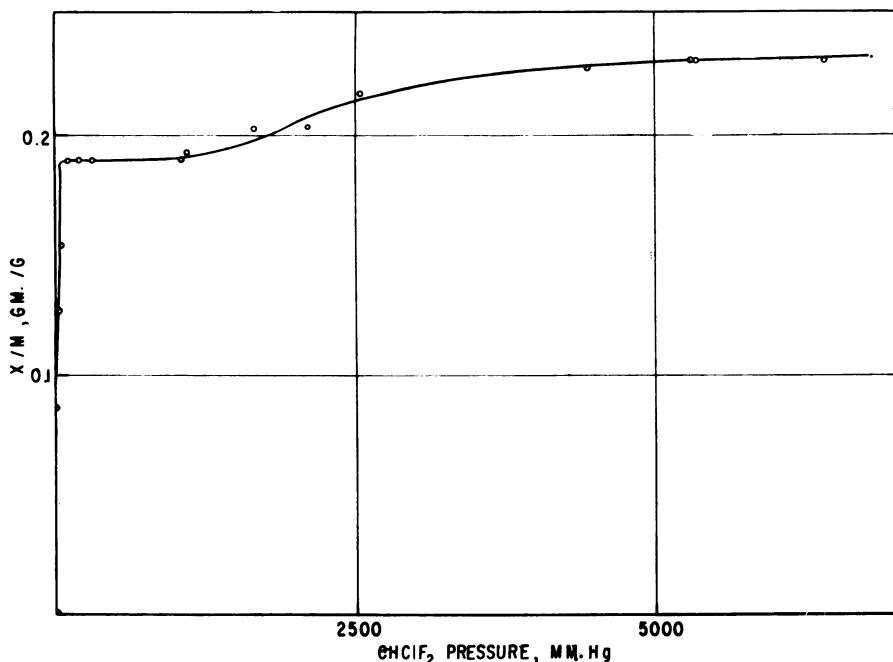


Figure 2. Isotherm of CHClF_2 on halozeolite at 29.6°C .
System fully reversible

clean zeolite. Thus, the surface energy of the solid appeared to be substantially lowered as a result of the halogenation reaction.

The adsorption of argon at low temperatures on this halozeolite also confirms these observations. The low pressure data obtained at 77.4 and 90.2° K are shown on Figure 3 and the isosteric heat of adsorption on Figure 4. The high pressure data conform to a Type I isotherm. It is immediately evident that there is a considerable difference between these results and the type of result normally obtained with these solids (we are comparing thermodynamically inexact quantities and a direct interpretation of the value of an isosteric heat is not possible). This sort of data is best converted into an exact differential or even a molar integral quantity (see Figure 5) before attempting analysis. Exceptions to these statements occur only at integral values of Θ .

Discussion

We may write a total interaction energy between a gas and a solid thus:

$$U = - \left(\frac{\delta \ln Q_N}{\delta \beta} \right) V$$

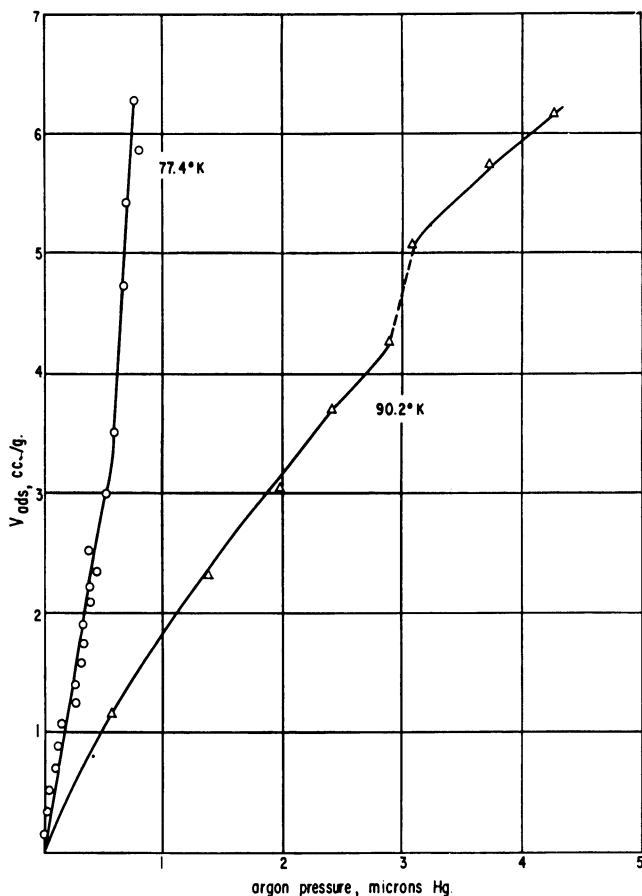


Figure 3. Low pressure isotherm data for argon on halozeolite

Small reversal of slope in 90.2° K plot appears reproducible

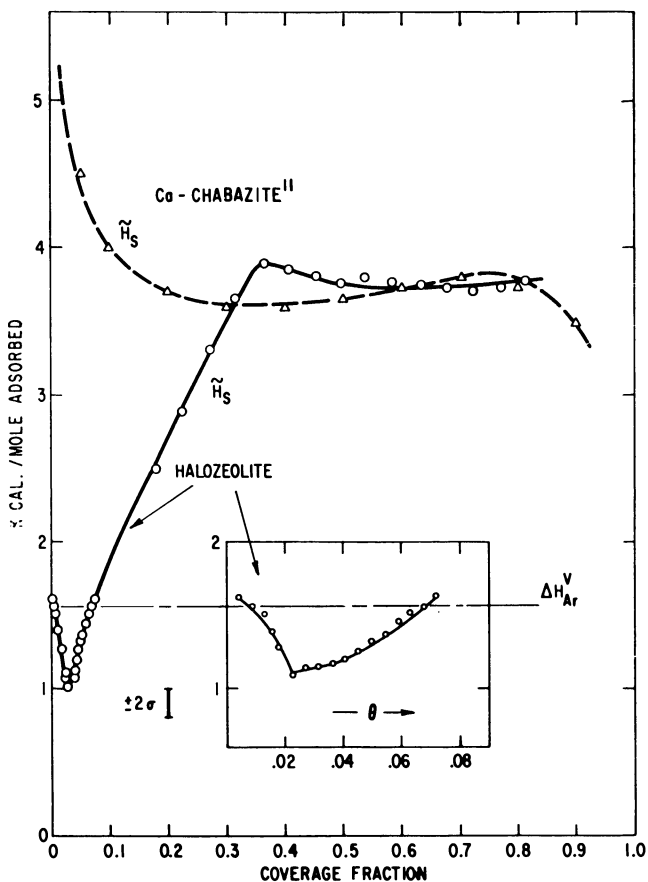


Figure 4. Isosteric heats of adsorption of argon on halozeolite and on Ca-chabazite (11)

$$\bar{T} = 83.8^\circ \text{K}$$

where Q_N is the partition function describing the number of states accessible to the system and where β contains T^{-1} . It is also possible to write this equation in terms of a sum of the kinetic and potential energies of the system by standard statistical mechanical methods. The variation of U (which is a molar integral quantity) with respect to the particle concentration, or surface coverage, then corresponds to the differential energy of adsorption. The only part of this quantity which can change in a nonlinear manner with respect to coverage (if there is no phase change in the ad-film) consists of the potential terms, which can be expressed in the integral form for a two-particle (gas-solid) system thus:

$$U = \text{kinetic energy} + A\left(\frac{r}{r_o}\right)^{-6} + B\left(\frac{r}{r_o}\right)^{-8} + C\left(\frac{r}{r_o}\right)^{-10} + D\left(\frac{r}{r_o}\right)^{-12}$$

where $A, B, C,$ and D are constants and $\left(\frac{r}{r_o}\right)$ is the ratio of average interparticle distance to equilibrium separation distance in the bulk case. It is evident that r is inversely proportional to the square root of particle density or coverage fraction

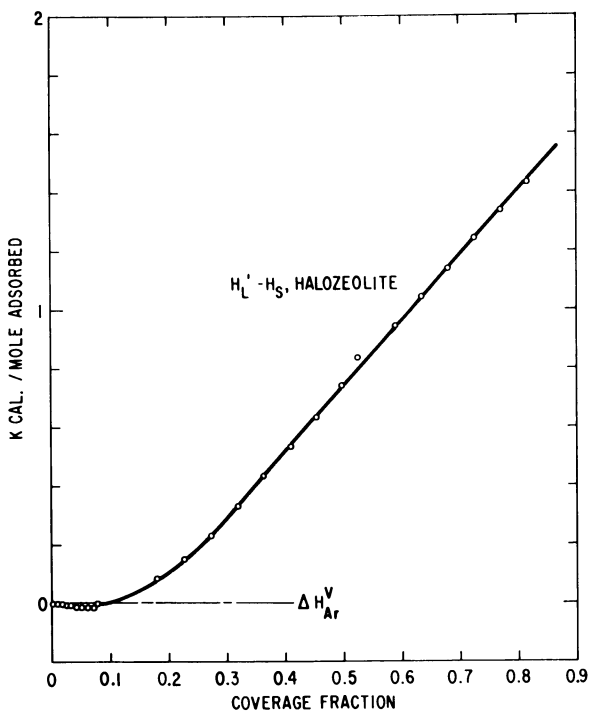


Figure 5. Molar integral heat of adsorption ($H_L' - H_S$) of argon on halozeolite

$$\bar{T} = 83.8^\circ \text{K}$$

for a two-dimensional film, and that at large values of $\left(\frac{r}{r_0}\right)$ (low coverage), only the terms with the smallest exponent will be significant.

It is possible to give physical significance to the various power terms. Thus:

$\left(\frac{r}{r_0}\right)^{-6}$ contains dispersion-attraction energy plus dipole-dipole attraction.

$\left(\frac{r}{r_0}\right)^{-8}$ contains dipole-quadrupole attraction.

$\left(\frac{r}{r_0}\right)^{-10}$ contains quadrupole-quadrupole attraction.

$\left(\frac{r}{r_0}\right)^{-12}$ contains dispersion-repulsion energy.

As might be expected, there is a very large variation in the magnitudes of these terms at some normal or standard concentration. Thus, at a monolayer coverage, these terms will have approximate upper limits of 10^4 , 10^3 , 10^2 , and 10^1 cal. per mole, respectively, when the induced moments are taken into account along with the permanent ones. At low coverages, the relative differences will be even greater, and we may expect to be able to account for the observed interaction heats on the basis of pure dispersion-attraction and simple dipole interactions.

The present results fall in line with this picture. If we consider the components of the lattice which the argon is likely to see, we must include F, F^- , Cl, Cl^- , O^{-2} , and Ca^{+2} , though, in view of the stability of $CHClF_2$ in this adsorbent,

it seems unlikely that any Ca^{+2} ions are in fact exposed. Additional support for the nonexposure of Ca^{+2} is gained by the nonappearance of a superlattice x-ray diffraction pattern when vapors are adsorbed on the halozeolite. In the case of the parent zeolite, the intensification of lines at $d \sim 2a_0$ was interpreted (6) on the basis of a migration and ordering of the cations together with the adsorbed phase.

In order to compute the approximate magnitude of the term in r^{-6} , it is necessary to know the polarizabilities and diamagnetic susceptibilities of the components considered in the interaction. Where these could not be found in the literature, they were calculated from the Slater average electron orbit radii using the relations

$$\bar{r}_k^i = \left[\frac{2(Z - S_i)}{n_i^*} \right]^k \left[\prod_{j=1}^k (2n_j^* + j) \right] a_0^k$$

$$\alpha = \frac{4}{9a_0} \sum_i (\bar{r}_i^2)^2$$

$$\bar{N}_X^{(m)} = \frac{Ne^2}{6mc^2} \sum_i \bar{r}_i^2$$

where \bar{r}_i is the k th power of the average orbital radius of the i th electron, n_i is the effective principal quantum number of the shell, Z is the atomic number, S_i is the Slater screening constant associated with the i th electron, and a_0 is the Bohr radius of hydrogen.

The values so derived are then used in the well known Kirkwood-Müller expression

$$E = 6mc^2 \frac{\alpha_1 \alpha_2}{x_1 + x_2} \frac{1}{d^6}$$

where subscripts 1 and 2 refer to the two components of the system, and d is a characteristic interparticle distance. The values of d used here are the arithmetic means of the ionic or atomic radii of the solid component and the van der Waals radii of the sorbate in the liquid state.

The following values are then obtained:

Ar/F	0.83 kcal./mole
Ar/F ⁻	2.2 kcal./mole
Ar/Ca ⁺²	7.4 kcal./mole

Since these values are controlled primarily by the state of the outermost electron shell, the values for Ar-Cl and Ar-Cl⁻ are like those given for F and F⁻. It is immediately apparent that the integral heat of adsorption of argon near $\theta = 0$ on our halozeolite is explicable on the basis of an interaction between argon and the electronegative components of the lattice, and because of the initially flat nature of the heat plot, there is no indication of any interaction with the Ca^{+2} ions. The relatively linear increase of the observed heat at higher coverages is apparently due to the commencement of Ar-Ar interactions with a normal energy value, heightened slightly by the unusual geometry of the lattice.

Influence of a Permanent Electric Moment on the Heat of Adsorption of a Gas or Vapor

So far in this discussion, the contribution of an electric moment interaction with an ionic field has been neglected. This is justifiable on the basis of the observed results, but Kington and Macleod (11) recently found a correlation between a heat of adsorption term and the permanent quadrupole moment of the gas involved, and from this correlation they concluded that a major part of the energy heterogeneity in adsorption may be laid to the interaction between the quadrupole and the position-dependent field gradient in the solid. It is therefore necessary to examine this idea in the present context.

Kington and Macleod's energy term consists of the difference between the isosteric heat values observed at two coverages for a variety of gases on a sample of chabazite. Since this corresponds to the difference between two (inexact) differential coefficients, it is not easy to give this quantity any physical significance. These terms were found to give a linear correlation with the quadrupole moment of the gas. Assuming for the moment that the heat term does reflect some direct measure of the quadrupole-ion field interaction, we may evaluate the magnitude of this interaction from the quadrupole moment times the ion field gradient. This amounts to approximately the same amount of energy as that in a simple dipole-dipole interaction. This part of the dispersion interaction energy between an ion of charge C_b and a (nonpolar) molecule a is given by the second term in the equation

$$\phi = -\frac{C_b^2 \alpha_a}{2r^2} - \frac{3\alpha_a \alpha_b h\nu_0}{4r^6}$$

For monopositive ions and the gases Ar, H₂, O₂, N₂, and CO₂, the second term is between 18 and 60% as large as the first, which corresponds to the ion-induced dipole interaction. For bipositive ions, the contribution of the second term is only 5 to 15% that of the first. Thus, although the ion-quadrupole interaction is not negligible, it is small compared with the total. The pure quadrupole-quadrupole interaction is of course a much smaller contribution. The absolute maximum magnitude of the second term above is about 1300 cal. per mole for any of the above combinations (CO₂ and Li⁺) and the minimum value is about 700 cal. per mole (H₂ and K⁺).

For argon-Ca⁺², the only case to be considered in the present study, the appropriate value of field-quadrupole interaction is approximately 1300 cal. per mole, but the ion-induced dipole-ion field interaction is nearly 6000 cal. per mole, the sum of both being directly comparable with the value derived earlier for this pair from the Kirkwood-Müller expression. Since one may resort to complex reasoning for interpretive purposes only if a rationale cannot be achieved with simple truths (12), it is evident that we cannot *a priori* use the ion-quadrupole interaction to explain the results.

Part of this dilemma may be resolved by considering the earlier remarks regarding the integral nature of energies evaluated from the above type of calculation. If we are to succeed in correlating these quantities with any of the observed data, we might expect to have to use sums rather than differences of the isosteric heat values. When this is done, using Kington and MacLeod's data, the results are as shown in Table III.

On the basis of the above equation for the interaction energy of a gas molecule with a charged ion, we may reasonably expect a primary correlation to exist between the total heat and the polarizability of the gas. This is shown on Figure

Table III. Heat Terms Derived from Experimental Data (11)

Gas	$(q_{s^{10.01}} - q_{s^{10.30}})$, Cal./Mole	Est. Integral Heat = $\frac{(q_{s^{10.01}} + q_{s^{10.30}})}{2} - 2\Delta H^v$, Kcal./Mole
N ₂	1800	2.60
O ₂	560	1.14
Ar	420	1.18
CO	2400	3.6
CO ₂	4200	8.0
H ₂	1050	1.92

6, A, and the result is good. The only serious deviation from linearity is with H₂, the PVT behavior of which at low temperatures is subject to large quantum mechanical effects. Figure 6 also shows a fair correlation, B, between the total heat and a term α/d^2 , where d is as defined earlier, this term corresponding to the energy involved in field-induced polarization.

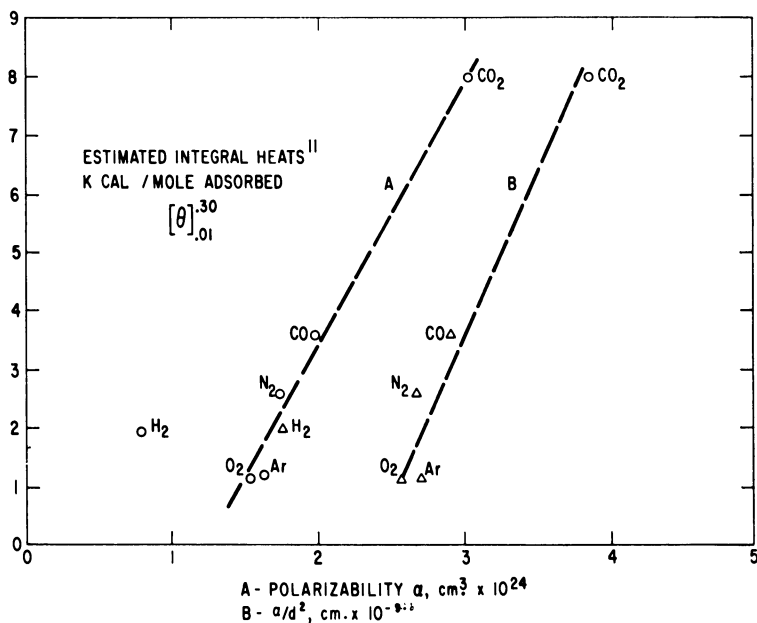


Figure 6. Correlation between integral heats of adsorption and electronic polarizabilities for various gases on Ca-chabazite (11)

Thus, the total ion-induced interaction energies correlate well with the experimental data, when the latter are handled in integral form, and under these circumstances, the excellence of the correlation of quadrupole moments with the experimental quantities is destroyed. Further, not only do the calculated quantities give a good correlation but they are sufficiently large to account for the estimated integral heats. It seems necessary to conclude that although ion-quadrupole interactions should not be neglected as a source of energy in adsorption (especially where monovalent ions are involved), they cannot be said to control the process, even in the case of unsubstituted Ca chabazite, and certainly not in the present

case, where the mutual induced-dipole interaction, or r^{-6} dispersion energy, will more than account for the observed energy release.

Literature Cited

- (1) Barrer, R. M., Baynham, J. W., Bultitude, F. W., Meier, W. M., *J. Chem. Soc.* **1959**, 195.
- (2) Barrer, R. M., Stuart, W. I., *Proc. Roy. Soc. (London)* **A242**, 172 (1957).
- (3) Breck, D. W., Eversole, W. G., Milton, R. M., Reed, T. B., Thomas, T. L., *J. Am. Chem. Soc.* **78**, 5963 (1956).
- (4) Cannon, P., *Ibid.*, **80**, 1766 (1958).
- (5) Cannon, P., *J. Phys. Chem.* **63**, 160 (1959).
- (6) *Ibid.*, p. 1292.
- (7) *Ibid.*, **64**, 858 (1960).
- (8) Cannon, P., *Rev. Sci. Instr.* **29**, 1115 (1958).
- (9) Gaines, G. L., *J. Phys. Chem.* **62**, 1526 (1958).
- (10) Kington, G. L., *Trans. Faraday Soc.* **52**, 475 (1956).
- (11) Kington, G. L., Macleod, A. C., *Ibid.*, **55**, 1799 (1959).
- (12) Occam, William of, "Dialogus," The Bavarian Court, ca. 1343.

RECEIVED June 27, 1961.

Pore Size Distribution of Porous Systems as Determined with an Automatic Adsorption Apparatus and Digital Computer

E. V. BALLOU¹ and R. T. BARTH

Gulf Research & Development Co., Pittsburgh, Pa.

An automatic apparatus for the determination of nitrogen adsorption and desorption isotherms has been used to characterize the pore size distributions of catalytic materials. Automatic operation allows either nitrogen adsorption to sample saturation, followed by desorption, or successive adsorption isotherms on successive samples. Data from the isotherms are transferred to punch cards for BET surface area and pore size distribution calculation by a digital computer. With the use of these mechanical and electronic aids, it is possible to study the structural effects of catalyst preparation techniques, sintering, metal impregnation, fluorination, and coking, on a scale heretofore practically impossible because of manpower and laboratory costs. In this manner, the original promise of these experimental and calculation methods is being fulfilled in research and development programs.

The design and operation of an automatic nitrogen adsorption apparatus have been described (1). The apparatus depends on the use of mercury pressure switches to control the action of electric valves, and thereby to introduce or remove unit quantities of vapor to or from the adsorption system. The essential features of the gas-handling system are shown in Figure 1.

The data output of the automatic apparatus is in the form of a pressure-volume record on a strip chart. The chart advance and chart pen drive operate in such a manner that the relative pressure scale reads horizontally and the volume scale reads vertically. The horizontal pen position records the difference in pressure between the vapor in equilibrium with the sample and that in a liquid nitrogen thermometer in the sample bath. The chart drive mechanism moves the chart 0.1 inch for each valve cycle involved in adding, or removing, a unit quantity of nitrogen gas.

¹ Present address, Missiles & Space Division, Lockheed Aircraft, Sunnyvale, Calif.

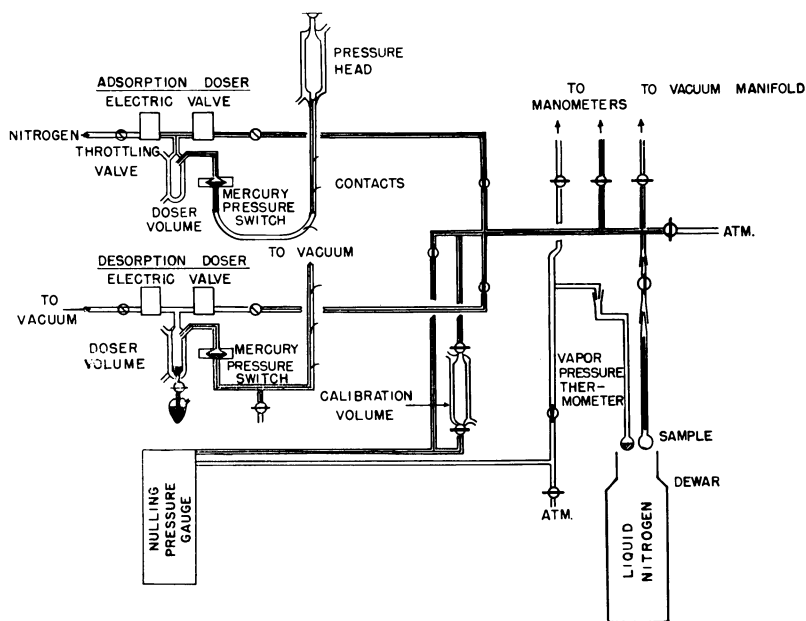


Figure 1. Gas-handling system of automated adsorption apparatus

The resulting chart record contains a point by point representation of each dose cycle. The apparatus has usually been programmed to deliver four or five consecutive doses, and then wait for equilibration. Only the equilibration points are read from the chart. The points on the chart record represent a pressure-volume relation which has not been corrected for the amount of vapor not adsorbed by the sample, the so-called "dead space correction."

The Barrett, Joyner, and Halenda (2) method of pore size distribution calculation requires data for the volumes of vapor adsorbed at 64 relative pressures, between 0.046 and 0.967. The volume of gas in the system at these pressures may be read from a smooth curve drawn through the equilibration points of the chart record or may be interpolated mathematically from a set of data points. In the procedure used, the pressure-volume points, and other data pertinent to the sample and the experiment, are listed in a form convenient to transcribe by key punch to IBM cards. The arrangement of the data on the punch cards is determined by the particular computer program. In this case, a program of the Barrett, Joyner, and Halenda method of pore size distribution calculation had been written for an IBM 704 data-processing unit.

Pore Size Distribution Data

The recorder chart record, and a portion of the data print-out sheet for an impregnated alumina sample, are shown in Figure 2. In the chart at the right, the nitrogen adsorption record starts at the bottom and proceeds stepwise across the chart. The record of the desorption curve then proceeds toward the upper left of the chart, inverting the usual representation of the desorption branch of the isotherm. The desorption process is discontinued before the pressure returns to zero. Two sections of the IBM 704 output sheet are at the left of the chart in Figure 2. The top section gives the data for the median and average pore radii of the sample,

```

PORE VOLUME DISTRIBUTION          FILE NUMBER      12424
AVERAGE RP      51.9
TOTAL PORE VOLUME 0.4683
SUM AP      193.5
2V/A      55.0
BE1 AREA      170.3
SLOPE      0.026
ADSORPTION CC PER DOSE      2.032

```

```

PORE VOLUME DISTRIBUTION          FILE NUMBER      12424
PORE RADIUS      VOL. PER CENT      AREA PER CENT
300 - 250      1.1      0.2
250 - 200      2.3      0.5
200 - 150      3.3      0.9
150 - 100      5.5      2.1
100 - 90      1.6      0.8
90 - 80      2.5      1.4
80 - 70      4.0      2.5
70 - 60      6.6      4.6
60 - 50      16.7      13.5
50 - 45      10.1      9.3
45 - 40      9.2      9.4
40 - 35      7.1      8.1
35 - 30      10.5      13.5
30 - 25      7.6      11.3
25 - 20      11.8      22.0
20 - 15      0.      0.
15 - 10      0.      0.
10 - 7      0.      0.

```

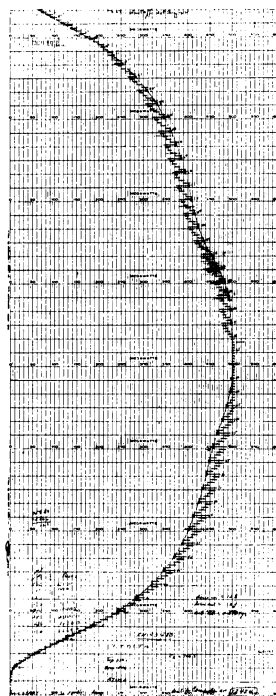


Figure 2. Chart record and portion of data print-out on an impregnated alumina of medium pore size

the BET surface area, and the sum of the pore areas. The bottom section gives the pore distribution in both volume per cent and area per cent in 18 pore radius ranges.

The complete output sheet from the computer contains a more detailed record of the calculated pore distribution, as well as the calculated isotherm. The complete output sheet for the sample mentioned above is shown in Figure 3. Details of the numerical data are not pertinent to this discussion. However, the type of data presented is of interest. The following information has been included:

At the top of the sheet, the sample file number, weight, and other descriptive material for the experimental run are given. Immediately below these, are listed the cubic centimeters of nitrogen, at standard temperature and pressure, adsorbed per gram of sample at the 64 pressure points used in the Barrett, Joyner, and Halenda calculation method.

Below the adsorption isotherm data, the detailed pore size distribution data are listed in seven columns. These include the pore radii corresponding to the 64 data points, the volume of liquid nitrogen desorbed at each step, the mean pore radii corresponding to each of the desorbed decrements, the pore volume per unit change in radius ($\Delta V/\Delta r$), the cumulative pore volumes at each pore radius, the calculated surface area in each of the pore radius steps, and the cumulative pore areas in pores larger than each of the listed radii. The print-out sheet is completed with the two sections discussed in connection with Figure 2.

PORE VOLUME DISTRIBUTION				FILE NUMBER		12424
CC PER DOSE	VAPOR OF NITROGEN	DEAD VOLUME FACTOR	WEIGHT OF SAMPLE	WT OF ADSORPTION	AMOUNT OF ADSORPTION	
1689	76.7	0.956	0.5947	240.0		
VOLUME - CC PER GRAM						
301.1	300.2	299.4	299.1	298.2		
297.6	296.3	295.3	293.4	292.3		
293.4	290.7	289.9	289.4	288.2		
287.4	287.1	285.7	284.9	284.1		
282.7	282.2	280.3	280.0	278.7		
277.0	273.4	274.3	271.8	270.9		
269.5	267.2	264.7	261.3	257.9		
232.4	244.0	238.3	221.9	204.2		
183.7	164.3	149.3	128.1	111.1		
93.7	89.6	86.1	82.6	78.4		
76.8	70.8	66.6	63.6	60.8		
38.6	33.9	33.3	31.0	27.7		
64.6	41.1	0.	0.			

PORE VOLUME DISTRIBUTION				FILE NUMBER		12424
RP	SV	PORE RADIUS	V=V/R-R	SUM VP	AP	SUM AP
43.	0.0289	47.3	0.0066	0.2931	18.20	87.26
40.	0.0233	42.3	0.0066	0.2383	13.61	102.87
35.	0.0333	37.3	0.0098	0.3776	10.17	129.04
30.	0.0264	32.3	0.0071	0.4129	7.13	150.89
25.	0.0271	27.3	0.0070	0.4679	5.69	176.58
24.	0.0264	24.3	0.0090	0.4569	7.37	183.76
23.	0.0254	23.3	0.0070	0.4640	3.99	189.73
22.	0.0254	22.3	0.0043	0.4693	3.81	193.23

PORE VOLUME DISTRIBUTION				FILE NUMBER		12424
RP	SV	PORE RADIUS	V=V/R-R	SUM VP	AP	SUM AP
299.	0.0014	295.0	0.0002	0.0016	0.11	0.11
280.	0.0014	285.0	0.0002	0.0002	0.11	0.22
270.	0.0004	275.0	0.0000	0.0000	0.03	0.25
260.	0.0014	265.0	0.0002	0.0002	0.12	0.37
250.	0.0013	255.0	0.0001	0.0007	0.12	0.49
240.	0.0018	245.0	0.0002	0.0007	0.17	0.63
230.	0.0013	235.0	0.0001	0.0002	0.13	0.78
220.	0.0002	225.0	0.0004	0.0001	0.06	1.12
210.	0.0018	215.0	0.0002	0.0001	0.19	1.31
200.	0.0011	205.0	0.0001	0.0000	0.13	1.44
193.	0.0014	197.3	0.0003	0.0000	0.17	1.61
190.	0.0013	192.3	0.0003	0.0000	0.16	1.77
183.	0.0014	187.3	0.0003	0.0000	0.18	1.94
180.	0.0013	182.3	0.0003	0.0000	0.17	2.11
173.	0.0009	177.3	0.0002	0.0000	0.12	2.23
170.	0.0006	172.3	0.0002	0.0000	0.11	2.33
163.	0.0022	167.3	0.0006	0.0000	0.33	2.66
160.	0.0013	162.3	0.0003	0.0000	0.19	2.83
153.	0.0013	157.3	0.0003	0.0000	0.19	3.04
150.	0.0021	152.3	0.0003	0.0000	0.33	3.39

PORE VOLUME DISTRIBUTION				FILE NUMBER		12424
AVERAGE RP	SV	PORE RADIUS	V=V/R-R	SUM VP	AP	SUM AP
TOTAL PORE VOLUME 0.4693						
SUM AP 193.3						
2V/A 55.0						
RET AP 170.3						
SLOPE 0.026						
ADSORPTION CC PER DOSE 2.032						

PORE VOLUME DISTRIBUTION				FILE NUMBER		12424
RP	SV	PORE RADIUS	V=V/R-R	SUM VP	AP	SUM AP
143.	0.0008	147.3	0.0002	0.0001	0.12	3.51
140.	0.0008	142.3	0.0007	0.0004	0.06	3.97
133.	0.0008	137.3	0.0002	0.0003	0.13	4.11
130.	0.0000	132.3	0.0003	0.0000	0.08	4.49
123.	0.0008	127.3	0.0007	0.0002	0.02	5.01
120.	0.0021	122.3	0.0003	0.0000	0.06	5.45
113.	0.0000	117.3	0.0003	0.0004	0.03	5.89
110.	0.0009	112.3	0.0010	0.0004	0.00	6.78
103.	0.0013	107.3	0.0004	0.0000	0.03	7.13
100.	0.0004	102.3	0.0006	0.0004	0.00	7.73
93.	0.0003	97.3	0.0009	0.0007	0.06	8.61
90.	0.0009	92.3	0.0010	0.0000	1.11	9.71
83.	0.0000	87.3	0.0013	0.0003	1.04	11.23
80.	0.0003	82.3	0.0013	0.0000	1.00	13.06
73.	0.0003	77.3	0.0003	0.0004	2.93	16.01
70.	0.0102	72.3	0.0000	0.0000	3.96	19.96
63.	0.0117	67.3	0.0003	0.0003	4.90	24.86
60.	0.0208	62.3	0.0000	0.0000	12.13	36.99
53.	0.0273	57.3	0.0001	0.0000	14.07	51.07
50.	0.0319	52.3	0.0000	0.0000	16.02	67.08

PORE VOLUME DISTRIBUTION				FILE NUMBER		12424
PORE RADIUS	VOL. PER CENT	AREA PER CENT				
300 - 250	1.1	0.2				
250 - 200	2.3	0.5				
200 - 150	3.3	0.9				
150 - 100	3.3	2.1				
100 - 90	1.4	0.8				
90 - 80	2.3	1.4				
80 - 70	4.0	2.9				
70 - 60	6.4	4.6				
60 - 50	16.7	13.3				
50 - 45	16.1	9.3				
45 - 40	9.2	6.0				
40 - 35	7.1	5.1				
35 - 30	10.0	13.3				
30 - 25	7.6	11.3				
25 - 20	11.8	22.0				
20 - 15	0.	0.				
15 - 10	0.	0.				
10 - 7	0.	0.				

Figure 3. Complete output data sheet from pore size distribution program on IBM 704 computer

Application of Automated Procedure and Computations to Catalyst Samples

Catalyst Impregnation. The adsorption and desorption isotherm record, and the essential pore size distribution data for a small pore silica-alumina catalyst, are shown in Figure 4. The sample pore size distribution was fairly sharp, in the 15- and 30-A. radii range, and the median pore radius was 27 A.

PORE VOLUME DISTRIBUTION FILE NUMBER 12437

AVERAGE RP 26.6

TOTAL PORE VOLUME 0.6572

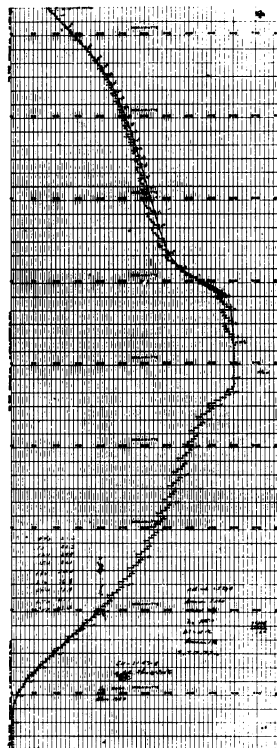
SUM AP 491.9

ZV/A 29.1

BET AREA 451.6

SLOPE 0.010

ADSORPTION CC PER DOSE 2.032



PORE VOLUME DISTRIBUTION		FILE NUMBER	
PORE RADIUS	VOL. PER CENT	12437	
300 - 250	0.3	0.0	
250 - 200	0.6	0.1	
200 - 150	0.7	0.1	
150 - 100	0.9	0.2	
100 - 90	0.3	0.1	
90 - 80	0.1	0.0	
80 - 70	0.3	0.1	
70 - 60	0.4	0.2	
60 - 50	1.1	0.5	
50 - 45	0.8	0.4	
45 - 40	1.3	0.8	
40 - 35	2.6	1.6	
35 - 30	4.9	3.5	
30 - 25	17.5	14.4	
25 - 20	50.9	54.2	
20 - 15	17.2	23.9	
15 - 10	0.	0.	
10 - 7	0.	0.	

Figure 4. Small-pore silica-alumina catalyst before impregnation

The adsorption and desorption record and calculated data for the same sample, after metal impregnation, are shown in Figure 5. The pore volume had dropped from 0.66 to 0.43 cc. per gram, the BET surface area had dropped from 452 to 351 sq. meters per gram, and the sum of the pore areas had dropped from 492 to 358 sq. meters per gram. At the same time, the median pore radius showed a small decline, from 27 to 24 A., and the pore size distribution had shifted slightly downward. A first step toward interpretation of these findings would be that this particular impregnation technique appeared to coat the surface of the catalyst uniformly in all size pores.

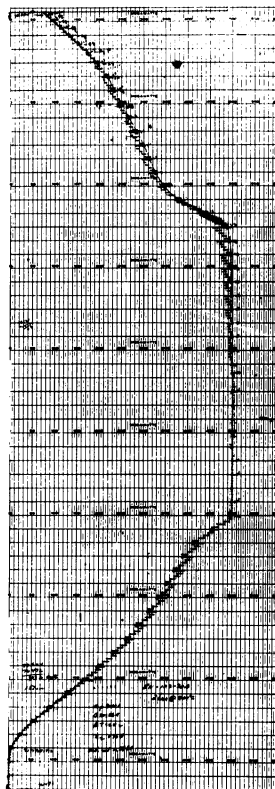
Catalyst Fluorination. The adsorption and desorption record and calculated data for a silica-alumina catalyst of low alumina content and a median pore radius of 78 A. were obtained. This indicated a fairly wide distribution of pore sizes in this material.

Fluorination of this catalyst altered the pore structure in the following way. The sample pore volume increased from 0.78 to 1.42 cc. per gram, and the median pore radius increased to 154 A. However, the BET surface area of the sample remained close to 228 sq. meters per gram. The total calculated pore area changed only from 226 to 216 sq. meters per gram. The surface area had probably de-

creased per unit particle volume, but remained the same per unit weight of catalyst. The data suggest that the fluorination step enlarged existing pores, but did not create new pores.

PORE VOLUME DISTRIBUTION
 AVERAGE RP 24.1
 TOTAL PORE VOLUME 0.4331
 SUM AP 358.6
 2V/A 24.7
 BET AREA 351.3
 SLO. λ 0.012
 ADSORPTION CC PER DOSE 2.032

FILE NUMBER 12431



PORE RADIUS	VOL. PER CENT	AREA PER CENT
300 - 250	0.6	0.0
250 - 200	0.7	0.1
200 - 150	0.8	0.1
150 - 100	0.6	0.1
100 - 90	0.2	0.1
90 - 80	0.3	0.1
80 - 70	0.6	0.2
70 - 60	0.7	0.3
60 - 50	1.1	0.5
50 - 45	0.6	0.3
45 - 40	0.8	0.4
40 - 35	2.1	1.2
35 - 30	4.4	2.8
30 - 25	9.8	7.3
25 - 20	43.3	41.8
20 - 15	26.0	33.2
15 - 10	7.3	11.6
10 - 7	0.	0.

PORE VOLUME DISTRIBUTION
 FILE NUMBER 12431

Figure 5. Small-pore silica-alumina catalyst after metal impregnation

Catalyst Coking. The adsorption and desorption records and the calculated data for a medium pore size, metal-impregnated, natural silica-alumina catalyst were obtained. The sample was tested in a pilot process unit until deactivated by coking. After coking, the pore volume dropped from 0.51 to 0.13 cc. per gram, the BET surface area dropped from 191 to 48 sq. meters per gram, and the calculated pore area dropped from 215 to 62 sq. meters per gram. There was a less marked decrease in the median pore radius, from 53 to 40 A., and the pore size distribution in general had shifted to smaller pore sizes. It is difficult to determine from these measurements alone how much coke covered the catalyst surface, and how much created new surface. Both area and pore volume in pores larger than 50-A. radius were practically eliminated by the coking.

General Application. The results treated above are a few examples of the type of catalyst modification which can be determined by nitrogen adsorption and de-

sorption experiments and pore size distribution calculations. In each case a more complete treatment could be made from the detailed pore size distribution results at small radius increments. The techniques of nitrogen adsorption and computation described here are not novel, but the use of automated equipment and electronic data processing allows pore size distribution data to be obtained in a routine manner, and for a large number of samples.

Possibilities of Further Automation

A further step in the application of automatic adsorption apparatus is to run a sequence of samples without operator attention. This has been accomplished for adsorption data alone, and, in principle, is possible with complete adsorption-desorption data.

A further step in automation would be to print out the pressure-volume data on tape, suitable for automatic transcription to punch cards. The prospects that this particular step will be of great value are limited by the slow rate at which adsorption and desorption data are accumulated.

Acknowledgment

O. K. Doolen, Instrument Development Division, Gulf Research & Development Co., largely devised the multiple sample apparatus. P. Ross and W. Frazier obtained the experimental data discussed.

Literature Cited

- (1) Ballou, E. V., Doolen, O. K., *Anal. Chem.* **32**, 532 (1960).
- (2) Barrett, E. P., Joyner, L. G., Halenda, P. P., *J. Am. Chem. Soc.* **73**, 373 (1951).

RECEIVED May 12, 1961.

Sticking Coefficients

FRANK M. WANLASS and HENRY EYRING

*University of Utah,
Salt Lake City, Utah*

Absolute reaction rate theory starts with the equilibrium concept for the transition state and then corrects the calculated equilibrium rate of change to nonequilibrium conditions by multiplying by a transmission coefficient, Ξ . For the sticking of molecules to a surface, the sticking coefficient is just this transmission coefficient. For the reverse process, of sublimation or of evaporation, the transmission coefficient is likewise required to correct the calculated equilibrium rate which is in general equal to the sticking coefficient. If one regards a condensed phase as a giant molecule, then evaporation or sublimation is a special kind of unimolecular reaction so that understanding such processes illuminates the entire field of unimolecular reactions. By taking account of the fact that the evaporation of physically adsorbed nitrogen molecules on tungsten is competitive with passage to the chemisorbed atomic state, the sticking coefficient can be explained. With increased surface coverage, the nitrogen molecules are more loosely held with a corresponding exponential increase in the rate of evaporation. Thus an interesting beginning has been made in understanding of rates of surface adsorption.

For reactions such as



the specific rate at which product is formed at equilibrium is very closely the specific reaction rate in the absence of products. Thus in the usual expression for the specific reaction rate constant

$$k' = \Xi \frac{kT}{h} K \neq \quad (2)$$

the transmission coefficient, Ξ , which corrects the equilibrium specific rate to non-equilibrium conditions is almost unity. On the other hand two hydrogen atoms, colliding in the absence of a third body, are stabilized to form a molecule only in the extremely rare circumstance that quadrupole radiation is emitted. Since about every eighth collision between three hydrogen atoms (3) at atmospheric pressure yields a stable molecule, a three-body collision is the important method for homogeneous recombination. The only factors difficult to estimate fairly accurately in Equation 2 are the activation energy, E_0 , which occurs in K^\ddagger , and the transmission coefficient, Ξ . Thus in the recombination of atoms or radicals where $E_0 \approx 0$ the only serious uncertainty is in Ξ . Similarly, the adsorption of molecules from a surface usually involves little or no activation energy, so that again the only uncertainty is in the sticking coefficient, S . S is just the transmission coefficient, Ξ , for the adsorption process.

Understanding the sticking coefficient is not only important for dealing with adsorption; it is also fundamental to a proper understanding of the general theory of all association reactions.

Pools at Equilibrium

When Equation 2 is written in the equivalent form

$$k' = \left(\Xi \frac{kT}{h} F^\ddagger e^{-\frac{E_0}{kT}} \right) / F_i \quad (3)$$

the quantity in parenthesis refers to the activated state and F_i is the partition function for the initial state. When the activated complex and the initial state are separated in space, they may be subjected to different conditions. Thus in homogeneous diffusion or passage across a phase boundary as in sublimation or vaporization, the activated complex and reactants may be environments with different temperatures, different concentrations, different dielectric constants, etc. Thus the question arises as to whether the reactant continually equilibrates with its surroundings or whether the activated complex still retains the properties it had at the last potential minimum even as it reaches and passes through the transition state.

The vaporization of a pure liquid or the reverse process, the condensation of the liquid, provides an interesting test of this delayed equilibration hypothesis. Thus as a hydrogen-bonded molecule, which vibrates in the liquid, separates from the surface it frees itself from the potential energy restrictions which prevented rotation. However, in so far as the evaporating molecule has insufficient collisions with neighbors to equilibrate to the free rotational partition function, f_g , of the gas, it will retain substantially the partition function, f_l , of the condensed phase even in the activated complex. Consequently for the condensation process the usual formula for molecules colliding, $\frac{p}{\sqrt{2\pi mkT}}$, per second per square centimeter must be multiplied by the factor f_l/f_g to give the rate of sticking to the surface. Thus f_l/f_g is the sticking coefficient, S , for liquids (5) in agreement with the available experimental evidence. Atoms, which have only translational degrees of freedom, do not necessarily stick on each collision with a surface and only every eighth triple collision between three hydrogen atoms redistributes energy sufficiently to yield a molecule (3). Delayed nucleation on a solid surface or in a solution is another example where sticking of atoms may be incomplete. Delayed equilibrium of energy in the coordinate joining a nitrogen molecule to a surface may thus decrease sticking by another factor in addition to that for rotation.

Sticking Probability for N_2 on Bare Tungsten as a Function of Temperature

Figure 1 shows the results of two experiments (2, 4) for the temperature-dependent sticking probability, S , of N_2 on a clean tungsten surface. Curve *A* is drawn through the experimental points obtained by Ehrlich; curve *B* is drawn through Kisiulik's data. Ehrlich claims his data, in addition to giving temperature dependence, is correct to within 5% in magnitude. Kisiulik's data are proportional only to S , thereby giving only the temperature dependence.

It is important to note in Figure 1 that both curves show a decrease with temperature, and it should be possible to fit *B* smoothly onto *A* by multiplying by a suitable scale factor, possibly as shown by the dashed line. To explain the data shown in Figure 1 the temperature dependence of f_g/f_θ is needed. The rotational partition function for a diatomic molecule that is free is

$$f_\theta = \frac{2IkT}{\sigma\hbar^2}$$

The rotational partition function for an N_2 molecule bound to a tungsten surface is more in doubt, but it would probably have very little temperature dependence if the molecule could turn or vibrate on the surface only with difficulty.

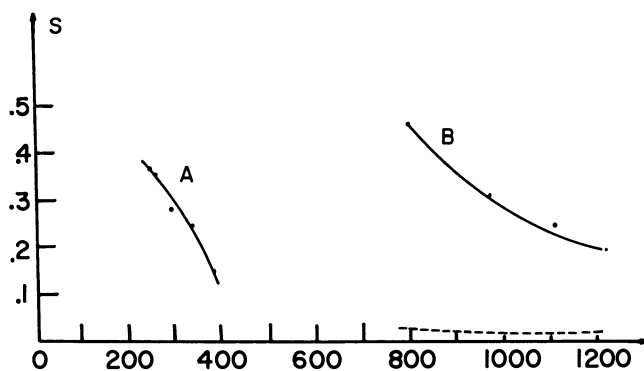


Figure 1. Comparison of data on sticking probability, S , of nitrogen on tungsten

It, therefore, might be reasonable for $S = \text{const } 1/T$. At least S now qualitatively decreases with temperature, as indicated in Figure 1. Further investigation is proceeding to see how well the data shown in Figure 1 can be fitted quantitatively and what account should be taken of slowness of translational degrees of freedom of the nitrogen to equilibrate.

Temperature Coefficient and Surface Coverage Dependence of Sticking Coefficient of N_2 on Tungsten

When a nitrogen molecule hits a tungsten surface, there will be some probability that it will be physically adsorbed. We denote this by S_0 and expect it will be essentially equal to the ratio of the adsorbed to the gas rotational partition functions of nitrogen. After the molecule is physically adsorbed, it will have to diffuse thermally to a strong binding site where it can stay permanently and thus be considered chemically bound. The rate of finding a particular type of

permanent site should be $k_1 \left(1 - \frac{\sigma}{\sigma_0}\right)$, where σ_0 is the number of permanent sites per square centimeter of surface and σ is the number already filled. There is the competing probability, k_2 , of a molecule's leaving the surface before it is chemically bound.

The sticking probability will, therefore, be

$$S = S_0 \frac{k_1 \left(1 - \frac{\sigma}{\sigma_0}\right)}{k_1 \left(1 - \frac{\sigma}{\sigma_0}\right) + k_2} \quad (4)$$

Rates k_1 and k_2 will both be of the form $\nu e^{-E_1/kT}$ and $\nu e^{-E_2/kT}$. We are going to assume that the desorption energy depends on surface coverage in the manner $E_2 = E_{20} - \alpha\sigma$, as Becker (1) found for cesium atoms on tungsten. Rewriting Equation 4 so that the dependence on surface coverage is plain, we get

$$S = \frac{S_0}{1 + \frac{b e^{a\sigma}}{\sigma_0 - \sigma}} \quad (5)$$

S_0 and b will both have temperature dependence, but we will not worry about checking their temperature dependence here. If b/σ_0 is small enough, S_0 should be the ordinate intercept of the curves in Figure 2; therefore S_0 should be easy to estimate for each curve.

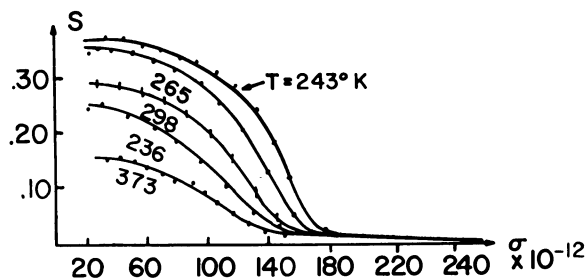


Figure 2. Temperature coefficient and surface coverage dependence of sticking coefficient of nitrogen on tungsten

In the following, Equation 5 will be fitted to the 298° K curve in Figure 2. For this curve we take $S_0 = 0.286$. Equation 5 can be rewritten as

$$\frac{b e^{a\sigma}}{\sigma_0 - \sigma} = \frac{S_0 - S}{S} = \frac{0.286 - S}{S} \quad (6)$$

There are three parameters, b , a , and σ_0 , to determine in this equation; therefore three points on the experimental curve will be needed. When the coordinates of three experimental points are put into Equation 6 three times, one obtains

$$\frac{b e^{72a}}{\sigma_0 - 72} = \frac{26}{260}, \quad \frac{b e^{117a}}{\sigma_0 - 117} = \frac{133}{153}, \quad \frac{b e^{145a}}{\sigma_0 - 145} = \frac{243}{43} \quad (7)$$

Eliminating b and a between the previous equations, one obtains

$$e^{45a} = 8.69 \left(\frac{\sigma_0 - 117}{\sigma_0 - 72}\right), \quad e^{73a} = 56.5 \left(\frac{\sigma_0 - 145}{\sigma_0 - 72}\right) \quad (8)$$

$$\left(\frac{\sigma_0 - 117}{\sigma_0 - 72}\right)^{1.62} = 1.712 \left(\frac{\sigma_0 - 145}{\sigma_0 - 72}\right) \quad (9)$$

It is found that $\sigma_0 = 262$ satisfies Equation 9, and using this value from Equation 8 we get $a = 0.042$, and from Equation 7 we get $b = 0.926$. Therefore, Equation 5 becomes

$$\frac{S}{S_0} = \frac{1}{1 + \frac{0.926e^{0.042\sigma}}{262 - \sigma}} \quad (10)$$

From Equation 10 it is justifiable that we assumed b/σ_0 to be small, since it was found to have the value $\frac{0.926}{262}$. Now we can write Equation 5 as

$$\ln(\sigma_0 - \sigma) + \ln \frac{S_0 - S}{S} = \ln b + a\sigma$$

or

$$\ln(262 - \sigma) + \ln \frac{0.286 - S}{S} = \ln b + a\sigma \quad (11)$$

If the left side of Equation 11—which can be obtained from the experimental curve—is plotted against σ , we should get a straight line if the theory we have proposed properly explains the data. Figure 3, which tests our hypothesis, is

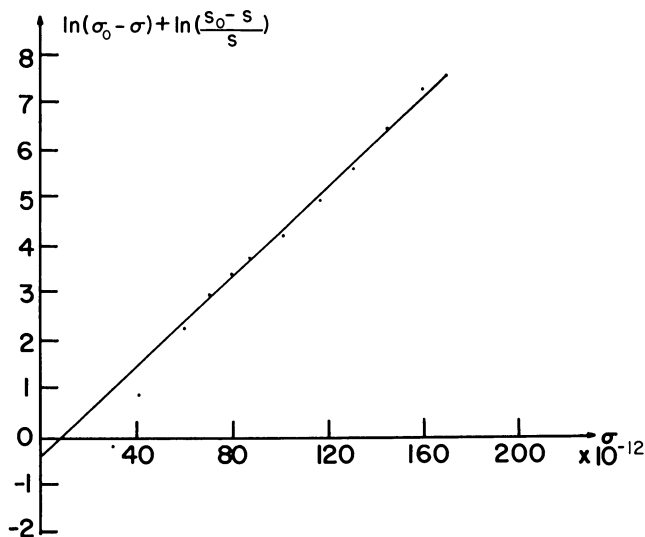


Figure 3.

satisfactory except near the origin. A slightly more complicated equation than $E_2 = E_{2_0} - a\sigma$ for the dependence of the energy of adsorption on surface coverage would improve the agreement. However, $k_1 \left(1 - \frac{\sigma}{\sigma_0}\right)$ stands for a rate which is to some extent composite, since it is the sum of the rates by which all other types of adsorption go over into adsorbed nitrogen atoms, while k_2 is the sum of the rates of all the ways the various adsorbed molecules, not yet adsorbed as nitrogen atoms, can disappear without being adsorbed as atoms. It will be interesting to continue the analysis further by breaking down these composite rate expressions.

Literature Cited

- (1) Becker, J., *Trans. Am. Electrochem. Soc.* **55**, 153 (1929).
- (2) Ehrlich, G. *J. Chem. Phys.* **34**, 29 (1961).
- (3) Eyring, Henry, Gershinowitz, Harold, Sun, C. E., *Ibid.*, **3**, 786 (1935).
- (4) Kisliuk, P., *Ibid.*, **30**, 174 (1959).
- (5) Mortensen, E. M., Eyring, Henry, *J. Phys. Chem.* **64**, 846 (1960).

RECEIVED July 17, 1961.

The Rate of Physical Adsorption at Low Surface Coverage

VICTOR R. DEITZ and FRANK G. CARPENTER

National Bureau of Standards, Washington, D. C.

The pressure decrease, following introduction of small amounts of argon or nitrogen to a freshly outgassed sample (diamond or graphite), showed a marked delay in adsorption at 77° or 90° K. The slow decrease was followed by a more rapid pressure decrease and then by a slower decrease until a steady state was reached. Delays up to 200 minutes were observed. Second and further additions showed no delay. A marked dependence was found on the temperature of pretreatment of the solid, which was systematically varied from -78° to 600° C. The behavior was highly reproducible. The coverage at steady-state adsorption was varied from 0.01 to 0.05. The delay does not appear to be due to limited heat transfer to the refrigerant. It was found to depend on the total time of cooling and not the time in contact of the solid with the adsorbate. This suggests that it may be due to a change in the adsorbing surface and is a function of the time that the surface spent at 90° K. after the thermal deactivation. The observed rate of adsorption is thus independent of the gas adsorption process.

The kinetics of physical adsorption were reviewed by Brunauer in 1943 (5). A careful literature survey (6) reveals that the present status of the subject is substantially unchanged. Elementary considerations indicate that the process of physical adsorption should proceed very rapidly and be practically complete within the order of magnitude of one minute, and indeed, experiment usually confirms this. Deviations from this behavior have been accounted for by the time required to dissipate the heat of adsorption or by a very slow surface diffusion into a microporous structure.

In the course of a study in this laboratory of the physical adsorption of argon and nitrogen on diamond and mineralogical graphite at 77° and 90° K and at low

coverages (8), a relatively slow rate of adsorption was sometimes observed. In view of the crystallinity of diamond and mineralogical graphite, the adsorption rate could not be ascribed to the porosity of the material. Only a minor fraction of the adsorbate could be accommodated by the cracks and fissures in the crystals. Neither can the new feature be attributed to the dissipation of the heat of adsorption or the sensible heat upon cooling.

The delay in adsorption takes place only upon the first introduction of gas to the solid and only when a very small amount of gas is introduced. The surface coverage corresponding to the final steady state is of the order of 1 to 5%. Moreover, the delay is very strongly dependent upon the thermal pretreatment of the solid.

This paper is concerned with a description of the experimental findings including the influence of thermal pretreatment. A subsequent paper will be concerned with the influence of the amount of gas introduced. The range of surface coverage which leads to the delay in adsorption is far removed from the usual region in which physical adsorption measurements are made, for example, in surface area determinations. This may be one reason why the delay has not been reported before.

Materials and Apparatus

The samples of mineralogical graphite and diamond used in these experiments have been described (8). Reproducible adsorption isotherms were reported at both 77° and 90° K for nitrogen and argon over a wide range of relative pressures. The volume of gas adsorbed at monolayer coverage for the diamond was 0.29 ml. per gram and for the mineralogical graphite 0.20 ml. per gram, corresponding to a surface area of about 1 sq. meter per gram. The industrial diamond powder used in the present experiments was further purified by repeated extraction with hydrochloric and hydrofluoric acids, washing to the disappearance of halides, and evacuation at 600° C. The chemical composition as determined by emission spectroscopy showed only traces of impurities at the limits of detection. The argon was passed through a charcoal trap immersed in liquid oxygen and a portion of this was introduced into the apparatus after repeated flushing of the dosing system. The nitrogen was purified by passing over hot copper to remove traces of oxygen.

A diagrammatic sketch of the apparatus used in the present work is shown in Figure 1. The sample (20 grams) covered the bottom of a Vycor tube 50 mm.

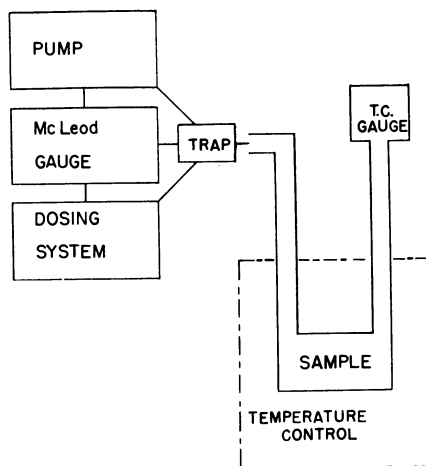


Figure 1. Diagrammatic sketch of apparatus

long and 35 mm. in diameter. This tube was connected to the apparatus through graded borosilicate glass-quartz seals located outside the furnace zone. A thermocouple gage (RCA 1946) was sealed to one outlet and the second outlet was connected to two U-shaped traps in series to block mercury vapor. The traps were immersed in liquid oxygen for the entire duration of the experiment.

The flow of gas was controlled with mercury cutoffs. The pertinent volumes of the apparatus were determined by expansion of argon or helium from the calibrated volume of the McLeod gage and the pressure differences were observed with a cathetometer. The reproducibility of the McLeod gage measurements was 1% or better in the pressure range used in these measurements.

Outgassing Technique

Past experience by the authors and many other investigators in outgassing diamond powder and graphite samples has been unsatisfactory, in that no quantitative measure was available of the extent of outgassing. The excellent vacuum ($<10^{-6}$ mm. of Hg) realized on cooling the sample is a necessary behavior, but this may be partially the result of adsorptive cleanup by the sample itself. Since 1958 the authors have monitored the extent of outgassing by measuring the rate of gas evolution at the elevated temperature. A simple measure was obtained from the pressure increase when the heated sample was cut off from the pumps for one hour. A typical record is given in Figure 2. The solid appears to have a good memory of the time evacuated at the elevated temperature and the rate of outgassing correspondingly decreases. Points A and B are typical of successful behavior and were determined before and after a series of adsorption measurements. Point C indicates an unsatisfactory situation that resulted from an inter-

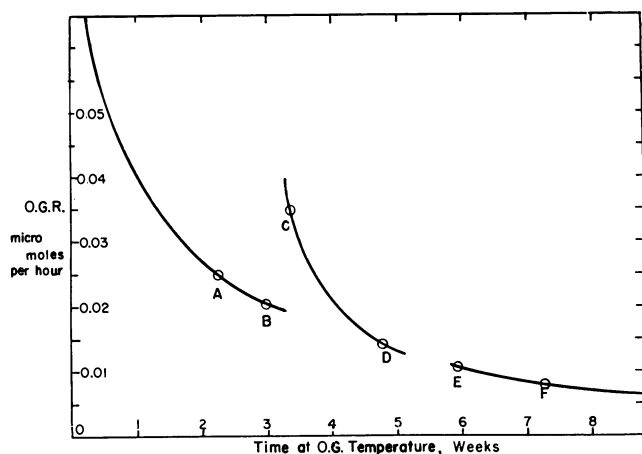


Figure 2. Typical record of outgassing of diamond dust at 600° C.

ruption in pumping due to power failure and the back-diffusion of oxygen to the heated sample. Adsorption measurements were not made with this sample until the outgassing had progressed to the rate given by point D.

The rate of adsorption measurements at 90° and 77° K reported in this paper were bracketed between values of the outgassing rate that decreased steadily from 0.008 to 0.005 μ mole per hour at 600° C. for a 20-gram sample.

Results

The typical rate curve shown in Figure 3 was observed for nitrogen adsorbed on the diamond dust at 90.1° K. The points in circles are based on McLeod gage readings and the balance of the curve was recorded from the thermocouple gage data. A steady-state surface coverage (θ) of 0.055 (10.1-micron pressure) was realized after only about 200 minutes. All pressure measurements have been corrected for thermomolecular diffusion.

Heat Transfer Considerations. From a qualitative point of view the observed effect appears explicable in terms of a slow cooling of the solid. However, when examined more closely, the actual heat transfer can account for only a very small part of the observed delay. Three questions may be raised concerning the cooling of the sample:

1. How closely must the temperature of the sample approach that of the bath, if the temperature difference is no longer to have a significant influence on adsorption?
2. What is the amount of heat to be transferred?
3. What is the rate at which the heat is transferred?

The influence of each will be examined in this order and the answer should indicate how much of the delay might be due to slow cooling of the adsorbent.

Significance of Temperature Difference. Physical adsorption is so strongly temperature-dependent that it is pertinent to estimate the temperature of the sample that would account for the entire effect.

In the vicinity of 90° K the temperature coefficient of the amount adsorbed can be estimated from the published isotherms (8). This coefficient is, of course, dependent upon the pressure and the apparatus dimensions. In the pressure range where the delay occurred, and on the basis of the dimensions of the apparatus, the temperature coefficient of the amount adsorbed was calculated to be about 2% per °K. The temperature coefficient of residual pressure was of the order of 20% per °K. The greater temperature sensitivity of the residual pressure suggests that this measurement might account for the delay, but the observed pressure changes associated with delay are relatively very large.

It is probably not appropriate to apply the above temperature coefficients to a situation far removed from steady-state pressure conditions. However, in the later stages, using the data of Figure 3 as an example, it may be seen that after 150 minutes when the delay was almost over, the pressure was still 100% greater than the steady-state value. This pressure is equivalent to an average adsorbent temperature of 5°K above the bath temperature. It is evident, therefore, that a lack of temperature equilibration amounting to several degrees would be required to account for the measurements. Differences of less than 1° would be quite insignificant. Hence, the heat transfer problem can be reduced to the question of how long it would take for the solid to cool to within about 1° of the bath temperature.

Amount of Heat to Be Transferred. The combination of low surface area, low fractional coverage, and low heat of adsorption results in a very low total heat of adsorption. In the example given in Figure 3, the total amount of nitrogen adsorbed at 90° K at the steady state was 0.71 μ mole per gram of diamond. When multiplied by a molar heat of adsorption of approximately 2000 cal., this results in the liberation of only 0.0014 cal. per gram. Since the specific heat of diamond at 90° K is 0.0025 cal. per gram, this could raise the temperature of the

system by about 0.5°K if the heat of adsorption were not dissipated. This is a relatively small heat quantity.

A much greater heat quantity is involved in cooling the diamond from 550°C . to 90°K . The specific heat of diamond at 500° is about $0.4 \text{ cal./g. }^\circ\text{C}$. and this decreases to only $0.0025 \text{ cal./g. }^\circ\text{C}$. at 90°K . The average specific heat over this temperature range is about $0.23 \text{ cal./g. }^\circ\text{C}$. and the sensible heat is, therefore, $160 \text{ cal. per gram}$. This is about 10^5 times greater than the heat of adsorption.

Rate of Heat Transfer. Whatever the source of the heat, the principal method for its dissipation is undoubtedly conduction through the bed to the container walls, and thence, to the boiling liquid bath. Radiation, being proportional to the fourth power of the absolute temperature, is negligible. Some natural convection in the gas above the sample will occur and help to cool the top surface of the bed as well as the sides. The outside of the bed will cool quickly to bath temperature, but the center of the bed will cool much more slowly. This is the well known (9) cooling rate problem, for which mathematical solutions have been developed giving the temperature at various points in the bed. These solutions always involve some sort of exponential approach to thermal equilibrium and the physical constants of the system appear in the following expression:

$$\frac{dC_p x^2}{k}$$

where d = density of bed

C_p = specific heat

x = linear dimension from point under consideration (center) to surface of bed

k = thermal conductivity of bed

This expression has the units of time and is customarily termed the "thermal conduction time constant." It is the time required for the temperature difference between the cooling bath and a point under consideration in the sample to drop to $1/e$ of its previous value. Conversely, if the cooling curve is known, the time constant is the time required for 63% of the eventual temperature change to be completed. Thus, the time constant can be estimated from a cooling curve as well as from the physical constants of the system.

When determined from the physical constants, the values of the time constant are found to vary because of the appreciable change of the specific heat with temperature. The precision is limited by the uncertainties in the values of the thermal conductivity of powders. Large single diamond crystals have a high thermal conductivity (see Table I), being of the same order of magnitude as for silver

Table I. Pertinent Thermal Conductivities for the System Investigated

Substance	k , Cal./Cm. Sec., $^\circ\text{C}$.
Argon gas at 90°K (1 mm. Hg)	1.42×10^{-5}
Helium gas at 90°K (1 mm. Hg)	14.8×10^{-5}
Diamond, single crystal, 90°K	12
Diamond, single crystal, 300°K	5
Graphite, consolidated	0.4
Graphite, 90°K	0.2
Graphite, 100-mesh powder	0.0004

and copper (1, 2, 3), but powders have extremely low thermal conductivities, sometimes approaching that of the gas contained in the interstices.

Some pertinent conductivities are given in Table I. The tremendous difference between powdered and consolidated graphite may be noted. No measure-

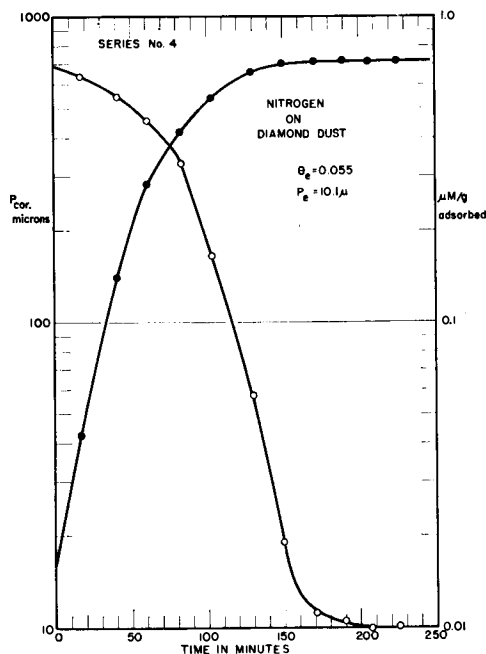


Figure 3. Pressure decrease and micro-moles adsorbed for nitrogen adsorbed on diamond dust at 90.1° K

Steady-state surface coverage = 0.055

ments have been reported for the thermal conductivity of powdered diamond, but when the available correlations (7, 14, 16, 17, 18) are applied conservatively, one arrives at a value not too different from that for graphite powder given in Table I. The measured thermal conductivity of both diamond and graphite crystals (1, 2, 3) is interesting in that both have a maximum in the general neighborhood of 90° K. The graphite used in this work was large flakes of about 1-mm. diameter and doubtless had a conductivity higher than that given in Table I. As a conservative estimate, however, the value of 0.0004 cal./cm. sec. °C. was used for the conductivity of both diamond and graphite beds.

The specific heat of both diamond and graphite decreases sharply on cooling to 90° K. Using diamond as an example, values are listed in Table II at several

Table II. Heat Capacity and Thermal Time Constant for Diamond Powder

Temp., °C.	c_p , Cal./G. °C.	$dc_p x^2/k$, Min.
500	0.38	16
200	0.26	11
25	0.12	5
-78	0.05	2
-183 (90°K)	0.0025	0.1

temperatures with the corresponding calculated time constants. The large decrease in the time constant as the bath temperature is approached greatly speeds the approach to thermal equilibrium. A calculation of the cooling time is given

Table III. Time of Cooling of Diamond Powder Immersed in Boiling Liquid Oxygen (90° K)

Step	Beginning of Step		End of Step		Time, Minutes	
	T^a	ΔT^b	T	ΔT	Increment	Total
1	773	683	340	250	12.5	12.5
2	340	250	182	92	4.5	17.0
3	182	92	124	34	1.5	18.5
4	124	34	102	12	0.5	19.0
5	102	12	94.6	4.6	0.2	19.2
6	94.6	4.6	91.7	1.7	0.1	19.3
7	91.7	1.7	90.6	0.6	0.05	19.35
8	90.6	0.6	90.2	0.2	0.05	19.40

^a T . Temperature at center of sample, °K.

^b ΔT . Temperature difference between center of sample and bath ($T - 90.0^\circ$).

in Table III, where it is assumed that the cooling occurs from 500° C. (773° K.) to 90° K. Each step drops the temperature difference to $1/e$ of the previous value. If the thermal time constant were truly constant over this temperature range, each step would correspond to equal time intervals. However, the thermal time constant decreases radically with temperature and, using the average value over each step, the total time for 8 steps was calculated as shown in Table III. According to this approximation, thermal equilibrium is established in about 20 minutes. A similar value is obtained for graphite. Both values are conservative estimates and the total time is probably less than 20 minutes.

Additional evidence that the observed delay is not due to the lack of thermal equilibrium was obtained from adsorption measurements in which the refrigerant was changed from liquid oxygen to liquid nitrogen after a steady state had been reached. The time constant was estimated from the time required for 63% of the eventual pressure change to occur—about 2 minutes. When the refrigerant was changed back to liquid oxygen, the time constant was also about 2 minutes. This has been repeated many times at different pressure levels and the time constant has always been observed to range between 2 and 4 minutes. This, however, was the pressure time constant and included the actual adsorption or desorption process, the time for flow of gas through the bed and other parts of the apparatus, the time of response of the thermocouple gage and recorder, and heating or cooling the walls of the vessel as well as heating or cooling the bed. A value of 2 to 4 minutes is, therefore, not inconsistent with the values given in Table II at the lower temperatures.

Thermal conductivity of beds of solids has always been found to depend very much upon the conductivity of the continuous phase, and very little upon the conductivity of the solid (7, 14, 16, 17, 18). By introducing a gas of much higher conductivity into the bed, the attainment of thermal equilibrium should be much enhanced, and if indeed the delay in adsorption were due to insufficient cooling, the delay should be greatly shortened. To test this hypothesis, some rate measurements were made in which the diamond sample was first cooled in the presence of helium at pressures of 1 to 7 mm. The thermal conductivity of helium is ten times greater than argon in this pressure range. After 10 to 30 minutes the helium was removed and argon admitted. The delay occurred exactly as before. This indicates that the delay is not associated with the cooling of the sample and, further, that the sample must be cooling in only a very few minutes in either argon or helium.

It is very improbable that the whole phenomenon is due to the time required

for cooling the bed. From three independent methods—estimation of the thermal constants of the system, rapid response of adsorption-desorption process on changing bath temperatures, and no influence in precooling the sample in helium—it is estimated that the cooling time is only a few minutes, certainly no more than 20 minutes, in order to reach within a fraction of a degree of the bath temperature. In contrast, delays amounting to hours have been observed, and, therefore, this behavior must represent a bona fide surface phenomenon.

Measurements subsequent to those reported in this paper have demonstrated a rapid cooling of several adsorbent materials when submerged in liquid oxygen. A very fine copper-constantan thermocouple (No. 36 wire) was centered in a bed of the material (2 cm. in diameter) and a cooling curve recorded. The time required to cool from room temperature to within 1° C. of the bath temperature was found to be 2 minutes with a sample of the mineralogical graphite used in this investigation. Many other solids were investigated in this way. Finely powdered materials, such as precipitated hydroxyapatite and a silica aerogel at a low residual gas pressure, required the longest time, but in no case was a period longer than 18 minutes required.

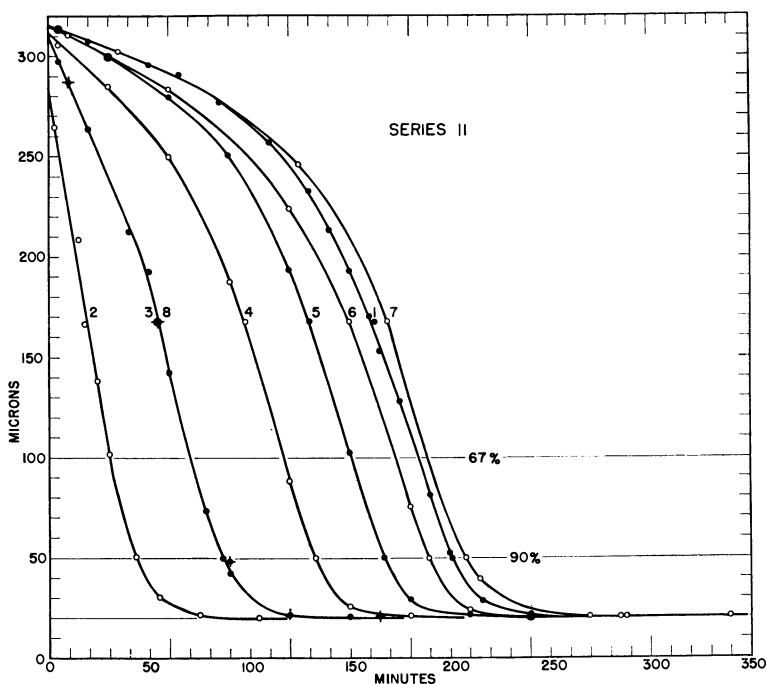


Figure 4. Rates of adsorption of argon on diamond dust at 90° K after pretreatment

1. Evacuation at 600° C.
 2. Desorption of argon at 203° K with no pumping
 3. 297° K
 4. 435° K
 5. 575° K
 6. 674° K
 7. 779° K
 8. 296° K
- Steady-state adsorption in all cases at $\theta = 0.032$

Sequence of Operations. The delay in adsorption was reproducible and can be considered as evidence for a memory effect of the solid. Accordingly, the sequence of operations in contacting gas and solid should be very important in understanding the adsorption process. The following combinations have been investigated:

1. Heat, cool to 90° K., and add gas at once.
2. Heat, add gas during cooling to room temperature, and then cool to 90° K.
3. Add gas, heat to elevated temperature, and cool to 90° K.
4. Heat, cool to 90° K. for various times, and then add gas.

No difference in behavior in the rates of adsorption was observed between sequences 1 and 2. Sequence 3, however, revealed an interesting behavior (Figure 4). In this experiment the sample of diamond was first evacuated at 600°. After it had been immersed in liquid oxygen for 7 minutes, 9.64 μ moles of argon were introduced. This corresponds to sequence 1 and the observed pressure decrease is represented by curve 1. After the steady state was attained (at 15.6-micron pressure and $\theta = 0.032$), the liquid oxygen bath was replaced by a dry ice mixture (approximately -70° C.) and the argon desorbed overnight. Upon replacing the liquid oxygen around the sample, the pressure decreased according to curve 2. This procedure, now corresponding to sequence 3, was repeated, raising the temperature in stages until 506° C. was reached. Finally, upon returning to room temperature, excellent reproducibility was obtained in the rate of adsorption as shown by the superposition of curves 3 and 8, Figure 4.

A series of operations involving sequences 3 and 4 proved to be of special significance (Figure 5). Curve 16A was observed upon introducing 8.42 μ moles of argon into the evacuated sample after it had been precooled in liquid oxygen for 23 hours. The rate of adsorption was very rapid, initial observations being limited by the response of the 1-second recorder. Immediately following the attainment of the steady state, the liquid oxygen bath was removed and the sample heated to 540° C. for 60 minutes. Upon replacement of the liquid oxygen bath,

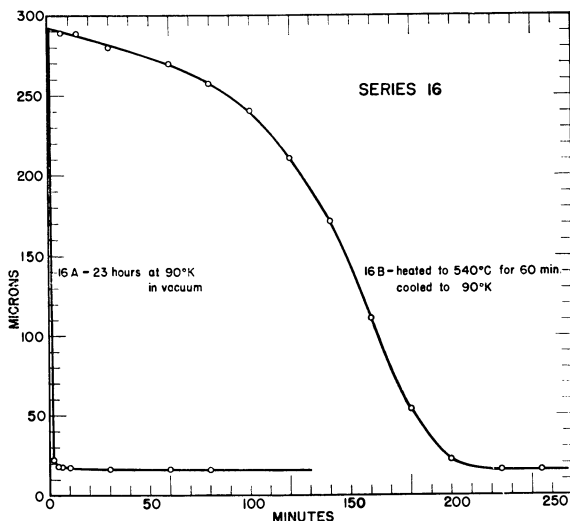


Figure 5. Rates of adsorption of argon on diamond dust

- 16A. After 23-hour storage of diamond at 90° K in vacuum
 16B. After subsequent heating to 540° C. for 60 minutes

rate curve 16B was observed, which resembles exactly the behavior given by curve 6 in Figure 4. Both curves 16A and 16B decayed to the same steady state—namely, 11.2 microns and 0.37 mole adsorbed per gram ($\theta = 0.029$).

The behavior shown in Figure 5 suggested at once that the observed delay in adsorption might be due to a change in the adsorption sites. In short, the adsorption process of argon had nothing to do with the rate-determining process of the observations; indeed, the adsorption of argon might be simply viewed as an index, or probe, as to some change in the surface itself. Accordingly, a number of rates were observed with different periods of precooling at 90° K. after identical heat treatment at 600° C. The results are shown in Figure 6. The ordinate is the relative pressure drop calculated as $(p_t - p_\infty)/(p_0 - p_\infty)$, where p_0 is the initial pressure, p_∞ is steady-state pressure, and p_t is pressure at time t . The family of curves shown in Figure 6 are closely analogous to those given in Figure 4,

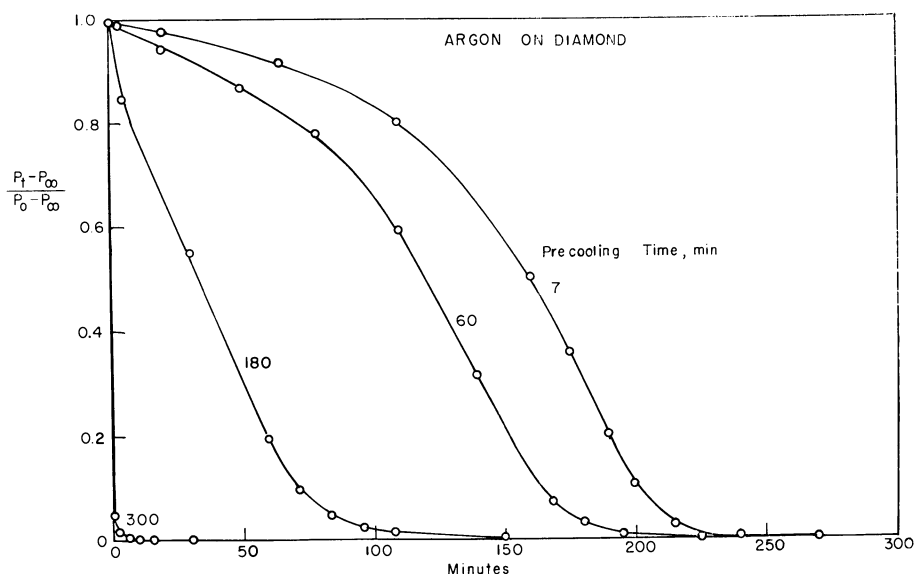


Figure 6. Rate curves of argon on diamond at designated precooling times before addition of argon

where the sample had been heated to different temperatures. A more striking way to present the same data is given in Figure 7, where the time variable is the total cooling time, rather than only the time of exposure of argon to the sample. Figure 7 demonstrates, in a striking way, the memory of the solid as to the length of time that it had spent at 90° K.

Discussion

It is tempting to explain away the above observations in terms of abnormal slow rates of cooling, but the actual transfer of heat to the refrigerant is too rapid to make this plausible.

It would appear from the above behavior that the actual physical adsorption of argon on a surface sufficiently aged at the temperature of the adsorption always takes place very rapidly. It is impossible at present to advance more than a con-

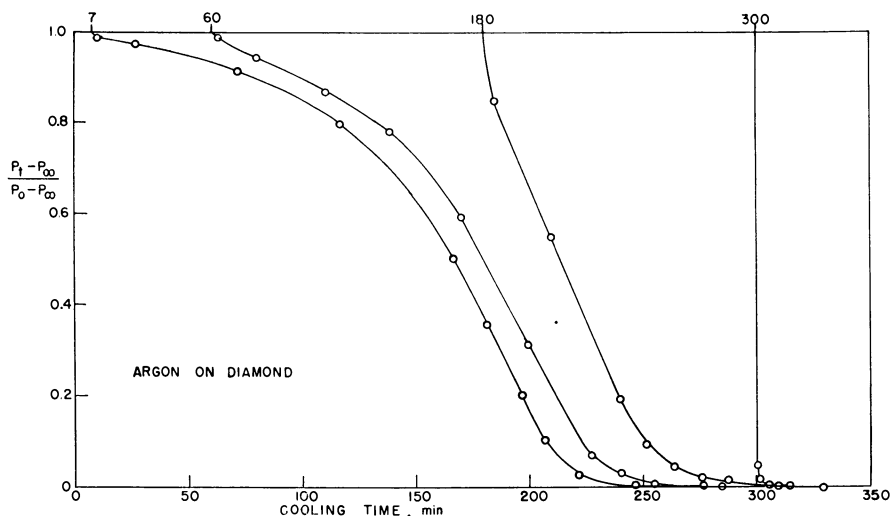


Figure 7. Rate curves of argon on diamond using total time at 90° K as abscissa

jecture as to the theoretical nature of the observed delay. One explanation might involve a thermal deactivation process during the pretreatment of the sample. Upon heating of the solid to an elevated temperature, the sites responsible for steady-state adsorption might be converted into a nonadsorbing species, which upon cooling to 90° K. might slowly revert to their normal behavior. It is suggested that the classical "inert" surface, that has been adequate heretofore in the study of physical adsorption, might actually be subject to change during an outgassing treatment. This is quite unexpected for relatively nonreactive solids such as diamond and graphite. The pretreatment operation of a solid thus assumes a very important role in physical adsorption at low surface coverage, as it already does to a much greater degree in chemisorption processes.

Preliminary to a more detailed theoretical treatment of the problem, it may be of interest to express the above observations from another point of view. One characteristic of the surface behavior of a solid is the adsorption isotherm. If it were possible within a few minutes to obtain a sufficient number of points to construct an isotherm, it would be most interesting to follow the changes in the adsorption isotherm of the diamond surface as it decays to its normal surface behavior. Figure 7 indicates that the decay is almost independent of the presence of argon. One possible procedure is to introduce different amounts of argon to the evacuated sample and by making a cross plot of the amounts adsorbed at constant time of cooling construct the desired isotherms.

The data for argon on diamond at 90° K. have been plotted from this point of view (Figure 8). The number on each curve signifies the time that the diamond had been kept at 90° K. With passage of time at 90° K. there are changes in both shape and ordinate magnitude. These move in the direction of greater adsorption and gradually converge upon the upper left curve, which represents the steady-state behavior. A similar analysis has been made for nitrogen adsorbed on diamond dust at 90° K. (Figure 9). It may be possible to interpret each curve in terms of corresponding values for the constants used to define adsorption isotherms. This has been done for a number of steady-state isotherms by Ross and Olivier (12) in terms of the number and energy distribution of the adsorption sites.

The maximum surface coverage in these experiments after the steady state had been reached was 0.032 with argon and 0.055 with nitrogen. It is, therefore, plausible that only small changes in the surface are responsible for the changing character of the adsorption process as a result of the thermal treatment.

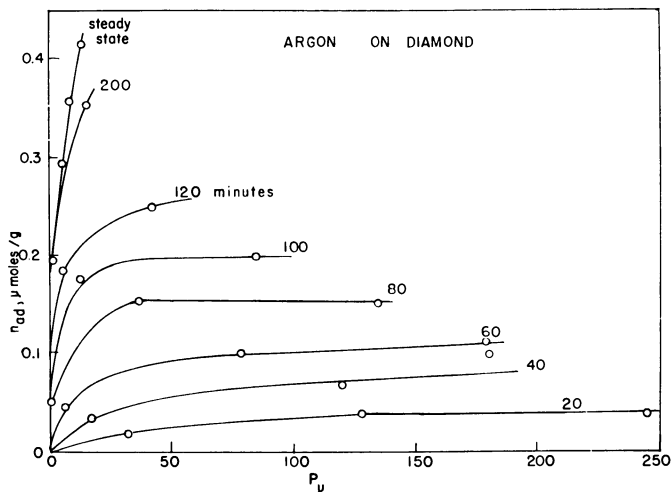


Figure 8. Instantaneous isotherms of argon on diamond dust corresponding to designated times at which sample was at 90° K

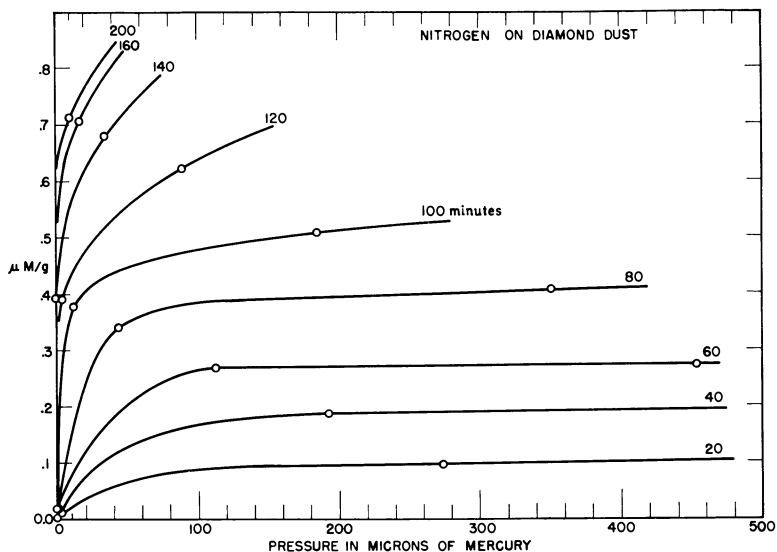


Figure 9. Instantaneous isotherms of nitrogen on diamond dust corresponding to designated times of sample at 90° K

The adsorption measurements reported were done at a temperature above the two-dimensional critical temperature of the adsorbate (see Table IV). In

Table IV. Three- and Two-Dimensional Critical Temperatures

	N_2 , °K	Ar , °K
T_{3c}	126.0	151.1
T_{2c}	63.0	75.5

other words, the model is that of a two-dimensional gas spreading over the surface. Evidence for this was based on the calculation of the spreading pressures from the steady-state adsorption isotherm of these materials at both 90° and 78° K (8). Typical two-dimensional gas film behavior was obtained. Consequently, phase transitions, such as those reported in two-dimensional liquid and solid films, must be ruled out as an explanation of the observed facts.

One might well raise the question as to how typical these observations are of adsorption phenomena in general at low pressures. Shereshefsky and Weir (15) reported the adsorption of nitrogen and oxygen on various packings of glass spheres at liquid air temperature. They discovered after the measurement of several adsorption points that there was a rapid pressure fall accompanied by a large increase in the adsorption of the gas. The behavior was analogous to shifting from the 20-minute to the steady-state isotherms in Figures 8 and 9. This was found to be influenced by the temperature at which the glass spheres were heated preliminary to the adsorption. Ross and Winkler (13) also observed a similar behavior in the adsorption of ethane on crystals of mineralogical asbestos at 90° K. These authors, too, found after a number of adsorption points at low pressure that there was a sudden decrease in pressure with a corresponding increase in adsorption. Different behavior was found when the asbestos was heated either to room temperature or to 130° to 150° C. Ross and Winkler offered an explanation in terms of "supersaturation phenomena." It is possible that the above two systems in reality were behaving similar to argon on diamond as reported in this paper and that long periods may be needed in some cases to bring about steady-state distributions of sites.

At low surface coverage (<5%) it is often difficult to distinguish clearly between physical adsorption and chemisorption. In this range there is an upward trend in the heats of physical adsorption with decrease in coverage to a value that makes this criterion of differentiation uncertain. The rate of adsorption of argon on diamond has been shown in this work to be either fast or slow, depending on the thermal history of the solid. Boudart (4) recently emphasized the possibility that the activation energy of a chemisorption process may in some cases be supplied entirely by the solid. Boudart refers to earlier work by Pace and Taylor (10) and by himself (11) to support this possibility. Identical values were found for the rates of adsorption of hydrogen and deuterium on Cr_2O_3 , $ZnO-Cr_2O_3$, and Ni supported on kieselguhr at 110°, 132°, and 184° C. The process, therefore, was not dependent upon the gas. The generation of an active site by the solid itself may thus be the slow step of the adsorption process. This is a very intriguing situation and, if also applicable to physical adsorption at low coverage, it merits additional study.

Literature Cited

- (1) Berman, R., "Industrial Carbon and Graphite," pp. 42-5, Soc. Chem. Ind., London, 1958.
- (2) Berman, R., *Proc. Phys. Soc.* **A65**, 1029 (1952).
- (3) Berman, R., Foster, E. L., *Proc. Roy. Soc. (London)* **A237**, 344-54 (1956).
- (4) Boudart, M., "Adsorption and Chemisorption," pp. 409-20, "The Surface Chemistry of Metals and Semiconductors," H. C. Gatos, ed., Wiley, New York, 1960.

- (5) Brunauer, S., "Adsorption of Gases and Vapors. I. Physical Adsorption," Chap. XIII, Princeton Univ. Press, Princeton, N. J., 1943.
- (6) Deitz, V. R., "Bibliography of Solid Adsorbents," Vol. 1, 1900-42, Vol. 2, 1943-53, Natl. Bur. Standards Circ. 566.
- (7) Loeb, A. L., *J. Am. Ceram. Soc.* **37**, 96 (1954).
- (8) Lopez-Gonzalez, J. de D., Carpenter, F. G., Deitz, V. R., *J. Phys. Chem.* **65**, 1112-19 (1961).
- (9) McAdams, W. H., "Heat Transmission," 2nd ed., p. 31, McGraw-Hill, New York, 1942.
- (10) Pace, J., Taylor, H. S., *J. Chem. Phys.* **2**, 578-80 (1934).
- (11) Parravano, G., Friedrick, H. G., Boudart, M., *J. Phys. Chem.* **63**, 1144-6 (1959).
- (12) Ross, S., Olivier, J. P., *Ibid.*, **65**, 608-15 (1961).
- (13) Ross, Sidney, Winkler, Werner, *J. Am. Chem. Soc.* **76**, 2637-40 (1954).
- (14) Russell, H. W., *J. Am. Ceram. Soc.* **18**, 1 (1935).
- (15) Shereshefsky, J. L., Weir, C. E., *J. Am. Chem. Soc.* **58**, 2022-9 (1936).
- (16) Verschoor, H., Schuit, G. C. A., *Appl. Sci. Research A2*, 97-119 (1950).
- (17) Wilhelm, R. H., Johnson, W. C., Winkopp, R., Collier, D. W., *Chem. Eng. Progr.* **44**, 105 (1948).
- (18) Yagi, S., Kunii, D., *A.I.Ch.E. Journal* **3**, 373 (1957).

RECEIVED May 25, 1961.

Streaming Potential Measurements on Paraffin Wax

H. C. PARREIRA and J. H. SCHULMAN

*Stanley-Thompson Laboratories, Henry Krumb School of Mines,
Columbia University, New York, 27, N. Y.*

The streaming potentials of a solid paraffin sample were determined for aqueous solutions of various inorganic ions. Very high values were obtained for dilute solutions. The zeta potentials and the surface charge densities were also calculated. The surface isotherms obtained in the presence of the halide ions investigated suggest that adsorption of the ions takes place in an increasing order, $\text{Cl}^- < \text{Br}^- < \text{I}^-$. In the presence of H^+ and OH^- ions the paraffin surface behaves as a weak acid. The determination of streaming potentials and the surface properties of paraffin may be of interest to the oil industry and flotation.

Adsorption studies of ionic species at the solid-liquid or liquid-liquid interfaces can be carried out using data obtained from electrokinetic measurements (1, 6, 7, 12, 13, 14, 26, 27, 29, 30, 37, 41, 44). In the case of solid-water most of the measurements have been obtained by using either the streaming potential technique or microelectrophoresis. Since the hydrocarbons investigated previously were liquid, the microelectrophoretic technique was used (7, 37, 41, 44). It is not an easy task to obtain precise results on ζ potentials of oil droplets from mobility measurements unless a certain number of corrections are introduced (4, 5, 20, 21, 22).

Since the streaming potential determination is easier to carry out and is less subject to corrections than microelectrophoresis, it was used in the present work to study the behavior of the solid paraffin-water interface.

Most of the disagreement among streaming potential workers appears to be due to experimental difficulties that are probably caused by the electrodes (22, 46). It has been shown recently (22, 46) that electrode polarization and other effects due to flow of the liquid past the electrodes appear to be responsible for the experimental difficulties encountered in the streaming potential technique. However, appropriate streaming cell design and measuring apparatus appear to lead to precise and reliable streaming potentials.

Experimental

Materials. The crystalline quartz used in this work was crushed and sized and the 28/35-mesh fraction was collected. This fraction was leached repeatedly

with hot concentrated hydrochloric acid until the complete absence of iron was ensured. The material was then washed with conductivity water until the supernatant showed no traces of chloride ion. Gulfwax paraffin was used and had the following properties: normal paraffin, 95%; isoparaffin, 5%; nonsaturated hydrocarbons, none; m.p., 55° C.; contact angle, 105° .

The paraffin was cut into small pieces (0.8 to 1.0 mm.) which were large enough to be retained in the streaming cell.

The water used had a conductivity of ca. 1×10^{-6} ohm $^{-1}$ cm. $^{-1}$ All chemical reagents were analytical grade and were used without further purification. The temperature was kept at $25^{\circ} \pm 0.5^{\circ}$ C. for the paraffin work. The stearic acid used was a specimen 99% pure.

Apparatus and Procedure. The material studied was placed in the streaming cell and packed in such a manner as to give a porous plug.

A streaming cell made of Perspex, holding a small amount of material (2 to 4 cc.), was used. The details of its construction have been published (34). The cell was fitted with two platinized platinum electrodes and two Ag/Ag halide electrodes and is shown in Figure 1. This cell was coupled with two Keithley electrometers Model 610A (one electrometer for each pair of electrodes), whose outputs were fed into a Varian double-channel recorder. Streaming potentials could, thus, be measured simultaneously using two different kinds of electrodes for comparison purposes.

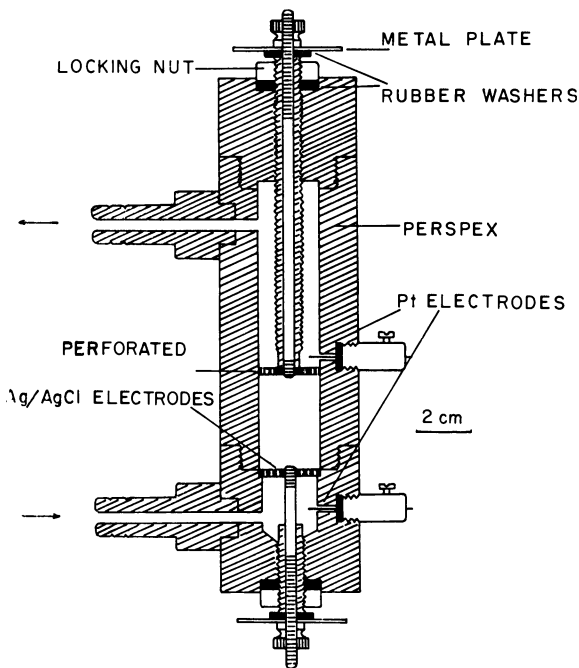


Figure 1. Streaming potential cell

The resistance of the plug was measured with a General Radio impedance bridge Model 650-PI. For plugs of resistances above 1 megohm an appropriate precision resistance was connected in parallel with the cell. This procedure was later checked using a General Radio impedance bridge Model 1650-A, which allowed resistance measurements up to 10 megohms to be made. Resistances of

3 megohms were obtained when water was streamed past the paraffin wax plugs. The streaming potentials were plotted against the driving pressure and the slope of

the best straight line was used for calculations of the ζ potential. Generally the direction of streaming did not affect the streaming potential; this is shown in Figure 2.

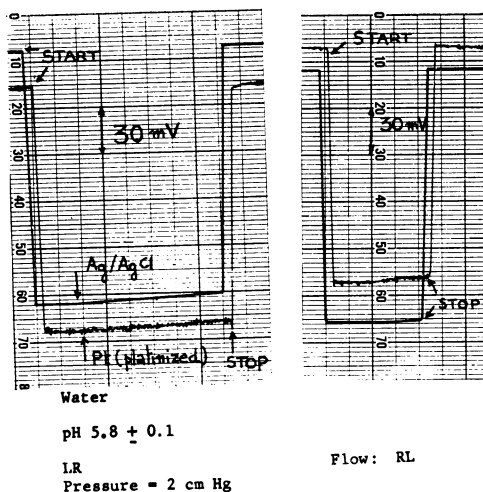


Figure 2. Recording chart of streaming potential for paraffin

Ag/AgCl and platinized platinum electrodes used simultaneously

It has been shown by Rutgers and collaborators (38, 39) that turbulence may have an effect on streaming potentials. To avoid this problem and ensure laminar flow, the driving pressure never exceeded 10 cm. of Hg.

Preparation of Electrodes. The Ag/AgBr and Ag/AgI electrodes were prepared by anodic electrolysis of the appropriate sodium salt solution (1N) at 6.5 ma. per sq. cm. for 5 minutes. The two electrodes to be coated were connected and dipped into the solution; a wire of pure silver was used as the cathode. In the case of the Ag/AgCl electrode 1N HCl was used. Just after preparation the electrodes were immersed in the appropriate halide solution (10^{-3} M). The Ag/Ag halide electrodes prepared in this manner showed a difference of potential of 0.3 to 0.5 mv. in the presence of 10^{-5} M solution of sodium halide. This potential will be referred to as rest or nonflow potential.

The platinized platinum electrodes were prepared by electrolyzing a solution of chloroplatinic acid containing no lead acetate (23). The metal deposition was stopped as soon as a light brown color appeared on the platinum wire. They were then immersed in 1N H_2SO_4 and electrolyzed again; their polarity was alternated every 2 minutes for 20 minutes. The platinum electrodes were washed thoroughly with distilled water and soaked in conductivity water for one week before they were used.

Many investigations on streaming potentials were performed in the presence of surface active agents (12, 13, 14). Since it is known that the surface active agents adsorb on the Ag/Ag halide electrodes (25, 31), a few experiments were carried out to see whether the surface active agent had any influence on the electrode behavior in the presence and absence of flow. For this purpose two identical Ag/AgCl electrodes were immersed in solutions of KCl of varying concentration and their difference of potential was measured with a Keithley electrometer. The rest potential of the Ag/AgCl electrodes varied from 0.1 to 0.5 mv. in KCl solutions in the range of 10^{-2} M to 10^{-5} M.

The addition of surface active agents such as sodium dodecyl sulfate, dodecylamine hydrochloride, and dodecyl pyridinium chloride to the KCl solution, giving concentrations of the agent ranging from 10^{-2} to 10^{-5} M, did not show any effect on the rest potential of these electrodes. Dodecylamine hydrochloride and dodecyl pyridinium chloride have a common ion to the Ag/AgCl electrode. It is known that the higher the concentration of one of the potential determining ions of the Ag/AgCl electrode, the smaller will be the effect of flow on the electrodes (46). The same characteristic was found in this work to be true for the Ag/AgBr and Ag/AgI electrodes. Thus the highest flow potential is expected to develop when distilled water flows past the electrodes with no plug in the streaming cell. The flow potential for the Ag/AgCl electrodes (no material in the cell) in the presence of distilled water flowing under a driving pressure of 10 cm. of Hg was ~ 1.4 mv. (the rest potential in water was found to be ~ 0.5 mv.). This pressure corresponds of a flow of 7.7 cc. per second. When a 28/35-mesh plug was placed in the cell, the same driving pressure gave a flow of 4.5 cc. per second, which probably corresponds to a much smaller flow potential.

Martinez and Zucker (26) carried out their work on asbestos using the Ag/AgCl electrodes in the presence of KCl in order to reduce the flow effects on the electrodes. In pure water the use of the platinized platinum electrodes seems to be unavoidable, since any of the Ag/Ag halide electrodes would release ions into the system.

The flow effects were more pronounced the older the Ag/Ag halide electrodes. Even in 10^{-3} M KCl a flow potential was observed for the Ag/AgCl electrodes; this effect disappeared, however, after the electrodes were freshly electroplated.

The behavior of the platinized platinum electrodes is entirely different from that of the Ag/Ag halide electrodes, both under flow conditions and at rest. Whereas the nonflow potential for the nonpolarizable electrodes remained constant with time, the rest potential for two platinized platinum electrodes increased with time. Also, the flow of liquid produced a more pronounced effect on the platinum electrodes than on the Ag/Ag halide electrodes. The erratic behavior of the platinum electrodes appears to be due to polarization effects which are difficult to eliminate. In Figure 3 the effect of flow on both Ag/AgCl and platinized electrodes can be assessed. The effect of flow on the platinum electrodes was known to Helmholtz (19) and still appears to remain unexplained.

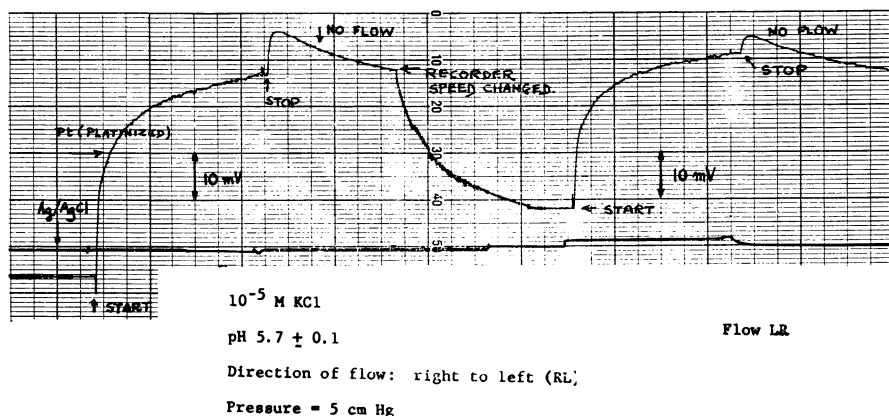


Figure 3. Effect of flow on Ag/AgCl and platinized platinum electrodes in presence of KCl

In Figure 4 the effect of flow on both Ag/AgCl and platinized platinum electrodes is shown to exist in the presence of surface active agent. The Ag/AgCl electrodes used were not fresh and show an appreciable flow potential (~ 7 mv.), which is reduced to 2.5 mv. in the presence of 10^{-4} M sodium dodecyl sulfate and 10^{-4} M KCl. The difference of potential between the platinized electrodes (measured after 6.5 seconds after flow was started) appears to be 20 mv.; this difference seems to decrease to about 16 mv. in the presence of 10^{-4} M sodium dodecyl sulfate and 10^{-4} M KCl. Higher concentrations of KCl and sodium dodecyl sulfate were tried; dodecylamine hydrochloride was also investigated. The efforts followed the same trend—i.e., the surface active agent appears to decrease somewhat the flow effects on both Ag/AgCl and platinum electrodes. Despite the different behavior of the Ag/Ag halide electrodes and the platinized platinum electrodes, it is possible to obtain the same value for the streaming potential (22) and consequently, the same ζ potential.

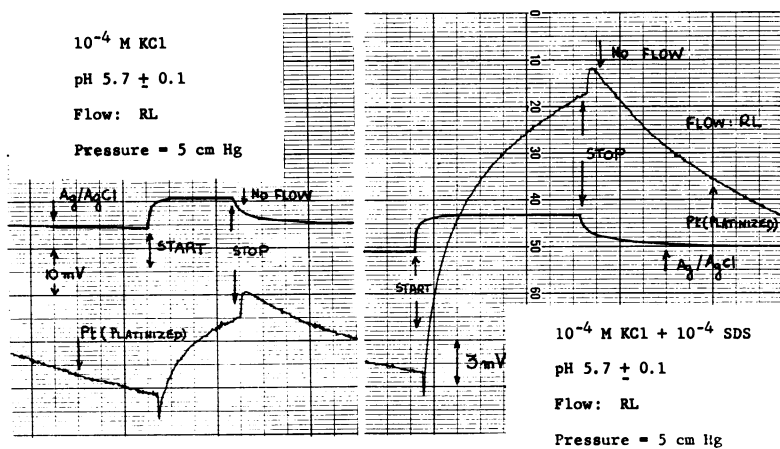


Figure 4. Effect of flow on Ag/AgCl and platinized platinum electrodes in presence of sodium dodecyl sulfate

For the curves shown in Figure 5 the electrometer was set at the maximum sensitivity and a streaming potential of 2 mv. was measured for the paraffin with both Ag/AgCl and Pt electrodes. The same value was measured for both directions of streaming. This is an interesting result, since the streaming potential is small and the flow effects on the Ag/AgCl are nondirectional under these experimental conditions (see Figure 5). Simultaneous recordings of the streaming potentials for paraffin plugs using any of the Ag/Ag halide and platinized platinum electrodes show that their values are the same for both kinds of electrodes, even though polarization effects on the Pt electrodes are present. The behavior of the Ag/AgCl and platinum electrodes in the absence of surface active agents has been studied by Zucker (46) and more recently by Korpi (22).

Theoretical Introduction

In the present investigation the Stern theory (42) is assumed to hold and consequently,

$$-\sigma_0 = \sigma_1 + \sigma_2 \dots \quad (1)$$

where σ_0 , σ_1 , and σ_2 are the surface charge densities at the paraffin surface, Stern

layer, and diffuse layer, respectively. It appears that the paraffin surface behaves as a nonionogenic surface (41) and, consequently, $-\sigma_1 = \sigma_2$. Thus the potential at the surface, Ψ_0 , will be equal to Ψ_δ , the Stern potential or the potential at the outer boundary of the Stern layer. It is common practice to assume that $\Psi_\delta = \zeta$ (45), despite the uncertainty of the location of the slipping plane and therefore $\Psi_0 = \zeta$. It has been shown recently by Haydon (18) that the potential in the plane of closest approach of the counter ions to the adsorbed ions converges to the value of ζ at low charge density. Haydon (18) reaches this conclusion for droplets of petroleum ether in the presence of NaCl and dodecyl trimethyl ammonium bromide, provided the surface charge density is below 2×10^{-4} e.s.u. per sq. cm.

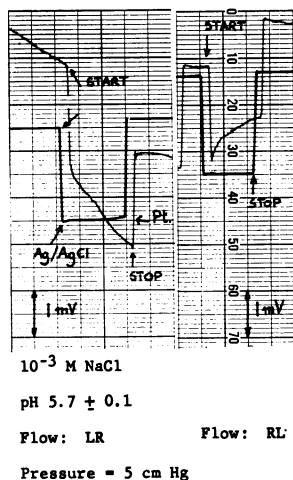


Figure 5. Recording chart for low streaming potentials

Measured with Ag/AgCl and platinumized platinum electrodes simultaneously

The surface charge density at the slipping plane or electrokinetic surface charge density may be calculated from the ζ potential by means of the Gouy theory (17) which for a plane surface gives:

$$\sigma'_2 = \pm \left(\frac{\epsilon RT}{2\pi} \right)^{1/2} \left\{ \sum_i n_i \left[\exp \left(- \frac{z_i e \zeta}{kT} \right) - 1 \right] \right\}^{1/2} \quad (2)$$

- where σ'_2 = electrokinetic surface charge density
- ϵ = dielectric permeability at the slipping plane considered equal to the bulk permeability
- n_i = bulk concentration of ionic species i , gram ions per cc.
- z_i = valence of ion i (including sign)
- e = electronic charge

For a uni-univalent electrolyte, at 25° C., Equation 2 becomes

$$\sigma'_2 = \pm \frac{c^{1/2}}{134} \sinh \frac{\zeta}{51.5} \quad (3)$$

where ζ is expressed in millivolts and c in moles per liter; σ'_2 (hereafter represented by σ) is given in electron charge per square angstrom. The sign of σ is the

same as that of the ζ potential. This potential was calculated using the classical Helmholtz-Smoluchowski equation:

$$\zeta = -\frac{4\pi\eta}{\epsilon} \lambda \frac{\Delta V}{\Delta P} \quad (4)$$

where η = viscosity coefficient of the streaming liquid

λ = conductivity of the liquid within the pores of the plug

ΔV = difference of potential (streaming potential) between the ends of the plug

ΔP = pressure drop between the ends of the plug

A few corrections have been proposed to modify the Helmholtz-Smoluchowski equation (3, 16, 28). Under certain experimental conditions many of these corrections become too small to be considered (6). However, these corrections are not as important as those that have to be introduced when ζ potentials are calculated from mobility data (4, 5, 20, 21, 32, 33).

A theoretical work has been published recently by Dukhin and Derjaguin (8), where they demonstrate that the streaming potential (and the ζ potential) is a function of the diffusion coefficients of both the positive and negative ions. This implies that the total ζ potential is composed of a positive and a negative component. They also showed that the influence of the diffusion of the ionic species on the streaming potential varies according to the hydrodynamic conditions of the system.

Results

The ζ potentials were calculated using Equation 4, which, at 25° C., becomes:

$$\zeta = -9.75 \cdot 10^4 \alpha C/R$$

where α is the slope of the ΔV vs. ΔP curves (in millivolts per centimeter of Hg) and R is the resistance of the liquid-plug system. The cell constant, C , was de-

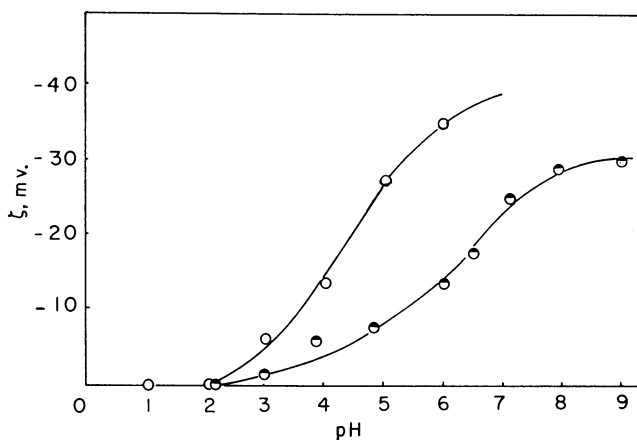


Figure 6. Potential vs. pH curves for quartz at varying and constant ionic strength

$I = 0.01$
 ○ Varying ionic strength
 ● Constant ionic strength

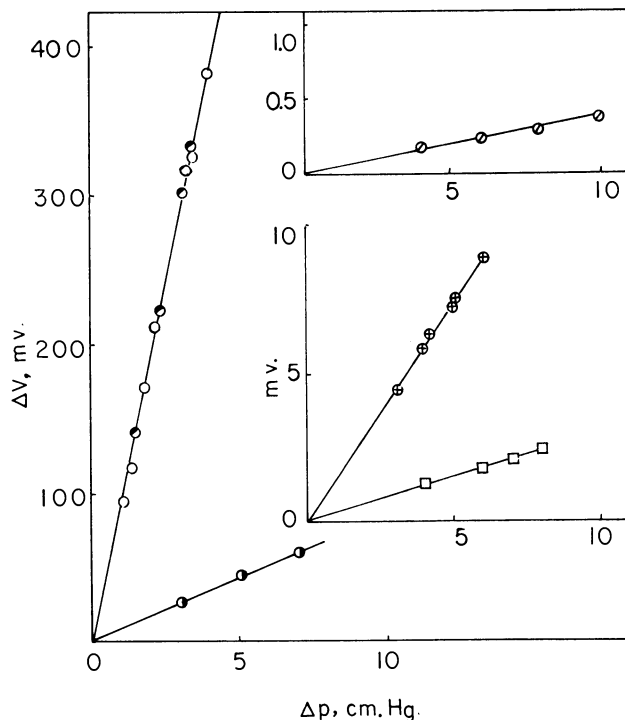


Figure 7. Streaming potential vs. pressure curves for paraffin wax in different pH values

- ⊙ pH 2.2
- pH 3.1
- ⊕ pH 3.8
- pH 5.1
- pH 5.8
- pH 5.8, after streaming with 0.01N HCl and washing with ca. 30 ml. of distilled water

terminated with 0.0200M KCl solution; the ζ potential is given in millivolts. The values for the conductivity of the streaming liquid measured with a conventional conductivity cell were in good agreement with C/R , except for very low values of the electrolyte concentration ($\sim 10^{-5}$ to 10^{-6} M). The surface charge densities were calculated using Equation 3.

Quartz. The ζ potential for the quartz sample under various conditions was investigated, since there still appears to exist some disagreement concerning the zero point of charge density for the quartz surface (13, 46). The ζ vs. pH curves at constant ionic strength ($I = 0.01$) (obtained with mixtures of KOH + KCl + HCl) and varying ionic strengths are given in Figure 6. It is apparent that the quartz surface is negatively charged above pH 2.0; in the pH range 1.0 to 2.0 the surface charge density is zero. No reversal of charge was ever observed.

The ζ potential in water ($\text{pH } 5.9 \pm 0.1, T = 26^\circ \pm 0.5^\circ \text{ M.}$) was found to be -34 mv.; this value is in good agreement with the -36 mv. obtained by Gaudin and Sun (15) from microelectrophoretic measurements. Other investigators (43) using microelectrophoresis gave values which are also in fair agreement with those obtained here. The ζ vs. c plot for quartz in KCl shows that the

ζ potential remains practically constant and equal to -36 mv. from $10^{-6} M$ up to $5 \times 10^{-4} M$ KCl (pH 5.8 ± 0.1 , $T = 27^\circ C.$). This is close to the -39.6 mv. obtained for the same sample using a different measuring device. The values reported here are, however, lower than those obtained by other workers using the streaming potential technique. For example, Fuerstenau (11) finds -70 mv. for quartz in water; Overbeek and Wijga (33) report a value of -98 mv. in $2 \times 10^{-4} M$ KCl.

Paraffin. The paraffin surface, which is known to be highly hydrophobic, shows very high streaming potentials at low ionic strength. For water at pH 5.8 ± 0.1 , potentials of nearly 1 volt were obtained under streaming pressures of ca. 10 cm. of Hg. A few ΔV vs. ΔP curves are shown in Figure 7. After stream-

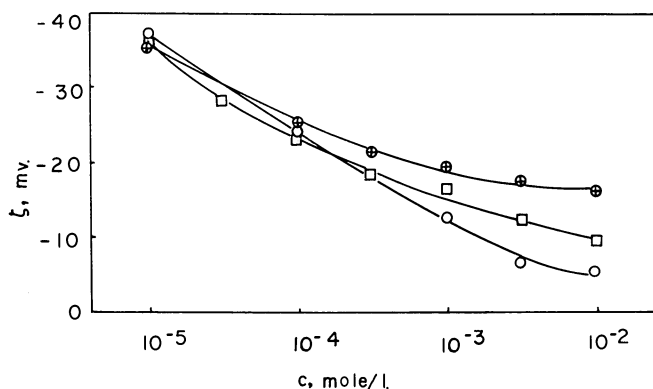


Figure 8. ζ potential vs. c curves for paraffin wax in different sodium halides

○ NaCl
 □ NaBr
 ⊕ NaI

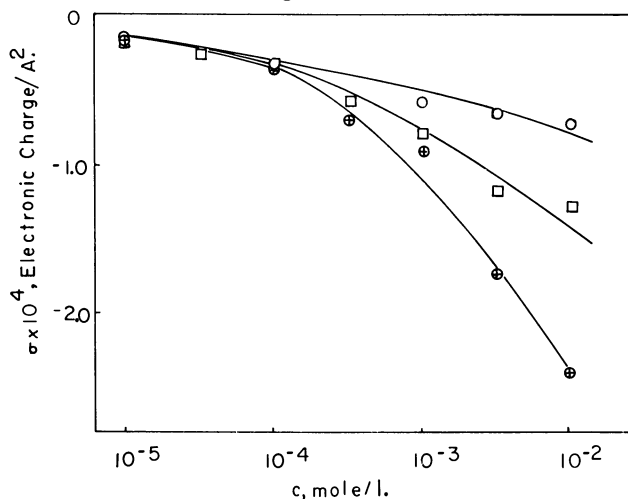


Figure 9. σ vs. c curves for paraffin wax in different sodium halides

○ NaCl
 □ NaBr
 ⊕ NaI

ing with 10^{-2} M HCl or NaOH, the streaming potential obtained in water could be reproduced by washing the paraffin with ca. 30 ml. of distilled water.

The ζ potentials *vs.* c curves for the different sodium halides are shown in Figure 8.

Discussion

Adsorption Isotherms. The adsorption of the halide ions on the paraffin surface can be better visualized with the help of the σ *vs.* c curves which are given in Figure 9. These isotherms show the increasing adsorption of the halide ions to occur in the order, $\text{Cl}^- < \text{Br}^- < \text{I}^-$. This behavior appears to be similar to what is observed for the adsorption of the halide ions at the A/W interface, which increases its negative charge in the same order (10). According to Samoilov (40) the energies of hydration of the halide ions are -0.27 , -0.29 , and -0.32 kcal. per mole for the Cl^- , Br^- , and I^- ions, respectively. The adsorption of the halide ions appears to increase according to the increasing order of the hydration energies. Also, it takes place in the increasing order of the polarizabilities of the halide ions (24).

The adsorption of the halide ions may be explained as follows: Probably the paraffin surface presents more hydrogen atoms in contact with the liquid phase than carbon atoms. The latter bears a residual negative charge, whereas the hydrogen atoms are polarized positively (44); therefore, the halide ions would preferentially adsorb on the hydrogen atom of the paraffin surface. The $\log \sigma$ *vs.* $\log c$ plots for the Br^- and I^- ions are very good straight lines up to 10^{-3} M. The curve for the Cl^- ion deviates from linearity at ca. 5×10^{-4} M. The $\log \sigma$ *vs.* $\log c$ plots show that the adsorption of the halide ions follows a relationship of the Freundlich type—namely, $\sigma = kc^{1/n}$ where n is very nearly 3 for the three halide ions studied. The values of k as obtained from the σ *vs.* $c^{1/n}$ plots are 8.7×10^{-3} , 7×10^{-3} , and 7.6×10^{-3} for I^- , Br^- , and Cl^- , respectively. A relationship of the Freundlich type was derived recently by Benton and Elton (2), using Equation 2 and assuming a mobile film to exist at a solid surface. The data presented here appear to agree with the predictions of Benton and Elton, although their treatment has been criticized (35).

The results for the adsorption of the halide ions on the paraffin surface seem to indicate that valence alone cannot explain ionic adsorption. However, an explicit form for the adsorption isotherms that takes into consideration factors such as the polarizability and the hydration energy of the ions is not easy to visualize at the present moment.

The ζ *vs.* pH Relationships. The pure paraffin surface is negatively charged above pH 5.0 and positively charged below that pH value (Figure 10). The characteristics of the ζ *vs.* pH curve suggest that the paraffin surface behaves as a weak acid. The H^+ and OH^- ions appear to be the potential-determining ions, although they do not belong to the hydrocarbon lattice. The strong influence of the H^+ and OH^- ions supports the views of Perrin (36), who maintained that these ions play a predominant role in charging a neutral wall. Perrin (36) attributed the effects of H^+ and OH^- ions to their ionic mobilities. Observation of the ζ *vs.* pH curve shows that there seems to exist a preferential adsorption of OH^- as compared to the H^+ ions.

The residual positive charge on the hydrogen atom appears to be one of the predominant factors responsible for the OH^- ion absorption, as it also appears to be a factor in the adsorption of the halide ions. Strong evidence for OH^- ion

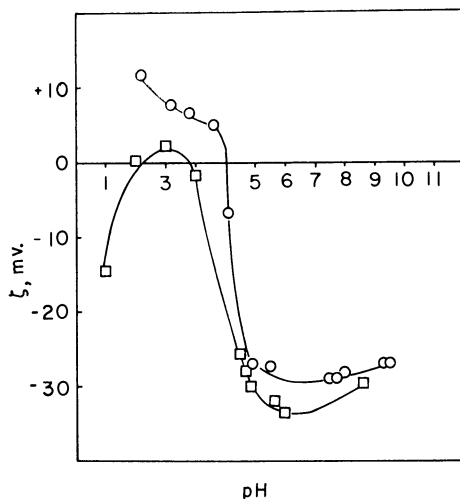


Figure 10. ζ potential vs. pH curves for paraffin wax in presence and absence of stearic acid

○ Paraffin wax
 □ Paraffin wax containing 0.1% of stearic acid

adsorption was also found for hydrocarbons such as octadecane (7), dodecane (44), and Decalin (41). The OH^- ion adsorption on Decalin was explained by Taylor and Wood (41) in terms of hydrogen bonding between the ion and a water sheath that surrounds the hydrocarbon surface.

Below pH 6.0 adsorption of H^+ ions probably occurs on the carbon atoms, thus rendering the surface less negative. Below pH 5.0 the surface becomes positive even in the presence of Cl^- ions, indicating the preferential adsorption of H^+ ions.

The ζ vs. pH curve for the paraffin wax containing 0.1% of stearic acid is also shown in Figure 10. In the presence of COO^- groups the H^+ ions are preferentially adsorbed on the surface, which becomes less negative. The curious shape of the ζ vs. pH curve below pH 3.8 appears to be due to Cl^- ion adsorption on the surface, which becomes markedly negative at pH 1.0. A possible site for the Cl^- ion adsorption can be the carbon atom of the COOH group, since the carbon atom in this group has a positive residual charge. Also, the Cl^- ion does not appear to adsorb on the hydrogen atoms of the hydrocarbon chains at low pH values. It is worthwhile to recall here some early experiments of Ellis (9) on the electrification of the paraffin surface in contact with aqueous solutions of inorganic acids. Although the ζ vs. pH curves are not given (9), his results appear to fit the curve for paraffin containing stearic acid. Since the presence of long-chain fatty acids gives a characteristic ζ vs. pH curve below pH 3.8, it is probable that the paraffin sample used does not contain any long-chain organic acid as impurities.

Acknowledgment

The authors thank the General Electric Co., Schenectady, N. Y., for the sample of quartz and the Gulf Oil Corp., New York, N. Y., for the information on

the properties of the paraffin used in this work. They are indebted to R. H. Ottewill, Department of Colloid Science, The University, Cambridge, England, for measurement of zeta potential of quartz in the presence of 5×10^{-4} M KCl.

Literature Cited

- (1) Anderson, P. J., *Trans. Faraday Soc.* **54**, 130 (1958).
- (2) Benton, D. P., Elton, G. A. H., Proc. 2nd Intern. Congr. Surface Activity, London, Vol. III, p. 28, 1957.
- (3) Bieffer, G. J., Mason, S. G., *Trans. Faraday Soc.* **55**, 1239 (1959).
- (4) Booth, F., *J. Chem. Phys.* **18**, 1361 (1950).
- (5) Booth, F., *Proc. Roy. Soc. (London)* **A203**, 514 (1950).
- (6) Buchanan, A. S., Heymann, E., *Ibid.*, **A195**, 150 (1948).
- (7) Carruthers, J. C., *Trans. Faraday Soc.* **34**, 300 (1938).
- (8) Dukhin, S. S., Derjaguin, B. V., Proc. 3rd Intern. Congr. Surface Activity, Cologne, Vol. II, p. 324, 1960.
- (9) Ellis, R., "Two Monographs on Electrokinetics," Engineering Research Institute, University of Michigan, p. 158, 1951.
- (10) Frumkin, A., *Z. physik. Chem.* **109**, 34 (1924).
- (11) Fuerstenau, D. W., *J. Phys. Chem.* **60**, 981 (1956).
- (12) Fuerstenau, D. W., Modi, H. J., *J. Electrochem. Soc.* **106**, 336 (1959).
- (13) Gaudin, A. M., Fuerstenau, D. W., *Trans. Am. Inst. Mining Met. Engrs.* **202**, 66 (1955).
- (14) *Ibid.*, p. 958.
- (15) Gaudin, A. M., Sun, S. C., *Ibid.*, **169**, 347 (1946).
- (16) Ghosh, D. N., Choudhury, B. K., De, P. K., *Trans. Faraday Soc.* **50**, 955 (1954).
- (17) Gouy, G., *J. phys. radium* **9** (4), 457 (1910).
- (18) Haydon, D. A., Proc. 3rd Intern. Congr. Surface Activity, Cologne, Vol. II, p. 341, 1960.
- (19) Helmholtz, H., "Two Monographs on Electrokinetics," Engineering Research Institute, University of Michigan, p. 101, 1951.
- (20) Henry, D. C., *Proc. Roy. Soc. (London)* **A133**, 106 (1931).
- (21) Jordan, D. O., Taylor, A. J., *Trans. Faraday Soc.* **48**, 346 (1952).
- (22) Korpi, G. K., M.Sc. thesis, Massachusetts Institute of Technology, Cambridge, Mass., 1960.
- (23) Kortum, G., Bockris, J. O'M., "Textbook of Electrochemistry," Vol. II, p. 564, Elsevier, Amsterdam, 1951.
- (24) *Ibid.*, p. 630.
- (25) Mackor, E. L., *Rec. trav. chim.* **70**, 663, 747 (1951).
- (26) Martinez, E., Zucker, G., *J. Phys. Chem.* **64**, 924 (1960).
- (27) Modi, H. J., Fuerstenau, D. W., *Ibid.*, **61**, 640 (1957).
- (28) Neale, S. M., *Trans. Faraday Soc.* **42**, 473 (1946).
- (29) O'Connor, D. J., Proc. 2nd Intern. Congr. Surface Activity, London, Vol. III, p. 319, 1957.
- (30) O'Connor, D. J., Johansen, P. G., Buchanan, A. S., *Trans. Faraday Soc.* **52**, 229 (1956).
- (31) Ottewill, R. H., Dept. of Colloid Science, University, Cambridge, England, personal communication.
- (32) Overbeek, J. Th. G., *Kolloid Beih.* **54**, 287 (1943).
- (33) Overbeek, J. Th. G., Wijga, P.W.O. *Rec. trav. chim.* **65**, 556 (1946).
- (34) Parreira, H. C., Ottewill, R. H., *An. acad. brasil. cienc.* **32**, 35 (1960).
- (35) Parsons, R., Proc. 2nd Intern. Congr. Surface Activity, London, Vol. III, p. 118, 1957.
- (36) Perrin, J., *J. chim. phys.* **2**, 601, 635 (1904); **3**, 50 (1905).
- (37) Powney, J., Wood, L. J., *Trans. Faraday Soc.* **36**, 57 (1940).
- (38) Rutgers, A. J., De Smet, M., DeMoyer, G., *Experientia* **12**, 371 (1956).
- (39) Rutgers, A. J., De Smet, M., DeMoyer, G., *Trans. Faraday Soc.* **53**, 393 (1957).
- (40) Samoilov, O. Ya., *Discussions Faraday Soc.* **24**, 141 (1957).
- (41) Taylor, A. J., Wood, F. W., *Trans. Faraday Soc.* **53**, 523 (1957).
- (42) Verwey, E. J. W., Overbeek, J. Th. G., "Theory of the Stability of Lyophobic Colloids," p. 22, Elsevier, New York, 1948.
- (43) Whitney, W. R., Blake, I. C., *J. Am. Chem. Soc.* **26**, 1939 (1904).
- (44) Williams, G. C., *Trans. Faraday Soc.* **36**, 1042 (1940).
- (45) Zieglaflaff, C. L., Mazur, I., *J. Colloid Sci.* **15**, 437 (1960).
- (46) Zucker, G. L., Sc. D. thesis, Columbia University, 1959.

RECEIVED August 8, 1961,

Surface Diffusion of Low Boiling Gases on Saran Charcoal

J. R. DACEY

*Chemistry Department, Royal Military College of Canada,
Kingston, Ontario, Canada*

Hydrogen, deuterium, neon, argon, and methane flow through saran charcoal by both Knudsen and surface flow. The latter is effected by the adsorbed molecules sliding from site to site across the surface. This is equivalent to a two-dimensional Knudsen flow where the adsorption site acts as the wall of the three-dimensional case, and a slide across the surface is the same as a flight across the pore. The activation energy for surface diffusion is 75 to 80% of the heat of adsorption. It is possible to calculate theoretically the relative contribution of each mechanism, while comparison with He, which does not adsorb, permits its experimental determination. The efficiency of surface flow is the ratio of the measured to the calculated value; this decreases as the size of the molecule increases, being 80% for Ne and 12% for CH₄.

When a gas passes, because of a pressure gradient, through a system of fine pores, the pressure may be sufficiently low and the pores sufficiently fine that the mean free path of the gas molecules is greater than the pore diameter. When this is so, the gas is transported by Knudsen flow and the amount of gas flowing is independent of the mean pressure but depends only on the pressure difference. When the pores are larger and the pressure is higher, the mean free path is smaller than the pore diameter. The gas is then transported by Poiseuille flow and the rate varies inversely as the gas viscosity. In this case the amount flowing at constant pressure gradient increases with the mean pressure. In any given case one may distinguish between these two methods of flow, as was shown by Adzumi, by plotting the amount flowing for constant pressure difference against the mean pressure (1). A horizontal line indicates Knudsen flow, while a sloping line indicates Poiseuille flow in addition. In the latter case the slope gives the Poiseuille flow and the intercept the Knudsen flow. When absorption occurs on the walls of

the pores, the adsorbed molecules may in some cases move along the surface, resulting in a transport of gas in the adsorbed phase. Such behavior has been found by Flood (8), Barrer (2, 3, 4), Carman (5), and others for a variety of porous solids. The present paper deals with the flow of small molecules through a porous form of carbon known as saran charcoal.

Poly(vinylidene chloride) may be obtained from The Dow Chemical Co. as a white powder, designated saran A. To prepare saran charcoal from this powder it is first pressed into a convenient shape by use of a hydraulic press and steel die at a pressure of 15,000 p.s.i. The compressed polymer is then heated slowly in vacuo, starting at 125° C. and gradually increasing the temperature up to 750° C. The heating process takes about 3 weeks and the resulting piece of carbon retains the shape of the original polymer but is reduced in size in all directions by about 20%.

Saran charcoal is a hard, strong, and highly porous form of carbon. The pores are believed to be very fine and uniform, slotlike in cross section, and between 12 and 15 Å. in width in their narrowest dimension (6).

In saran charcoal the pores are so small that molecules of the size of branched hydrocarbons, such as neopentane, iso-octane, and 2-methylpentane, to be in the pores at all are also on the pore walls. When such molecules are adsorbed, they pass into the charcoal by a process similar to the surface flow of adsorbed molecules in larger pores. Such molecules move by an activated diffusion and activation energies have been determined from the temperature dependence of the rates of adsorption (6). Larger molecules such as α -pinene, tetraethylmethane, and sulfur hexafluoride, adsorb with great slowness, being too large to enter the pores easily. With small molecules up to 4 or 5 Å. in diameter, Knudsen flow should be possible. However, gases such as H₂, D₂, Ne, and Ar are adsorbed so rapidly that their rates of adsorption cannot be readily measured. The present paper describes experiments designed to determine the flow mechanism of these small molecules through saran charcoal by measuring the transport of the gas under a pressure gradient through a thin diaphragm.

Experimental Methods

Preliminary experiments indicated that a convenient charcoal diaphragm, permitting a reasonable flow rate of gas, was about 1 cm. in diameter and 0.2 to 1.0 mm. thick. A number of disks of carbon were made of this size by carbonizing slightly larger disks of compressed poly(vinylidene chloride) and smoothing them on each side by rubbing on fine emery paper. This made them flat, so that their thickness could be measured accurately. The disks were handled by dry-box technique to avoid adsorption of water or other contaminants from the air.

The disk was mounted with Epon resin across the open end of a glass tube and the tube assembled as the inner tube of an ordinary trap. This trap is connected to the gas metering apparatus shown in Figure 1. This consists of a standard-bore tube of accurately known diameter, *B*, which contains the gas under investigation. The pressure is maintained constant by means of the tungsten contacts, *E*, which operate a relay, *F*, controlling a valve so that as the pressure drops the gas which has passed through the diaphragm is replaced by mercury, thus restoring the pressure. A similar metering device on the other side of the diaphragm measures the volume and maintains constant pressure of the gas leaving the charcoal. The rate of flow of the gas is measured by observing the level of the mercury in the standard bore tube by a cathetometer. The charcoal is located at *C* and may be held at constant temperature by immersion in a thermostat bath. The thermostat was a Dewar flask containing water for temperatures between 0° and 100° C., and acetone or Freon for temperatures below zero. Cooling was accomplished by using an outer Dewar, the annular space be-

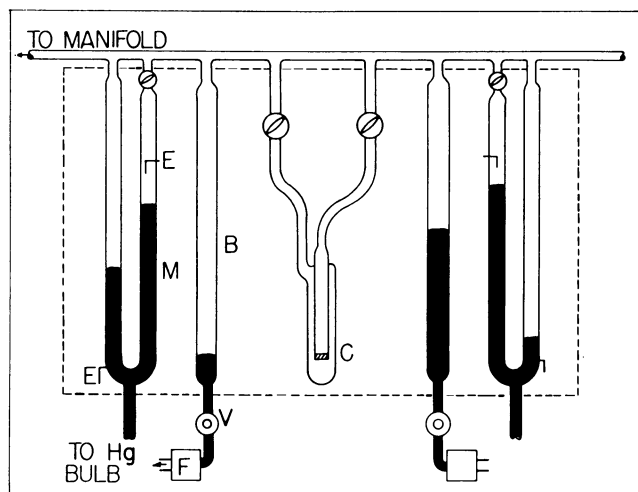


Figure 1. Apparatus

tween being filled with liquid air. The gas pressure between the walls of the inner Dewar could be controlled to regulate the rate of cooling. A resistance wire wound around a support on the inner wall of the inner Dewar was used for heating. Temperature measurement and control to 0.01°C . were accomplished by a platinum resistance thermometer and a Müller bridge. The off-balance current of the latter was amplified and used to operate the heating relay.

Before being used for flow experiments, each disk was tested with helium for acceptability. The rate of helium flow at 10-cm. pressure gradient across the disk was measured at several mean pressures between 5 and 50 cm. Unless the mass of gas passing per unit time was constant—i.e., the flow through the disk followed Knudsen's law—the disk was rejected. About one disk in ten passed this test; the others showed increased flow at high pressures.

Reproducible flow rates in the Knudsen region could be achieved with adsorbable gases only if the total amount adsorbed was small. Adsorption of 10% by weight, or greater, altered the permeability of the carbon. This effect on permeability may have been due in part to loosening of the cement but could not be wholly corrected by recementing. It is believed that the internal structure of the charcoal was altered in critical regions by strains produced by the adsorption of considerable amounts of adsorbate. For this reason all experiments on flow were carried out with less than 3% by weight adsorbed. Under these conditions results reproducible to within 5% were possible on any favorable sample for a considerable time. However, a charcoal disk would eventually change its flow properties, suddenly increasing in permeability. This may have been due to thermal shock, accidental exposure to too high a pressure, or some other cause. For this reason only a limited number of data were obtained from any one carbon disk and a number of different disks had to be used. During any series of runs the flow of helium was measured from time to time as a check on the condition of the carbon disk.

A series of tests was made by measuring the helium flow rate after successive adsorption and desorption of ethane to 10% of the weight of the carbon. With a disk which originally exhibited only Knudsen flow, Poiseuille flow appeared and

the Knudsen flow increased. After eight or nine cycles of adsorption and desorption the increase in flow stopped and a reproducible helium flow rate was established with a combination of Poiseuille and Knudsen flow.

The adsorption isotherms were determined either gravimetrically with a quartz spiral balance or volumetrically by means of a modified BET apparatus (9).

The helium, argon, neon, and hydrogen were supplied by the Air Reduction Co. The methane was supplied by Phillips Petroleum Co. The deuterium was prepared from heavy water provided by Atomic Energy of Canada. The heavy water was reacted with an excess of the liquid alloy of Na and K, by breaking an ampoule of the alloy in the presence of 5 grams of heavy water contained in a closed system of 3-liter volume.

Experimental Results

A BET plot of the adsorption data for argon at its boiling point gave a linear portion over the range $p/p_0 = 0.001$ to 0.20. Taking 14.6 Å. as the area of the argon atom, this gives a surface area for the carbon of 590 sq. meters per gram. The porosity of the carbon was calculated from the difference between helium and mercury displacement densities. The average value of ten disks, which agreed between themselves within 6%, was 0.44 cc. per gram. From these data an average pore radius, γ , may be determined by using the relation $\gamma = 2\epsilon/A$ (7), where ϵ is the porosity and A the area. The value obtained is 15 Å. This assumes that the charcoal is made up of a large number of cylindrical pores. We know this is not true; the evidence of rates of adsorption shows that the pores are slotlike and less than 15 Å. in diameter rather than radius (6).

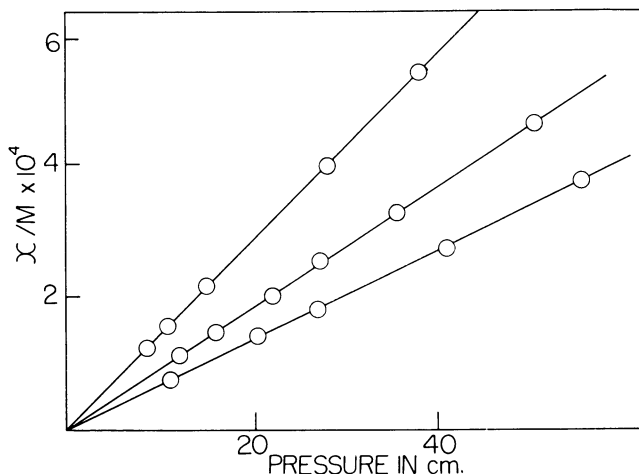


Figure 2. Adsorption of neon at -35.0° , -55.3° , and -75.8° C.

Figures 2 through 6 show the isotherms for neon, argon, hydrogen, deuterium, and methane. Heats of adsorption were calculated from these isotherms: Ne 1650, H₂ 2350, D₂ 2400, Ar 4900, CH₄ 5900 cal. per mole.

The carbon disks used for these experiments had been selected so that the

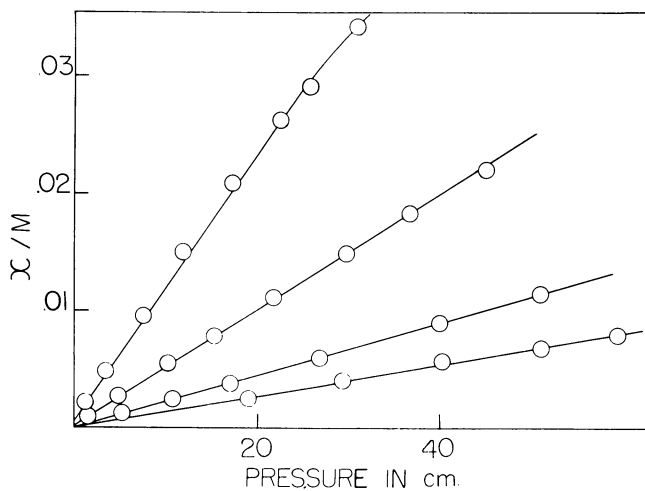


Figure 3. Adsorption of argon at -30° , 0° , 30° , and 60° C.

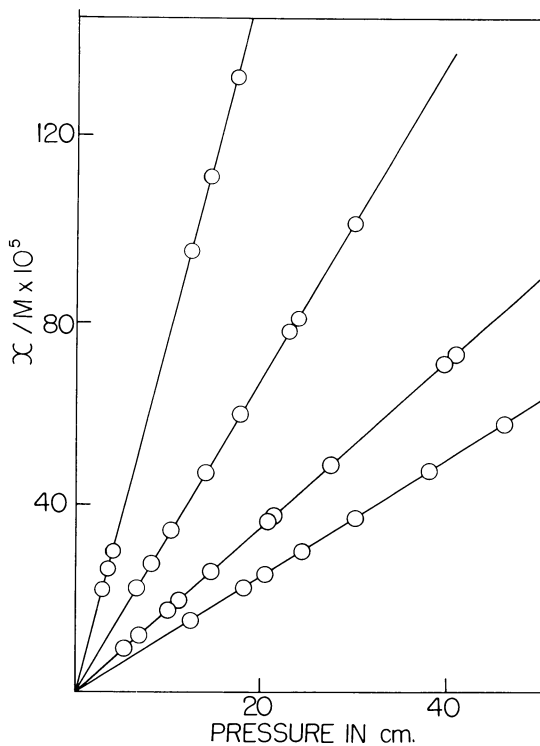


Figure 4. Adsorption of hydrogen at -100° , -70° , -35° , and 0° C.

flow of helium was entirely Knudsen flow according to the Adzumi plot. This was confirmed by the measured temperature dependence, as seen in Figure 7 where the total amount of gas passing per unit time at constant pressure gradient

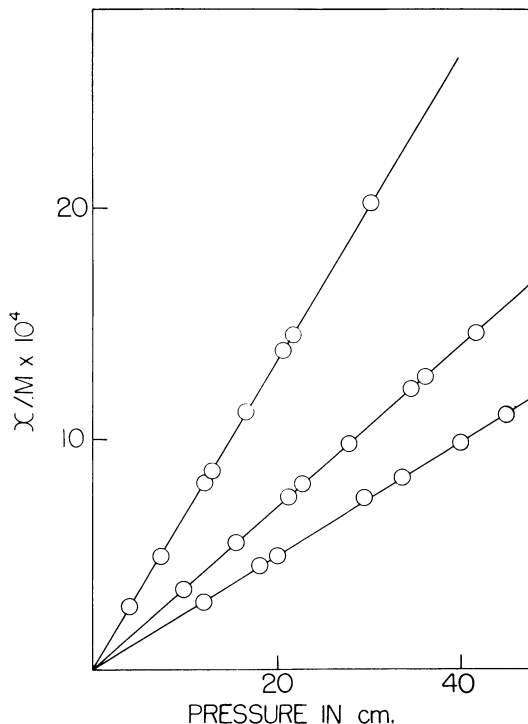


Figure 5. Adsorption of deuterium at -70° , -35° , and 0° C.

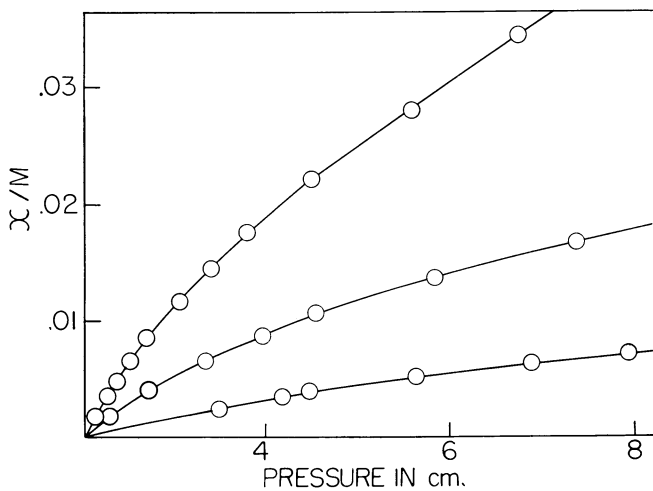


Figure 6. Adsorption of methane at -30° , 0° , and 30° C.

varies inversely as the square root of the temperature. The helium flow is therefore taken to be a measure of the Knudsen permeability of the carbon disk and from it the Knudsen flow for any other gas can be calculated.

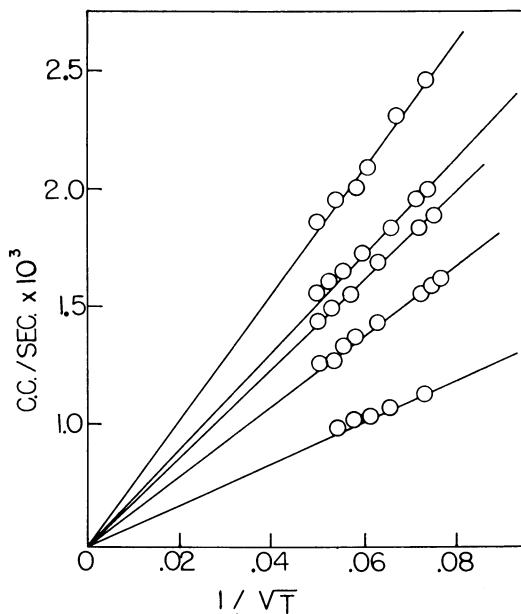


Figure 7. Flow of helium through several different disks as a function of pressure

All disks have approximately same thickness, 0.4 mm.

The other gases used were examined in the same way as helium. In all cases the flow exceeded the Knudsen flow as predicted from the helium data. Figure 8 gives typical data; the flow in excess of the calculated Knudsen flow is attributed to surface diffusion of the adsorbed molecules.

Instead of maintaining a pressure difference of 10 cm. across the carbon disk, one may select the proper pressures by reference to the adsorption isotherms so that the concentration gradient in the adsorbed phase remains constant. A pressure gradient from 0.5 to 1% was chosen as suitable. Of the gases used, this technique is possible only with argon and methane, unless one uses very high pressures. The data in Table I were obtained in this way.

Table I. Flow of Gases for a Concentration Gradient in Adsorbed Phase of 0.005 to 0.010 Gram per Gram of Carbon

Temp., °C.	Total Flow, Cc./Sec. × 10 ³	Knudsen Flow, Calcd. from Helium Data, Cc./Sec. × 10 ³	Surface Flow, Cc./Sec. × 10 ³
Argon			
-30	3.57	2.51	1.06
0	8.32	5.60	2.72
30	15.98	11.12	4.86
50	22.09	15.18	6.91
Methane			
-30	1.87	1.68	0.19
0	4.80	4.25	0.55
30	13.48	11.94	1.54
60	28.15	24.17	3.98

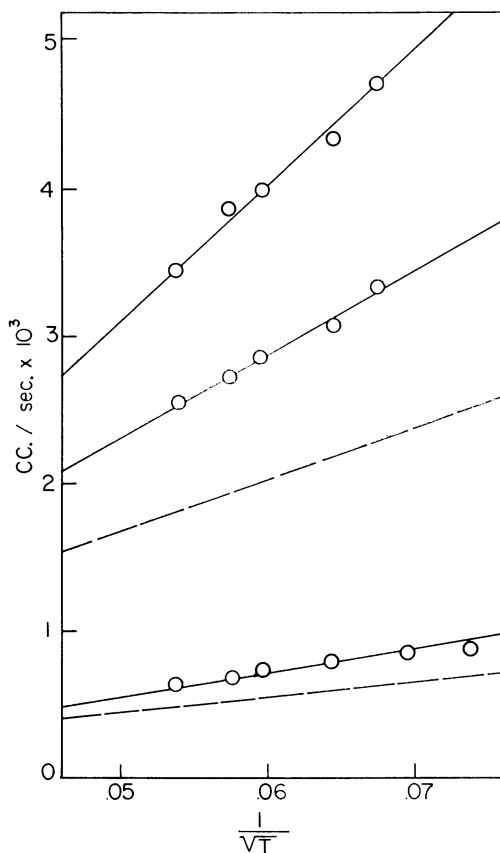


Figure 8. Gas flow as a function of pressure

Upper curves. Hydrogen and deuterium as compared with helium. Dashed line, disk 8
 Lower curves. Neon and calculated Knudsen flow of neon for disk 2

Discussion

The Knudsen permeability of a porous system of unit area and thickness is given by $K = \frac{8\epsilon}{3\kappa A} \frac{2RT}{\pi M}$ for unit pressure gradient, where κ is a structural constant or shape factor. For any system of ideal cylindrical pores κ is equal to unity. With helium flowing through saran charcoal disks, the measured permeability is between 4 and 8.5% of the ideal value. This means that κ lies between 25.0 and 11.7.

The high value for κ indicates that this carbon does not resemble a system of ideal cylinders but rather that only a fraction of the void volume supports flow, the remainder being shut off from a continuous path or otherwise not functional.

As can be seen from Figure 7, the resistance to flow of various disks is not proportional to the disk thickness. In fact, the value for κ for different disks varies over a range of about 200%, while the porosity varies only about 5%. The

proportion of pores supporting Knudsen flow in any given disk probably depends on random effects operating during its production. For this reason we cannot say that resistance to flow is the same at all depths throughout a single disk, and the pressure drop across a disk need not be linear with thickness.

Hydrogen and deuterium both exhibit considerable surface flow, as seen in Figure 8. In both cases the temperature dependence gives an activation energy for surface diffusion of 1850 cal. per mole or 77% of the heat of adsorption. With these gases the total flow is always in the ratio $1:\sqrt{2}$. Since this is the expected ratio for Knudsen flow, it follows that the surface flow also varies inversely as the square root of the molecular weight. It is therefore suggested that surface diffusion is a two-dimensional Knudsen flow where fixed adsorption sites play the role of the walls and a slip across the surface is equivalent to that of a flight across a pore. The activation energy for surface diffusion is therefore the energy necessary to break the bonds holding the molecule to the adsorption site while it still remains on the surface but is not free to slide to an adjacent site. This is to be contrasted with the activation energy for ordinary Knudsen flow, which is that necessary to remove the molecule from the surfaces and allow a free flight across a pore. The latter is equal to the heat of adsorption. Knudsen flow is not affected by the extent of adsorption. If two molecules of the same molecular weight have the same Knudsen flow—e.g., He and D_2 —the former is not absorbed but the latter is. A molecule of a species which is strongly adsorbed spends a longer time on the wall than one of a more lightly adsorbed species, but at any instant the total number in flight across a pore is the same for each. For two-dimensional Knudsen flow the same should be true. The species with higher surface concentration, for any given pressure, is more difficult to move laterally across the surface and spends more time at each fixed site than the less adsorbed one. As long as the ratio of the activation energy, E , for surface diffusion to the heat of adsorption, ΔH , is the same for two gases, the surface diffusion would be expected to be proportional to $1/\sqrt{M}$. As seen below, size may play a part in surface diffusion; and the above statement may be true only if both species are of similar size.

Both the adsorption of neon and its surface flow are small. The accuracy of determining the activation energy for surface diffusion is therefore poor. An average value of 1250 cal. is calculated from the data in Figure 8. This value is considerably greater than RT , indicating that we do have activated diffusion and not a mobile film.

The data for argon and methane appear in Table I. The activation energies for these gases are, respectively, 3800 and 4450 cal. per mole.

The ratio of $e^{-E/RT}$ to $e^{\Delta H/RT}$ should give the number of times a molecule slides to an adjacent site within the surface for each time it leaves the surface for a flight across a pore. One would expect a single slip across the surface to be less effective in advancing the molecule than a single flight across a pore. Adsorption sites are perhaps only 2 or 3 Å. apart, while a flight across a pore would advance a molecule 15 to 20 Å. If we assume a factor of 7 for the relative value of a flight compared to a slip, we can arrive at an efficiency index for surface flow for each gas. For neon 2.6 surface slips occur for every Knudsen flight, but each flight is 7 times as effective as a slip; therefore, the calculated ratio of surface to volume flow is 0.37, the actual value is 0.29, and the efficiency for surface flow for neon is 78%. For methane the efficiency is only 12%. Figure 9 shows the efficiency plotted against the molecular diameter for the five gases used. On the assumption that molecular size does not affect ordinary Knudsen flow, one can conclude that

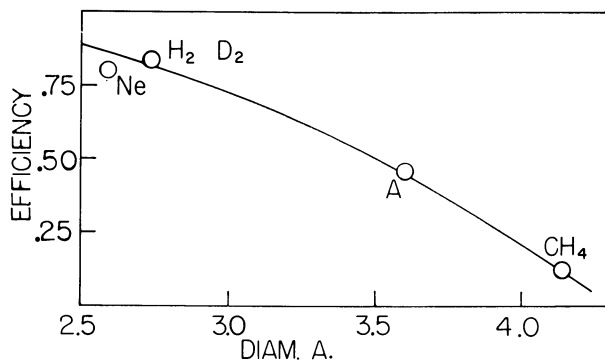


Figure 9. Efficiency of surface flow as a function of molecular diameter

small molecules like Ne, H₂, and D₂ move very efficiently across the surface while larger ones meet with surface hindrances and in effect must traverse a longer path.

Acknowledgment

We acknowledge the financial assistance of the Defence Research Board of Canada under Grant 8220/12.

Literature Cited

- (1) Adzumi, H., *Bull. Chem. Soc. Japan* **12**, 285 (1937).
- (2) Barrer, R. M., Barrie, J. A., *Proc. Roy. Soc. (London)* **A213**, 250 (1952).
- (3) Barrer, R. M., Grove, D. M., *Trans. Faraday Soc.* **47**, 837 (1951).
- (4) Barrer, R. M., Strachan, E., *Proc. Roy. Soc. (London)* **A231**, 52 (1955).
- (5) Carman, P. C., Raal, F. A., *Ibid.*, **A209**, 38 (1951); *Trans. Faraday Soc.* **50**, 842 (1954).
- (6) Dacey, J. R., Thomas, D. G., *Ibid.*, **50**, 740 (1954).
- (7) Emmett, P. H., de Witt, T. W., *J. Am. Chem. Soc.* **65**, 1253 (1943).
- (8) Flood, E. A., Tomlinson, R. H., Leger, A. E., *Can. J. Chem.* **A30**, 348, 372, 389 (1952).
- (9) Young, D. M., Beebe, R. A., Bienes, H., *Trans. Faraday Soc.* **47**, 1086 (1953).

RECEIVED June 19, 1961.

Thiophene Desulfurization by a Microreactor Technique

P. J. OWENS and C. H. AMBERG

Division of Applied Chemistry, National Research Council, Ottawa 2, Canada

The hydrodesulfurization of thiophene was investigated over chromia and supported cobalt molybdate catalysts in a microreactor permitting the use of both flow and pulse techniques. The rates of various steps in the reaction were studied independently, the results supporting the view that C-S bond cleavage rather than thiophene hydrogenation was the initial step. The apparent activation energy for the flow reaction over Co molybdate was 25 kcal. per mole. Adsorption of both reactants and products on this catalyst was examined under operating conditions. Peak elution time of C₄'s and thiophene was principally governed by temperature. The C₄'s desorbed much faster than thiophene and had a relatively small effect on the rate of desulfurization. H₂S adsorbed rapidly; its desorption rate was dependent on the total H₂S content of the catalyst. Adsorbed H₂S markedly suppressed butene hydrogenation, affecting the desulfurization to a smaller extent.

The mechanism of hydrodesulfurization of thiophene has been studied by a number of workers and results up to 1957 have been reviewed by McKinley (22). The reaction probably always proceeds in a series of consecutive steps between thiophene and the final butane and H₂S product (19), but there have been various opinions as to the exact nature of the steps involved for different catalysts. Thus the first step has been said to involve ring saturation (5, 6, 23, 24) or ring opening to form 1-butadienethiol (19). Traces of butanethiol and tetrahydrothiophene have been found in the products of thiophene desulfurization over various catalysts, but it has not always been clear whether these were intermediates or by-products. There have been few studies of the kinetics of the reaction (14, 25, 27) and even less of relevant adsorption phenomena (10, 27).

It seemed possible that the microreactor technique developed by Emmett

and coworkers (8, 9, 12, 13, 18) would lend itself not only to the detection of chemical intermediates in the reaction, but also to the separate study of the rates of reaction of those intermediates, if the latter were stable. In fact, butadiene and the butenes were found to be intermediates under the conditions used and were studied in this way. In addition, band spreading and peak retardation caused by the slow desorption of some reaction products from the catalyst surface led to a study of the way in which adsorption and desorption of reactants and products might influence the over-all reaction rate.

Since conditions are not quite the same for a catalyst used intermittently to study 5-mg. samples in a stream of pure hydrogen as they are for one under normal continuous flow operation, some continuous flow experiments were done for comparison.

Experimental

The apparatus used for most of the work was similar in layout to that described by Emmett and coworkers (8, 9, 12, 13, 18).

A stream of hydrogen flowed first through the reactor and then through an analytical column, serving both as a reactant and as a carrier gas. Samples of the other reactant—e.g., thiophene—were injected through a serum cap above the catalyst. The products flowed to the analytical column and were analyzed immediately. In this type of experiment the hydrogen-thiophene ratio is difficult to measure and varies from point to point in the thiophene band. The smallest practicable thiophene shots were therefore used to keep this ratio high while studying other variables such as temperature and H_2S poisoning.

Modifications of Apparatus. High flow rates through the catalyst were obtained by allowing most of the gas to pass to a metered blowoff between the reactor and the analysis column.

Ordinary flow reactions were carried out by using two entirely separate gas streams. A saturator was used to maintain a steady concentration of thiophene in the reactor feed, and gas samples from the reactor product line were transferred to the analysis column by syringe.

Some of the measurements of peak delay caused by adsorption on the catalyst were made more conveniently by dispensing with an analytical column and connecting the reactor and katharometer together directly.

Reactor Dimensions. Borosilicate glass tube, 10-mm. i.d., with 6-mm. o.d. thermocouple well down the center. The catalyst was supported on a sintered-glass disk. The empty tube was tested for catalytic activity and found inactive towards thiophene at temperatures up to 550° C.

Catalysts. Chromia prepared by the method of Burwell and others (3, 4). Weight 0.86 gram. Treated with continuous flow of hydrogen and thiophene for 2 hours at 400° C. before use. This particular catalyst deteriorated rather rapidly.

Cobalt molybdate, Girdler No. G35A, received as pellets, then crushed and sieved to 35 to 65 mesh. 1.3% Co + 6.1% Mo on alumina; BET nitrogen surface area 241 sq. meters per gram; stabilized with thiophene in a flow reaction at 400° C. before use. Weight of catalyst used is noted with each set of results.

Materials. Hydrogen, purified by passage through a palladium catalyst and drying column to remove oxygen and water.

Thiophene, Matheson 5876, > 99% pure by gas chromatography, used as received.

C_4 hydrocarbons, Phillips research grade, used as received.

Analytical Columns. To measure activities, 6-foot squalane column at 90° C., 25% w./w. on Chromosorb.

To separate C_4 products, 25-foot or 50-foot propylene carbonate columns at 23° C., 30% w./w. on Chromosorb (21) (results in Table I obtained with 18-foot tricresyl phosphate column at 23° C., 40% w./w. on C_{22} firebrick).

Table I. Analysis of C₄ Products Obtained over Chromia Catalyst(0.86 g. chromia catalyst at 415°C., 9 liters H₂/hr.,
10- μ l. liquid, 0.5-cc. gas samples)

Reactant	Product, % of C ₄ Fraction				
	Isobutane	<i>n</i> -Butane	1-Butene + isobutene ^a	<i>trans</i> -2- Butene	<i>cis</i> -2- Butene + butadiene
Thiophene	0	8.6	30.1	27.4	33.9 ^b
1,3-Butadiene	0	2.0	23.1	36.7	38.2 ^b
1-Butene	0	8.9 ^c	42.1	26.6	22.4
<i>trans</i> -2-Butene	0	1.9	22.3	52.4	23.5
<i>cis</i> -2-Butene	0	2.0	21.2	37.6	39.2
Isobutene	2.0	0	98	0	0
<i>n</i> -Butane	..	100	0	0	0
<i>n</i> -Butene (equil. in gas phase)			20	48	32

^a Presumed absent wherever isobutane was absent.^b Butadiene present.^c May be high because of impurity.

Results and Discussion

Reaction Products. No mercaptan or tetrahydrothiophene intermediates were found in the products of shot reactions over either catalyst. Instead thiophene reacted by rejecting its hydrocarbon portion either as a butadiene-butene mixture (from chromia) or a butene-butane mixture without butadiene (from cobalt molybdate). In both cases, the sulfur was left on the catalyst as adsorbed H₂S. No H₂S peak was observed following any such reaction and subsequent experiments with H₂S showed that the rate of desorption of H₂S was negligible until much higher concentrations on the catalyst surface had been reached.

Chromia Catalyst. SEQUENCE OF REACTIONS. The reactions of the C₄ hydrocarbons on the sulfided chromia catalyst were investigated at 415° C. and the products compared with those of thiophene (Table I).

The conversion of any of the butenes to butane was very slow compared with the conversion of butadiene to butene, the 2% conversion of butene as against an estimated 90 to 98% conversion of butadiene (which was incompletely resolved from *cis*-2-butene) indicating that a factor of at least 50 was involved.

No appreciable skeletal isomerization of the butenes occurred.

Both *cis*-*trans* isomerization and double bond shift were incomplete under these conditions, and the product obtained from thiophene contained an excess of 1-butene over the thermodynamic equilibrium amount.

Dehydrogenation of butane or butene did not occur, and was therefore ignored in drawing Figure 1.

The heavy lines in Figure 1 indicate reactions which were experimentally shown to occur—the conversion of thiophene to butadiene in one step, followed by hydrogenation of the butadiene to butene, for example. The results do not eliminate the possibility of two hydrogenation steps occurring on one site (see dashed lines in Figure 1).

No attempt has been made in Figure 1 to indicate the detailed mechanism of the reaction. One such mechanism has been suggested by Komarewsky and Knaggs (19); this specifies butadiene as an intermediate, but also involves mercaptans which were not found in the present study. The mechanism proposed by Griffith, Marsh, and Newling (10) involves stepwise conversion of thiophene to butene on one site and thus does not allow butadiene formation. The present

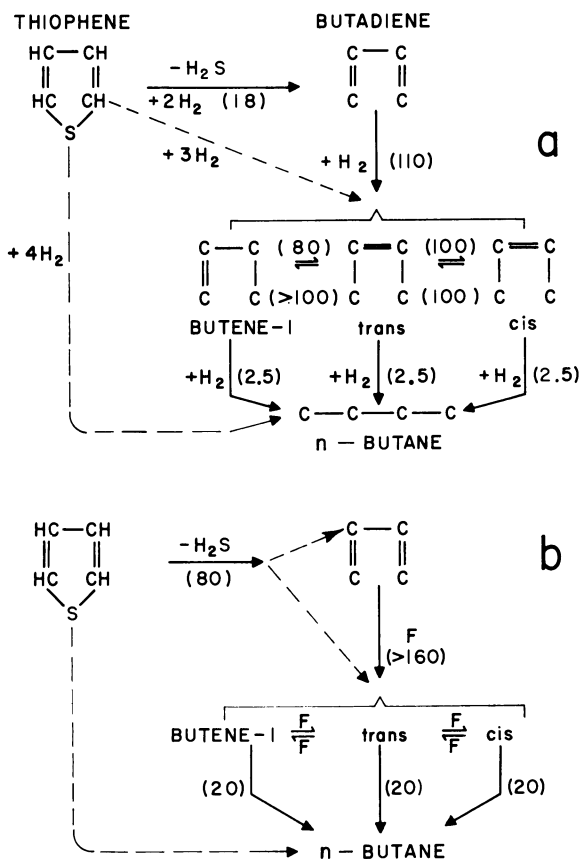


Figure 1. Reaction schemes and estimates of rates of steps

Micromoles per gram of catalyst per second

a. Chromia at 415° C.

b. Cobalt molybdate at 400° C.

results, however, support the view of these authors that the first step in the reaction is C—S bond cleavage rather than hydrogenation of the ring.

The figures in parentheses in Figure 1 are estimates of the rates of the various reaction steps in micromoles converted per gram of catalyst per second. They were calculated from results on thiophene, butadiene, and the butenes such as those shown in Table I, and should be regarded only as a rough indication of relative values. It is hoped to publish further data at a later date.

Cobalt Molybdate Catalyst. SEQUENCE OF REACTIONS. Similar reactions were observed over the more active commercial cobalt molybdate catalyst. This effected 82% conversion of a 5- μ l. thiophene shot at 400° C.

The hydrocarbon product obtained at 400° C. was analyzed in detail. No isobutene, isobutane, or butadiene was found. The reaction was then carried out at a series of temperatures down to 274° C. and at much higher flow rates; the relative amounts of the different C₄'s obtained were similar at all temperatures and no butadiene was found under any conditions.

The reactions of the individual C₄ hydrocarbons were also investigated. At

350° C. butadiene and the butenes were almost entirely converted to butane, though the C₄ product from thiophene contained only 21% butane, the other 79% being butene.

Since H₂S was very strongly adsorbed by the catalyst, it seemed likely that under flow reaction conditions the catalyst would always be effectively saturated with H₂S. Accordingly, 2- to 10-cc. samples of H₂S, judged to be well in excess of saturation, were put on the catalyst to test their effect on thiophene conversion and butene hydrogenation. Thiophene conversion was lowered appreciably (Figure 2). The effect on butene hydrogenation was greater still. In a typical experiment at 350° C. a butene shot was 93% hydrogenated in the absence of H₂S, while immediately after injection of 2 cc. of H₂S the butene conversion obtained was less than 5%. In each case, smaller amounts of H₂S caused smaller changes in conversion.

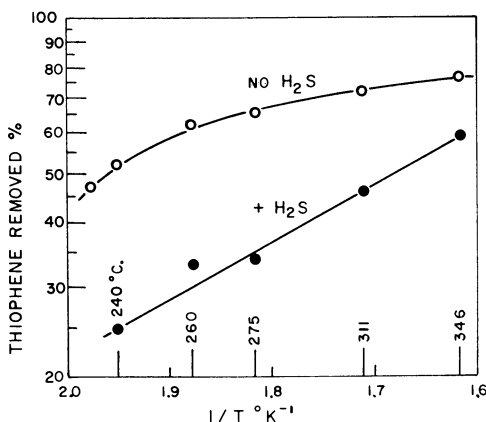


Figure 2. Effect of preadsorbed H₂ on per cent desulfurization of thiophene shots

3.6 grams of cobalt molybdate catalyst
6.0 liters of H₂ per hour
5-cc. H₂S shots injected 3 to 5 seconds before
5 μl. of thiophene

On the other hand, H₂S did not prevent cis-trans isomerization and double bond shift reactions from going to completion at 300° or 350°, and the olefin mixtures analyzed were always found to be close to thermodynamic equilibrium, whether they had been formed from thiophene, butadiene, or one of the olefins themselves. Nor did H₂S prevent the total conversion of butadiene to butene, even when 10- to 20-cc. samples were used at reaction temperatures down to 200° C. and flow rates up to 10 liters per hour. This may be the explanation of the absence of butadiene from the thiophene reaction products over cobalt molybdate—that if it had been formed as it was over chromia, it would have reacted further too rapidly to survive.

Figure 1, *b*, shows the reaction scheme for cobalt molybdate, with estimates for the rates of the steps observed.

EFFECT OF TEMPERATURE ON REACTIONS. The hydrocarbon products given by single shots or slugs of thiophene on cobalt molybdate catalyst were analyzed at various temperatures in the range 400° to 274° C. There was little change in percentage unsaturation or in the relative amounts of the various C₄ olefins pro-

duced as reaction temperature was lowered, a typical analysis of the C_4 product at any temperature being *n*-butane 21%, 1-butene 20%, *trans*-2-butene 37%, and *cis*-2-butene 22%.

The effect of temperature on the percentage conversion of the thiophene was marked (Figure 3). Data from a normal flow experiment gave a typical plot with an apparent activation energy in the linear portion of 25 kcal. per mole, the figure obtained by Van Looy and Limido (27) using a supported chromia catalyst.

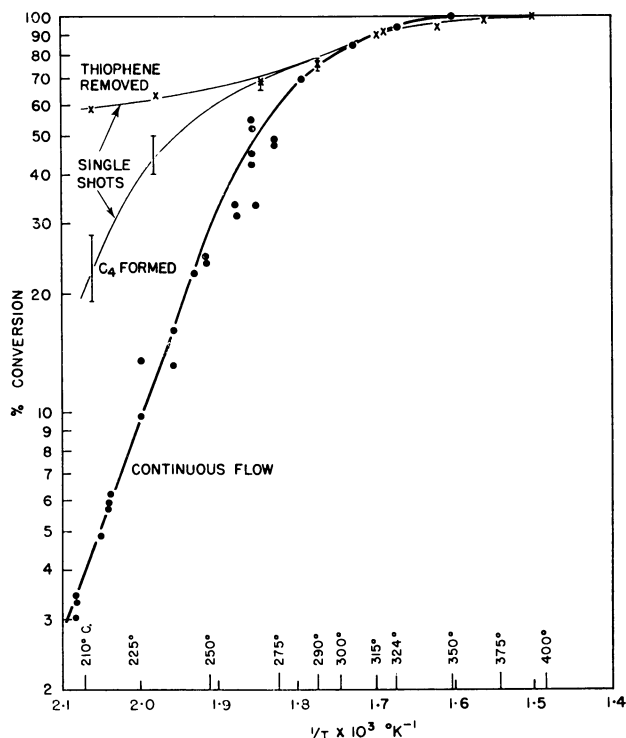


Figure 3. Effect of temperature on conversion for flow and single-shot reactions

5.4 grams of presulfided cobalt molybdate catalyst

5.2 liters of H_2 per hour containing 2 mole % of thiophene in flow experiment

7.0 liters of H_2 per hour and 5- μ l. thiophene shots in single-shot experiments

The single-shot experiments gave very different results. Above about 300° the curve is essentially similar to that of the flow experiment; the flow results lie a little higher, but it is probable that in this case, with 50 moles of hydrogen supplied per mole of feed, hydrogen was more readily available than in the shot experiments. There, the 5- μ l. shots used traversed the catalyst as a band, the center of which probably contained a hydrogen-thiophene ratio of much less than 50 to 1. Smaller shots did give somewhat higher percentage conversions, as shown (for a smaller sample of catalyst) in Figure 4.

Below 300° C. there is a much larger difference between the curves. In this temperature range adsorption on the catalyst caused widening and tailing of the

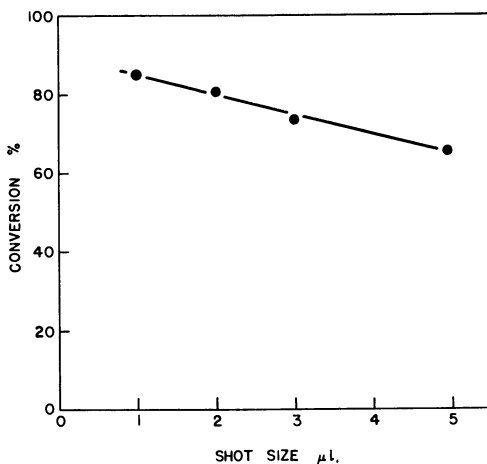


Figure 4. Effect of shot size on thiophene conversion

3.6 grams of cobalt molybdate catalyst at 292° C.
6.8 liters of H₂ per hour

C₄ peak on the shot reaction chromatogram, making measurement difficult. The estimated probable error has been indicated by bars in Figure 3. (A typical peak is shown in Figure 5, *d*; the dashed line shows the peak width for a shot passed through the analytical column alone.) There was also a loss of material in the shot reactions—i.e., the difference between the initial and final quantities of thiophene (upper curve, Figure 3) was greater than the C₄ produced (middle curve). Presumably the loss was due to irreversible adsorption of either butene or thiophene, possibly as a polymer.

Even when taken at their lowest value—namely, as C₄ obtained—shot conversions were still much higher than the corresponding flow conversions at low temperature. This is thought to be due to the effective increase in shot reaction time, as adsorption on the catalyst caused the thiophene band to move more slowly through the catalyst (Figure 6). Thus at 212°, where thiophene in a shot reaction took 68 seconds to pass through the catalyst (Figure 6), the contact time in the flow reaction, assuming piston flow, was 2.3 seconds. Such a change in reaction time would completely overshadow any differences in hydrogen-thiophene ratio, thus accounting for the observed high shot conversions. This implies that flow conversions in the linear portion of the curve were limited by the fact that the active sites were occupied for an appreciable time before either products or unreacted material desorbed, thus preventing further molecules from adsorbing. Successive shots at 212° C. supported this view; the quantities of thiophene desorbing after the second, third, and fourth shots (at 90-second intervals) became progressively larger and their desorption times decreased (Figure 6, points joined by arrow). Five microliters of thiophene can cover only approximately 1% of the surface and a large fraction of this will have eluted during the 90-second period.

Adsorption Studies on Cobalt Molybdate Catalyst. THIOPHENE AND C₄ HYDROCARBONS. The peak delay due to slow desorption of thiophene and its C₄ product from the catalyst in single-shot experiments was investigated further, as it seemed probable that the desorption was slow enough to have a considerable effect on the over-all rate of reaction. The delay in appearance of the peak maximum

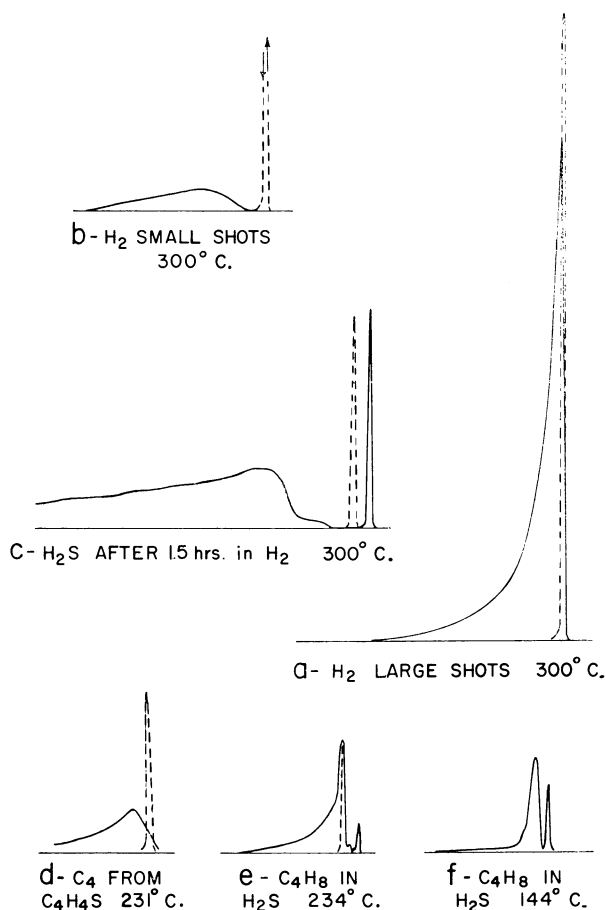


Figure 5. Typical peak shapes for adsorbing gases

--- Hypothetical peak for gas not adsorbed by catalyst

- a. 2 cc. of H_2 , 3.2 liters of N_2 per hour
- b. 0.5 cc. of H_2 , 3.2 liters of N_2 per hour
- c. 2 cc. of H_2S , 6.7 liters of H_2 per hour
- d. C_4 from 5 μ l. of thiophene approximately 50% desulfurized on 5.4 grams of catalyst. 7.0 liters of H_2 per hour
- e. 0.5 cc. of butene in 5 cc. of H_2S . 6.0 liters of H_2 per hour
- f. 0.5 cc. of butene in 5 cc. of H_2S plus helium marker. 5.6 liters of H_2 per hour

was used as a measure of the rate of such desorption, though the delay in the peak front could also have been used.

An attempt was made to study thiophene and C_4 adsorption using nitrogen as carrier gas, and thus remove the complications caused by reaction products. However, adsorption appeared to be very much stronger in nitrogen than in hydrogen, and at 300° and 400° C: up to half the thiophene sample and even more of the butene and butadiene stayed bound to the surface and did not desorb at all. Presaturation of the catalyst with hydrogen before injection of the sample did not prevent this loss, though some thiophene apparently desorbed when more hydrogen was added subsequently and a small amount of bound thiophene was shown to react with hydrogen added as much as 5 minutes later. Thiophene

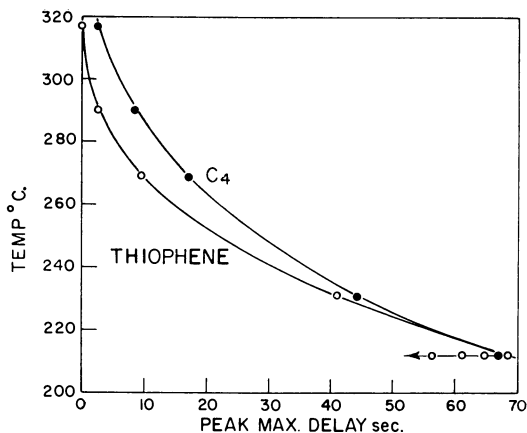


Figure 6. Peak delay due to adsorption on catalyst as function of temperature

5 μ l. of thiophene on 5.4 grams of cobalt molybdate catalyst, bed depth 80 mm., 7.0 liters of H_2 per hour

which did desorb showed some peak broadening even at 400° C., and probably very strong adsorption of butene and thiophene in the absence of hydrogen leads ultimately to carbon formation. For these reasons it was necessary to use hydrogen as the carrier gas, in order to preserve the catalyst surface and to obtain results which would be applicable to reaction conditions. This meant that to observe the thiophene peak behavior it was first necessary to separate it from its C_4 product, which was accomplished by using the 6-foot squalane column. The hypothetical peak maximum position for thiophene which did not adsorb at all on the catalyst was calculated by measuring the retention time for thiophene on the analytical column and adding to this a small helium dead space correction for the reactor. The latter was obtained as the difference between total helium retention time and that of the column alone.

The results in Figure 7 were obtained between 233° and 125° C., and thus extend into the reaction region, since C_4 formation occurred at temperatures down to and including 200° C. Some peak retardation was noticed even at 317° C.; being small, it could not be measured accurately by this method, but was not inconsistent with the extrapolated data of Figure 7. The effect of H_2S on thiophene peak delay was investigated at three temperatures; the peak delay was reduced by 10 to 30% by saturating the catalyst with 5 cc. of H_2S injected immediately before the thiophene shot. The effect of sample size was also investigated (Figure 8).

A modified technique was used to obtain the C_4 data shown in Figures 7 and 8. Attempts to employ an analytical column to separate all the C_4 's and measure the peak retardation of each individually indicated that each of the C_4 's was retarded by a similar amount, but failed at low temperatures because peak widening destroyed the separation. In addition, the butenes could be prevented from converting completely to butane only by saturating the catalyst with H_2S , and some means of eliminating the H_2S before the detector was necessary. Accordingly, the reactor was connected to the Gow-Mac detector through a short column of Ascarite which absorbed H_2S without affecting any of the other components, and the

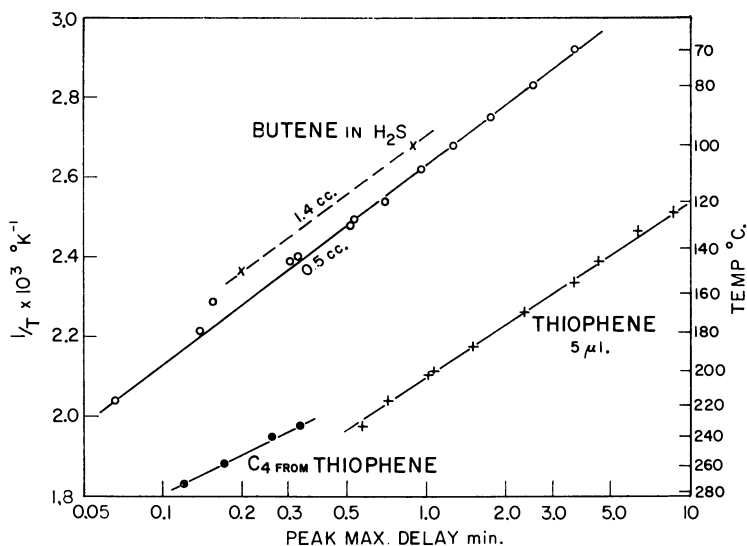


Figure 7. Effect of temperature on butene and thiophene adsorption
 3.6 grams of cobalt molybdate catalyst, bed depth 54 mm., 6.0 liters of H₂ per hour

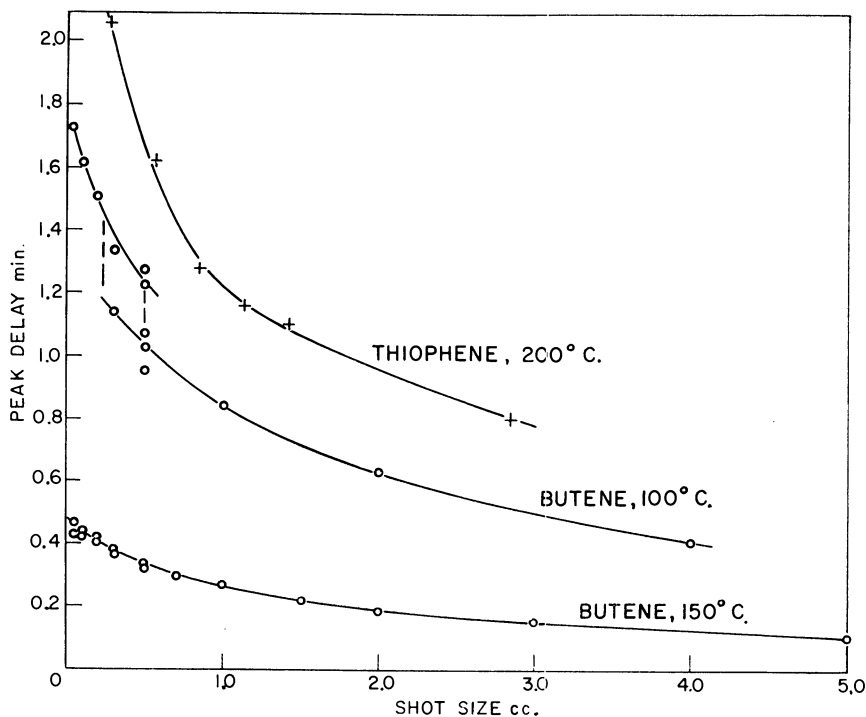


Figure 8. Effect of sample size on peak delay
 3.6 grams of cobalt molybdate catalyst, 54 mm. deep, 5.8 liters of H₂ per hour

analytical column was dispensed with. The butene points were then obtained directly by measuring the separation between helium and butene peak maxima, since separation occurred only on the catalyst (see Figure 5,f; small peak is helium). A 5-cc. syringe was used, containing 0.5 cc. (usually) of *trans*-2-butene, a small quantity of helium marker, and about 4 cc. of H₂S drawn into it in that order. No attempt was made to mix the gases in the syringe, in the hope that upon injection the butene band would be preceded on the catalyst by the excess H₂S. The results lie in the range 70° to 214° C.; above this range separation of butene and helium was incomplete on the length of catalyst column used.

Some experiments with 1,3-butadiene (which hydrogenated immediately to butene) and *n*-butane gave results similar to those obtained with butene; in fact, the two butene curves of Figure 8 were duplicated by butane within the limits of reproducibility. Finally, some peak delay experiments with thiophene were repeated to check that the catalyst had not altered; agreement with previous results was satisfactory.

The results obtained with butene depended to some extent on catalyst history. The 100° C. curve in Figure 8 is an example of this; the catalyst was left for some hours in flowing hydrogen after determining the delays for larger shot sizes, and apparently increased in adsorptive power before the other half of the curve was determined. Heating the catalyst to 400° C. in hydrogen had a similar effect, due apparently to removal of strongly adsorbed material, but in most cases the catalyst reverted to normal behavior after two or three samples at 100° C.

The results show a strong dependence of peak delay on temperature for both thiophene and butene (Figure 7), with a smaller but by no means negligible dependence on sample size (Figure 8). The temperature coefficients calculated from Figure 7 after making corrections to standard conditions are 9.5 ± 1 kcal. per mole for thiophene, and 8.5 ± 0.5 kcal. for butene. Cremer (7) and Habgood and coworkers (1, 11) have shown that for weak adsorption, where equilibrium between adsorbed and gaseous phases can be assumed, temperature coefficients are equal to the heats of adsorption. Whether such assumptions can fairly be made in this case is open to doubt; possibly at higher temperatures, where peak delay is small and mass transfer between the phases is rapid, one could argue an approximation to equilibrium conditions.

A few results using different sample sizes indicated that the temperature coefficient did not vary greatly with coverage in the range examined, in spite of the effect of sample size on peak delay at a given temperature.

The only heat of adsorption we have found in the literature is a figure of 17 kcal. per mole (27) for thiophene on a supported chromia catalyst. This figure was obtained by analysis of reactions carried out in a static system, assuming a Langmuir mechanism for thiophene and hydrogen adsorption and neglecting the effects of H₂S and butene adsorption.

The large difference in peak maximum delay between butene shots in H₂S on the one hand and butene formed from thiophene on the other (Figure 7) requires some explanation. Various factors may have contributed to this. First, there was some evidence that above 200° C. some butene also adsorbed on stronger sites: At 234° C., for example, butene showed considerably more tailing (Figure 5,e) than at lower temperatures (Figure 5,f). Removal of hydrogen from the catalyst by reaction with thiophene may also have contributed to the delay of butene product peaks, since butene was found to sorb very strongly on a catalyst which was deficient in hydrogen—in nitrogen and helium carrier gases, for example. Finally, the main factor causing retardation and spreading of the C₄ peak

was probably the slow advance of the parent thiophene through the catalyst before reaction occurred. Peak delay of C₄ formed from thiophene is thus a complex phenomenon not related in a simple manner to the rate of C₄ desorption.

In view of the difference of a factor of 10 or more in peak delay between butene and thiophene at similar temperatures, butene adsorption was checked to see that chemisorption was in fact occurring below 200° C. Using the 50-foot propylene carbonate column, it was found that some butane was formed in spite of the H₂S present down to 150° C. (without H₂S butene was almost completely hydrogenated at this temperature) and both cis-trans and double bond isomerization of the butenes went to completion at temperatures below 100° C., indicating that chemisorption of butene must have occurred. It is therefore felt that extrapolation of the butene sorption results obtained to the temperature range of the desulfurization reaction (above 200° C.) should be valid.

As has already been demonstrated, the adsorption of butene was weaker by a large factor (10 to 15×) than the adsorption of thiophene. Also, the poisoning effect of H₂S on butene hydrogenation was about 10 times greater than its effect on thiophene desulfurization, suggesting that the two may occur on different sites, at least to some extent. Further evidence in support of this view will be cited in a forthcoming publication. For these reasons, butene adsorption should not have a large effect on the over-all reaction rate by blocking desulfurization sites.

Kirsch, Heinemann, and Stevenson (16) have reported some olefin addition experiments that support this view. Working with 2.6% thiophene in *n*-heptane, they found that replacement of 20% of the heptane by heptene reduced the per cent conversion of the thiophene from 79% to 65%, a small enough change for the addition of nearly 8 moles of olefin per mole of thiophene. Most of the heptene was hydrogenated.

The results in Table II show the effect of adding hexene to thiophene in single-shot experiments. Cyclohexene had a similar effect; cyclohexane, *n*-hexane, and benzene had no effect, though all were shown to adsorb on the catalyst. Thus the effect of adding 3 moles of hexene per mole of thiophene was to lower thiophene conversion by 21%; 1 mole per mole of thiophene cut conversion by only 4.5%, so that assuming that butene and hexene behave similarly, the 1 mole of butene formed from each mole of thiophene probably would not retard the reaction appreciably.

Table II. Effect of Hexene on Thiophene Conversion at 250° C.

<i>Sample</i>	<i>Thiophene Conversion, %</i>
5 μ l. thiophene only	65.4 65.6
+ 5 μ l. hexene	62.7
+ 15 μ l. hexene	51.5

ADSORPTION OF HYDROGEN. Strong adsorption of hydrogen on the catalyst could be observed by using N₂ or He as carrier gas. Large samples of H₂ admitted to a catalyst in a nitrogen stream at 300° or 400° C. produced peaks shaped like Figure 5,*a*, while smaller samples (0.5 cc. or less) produced peaks like that of Figure 5,*b*. The first part of the peak in Figure 5,*a*, appeared with no measurable delay, and was at first thought to contain the excess hydrogen which was not adsorbed by the catalyst at all. The second part of the peak, which is also represented by Figure 5,*b*, contained hydrogen which had adsorbed

but which apparently all desorbed within 3 to 4 minutes. There may also have been some further slow desorption, but this is not certain.

Some preliminary experiments on the slower rate of desorption, as exemplified by Figure 5,*b*, indicated that hydrogen behaved in the same way as H₂S (below) in that the rate of emergence of a peak depended on sample size and also on the hydrogen already present on the catalyst.

These experiments were not pursued further, however, because of the results shown in Table III. These are the results of experiments intended to find out which mode of hydrogen sorption was important under reaction conditions. To carry out the experiments, the catalyst was first saturated with hydrogen (helium being used as carrier gas) and then after a measured time interval the hydrogen was followed by a shot of thiophene or butene. It can be seen from Table III that although thiophene reacted to a greater extent than butene with the moderately slowly desorbing hydrogen of the type shown in Figure 5,*b*, reaction occurred primarily with the rapidly desorbing hydrogen.

Table III. Reaction of Thiophene and Butene Shots with Preadsorbed Hydrogen at 297° C.

	(Time required for hydrogen to pass through catalyst in plug flow, 28 seconds)					
	<i>Thiophene</i>			<i>Butene</i>		
Time between H ₂ and reactant shots, sec.	30	60	120	30	60	
% reaction	70	25	6	21	4.5	
Hydrogen used up by reaction, cc.	0.5	0.2	0.05	0.05	0.015	

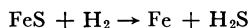
Following the method of Tamaru (26), hydrogen adsorption was also studied at 300° C. on a catalyst saturated with thiophene, by using nitrogen as a carrier gas and presaturating it with thiophene at room temperature. No change in the behavior of hydrogen was observed, from which it would appear that thiophene cannot compete successfully for hydrogen adsorption sites. The converse may be expected to be true; indeed, thiophene and butene adsorbed much less strongly in hydrogen carrier gas than in nitrogen, and when strong adsorption of thiophene had occurred in nitrogen carrier gas a portion of the adsorbed thiophene could be flushed off by a hydrogen shot. Thus, adsorbed hydrogen seemed to have an important role to play in modifying the adsorption of thiophene and C₄'s, while more loosely bound or perhaps completely free hydrogen was necessary for reaction to occur.

ADSORPTION AND DESORPTION OF H₂S. H₂S showed stronger interaction with the catalyst than thiophene or any of the C₄ hydrocarbons. When produced by the reaction of a single shot of thiophene in hydrogen carrier gas, it did not desorb at all, but remained strongly bound to the surface. Larger amounts (1 to 5 cc.) injected from a syringe adsorbed immediately and completely, but desorbed slowly, giving peaks similar to Figure 5,*a*, though with longer tails. Some small shots gave peaks of the type shown in Figure 5,*c*. The quantity desorbed, calculated from the area under the curve, was found to be an approximately linear function of the logarithm of the time. All experiments were performed on a fully presulfided catalyst containing 2.8% S.

H₂S sample size was found to govern not only the rate of desorption from the catalyst, but also the delay before desorption began. This break-through delay time, *t'* (measured to the front of the main peak), was studied under a variety of

conditions. It was found that its inverse, $1/t'$, which is a measure of the rate of passage of H_2S through the catalyst, correlated well with sample size under comparable conditions of the catalyst surface. Thus, if the catalyst was left 3 hours in hydrogen between shots at $293^\circ C.$, a smooth plot of $1/t'$ vs. shot size was obtained. Delay times of shots spaced more closely than this were influenced by the size of the preceding shot, but it was found that by injecting always at the same concentration in the tail of the preceding peak smooth plots were again obtained. The residual H_2S contents of the catalyst (above the "equilibrium" value after very long times), associated with a given point in the tail of the H_2S peak, were then estimated by integrating the appropriate areas under the desorption curve. The figures so obtained could be used to correct the injected sample size for the H_2S already present on the catalyst, so as to reduce all the data to a single plot for that temperature ($293^\circ C.$). This is shown in Figure 9, along with a few results at $343^\circ C.$

It was thought that some desulfiding of the catalyst might occur, by a reaction similar to that reported by Ivanovskii for iron sulfide desulfurization catalysts (15):



To check this, experiments on H_2S desorption were done using nitrogen and helium carrier gases. Few detailed measurements were made; the same type of behavior occurred as in hydrogen. Even the very slow removal of H_2S which still went on after several hours in hydrogen at 250° also took place in helium; this would seem to indicate that most of the H_2S was chemisorbed rather than converted to a metal sulfide.

At $400^\circ C.$, hydrogen was able to displace H_2S more quickly than helium, because it was possible to produce small H_2S peaks by injecting hydrogen into the reactor while H_2S was still slowly desorbing in a helium stream. This could conceivably have involved some desulfiding, but clearly the rest of the phenomena observed were due to desorption.

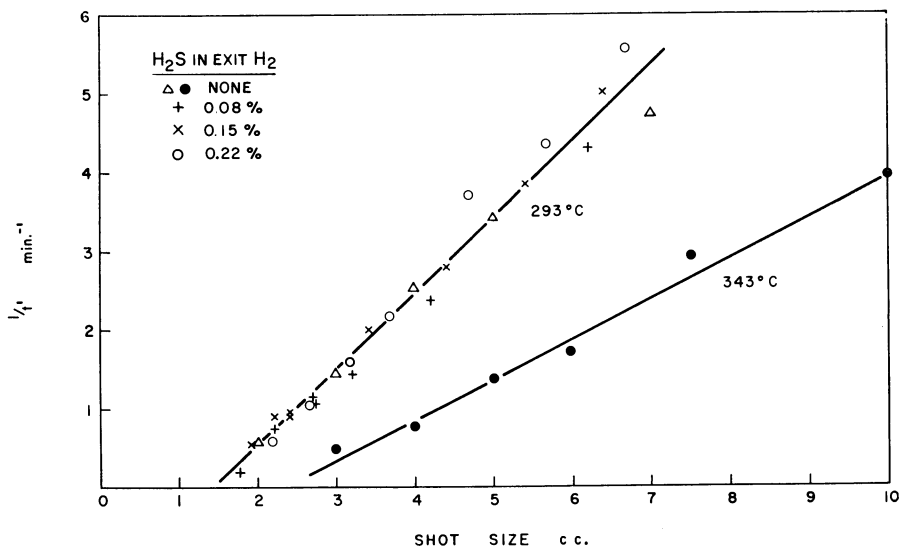


Figure 9. Correction of H_2S break-through times to clean surfaces
3.6 grams of cobalt molybdate catalyst, 54 mm. deep, 6.6 liters of H_2 per hour

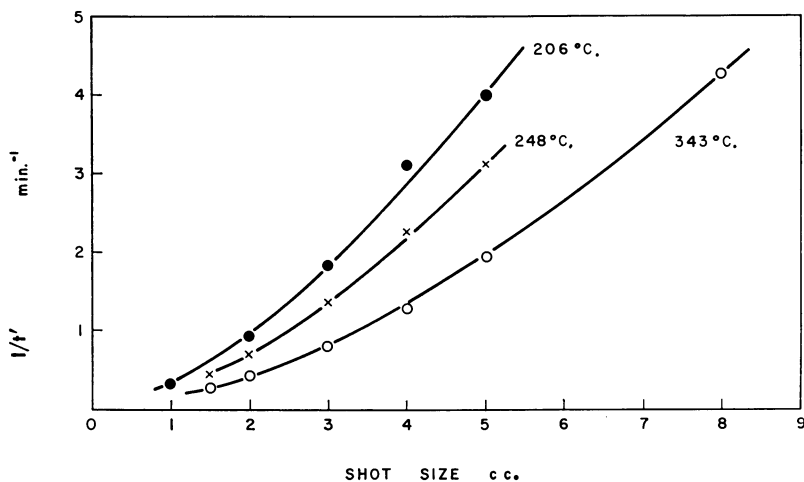


Figure 10. H_2S break-through rates at various temperatures

Shots after 1 hour in 7.1 liters of H_2 per hour
3.6 grams of cobalt molybdate catalyst, 54 mm. deep

The effect of temperature on the curves of break-through rate vs. shot size was fairly small compared to the effect of sample size (Figure 10). On the other hand, a catalyst cleaned by heating to $400^\circ C$. in hydrogen and then cooled to 250° was found to adsorb about 1.5 cc. of H_2S per gram of catalyst completely before allowing any additional amounts injected to desorb, so that there appeared to be a change in equilibrium sulfur content with temperature.

The points in Figure 10 were determined at intervals of exactly 1 hour, and in consequence show rather less scatter than the points for "clean" catalyst in Figure 9, which were determined as occasion arose between experiments at higher catalyst contents of H_2S . Probably the best line through the points for clean catalyst in Figure 9 should also pass through the origin, as do the curves in Figure 10. The rest of the data in Figure 9 are for shots put on catalyst which already contained between 1.2 and 1.7 cc. of H_2S more than clean catalyst, corrected by the corresponding amounts; the intercept on the x axis simply reflects this. Both the break-through rate and the rate of removal of H_2S from the surface were found to be directly proportional to the carrier gas flow rate.

The rate of break-through of an H_2S peak front thus depends on H_2S sample size (including the amount of H_2S remaining on the catalyst from previous experiments), the catalyst temperature, the carrier gas flow rate, and finally (to a small extent) the nature of the carrier gas.

The results on H_2S desorption can perhaps best be explained by a fast adsorption step, followed by desorption at a rate proportional to surface coverage and carrier gas flow rate. The "equilibrium" quantity of H_2S still held by the catalyst after long periods in hydrogen is different at different temperatures, and the proportionalities hold only at catalyst contents of H_2S above the equilibrium amounts.

The importance of H_2S adsorption from the point of view of the over-all reaction is shown by its effect on butene hydrogenation and on thiophene conversion (Figure 2). These indicate that H_2S adsorption competes for sites which are essential to the reaction. Since its effect on thiophene adsorption was to cut peak delay by only 10 to 30%, it may be that H_2S competes for hydrogen adsorption

sites. This was also suggested by the experiments in helium carrier gas mentioned above, in which hydrogen shots displaced H₂S from the surface.

Summary and Conclusions

Examination of the reaction products indicated that the primary products of reaction were probably butadiene and H₂S. The rates of hydrogenation of butadiene and butene were found to be consistent with the amounts appearing in the reaction products (provided, in the case of cobalt molybdate catalyst, that H₂S was present to simulate reaction conditions). The results support the view that C-S bond cleavage is the first step in thiophene desulfurization, rather than hydrogenation of the ring.

The flow reaction over cobalt molybdate catalyst had an apparent activation energy of 25 kcal. per mole. Shot reactions showed comparatively high conversions at low temperatures, due possibly to the absence of blocked sites.

The adsorption of each of the reactants and products on cobalt molybdate was studied under conditions as close as possible to reaction conditions. Butene and thiophene both showed strong temperature dependence, adsorption of the latter in particular being slow at the lower reaction temperatures. The temperature coefficients were 8.5 and 9.5 kcal. per mole, respectively. H₂S adsorbed quickly and desorbed at a rate proportional to coverage, and hydrogen apparently behaved in the same way. Only relatively weakly bound or free hydrogen appeared to be reactive, but adsorbed hydrogen probably modified the adsorption of thiophene and of butene.

Adsorbed H₂S had an appreciable effect on the rate of desulfurization, and a very marked effect on the rate of butene hydrogenation. Olefins were weakly adsorbed and had only a small effect on desulfurization.

It may be that on cobalt molybdate, olefins can adsorb on sites other than the desulfurization sites. If so, it would be in accordance with conclusions reached by Hammar (14), and would also explain the selective poisoning reported with nitrogen compounds and CO (17, 20), which are strongly adsorbed reversible poisons like H₂S (2, 17). These poisons offer one of the few ways at present available of improving selectivity and so lowering hydrogen consumption when desulfurizing olefinic feeds.

Acknowledgment

The authors thank D. Kulawic for technical assistance.

Literature Cited

- (1) Bassett, D. W., Habgood, H. W., *J. Phys. Chem.* **64**, 769 (1960).
- (2) Blue, E. M., Spurlock, B., *Chem. Eng. Progr.* **56**, (4) 54 (1960).
- (3) Burwell, R. L., Jr., Littlewood, A. B., Cardew, M., Pass, G., Stoddart, C. T. H., *J. Am. Chem. Soc.* **82**, 6272 (1960).
- (4) Burwell, R. L., Jr., Taylor, H. S., *Ibid.*, **58**, 697 (1936).
- (5) Cawley, C. M., Proc. 3rd World Petrol. Congr., The Hague, 1951, Sect. IV, p. 294.
- (6) Cawley, C. M., Hall, C. C., *J. Soc. Chem. Ind. (London)* **62**, 116 (1943).
- (7) Cremer, E., *Angew. Chem.* **71**, 512 (1959).
- (8) Emmett, P. H., *Advances in Catalysis* **9**, 653 (1957).
- (9) Emmett, P. H., Kokes, R. J., Tobin, H. H., U. S. Patent **2,905,536** (Sept. 22, 1959).
- (10) Griffith, R. H., Marsh, J. D. F., Newling, W. B. S., *Proc. Roy. Soc. (London)* **A197**, 194 (1949).
- (11) Habgood, H. W., Hanlan, J. E., *Can. J. Chem.* **37**, 843 (1959).

- (12) Hall, W. K., Emmett, P. H., *J. Am. Chem. Soc.* **79**, 2091 (1957).
- (13) Hall, W. K., Emmett, P. H., *J. Phys. Chem.* **63**, 1102 (1959).
- (14) Hammar, C. G. B., Proc. 3rd World Petrol. Congr., The Hague, 1951, Sect. IV, p. 295.
- (15) Ivanovskii, F. P., Kalvar'skaya, R. S., Beskova, G. S., Sokolova, N. P., *Zhur. Fiz. Khim.* **30**, 1860 (1956).
- (16) Kirsch, F. W., Heinemann, H., Stevenson, D. H., *Ind. Eng. Chem.* **49**, 646 (1957).
- (17) Kirsch, F. W., Shalit, H., Heinemann, H., *Ibid.*, **51**, 1379 (1959).
- (18) Kokes, R. J., Tobin, H., Emmett, P. H., *J. Am. Chem. Soc.* **77**, 5860 (1955).
- (19) Komarevsky, V. I., Knaggs, E. A., *Ind. Eng. Chem.* **43**, 1415 (1957).
- (20) Lachowicz, S., French Patent **1,132,241** (March 6, 1957).
- (21) McKenna, T. A., Idleman, J. A., *Anal. Chem.* **31**, 2000 (1959).
- (22) McKinley, J. B., *Catalysis* **5**, 405 (1957).
- (23) Moldavskii, B. L., Kumari, Z. I., *Zhur. Obshchei Khim.* **4**, 298 (1934); *Chem. Abstr.* **29**, 1814 (1935).
- (24) Moldavskii, B. L., Prokopchuk, N., *Zhur. Priklad. Khim.* **5**, 619 (1932); *Chem. Abstr.* **27**, 274 (1933).
- (25) Pease, R. N., Keighton, W. B., Jr., *Ind. Eng. Chem.* **25**, 1012 (1933).
- (26) Tamaru, K., *Nature* **183**, 319 (1959).
- (27) Van Looy, H., Limido, G., *Compt. rend. congr. intern. chim.* **31**^e, Liège 1958, **1**, 645.

RECEIVED June 22, 1961. Work conducted during P. J. Owens' tenure of a National Research Council Postgraduate Fellowship, 1959-1961.

Development of Surface in the Hydration of Calcium Silicates

DAVID L. KANTRO, STEPHEN BRUNAUER, and CHARLES H. WEISE

Portland Cement Association Research and Development Laboratories, Skokie, Ill.

The paste hydration of β - Ca_2SiO_4 , Ca_3SiO_5 , and alite has been investigated at 5° , 25° , and 50° , for periods ranging from 1 to 400 days. A high-surface calcium silicate hydrate, tobermorite, was formed in all these reactions, and the surface development was primarily dependent on the degree of hydration of the paste. The stoichiometry of the reactions was variable, depending on the original silicate, time, and temperature; and this variation had important effects on surface development. A linear relationship was obtained between the surface area and the CaO/SiO_2 ratio of the tobermorite. From this relationship and other considerations, conclusions were drawn about the composition and structure of stable tobermorites as well as the composition of the tobermorite surface. The unstable tobermorites, obtained in the early part of the hydration, are briefly discussed.

Tricalcium silicate, Ca_3SiO_5 , and β -dicalcium silicate, β - Ca_2SiO_4 , are the two calcium silicates found in portland cement and comprise the major portion of this important construction material. The hydration reactions of these calcium silicates are complicated processes now undergoing a thorough investigation with an aim toward understanding the even more complicated processes of cement hydration.

Previous investigations of these hydration reactions at room temperature have been reviewed recently (4). Research in this laboratory has included the stoichiometry of the hydration of both silicates, employing different methods of hydration (2, 3, 5, 21), and a determination of the surface energy of tobermorite, the calcium silicate hydrate produced in the hydration of both silicates under most experimental conditions(8). The surface area and the surface energy of tobermorite are briefly discussed by Brunauer (1). These properties play vital roles in determining the strength, dimensional stability, and other important engineering properties of hardened portland cement paste, concrete, and mortar.

In the previous investigations in this laboratory, most of the data were obtained on well-hydrated specimens prepared at room temperature. The present investigation includes specimens of this type, as well as specimens hydrated for shorter periods of time. Three temperatures were used—5°, 25°, and 50°. The hydration of alite, the form of Ca_3SiO_5 found in portland cement, was also investigated under the same conditions. In addition to time and temperature, the effect of stoichiometry on the development of surface area was investigated.

The crystal structure of the natural mineral tobermorite was partly worked out by Megaw and Kelsey (22). Taylor and coworkers (15, 17, 26, 27) have carried out detailed investigations of tobermorite prepared synthetically, and correlated their structural features with those of the natural mineral structure. However, little was known about the nature of the surface, except what may be deduced from the surface energy results, the surface energy being approximately the geometric mean of the surface energies of calcium hydroxide and hydrous amorphous silica.

Experimental

Preparation of Silicates. The $\beta\text{-Ca}_2\text{SiO}_4$ and Ca_3SiO_5 were prepared from U.S.P. calcium carbonate and ground quartz, the latter containing 99.9% SiO_2 . Approximately 0.5% B_2O_3 , as U.S.P. boric acid, was added to the Ca_2SiO_4 raw mix as a stabilizer. The burning procedure was as described previously (9), but the burns were made in a six-burner gas-fired kiln which had a larger capacity than the two-burner kiln previously used. The $\beta\text{-Ca}_2\text{SiO}_4$ mixture was twice heated at 1450° for 3 hours, with intervening grinding and remixing. Since the mixing operations were carried out in a 22-quart dough mixer, the mixtures obtained were more homogeneous than those previously obtained and no "dusting" (inversion to the γ form of Ca_2SiO_4) occurred at any time. The Ca_3SiO_5 was twice heated to 1600° with intervening grinding and remixing. Alite- Ca_3SiO_5 to which small amounts of alumina, magnesia, and additional lime were added to give the mix the over-all composition $52\text{Ca}_3\text{SiO}_5 \cdot 6\text{CaO} \cdot \text{Al}_2\text{O}_3 \cdot \text{MgO}$ —was prepared in exactly the same manner as Ca_3SiO_5 . Reagent grade hydrous alumina and magnesium oxide were used.

All three preparations were ground in porcelain jar mills with flint pebbles. A portion of each preparation was ground to a Blaine surface area (ASTM designation C-204-51) of about 4500 sq. cm. per gram.

The analyses and compound compositions of these preparations are given in Table I. The compound compositions were adjusted to 100% by assuming that the missing percentage in the Ca_2SiO_4 preparations was Ca_2SiO_4 , and that in the Ca_3SiO_5 and alite preparations it was Ca_3SiO_5 .

Preparation of Hydrated Silicates. The hydrated silicate specimens used were all in the paste form—that is, mixtures of one of the calcium silicates with a limited amount of water to form a slurry, which sets and hardens as portland cement itself does. These pastes were prepared by the vacuum mixing procedure described by Powers, Copeland, Hayes, and Mann (23), adapted so that the temperature of the mix upon removal from the mixer was the temperature at which the specimen was to be hydrated. The 5° specimens were made by starting with an ice-water mixture; the 50° specimens by starting with preheated water. A manostat was incorporated into the pumping system to prevent the pressure from dropping below the vapor pressure of water at the desired final temperature. This was especially important for the 50° mixes, to prevent excessive cooling.

The mixing of specimens consisted of two 1-minute mixing periods separated by a 3-minute standing period for the 5° and 25° specimens, and by a 2-minute standing period for the 50° specimens. In all but a few mixes, the water-solid ratio was 0.70. Four or five specimens were obtained from each mix. The

Table I. Compositions of Unhydrated Calcium Silicates

Component	Material, %		
	β - Ca_2SiO_4	Ca_3SiO_5	Alite
CaO	65.43	73.57	73.62
SiO ₂	33.56	25.69	24.93
Al ₂ O ₃	0.12	0.20	1.01
MgO	0.05	Nil	0.37
B ₂ O ₃	0.47	—	—
Total	99.63	99.46	99.93
Ca ₃ SiO ₅	2.36	98.18	94.77 ^b
Ca ₂ SiO ₄	97.01 ^a	—	—
Ca ₃ Al ₂ O ₆	0.32	0.53	2.68
MgO	0.05	—	0.37
Free CaO	0.20	1.29	2.18
Insol. residue (SiO ₂)	0.06	—	—
Total	100.00	100.00	100.00

^a Total Ca_2SiO_4 taken as sum of Ca_2SiO_4 (94.65%) and B_2O_3 expressed as $5\text{CaO} \cdot \text{B}_2\text{O}_3$ (2.36%).

^b Total alite (97.82%) taken as sum of Ca_3SiO_5 , $\text{Ca}_3\text{Al}_2\text{O}_6$, and MgO.

specimens were transferred from the mixing vessel to temperature-resistant polyethylene or polypropylene test tubes, in which they were allowed to hydrate. The 5° and 25° specimens thus obtained were placed in suitable temperature-controlled baths, and the 50° specimens in a temperature-controlled oven for the duration of the hydration period.

Each specimen was removed from its test tube mold at the end of a prescribed hydration period. In most cases the specimen had set. If so, the top and bottom half inch of material were removed by means of a small diamond saw and discarded. The remaining cylinder was sawed into two pieces axially. The specimen was then dried for 1 to 2 days in a vacuum drying apparatus of the type described by Copeland and Hayes (12), after which the material was placed in a gloved box containing a CO₂-free atmosphere. Here the specimen was ground to pass a U.S. Standard No. 200 sieve. (A few specimens were ground to pass only a U.S. Standard No. 80 sieve.) Each specimen was then placed in tared weighing bottles which were placed back in the vacuum drying apparatus and dried to equilibrium at the vapor pressure of ice at -78.5° (5×10^{-4} mm.).

This paper reports results obtained for a number of very well hydrated older specimens, prepared from other batches of Ca_2SiO_4 and Ca_3SiO_5 than those described above (5, 9). The compositions of these older unhydrated materials were given by Brunauer (Table I, 9). The paste preparation was identical with that described above, except in two respects: The specimens were hydrated in glass molds lined with a polyvinyl plastic paint, and the room temperature specimens were hydrated in air in a temperature-controlled room. Specimens hydrated at higher temperatures were hydrated in temperature-controlled water baths. After 2 months of hydration at these higher temperatures (50° and 80°), the controls were turned off and the baths were allowed to cool to room temperature. Eventually the samples were removed from the baths and stored in air in the temperature-controlled room until they were used. Grinding and drying were accomplished as described above.

Analysis and Surface Determination. Loss-on-ignition and carbon dioxide content were determined for each specimen. Complete chemical analyses were also performed on many of the pastes. These analyses were found to agree with those of the original unhydrated materials; in the end, one chemical analysis was used for all pastes made from the same original material. The analyses reported in Table I are the averages of those obtained for various pastes and respective unhydrated materials.

Free calcium hydroxide was determined by a modified Franke extraction procedure (24), most of the data having been obtained by the time-variation method (TVM). The unhydrated material was determined by x-ray quantitative analysis, using magnesium hydroxide as an internal standard, as described previously (21). The calibration equations for all three calcium silicates were of the form

$$\frac{I_x}{I_0} = k \frac{w_x}{w_0} \quad (1)$$

where I_x and I_0 are integrated intensities of suitably chosen calcium silicate and internal standard diffraction lines, respectively, w_x and w_0 are weight fractions of these substances, and k is a constant (10). The values of k for Ca_2SiO_4 , Ca_3SiO_5 , and alite, obtained from calibration mixtures, are 0.288 ± 0.006 , 0.338 ± 0.006 , and 0.332 ± 0.009 , respectively.

Surface areas were determined by the BET method using water vapor adsorption. The adsorption data were obtained gravimetrically in modified vacuum desiccators, such as that shown in Figure 1.

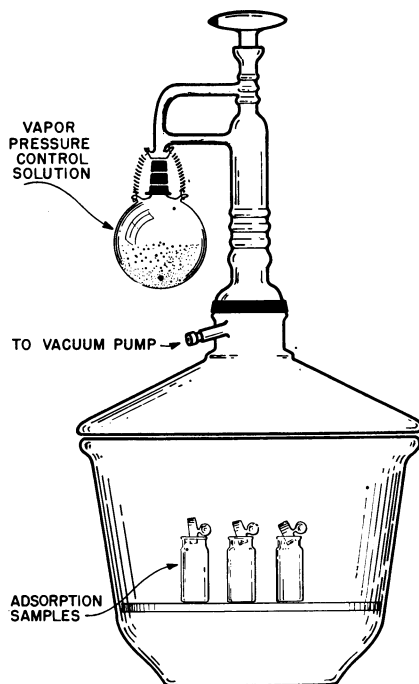


Figure 1. Water vapor adsorption apparatus

The desiccator lid was manufactured with a ring stopcock through which evacuation was accomplished. A center tube was sealed on the lid, connecting it to a bulb. The bulb contained the saturated salt solution that maintained a constant water vapor pressure over the specimens. The bulb was isolable by means of a stopcock, so that the saturated salt solution could be stored under vacuum while samples were being changed. A ground joint connection made it possible to remove the whole upper assembly from the lid. Six such desiccators were employed, a different water vapor pressure being maintained in each. The relative

pressures ranged from 0.07 to 0.33. Duplicate samples were exposed to each pressure for 7 days before weighing.

Table II. Compositions of Older β - Ca_2SiO_4 and Ca_3SiO_5 Pastes

(Grams per gram ignited weight)

Paste ^a	Age	Temp. of Hydration, °C.	Ca(OH) ₂ G./G.	Unhydrated Material, G./G.	Minor Constituents, ^c G./G.	
Pastes of Ca_2SiO_4						
C-23	17 mo.	25	0.102	0.306	0.024	
C-51	4.25 yr.	25	0.127	0.147	0.028	
C-29	21 mo.	50 ^b	0.059	0.355	0.040	
C-57	5.2 yr.	80 ^b	0.060	0.310	0.028	
Paste ^a	Age	Temp. of Hydration, °C.	Tobermorite, G./G.	CaO/SiO ₂ , Moles/Mole	H ₂ O/SiO ₂ , Moles/Mole	Tobermorite Area, Sq. M./G.
C-23	17 mo.	25	0.683	1.65	1.15	280.1
C-51	4.25 yr.	25	0.835	1.63	1.09	305.7
C-29	21 mo.	50 ^b	0.656	1.73	1.19	264.1
C-57	5.2 yr.	80 ^b	0.720	1.75	1.29	242.0
Paste ^a	Age	Temp. of Hydration, °C.	Ca(OH) ₂ G./G.	Unhydrated Material, G./G.	Minor Constituents, G./G.	
Pastes of Ca_3SiO_5						
C-17	17 mo.	25	0.464	0.000	0.016	
C-52	5 yr.	25	0.452	0.000	0.022	
C-27	21 mo.	50 ^b	0.443	0.000	0.018	
C-55	5.2 yr.	80 ^b	0.359	0.159	0.014	
Paste ^a	Age	Temp. of Hydration, °C.	Tobermorite, G./G.	CaO/SiO ₂ , Moles/Mole	H ₂ O/SiO ₂ , Moles/Mole	Tobermorite Area, Sq. M./G.
C-17	17 mo.	25	0.725	1.54	1.10	285.9
C-52	5 yr.	25	0.734	1.56	1.14	267.6
C-27	21 mo.	50 ^b	0.744	1.58	1.13	296.5
C-55	5.2 yr.	80 ^b	0.646	1.63	1.29	289.3

^a All pastes made from 0.7 water–solid ratio mixes.

^b Paste hydrated 2 months at indicated temperature, remainder of time at room temperature.

^c Minor constituents consist of CaCO₃, Mg(OH)₂, Ca₃Al₂O₆·6H₂O, Na₂SO₄, and in case of Ca₂SiO₄ pastes, H₂BO₃ also.

Results

The compound composition of each paste was calculated from the chemical analysis in terms of oxides (CaO , SiO_2 , Al_2O_3 , MgO , B_2O_3 , CO_2 , and H_2O), the free calcium hydroxide, and the unhydrated material present. The amount and composition of the tobermorite present were obtained from the difference between the total analysis and the amounts of the oxides required to account for calcium hydroxide and the unhydrated material. Allowance was made for minor impurities such as calcium carbonate.

Tobermorite has a variable composition. The composition in any given paste may be expressed as $x\text{CaO}\cdot\text{SiO}_2\cdot y\text{H}_2\text{O}$, where x and y represent the molar $\text{CaO}/$

Table III. Compositions of Ca_2SiO_4 Pastes

Paste	Age, days	$\text{Ca}(\text{OH})_2$, G./G.	Ca_2SiO_4 , ^b G./G.	Minor Constituents, ^c G./G.	Tobermorite, G./G.	CaO/SiO_2 , Moles/Mole	$\text{H}_2\text{O}/\text{SiO}_2$, Moles/Mole	Tobermorite Area, Sq. M./G.
Hydrated at 5°								
R	1	0.033	0.903	0.025	0.050	1.04	0.00	169.2
V	1	0.035	0.877	0.025	0.075	1.27	0.00	94.1
S	2	0.047	0.910	0.021	0.037	0.57	0.05	224.9
T	4	0.064	0.858	0.019	0.077	0.89	0.09	392.6
S	7	0.081	0.841	0.019	0.083	0.76	0.00	478.3
V	9	0.078	0.821	0.017	0.108	0.97	0.12	397.2
T	11	0.079	0.826	0.017	0.104	0.93	0.23	488.6
V	14	0.088	0.820	0.017	0.103	0.84	0.20	537.0
T	17	0.102	0.782	0.016	0.132	0.92	0.16	457.8
S	21	0.099	0.759	0.016	0.159	1.06	0.24	408.2
V	28	0.099	0.768	0.015	0.155	1.04	0.39	497.8
S	50	0.114	0.643	0.014	0.277	1.31	0.47	364.0
T	74	0.111	0.591	0.014	0.346	1.43	0.75	358.7
L	100	0.111	0.470	0.018	0.472	1.56	0.71	260.3
L	199	0.151	0.300	0.019	0.640	1.55	0.94	299.6
Hydrated at 25°								
F	1	0.046	0.855	0.025	0.094	1.20	0.47	303.8
F	2	0.063	0.798	0.024	0.136	1.26	0.18	247.7
Q	5	0.091	0.747	0.021	0.168	1.17	0.08	319.8
F	8	0.085	0.738	0.020	0.193	1.27	0.46	350.3
Q	11	0.104	0.617	0.018	0.306	1.41	0.43	298.1
F	14	0.114	0.641	0.019	0.283	1.30	0.71	372.8
Q	18	0.104	0.484	0.022	0.457	1.58	0.69	257.7
H	21	0.117	0.511	0.021	0.419	1.49	0.69	301.1
H	28	0.114	0.447	0.021	0.496	1.57	0.79	276.0
Q	41	0.122	0.433	0.027	0.582	1.52	0.86	325.4
C	72	0.132	0.344	0.017	0.616	1.59	1.07	284.0
H	100	0.141	0.268	0.020	0.685	1.60	0.99	288.1
H	200	0.157	0.214	0.020	0.736	1.58	1.02	284.3
C	330	0.158	0.150	0.021	0.806	1.62	1.03	304.9
C	400	0.160	0.207	0.032	0.740	1.55	1.08	314.8
C' ^a	127	0.128	0.274	0.014	0.696	1.65	1.03	244.3
Hydrated at 50°								
O	1	0.072	0.757	0.023	0.175	1.32	0.31	263.4
O	2	0.089	0.716	0.023	0.212	1.28	0.54	295.0
O	8	0.099	0.516	0.024	0.433	1.56	0.89	270.6
O	14	0.094	0.487	0.021	0.476	1.63	0.99	296.9
P	21	0.104	0.444	0.021	0.520	1.62	1.04	302.6
P	28	0.105	0.403	0.023	0.562	1.64	1.01	280.9
P	100	0.111	0.299	0.022	0.672	1.68	0.98	264.9
P	200	0.105	0.303	0.021	0.688	1.70	1.18	268.7

^a 3500 sq. cm. Blaine surface Ca_2SiO_4 used.

^b Total Ca_2SiO_4 includes Ca_2SiO_4 and $5\text{CaO}\cdot\text{B}_2\text{O}_3$.

^c Minor constituents include CaCO_3 , $\text{Mg}(\text{OH})_2$, $\text{Ca}_3\text{Al}_2\text{O}_6\cdot 6\text{H}_2\text{O}$, Ca_3SiO_5 , and H_3BO_3 .

SiO₂ and H₂O/SiO₂ ratios in the tobermorite. The compound compositions and the tobermorite compositions, the latter expressed in terms of CaO/SiO₂ and H₂O/SiO₂ ratios, for the older Ca₂SiO₄ and Ca₃SiO₅ pastes are given in Table II. The results for Ca₂SiO₄, Ca₃SiO₅, and alite pastes (compositions in Table I) are given in Tables III, IV, and V, respectively. The weights of the constituents are given in grams per gram of ignited weight, and not as grams per gram of paste. Thus, their sum is always greater than 1 gram.

Table IV. Compositions of Ca₃SiO₅ Pastes

Paste		Ca(OH) ₂ , G./G.	Ca ₃ SiO ₅ , G./G.	Minor Constit- uents, ^c G./G.	Tober- morite, G./G.	CaO/ SiO ₂ , Moles/ Mole	H ₂ O/ SiO ₂ , Moles/ Mole	Tober- morite Area, Sq. M./G.
Mix	Age, days							
Hydrated at 5°								
K	1	0.121	0.694	0.012	0.214	1.86	0.32	201.7
K	2	0.197	0.542	0.012	0.332	1.72	0.89	324.7
K	8	0.288	0.362	0.010	0.466	1.64	1.08	340.4
K	14	0.341	0.294	0.012	0.495	1.53	1.01	341.1
L	21	0.360	0.242	0.010	0.544	1.56	1.12	326.6
L	28	0.368	0.194	0.011	0.587	1.62	1.08	351.8
L	100	0.463	0.094	0.011	0.621	1.43	1.09	357.1
L	200	0.473	0.030	0.009	0.683	1.51	1.05	326.3
Hydrated at 25°								
Q	1	0.148	0.654	0.010	0.244	1.76	0.63	306.2
Q	1.5	0.173	0.642	0.012	0.238	1.56	0.71	372.8
Q	2	0.189	0.580	0.011	0.289	1.66	0.63	312.5
Q	4	0.225	0.514	0.009	0.338	1.62	0.78	359.8
F	8	0.264	0.422	0.011	0.411	1.63	0.91	352.2
F	14	0.329	0.304	0.012	0.487	1.57	0.90	354.9
H	21	0.380	0.245	0.014	0.512	1.47	0.92	387.6
H	28	0.400	0.191	0.014	0.559	1.49	1.00	355.6
C	72	0.444	0.074	0.010	0.655	1.55	1.00	356.8
H	100	0.489	0.045	0.012	0.649	1.44	0.97	357.5
H	200	0.504	0.024	0.016	0.662	1.42	1.01	328.6
C	300	0.482	0.000	0.013	0.709	1.53	1.07	357.5
C	400	0.500	0.000	0.028	0.681	1.44	0.98	329.7
B ^a	72	0.440	0.096	0.012	0.633	1.52	1.00	352.9
C ^b	72	0.401	0.143	0.013	0.625	1.57	1.00	359.8
Hydrated at 50°								
P	1	0.164	0.628	0.012	0.260	1.69	0.74	315.2
P	2	0.199	0.533	0.012	0.335	1.73	0.74	290.8
P	8	0.270	0.388	0.014	0.446	1.66	1.00	323.2
P	14	0.297	0.345	0.015	0.483	1.62	1.24	358.7
O	21	0.325	0.268	0.012	0.539	1.66	1.08	303.4
O	28	0.357	0.232	0.013	0.554	1.59	1.10	326.3
O	100	0.420	0.082	0.013	0.675	1.61	1.17	303.4
O	200	0.444	0.038	0.012	0.707	1.59	1.20	310.3
D ^a	90	0.431	0.080	0.011	0.667	1.58	1.12	334.3

^a Water-solid ratio in mix: 0.57.

^b Water-solid ratio in mix: 0.45.

^c Minor constituents include CaCO₃ and Ca₃Al₂O₆·6H₂O.

The extent to which any paste is hydrated may be expressed by the ratio of the amount of unhydrated material that has disappeared to the amount present originally. This ratio will be called the degree of hydration. In the case of Ca₂SiO₄, a correction was made for the small amount of Ca₃SiO₅ present. The latter was assumed to hydrate at the same rate as in Ca₃SiO₅ pastes under comparable conditions. Thus, the amount of Ca₃SiO₅ remaining unhydrated in a Ca₂SiO₄ paste could be estimated and subtracted from the total amount of remaining unhydrated material, the difference being the amount of unhydrated Ca₂SiO₄.

Table V. Compositions of Alite Pastes

Paste		Ca(OH) ₂ , G./G.	Alite, ^b G./G.	CaCO ₃ , G./G.	Tober- morite, G./G.	CaO/	H ₂ O/	Tober- morite Area, Sq. M./G.
Mix	Age, days					SiO ₂ , ^c Moles/ Mole	SiO ₂ , ^c Moles/ Mole	
Hydrated at 5°								
M	1	0.102	0.781	0.002	0.147	1.79	0.46	231.0
M	2	0.217	0.542	0.004	0.318	1.62	0.77	311.9
M	8	0.348	0.251	0.003	0.544	1.61	1.04	307.6
M	14	0.385	0.198	0.003	0.582	1.56	1.19	332.0
N	22	0.451	0.146	0.003	0.577	1.41	0.98	335.0
N	28	0.454	0.118	0.004	0.605	1.44	1.01	339.2
N	100	0.452	0.061	0.004	0.676	1.54	1.11	325.9
N	200	0.477	0.062	0.003	0.661	1.46	1.16	365.9
Hydrated at 25°								
I	1	0.179	0.621	0.004	0.264	1.65	0.80	294.2
I	2	0.237	0.521	0.001	0.328	1.57	0.76	289.7
I	8	0.329	0.359	0.004	0.435	1.47	0.90	349.9
I	14	0.392	0.256	0.004	0.502	1.41	0.97	377.7
G	21	0.435	0.191	0.006	0.534	1.37	0.92	366.7
G	28	0.452	0.139	0.007	0.582	1.40	1.01	346.8
G	72	0.501	0.049	0.007	0.647	1.40	1.05	387.8
G	100	0.511	0.033	0.010	0.650	1.38	1.00	357.5
G	200	0.525	0.000	0.010	0.673	1.39	0.96	336.6
A ^a	72	0.427	0.102	0.006	0.652	1.55	1.15	319.4
Hydrated at 50°								
R	1	0.218	0.583	0.003	0.272	1.48	0.69	333.9
R	2	0.274	0.502	0.004	0.318	1.37	0.77	377.7
R	8	0.394	0.254	0.005	0.504	1.40	1.02	389.5
R	14	0.436	0.195	0.006	0.536	1.36	1.02	385.0
Q	22	0.453	0.130	0.006	0.597	1.42	1.08	385.3
Q	28	0.453	0.130	0.008	0.591	1.41	1.15	390.7
Q	100	0.494	0.032	0.014	0.669	1.43	1.09	328.2
Q	200	0.492	0.000	0.012	0.707	1.49	1.10	313.7

^a Water-solid ratio in mix: 0.45.

^b Sum of Ca₃SiO₅, Ca₃Al₂O₆, and MgO.

^c SiO₂ includes Al₂O₃ which substitutes in lattice for SiO₂.

The degrees of hydration of Ca₂SiO₄, Ca₃SiO₅, and alite pastes as functions of time at the three temperatures are given in Figures 2, 4, and 6, respectively. The data, obtained from pastes whose compositions are given in Tables III, IV, and V, are plotted on a logarithmic time scale only as a matter of convenience.

The V_m values for Ca₂SiO₄, Ca₃SiO₅, and alite pastes are plotted as functions of time at the three temperatures in Figures 3, 5, and 7, respectively. (The specific surface areas shown in the last columns of Tables III, IV, and V were calculated from these V_m values.) In these figures, too, the logarithmic time scale has been used for convenience.

Discussion

Progress of Surface Formation. During the early stages of reaction, the hydration of β -Ca₂SiO₄ depends on temperature in much the same manner as most chemical reactions. As can be seen in Figure 2, at any given time during the early stages, hydration of β -Ca₂SiO₄ has proceeded to the greatest extent at the highest temperature of hydration. This temperature dependence is not maintained, however, in the later stages of reaction. The degree of hydration of β -Ca₂SiO₄ at 50° is less than that at 25° at any given age beyond 60 days, although at 60 days only about 65% of the β -Ca₂SiO₄ has disappeared.

A comparison of Figures 2 and 3 shows that the degree of surface area de-

velopment behaves in about the same manner. Because the specific surface areas of the calcium silicates are three orders of magnitude smaller than those of the hydration products, the V_m values are almost entirely dependent on the surfaces of the hydration products. As Figure 3 shows, the V_m data, like the degree of hydration data, are lower for 50° pastes older than 60 days than for 25° pastes of the same ages. This parallelism is only semiquantitative, however, for as can be seen from a comparison of Figures 2 and 3, the detailed shapes of the corresponding temperature curves differ in some respects. Relationships between V_m and other variables are discussed later.

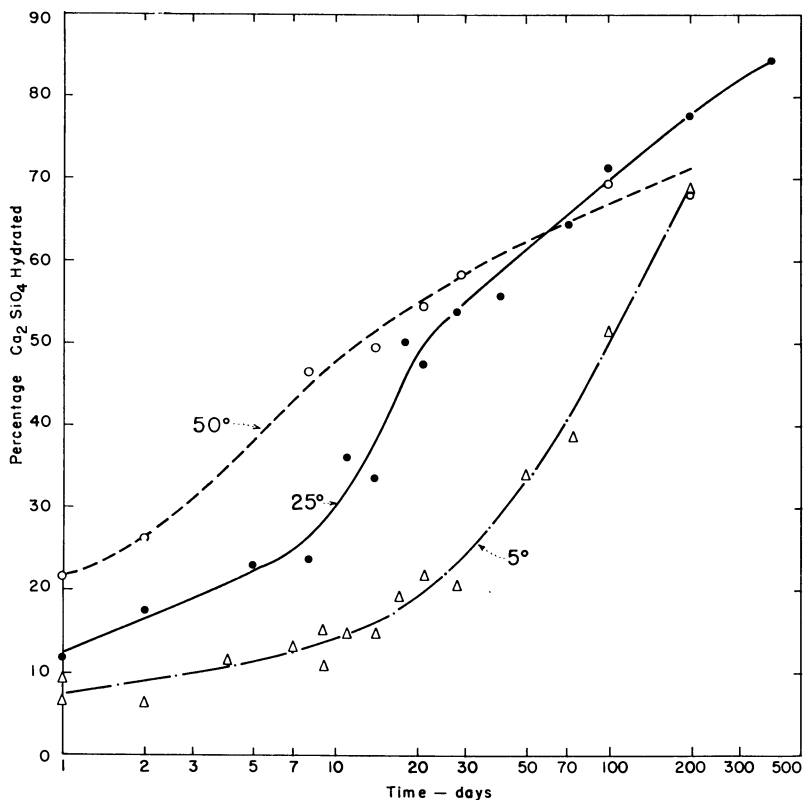


Figure 2. Percentage hydration of Ca_2SiO_4 vs. time

The degree of hydration results for Ca_3SiO_5 (Figure 4) have relationships different from those for $\beta\text{-Ca}_2\text{SiO}_4$. First of all, the temperature dependence of the hydration of Ca_3SiO_5 is considerably smaller than that of Ca_2SiO_4 ; the curves at the three temperatures are much closer to each other in Figure 4 than in Figure 2. In the second place, the Ca_2SiO_4 curves show only one crossing between 1 and 100 days of hydration, whereas the Ca_3SiO_5 curves show four crossings. The V_m curves for Ca_3SiO_5 (Figure 5) also exhibit four crossings between 1 and 100 days. The crossings do not occur at exactly the same ages in Figures 4 and 5, because V_m is a function not only of the degree of hydration but also of the stoichiometry of the hydration. Nevertheless, the 25° curve indicates a lower degree of hydration between 1.5 and 10 days and a higher degree of hydration after 20 days than

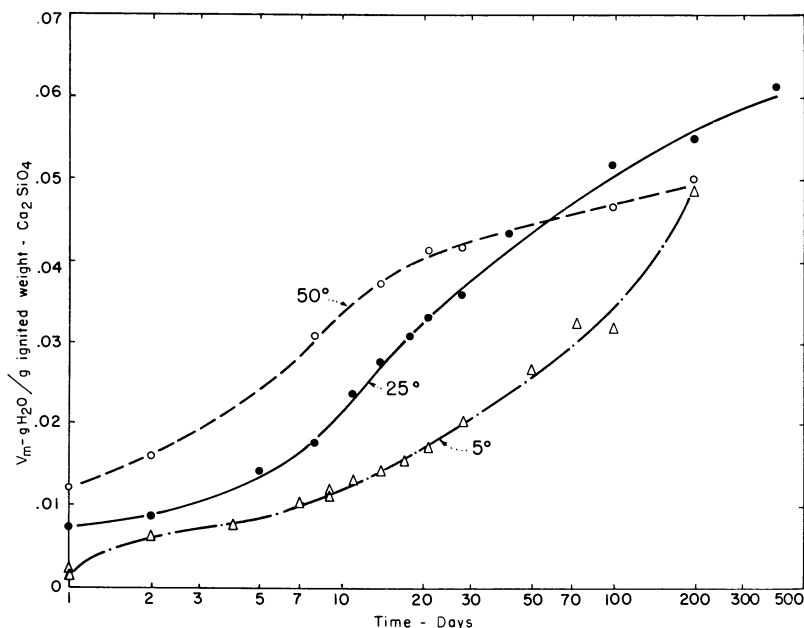


Figure 3. Surface development in hydration of Ca_2SiO_4 vs. time

the 5° and 50° curves (Figure 4) and, similarly, the 25° curve indicates a lower surface between 1.7 and 4 days and a higher surface after 20 days than the 5 and 50° curves (Figure 5). Figure 4 shows a region in the vicinity of 14 days in which inverse correlation with temperature exists, the 5° paste being the most hydrated, the 50° paste the least. A similar region of inverse temperature dependence is found for V_m in Figure 5, at about the same age.

The hydration of alite is of interest because of the similarity of this material to Ca_3SiO_5 . The alite used was stabilized by Al_2O_3 and MgO as described in an earlier investigation (11). Thus, alite is slightly different from Ca_3SiO_5 in composition, but more important is the fact that Ca_3SiO_5 and alite are crystallographically dissimilar. Ca_3SiO_5 is triclinic and alite is monoclinic, as was shown by Jeffrey (19) and confirmed by Yamaguchi and Miyabe (28).

The curves of degree of hydration vs. time for alite (Figure 6) bear a strong resemblance to those of Ca_3SiO_5 (Figure 4). However, for alite the pastes hydrated at 50° are at all times more hydrated than corresponding 5° and 25° pastes. The 5° and 25° curves, however, behave relative to each other in much the same way as the corresponding Ca_3SiO_5 curves. Comparison of the V_m vs. time curves of alite (Figure 7) with the degree of hydration vs. time curves (Figure 6) reveals a similarity in behavior, as in the previous cases.

No attempt is made here to explain the intricate temperature dependence of the hydrations of the three calcium silicates. Work on the kinetics of these hydration processes is not complete, so the authors could give at present only highly tentative and speculative explanations. The conclusion from Figures 2 to 7 for the purposes of this paper is that the surface area development in pastes of all three silicates is determined primarily by the degree of hydration of the silicate. For a simple reaction, in which the reactants have negligible surface areas compared with the reaction products, such a conclusion would be trivial. However, for as complex

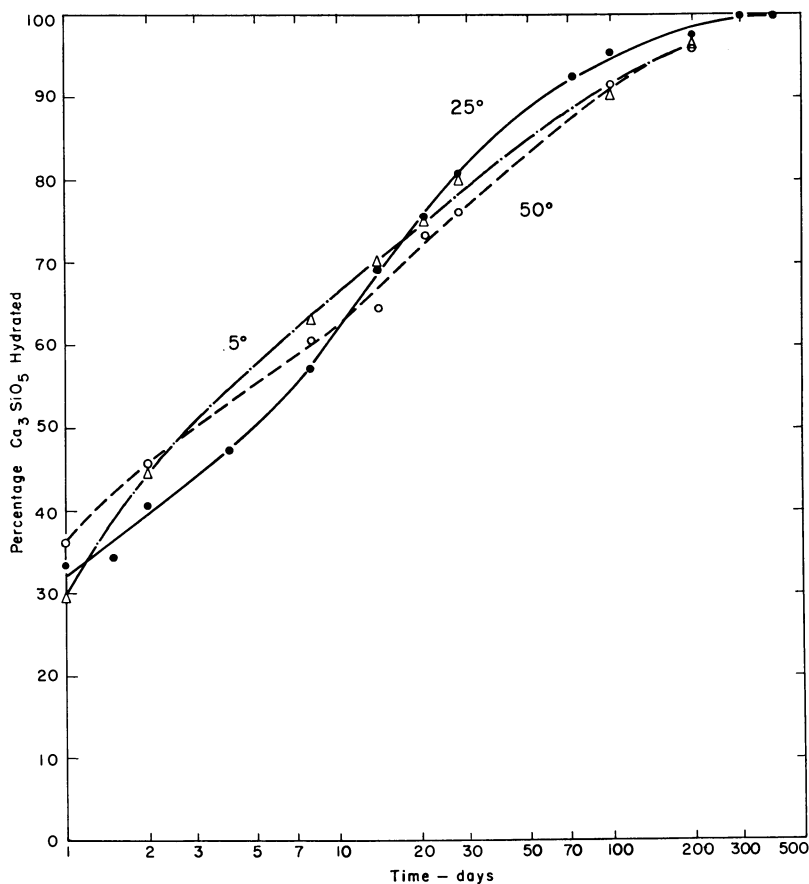
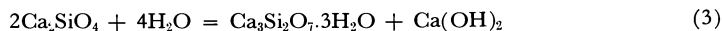
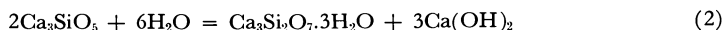


Figure 4. Percentage hydration of Ca_3SiO_5 vs. time

reactions as the three discussed here, through all the intricate and not easily explainable crisscrossings of the hydration curves, the surface area development, by and large, faithfully follows the degree of hydration. Consideration of the secondary factors leads to more interesting conclusions, because these factors reveal important information about the mechanism of surface formation and the nature of the tobermorite surface.

Stoichiometry of Hydration Reactions. The stoichiometry of the hydration reactions has a significant influence on surface formation. In previous investigations of Ca_3SiO_5 and $\beta\text{-Ca}_2\text{SiO}_4$ pastes hydrated at room temperature for long times (3, 5), the stoichiometry of the hydration process was found to be represented by the following equations:



The calcium silicate hydrate formed in both cases appears to be a very poorly crystallized version of the natural mineral tobermorite. The use of the name tobermorite for the calcium silicate hydrate obtained in the hydration of Ca_3SiO_5 and Ca_2SiO_4 is not fully justified; nevertheless, because in all publications from this laboratory that name was used, the usage is retained in this paper.

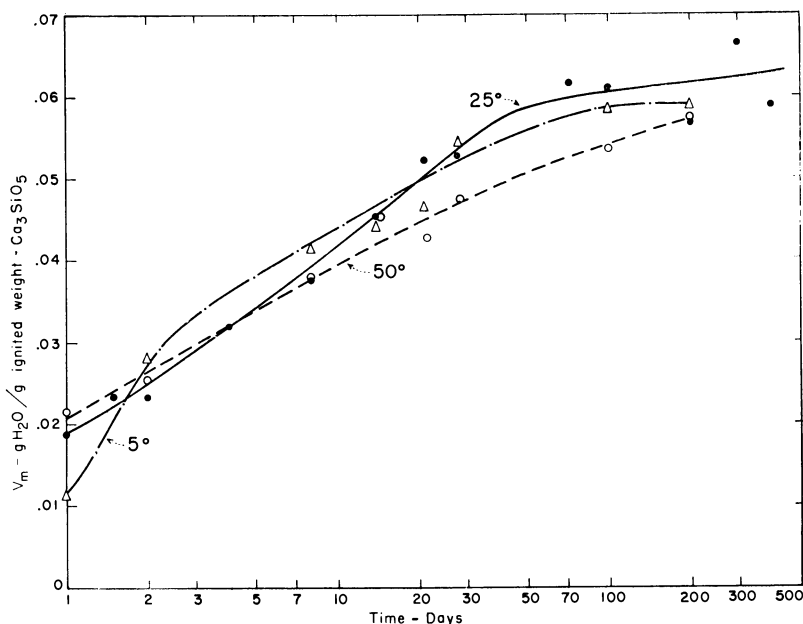


Figure 5. Surface development in hydration of Ca_3SiO_5 vs. time

Prior to analysis and surface area determination, the tobermorite was dried, as described before. In this drying, one molecule of water was lost, so the formula of the tobermorite was $\text{Ca}_3\text{Si}_2\text{O}_7 \cdot 2\text{H}_2\text{O}$. This formula, however, is only an approximation even for pastes hydrated at room temperature for long times. As Table II shows, the CaO/SiO_2 ratio in the tobermorite prepared at 25° is not 1.50, but 1.64 for hydrated Ca_2SiO_4 and 1.55 for hydrated Ca_3SiO_5 ; and the $\text{H}_2\text{O}/\text{SiO}_2$ ratio is not 1.00, but about 1.12. As Tables III, IV, and V show, the CaO/SiO_2 and $\text{H}_2\text{O}/\text{SiO}_2$ ratios in the tobermorites depend on temperature, time of hydration, and starting material (Ca_2SiO_4 , Ca_3SiO_5 , or alite). In Table V, the SiO_2 values include the Al_2O_3 which substitutes in the tobermorite lattice for 2SiO_2 in a manner analogous to that described for alite (19).

Examination of the data of Tables III, IV, and V reveals certain trends in the CaO/SiO_2 ratios of tobermorite. Table III indicates that in the hydration of Ca_2SiO_4 , the CaO/SiO_2 ratio at 5° starts with a low value, then builds up to higher values as the reaction progresses. Because the reaction is faster at 25° and still faster at 50° , and because no pastes less than 1 day old were investigated so far, the CaO/SiO_2 values for the youngest pastes at 25° are higher than at 5° , and still higher at 50° . The ultimate CaO/SiO_2 ratio seems to be reached at about 50% hydration, which, as Figure 2 shows, is reached in about 14 days at 50° , 18 days at 25° , and 100 days at 5° . The values of the final CaO/SiO_2 ratios are 1.65, 1.58, and 1.55 at 50° , 25° , and 5° , respectively. These results are consistent with those of Funk (14), who reported increasing CaO/SiO_2 ratios with increasing temperatures between 50° and 100° for tobermorites produced in the hydration of $\beta\text{-Ca}_2\text{SiO}_4$.

The course of the $\text{H}_2\text{O}/\text{SiO}_2$ ratio in the tobermorites of Table III is similar to the course of the CaO/SiO_2 ratio. The $\text{H}_2\text{O}/\text{SiO}_2$ ratio also starts with low values at each temperature and builds up to higher values as the reaction progresses. The

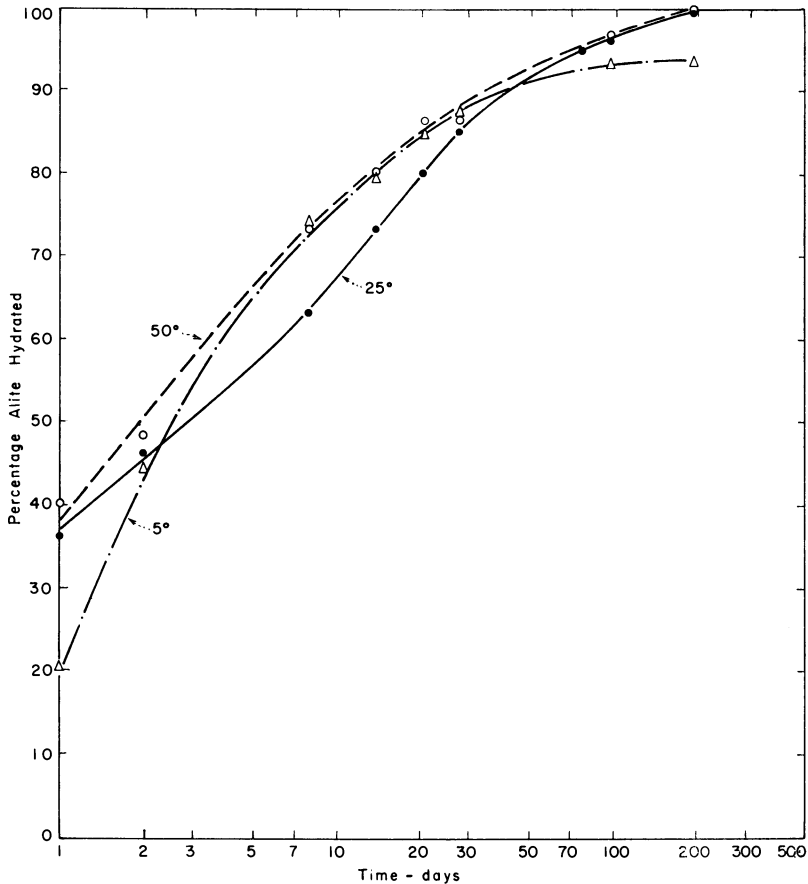


Figure 6. Percentage hydration of alite vs. time

combined water, initially, is very loosely bound, so that several of the 5° early age pastes show zero or close to zero H_2O/SiO_2 ratios under the drying conditions employed in the present work. The H_2O/SiO_2 ratio increases to its final value more slowly than the CaO/SiO_2 ratio, and the ultimate values are not reached at 50% hydration. The values observed for the oldest pastes in the present work are 0.94, 1.08, and 1.18 at 5°, 25°, and 50°, respectively. Indication from earlier work (4) is that the 25° and 50° values, obtained for the 400- and 200-day pastes, respectively, are ultimate values, but the 5° value, obtained for a 200-day paste, is not. The ultimate value for the 5° paste should be in the vicinity of 1.05.

In contrast with the Ca_2SiO_4 results, the CaO/SiO_2 ratios for tobermorites obtained from the hydration of Ca_3SiO_5 and alite, shown in Tables IV and V, exhibit a decreasing trend with time. This can be explained in a crude way, if it is assumed that the first step in the hydration of both Ca_2SiO_4 and Ca_3SiO_5 is the loss of one molecule of CaO , and that the hydration, in its early stages, takes place on the surface of the silicate. In this case, the initial CaO/SiO_2 ratio in the tobermorite would be 1.0 for Ca_2SiO_4 and 2.0 for Ca_3SiO_5 . Because the ultimate ratio for both tobermorites is in the vicinity of 1.5, the ratio for Ca_2SiO_4 should show an increasing trend with time, and for Ca_3SiO_5 and alite, a decreasing trend.

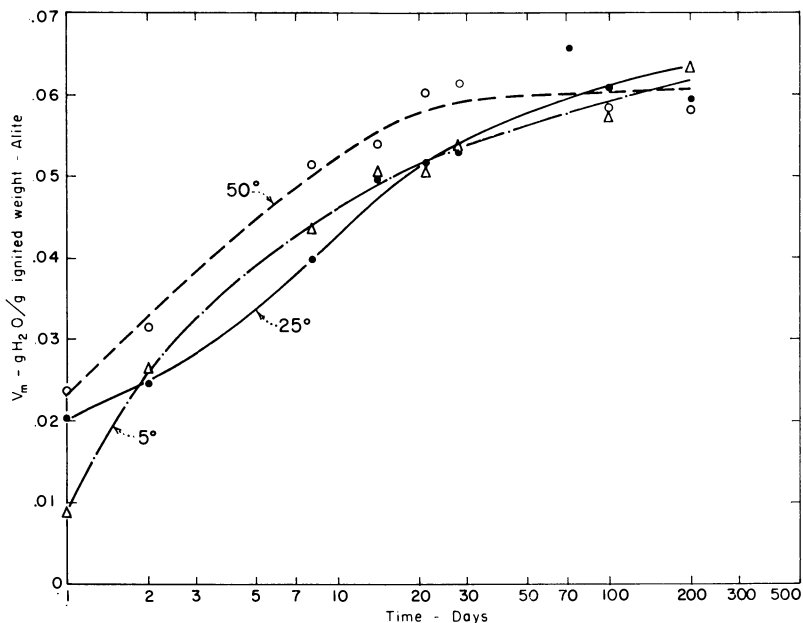


Figure 7. Surface development in hydration of alite vs. time

The loss of one molecule of lime is not accompanied by an immediate uptake of one molecule of water. The $\text{H}_2\text{O}/\text{SiO}_2$ ratios for the tobermorites in all 13 Ca_2SiO_5 and alite pastes that are 2 days old or younger are significantly less than 1.0. Subsequently, the $\text{H}_2\text{O}/\text{SiO}_2$ ratio increases to an ultimate value, while the CaO/SiO_2 ratio decreases to an ultimate value. In the hydration of Ca_2SiO_4 , both ratios increase, but the uptake of water is slower than the uptake of lime, as pointed out above.

Although there is no definite relation between the CaO/SiO_2 and $\text{H}_2\text{O}/\text{SiO}_2$ ratios while these ratios are in a process of change, there is a definite relation between the final values (4). Higher CaO/SiO_2 ratios go with higher $\text{H}_2\text{O}/\text{SiO}_2$ ratios, as pointed out above for the Ca_2SiO_4 pastes. The same is true for the Ca_3SiO_5 pastes. The ultimate CaO/SiO_2 ratios in Table IV are 1.53, 1.48, and 1.59 at 5°, 25°, and 50°, respectively, and the corresponding $\text{H}_2\text{O}/\text{SiO}_2$ ratios are 1.07, 1.00, and 1.15. The smallest values of both ratios are at 25°, and the same is true for alite pastes. The ultimate CaO/SiO_2 ratios in Table V are 1.46, 1.39, and 1.42 at 5°, 25°, and 50°, respectively, and the corresponding $\text{H}_2\text{O}/\text{SiO}_2$ values are 1.06, 0.99, and 1.08. There appears to be no unidirectional change with temperature in the ultimate ratios for Ca_3SiO_5 and alite pastes, in contrast with the Ca_2SiO_4 results.

Stoichiometry and Surface Development. SOME ASPECTS OF TOBERMORITE STRUCTURE. Prior to the discussion that follows, it is necessary to point out certain features of the tobermorite structure. Tobermorite has a layer structure, like the clay minerals montmorillonite and vermiculite. Megaw and Kelsey (22) found that each layer of the natural mineral tobermorite was actually a triple layer: a CaO_2 layer in the center, similar to a distorted $\text{Ca}(\text{OH})_2$ layer from which all hydrogen atoms have been removed, and on both sides of this layers of metasilicate chains. This 2:1 layer is called one layer in the following discussion.

The basic layer has a CaO/SiO_2 ratio of 2/3, but all tobermorites, natural or synthetic, have ratios higher than this. The natural mineral has a CaO/SiO_2 ratio of 0.83; the synthetic tobermorites, prepared in the temperature range 5° to 50° , have CaO/SiO_2 ratios ranging from about 0.80 to 1.75, and possibly higher. Except in the last section of this paper, only tobermorites with a relatively stable structure are discussed—i.e., those which have already reached the final CaO/SiO_2 ratios. In the process of formation, the CaO/SiO_2 ratio may be as high as 2.0—the highest value actually observed was 1.86 (Table IV). However, the maximum ultimate ratio reported in this paper for the temperature range 5° to 50° is 1.73 (Table II).

The low-lime tobermorites, with CaO/SiO_2 ratios of about 0.8 to 1.5, are poorly crystallized—their x-ray diffraction patterns consist of a dozen lines or fewer, and their electron micrographs show crumpled sheets (16). The high-lime tobermorites, with CaO/SiO_2 ratios of about 1.4 to 1.75 (or higher), are even more poorly crystallized—their x-ray diffraction patterns consist of only three lines, and their electron micrographs show fibers (13, 16). These fibers are actually rolled-up sheets (1). The overlapping in CaO/SiO_2 ratios between low- and high-lime tobermorites is probably real. All work reported in this paper refers to high-lime tobermorites, and the lowest ultimate value reported here is 1.39. There is considerable evidence that the upper limit of low-lime tobermorites is 1.5 (4), though one cannot rule out the possibility of some high-lime tobermorite in the low-lime preparations. Kalousek and Prebus (20) consider 1.33 the upper limit of the low-lime tobermorites.

If the layer has a CaO/SiO_2 ratio of 0.67, the question is: Where is the rest of the lime? Taylor (26) demonstrated that the ($hk0$) spacings do not change with increasing CaO/SiO_2 ratios, which indicates that the extra lime is not in the 2:1 layers but outside these layers. Grudemo (16) showed that the ($00l$) spacings diminish with increasing CaO/SiO_2 ratios, indicating that the extra lime is between the layers. Taylor (26) showed that the ($hk0$) spacings change only very slightly with increasing $\text{H}_2\text{O}/\text{SiO}_2$ ratios, but the ($00l$) spacings increase markedly with increasing $\text{H}_2\text{O}/\text{SiO}_2$ ratios. Finally, Brunauer, Kantro, and Copeland (5) showed that the decrease in ($00l$) spacings caused by the addition of a mole of CaO was approximately equal to the increase in spacings caused by the addition of a mole of H_2O ; thus, the simultaneous addition of both results in no appreciable change. Increase in the CaO/SiO_2 ratio is accompanied by an equimolar increase in the $\text{H}_2\text{O}/\text{SiO}_2$ ratio (4), and the results discussed above indicate that this relationship holds approximately for the ultimate CaO/SiO_2 and $\text{H}_2\text{O}/\text{SiO}_2$ ratios in the tobermorites obtained in the hydration of Ca_2SiO_4 , Ca_3SiO_5 , and alite.

The unit cell of tobermorite is orthorhombic (17). For simplicity, a pseudocell, which contains one molecule, will be described. The b dimension of the pseudocell is the distance between neighboring silicon atoms in the silicate chains, and the a dimension is perpendicular to the b dimension within the layer. The values of a and b are 5.59 and 3.64 Å, respectively, under the drying conditions used in the present work. Changing the CaO/SiO_2 ratio has no effect, and changing the $\text{H}_2\text{O}/\text{SiO}_2$ ratio has a negligible effect (less than 1%) on the a and b dimensions; consequently, area ab is constant, and it is 20.35 sq. Å.

The three x-ray spacings exhibited by all tobermorites discussed in this paper are ($hk0$) spacings; the ($00l$) spacings are absent. In previous work, the density of tobermorite having a composition of $\text{Ca}_3\text{Si}_2\text{O}_7 \cdot 2\text{H}_2\text{O}$ was determined (5), and from the density of 2.86 ± 0.02 grams per cc. the value of 9.3 ± 0.1 Å. was calculated for the c dimension of the pseudocell. This is the distance between neighbor-

ing layers in the tobermorite sheets under the drying conditions used, when the pseudo-cell contains one molecule of $\text{Ca}_3\text{Si}_2\text{O}_7 \cdot 2\text{H}_2\text{O}$.

In the following discussion, it is assumed that the pseudo-cell always contains one molecule of tobermorite, regardless of composition. This means that the weight of the pseudo-cell increases as the CaO/SiO_2 ratio increases—for example, an increase in the CaO/SiO_2 ratio from 1.50 to 1.60 means the addition of 0.10 molecule of CaO and 0.10 molecule of H_2O to the pseudo-cell. This, naturally, should be understood in the average sense—i.e., one molecule of lime and one molecule of water are added to one pseudo-cell out of ten.

SURFACE AREA OF TOBERMORITE. From the dimensions of the pseudo-cell, given above, the specific surface area can be calculated for tobermorite sheets that have thicknesses of any number of layers. For a tobermorite having the formula $\text{Ca}_3\text{Si}_2\text{O}_7 \cdot 2\text{H}_2\text{O}$, the specific surface area for sheets consisting of one, two, and three layers is 755, 377, and 252 sq. meters per gram, respectively. The calculation is described elsewhere (1). It is assumed in the calculation that the areas along the thin edges of the large sheets make negligible contributions to the surface area.

The specific surface areas of Ca_2SiO_4 , Ca_3SiO_5 , and alite are negligible compared to those of the hydration products. Actually, the unhydrated silicates have specific surface areas well under 1 sq. meter per gram. The calcium hydroxide produced in the hydration reactions, likewise, has a negligible surface area (3, 4, 8). Thus, the V_m values obtained for the pastes of the silicates can be assigned entirely to tobermorite, well within the experimental errors. The specific surface areas were calculated from the V_m values, by assuming that the area of an adsorbed water molecule is 11.59 Å. (5). The areas thus calculated are shown in the last columns of Tables III, IV, and V. Comparison of these values with the values given in the previous paragraph indicates that for most tobermorites, which have reached ultimate CaO/SiO_2 ratios, the surface areas fall between those given for the two-layer and the three-layer sheet. More accurate calculations, presented later, show that all surface areas measured fall between the areas expected for two-layer and three-layer sheets. It is concluded, therefore, that all stable tobermorites obtained in the present work consist of mixtures of two-layer and three-layer sheets.

EFFECT OF CaO/SiO_2 RATIO ON TOBERMORITE SURFACE. The specific surface areas of the tobermorites were plotted against the final CaO/SiO_2 ratios. Although there was considerable scatter in the points, the data fell on a straight line. The equation of the least squares straight line, based on 44 pastes whose CaO/SiO_2 ratios and specific surface areas are given in Tables III, IV, and V, is

$$A = 865.0 \pm 42.9 - (354.7 \pm 39.9)(\text{CaO}/\text{SiO}_2) \quad (4)$$

where A is the specific surface area in square meters per gram, and $(\text{CaO}/\text{SiO}_2)$ is the molar CaO/SiO_2 ratio. The empirical equation indicates that the more lime is in the tobermorite the lower the specific surface, which in turn indicates that increase in the lime content results in a larger fraction of three-layer and a smaller fraction of two-layer sheets. It has been suggested that lime has the ability to cement neighboring crystals of tobermorite together (15). Equation 4 indicates that lime can cement the layers of tobermorite, within a crystal, to each other.

The specific surface areas were calculated above for two- and three-layer tobermorites, both having CaO/SiO_2 ratios of 1.5. Those, however, are only "zeroth approximation" values, because Equation 4 indicates that the two- and three-layer tobermorites have different CaO/SiO_2 ratios, and neither has a ratio of 1.5; the former has a lower, the latter a higher ratio. Combining the calculation of

the specific surface area from the x-ray data with Equation 4 shows that the pure two-layer tobermorite has a CaO/SiO_2 ratio of 1.33 and a specific surface area of 393 sq. meters per gram, and the pure three-layer tobermorite has a CaO/SiO_2 ratio of 1.77 and a specific surface area of 237 sq. meters per gram. Unfortunately, the slope of the straight line in Equation 4 has a standard error of 11%, which makes these values somewhat uncertain; nevertheless, Tables III, IV, and V indicate that the values cannot be far from the true values. The lowest and highest values of the CaO/SiO_2 ratio reported in this paper for stable tobermorites are 1.39 and 1.73, and the highest and lowest specific surface areas are 391 and 244 sq. meters per gram—all within the calculated ranges and all close to the calculated extreme values. Close though the agreement is in this first approximation calculation, a second approximation is presented below, after discussion of the composition of the tobermorite surface.

Another interesting conclusion can be drawn from the slope of the straight line of Equation 4. The slope indicates that a unit increase in the molar CaO/SiO_2 ratio produces a decrease of 354.7 sq. meters per gram in the surface area. The decrease per molecule of tobermorite is 19.4 sq. A., if the calculation is made for a tobermorite of average composition—i.e., one having a CaO/SiO_2 ratio of 1.55. The area contributed by a pseudocell to the surface of a two- or three-layer tobermorite is ab , which is 20.35 sq. A. The 19.4 sq. A. value calculated differs from this by less than 5%, whereas the 19.4 sq. A. value itself has a standard error of 11%. Thus, it appears that a unit change in the molar CaO/SiO_2 ratio is accompanied by the disappearance of a unit surface, the surface contributed by a pseudocell.

A pseudocell of tobermorite contains two SiO_2 molecules, with variable amounts of CaO . A unit increase in the molar CaO/SiO_2 ratio, therefore, means the addition of two CaO molecules to the pseudocell. The conclusion from these considerations is that the addition of two molecules of CaO results in the disappearance of one pseudocell surface.

One can visualize this situation by considering six pseudocells as constituents of two- and three-layer tobermorite sheets. The number of SiO_2 molecules in the six pseudocells is 12, and the two-layer structure has, let us say, 17 CaO molecules in the six cells. The CaO/SiO_2 ratio is 1.42. The six cells in the two-layer sheet contribute six unit areas, in the three-layer sheet four unit areas. Thus, in the conversion from the two- to the three-layer sheet, two pseudocell areas disappear. The cementing action requires four CaO molecules; consequently, the six cells in the three-layer sheet have 21 CaO and 12 SiO_2 molecules, and the CaO/SiO_2 ratio becomes 1.75.

EFFECT OF CaO/SiO_2 RATIO ON TOBERMORITE SURFACE WITH OTHER MODELS. Taylor and Howison (27) have advanced a hypothesis, according to which the addition of calcium to the basic tobermorite structure is accompanied by the removal of SiO_2 from the 2:1 layer. This hypothesis, with a modification proposed by Brunauer and Greenberg (4), leads to an almost constant weight of the pseudocell. In the entire CaO/SiO_2 ratio range investigated here, from 1.39 to 1.73, the weight change is 1.1%, which is neglected in the following calculations.

For a CaO/SiO_2 ratio of 1.5, the pseudocell of the modified Taylor-Howison hypothesis contains 3.30 molecules of CaO , 2.20 molecules of SiO_2 , and 2.20 molecules of H_2O . Thus, the cell is 10% heavier than the one in the model discussed before, which results in a 10% smaller specific surface area. The specific surface area for the two-layer tobermorite is 343 sq. meters per gram; for the three-layer tobermorite, 229 sq. meters per gram. The corresponding CaO/SiO_2 ratios, from

Equation 4, are 1.47 and 1.79, respectively. Although the latter value is inconsistent with the Taylor-Howison hypothesis, because according to it the maximum CaO/SiO₂ ratio is 1.75, the uncertainty in the slope of the straight line explains the discrepancy easily. Because many of the pastes investigated have CaO/SiO₂ ratios lower than 1.47 and specific surface areas higher than 343 sq. meters per gram, the modified Taylor-Howison hypothesis indicates the presence of one-layer tobermorite sheets in these pastes.

In the model described earlier, the addition of two molecules of lime results in the disappearance of a unit surface. A similar calculation, based on the modified Taylor-Howison hypothesis, leads to the conclusion that the substitution of 0.78 molecule of CaO for SiO₂ causes the disappearance of a unit surface. This substitution is equivalent to the replacement by CaO of one molecule of SiO₂ out of 8.58 molecules.

Considering everything, the model proposed is more consistent with the data presented in this paper than the Taylor-Howison model. Nevertheless, the latter model does not lead to absurd results. There is some evidence (4) for the constancy of the weight of the pseudocell with changing CaO/SiO₂ ratio, and further work is contemplated to ascertain this.

Recently, Gard, Howison, and Taylor (15) have advanced a hypothesis for the structure of high-lime tobermorites, according to which the basic layer is not the triple 3:1 layer of Megaw and Kelsey (22), but a double 1:1 layer, of which one is a lime and the other is a silica layer. The results of this paper, as well as earlier results (1), disagree with this hypothesis. However, Gard, Howison, and Taylor rather suggested than developed their model, so it is possible that complete development of the hypothesis may change this conclusion.

COMPOSITION OF TOBERMORITE SURFACE. When silica surfaces are in contact with water for longer times, the surfaces are covered with silanol (SiOH) groups (18). In alkaline solutions, the silanol groups hydrolyze to negatively charged siloxane (SiO⁻) groups. One would expect the silica groups on the tobermorite surfaces to behave in the same way. Stein (25) showed that tobermorite particles are negatively charged when the lime concentration is low in the surrounding solution, but at higher lime concentrations they are positively charged because of adsorption of Ca⁺² ions from the solution. The tobermorites discussed here were in equilibrium with saturated calcium hydroxide solutions.

Other evidence for the presence of calcium on the surface of tobermorite comes from work on the surface energy of tobermorite. The surface energy of calcium hydroxide is 1180 ergs per sq. cm. (6), that of a pure silanol surface is 129 (7), and that of tobermorite is 386 (8), which is close to the geometric mean of the two other figures.

The area contributed by a pseudocell in both two- and three-layer tobermorites is 20.35 sq. A., and the area of an adsorbed water molecule is 11.4 sq. A. The ratio is 1.78. In the model proposed in this paper, there is one silica molecule in the surface. If the area of a water molecule adsorbed on surface silica is the same as that adsorbed on surface lime, the ratio indicates that there is 0.78 molecule of lime on the surface. Almost the same result can be obtained in a different way. The area of a water molecule adsorbed on hydrous amorphous silica is 12.5 sq. A. (7), and the area of water adsorbed on calcium hydroxide is 10.3 sq. A. (6). If it is assumed that water adsorbed on the silica part of the tobermorite surface is 12.5 sq. A., and that adsorbed on the lime part is 10.3 sq. A., calculation gives 0.76 as the number of lime molecules on the pseudocell surface.

The aqueous phase in contact with Ca₃SiO₅ and alite becomes saturated with

respect to $\text{Ca}(\text{OH})_2$ in a few minutes. Lime saturation is much more slowly established for the Ca_2SiO_4 pastes; even so, all stable tobermorites discussed here were in equilibrium with saturated $\text{Ca}(\text{OH})_2$ solutions. It can be assumed, therefore, that the surfaces of all tobermorites contained one molecule of silica and 0.77 molecule of lime per pseudocell, regardless of the CaO/SiO_2 ratio in the tobermorite. This implies that the tobermorite surface and the aqueous phase were in equilibrium with each other, but the aqueous phase and the inside of the tobermorite sheet were not.

In a saturated $\text{Ca}(\text{OH})_2$ solution, one would expect lime to be taken up by the tobermorite until the maximum CaO/SiO_2 ratio is established, which is about 1.75, in the temperature range investigated. Likewise, because of the much larger surface free energy of the two-layer sheet, one would expect it to be converted in time to the three-layer sheet. Thus, the three-layer sheet, with CaO/SiO_2 ratio of about 1.75, appears to be the thermodynamically stable form of high-lime tobermorite. The expression "stable tobermorite" has been used in this paper to designate tobermorites that had reached a final and apparently constant CaO/SiO_2 ratio. This, however, did not mean to imply thermodynamic stability.

The uptake of lime from the solution by the surface of the tobermorite should be much faster than the uptake by the inside of the sheets. It is not unreasonable to assume, therefore, that the surface was in equilibrium with the aqueous phase, whereas the inside was not. The structures of two- and three-layer tobermorite sheets, based on these considerations, as well as on considerations advanced earlier in this paper, are shown in Figure 8: a section consisting of two pseudocells for the two-layer sheet and of three pseudocells for the three-layer sheet. The CaO/SiO_2 ratio of the two-layer sheet is 1.39, and the lowest ratio obtained in the present investigation was 1.39. According to Equation 4, formation of the three-layer sheet involves the addition of two molecules of CaO for the disappearance of unit surface, which leads to the structure shown on the right side of Figure 8. The CaO/SiO_2 ratio here is 1.72, and the largest ratio reported in this paper is 1.73. The calculated specific surface areas for the two- and three-layer sheets are 387 and 240 sq. meters per gram, respectively, and the largest and smallest values in the present work are 391 and 244 sq. meters per gram, respectively. Equation 4 gives specific surface areas of 372 and 255 sq. meters per gram for CaO/SiO_2 ratios of 1.39 and 1.72, respectively; these values differ by 3.9 and 6.2% from the calculated values, differences well within the standard error of the curve.

The Taylor-Howison hypothesis gives an almost identical structure for the three-layer tobermorite with the one shown in Figure 8; the pseudocell surface contains one molecule of SiO_2 and 0.75 molecule of CaO , and the CaO content of the layers between the pseudocells is 1.50 molecules. The two-layer structure, however, shows greater differences. The surface is not very different; it contains

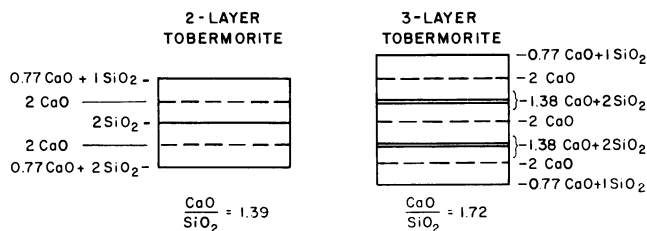


Figure 8. Two- and three-layer tobermorites

1.14 molecules of SiO_2 and 0.60 molecule of CaO for a tobermorite having a CaO/SiO_2 ratio of 1.40. However, in Figure 8, the two-layer structure has 2 SiO_2 molecules and no CaO between the pseudocells, whereas the Taylor-Howison model has 2.29 molecules of SiO_2 and 1.21 molecules of CaO between the pseudocells. Only future work can decide which model is correct.

If V_m is expressed in moles of water, then V_m/SiO_2 , expressed as moles of water per moles of silica, on the basis of the present model should be 0.88 for the two-layer and 0.59 for the three-layer tobermorite. The average value of this ratio for all stable tobermorites obtained from the hydration of Ca_3SiO_5 and alite is 0.82, and the average value for those obtained from the hydration of Ca_2SiO_4 is 0.65. Thus, the hydration of Ca_3SiO_5 and alite produces predominantly two-layer, the hydration of Ca_2SiO_4 predominantly three-layer tobermorites.

UNSTABLE TOBERMORITES. Tobermorites obtained in the earlier stages of hydration, prior to the attainment of the ultimate CaO/SiO_2 and $\text{H}_2\text{O}/\text{SiO}_2$ ratios, may be called unstable tobermorites.

The 5° series of Ca_2SiO_4 pastes alone furnishes extensive information about the early stages of hydration. Between 0 and 21% hydration, data are given in Table III for 11 pastes; in the same hydration range there are between 0 and 2 pastes in the eight other series. Extensive work will soon be started in this laboratory on the early hydration of all three silicates at all three temperatures.

The 5° pastes exhibit very low specific surface areas at 1 day; the average of the two values in Table III is about 130 sq. meters per gram. This corresponds roughly to a six-layer sheet. The surface then rises sharply; the eight pastes between 4 and 28 days all have specific surface areas greater than that corresponding to a two-layer sheet, clearly indicating the presence of one-layer sheets. Perhaps tobermorite forms initially in thick layers on the surfaces of Ca_2SiO_4 grains, then single layers peel off this unstable intermediate, giving rise to the large surface values.

The maximum specific surface area is reached in 14 days: 537 sq. meters per gram, with a CaO/SiO_2 ratio of 0.84. Equation 4 was obtained from data for stable tobermorites, all consisting of two- and three-layer sheets; nevertheless, this particular tobermorite falls on the extrapolation of the straight line. For a CaO/SiO_2 ratio of 0.84, the line indicates a surface of 567 sq. meters per gram, which differs from the experimental value by only 5.6%. If this tobermorite is assumed to be a mixture of one- and two-layer sheets, the surface indicates that 41% of the tobermorite is in one-layer sheets; if some of the tobermorite is in three-layer or thicker sheets, the fraction of one-layer sheets is even greater. The one-layer sheets are unstable because of their large surface free energies; consequently, they join up to form thicker sheets. This results in the decrease in the specific surface area shown by pastes older than 14 days.

Only further work can reveal whether a similar course of surface development takes place in the other eight series. The data for all eight series (Tables III, IV, and V) indicate an initial increase in surface, which can be interpreted as the building up of unstable thicker sheets on the grains of the silicates and the peeling off of thinner sheets. However, none of the pastes of the eight series indicates the presence of one-layer sheets. All pastes of the eight series, with the exception of the 1-day Ca_3SiO_5 and the 1-day alite paste at 5° , exhibit surface areas in the range of two- and three-layer sheets. Seven of the eight series, alite at 5° being the exception, show a decrease in surface area after the increase. This can be interpreted as the conversion of two-layer tobermorite sheets to three-layer sheets.

Acknowledgment

The authors express their thanks to William Hime and his coworkers for the numerous chemical analyses on the various specimens, to Elaine Anderson who obtained all of the hundreds of x-ray diffraction patterns used in this investigation, and to Donn Hathaway, who was of invaluable assistance in most operations connected with these investigations.

Literature Cited

- (1) Brunauer, S., *ADVANCES IN CHEM. SER.*, No. 33, 5 (1961).
- (2) Brunauer, S., Copeland, L. E., Bragg, R. H., *J. Phys. Chem.* **60**, 112 (1956).
- (3) *Ibid.*, p. 116.
- (4) Brunauer, S., Greenberg, S. A., Fourth International Symposium on Chemistry of Cement, 1960, in press.
- (5) Brunauer, S., Kantro, D. L., Copeland, L. E., *J. Am. Chem. Soc.* **80**, 761 (1958).
- (6) Brunauer, S., Kantro, D. L., Weise, C. H., *Can. J. Chem.* **34**, 729 (1956).
- (7) *Ibid.*, p. 1483.
- (8) *Ibid.*, **37**, 714 (1959).
- (9) Brunauer, S., Kantro, D. L., Weise, C. H., *J. Phys. Chem.* **60**, 771, (1956).
- (10) Copeland, L. E., Bragg, R. H., *Anal. Chem.* **30**, 196 (1958).
- (11) Copeland, L. E., Brunauer, S., Kantro, D. L., Schulz, E. G., Weise, C. H., *Ibid.*, **31**, 1521 (1959).
- (12) Copeland, L. E., Hayes, J. C., *ASTM Bull.*, No. 194, 70 (1953).
- (13) Copeland, L. E., Schulz, E. G., Brunauer, S., *Silikat Techn.* **11**, 367 (1960).
- (14) Funk, H., *Z. anorg. allgem. Chem.* **291**, 276 (1957).
- (15) Gard, J. A., Howison, J. W., Taylor, H. F. W., *Mag. of Concrete Research* **11**, 151 (1959).
- (16) Grudemo, A., Swedish Cement and Concrete Research Institute Proc. (Handlingar), No. 26, 1955.
- (17) Heller, L., Taylor, H. F. W., *J. Chem. Soc.* **1951**, 2397.
- (18) Iler, R. K., "Colloidal Chemistry of Silica and Silicates," p. 242, Cornell Univ. Press, Ithaca, N. Y., 1955.
- (19) Jeffrey, J. W., Proceedings of Third International Symposium on Chemistry of Cement, 1952, p. 30, Cement and Concrete Association, London, 1954.
- (20) Kalousek, G. L., Prebus, A. F., *J. Am. Ceram. Soc.* **41**, 124 (1958).
- (21) Kantro, D. L., Brunauer, S., Weise, C. H., *J. Colloid Sci.* **14**, 363 (1959).
- (22) Megaw, H. D., Kelsey, C. H., *Nature* **177**, 390 (1956).
- (23) Powers, T. C., Copeland, L. E., Hayes, J. C., Mann, H. M., *J. Am. Concrete Inst. Proc.* **51**, 285 (1954).
- (24) Pressler, E. E., Brunauer, S., Kantro, D. L., Weise, C. H., *Anal. Chem.* **33**, 877 (1961).
- (25) Stein, H. N., *J. Colloid Sci.* **15**, 578 (1960).
- (26) Taylor, H. F. W., *J. Chem. Soc.* **1950**, 3682.
- (27) Taylor, H. F. W., Howison, J. W., *Clay Minerals Bull.* **3**, 98 (1956).
- (28) Yamaguchi, G., Miyabe, H., *J. Am. Ceram. Soc.* **43**, 219 (1960).

RECEIVED May 29, 1961.

Surface Condensation Forces

MELVIN A. COOK

*Institute of Metals and Explosives Research, Department of Metallurgy,
University of Utah, Salt Lake City, Utah*

Hard sphere adsorbate–inert adsorbent, polarized adsorbate–inert adsorbent, and hard sphere adsorbate–polarized adsorbent models of the Type II isotherm are considered in terms of various theoretical adsorption potentials. Solid surface and adsorbate polarizations in first-layer adsorption are discussed along with dilatation of the adsorbent by physical adsorption of inert gases demonstrated especially by Yates. Structural adsorption occurs also in chemisorption. Supporting evidence is cited, including derivations of the Elovich equation for the rate of activated adsorption, the Becker equation for the rate of desorption, and the Temkin and Freundlich isotherms. Differential infrared spectrograms, showing structural adsorption effects in the adsorbent, are also discussed and suggestions made for demonstrating first-layer adsorbate polarization.

Theoretical models of physical adsorption may be classified as follows:

Model 1. Inert adsorbent–hard sphere adsorbate—the BET model and its early modifications.

Model 2. Inert adsorbent–polarized adsorbate.

Model 3. Polarized adsorbent–hard sphere adsorbate (“structural adsorption”).

Model 4. Polarized adsorbent–polarized adsorbate (not yet studied).

The important advances in adsorption technology made possible by the BET theory (3, 4) clearly justify Model 1 in many applications. But one of the Models 2, 3, or 4 is apparently required for first-layer adsorption in a Type II isotherm. That an important condensation potential at the solid-gas interface is the Lennard-Jones 3-9 potential now seems well established (3, 7, 9, 10, 15). Equally clear is the fact that this potential is not solely responsible for physical adsorption; the type of surface polarization predicted by the theory of “structural adsorption” (10) has been demonstrated by observed changes due to adsorption in linear

dimensions of the adsorbent (5, 12, 18, 26). Model 2 could be used with appropriate assumptions to extend curve fitting in some cases to include the entire Type II isotherm. While Model 2 might thus be considered adequate in physical adsorption, since surface polarization (Model 3) has been demonstrated, a necessary compromise may therefore be Model 4. In addition to a consideration of these models, the influence of adsorption polarization is discussed in connection with activated adsorption, adsorption bands in infrared spectroscopy, and studies by Pitt and Wadsworth of the adsorption and desorption of CO₂ on thoria.

General Equations

Following the detailed balancing methods of Brunauer, Emmett, and Teller (BET) (3, 4), the equations for adsorption of gaseous adsorbates on solid adsorbents may be presented in a sufficiently general form to take into account van der Waals, structural adsorption, and other adsorption potentials (7, 9, 10) as follows:

$$\begin{aligned} p s_0 / s_1 &= g_1^{-1} e^{-\epsilon_1 / kT} \\ p s_1 / s_2 &= g_2^{-1} e^{-\epsilon_2 / kT} \\ &\vdots \\ &\vdots \end{aligned} \tag{1}$$

$$\begin{aligned} p s_{(i-1)} / s_i &= g_i^{-1} e^{-\epsilon_i / kT} \\ g_1 &= g_2 = \dots = g_i \\ \epsilon_1 &= \alpha f_1(\theta_1) + \beta [1 - h(\theta_1)] + 2\gamma/3 + C(\theta_1) \\ \epsilon_2 &= \alpha f_2(\theta_2) + \gamma/8 \\ \epsilon_3 &= \alpha f_3(\theta_3) + \gamma/27 \end{aligned} \tag{2}$$

$$\begin{aligned} &\vdots \\ &\vdots \\ \epsilon_i &= \alpha f_i(\theta_i) + \gamma/i^3 \\ &\vdots \\ &\vdots \\ \epsilon_\infty &= \alpha \end{aligned} \tag{3}$$

Then

$$v/v_m = \frac{\sum_{i=1}^{\infty} i x^i \exp(\epsilon_1 + \epsilon_2 + \dots + \epsilon_i - i\alpha) / kT}{1 + \sum_{i=1}^{\infty} x^i \exp(\epsilon_1 + \epsilon_2 + \dots + \epsilon_i - i\alpha) / kT} = \frac{\sum_{i=1}^{\infty} i x^i d_i}{1 + \sum_{i=1}^{\infty} x^i d_i} \tag{4}$$

where

$$d_i = \exp [(\zeta_i - i\alpha) / kT] \tag{5}$$

and

$$\zeta_i = C + \alpha \sum_{j=1}^i f_j(\theta_j) + \beta(1 - h) + \gamma \left(\sum_{j=1}^i i^{-3} - 1/3 \right) \tag{6}$$

- where α = heat of liquefaction
- β = structural adsorption potential at zero first-layer coverage
- γ = van der Waals adsorbate-adsorbent attractive potential, the coefficient of γ in ϵ_1 —namely, 2/3—being based on the Lennard-Jones 3-9 (surface representation)
- C = chemisorption potential which is evidently itself a function $C(\theta)$ of first-layer coverage θ
- $(p_0/g)e^{-\alpha/kT} = 1$; $p/p_0 = x$
- θ_i = fraction of i th surface covered by adsorbate

- $\epsilon(\theta_i)$ = function expressing the variation of relative adsorbate-adsorbate correlation z_i/z_L with coverage of the i th layer, where z_i is the effective correlation number for the i th layer and z_L that for the bulk liquid
- $h(\theta_1)$ = function expressing the change (decrease) in the structural adsorption potential with increasing first-layer coverage

This formalism includes the suggestion that the adsorbate-adsorbent interaction should be the Lennard-Jones 3-9 potential for interaction with an infinite surface. In detailed balancing this term generates the last term in Equation 6. The formalism of Equation 1 to 6 also includes the structural adsorption potential postulated by this school (10)—i.e., the $\beta(1-h)$ term, considered to apply only in first-layer adsorption (generating the next to last term in Equation 6) or an equivalent potential—since this form seems to agree with observations. The term $f_i \alpha$ may be considered to be generated by adsorbate-adsorbent interactions expressing these interactions in the form convenient for introducing coordination symmetry. When the C term exists—i.e., in chemisorption—it has been conventional to assume that all others in Equation 6 are relatively unimportant and one has then simply a Langmuir equation. Even when C is large, however, surface and adsorbate polarization may be sufficient to require $C = C(\theta_1)$, providing, as shown below, a Temkin and/or Freundlich type fitting of the chemisorption isotherm.

The isotherms (v/v_m vs. x) for multimolecular adsorption might perhaps more conveniently be expressed in other forms, but the form presented above can, if desired, include all other fundamental developments concerning physical adsorption and chemisorption. Whether this form is a useful one will, of course, depend on whether suitable generating functions can be defined that permit mathematical conversion of the infinite series in Equation 4 to closed, polynomial form and still retain the fundamental description of the adsorption potential for the particular model in question. Tractability by this formalism was so readily accomplished in the BET model as to prompt the author to attempt it in a more accurate description of adsorption potentials but still within the framework of Model 1. The success of this approach in providing a representation of the $0.05 < x < 1.0$, or the multilayer region of the Type II isotherm, thus contributed significantly to the BET model (9). Application of the predicted linear form $k\theta$ for $h(\theta)$ of the structural adsorption concept for first-layer adsorption used in conjunction with the functions for multimolecular adsorption permitted fairly accurate fitting of the entire adsorption isotherm for argon, nitrogen, and oxygen, and mixtures of nitrogen and oxygen on anatase and for other systems studied also within this framework.

Perhaps the most significant achievement of the structural adsorption refinement of the BET model was its prediction that "physical" adsorption even of inert gases should modify the surface and cause dilatation of the adsorbent. This prediction was strikingly verified in the work of Yates (26), who demonstrated a surprisingly large dilatation of the adsorbent in the physical adsorption of inert gases on various adsorbents. Further support is found in the work of Emmett (12), Brunauer, Kantro, and Weise (5), and Peticolas (18). Further evidence interpreted as supporting structural adsorption was the fact that N_2 exhibited a stronger adsorption potential for adsorption on anatase than O_2 in the low pressure region.

Most treatments of physical adsorption and even chemisorption have assumed a rigid, immobile, and physically inert adsorbent surface. That adsorption even of an inert gas such as helium, argon, or nitrogen should distort the surface of the solid was suggested by a consideration of the free radical nature of solids, at least

those solids involving strong chemical binding—metals, ionic crystal, valence crystal, and semiconductors. If adsorption were capable of distorting the adsorbent, it would also be capable of distorting or polarizing the adsorbate molecules, particularly in first-layer adsorption (11,21). Indeed, it is not unlikely that adsorbate distortion or polarization may take place in second ($i = 2$), third ($i = 3$), and perhaps even higher layers, of course, to an extent diminishing rapidly as i increases.

Specific Models

Model 1. It is convenient and sufficiently reliable in many applications to separate the Type II isotherm into two parts: the region above “point B” or the multimolecular region, and the region below “point B” or the monolayer region. Cook and Pack (9) showed that an excellent representation of the region from point B to $x = 1.0$ may be obtained by representing ζ_i in Equation 6 by the relation

$$\zeta_i = \alpha \sum_1^i [c_1 + i - 1]/i + \gamma \left(\sum_1^i i^{-3} - 1/3 \right) \quad (6a)$$

This representation is based on the following assumptions:

1. The Lennard-Jones 3-9 potential is assumed for the adsorbate-adsorbent interaction in which the attractive term is γ/i^3 and the repulsive term amounts to $\gamma/3$ in the first layer and is negligible for $i \geq 2$.

2. The (hard-sphere) adsorbate-adsorbate interactions are assumed to involve effectively only nearest neighbors, each near neighbor molecule contributing the same interaction potential as in the bulk-liquid state.

3. The $f_i(\theta)$ relationship is assumed to be $f_i(\theta_i) = c_i = (c_1 + i - 1)/i$. This form of f_i , besides providing a tractable generating function relating the c_i 's, assigns an average value for the relative (hard-sphere) adsorbate-adsorbate correlation number and thus neglects any variations of c_i with θ_i or convergence on any adjacent layers.

The application of the 3-9 surface potential in physical adsorption was lucidly discussed by Brunauer (3) and later used by Hill (15) in Model 1 adsorption about the same time that the BET theory was reworked by the author and Pack (7, 9) on the basis of Equation 6a as the adsorption potential function.

Model 2. There seems to be no way to fit first-layer adsorption by Model 1; a model based on adsorbate polarizations, adsorbent polarization, or both is needed to treat first-layer adsorption in a Type II isotherm. Sinanoglu and Pitzer (21) gave a fundamental discussion of the importance of adsorbate polarization in first-layer adsorption following experimental proof of such polarization by Ehrlich and Hudda (11). It is interesting therefore to compare the type of physical adsorption potential for first-layer adsorption discussed by them with the observed potential for typical Type II isotherms. Rather than attempting the arduous task of fitting the experimental curves for first-layer adsorption into the BET scheme, modified to include the Sinanoglu-Pitzer potential, it is simpler and quite as reliable to consider merely the approximate form of the potential function needed to obtain agreement between theory and observations. The type of potential function needed to fit the experimental curve of Arnold (1), for example, is one which decreases uniformly over the range from $\theta = 0$ to $\theta > 0.5$. This seems to be a representative condition, moreover, for many Type II isotherms in the low pressure region. It thus appears that the potential function in first-layer physical adsorption follows approximately the form

$$\zeta = a + b\theta \quad (6b)$$

where a is the adsorption potential at zero coverage and b is a constant.

In addition to the form of ζ in first-layer adsorption, its magnitude is also of significance as regards validity or relative importance of Model 2. Here it is assumed that Model 2 may be based on dispersion forces with polarizations to produce larger than normal first-layer adsorbate-adsorbent potentials (the a term in Equation 6b) and longer than normal range adsorbate-adsorbate repulsions. One may evaluate a and b by curve fitting as follows:

Substitution of Equation 6b in 4 for first-layer adsorption gives

$$\theta = x \exp(a + b\theta - \alpha)/kT / [1 + x \exp(a + b\theta - \alpha)/kT]$$

Whence,

$$a \doteq \alpha + 2.3 kT \log \theta/x_i \text{ for } \theta \rightarrow 0 \quad (7b)$$

To obtain b one may evaluate ζ at some finite value of θ (say θ') by means of the relation

$$b = -a + 2.3 kT \log [\theta'/x'(1 - \theta')] \quad (8b)$$

Using Equations 7c and 8c together with the data of Arnold (1) for oxygen and nitrogen on anatase, one obtains the results shown in Table I.

Table I. Magnitudes of Adsorption Potential Parameters for Adsorption of O₂ and N₂ on Anatase at T = 78.2° K.^a

	O ₂ , Kcal./Mole	N ₂ , Kcal./Mole
a	3.08	3.38
b	-0.47	-1.11
α	1.72	1.34
γ	1.41	1.47
c_1	0.845	0.784
$\zeta_1(6a)^a$	2.39	2.03
$\zeta_1(6b)^b$	2.61	2.27

^a Using isotherms observed by Arnold(1).

^b Values of ζ_1 correspond to $\theta = v/v_m = 1$ as determined from Equations 6a and 6b.

To determine how smoothly Equation 6b fits into Equation 6a when $\theta \rightarrow 1.0$ —i.e., at point B—the value of ζ obtained from Equation 6a for this point is given also in Table I along with its parameters γ and c_1 . These comparisons suggest that the long-range repulsion might have to be larger in the range $0.5 < \theta < 1.0$ than at lower coverage. Part of the difference, however, is associated with the fact that the first-layer coverage at point B is only 0.89, with the remaining 0.11 in the second and higher layers in each case according to computations by Pack (17). The adsorption potential in the second layer is only slightly higher than α and so ζ_1 (6b) values in Table I should really be lowered about 0.07, thus accounting for about a third of the difference.

In Model 2 the ratio $3a/2\gamma$ may be considered approximately to represent the ratio of the dispersion interaction potential between an adsorbate molecule and a solid surface for a polarized as against a rigid, unpolarized adsorbate molecule, assuming in both cases that the potential may be represented by the 3-9 Lennard-Jones (surface) function. This approximation is based additionally on the assumption that the adsorbate is effectively hard sphere in the multilayer region. This ratio turns out to be 3.3 and 3.5 for O₂ and N₂ on anatase, respectively. Furthermore, the adsorbate-adsorbent interactions in the adsorbate-polarization case must evidently amount to 1.8 E_L and 2.5 E_L for O₂ and N₂ on anatase, re-

spectively, as far as conditions at zero coverage are concerned. These ratios are surprisingly large if they are considered to represent simply the influence of polarization on the magnitude of dispersion forces.

The application of dispersion forces with surface polarization to account for a potential function in first-layer adsorption such as that described by Equation 7a, in which correlations with other adsorbate molecules result only in repulsion over the entire first-layer filling, seems more difficult to justify. Thus, b is apparently negative for the entire region below point B in most typical Type II isotherms, at least those in which point B appears at $x < 0.05$. If molecules adsorbed on the first layer of a Type II isotherm were to cause only repulsion, one would expect them to adsorb always in a pattern such as to remain as far apart as possible. But then when they are all a long distance from each other, as they would be near zero coverage, a repulsion term of sufficiently long range to account for a linear $b\theta$ relationship is difficult to explain. Perhaps it may be possible to explain this situation in a Model 4 type adsorption process—i.e., in a model in which both the adsorbate and the adsorbent suffer polarization upon adsorption.

Model 3. Cook, Pack, and Oblad (10) gave a treatment of the first-layer region of a Type II isotherm by Model 3 in which ζ was given by the equation

$$\zeta = \beta[(1 - h(\theta))] + c_1\theta\alpha + 2\gamma/3 \quad (6c)$$

with $h(\theta)$ defined by

$$h(\theta) = \begin{cases} \epsilon^{-1}\theta; & \theta < \epsilon \\ 0; & \theta > \epsilon \end{cases}$$

This potential for first-layer adsorption agreed closely with the experimental one in the cases analyzed. The assumptions leading to Equation 6c were:

1. Second- and higher-layer adsorption can be neglected over most of the region of first-layer filling, becoming important only as v/v_m approaches unity.
2. $C = 0$ (no chemisorption potential).
3. The relative correlation number, z_1/z_L , increases linearly with θ from zero at $\theta = 0$ to c_1 at $\theta = 1.0$.
4. The "structural adsorption" potential is a maximum at $\theta = 0$ and decreases linearly with θ , reaching zero at $\theta = \epsilon$. This assumption was justified from the consideration that surface strain on a bare surface should be long range. It results from elimination of the otherwise high energy of free radical structures by surface bonding, a condition possible only under strong surface distortion. It was considered, since structural adsorption involves strained chemical bonds, that β should fall somewhere between a chemisorption potential C and the physical adsorption potential. This situation is satisfied by the data in Table I; β in Equation 6c has the value $a - 2\gamma/3$, which for O_2 and N_2 on anatase amounts to 2.14 and 2.4 kcal., respectively. In terms of the function 6c, however,

$$\theta = v/v_m = xd_1/(1 + xd_1) \underset{x \rightarrow 0}{\doteq} xd_1 = \exp[\beta - \alpha + 2\gamma/3]$$

Whence

$$\beta = kT \log \theta/x + \alpha - 2\gamma/3 \quad (7c)$$

The constant ϵ should be about 0.5 according to the arguments presented by Cook, Pack, and Oblad (10). However, if desired, ϵ may be used as an adjustable constant and defined by a point on the $\theta(x)$ curve as follows:

$$\epsilon = \{1 + c_1\alpha/\beta + 2\gamma/3\beta\theta' - (2.3/\beta\theta')kT \log \theta'/x'(1 - \theta')\}^{-1} \quad (8c)$$

Surface Polarization in Chemisorption

The evidence for structural adsorption (or surface polarization in first-layer physical adsorption) (5, 12, 18, 26) may be augmented by various considerations

prompted by the theory as applied to chemisorption. That surface polarization should occur strongly in chemisorption is, of course, more readily understandable than in physical adsorption. Some types of evidence for it, however, are strongly suggestive of the type of polarization involved in structural adsorption in first-layer physical adsorption. For example, the chemisorption potential seems frequently to follow the same linear decay in θ described above for Models 2 and 3—that is, for chemisorption ζ seems frequently to follow the equation

$$\zeta = C_0 + C_1\theta \quad (7d)$$

where again C_0 is the initial chemisorption potential and C_1 the slope of the curve of ζ against θ . The author and Oblad (8) showed that this type of potential function, assumed to apply both to the “chemisorption band” and the activated complex, accounts for the Elovich-Taylor-Thon (22, 25, 27) equation for the rate of activated adsorption—namely,

$$d\theta/dt = a'c - b'\theta \quad (9)$$

in which constants a' and b' were defined by the parameters of absolute reaction rate theory as follows:

$$a' = (kT/h)e^{-\Delta F_0^\ddagger/kT}f \quad (10)$$

$$b' = b_0\theta/RT \quad (10)$$

$$\Delta F^\ddagger(\theta) = \Delta F_0^\ddagger + b_0\theta \quad (11)$$

the activation energy of activated adsorption $\Delta F^\ddagger(\theta)$, decreasing linearly with θ because of structural adsorption of the adsorbate as shown by Equation 11. Here f is the true order of the reaction rate process. By this means a previously anomalous, apparently exponential-order, law was explained on the basis that the order law was not really an exponential one, but one which merely appeared to be so because the structural adsorption potential influenced not only the free energy of adsorption of the chemisorption product but also that of the activated complex.

Wadsworth and coworkers (13, 14) have found considerable evidence for surface polarization in double-beam infrared spectroscopy. Not only do new differential peaks due to adsorption appear in the spectrograms but also the bands due entirely to the adsorbent are frequently appreciably shifted by adsorption. This occurred, for example, in calcium fluorite treated with oleic acid, in samples of bentonites taken from aqueous solutions of different pH, and in various minerals treated by flotation collectors. In fact, it is more the rule than the exception that the spectrograms of finely divided solids dispersed in the KI or KBr window exhibit distortion due to adsorption, whether adsorption occurs at the solid-aqueous solution or at the solid-vapor interface. For example, Eyring and Wadsworth (13) found that two (differential) peaks were produced by adsorption on willemite either from the vapor or aqueous solution of hexanethiol. These peaks were due to the influence of adsorption of the hexanethiol on the Si-O bands of the willemite and occurred at about 9.2 and 12.3 microns.

One should be able to observe shifts in the infrared adsorption bands of various adsorbents as a function θ in first-layer physical adsorption if Model 3 is a correct one. Furthermore, if Model 2 applies, the infrared technique of Wadsworth *et al.* (14), Mapes and Eischens (16), and others should be capable of demonstrating the predicted polarization effects by using the KI or KBr window and double-beam technique. So far as the author is aware, studies of this sort have not yet been attempted.

As further evidence for the Model 3 adsorption process the work of Pitt and Wadsworth (19, 20) on the adsorption and desorption of CO₂ on thoria is here summarized. To account for the adsorption isotherm they used for the free energy of adsorption the relation

$$\Delta F = \Delta F_0 + b'\theta \quad (12)$$

where ΔF_0 is the free energy of adsorption at zero coverage and b' is a constant, recognizing again the linear variation of ΔF with coverage. This, of course, neglects secondary forces other than the structural adsorption potential in the chemisorption process. The equilibrium relation for adsorption of CO₂ on thoria was given as



The adsorption equilibrium constant, K , was then given by

$$K = \theta/(1 - \theta)p_G = e^{-\Delta F/RT} \quad (14)$$

The substitution of Equation 12 for ΔF into Equation 13 then gives

$$\ln \theta/(1 - \theta) + (\Delta F_0)/RT + b'\theta = \ln p_G \quad (15)$$

Here S is a surface site, SG the covered site, G the adsorbent gas, and p_G the CO₂ pressure. Under three different approximations Equation 15 becomes alternately the Langmuir equation, the Temkin (23) equation $\theta = f^{-1} \ln(a_0 p)$, and the Freundlich equation $\theta = kp^{1/n}$. In the first instance the approximation is, of course, $\Delta F_0 \gg b'\theta$. In the second, Brunauer, Love, and Keenan (6), recognizing the approximate linear variation of ΔF with θ , showed by taking $b'/RT = f'$ and $\Delta F_0/RT = -\ln a_0$ and by assuming $b'\theta/RT \gg \ln \theta/(1 - \theta)$ that Equation 15 becomes the Temkin equation. Using again the same approximation as employed by Brunauer *et al.* in deriving the Temkin equation and the additional approximation $\ln \theta = (\theta - 1)$ (a good approximation in the range $0.5 < \theta < 1.0$ where the Freundlich equation is applicable), Pitt and Wadsworth derived the Freundlich equation. Clearly, therefore, both the Freundlich and Temkin isotherms depend on the linear variation of ΔF with θ attributed by the author and associates to structural adsorption.

In accord with predictions of Trapnell (24), there were shown to be really two types of surface sites in the adsorption of CO₂ on thoria, both of which exhibited the linear variation of adsorption potential with coverage. Thus, plots of $\Delta F(\theta) [= p_{\text{CO}_2} (1 - \theta)/\theta]$ against θ gave two series of straight lines in which for temperatures above 150°C. one type of site only was active but below 150°C. both were active. The observed adsorption constants are shown in Table II. Both the b' values and the ΔF_0 's varied nearly linearly with θ . This perhaps reflects the influence of temperature on the magnitude of structural adsorption in which increased temperature appears to diminish surface strain as anticipated by the theory of structural adsorption.

While Cook and Oblad showed that structural adsorption causes ΔF^\ddagger for activated adsorption to increase linearly with θ and thereby accounts for the equation for the rate of activated adsorption (Equation 9), Pitt and Wadsworth demonstrated that desorption of CO₂ from thoria followed the equation of Becker (2) for desorption—namely,

$$(-d\theta)/dt = a''\theta e^{b''\theta} \quad (16)$$

From absolute reaction rate theory they gave

$$(-d\theta)/dt = k''\theta kT/h e^{-\Delta F^\ddagger/RT} \quad (17)$$

Table II. Adsorption Constants for CO₂ on Thoria (I9)

<i>T</i> , °K	$-\Delta F_{01}$, Kcal./Mole	b_1' , Kcal./Mole	$-\Delta F_{02}$	b_2'
823	11.80	37	(-18.1)	(3.3)
723	12.60	37.1	(-13.7)	(3.7)
623	13.25	37.5	(-9.3)	(3.8)
523	13.95	37.6	(-4.9)	(3.9)
473	14.35	37.6	(-2.7)	(4.0)
423	14.70	37.8	-0.50	4.10
373	(15.10) ^a	(37.90)	1.80	4.20
323	(15.40)	(38.00)	3.90	4.30

^a Values in () extrapolated from parts of curves extending across boundary of change.

where ΔF^\ddagger is the free energy of desorption and k'_0 a concentration term. On the basis of the theory of the "chemisorption band" (8) the linear potential term was again given by

$$\Delta F^\ddagger = \Delta F_0^\ddagger - b'''\theta \quad (18)$$

By substituting Equation 18 into 17 and rearranging, they obtained

$$b'''\theta/T + 2.3 K \log b'''\theta = \Delta H_0^\ddagger/T - K' \quad (19)$$

where K' is a (concentration and entropy) constant given by

$$K' = 4.6R + \Delta S_0^\ddagger + 2.3K \log k'_0 k/Rh$$

k and h being the Boltzmann and Planck constants. Plotting the l.h.s. of Equation 19 against T^{-1} gave a straight line of slope $\Delta H_0^\ddagger = 22.5$ kcal. Also, the value $\Delta S_0^\ddagger = -51.5$ E.U. for CO₂ desorption from thoria was obtained.

Literature Cited

- (1) Arnold, J. R., *J. Am. Chem. Soc.* **71**, 104 (1949).
- (2) Becker, J., *Trans. Am. Electrochem. Soc.* **55**, 153 (1929).
- (3) Brunauer, S., "Physical Adsorption," Princeton University Press, Princeton, N. J., 1945.
- (4) Brunauer, S., Emmett, P. H., Teller, E., *J. Am. Chem. Soc.* **60**, 309 (1938).
- (5) Brunauer, S., Kantro, D. L., Weise, C. H., *Can. J. Chem.* **34**, 729 (1956).
- (6) Brunauer, S., Love, K. S., Keenan, R. G., *J. Am. Chem. Soc.* **64**, 751 (1952).
- (7) Cook, M. A., *Ibid.*, **70**, 2925 (1948).
- (8) Cook, M. A., Oblad, A. G., *Ind. Eng. Chem.* **45**, 1456 (1953).
- (9) Cook, M. A., Pack, D. H., *J. Am. Chem. Soc.* **71**, 791 (1949).
- (10) Cook, M. A., Pack, D. H., Oblad, A. G., *J. Chem. Phys.* **19**, 367 (1951).
- (11) Ehrlich, G., Hudda, F. G., *Ibid.*, **30**, 493 (1959).
- (12) Emmett, P. H., *J. Phys. Chem.* **63**, 449 (1959).
- (13) Eyring, E. M., Wadsworth, M. E., *Min. Eng.*, **1956**, 531.
- (14) French, R. O., Wadsworth, M. E., Cook, M. A., Cutler, I. B., *J. Phys. Chem.* **58**, 805 (1954).
- (15) Hill, T. L., *J. Chem. Phys.* **15**, 767 (1947); **14**, 263, 268, 441 (1946); *Advances in Catalysis* **4**, 212 (1952).
- (16) Mapes, J. E., Eischens, R. P., *J. Phys. Chem.* **58**, 1059 (1954).
- (17) Pack, D. H., "Theory of Physical and Structural Adsorption," Ph.D. thesis, University of Utah, 1950.
- (18) Peticolas, W. L., *J. Chem. Phys.* **27**, 436 (1957).
- (19) Pitt, C. H., "Kinetic Study of Nickel Corrosion," Ph.D. thesis, University of Utah, 1959.
- (20) Pitt, C. H., Wadsworth, M. E., "Carbon Dioxide Adsorption on Thoria," University of Utah, Tech. Rept. **1** (Feb. 15, 1958).
- (21) Sinanoglu, O., Pitzer, K. S., *J. Chem. Phys.* **32**, 1279 (1952).
- (22) Taylor, H. A., Thon, N., *J. Am. Chem. Soc.* **74**, 4169 (1942).
- (23) Temkin, A., Slygin, A., *Acta Physicochim. U.R.S.S.* **3**, 791 (1935).
- (24) Trapnell, B.M.W., "Chemisorption," p. 73, Academic Press, New York, 1955.
- (25) Twigg, G. H., *Discussions Faraday Soc.* No. **8**, 152 (1950).
- (26) Yates, D. J. C., *Advances in Catalysis* **12**, 265 (1960).
- (27) Zeldovich, Y., *Acta Physicochim. U.R.S.S.* No. **3/4**, 449 (1934).

RECEIVED May 9, 1961.

Adsorption Studies on Metals

X. 1-Propanol on Germanium Powders

A. C. ZETTEMAYER, CARL H. HASSIS,
J. J. CHESSICK, and GANAPATHY SRINIVASAN

*Surface Chemistry Laboratory,
Lehigh University, Bethlehem, Pa.*

A series of four *n*-type germanium crystals of differing resistivities was crushed in air and then studied by adsorption techniques. Argon isotherms were measured to monitor the surface areas as a function of outgassing temperature from 25° to 500° C. Both the physical and chemical adsorption of propanol was measured at 25° also as a function of the outgassing temperature. The chemisorption was found to decrease with decrease in the resistivity. Thus, the adsorption responds to the semiconductivity of the bulk germanium. It is believed that the slow states on the oxide coating tend to trap electrons more readily the higher the conductivity. According to the proposed molecular mechanism, these trapped electrons then tend to repel the donor oxygen of the propanol.

That supported metal catalysts are influenced by the support has been suspected for some time. Several lines of evidence developed by Schwab (9-12) in recent years have confirmed this supposition. His group has been able to demonstrate, for example, that the activity for the hydration of ethylene over nickel is strongly influenced by the nature of the zinc oxide support on which the nickel catalyst is reduced. The addition of lithium to the zinc oxide decreases the activation energy and thereby increases the reaction rate; the addition of gallium has an opposite effect. These findings coincide with the changes in the *n*-conductivity provided by the doping of the zinc oxide substrate. The gallium increases the *n*-conductivity and the lithium reduces it. With increased *n*-conductivity of the support, the electron density in the nickel is increased. Then, in the case of the gallium-doped zinc oxide, the tendency toward chemisorption is reduced and the activation energy rises. The reverse effects are achieved by doping with lithium.

The question arises naturally, therefore, as to whether the conductivity type

and amount in a metal substrate affect the chemisorption on an oxide film supported thereon. An excellent opportunity is provided by germanium semiconductors, in which the amount of *n*- or *p*-type doping can be readily varied. Beyond the scientific interest in the problem, there is considerable technological interest as well because it is recognized that the surface properties may affect the behavior of semiconductor devices.

Four *n*-type germanium crystals of differing resistivities and one *p*-type were chosen for this initial investigation. 1-Propanol was chosen as the adsorbate. Before the results of the adsorption measurements are summarized, it seems desirable to review briefly some of the pertinent information already available concerning the surface of germanium.

Surface States of Oxide-Coated Germanium

Two to three layers of oxide are formed on freshly prepared or reduced germanium surfaces in the first few days when stored in oxygen (6). Thereafter, the oxide film growth is slow. The same reaction kinetics appear to be followed for both *p*- and *n*-type crystals. The oxygen uptake corresponds to one oxygen atom per germanium atom up to a coverage of seven tenths of a monolayer. Then, a logarithmic uptake rate (3) is followed, the rate of growth being proportional to $P_{O_2}^{1/2}$. In the presence of water vapor, hydroxyl groups are probably developed on the outer surface. However, the stability of these hydroxyls to heat and vacuum is not established, as is the case for silica surfaces. There is some evidence (to be published later) that the *p*- and *n*-type oxide-coated crystals respond differently to water adsorption.

Upon heating, the GeO_2 reacts with germanium to form GeO , which then evaporates. Thus, a reduced surface can be obtained by heating under vacuum, but an ultrahigh vacuum is, of course, required if the bare surface is to be maintained. At 10^{-6} mm. of Hg, extrapolated data indicate (5) that about one layer per minute would be lost at 400° , and about one tenth of a layer per minute at 350° . However, it is doubtful whether the first adsorbed layer of oxygen is removed under these conditions. At 200° , the loss is estimated to be extremely slow or negligible.

It is recognized in device technology (2, 7, 8, 13) that oxide-coated germanium crystals possess both fast and slow surface states. The fast states, corresponding to rapid relaxation times, are believed to reside at the oxide-germanium interface; they act as electron traps and have a density of about 10^{11} states per sq. cm. They interact with the bulk electrons in a matter of microseconds. The slow states, on the other hand, are believed to reside at the oxide-air interface or in the oxide layer; their density is of the order of 10^{14} states per sq. cm. They respond slowly, in a matter of seconds, minutes, or hours, to bulk electrical impulses or to changes in ambient conditions. It is the slow states which would be expected to be most affected and effective in interaction with adsorbates. These states are also most influential because of their density, in creating a space charge region in the semiconductor and thereby influencing bulk properties. The interest in direct adsorption measurements is thus heightened.

The spectrum of energy levels for electrons at the germanium surface usually differs from that in the interior of the crystal. This situation arises because of the unsaturated energy levels of the surface atoms, misfits in the structures of germanium and the oxide, and other impurities like chemisorbed gases. All these factors, either independently or combined together, result in the formation of the

surface states which act as traps for the carriers. Band diagrams, as given in Figure 1, elucidate the characteristics of the surface states. When electrons are trapped in the surface states, the potential energy of electrons is greatly increased at the surface. Electroneutrality is maintained by the migration of oppositely charged holes to the vicinity of the surface region. A space charge region (1) is formed near the surface having a thickness of 10^{-7} to 10^{-4} cm. If the concentration of the electrons trapped in the surface states is considerable, the space charge region becomes an inversion layer for *n*-type germanium (Figure 1, *a*) and an accumulation layer for a *p*-type semiconductor (Figure 1, *b*). It will be of interest to consider how these band diagrams might respond to adsorption by the oxide layer.

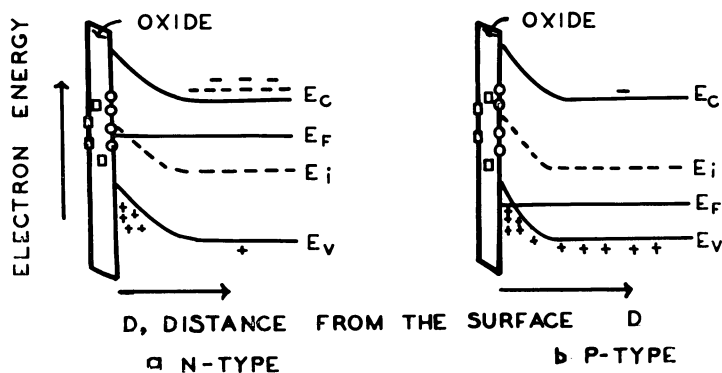


Figure 1. Energy diagrams at germanium surfaces

- Slow states
- Fast states
- E_c . Bottom of conduction band
- E_f . Fermi level
- E_i . Middle of energy gap
- E_v . Top of valence band

Experimental

Germanium single crystals of the four *n*-type samples, with 0.14-, 1.8- to 2.1-, 5.5- to 10-, and 20- to 30-ohm-cm. resistivities, were crushed in an agate mortar and stored in air for 15 days before measurements were begun. Both argon surface areas and propanol isotherms were determined after activation for 15 hours at better than 10^{-5} mm. of Hg at six different temperatures ranging from 25° to 500° C. Even after outgassing at 500° where oxide film is lost by reduction and subsequent evaporation, additional oxide forms instantaneously at the ordinary vacuum employed and over the relatively small surface areas in the sample tube totally about 1 sq. meter.

The organic adsorption apparatus, based on a glass Bourdon gage and Teflon stopcocks, has been described (14). After each activation, the first propanol isotherm, measured at 25°, gave the total amount adsorbed. The "B point" was employed as a measure of the monolayer capacity, but there was a general agreement with the V_m 's estimated from BET plots.

After the total isotherm was determined, the physically adsorbed propanol was pumped off at 25° C. and $< 10^{-5}$ mm. of Hg for 48 hours. The propanol which remains adsorbed is called "chemisorbed," although it is recognized that this is not a strong criterion (4). A second isotherm was then determined to

yield the physically adsorbed monolayer capacity. The difference between the two isotherms, after each activation, gave measure of the chemisorbed portion.

Table I. Propanol Adsorption

Temp., °C.	Argon Area, Sq. M./G.	$V_{ads.}$, ML./Sq. Meter			Propanol Total
		Total	Phys.	Chem.	
20- to 30-Ohm-Cm. Sample					
25	0.112	0.142	0.056	0.086	0.107
100	0.122	0.069	0.026	0.043	0.057
200	0.115	0.098	0.024	0.074	0.076
300	0.130	0.105	0.040	0.065	0.092
400	0.129	0.116	0.049	0.067	0.101
500	0.128	0.159	0.055	0.104	0.136
0.14-Ohm-Cm. Sample					
25	0.156	0.115	0.048	0.067	0.121
100	0.161	0.057	0.022	0.035	0.067
200	0.164	0.064	0.021	0.043	0.071
300	0.173	0.091	0.030	0.061	0.105
400	0.194	0.080	0.033	0.047	0.104
500	0.200	0.098	0.032	0.066	0.131

The measurements at each activation temperature were made on the same crushed sample.

Results and Discussion

Table I lists the adsorption results of two *n*-type samples which fell at the two extremes of the resistivity range studied. The extent of chemisorption per unit area of the surfaces of the *n*-type samples is much more than the amounts physically adsorbed, indicating that the larger fraction of the surface enters into strong interaction with propanol.

The surface area as measured by argon adsorption undergoes a small increase between the 100° and 200° outgassing steps for the 20- to 30-, 5.5- to 10-, and 1.8- to 2.1-ohm-cm. *n*-type samples. Above 300°, the changes in argon areas are negligibly small for these three samples. The 0.14-ohm-cm. germanium, on the other hand, exhibits a uniform increase in the area during the entire temperature range.

The area per adsorbed propanol molecule at 25° activation is calculated to be within the range 27 to 36 sq. Å. for the four *n*-type germanium samples. Therefore, the adsorbate is fairly closely packed. The initial high chemisorption of propanol at 25° compared to water (the results of water adsorption on germanium are to be published elsewhere) on 5.5- to 10- and 0.14-ohm-cm. germanium powders surprisingly suggests that the presence of preadsorbed water on the surface is not critical in deciding the strong propanol adsorption. Nevertheless, it appears that a complete monolayer coverage is obtained only for the 20- to 30-ohm-cm. sample at the 500° outgassing step, as indicated by the ratio of propanol to argon areas.

The dependence of propanol adsorption capacity of the germanium surfaces on the outgassing conditions is essentially decided by the chemisorption, since

on *n*-Type Ge

Area, Sq. Meter/G.		Propanol Molecule Area (Total), Sq. A.	Ratio of Propanol to Argon Area		
Phys.	Chem.		Total	Phys.	Chem.
20- to 30-Ohm-Cm. Sample					
0.042	0.065	26.6	0.955	0.370	0.577
0.021	0.035	54.1	0.468	0.180	0.288
0.019	0.057	38.1	0.670	0.165	0.505
0.035	0.057	35.5	0.708	0.269	0.439
0.042	0.059	32.2	0.783	0.326	0.457
0.047	0.089	23.4	1.060	0.368	0.692
0.14-Ohm-Cm. Sample					
0.050	0.071	32.4	0.803	0.319	0.484
0.024	0.044	65.5	0.398	0.161	0.237
0.024	0.047	58.3	0.482	0.139	0.343
0.034	0.071	41.0	0.578	0.201	0.377
0.043	0.061	46.6	0.510	0.226	0.284
0.043	0.088	38.1	0.625	0.225	0.400

both total adsorption and chemisorption respond in a similar manner to the thermal activation.

The chemisorbed portions for the four *n*-type samples are plotted in Figure 2

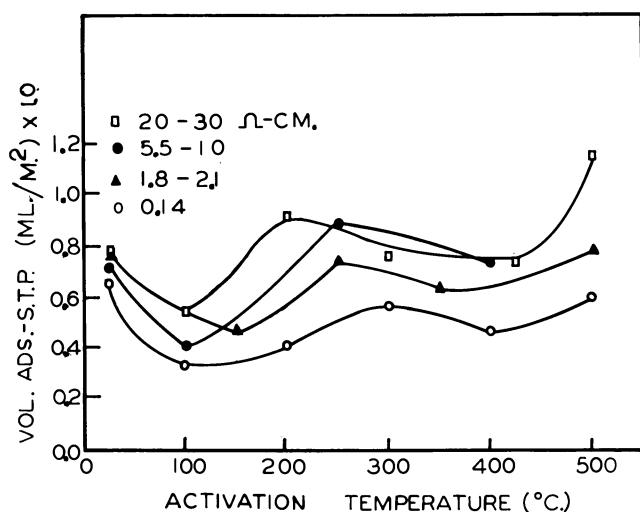


Figure 2. Chemisorption of propanol on *n*-type germanium samples of different resistivities as a function of activation temperature

against the activation temperature. There is a large adsorption after 25° outgassing. The curves show considerable similarity, in marked contrast to the water adsorption characteristics. They fall rapidly at 100° outgassing, then generally show a peak in an intermediate region before they rise again to high values upon outgassing at 500°.

The events are complicated by several factors. On the one hand, there is the loss of physically and strongly bound water in the monolayer with increasing activation temperature. Also, it is not established whether or not this combined water resides as hydroxyl groups. Finally, the response of Ge-O-Ge groups, if formed, to interaction with propanol (or to water) as a function of strain removal by heat treatment (cf. silica and alumina surfaces) is not at all understood.

It appears desirable to compare the adsorptive properties of the various samples after activation at 200° C. Upon outgassing at this temperature at 10^{-5} to 10^{-6} mm. of Hg, the physically adsorbed water is mostly removed. In addition, at this temperature there is a negligible loss of oxide film. For three out of the four samples, there is little change in the argon surface area above this temperature. At this temperature and close thereto, the amounts chemisorbed on the *n*-type samples, as depicted in Figure 2, increase with increasing resistance. This pattern exists for three of the samples at all temperatures, although there is some exception for the 5.5- to 10-ohm-cm. resistivity sample. Lack of complete agreement for the 5.5- to 10-ohm-cm. sample may be due to inhomogeneities. In addition, inconsistencies in the low temperature results may be due to incomplete removal of propanol at the next higher temperature. The 100° data were taken on the same material which had just previously been used for the 25° data. No capillary effects are to be expected, because single crystals were crushed to produce the adsorption samples; in turn, the germanium surfaces were coated with only two to three oxide layers. An interpretation was sought from the energy diagrams of the germanium surface.

Suppose the alcohol molecules adsorb donor fashion with the positive ends of the dipole oriented toward the surface. Figure 3 shows the effect of adsorption

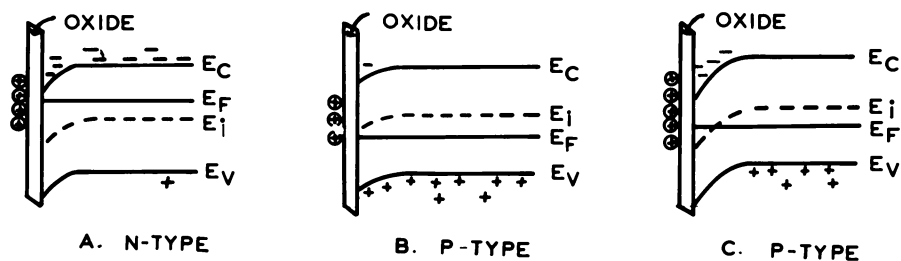


Figure 3. Effect of trapped charges or adsorption on energy diagrams of germanium

Positive charges either trapped or formed because of adsorption on Ge surfaces produce

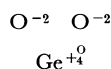
- A. Accumulation space charge region
- B. Depletion region
- C. Inversion region

of such donor molecules or atoms on the oxide-covered germanium surface. The electrons in the bulk move to the surface to restore the electroneutrality upset created by the adsorbed species. Now a space charge region is formed which constitutes an accumulation layer of electrons in the case of *n*-type germanium as

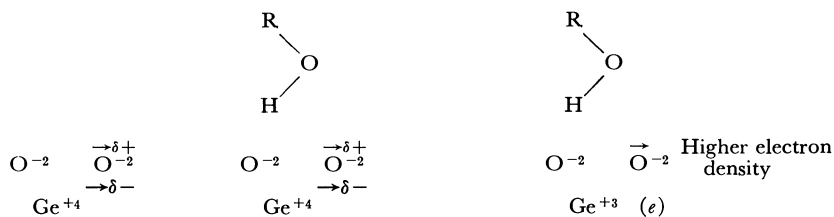
shown in Figure 3, A. If the extent of such chemisorption on *p*-type germanium is small, the majority carriers—viz., holes—will be repelled by the adsorbed dipole. So the concentration of the holes will be smaller just below the surface than in the interior. This situation leads to a depletion layer of space charge, as shown in Figure 3, B. On the other hand, if the adsorption on *p*-type germanium becomes large, the minority carriers migrate to the surface for electrical balance. An inversion layer, as shown in Figure 3, C, of opposite conductivity type will be the result.

For *n*-type germanium samples of different resistivities the concentration of electrons in the conduction band will be larger the lower the resistivity. If the situation in Figure 3, A, is considered, the repulsion offered by the sample for any donor-type molecule will be greater, the lower the resistivity of the germanium. Consequently, the extent of adsorption of such a molecule will decrease with decreasing resistivity. The observed decreasing propanol chemisorption with decreasing resistivity can thus be explained. The molecular mechanism must now be considered.

The interaction of the propanol with the oxide-covered germanium can be considered in terms of the surface both with and without hydroxyls. Suppose the surface oxide is as follows:



The highly charged germanium cation possesses a tendency to polarize the oxygen anions, drawing the charge density toward it. However, the exact nature of the local situation should be considered in terms of the charge carriers available in the interior. The conduction electron of an *n*-type germanium could be trapped at the cation Ge^{+4} site and thus reduce its effective charge. This migration of the conduction electron will be facilitated at the higher outgassing temperatures. Consequently, there will be a diminution in the polarization effect of the cation on the oxide anion and the electron density at the outermost periphery of the oxide ion will increase. This electron density is expected to increase with decreasing resistivity which represents increased availability of electrons. One can therefore expect the extent of R-OH-oxide interaction to increase with decrease in the resistivity of the *n*-type powders. The following representation clarifies this point.



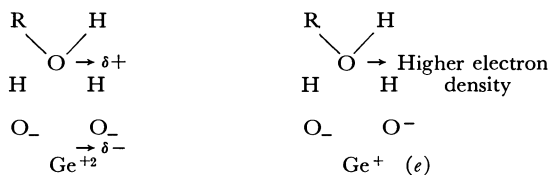
Polarization of O^{-2} ion by germanium cation

High resistivity sample; reduced R-OH-oxide interaction

Low resistivity sample with depolarized O^{-2} ion; strong R-OH-oxide interaction; (*e*) trapped electron

The experimental findings are contrary to the conclusions reached on the basis of this mechanism.

Suppose, on the other hand, hydroxyls are present on the surface. The negativity of the outer periphery of the hydroxyl will be higher for the low resistivity sample. If the alcohol adsorbs donor fashion, the situation illustrated below prevails.



High resistivity sample; strong interaction between R-OH and the surface

Low resistivity sample; weak interaction between R-OH and surface; (*e*) trapped electron

Enrichment of the surface layer with electrons, as happens for the low resistivity sample, makes the surface less attractive for molecules with $-\text{OH}$ groups like R-OH, H_2O , etc. This mechanism is in accord with the experimental results depicted in Figure 2.

The propanol chemisorption ranges from 0.05 to 0.09 ml. per sq. meter—i.e., about 1.3 to 2.4×10^{14} molecules per sq. cm. These values are only slightly higher than the reported density of the slow surface states—viz., 10^{13} to 10^{14} per sq. cm. Whether the chemisorption of foreign gases can be quantitatively related to the slow states remains undecided. The slow states are measured electrically, so that a bias is imposed on the crystal (2, 7, 8, 13). This bias was, of course, not present during the adsorption measurements reported here.

Similar adsorption studies were conducted on a *p*-type germanium powder (2.5-ohm-cm. resistivity). The general trend of the total adsorption with increasing thermal outgassing was similar to that of the *n*-type samples, but it was chiefly decided by the physical adsorption, which in this case was always larger than the chemisorption. The chemisorption was small at 25° and gradually increased to a constant value above 300° . Compared to the *n*-type samples, the chemisorption on the *p*-type specimen was found to be considerably smaller; at 200°C. , it was about 30% less than for the *n*-type samples. Further investigation is under way to attempt to fit the adsorption characteristics of *p*-type germanium into the pattern developed for the *n*-type samples.

An interesting avenue for investigation is to examine the adsorption characteristics on single crystals concurrently with electrical measurements. Thus, any relationship which possibly exists between the slow states and the chemisorption might be positively revealed. Examination of the adsorption characteristics of reduced germanium crystals and the effect of the fast states would also be of interest. These studies have been initiated. It remains clear at this time, however, that the semiconductor properties of the germanium influence the surface properties of the thin oxide films supported thereon. The influence is clear in the case of propanol adsorption and the differences are even more dramatic in the case of water adsorption.

Acknowledgment

Helpful discussions were held with Max Katz of the U. S. Signal Corp. Research Laboratory and with Richard Serrine of the General Electric Co.

Literature Cited

- (1) Bardeen, J., *Phys. Rev.* **71**, 717 (1947).
- (2) Garret, C. G., B., Brattain, W., Brown, W. L., Montgomery, H., "Semiconductor Surface Physics," R. H. Kingston, ed., p. 111, University of Pennsylvania Press, Philadelphia, 1957.
- (3) Green, M., "Progress in Semiconductors," A. F. Gibson, ed., Vol. 4, pp. 35-62, Heywood & Co., London, 1960.
- (4) Kipling, J. J., Peakall, D. B., "Chemisorption," W. E. Garner, ed., p. 59, Academic Press, New York, 1957.
- (5) Law, J. T., Meigs, P. S., "Semiconductor Surface Physics," R. H. Kingston, ed., p. 383, University of Pennsylvania Press, Philadelphia, 1957.
- (6) Ligenza, J. R., *J. Phys. Chem.* **64**, 1017 (1960).
- (7) Many, A., Gerlick, D., *Phys. Rev.* **107**, 404 (1957).
- (8) Morrison, S. R., "Semiconductor Surface Physics," R. H. Kingston, ed., p. 169, University of Pennsylvania Press, Philadelphia, 1957.
- (9) Schwab, G.-M., *Ibid.*, p. 283.
- (10) Schwab, G.-M., Block, J., Müller, W., Schultze, D., *Naturwissenschaften* **22**, 582 (1957).
- (11) Schwab, G.-M., Block, J., Schultze, D., *Angew. Chem.* **71**, 101-4 (1959).
- (12) Schwab, G.-M., Mutzbauer, G., *Naturwissenschaften* **46**, 13 (1959).
- (13) Statz, H., deMars, G. A., Davis, L., Adams, A., *Phys. Rev.* **101**, 1272 (1956).
- (14) Yu, Y.-F., Chessick, J. J., Zettlemoyer, A. C., *J. Phys. Chem.* **63**, 1626 (1959).

RECEIVED July 20, 1961. Work supported by the U. S. Signal Corps Research Laboratory, Fort Monmouth, N. J., Contract DA 36-039 SC-85130.

Editor's Note. The results reported by Zettlemoyer and associates are explained by a theory which has been very neatly corroborated by work on similar systems at the U. S. Army Signal Research and Development Laboratory. The following discussion is included with the consent of the symposium chairman.

Discussion of Adsorption Studies on Metals

X. *I*-Propanol on Germanium Powders

M. J. KATZ

U. S. Army Signal Research and Development Laboratory, Fort Monmouth, N. J.

Results obtained recently by us are entirely consistent with the model advanced here for adsorption on the semiconductor surface.

Starting from the theory of surface states, Zettlemoyer *et al.* are able to account for changes in chemisorption with the variation in conductivity of a series of samples. As the authors suggest, a direct confirmation of the relationship would require simultaneous measurement on a single crystal of chemisorption and the related electronic factors. This requirement is partially met in our experiments. Taken with the work described above, they provide a complementary aspect of the proposed model.

Before entering into a discussion of our results, it is appropriate to point out the essential differences in approach. The Lehigh group measured chemisorption on powdered samples and deduced the electronic interaction with the surface from a plausible model. We, on the other hand, measured the conductivity and lifetime

Literature Cited

- (1) Bardeen, J., *Phys. Rev.* **71**, 717 (1947).
- (2) Garret, C. G., B., Brattain, W., Brown, W. L., Montgomery, H., "Semiconductor Surface Physics," R. H. Kingston, ed., p. 111, University of Pennsylvania Press, Philadelphia, 1957.
- (3) Green, M., "Progress in Semiconductors," A. F. Gibson, ed., Vol. 4, pp. 35-62, Heywood & Co., London, 1960.
- (4) Kipling, J. J., Peakall, D. B., "Chemisorption," W. E. Garner, ed., p. 59, Academic Press, New York, 1957.
- (5) Law, J. T., Meigs, P. S., "Semiconductor Surface Physics," R. H. Kingston, ed., p. 383, University of Pennsylvania Press, Philadelphia, 1957.
- (6) Ligenza, J. R., *J. Phys. Chem.* **64**, 1017 (1960).
- (7) Many, A., Gerlick, D., *Phys. Rev.* **107**, 404 (1957).
- (8) Morrison, S. R., "Semiconductor Surface Physics," R. H. Kingston, ed., p. 169, University of Pennsylvania Press, Philadelphia, 1957.
- (9) Schwab, G.-M., *Ibid.*, p. 283.
- (10) Schwab, G.-M., Block, J., Müller, W., Schultze, D., *Naturwissenschaften* **22**, 582 (1957).
- (11) Schwab, G.-M., Block, J., Schultze, D., *Angew. Chem.* **71**, 101-4 (1959).
- (12) Schwab, G.-M., Mutzbauer, G., *Naturwissenschaften* **46**, 13 (1959).
- (13) Statz, H., deMars, G. A., Davis, L., Adams, A., *Phys. Rev.* **101**, 1272 (1956).
- (14) Yu, Y.-F., Chessick, J. J., Zettlemoyer, A. C., *J. Phys. Chem.* **63**, 1626 (1959).

RECEIVED July 20, 1961. Work supported by the U. S. Signal Corps Research Laboratory, Fort Monmouth, N. J., Contract DA 36-039 SC-85130.

Editor's Note. The results reported by Zettlemoyer and associates are explained by a theory which has been very neatly corroborated by work on similar systems at the U. S. Army Signal Research and Development Laboratory. The following discussion is included with the consent of the symposium chairman.

Discussion of Adsorption Studies on Metals

X. *I*-Propanol on Germanium Powders

M. J. KATZ

U. S. Army Signal Research and Development Laboratory, Fort Monmouth, N. J.

Results obtained recently by us are entirely consistent with the model advanced here for adsorption on the semiconductor surface.

Starting from the theory of surface states, Zettlemoyer *et al.* are able to account for changes in chemisorption with the variation in conductivity of a series of samples. As the authors suggest, a direct confirmation of the relationship would require simultaneous measurement on a single crystal of chemisorption and the related electronic factors. This requirement is partially met in our experiments. Taken with the work described above, they provide a complementary aspect of the proposed model.

Before entering into a discussion of our results, it is appropriate to point out the essential differences in approach. The Lehigh group measured chemisorption on powdered samples and deduced the electronic interaction with the surface from a plausible model. We, on the other hand, measured the conductivity and lifetime

of excess current carriers on single-crystal germanium as a function of the ambient. The crystals were *n*-type, about 30 ohm-cm., 0.5 mm. thick, polished and etched in 2 to 1 HNO₃ to HF. A number of adsorbates were scanned through, including O₂, H₂O, and some compounds of the series, R—X, R—NH₂, and R—OH. Our procedure was to pump the sample to a 10⁻⁶ mm. vacuum and to observe the change in lifetime (average life of injected current carriers) by measuring the decay in photovoltage with exposures to the adsorbate. In some cases, where the reaction seemed reversible, a new exposure was made after pumping at room temperature. Otherwise the sample was flashed at about 500° C. at 10⁻⁶ mm. before re-exposing it. This treatment will not remove all residual oxygen and/or hydroxyl so that our surfaces are similar in this respect to the powder surfaces. It seemed worthwhile to proceed in this way, although any given reaction must be understood in terms of previous sample history.

We cannot detail here the diverse effects of reversibility, rates, and pressure dependence of the reactions. Although there was no means of measuring the adsorption directly, we could control the extent of the reaction by varying the ambient pressure. In the present context, the following points should be made:

1. Systematic variations in lifetime and conductivity as a function of the ambient were obtained on *n*-type germanium.

2. Upon exposure to various alkanols and alkyl amines (not exceeding 4 carbons) carrier lifetimes increased up to about 50%, whereas the conductivities increased by 1%. Total conductivity was measured—i.e., bulk plus surface—and, therefore, the magnitude of the change does not reflect the true sensitivity of surface conductivity to the reaction.

3. The lifetime of a *p*-type crystal decreased on exposure to ethylamine—i.e., a change inverse to that obtained with an *n*-type crystal.

4. CH₃SH and alkyl halides produced no change in lifetime. Zettlemoyer has shown elsewhere that alkyl halides adsorb to a negligible extent, if at all, on oxidized germanium surfaces. In the case of CH₃SH, we have an interesting contrast to that of CH₃OH, which, as indicated above, produced a pronounced increase in lifetime. As the CH₃SH would not be expected to react as a donor, it would not tend to liberate trapped electrons.

5. Prolonged pumping on the adsorbed alcohols and amines at room temperature tended to decrease the lifetime. Thus, even the reversibly sorbed fraction may affect the trapped electrons—perhaps through a dipole-dipole interaction.

Essentially, the Lehigh theory envisages electrons trapped at surface cation sites where they will act to inhibit donor-type chemisorption. From our point of view, the process of donor chemisorption tends to release the trapped electron, thereby increasing the conductivity and increasing the lifetime by reducing the occupancy at recombination centers. As already noted, this process is observed during the adsorption of R—OH. The theory also predicts similar results for the adsorption of R—NH₂, which were in fact obtained, although detailed chemisorption data are not available for this case. Here again the amino group would be expected to exhibit donor properties.

RECEIVED October 17, 1961.

Utilization of Order-Disorder Theory in Physical Adsorption

II. The Square Lattice

JURGEN M. HONIG

*Lincoln Laboratory, Massachusetts Institute of Technology,
Lexington 73, Mass.*

The order-disorder formalism of Hijmans and de Boer has been applied to the interaction between a gas and a square lattice of adsorption sites, following the procedure of an earlier publication. The decomposition of the lattice into representative arrays and the process of setting up normalization, consistency, and equilibrium conditions are discussed. Procedural methods for obtaining numerical solutions are outlined. Representative isotherms are provided and some noteworthy features are pointed out.

In previous work the order-disorder formalism developed by Hijmans and de Boer (5) (the HB formalism) was applied to gas adsorption theory (1). It was shown that the well known Langmuir or Fowler-Guggenheim (3, 4) isotherm equations (F. G. approximation), which pertain to localized monolayer adsorption on uniform surfaces in the absence and presence of nearest neighbor lateral interactions, were obtained as special cases of this more general formulation. In an extension of the earlier work, the effect of next nearest neighbor interactions on the adsorption process was taken explicitly into account. The case treated by Bumble and Honig (1) pertained to a hexagonal lattice array, for which the ratio of next nearest to nearest neighbor distances is $R = \sqrt{3}/1$. If the predominant lateral interactions are due to van der Waals-London dispersion forces, the attractive energy varies with distance approximately as $r^{-1/6}$. Because of the rather large R ratio, only minor changes would be anticipated in passing from the Fowler-Guggenheim equation to the case where allowance is made for next nearest neighbor interactions. This is indeed the case; it was shown, however, that for relatively strong lateral interactions among adsorbate molecules on adjacent sites the corrections introduced in considering next nearest neighbor interactions are by no means negligible.

In the present paper the formalism is applied to the case of a square lattice of adsorption sites depicted in Figure 1. Here R has the value $\sqrt{2}/1$, so that the

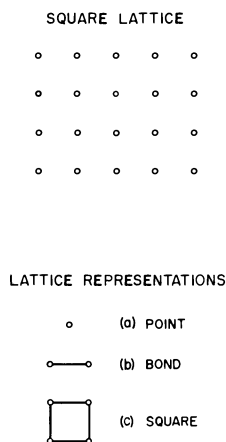


Figure 1. The square lattice and its simple representations

effect of next nearest neighbor interactions on the shape of the isotherm should be greater than for the hexagonal array of sites; this is found to be the case.

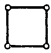

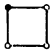


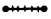





Bumble and Honig (1) have discussed the HB procedure as applied to gas adsorption and the approximations inherent in the model used below. Honig (6) gives additional background information, where the Fowler-Guggenheim isotherm equation is derived in an elementary fashion.

The Lattice Representation

To simplify the analysis, the lattice depicted in Figure 1 is decomposed into representations in which the most complicated figure is the square depicted in Figure 1, *c*; this is the so-called basic figure and is labeled with the index *c*. In addition, it is necessary to take account of the bond (Figure 1, *b*) and of the point (Figure 1, *a*), which represent so-called subfigures and are labeled *b* and *a*, respectively. Suppose the lattice proper consists of L adsorption sites; since each square is specified by four points and each site is shared by four adjacent squares, it is necessary to construct a c - array of L squares for the primary representation of the lattice. Included in this count are $4L$ bonds, since every square contains four sides. In the actual lattice there are only $2L$ bonds; to rectify this overcount it is therefore necessary to construct a b - array of $-2L$ bonds. The occurrence of negative numbers is an integral part of the HB formalism and has been discussed by Bumble and Honig (1). The number of points contained in the figures constituting the c - and b - representation are $4L$ and $-4L$, respectively, and cancel out; since the lattice contains L sites, it is necessary to construct an a - array of L points. We have thus succeeded in representing a square lattice as a superposition of L squares, $-2L$ bonds, and L points; the integers 1, -2 , and 1 are labeled $y_c^{(c)}$, $y_c^{(b)}$, and $y_c^{(a)}$, respectively.

It is now possible to specify the possible configurations or occupation states for each representation, as shown in Table I. A filled circle indicates a site occupied by an adsorbed atom. The symbol to the right of each figure represents the fraction of all members in each array in the specified configuration. The

Table I. Configurations, Multiplicities, and Energies Appropriate to the Representation of a Square Lattice

CONFIGURATIONS				CONFIGURATIONS			
	VARIABLE	MULTI-PLICITY	ENERGY		VARIABLE	MULTI-PLICITY	ENERGY
	$p_{j\xi^{(c)}}$	$\lambda_{j\xi^{(c)}}$	$\epsilon_{j\xi^{(c)}}$		$p_j^{(b)}$	$\lambda_j^{(b)}$	$\epsilon_j^{(b)}$
	γ_0	1	0		β_0	1	0
	γ_1	4	$-\epsilon$		β_1	2	$-\epsilon$
	γ_{21}	4	$-2\epsilon + w$		β_2	1	$-2\epsilon + w$
	γ_{22}	2	$-2\epsilon + w'$	<u>-2L BONDS</u>			
	γ_3	4	$-3\epsilon + 2w + w'$	$p_j^{(a)}$	$\lambda_j^{(a)}$	$\epsilon_j^{(a)}$	
	γ_4	1	$-4\epsilon + 4w + 2w'$		α_0	1	0
					α_1	1	$-\epsilon$
				<u>L POINTS</u>			
				<u>L SQUARES</u>			

multiplicity shows the number of equivalent ways in which the given occupation state may be reproduced by redistribution of the occupied sites in the figure while maintaining their relative geometric interrelation. Configurations 21 and 22 are not equivalent, since one cannot superpose the two figures on each other in such a way that all filled and all empty sites coincide. In contrast to the previous work (1), it is not necessary to introduce subscript r into the notation here, and index ξ is utilized only where needed in the c -array to distinguish between nonequivalent configurations; j designates the total number of occupied sites. The energy appropriate to each configuration is also shown in Table I; the energy difference between an isolated adsorbate atom at rest in the gas phase and in its ground state on an isolated surface site is designated as $-\epsilon$; the lateral interaction energy for adsorbate particles on adjacent and on next nearest neighbor sites is written as w and w' , respectively. It is important to note two assumptions which have been implicitly introduced: first, that all sites are associated with the same value of $-\epsilon$, and second, that the different types of interaction energies are linearly additive. In many cases of interest neither approximation is satisfactory.

Consistency and Normalization Conditions

In Table I are introduced 11 variables designated in general as $p_{j\xi^{(m)}}$, ($m = a, b, c$). To shorten the notation we frequently write $p_j^{(a)} \equiv \alpha_j$, $p_j^{(b)} \equiv \beta_j$, and $p_{j\xi^{(c)}} \equiv \gamma_{j\xi}$. The 11 variables are subject to constraints which reduce the number of independent $p_{j\xi^{(m)}}$ to six. One set of constraints arises from the definition of the $p_{j\xi^{(m)}}$ ($m = a, b, c$); the normalization conditions require that

$$\sum_{j\xi} \lambda_{j\xi^{(m)}} p_{j\xi^{(m)}} = 1 \quad (m = a, b, c) \quad (1)$$

where the $\lambda_{j\xi^{(m)}}$ are the multiplicities listed in Table I. As applied to the present case Equation 1 reads






$$\alpha_0 + \alpha_1 = 1 \quad (2)$$

$$\beta_0 + 2\beta_1 + \beta_2 = 1 \quad (3)$$

$$\gamma_0 + 4\gamma_1 + 4\gamma_{21} + 2\gamma_{22} + 4\gamma_3 + \gamma_4 = 1 \quad (4)$$

In addition there exist so-called consistency relations which basically arise from the fact that in the lattice proper only the subfigures exhibited in Table II are recognized as distinct. These configurations represent completely occupied

Table II. Distinct Occupied Subfigures, with Appropriate Occupation Variables, Multiplicities, and Designation of Occupation Variable in Table I

FULLY OCCUPIED SUBFIGURES	q VARIABLES	CORRESPONDING OCCUPATION VARIABLES
	q_1	$\alpha_1, \beta_1, \beta_2, \gamma_1, \gamma_{21}, \gamma_{22}, \gamma_3, \gamma_4$
	q_{21}	$\beta_2, \gamma_{21}, \gamma_3, \gamma_4$
	q_{22}	$\gamma_{22}, \gamma_3, \gamma_4$
	q_3	γ_3, γ_4
	q_4	γ_4

subfigures whose occupation variables are represented as $q_{k\eta}$ where $k\eta$ is a doublet of running indices analogous to $j\xi$. The consistency condition associated, for example, with q_{21} arises because in the lattice representation this occupation state would be designated by the distinct symbols $p_2^{(b)}$ or $p_{21}^{(c)}$ for the b - and c -arrays, whereas such a distinction is physically meaningless when referred to the lattice proper. The consistency conditions interrelate all the $p_{j\xi}^{(m)}$ which are associated with a given $q_{k\eta}^{(m)}$ by the equations

$$\lambda_{k\eta}^{(m)} q_{k\eta}^{(m)} = \sum_{j\xi} c_{k\eta;j\xi}^{(m)} \lambda_{j\xi}^{(m)} p_{j\xi}^{(m)} \quad (m = a, b, c) \quad (5)$$

where $c_{k\eta;j\xi}^{(m)}$ represents the number of distinct ways in which the completely occupied subfigure under study can be superposed on the j occupied sites of the various subfigures which occur in the lattice representations. The physical condition, that a fully occupied subfigure be associated with an occupation variable which should not depend on the size of the subfigure in the representation, is met by the requirement

$$\dots = q_{k\eta}^{(l)} = q_{k\eta}^{(m)} \equiv q_{k\eta} \quad (6)$$

The integers $c_{k\eta;j\xi}^{(m)}$ are readily determined by superposition of the figures in Table II onto those of Table I. In this manner one arrives at the matrices listed in Table III together with the associated multiplicities. [For the entries in row 1 of each matrix see (1) and the discussion centering about Equation 10.] For example, the fully occupied subfigure 21 can be superposed onto figure 3 of the c -array in two ways—namely, along the edges joining the filled sites. Hence entry 2 is placed in position $k\eta = 21$, $j = 3$ of the C -matrix. The negative signs will be introduced at a later stage.

From Table III one may read off numerical values to be inserted for c and λ in Equation 5. On applying Equation 6 it is found that

$$q_1 \equiv p_1^{(a)} = p_1^{(b)} + p_2^{(b)} = p_1^{(c)} + 2p_{21}^{(c)} + p_{22}^{(c)} + 3p_3^{(c)} + p_4^{(c)} \quad (7)$$

$$q_2 \equiv p_2^{(b)} = p_{21}^{(c)} + 2p_3^{(c)} + p_4^{(c)} \quad (8)$$

which are the desired consistency conditions. In view of Equations 2 to 4, 7, and 8, only five of the original 11 variables remain independent. It turns out convenient to select as independent variables the $q_{k\eta}$ listed in Table II or the equivalent occupation variables $\alpha_1, \beta_2, \gamma_{22}, \gamma_3,$ and γ_4 .

Table III. Matrices for Setting Up Consistency Conditions

Lower sign to be used in conjunction with equilibrium conditions. First row follows from the definition, Equation 10

C MATRIX		$\lambda_{j\xi}^{(c)}$	1	4	4	2	4	1
$\lambda_{k\eta}^{(c)}$			$j\xi$					
1	$k\eta$	0	1	± 1	1	1	± 1	1
4		1	0	1	± 2	± 2	3	± 4
4		21	0	0	1	0	± 2	4
2		22	0	0	0	1	± 1	2
4		3	0	0	0	0	1	± 4
1		4	0	0	0	0	0	1

B MATRIX		$\lambda_j^{(b)}$	1	2	1
$\lambda_k^{(b)}$			j		
1		0	1	± 1	1
2	k	1	0	1	± 2
1		2	0	0	1

A MATRIX		$\lambda_j^{(a)}$	1	1
$\lambda_k^{(a)}$			j	
1		0	1	± 1
1	k	1	0	1

B-11541

Equilibrium Conditions

To determine the above-mentioned unknowns it is necessary to impose the equilibrium condition that the entropy of the system be a maximum consistent with all constraints placed on the system. As shown by Bumble and Honig (1), this leads to the result

$$\sum_{m=a}^n y_n^{(m)} \sum_{j\xi} \lambda_{k\eta}^{(m)} B_{j\xi;k\eta}^{(m)} [\epsilon_{j\xi}^{(m)} + kT \ln p_{j\xi}^{(m)}] = \mu^{(G)} B_{1;1}^{(a)} \delta_{1k} \quad (9)$$

for all η consistent with a given k and for $k = 1, 2, 3$. The case $k = 0$ is excluded because q_0 is so defined as to satisfy the relation

$$q_0 \equiv \sum_{j\xi} \lambda_{j\xi}^{(m)} p_{j\xi}^{(m)} = 1 \quad (10)$$

By comparison with Equation 5 it follows that $B_{0;j\xi}^{(m)} = 1$ for all $m, k,$ and η . The coefficients $B_{j\xi;k\eta}^{(m)}$ can be shown (5) to be identical with the $c_{j\xi;k\eta}^{(m)}$ listed in Table III except for a change of sign whenever $|j - k|$ is odd. The order of the subscripts on B and c in Equations 9 and 5 is reversed; in carrying out the summation Equation 9, the second set of indices remains fixed. The symbol $\mu^{(G)}$ in Equation 9 designates the chemical potential of the gaseous species, and $\epsilon_{j\xi}^{(m)}$ refers to the energies listed in Table I. On inserting the appropriate numerical values in Equation 9 and taking antilogarithms on both sides one arrives at the following set of equilibrium conditions:

$$\frac{\alpha_1}{\alpha_0} \left(\frac{\beta_0}{\beta_1} \right)^4 \left(\frac{\gamma_1}{\gamma_0} \right)^4 = e^{[\mu^{(G)} + \epsilon]/kT} \quad (k = 1) \quad (11)$$

$$\frac{\beta_1^2}{\beta_0\beta_2} \left(\frac{\gamma_0\gamma_{21}}{\gamma_1^2} \right)^2 = C \equiv e^{-w/kT} \quad (k = 21) \quad (12)$$

$$\gamma_{22}\gamma_0/\gamma_1^2 = C' \equiv e^{-w'/kT} \quad (k = 22) \quad (13)$$

$$\gamma_3\gamma_1^3/\gamma_{22}\gamma_0\gamma_{21}^2 = 1 \quad (k = 3) \quad (14)$$

$$\gamma_0\gamma_4\gamma_{22}^2 \left(\frac{\gamma_{21}}{\gamma_3\gamma_1} \right)^4 = 1 \quad (k = 4) \quad (15)$$

Equations 2 to 4, 7, 8, and 11 to 15 represent 11 simultaneous equations which can be solved for the unknown $p_{j\dot{x}}^{(m)}$. Now, $\mu^{(G)} = \mu_0^{(G)}(T) + kT \ln P$, where P is the pressure or fugacity of the gas and $\mu_0^{(G)}$ is the chemical potential of the gas in its standard state. Hence the term on the right of Equation 11 may be replaced with P/P^o , where $P^o = \exp - [\mu_0^{(G)} + \epsilon]/kT$ is a constant for fixed temperatures, not to be confused with the saturation vapor pressure P_0 , occurring in the theory of multilayer adsorption. In this manner, Equation 11 represents an isotherm equation, once the various $p_{j\dot{x}}^{(m)}$ have been expressed in terms of $p_1^{(a)} \equiv \theta$, where θ is the fraction of lattice sites covered at pressure P .

Numerical Solutions

It remains to solve the equations mentioned earlier. Since the equilibrium relations are nonlinear, any attempt to find an analytical solution seems hopeless. One is thus forced to utilize an approximation method which requires, first, the specification of inputs reasonably close to the final answers, and second, the utilization of a self-consistent calculation cycle by which the final answer may be obtained in successive approximations.

To obtain inputs one may proceed as follows: Define a quantity K

$$K = \left[\frac{P}{P^o} \times \frac{\alpha_0}{\alpha_1} \right] \quad (16)$$

with which Equation 11 may be rewritten as

$$\gamma_1/\gamma_0 = K^{1/4}\beta_1/\beta_0 \quad (17)$$

In view of Equations 16 and 17, Equation 12 reads

$$\gamma_{21}/\gamma_0 = C^{1/2}K^{1/2}\beta_1\beta_2^{1/2}/\beta_0^{3/2} \quad (18)$$

Proceeding in similar fashion with the remaining equilibrium relations, one finds

$$\gamma_{22}/\gamma_0 = C'K^{1/2}(\beta_1/\beta_0)^2 \quad (19)$$

$$\gamma_3/\gamma_0 = CC'K^{3/4}\beta_1\beta_2/\beta_0^2 \quad (20)$$

$$\gamma_4/\gamma_0 = C^2(C')^2K(\beta_2/\beta_0)^2 \quad (21)$$

Finally, it is necessary to introduce the Fowler-Guggenheim isotherm equation (3, 6), ($Z = 4$)

$$P/P^o = [\theta/(1 - \theta)][(\beta - 1 + 2\theta)/2\theta]^4 C^{-4} \quad (22)$$

where

$$\beta = [1 + 4\alpha_0\alpha_1(C - \frac{1}{2})]^{1/2} \quad (23)$$

and the corresponding equilibrium condition (1, 5, 6)

$$\beta_0\beta_2/\beta_1^2 = C \quad (24)$$

The input data may then be obtained as follows: One specifies numerical values for C , C' and for a set of $p_1^{(a)} \equiv \theta$. From Equations 2, 3, 7, and 24 one then obtains α_0 and β_j ($j = 0, 1, 2$), with which the ratio P/P^0 may be determined via Equations 22 and 23, so that K may be computed according to Equation 16. With these preliminary values the ratios $\gamma_{j\bar{k}}/\gamma_0$ can be computed from Equations 17 to 21; in conjunction with Equation 4 the values of $p_{j\bar{k}}^{(c)}$ can be found individually. The various $p_{j\bar{k}}^{(m)}$ specified above and the ratio P/P^0 serve as the zero-order inputs.

To aid in the second step involving successive approximations it is convenient to "linearize" Equations 11 to 15, using the method outlined by Bumble and Honig (1). In essence, one rewrites each $p_{j\bar{k}}^{(m)}$ as $\Delta p_{j\bar{k}}^{(m)} + p_{j\bar{k}}^{(m,0)}$ where the latter symbol represents the zero-order inputs. The $\Delta p_{j\bar{k}}^{(m)}$ now represent the new unknowns; since they are presumed small, one can rewrite the equilibrium relations in linear form, involving first powers of $\Delta p_{j\bar{k}}^{(m)}$. For example, Equation 13 becomes

$$[p_{22}^{(c,0)} + \Delta p_{22}^{(c)}][p_0^{(c,0)} + \Delta p_0^{(c)}]/[p_1^{(c,0)} + \Delta p_1^{(c)}]^2 \cong \frac{p_{22}^{(c,0)}p_0^{(c,0)}}{[p_1^{(c,0)}]^2} \left[\frac{1 + \frac{1}{p_{22}^{(c,0)}} \Delta p_{22}^{(c)} + \frac{1}{p_0^{(c,0)}} \Delta p_0^{(c)}}{1 + \frac{2}{p_1^{(c,0)}} \Delta p_1^{(c)}} \right] = C'$$

or, approximately,

$$\frac{1}{p_0^{(c,0)}} \Delta p_0^{(c)} - \frac{2}{p_1^{(c,0)}} \Delta p_1^{(c)} + \frac{1}{p_{22}^{(c,0)}} \Delta p_{22}^{(c)} = \frac{C' [p_1^{(c,0)}]^2}{p_{22}^{(c,0)} p_0^{(c,0)}} - 1$$

Proceeding similarly with the remaining relations one obtains a set of "linearized" equilibrium conditions which together with the normalization and consistency conditions yield 11 simultaneous linear equations in the $\Delta p_{j\bar{k}}^{(m)}$. These may be solved by machine computation to obtain $\Delta P/P^0$. The resulting increments are added to their corresponding zero-order quantities to yield a set of first-order results $p_{j\bar{k}}^{(m,1)}$ which replace the $p_{j\bar{k}}^{(m,0)}$. The process of solving the linearized set is repeated until the increments become too small to be of consequence. The entire procedure is then repeated for other values of C and C' .

Results

Computations were carried through for values of $0.05 \leq \theta \leq 0.95$ in increments of 0.05 unit, with $C = 2, 3, 4$, and 5. It was assumed that lateral interactions were due to attractive van der Waals-London dispersion forces, where the leading term in the energy expansion varies with distance as $r^{-1/6}$; with $R = \sqrt{2}$ one finds $C' = C^{1/8}$. Calculations were also carried out in the Fowler-Guggenheim approximation; this simply requires the determination of the zero-order inputs $p_0^{(a,0)}$, $p_j^{(b,0)}$, and P/P^0 . The results are exhibited in Figures 2 and 3; the broken curves refer to isotherms calculated according to Equations 22 and 23.

Noteworthy Features. For a given value of C the isotherms depicted in Figures 2 and 3 are displaced towards larger values of P/P^0 than the corresponding isotherms of Bumble and Honig (1). This is a reflection of the fact that $Z = 6$ for the hexagonal lattice, whereas $Z = 4$ for the square lattice. Since the number of nearest neighbors to a given site is smaller in the latter case, it requires a larger pressure to reach a given θ value when lateral interactions are of the attractive type ($w < 0$).

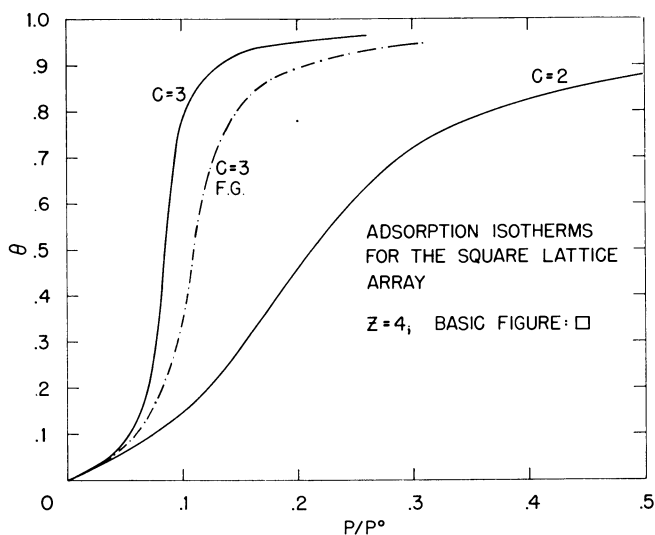


Figure 2. Adsorption isotherms calculated as described in text for $C = 2$ and 3

--- Fowler-Guggenheim isotherm

The occurrence of loops in the isotherms indicates the existence of two-dimensional condensation. This phenomenon sets in for a critical value C_0 which is greater than that encountered by Bumble and Honig (1)—i.e., to achieve two-dimensional condensation the lateral interactions must be stronger than those required in (1). Again, this is believed to be primarily due to the difference in Z values for the two cases.

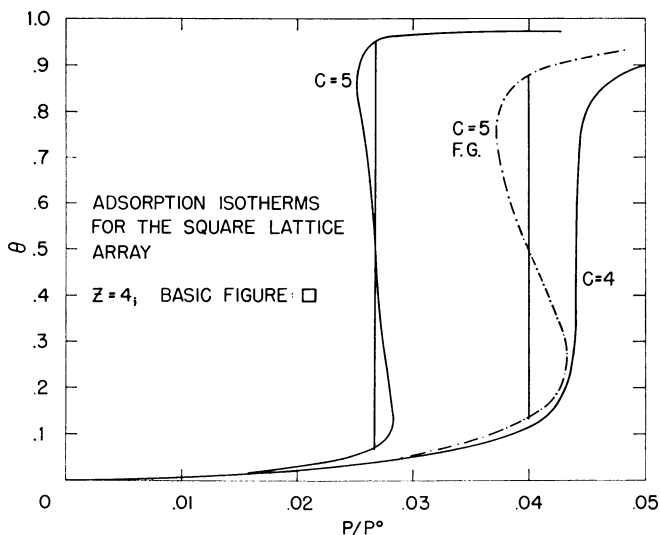


Figure 3. Adsorption isotherms calculated as described in text for $C = 4$ and 5

--- Fowler-Guggenheim isotherm

Table IV. C_0 Values

	Square Array $Z = 4$	Hexagonal Array $Z = 6$
F.G. approximation	4.00	2.25
Present analysis	4.80	2.62
Literature value	5.83	3.00

One would expect an appreciable change in the form of the isotherm for the square lattice array as one passes from the F. G. approximation ($C' = 1$) to the case where next nearest neighbor interactions are considered ($C' > 1$). Comparison with (1) shows that the changes encountered here indeed are greater and are in the anticipated direction. Thus, isotherms for which $C' > 1$ are displaced towards the lower end of the P/P^0 scale compared to those for which $C' = 1$. Furthermore, the vertical line connecting those portions of the isotherm that are separated by loops is longer in the former than in the latter case. This means that two-dimensional condensation sets in at a lower surface coverage and terminates at a higher surface coverage when the theory takes account of lateral interactions between next nearest neighbors than when these interactions are ignored.

The critical value, C_0 , is larger when $C' > 1$ than it is for the case $C' = 1$, as may be verified by direct calculation or by comparison of the size of the loops in Figure 3. This again is an expected result; for it is known that C_0 as determined from the Fowler-Guggenheim approximation is too low. Here, the exact solutions serve as a comparison standard; by sophisticated mathematical techniques reviewed in several articles (2, 7) it is possible to determine the exact value of C_0 for certain types of infinite two-dimensional lattices, the square and hexagonal arrays among them. Values for C_0 in the present approximation were obtained by trial and error techniques. The results are presented in Table IV.

In both types of lattices the C_0 value obtained in the present approximation is a significant improvement over that associated with the F. G. approximation. On the other hand, as judged by the trend of the entries in Table IV, convergence to the correct C_0 value is very slow, and considerable further refinement seems to be required to approach the exact quantities. Unfortunately, the next higher approximation becomes extremely cumbersome, since it can be shown that 30 additional variables are required to characterize the problem. It is likely that the next nearest neighbor approximation as given here represents an upper limit for practical calculations.

Acknowledgment

The author acknowledges the assistance of Seymour Hilsenrath in checking the derivations. He is greatly indebted to Ann Sherman and Cynthia Schweppe for the numerical calculations.

Literature Cited

- (1) Bumble, S., Honig, J. M., *J. Chem. Phys.* **33**, 424 (1960).
- (2) Domb, C., *Advances in Phys.* **9**, 149 (1960).
- (3) Fowler, R. H., Guggenheim, E. A., "Statistical Thermodynamics," Chap. X, Cambridge University Press, London, 1956.
- (4) Guggenheim, E. A., "Mixtures," Oxford University Press, Oxford, 1952.
- (5) Hijmans, J., de Boer, J., *Physica* **21**, 471, 485, 499 (1955).
- (6) Honig, J. M., *Trans. N. Y. Acad. Sci.* **22**, 313 (1960).
- (7) Newell, G. F., Montroll, E. W., *Revs. Modern Phys.* **25**, 353 (1953).

RECEIVED June 12, 1961. The Lincoln Laboratory is operated with support from the U. S. Army, Navy, and Air Force.

Adsorption Potentials, Adsorbent Self-Potentials, and Thermodynamic Equilibria

E. A. FLOOD

*Division of Pure Chemistry, National Research Council,
Sussex Drive, Ottawa, Canada*

The Gibbs potential, F_{ac} , of an adsorbate-adsorbent system may be considered as the sum of the intrinsic potentials of adsorbate, $F_{a'}$ and adsorbent, $F_{c'}$, together with a mutual interaction potential, ω_{ac} . When adsorbent-adsorbate potentials are small compared with adsorbent self-potentials, the interaction is largely confined to fields lying outside the adsorbent system and the energies, Gibbs potentials, stresses, etc., are additive, ω_{ac} approaching zero. In this case the free energy change of the adsorbent is measured by its change in state of stress. When adsorption potentials are comparable with adsorbent self-potentials, the Gibbs potentials and stresses are not additive and the free energy change of the adsorbent is not measured by its change in state of stress alone.

The change in Gibbs potential (δF) due to immersion of active carbon (F_c) in a relatively large mass of gas (F_g) at constant pressure (P_g) and temperature may be expressed by

$$F_g(p_g, m_g) + F_c(p_c = 0, m_c) = F_{ac}(p_g, m_g, m_c) + \delta F \quad (1)$$

or

$$\mu_g m_g + \mu_{co} m_c = \mu_g m_g + \mu_c m_c + \delta F$$

and

$$\delta F = (\mu_{co} - \mu_c) m_c = -\delta F_c$$

This equation will hold regardless of the kind of reaction involved, provided that no volatile or gas-soluble substance containing carbon is evolved. The equation is therefore applicable to a great variety of possible reactions and provides little or no information concerning the state of either adsorbate or adsorbent in the combined system.

If, however, a dividing surface exists which separates the adsorbent completely from the adsorbate, so that throughout the adsorption reaction no material, electrons, etc., can cross this dividing surface, we can considerably restrict the number of possible types of interaction. When such a surface exists, we can apply equations of the Polanyi (18) or Guggenheim (10) type [essentially variants of

Gibbs' 508, 514 (9)] and obtain expressions for the adsorbate "spreading pressure."

Assuming such spreading pressures to consist literally of purely hydrostatic stresses and these stresses to be in equilibrium with the accompanying purely mechanical stresses of the solid, we can write the approximate equation,

$$F_c = K\sigma\bar{\gamma} \quad (2)$$

where K is a proportionality constant, σ the surface area, and $\bar{\gamma}$ the mean surface mechanical stresses of the solid, or we may write the more general equation,

$$F_c = K'v_c\bar{p}_c^v \quad (3)$$

where v_c is the volume of the solid adsorbent and \bar{p}_c^v is the mean principal stress intensity.

Equation 2 has been used with some success by Bangham (1), McIntosh (5), Yates (20), and others to correlate adsorption extension data. Equation 3 has also been used with considerable success by McIntosh (15) and Dacey (6), and in some of my own work (8, 15).

If the adsorption reaction can indeed be represented as a purely mechanical interaction, then from the thermodynamic conditions for equilibrium of systems in purely hydrostatic states of stress, we can deduce

$$v_a\bar{p}_a^v + v_c\bar{p}_c^v = (v_a + v_c)P \quad (4)$$

where v_a is a volume which includes the effective field of the solid (for porous bodies v_a can be taken as either the whole of the void volume or as the micropore volume, and the value of \bar{p}_a^v changes accordingly); v_c is the solid volume; \bar{p}_a^v is the volumetric mean of the principal stress intensities acting on the external surfaces of the adsorbate volumes which contribute to v_a ; \bar{p}_c^v is the similar volumetric mean stress intensity of the solid; and P is the hydrostatic pressure of the fluid in which the system is immersed and with which it is in equilibrium. When the volume v_a is very small compared with v_c , so that v_a is virtually the "surface" of v_c , Equation 4 reduces to

$$v_c(\bar{p}^v - P) = \frac{2}{3}\sigma\bar{\gamma} \quad (5)$$

regardless of the shape of the solid.

Equations 4 and 5 may be compared with the very similar equations of classical elasticity (14, 16) theory as applied to isotropic bodies. Equation 5 is the same as Gibbs' 560. (Gibbs' 560 refers to spherical volumes, but it is easily shown that the equation applies to volumes of any shape.)

Adsorption-extension and permeability measurements provide fairly searching tests of the validity of the assumption that in physical adsorption reactions the adsorbate and adsorbent behave essentially as bodies of matter in mechanical equilibrium.

Ignoring shearing and similar work terms, the basic assumptions lead to the following equations:

$$\delta\bar{p}_c^v = \int_0^P \frac{\bar{p}_a}{\rho_g} dp_g = a\delta P \quad (6a)$$

where \bar{p}_a is the volumetric mean adsorbate density, ρ_g is the gas density, p_g is the gas pressure ($0 \leq p_g \leq P$), and a is defined by Equation 6a.

$$\delta\bar{p}_c^v = \left[1 + \frac{v_a}{v_c} (1 - a) \right] \delta P \quad (6b)$$

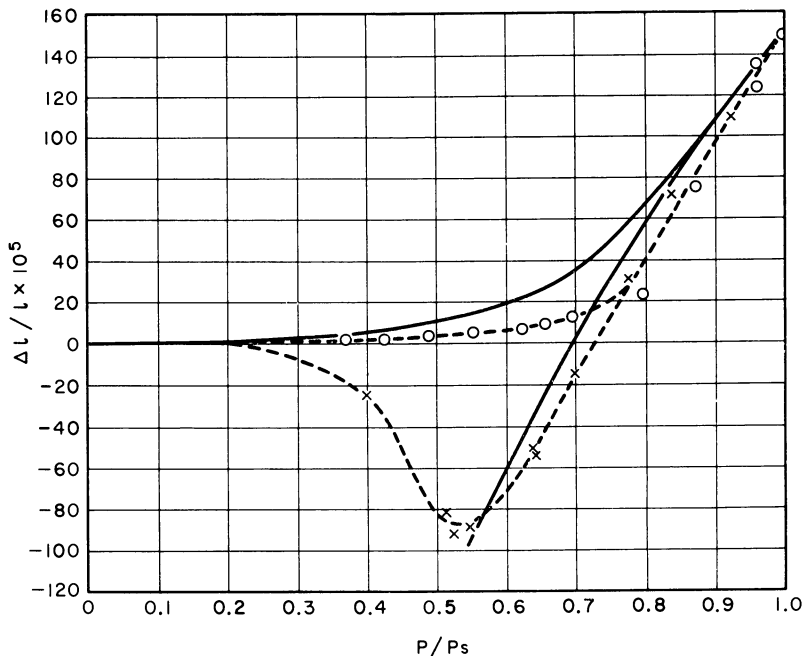


Figure 1. Adsorption extension data for water vapor on carbon

Data of Haines and McIntosh (1¹)

----- O. Adsorption. X. Desorption
 ————— Calculated from Equations 6d and 6e

A. $1.0 \times 10^{-7}/p.s.i.$

B. 0

$f(p) \cdot 1$

K. 4.76

v_a/v_c . 2.16 (observed value)

The dimensional change of the carbon may be represented by

$$\delta v_c/v_c = -A\delta\bar{p}_c^s(1 - B\delta\bar{p}_c^L) \quad (6c)$$

The dilation of the whole volume, $\delta v/v$, will not in general be equal to $\delta v_c/v_c$, even if the solid is reasonably isotropic elastically, unless $\delta\bar{p}_c^s$ is a change in uniform hydrostatic pressure, which it is very unlikely to be if the adsorption is appreciable. Hence we write more or less empirically

$$\delta v/v = (\delta v_a + \delta v_c)/(v_a + v_c) = -A\delta\bar{p}_c^L(1 - B\delta\bar{p}_c^L) \quad (6d)$$

and

$$\delta\bar{p}_c^L = \left[1 + f(p)K_s \cdot \frac{v_a}{v_c} (1 - a) \right] \delta P \quad (6e)$$

where K_s is a structure factor dependent only on the solid structure and constitutes a measure of the variation in wall thickness of representative filaments. $f(p)$ is a specific, pressure-dependent term, for each adsorbate. It may be regarded as a statistical factor correlating surface potentials and pore sizes. The implication is that both of these factors are reasonably close to unity.

The basic assumptions also lead to equations describing the micropore permeabilities of systems whose micropores are greater than a few adsorbate molecular diameters (12). One of these equations is

$$Q_m = \frac{A}{L\eta} \int_{P_1}^{P_2} \frac{\bar{p}_a^2}{\rho_a} dp_a \tag{6f}$$

These equations in fact describe a good deal of adsorption-extension data remarkably well, and also describe some permeability data (Figures 1 to 4).

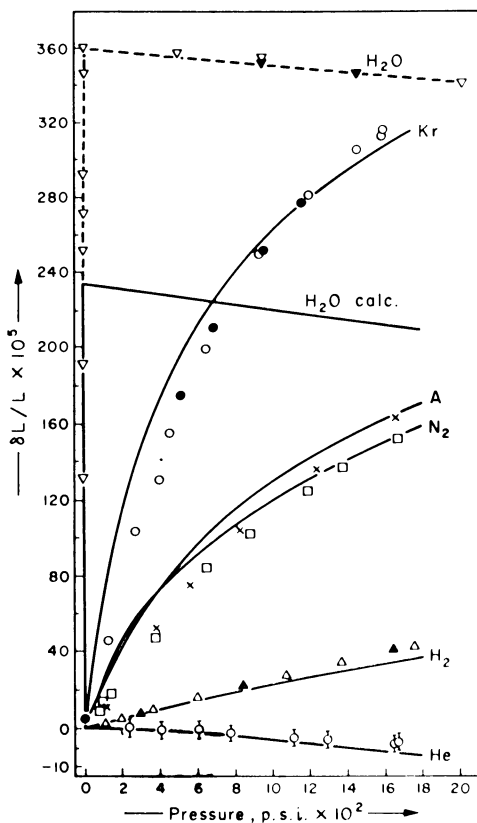


Figure 2. Adsorption-extension at 25° C.

○, ●. Krypton adsorption, desorption, etc.
 ——— Calculated from Equations 6d and 6e
 A. $2.40 \times 10^{-7}/p.s.i.$ B. $2/3 \times 10^{-5}/p.s.i.$
 $f_{(p)} = \frac{1}{K}$ 3.50
 $v_a/v_c = 1.304$ (observed)

The evidence lends considerable support to the basic assumptions. There are, however, some notable exceptions, especially where contractions occur instead of the predicted expansions. These contractions have been studied by Wiig (19), McIntosh (5), Yates (20), and Dacey (7), and in my laboratory (13) (Figures 5 and 6).

Evidently the previous thermodynamic treatment must have been oversimplified.

Revised Thermodynamic Treatment

If in the adsorbate-adsorbent system a surface exists dividing the system into two distinct parts, we can refer to the intrinsic energies, entropies, and Gibbs

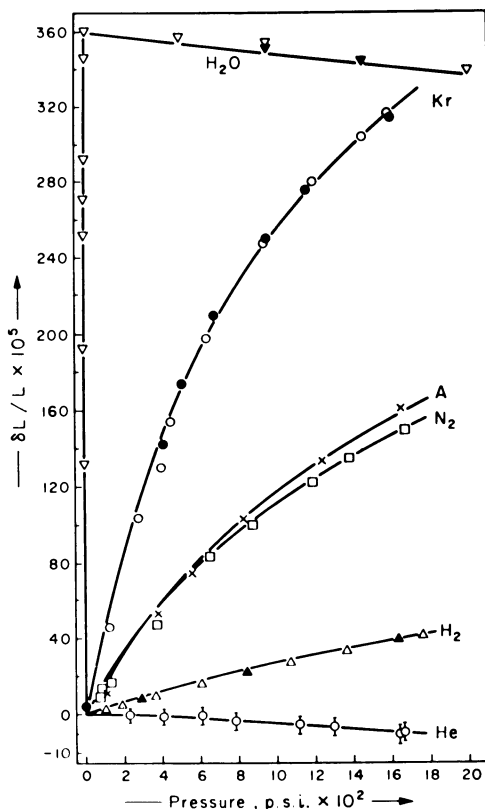


Figure 3. Adsorption-extension data as for Figure 2

- Calculated from Equations 6d and 6e
 A. $2.640 \times 10^{-7}/p.s.i.$
 B. $1/2 \times 10^{-3}/p.s.i.$
 $f_{(p)}, 1 - D\sqrt{a}$
 K. 3.834
 $v_a/v_c, 1.304$
 D. 0 for He and H_2O , 0.172 for H_2 ,
 0.168 for Ar and N_2 , 0.116 for Kr

potentials of the two parts separately. However, if these parts exert forces upon one another in addition to purely mechanical forces, there will also be a potential associated with these forces—i.e., with their mutual field. Since energies, entropies, volumes, etc., are additive properties, we may regard the energy, entropy, and volume of the whole system as equal to the sum of its parts. However, in general, pressures and displacement work terms such as pV terms are not necessarily additive properties. Thus, the Gibbs potential of the whole system is not necessarily equal to the sum of the intrinsic Gibbs potentials of its parts. When the adsorbate and adsorbent can both exist separately in equilibrium with externally applied forces in states that are identical with those of the combined system and which are both in equilibrium with the combined system—i.e., when the Gibbs potentials are additive—we can write $E'_a + E'_c = E_{ac}$, $S'_a + S'_c = S_{ac}$, $F'_a + F'_c = F_{ac}$, where the primes refer to the separate bodies of the adsorbate and of adsorbent, and hence,

$$v_a \bar{p}_a^v + v_c \bar{p}_c^v = (v_a + v_c)P \tag{7}$$

also

$$dF'_a + dF'_c = dF_{ac}$$

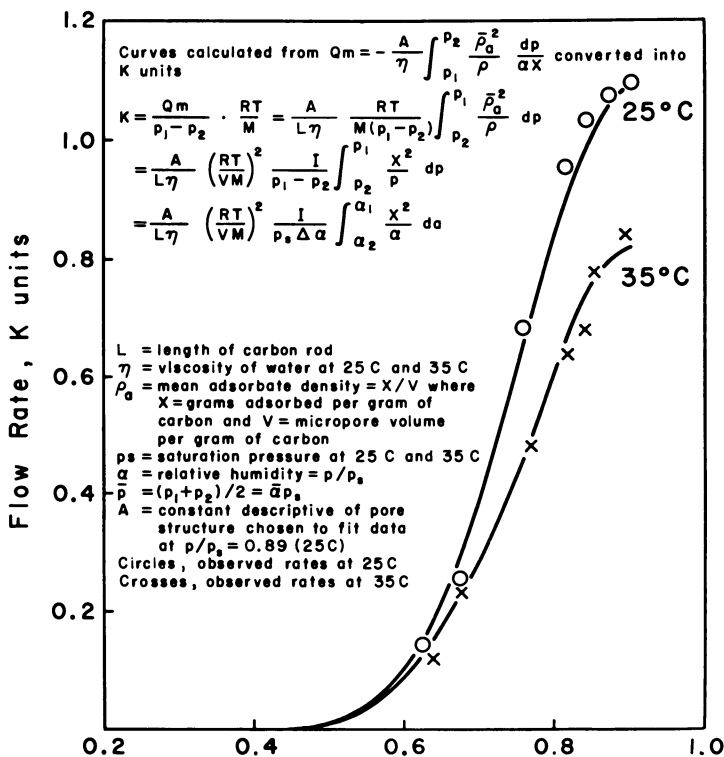


Figure 4. Flow rates of water vapor through micropore system of activated carbon rod having larger micropores than samples of Figures 2 and 3

———— Calculated from Equation 6f

and where only hydrostatic states of stress are involved

$$\int_0^{\bar{p}_a^v} v_a dp_a + \int_0^{\bar{p}_c^v} v_c dp_c = \int_0^P (v_a + v_c) dP$$

or

$$\bar{v}_a \bar{p}_a^v + \bar{v}_c \bar{p}_c^v = \overline{(v_a + v_c)} P$$

and hence

$$\bar{v}_a/v_a = \bar{v}_c/v_c = \overline{v_a + v_c} / (v_a + v_c)$$

Therefore, for small changes in volumes,

$$\delta v/v = \delta v_c/v_c = -A \delta \bar{p}_c^v (1 - B \delta \bar{p}_c^v)$$

Accordingly, $f(p)$ K_s in Equation 6e must be unity.

However, in the general case, the intrinsic potentials are not additive and we must write

$$F'_a + F'_c - \omega_{ac} = F_{ac} \quad (8)$$

where the primes refer to the intrinsic potentials of the two separate systems in identical states to those in the combined system and ω_{ac} is a measure of the displacement work done by the two systems upon one another, as the combined system grows, its nature and state, temperature, distribution of stress, etc., remaining constant.

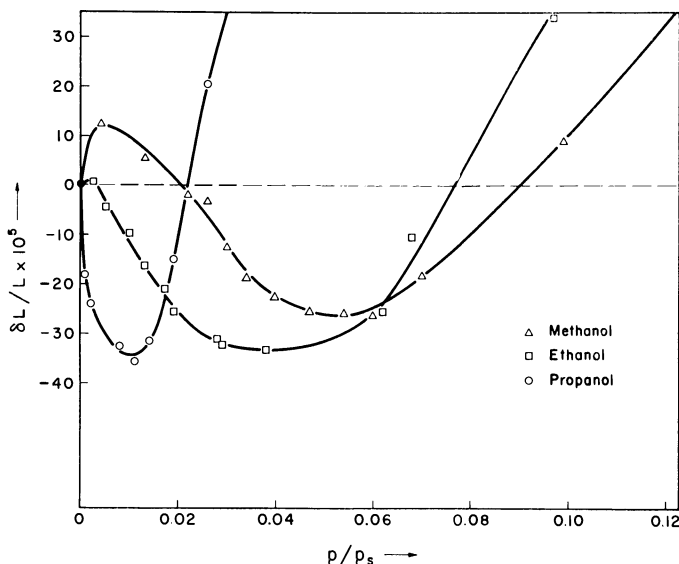


Figure 5. Elongation as a function of relative pressure, p/p_s , for some alcohols

Marked contractions are observed with CCl_4 but with neither methyl- or ethylamine

If in addition to $p dv$ work terms we include work terms at constant S , v , such as polarization terms, shear strains, etc., and these are included explicitly, we obtain the following revised equations:

$$v_a \bar{p}_a^* + v_c \bar{p}_c^* - \omega_{ac} = (v_a + v_c)P \quad (8a)$$

$$\bar{v}_a \bar{p}_a^* + \Phi_a + \bar{v}_c \bar{p}_c^* + \Phi_c - \omega_{ac} = \overline{(v_a + v_c)}P \quad (8b)$$

$$\delta \bar{p}_a^* = \int_0^P \frac{\bar{p}_a}{\rho_a} d p_a - \Phi'_a = a \delta P$$

Some interesting relations may be deduced from these equations. For example, if ω_{ac} and $\Phi_a = 0$ and adsorption is marked, when Φ_c is positive, $\delta v/v > \delta v_c/v_c$ but when Φ_c is negative, $\delta v/v < \delta v_c/v_c$. Thus, when the adsorption mechanism consists partly of a release of the compressive stress of the carbon and partly of a release of shear strain, $\delta v/v$ will be less than $\delta v_c/v_c$ —i.e., $f(p) K_s$ in Equation 6e would be less than unity and could even be negative.

However, to make any detailed use of these equations we must be able to impose limits on ω_{ac} , Φ_a , and Φ_c , especially upon ω_{ac} .

When $\omega_{ac} = 0$, the equations represent, formally, a mechanical interaction including shear strain, polarization, and similar potentials.

The ideas underlying Equations 7 and 8a may be illustrated as follows:

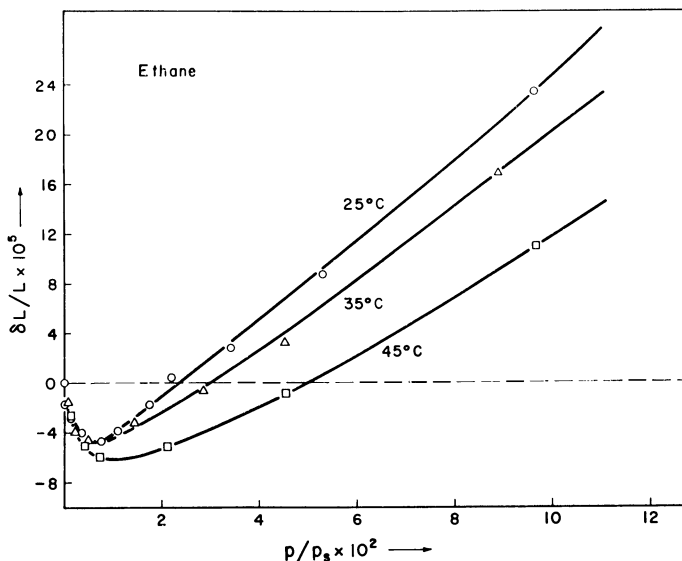


Figure 6. Adsorption-extension data for ethane

Temperature dependence. Elongation as function of p/p_s , where p_s is vapor pressure of ethane at 25° C. Critical temperature 32.1° C.

Let the change in energy of a body be represented by $dE = Tds - \bar{p}dv + \phi dq + f(x)dx + \mu dm$, where $p = \frac{1}{3}(p_x + p_y + p_z)$, p_x, p_y , and p_z being the principal stresses. If these stresses are not equal, dv must grow in a definite manner (constant shape) so that $\int_{v_1}^{v_2} p dv$ shall have a definite value dependent only on the limits. ϕdq are work terms at constant S, v, q, x , and m —i.e., ϕdq measures shear strains, polarization terms, etc. And $f(x)dx$ are work terms against scalar potential fields.

We suppose that the system can be in reversible equilibrium with these external forces and is capable of growth from a suitable source of m , the growth taking place reversibly while the nature and state of the body remain constant. We can write for the increment of energy E associated with this process, where T, \bar{p}, q, x , and μ remain constant during the growth or displacement process,

$$E = TS - \bar{p}v + \mu m$$

and

$$E - TS + \bar{p}v = \mu m = F$$

the Gibbs potential of the increment.

Also,

$$dF = -SdT + v d\bar{p} + \phi dq + f dx + \mu dm$$

Consider two distinct systems to which the following equations apply:

$$dE_1 = TdS_1 - \bar{p}_1 dv_1 + \phi_1 dq_1 + f_1 dx_1 + \mu_1 dm_1$$

$$dE_2 = TdS_2 - \bar{p}_2 dv_2 + \phi_2 dq_2 + f_2 dx_2 + \mu_2 dm_2$$

Let the two systems grow so that the relative volumes, masses, etc., remain constant—i.e., so that $\delta v_1/v_1 = \delta v_2/v_2, \delta m_1/m_1 = \delta m_2/m_2$, etc. We suppose that this can occur without terms of the type $f_1 dx_1, f_2 dx_2$ being involved. Then for the increment of energy

$$E = E_1 + E_2 = T(S_1 + S_2) - \bar{p}_1 v_1 - \bar{p}_2 v_2 + \mu_1 m_1 + \mu_2 m_2$$

and

$$E - T(S_1 + S_2) + \bar{p}_1 v_1 + \bar{p}_2 v_2 = \mu_1 m_1 + \mu_2 m_2$$

Van der Waals (6-12) crystal % E_0^*	Ionic crystal % E_0^*	Dividing Surface
65.5(68.1)	97.50	1st Molecular layer
93.0(96.1)	99.97	2nd Molecular layer
98.3	99.98	3rd Molecular layer
99.4	99.99	4th Molecular layer
...
100	100	∞ th Molecular layer

Figure 7. Van der Waals values of self-potentials at absolute zero

If the two systems together can also be in equilibrium with the hydrostatic pressure, P , during this displacement process, we can also write for both together

$$dE = TdS - Pdv + \mu_1 dm_1 + \mu_2 dm_2$$

where

$$v = v_1 + v_2$$

Hence

$$\bar{p}_1 v_1 + \bar{p}_2 v_2 = P(v_1 + v_2)$$

However, if the two parts to which the subscripts refer exert forces upon one another in addition to those implied by \bar{p}_1 and \bar{p}_2 , we must write

$$dE_1 = TdS_1 - \bar{p}_1 dv_1 + \phi_{12} dq_1 + f_{12} dx_1 + f_{12} \frac{\partial x_{12}}{\partial v_1} dv_1 + \mu_1 dm_1$$

$$dE_2 = TdS_2 - \bar{p}_2 dv_2 + \phi_{21} dq_2 + f_{21} dx_2 + f_{21} \frac{\partial x_{21}}{\partial v_2} dv_2 + \mu_2 dm_2$$

and writing $\pi_1 v_1$ for the integral $\int_0^{v_1} f_{12} \frac{\partial x_{12}}{\partial v_1} dv_1$, etc., we obtain $(\bar{p}_1 - \pi_1) v_1 + (\bar{p}_2 - \pi_2) v_2 = P(v_1 + v_2)$ or $\bar{p}_1 v_1 + \bar{p}_2 v_2 - \omega_{12} = P(v_1 + v_2)$, where ω_{12} is a measure of the interaction potential—i.e., the difference in net displacement work of the two separate systems (1 and 2) and that of the combined system.

If μ_1 and μ_2 refer to the same substance and this substance is in equilibrium throughout the system, so that $\mu_1 = \mu_2$, the above equations would describe, say, a self-gravitating spherical mass of liquid water divided into two arbitrary volumes. The values of \bar{p}_1 and \bar{p}_2 in this case would be the “external” compressive stresses on the surfaces of each of these volumes, not the volumetric means of the principal stresses on the surfaces of the elementary volumes into which each might have been subdivided. If the \bar{p}_i 's be the mean principal stresses on the elementary volumes of the whole of mass fluid mass, we would obtain

$$v(\bar{p}^* - \bar{\pi}^*) = vP = v\bar{p}^* - \omega$$

If the mass were large, P , the pressure at the surface of the spherical mass, might be very low while \bar{p}^* was of a very large magnitude.

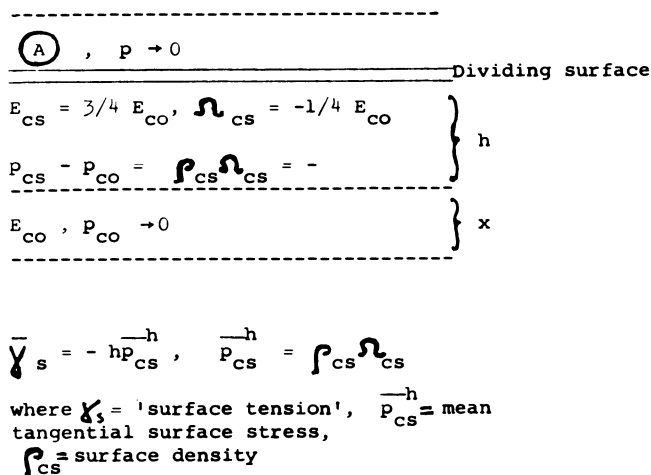


Figure 8. Surface potentials, stresses, etc., for disorganized carbon

Self-Potentials and Adsorption Potentials

If the attractive force of the adsorbent for the gas molecules is relatively strong and "pairwise" additive and varies inversely as the square of the distance between adsorbate and adsorbent molecules, then when the adsorbate density is at all large, ω_{ac} must be large, since both adsorbate and adsorbent will be attracted to their mutual center of "gravity." In this case the pressure acting on the outside surface of the whole system will be less than the pressure of either of the parts—i.e., P may approach zero while both p_a^v and p_c^v are large and positive.

If the attractive force between molecules varies more steeply than an inverse third power, the net attractive force of a semi-infinite solid slab on a single molecule has a finite value. Thus the cumulative effects of distant masses tend to vanish, which is not the case for an inverse square law; in the latter case the number of pairwise interactions increases more rapidly than the effective force per pair diminishes.

If E'_0 be the energy per gram of separating the atoms from the interior of a semi-infinite condensed system at absolute zero and E'_s be the corresponding energy for the surface layer, in general these two quantities must differ. These quantities are commonly called self-potentials (2). As the temperature is increased, the increase in energy will be largely a heat energy and the increased energy of the interior and of the surface will be about the same for substances of very low vapor pressures and compressibilities. Thus at ordinary temperatures there will be a "surface" energy or potential, $\Omega_s = E_s - E_0$, which is approximately equal to $E'_s - E'_0$. Hence, for an equilibrium to exist between the bulk material, the surface, and the vapor, the surface layer must contain other kinds of "potential" which offset the increase in Gibbs potential due to the surface "energy." The most immediately available "potential" is a negative surface stress, assuming the interior stress to be isotropic and that there is relatively little difference between the surface entropy and the bulk entropy, as found by Morrison (3).

Figure 7 shows the values of the self-potentials at absolute zero for a van der Waals (6-12) close-packed crystal and an ionic crystal. The values are due to Benson (4). The two figures in parenthesis are Barrer's (2).

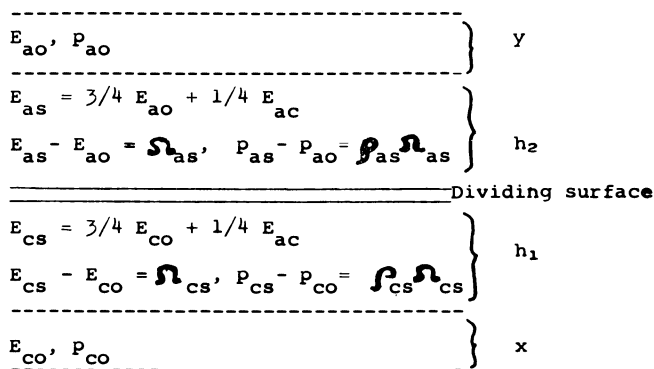


Figure 9. Interaction of carbon surface with gas or liquid

For disorganized carbon we might expect E_s/E_0 to be intermediate between the ionic and van der Waals crystals, perhaps closer to the latter. Thus we might represent the situation approximately as shown in Figure 8.

A molecule of carbon (*A*, Figure 8) near the surface must also experience a force toward the dividing surface, the force varying as an inverse fourth power of its distance from the surface, assuming a 6–12 potential. Thus the solid must “adsorb” its own vapor.

Figure 9 illustrates the interaction of the carbon surface with a gas or liquid.

When $E_{ao} = E_{ac} = 0$ and we suppose the solid enclosed by the dividing surface, the tangential surface forces corresponding to δp_{cs} must be balanced by stresses in the solid beyond the surface region and $v_{co}p_{co} + v_{cs}p_{cs} = v_c p_{co}$; or if $h_1 \ll x$, $v_c(p_c - p_{ao}) = \frac{2}{3} \sigma \gamma = -\frac{2}{3} \sigma h_1 \bar{p}_{cs}$.

When $E_{ao} \ll E_{ac} \ll E_{co}$, $p_{cs} - p_{co}$ will not be changed appreciably by the presence of the gas, but $p_{as} - p_{ao}$ can be large and will be positive. Accordingly the net surface tension will be reduced, both p_{cs} and p_{co} being reduced by very nearly equal quantities. Since the field passing the dividing surface is negligible, the stresses acting on the volume enclosed by the dividing surface must be balanced by stresses within the dividing surface, the interaction will still be essentially mechanical, and $v_c \bar{p}_c + v_a \bar{p}_a = (v_a + v_c) p_{ao}$, as before.

In this case also, if $h_1 + h_2 \ll x$, $v_c \delta p_c = \frac{2}{3} \sigma \delta \gamma$.

If, however, $E_{ac} \approx E_{co}$, there will be large fields operating across the dividing surfaces and if $h_1 \approx x$, a large fraction of the solid will undergo a positive pressure change, in addition to the change in stresses needed to balance the additional tangential forces.

In this case $v_a p_a + v_c p_c > (v_a + v_c) p_{ao}$.

If, however, $h_1 + h_2 \ll x$, we can still write $v_a p_a + v_c p_c = (v_a + v_c) p_{ao}$ approximately, and again $v_c \delta p_c = \frac{2}{3} \sigma \delta \gamma$. When $E_{ac} \approx E_{co}$ the heat of wetting or of immersion will be about 10^3 cal. per gram for carbons of surface areas of 10^3 sq. meters per gram. (The heat of combustion of such a carbon would be about 10 kcal. higher than that of graphite.) This is, of course, very much greater than normal heats of wetting.

Evidently the various effects are strongly dependent on the detailed surface interactions. Figure 10 illustrates a highly simplified surface system that is

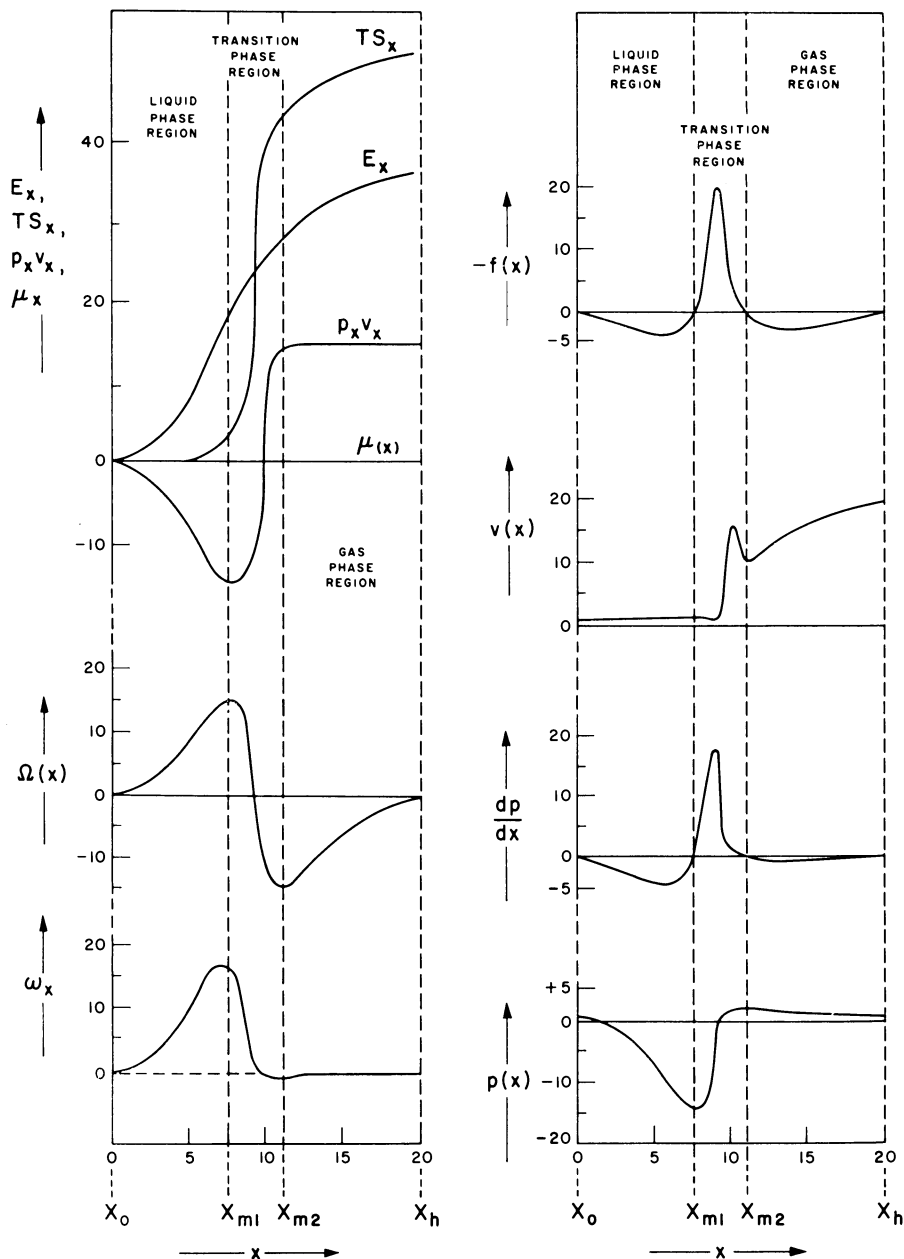


Figure 10. Diagrammatic representation of thermodynamic relations within an ideal liquid-vapor interfacial region

$$\mu_x = E_x - TS_x + p_x v_x, \text{ per gram}$$

$$\mu_x - \mu_{x0} = \int_{x_0, p_{x0}}^{x, p_x} (v_x dp_x + f_x dx) = 0 \quad \int_{x_0, p_{x0}}^{x, p_x} v_x dp_x = \int_{x_0, p_{x0}}^{x, p_x} f_x dx = -\Omega(x)$$

$$\rho_x \Omega_x = \omega_x = \text{potential per unit volume at } x$$

$$\text{Total surface potential} = h\sigma\bar{\omega} = h\sigma \int_{x_0}^x \omega_x dx$$

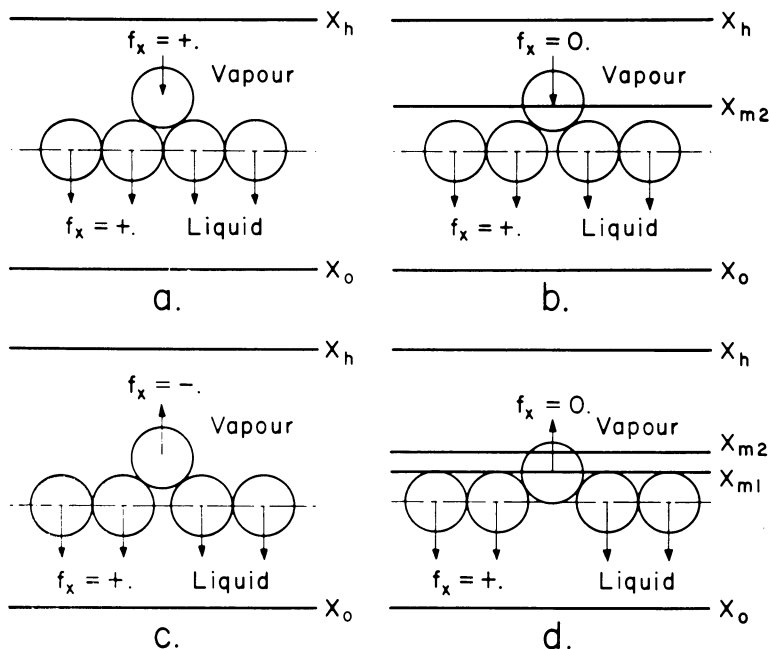


Figure 11. Dividing surface or interfacial transition region $x_{m2} - x_{m1} < \text{molecular radius}, r$

Surface region. $x_h - x_0 = 4 \text{ to } 20 r$

Liquid or condensed region extends from below x_0 to just above X_{m2}

Gas region, from just below x_{m2} to above x_h

thermodynamically consistent with a positive surface tension and might represent a liquid-gas interface. It is thermodynamically necessary that both attractive and repulsive forces exist in the surface region.

The transition region might arise from effects such as those illustrated in Figure 11, while Figure 12 illustrates possible effects of exposing the surface depicted in Figure 10 to a second gas.

Conclusions

When a definite more or less fixed dividing surface exists between the adsorbent and an adsorbable substance, the reaction will resemble a mechanical interaction—i.e., $\omega_{ac} \rightarrow 0$ and $v_a \bar{p}_a + v_c \bar{p}_c = (v_a + v_c) P$ —under the following conditions.

When the total volume of the solid is large compared with the volume of the surface region, regardless of the magnitude of the adsorption potential, E_{ac} .

When the surface coverage, ρ_{as} is very small.

When the adsorption potential, E_{ac} , is low compared with the adsorbent self-potential, E_{cs} , as is usually the case for adsorption on active carbon.

The adsorption reaction will probably not resemble a mechanical system—i.e., $\omega_{ac} \neq 0$ —when the BET surface area is very large—i.e., when the volume of surface region is comparable with the total solid volume and the net adsorption potential, $\rho_{as} E_{ac}$, is at all comparable with the heat of evaporation of the solid itself or with the net solid surface potential, $\rho_{cs} \Omega_{cs}$.

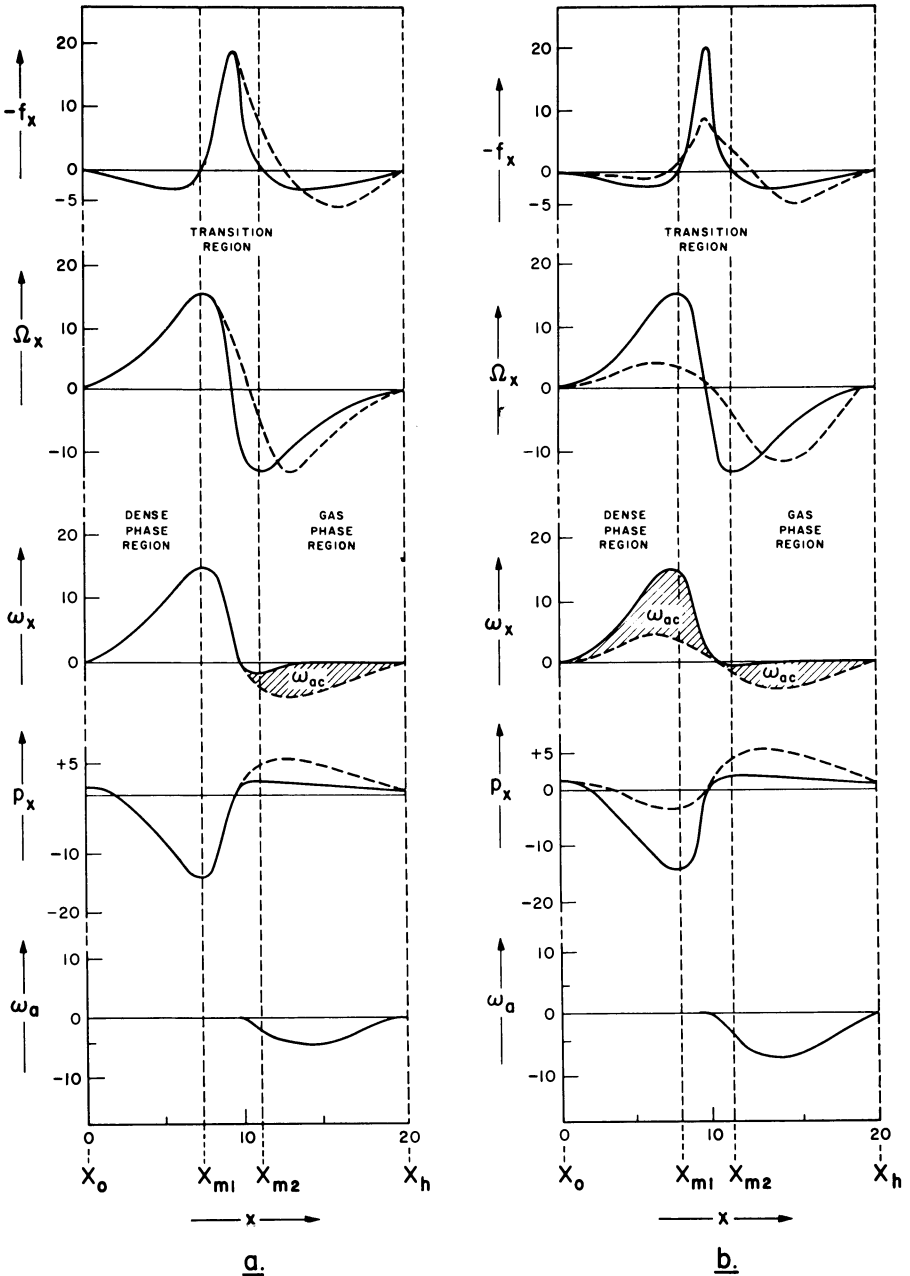


Figure 12. Interaction of adsorbable gas with ideal interface of Figure 10

- a. $\omega_{ac} \rightarrow 0$
- b. $\omega_{ac} \neq 0$

In general, the adsorption reaction will not resemble a mechanical reaction if the dividing surface largely ceases to exist because of solution of the gas throughout the solid, material of the solid dissolving directly or indirectly in the adsorbate,

the formation of a large number of bonds between the adsorbent and adsorbate, the bonds involving electron transfer across the surface, or the formation of entirely new dividing surfaces which are more or less separate and distinct from the original adsorbent. [Mrozowski (17) has shown that free valencies are largely absent from active carbons heated to temperature above 1000° C. Thus we can expect that the "dividing surface" exists for all ordinary physical adsorption on H-type active carbons which are reasonably pure carbons, such as "saran carbons."]

Evidently the majority of readily reversible physical adsorption reactions can be described thermodynamically in terms of the accompanying mechanical effect and we can write

$$\bar{v}_a \bar{p}_a^* + \Phi_a + \bar{v}_c \bar{p}_c^* + \Phi_c = (\bar{v}_a + \bar{v}_c)P$$

and

$$v_a \bar{p}_a^* + v_c \bar{p}_c^* = (v_a + v_c)P$$

where

$$\bar{p}_a^* = \int_0^P \frac{\bar{p}_a}{\rho_a} dp_a - \Phi_a' = aP$$

When the solid is comparatively incompressible, we can write

$$\frac{\delta v_a}{v_a} - \frac{\delta v_c}{v_c} = \frac{2(\Phi_a + \Phi_c)}{(P - \bar{p}_c^*)v_c}$$

Since $\delta v_a/v_a$ and $\delta v_c/v_c$ are small quantities (much less than unity), their differences are much less than unity. Accordingly when Φ_c is comparable in magnitude to $(P - \bar{p}_c^*)v_c$, Φ_a and Φ_c must be of nearly equal magnitudes but of opposite signs. From the elastic properties of carbons we can place an upper limit of about 10 cal. per mole of carbon on reversible values of Φ_c arising wholly from elastic mechanical strains. In many cases of physical adsorption of vapors near saturation integral δF_c values of about 200 cal. per mole of carbon are observed. In such cases δF_c values must be largely controlled by $v_c \delta p_c$ terms, but at lower surface coverages Φ_c terms may be relatively much larger. Values of Φ_a and Φ_c can be estimated from observed adsorption extension and isotherm data, together with differential and integral heats of adsorption and heats of wetting.

For one of our carbons we estimate that in some cases Φ_a and Φ_c are of the order of 20% of the adsorption potential, assuming a Poisson ratio of $1/3$. In these cases one may regard the adsorption potential as arising from a release of a compressive stress potential (80%) and a shear strain potential (20%).

The Gibbs adsorption equation should be valid when the total solid volume is large compared to the total solid volume and terms of the type Φ_a and Φ_c can be neglected.

The equation

$$\delta v/v = -A\delta \bar{p}_c^t(1 - B\delta \bar{p}_c^t)$$

$$\delta \bar{p}_c^t = \left[1 + f(p)K \frac{v_a}{v_c} (1 - a) \right] \delta P$$

may be regarded as reasonably valid for physical adsorption on "high temperature" carbons. The values of $f(p)$, K_s , etc., will be strongly dependent on pore-size distribution, surface potentials, and their correlations.

Acknowledgment

The author is very much indebted to G. C. Benson for carrying out the computer summations and calculations leading to the self-potentials given in Figure 7.

Literature Cited

- (1) Bangham, D. H., Razouk, R. I., *Proc. Roy. Soc. (London)* **A166**, 572 (1938).
- (2) Barrer, R. M., *Trans. Faraday Soc.* **50**, 1074 (1954).
- (3) Barron, T. K. H., Berg, W. T., Morrison, J. A., *Proc. Roy. Soc. (London)* **A250**, 70 (1959).
- (4) Benson, G. C., National Research Council, Ottawa, Canada, private communication.
- (5) Channen, E. W., McIntosh, R. L., *Can. J. Chem.* **33**, 172 (1955).
- (6) Dacey, J. R., Proceedings of Fourth Conference on Carbon, Pergamon Press, London and New York, 1960.
- (7) Dacey, J. R., Royal Military College, Kingston, Ontario, Canada, private communication.
- (8) Flood, E. A., Lakhanpal, M. L., Proceedings of Second International Congress on Surface Activity, Butterworths, London, 1957.
- (9) Gibbs, J. W., "The Collected Works of J. Willard Gibbs," Vol. I, pp. 230, 234, etc., Yale University Press, New Haven, Conn., 1957.
- (10) Guggenheim, E. A., "Statistical Thermodynamics," R. H. Fowler, E. A. Guggenheim, eds., pp. 422ff, Cambridge University Press, London, 1949.
- (11) Haines, R. S., McIntosh, R. L., *J. Chem. Phys.* **15**, 28 (1947).
- (12) Huber, M. E., Flood, E. A., Heyding, R. D., *Can. J. Chem.* **34**, 1284 (1956).
- (13) Lakhanpal, M. L., Flood, E. A., *Ibid.*, **35**, 887 (1957).
- (14) Love, A. E. H., "Treatise on the Mathematical Theory of Elasticity," 4th ed., pp. 175-6, Dover Publications, New York, 1944.
- (15) McIntosh, R. L., Queen's University, Kingston, Ontario, Canada, private communication.
- (16) Maxwell, J. C., "Equilibrium of Elastic Solids," in "Scientific Papers of James Clark Maxwell," Vol. I, W. D. Niven, ed., Librairie Scientifique, J. Herman, Paris, 1927.
- (17) Mrozowski, S., Andrews, J. F., Proceedings of Fourth Conference on Carbon, Pergamon Press, London and New York, 1960.
- (18) Polanyi, M., "Discussion of the Potential Theory of Adsorption" in "Adsorption of Gases and Vapors," by Stephen Brunauer, Princeton University Press, Princeton, N. J., 1947.
- (19) Wiig, W. A., Juhola, A. J., *J. Am. Chem. Soc.* **71**, 561 (1949).
- (20) Yates, D. J. C., *Advances in Catalysis* **12**, 265 (1960).

RECEIVED May 9, 1961.

The Adsorption of Gases on Ion Exchanged Mica

III. The Adsorption of Krypton

GEORGE L. GAINES, Jr.

General Electric Research Laboratory, Schenectady, N. Y.

The adsorption of krypton by ground muscovite mica bearing potassium, barium, or cesium as exchangeable ions has been studied at 77° and 90° K. Coverages in the first monolayer and slightly beyond were studied. The results are compared with previous measurements of argon adsorption. Whereas argon adsorption was found to be markedly influenced by the nature of the exchangeable ion, this controlled alteration of the mica surface has little effect on the adsorption of krypton. The adsorption of the larger krypton atom is also less affected by the geometric factors which appear to govern argon uptake in the first monolayer. The thermodynamic functions for krypton adsorption do not show the variation with coverage found for argon on potassium and barium mica. It is suggested that, whereas argon is first adsorbed in a substantially localized manner which becomes more mobile as the first monolayer is completed, the adsorbed krypton film behaves as a two-dimensional liquid over the range $0.2 < \theta < 0.8$.

We have previously reported (3, 5) studies of the adsorption of argon at 77° and 90° K on muscovite mica which had been treated to replace the exchangeable surface potassium ions with other cations. The adsorption isotherms and thermodynamic functions evaluated from them showed significant differences among the various ion exchanged forms of mica. We have now obtained data for the adsorption of krypton on these substrates, and wish to discuss the differences in the behavior of the argon-mica and krypton-mica systems.

Experimental

The mica samples were portions of the same 100- to 200-mesh potassium, barium, and cesium muscovite used in our previous work. They had been stored

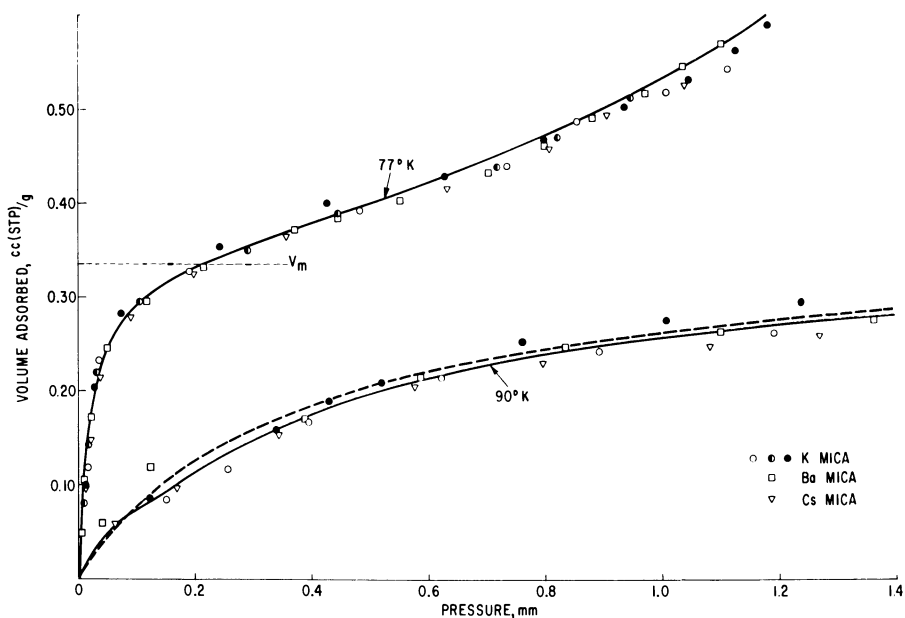


Figure 1. Adsorption of krypton on 100- to 200-mesh muscovite

under normal atmospheric conditions at room temperature in screw-capped bottles in the intervening two-year period. Adsorption measurements were carried out in a conventional glass volumetric system equipped with stopcocks and a thermistor gage; procedures were the same as previously described, but no very low pressure measurements were made. The thermistor gage was calibrated against a McLeod gage for the range 0.003 to 1.7 mm., and the precision of pressure measurement was about $\pm 3\%$, except at the lowest pressures, where the error could amount to ± 0.5 micron. Since dose pressures were limited by the gage response at higher pressures, the volume measurements at equilibrium pressures above 1.0 mm. are subject to considerable uncertainty.

All calculations were performed in the same manner as before, and saturation pressures used were those given in the previous papers (3, 5).

Results and Discussion

Isotherms and BET Surface Area. The adsorption isotherms on the various mica samples were found to be experimentally indistinguishable at both 77° and 90° K. They are shown in Figure 1, with points from replicate experiments with potassium mica (open, half-solid, and solid circles) showing scatter greater than any differences between the three kinds of mica over most of the range covered. At low coverage (up to 0.15 cc. adsorbed per gram) the barium mica 90° isotherm may differ slightly from those for potassium and cesium micas.

A BET plot of all the data at 77° is linear over a wide range, and least-squares analysis of all the experimental values in the monolayer region ($0.025 < p/p_0 < 0.20$) yields values of $v_m = 0.336$ cc. per gram and $c = 131$. While the c value is very close to that previously observed for krypton adsorption on this mica (5), the surface area is appreciably smaller. This decrease in v_m has occurred progressively with time for all our ground mica samples, and at present we have no

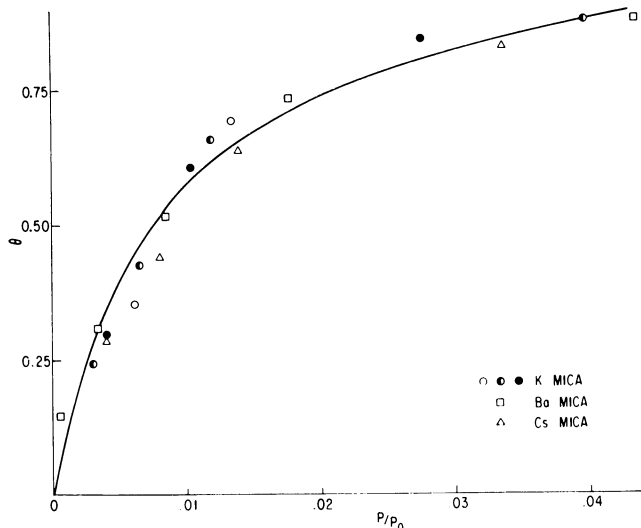


Figure 2. Adsorption of krypton at 77.4° K on 100- to 200-mesh muscovite

$$v_m = 0.336 \text{ cc. (STP) per gram}$$

— BET equation, $c = 130$

information on the nature of the change. It is possible that some particles have become joined through rebonding of cleavage planes. Krypton isotherms plotted in terms of $\theta = v/v_m$ are superimposable even when the measurements were made several years apart and the v_m values differ by 30%. We conclude, therefore, that the process producing the change in surface area has little effect on the nature or energetics of the surface remaining exposed. If this were not so, of course, the comparison which we wish to make between the present krypton adsorption measurements and the previous work with argon might not be valid.

As was previously noted (5), the data for krypton at 77° follow the BET isotherm closely down to low coverage. At 90°, our data are not sufficient at higher coverages to allow evaluation of meaningful BET parameters, but the general shape of the isotherm is consistent with a plot of the BET equation using reasonable constants. Thus, in Figure 1, the curve drawn through the 77° points is the BET isotherm with $c = 130$ and $v_m = 0.336$ cc. per gram, as evaluated from the surface area plots, and $p_o = 2.63$ mm. (Figure 2 depicts the first part of the 77° isotherm on an expanded scale.) The dashed line in the 90° plot represents the BET isotherm with $v_m = 0.336$, $c = 80$, and $p_o = 27.1$ mm. It is obvious that this curve represents the experimental observations very nearly as well as does the solid line, which has been used for evaluating the thermodynamic functions.

Heat and Entropy Functions. Both differential and integral heats and entropies of adsorption were evaluated from the data for argon adsorption on muscovite (3). The variations in these functions with coverage for the potassium and barium muscovite were discussed in terms of localized adsorption on the various kinds of geometrical sites on the mica surface. On the cesium mica, however, the heat of adsorption of argon was higher and more uniform than on the potassium and barium micas, and the entropy functions showed a monotonic decrease with coverage.

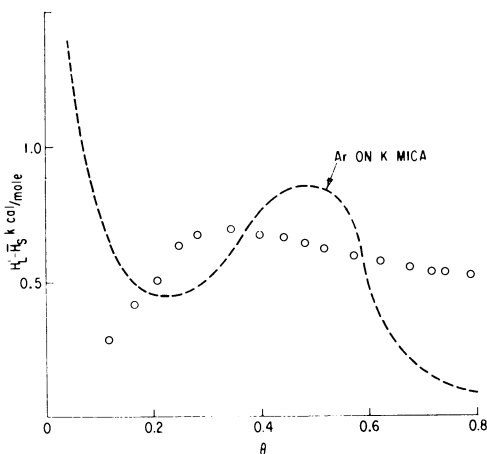


Figure 3. Net isosteric heat of adsorption of krypton on 100- to 200-mesh muscovite

Evaluated from solid lines in Figure 1

- - - Corresponding values for argon on potassium muscovite (3)

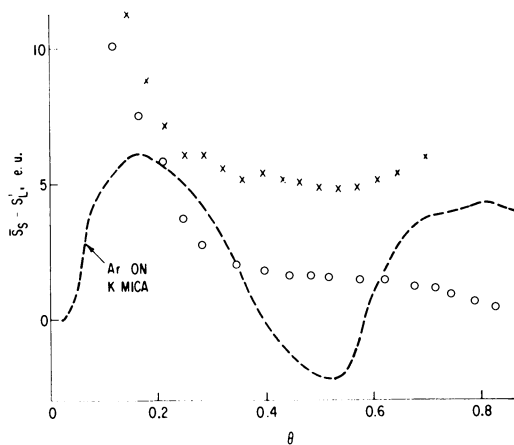


Figure 4. Net differential entropy of adsorption of krypton on ground muscovite

○ 100- to 200-mesh muscovite, from solid lines in Figure 1

× Corrected data for 60- to 80-mesh muscovite

- - - Corresponding values for argon on potassium muscovite (3)

From our krypton adsorption data, we must conclude that the adsorption energetics are the same within experimental error on all three mica samples for the range $0.2 < \theta < 0.8$ (with the possible exception of the barium muscovite up to $\theta \sim 0.4$, as noted above). We have calculated differential heats and entropies from the "average" isotherms (solid lines, Figure 1). These results are shown in Figures 3 and 4, along with some of the corresponding differential quantities

evaluated from the argon adsorption data. In both cases, θ values are estimated from the 77° isotherms. In the case of the krypton data, experimental uncertainty in the isosteric heat amounts to about 200 cal. at $\theta = 0.5$, and ranges upward to about 400 cal. at the highest and lowest coverages. The corresponding uncertainties in the entropy are about 2 and 4 e.u., respectively. [An error was made in the calculation of the differential entropy data for krypton on 60- to 80-mesh muscovite, shown in Figure 9 of paper II of this series (3). The correct data are shown by crosses in Figure 4.]

It is apparent that the thermodynamic functions for krypton show less variation with coverage than did those for argon on potassium (and barium) muscovite. They resemble the results for argon adsorption on cesium mica in this respect. Our suggestion of geometrical specificity in the argon-potassium mica and argon-barium mica systems is therefore supported by the present data. Any attempt to interpret the difference in absolute magnitude of the heats and entropies for the argon-cesium mica system as compared to the krypton results must allow for the uncertainty in the selection of the reference states for these two adsorbates at the temperatures used (3).

The similarity in the adsorption behavior of krypton on the three kinds of mica surfaces suggests that the adsorption here is primarily due to dispersion forces, with very little contribution from ion-induced dipole forces. The results of Barrer and Stuart (1) for the adsorption of argon on various ion-exchanged forms of faujasite are similar. They found that while calcium, strontium, and lithium faujasite—i.e., the materials containing cations with greater polarizing power—did show heat effects correlatable with ion-induced dipole interactions, no such effects were observed with sodium, potassium, or barium zeolites. With the latter materials, they also concluded that the adsorbed argon possessed appreciable mobility.

We may assume that both argon and krypton adsorbed on mica are essentially two-dimensional liquids at the completion of the first monolayer (2, 4). The rise in the entropy functions for argon adsorption on potassium and barium mica as the monolayer point is approached may then reflect the transition from substantially localized adsorption at lower coverages to a mobile film. No such phenomenon is observed with krypton, suggesting that there is no change in the behavior of the adsorbed phase during formation of most of the first monolayer.

A detailed investigation of these effects will require adsorption measurements of higher precision and over a much wider range of surface coverage.

Acknowledgment

I am indebted to C. P. Rutkowski and N. L. Keary for experimental assistance.

Literature Cited

- (1) Barrer, R. M., Stuart, W. I., *Proc. Roy. Soc. (London)* **A249**, 464, 484 (1959).
- (2) Cannon, P., Gaines, G. L., Jr., *Nature* **190**, 340 (1961).
- (3) Gaines, G. L., Jr., *J. Phys. Chem.* **62**, 1526 (1958).
- (4) Gaines, G. L., Jr., Cannon, P., *Ibid.*, **64**, 997 (1960).
- (5) Gaines, G. L., Jr., Rutkowski, C. P., *Ibid.*, **62**, 1521 (1958).

RECEIVED May 9, 1961.

A General Theory of Monolayer Physical Adsorption

WILLIAM A. STEELE

Department of Chemistry, The Pennsylvania State University, University Park, Pa.

A general theoretical approach to monolayer physical adsorption is discussed. In this theory, the isotherms and heats of adsorption at given μ, T are given as functions of the interaction energies of the adsorbed atoms with the solid and with each other. The general equations reduce to localized and mobile adsorption when the potential variations over the surface are either very large or very small. Intermediate cases are also included. Gas atom-solid interaction energy functions are computed from the known pair interaction potentials for several rare gas systems, and it is shown that a considerable amount of information can be obtained about the adsorption properties of such systems from these potential functions.

The relationship between the properties of a physical adsorption system and the energies of the adsorbed particles with each other and with the solid has been the subject of numerous investigations. In particular, reasonably good agreement has been obtained between theoretically calculated energies of adsorption and experimental heats at very low coverages on reasonably uniform surfaces (16). Halsey *et al.* (7, 22) have interpreted measurements of the high temperature interaction of dilute gases with solids as gas imperfection caused by the potential energy of gas atoms in the vicinity of the gas-solid interface. More recently, the formal equations necessary to express the properties of an adsorption system at any T, μ as functions of the interaction energies have been given (12, 23). In these treatments, it is assumed that the properties of the adsorbent surface remain essentially unperturbed by the presence of the adsorbed gas. This approximation allows one to identify the adsorption problem with that of a fluid in the external potential field which exists near the surface of the adsorbent. This approach was then used in a treatment of the specific problem of monolayer adsorption (11, 24) and it was shown that a general theory of monolayer adsorption could be obtained in which many of the assumptions made in previous theories were no longer necessary. In particular, the general theory contains both localized and mobile adsorption as special cases. In this paper, we bring together some of the results of the previous papers which are pertinent to the monolayer adsorption problem. The application of the theory to several simple adsorbate-adsorbent pairs is discussed,

and it is shown that one can obtain a great deal of information about the nature of the gas-solid potential energy function from an analysis of the experimental data for suitable systems.

Theoretical

Most experimental investigations consist in measurements of the isotherms, the heats of adsorption, or both. Therefore, we shall direct our attention to these two properties. From the point of view of a statistical mechanical calculation, the most convenient definition of the amount adsorbed, N_a , is:

$$N_a = \int_v [\rho^{(1)}(\mathbf{r}_1) - \rho_0] d\mathbf{r}_1 \quad (2.1)$$

where ρ_0 is the gas density in the adsorption volume, v , in the absence of gas-surface interactions, and $\rho^{(1)}(\mathbf{r}_1)$ is the density in the presence of the interactions. $\rho^{(1)}(\mathbf{r}_1)$ is, of course, a function of the position of atom 1 (denoted by \mathbf{r}_1), and is expected to be large compared to ρ_0 when atom 1 is in the vicinity of the surface, and to decrease rapidly to ρ_0 as the distance from the surface increases. Since adsorption systems are generally at known T , μ (the chemical potential of the adsorbed gas is obtained from the adsorption pressure), it is clear that it is most convenient to use the grand canonical ensemble in computing the properties of the system. In general, $\rho^{(1)}(\mathbf{r}_1)$ is defined as the probability that a molecule will be found at \mathbf{r}_1 , irrespective of the positions of the other molecules. Therefore, the expression for $\rho^{(1)}(\mathbf{r}_1)$ in a canonical ensemble of N particles is given by a Boltzmann factor which includes the interaction energies of all N atoms with each other and with the surface, integrated over all possible positions of all atoms except atom 1, and divided by the proper normalizing factor. In the grand canonical ensemble, N is unrestricted, and, therefore, one has a sum of Boltzmann factors, one for each possible value of N . When the proper normalizing and weighting factors are included, the classical statistical mechanical equation for $\rho^{(1)}(\mathbf{r}_1)$ is written:

$$\rho^{(1)}(\mathbf{r}_1) = \frac{1}{\Xi} \sum_{N \geq 1} \frac{z^N}{(N-1)!} \int \dots \int_v \exp[-U_N(\mathbf{r}_1, \dots, \mathbf{r}_N)/kT] d\mathbf{r}_2 \dots d\mathbf{r}_N \quad (2.2)$$

$$z = \exp(\mu/kT)/\Lambda^3 \quad (2.3)$$

$$U_N(\mathbf{r}_1, \dots, \mathbf{r}_N) = \sum_{i=1}^N u_s(\mathbf{r}_i) + \sum_{1 \leq i < j \leq N} u(r_{ij}) \quad (2.4)$$

$$\Xi = \sum_{N \geq 0} \frac{z^N}{N!} Z_N \quad (2.5)$$

$$Z_N = \int \dots \int_v \exp[-U_N(\mathbf{r}_1, \dots, \mathbf{r}_N)/kT] d\mathbf{r}_1 \dots d\mathbf{r}_N \quad (2.6)$$

where $u_s(\mathbf{r}_1)$ is the potential energy of interaction of atom 1 at position \mathbf{r}_1 with the solid, and $u(r_{ij})$ is the mutual interaction of atoms i and j separated by a distance r_{ij} .

Methods of computing $\rho^{(1)}(\mathbf{r}_1)$ from Equations 2.2 to 2.6 have been discussed (23); however, in the case of monolayer adsorption, it is often more convenient to deal directly with the grand partition function of the system. When Equation 2.2 is substituted in Equation 2.1 and the integrations are carried out, the amount adsorbed is given by

$$N_a = \frac{1}{\Xi} \sum_{N \geq 1} \frac{z^N}{(N-1)!} Z_N - N_o \tag{2.7}$$

where N_o is the total number of atoms which would be held in the adsorption container if there were no gas-surface interactions. It is now easy to show that the total number of gas atoms in the container ($N_a + N_o$) can be obtained directly from the grand partition function in the usual manner:

$$N_a + N_o = \frac{z}{\Xi} \left(\frac{\partial \Xi}{\partial z} \right)_{T,V} \tag{2.8}$$

However, the expression given in Equation 2.5 for the grand partition function can be written in a form which is better adapted to adsorption calculations. This is accomplished by dividing the volume of integration into two parts: a relatively small volume in the immediate vicinity of the adsorbent surface (denoted by V_s), and the remainder of the gas space volume (denoted by V_g). The dividing line is chosen to be at the point where the gas-surface interactions become negligibly small. [In most monolayer problems, the exact location of this boundary is unimportant, since all the adsorbed atoms will be found in a small region of maximum attractive energy; however, at sufficiently high temperatures, one must treat this problem somewhat more carefully (22).] For convenience, it will be assumed that the gas in the volume V_g is perfect. Then one can write

$$Z_N = Z_{sN} + NV_g Z_{sN-1} + \frac{N(N-1)}{2} V_g^2 Z_{sN-2} + \dots + V_g^N \tag{2.9}$$

where

$$Z_{sN} = \int \dots \int_{V_s} \exp [-U_N(\mathbf{r}_1, \dots, \mathbf{r}_N)/kT] d\mathbf{r}_1 \dots d\mathbf{r}_N \tag{2.10}$$

When Equation 2.9 is substituted in 2.5, and terms are collected, it emerges that

$$\Xi = \sum_{N \geq 0} \frac{z^N}{N!} Z_N \sum_{N \geq 0} \frac{z^N}{N!} V_g^N \tag{2.11}$$

z is the absolute activity of the adsorption system, and is equal to the absolute activity of the gas in equilibrium with the system. As is usual in treatments of ideal gases, we set $z = p/kT$ (10). Then the second sum in Equation 2.11 is just the grand partition function for an ideal gas in volume V_g . We define

$$\Xi^* = \sum_{N \geq 0} \frac{z^N}{N!} Z_{sN} \tag{2.12}$$

It is now easy to show that

$$N_a = z(\partial \ln \Xi^*/\partial z)_{T,V} \tag{2.13}$$

where it has been assumed that $V_g \simeq v$. The energy of the adsorbed phase E_a can also be obtained from the grand partition function in the usual manner:

$$E_a = kT^2(\partial \ln \Xi^*/\partial T)_{V,\mu} + N_a\mu \tag{2.14}$$

$$= kT^2(\partial \ln \Xi^*/\partial T)_{V,z} + E_{kinetic} \tag{2.15}$$

Up to this point, the theory has been presented in a form suitable only for adsorption systems which can be treated by classical statistical mechanics. When the quantization of the motion of the atoms is important, one must replace the Boltzmann factors in the integrals for Z_N by the appropriate Slater sums. After integrating over the coordinates, one obtains

$$(Z_{sN})_{\text{quantum}} = \Lambda^{-3N} \sum_{jN} \exp[-\epsilon(j_N)/kT] \quad (2.16)$$

$$\Lambda = (h^2/2\pi mkT)^{1/2} \quad (2.17)$$

$\epsilon(j_N)$ is the j th eigen value of the energy of a collection of N atoms in the adsorption volume V_s .

Equation 2.12 is in the form of the grand partition function for an imperfect gas, and the adsorption isotherm can be obtained by the usual methods of imperfect gas theory (10):

$$N_a = Z_{s1}(p/kT) + (Z_{s2} - Z_{s1}^2)(p/kT)^2 + \dots \quad (2.18)$$

If the surface of the adsorbent is homogeneous in the sense that it is made of N_s elements of area A_s , all of which are identical, Equation 2.18 can be put in a convenient form for the analysis of experimental data by making the substitutions:

$$kT/p_o = Z_{s1}/N_s = \int_{z_s} \int_{A_s} \exp[-u_s(\mathbf{r}_1)/kT] d\mathbf{r}_1 \quad (2.19)$$

$$\beta = N_s - Z_{s2}N_s/Z_{s1}^2$$

$$-\beta = \frac{\int_{z_s} \int_{A_s} \int_{z_s} \int_{A_s} f_{12} \exp\{-[u_s(\mathbf{r}_1) + u_s(\mathbf{r}_2)]/kT\} d\mathbf{r}_1 d\mathbf{r}_2}{\int_{z_s} \int_{A_s} \int_{z_s} \int_{A_s} \exp\{-[u_s(\mathbf{r}_1) + u_s(\mathbf{r}_2)]/kT\} d\mathbf{r}_1 d\mathbf{r}_2} \quad (2.20)$$

$$f_{12} = \exp[-u(r_{12})/kT] - 1$$

The isotherm equation becomes

$$\Theta = N_a/N_s = (p/p_o)[1 - \beta(p/p_o) + \dots] \quad (2.21)$$

At small p/p_o , higher terms can be omitted and Equation 2.21 can be written in a form which is particularly useful in the comparison of experiment with theory:

$$N_a/N_s = (p/p_o)/[1 + \beta(p/p_o)] \quad (2.22)$$

If N_a/p is plotted as a function of N_a , the slope at small N_a gives $-\beta/p_o$, and the intercept gives N_s/p_o . If an independent estimate of N_s is available—from multi-layer data, for instance—one can obtain both β and p_o .

The partial molar heat of adsorption can be derived either from Equation 2.15 or from the well known relation

$$q_{st} = R[\partial \ln p/\partial(1/T)]_{\Theta} \quad (2.23)$$

In either case, one obtains

$$q_{st} = R[\partial \ln p_o/\partial(1/T)] + [R\Theta/(1 - \beta\Theta)][\partial\beta/\partial(1/T)] + \dots \quad (2.24)$$

Equation 2.24 predicts that, unless β is constant, q_{st} will change with coverage even in systems which are topographically uniform—i.e., no imperfections in the lattice structure of the surface.

Calculation of Parameters

To carry out a complete and unambiguous computation of the parameters p_o and β , a detailed knowledge of the gas-surface potential function is necessary, as well as the gas-gas potential function. The computation of the gas-surface potential function for all possible positions of the gas atom relative to the surface

is extremely difficult, and it is much more likely that experimental results will be used to obtain information about this potential, than the converse. It is possible to simplify this process if one can approximate the gas-surface potential interaction as a relatively simple function of the position coordinates of the gas atom. This procedure is feasible only if it is assumed that monolayer adsorption is adsorption under conditions where all the adsorbed atoms are at distances from the surface which are very nearly equal to the distance corresponding to the minimum potential energy. This distance is denoted by z_m , and the gas-solid interaction energy at that point by ϵ_m . Also, let τ be a two-dimensional vector which is parallel to the plane of the adsorbent surface. In general, both z_m and ϵ_m will vary with τ (measured relative to some convenient origin). We define $\epsilon_\tau(\tau_i)$ to be the variation in ϵ_m due to changes in τ_i , $\epsilon_m(0)$ to be the potential energy at $\tau = 0$ and $z = z_m$, and $\epsilon_z(z - z_m)$ to be the change in the interaction energy as the z coordinate of the atom is changed from z_m . Then the gas-surface potential function in the neighborhood of the minimum can be written as

$$u_s(\mathbf{r}_i) = \epsilon_m(0) + \epsilon_\tau(\tau_i) + \epsilon_z(z - z_m) \quad (3.1)$$

where it has been assumed that ϵ_z has no appreciable dependence upon τ .

Equation 2.19 for p_o can now be written

$$1/p_o = (1/kT) \exp[-\epsilon_m(0)/kT] \int_{z_s} \exp[-\epsilon_z(z - z_m)/kT] dz \int_{A_s} \exp[-\epsilon_\tau(\tau_i)/kT] d\tau_i \quad (3.2)$$

In many systems, the variation of ϵ_z with z is sufficiently rapid that one cannot successfully use the classical integral with respect to z which appears in Equation 3.2; if this degree of freedom is considered to be quantized, the equation for p_o becomes

$$1/p_o = (\Delta kT)^{-1} \exp[-\epsilon_m(0)/kT] \sum_n \exp[-\epsilon_z(n)/kT] \int_{A_s} \exp[-\epsilon_\tau(\tau_i)/kT] d\tau_i \quad (3.3)$$

where $\epsilon_z(n)$ is the n th energy level for motion in the z direction. It is generally most convenient to choose $\tau = 0$ to be the point of maximum attractive energy; in this case, ϵ_τ will always be greater than or equal to zero, and $\tau = 0$ will correspond to the central point of an adsorption site.

The assumption that all atoms are at or very near to $z = z_m$ allows one to simplify the expression for β . The integrations over z (or sums over quantum states) in the numerator and denominator of Equation 2.20 are identical in this case, and cancel out. The resulting equation for β involves only the τ variable:

$$\beta = \frac{- \int_{A_s} \int_{A_s} f_{12} \exp\{-[\epsilon_\tau(\tau_1) + \epsilon_\tau(\tau_2)]/kT\} d\tau_1 d\tau_2}{\int_{A_s} \int_{A_s} \exp\{-[\epsilon_\tau(\tau_1) + \epsilon_\tau(\tau_2)]/kT\} d\tau_1 d\tau_2} \quad (3.4)$$

To progress further, the form of ϵ_τ as a function of τ must be specified. In previous work, it has often been assumed that ϵ_τ could be represented either as a sinusoidal or as a harmonic function of the two-dimensional position coordinates (8). However, direct calculations (24) of the potential energy of an atom interacting with the 100 face of a simple cubic solid showed that the best simple representation of ϵ_τ was as a linear function of the displacement from

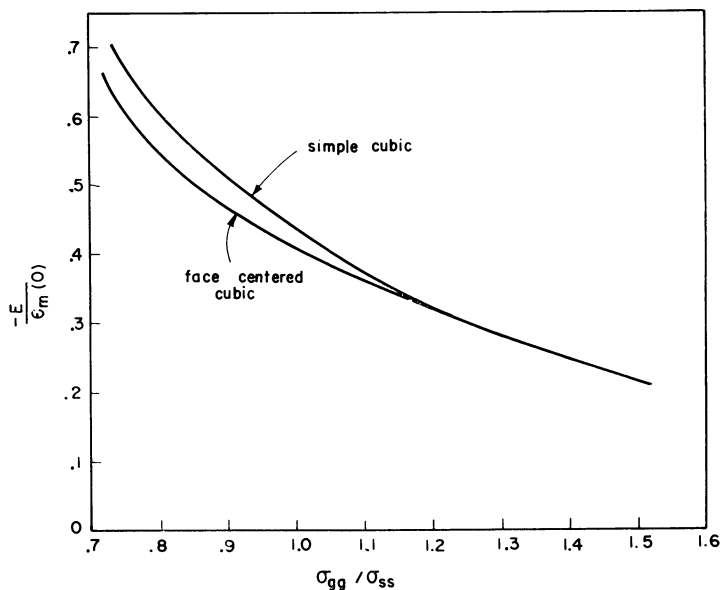


Figure 1. The fractional change in the minimum interaction energy as an adsorbed atom moves from a site center to the mid-point of a site edge is plotted against the ratio of σ_{gg} , the atomic diameter of an adsorbed atom, to σ_{ss} , the diameter of an atom of the solid. The fractional change in energy, $-E/\epsilon_m(0)$, was obtained by linear extrapolation of the theoretically computed change in ϵ_r near the site center

The two curves shown are for an atom over the 100 face of a simple cubic solid, and over the 100 face of a face-centered cubic solid

the site center [the site centers ($r = 0$) for a surface such as this occur at points equidistant from four surface atoms]. This potential was computed by assuming that the total interaction was equal to a sum of pairwise interactions between the gas atom and the atoms of the solid. The pair interactions were calculated from a Lennard-Jones potential function and the sums were carried out on an IBM 650 computer. Since extensive tabulations of these functions have been published (24), we merely point out here that the data show that the angular dependence of ϵ_r for such a lattice is reasonably small near the site center. In this region, ϵ_r can thus be represented by

$$\epsilon_r = 2Er/a \quad (3.5)$$

where a is the edge length of a site, r is the radial distance from the site center, and E is the change in the minimum of the energy between the site center and the mid-point of a site edge, calculated by linear extrapolation of the variation near the center. E was found to depend strongly upon the relative sizes of the gas atom and the solid atom. $-E/\epsilon_m(0)$, the extrapolated fractional change in energy between $r = 0$ and $r = a/2$, is shown in Figure 1 as a function of the ratio of the atomic diameters. The extrapolated fractional change in energy between the site center and the midpoint of a site edge for an atom adsorbed on the 100 face of a face-centered cubic crystal is also shown—the details of this calculation are discussed in the following section. As $E/\epsilon_m(0)$ approaches zero, the mono-

layer properties approach those of a completely mobile monolayer, and p_o and β become

$$1/p_o = (\Lambda kT)^{-1} A_s \exp [-\epsilon_m(0)/kT] \sum_n \exp [-\epsilon_z(n)/kT] \tag{3.6}$$

$$\beta = -1/A_s \int_A f_{12} d\tau \tag{3.7}$$

As expected, Equation 3.7 for β is similar to the surface second virial coefficient which occurs in the usual treatment of the two-dimensional gas approach to monolayer adsorption (9).

For $E/kT \gg 1$, p_o becomes

$$1/p_o = (\Lambda kT)^{-1} (\pi a^2/2) (kT/E)^2 \exp [-\epsilon_m(0)/kT] \sum_n \exp [-\epsilon_z(n)/kT] \tag{3.8}$$

Furthermore, the rapid variation in c_τ when $E/kT \gg 1$ means that there is negligible probability of the adsorbed atoms being anywhere other than at their site centers. In this case, the integrand in the denominator of Equation 3.4 is finite only when both atoms are at the centers of their sites. Thus,

$$\beta = 1 - c(\exp [-u(a_{ij})/kT] - 1) + \dots \tag{3.9}$$

where $u(a_{ij})$ is the interaction of a pair of atoms on one of the c pairs of nearest neighbor sites whose centers are separated by a distance a_{ij} . Higher terms in the series include similar contributions to β from next nearest neighbor sites, etc. $\beta = 1$ if interactions with atoms on neighboring sites are negligible; in this case, Equation 2.22 is identical to the Langmuir isotherm.

The calculation of β and p_o for intermediate values of E/kT requires considerable computational labor, and is discussed in detail elsewhere (11, 24).

Application

It is desirable to compare the predictions of the theory presented here with experimental results obtained on some systems in which an independent computation of the gas-surface potential function can be carried out. A calculation of the potential functions for the adsorption of rare gases on solid rare gases involves the least number of unknown parameters. The rare gases crystallize into face-centered cubic solids with known lattice constants. Furthermore, the parameters appearing in the Lennard-Jones potential functions for the gas-gas and the gas-solid atom interaction can be estimated to a good degree of accuracy from experiments on the gas properties as well as from the empirical combining laws for potential parameters. Furthermore, some experimental results have already been reported for these adsorption systems (18, 20).

In particular, the potential functions for helium adsorbed on argon and for neon, argon, and xenon adsorbed on xenon are shown here, and the theoretically predicted adsorption properties are compared with experiment, wherever possible. $u_s(\mathbf{r}_i)$ for a Lennard-Jones atom interacting with a crystalline solid is given by the equation:

$$u_s(\mathbf{r}_i) = 4\epsilon^* \rho^{*6} [-S_6(\rho) + \rho^{*6} S_{12}(\rho)] \tag{4.1}$$

$$\rho^* = \sigma/a, \quad \rho = z/a \tag{4.2}$$

where ϵ^* and σ are the usual parameters in the Lennard-Jones equation for the interaction between a pair of atoms (one gas atom and one solid atom) and a is

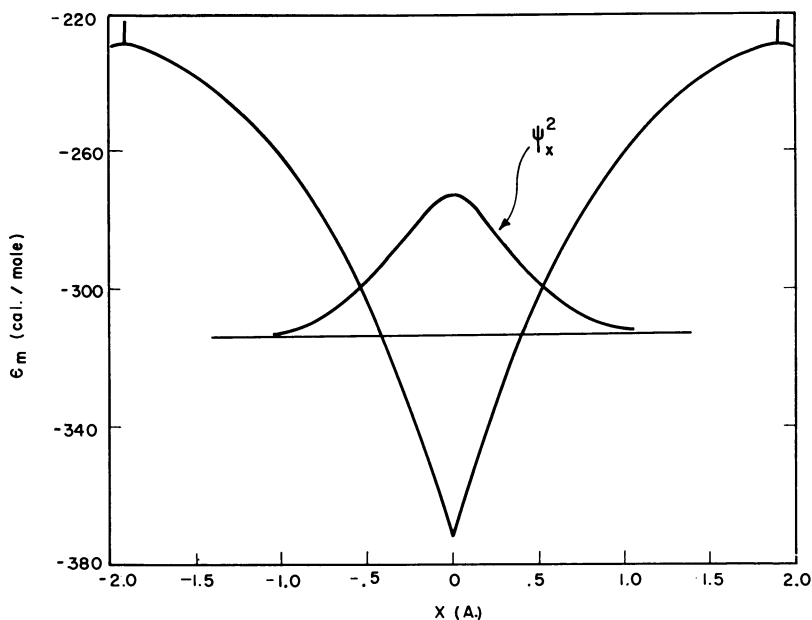


Figure 2. The minimum potential energy, ϵ_m , of a helium atom interacting with the 100 face of an argon crystal is plotted as a function of the position of the helium atom relative to the surface lattice

The origin of the x coordinate is at the center of a site, and the orientation of the x axis is parallel to the site edge. The horizontal line intersecting the potential curve shows the location of the ground state energy level of a helium atom vibrating along the x axis. ψ_x^2 is the probability amplitude in the x direction for an adsorbed helium atom in its ground state, plotted in arbitrary units

the lattice parameter of the solid. S_6 and S_{12} are the sums (over the entire solid) of the attractive and repulsive terms in the Lennard-Jones expression. These quantities depend upon the coordinates of the gas atom, as well as the symmetry of the lattice and the crystallographic indices of the exposed face. If it is assumed that the 100 face is exposed, S_6 and S_{12} for a face-centered cubic lattice can easily be obtained from the tabulated sums for a simple cubic lattice. The results show that the edge length of a repeating unit in the surface (or site) is $a/\sqrt{2}$, the distance of closest approach of two solid atoms in this lattice. Two of the corners of a site coincide with two atoms on an edge of a unit cell, and the other two corners coincide with atoms in the centers of the faces of two adjacent unit cells.

The parameters used in these calculations were calculated from the combining rules:

$$\epsilon^* = \sqrt{\epsilon_{11}^* \epsilon_{22}^*} \quad , \quad \sigma = (\sigma_{11} + \sigma_{22})/2 \quad (4.3)$$

The values used for ϵ_{11}^* , σ_{11} , etc., were taken from Dobbs and Jones (5); these authors also list the requisite lattice parameters for argon and xenon at 0° K. The values of the parameters used in the calculation are listed in Table I. The potential functions which were obtained when these parameters were substituted in Equation 4.1 are shown in Figures 2 and 3. The potential energy at $z = z_m$ is plotted as a function of x (or y), the displacement of an adsorbed atom from the site center parallel to a site edge. It was found that the best simple representation of ϵ_τ in the neighborhood of a site center on a face-centered cubic crystal is

$$\epsilon_r = (2\sqrt{2}E/a)(|x| + |y|) \tag{4.4}$$

where E is, as before the extrapolated difference in energy between the site center and the midpoint of a site edge. Theoretical values of the quantities pertinent to computations of adsorption data are shown in Table II. $\epsilon_z(n)$ are shown for $n =$

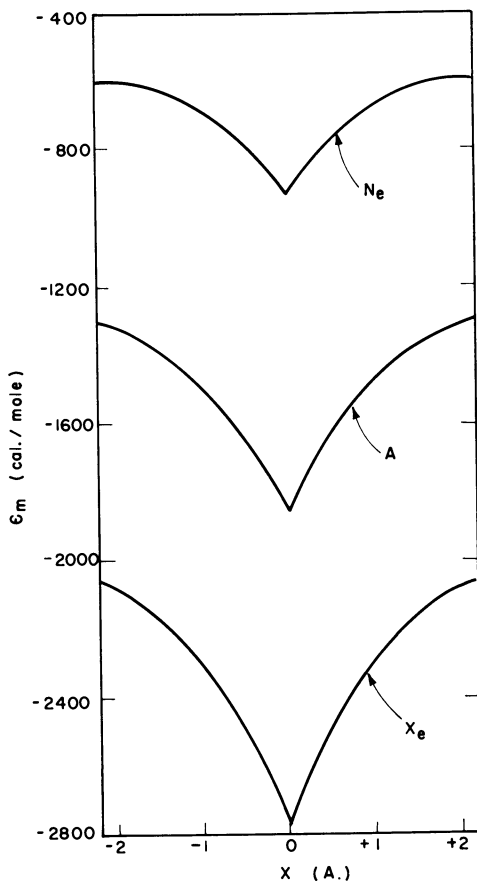


Figure 3. The minimum potential energies of several rare gases interacting with the 100 face of a xenon crystal are plotted here

The definition of the x coordinate is identical to that given in Figure 2

Table I. Interaction Parameters for Adsorbate-Adsorbent Pairs

Adsorbate-Adsorbent	$\epsilon^*/k, \text{ }^\circ K.$	$\sigma, \text{ \AA.}$	$a, \text{ \AA. at } 0^\circ K.$
He-A	35.6	3.00	5.31
Ne-Xe	89.5	3.41	6.1
A-Xe	166.0	3.74	6.1
Xe-Xe	225.0	4.07	6.1

0,1. These values were computed by fitting the calculated $u_s(z)$ curves in the neighborhood of z_m to perturbed harmonic oscillator functions [incidentally, these

Table II. Theoretical Minimum Interaction Energies and Energy Levels for Adsorbed Gases

(All energies given in units of cal./mole)

Adsorbate- Adsorbent	$\epsilon_m(0)$	$\epsilon_x(0)$	$\epsilon_x(1)$	E	$-E/\epsilon_m(0)$	$\epsilon_x(0)$	$\epsilon_x(1)$	$u(a_{ij})$
He-A	-370	66	172	250	0.69	60	140	-4.1
Ne-Xe	-937	66	184	660	0.71	60	140	-18.0
A-Xe	-1862	73	214	875	0.52	59	135	-177.0
Xe-Xe	-2756	59	175	1150	0.42	47	108	-370.0

calculations indicated that $\epsilon_x(n)$ has a negligible dependence upon τ for the systems considered]. Also shown is the value of the interaction energy of a pair of gas atoms which are assumed to be completely localized at the centers of two nearest neighbor sites [$u(a_{ij})$].

In view of the rapid variation of potential energy with distance shown in Figures 1 and 2, it seemed worthwhile to calculate the energy levels for motion of the adsorbed atoms in the x or y directions. The Schrodinger equation has been solved elsewhere for the potential function of Equation 4.4 (20); the results can be summarized as:

$$\begin{aligned}\epsilon_x(m) &= \xi_m \alpha (2\sqrt{2}E/a) \\ \alpha &= (9ah^2/64\sqrt{2}\pi^2ME)^{1/3}\end{aligned}\quad (4.5)$$

where M is the mass of the adsorbed atom, and ξ_m is a numerical factor having the values 0.778, 1.875, 3.480, . . . for $m = 0, 1, 2, \dots$. The ground and first excited states for motion in the x direction were calculated from Equation 4.5 for the various adsorption systems, and are listed in Table II. The horizontal line in Figure 2 shows the net energy of an adsorbed helium atom after $\epsilon_x(0)$ is added to the total potential energy; the probability amplitude in the x direction for an atom in the ground state (ψ_x^2) is also plotted in arbitrary units. It is clear that the zero point energy and zero point motion of an adsorbed atom are large in this system, and in fact, the total zero point energy (summed over all three degrees of freedom) amounts to 190 cal. per mole. Therefore, helium atoms adsorbed on an argon surface must be treated as completely quantized at experimental temperatures ($\sim 20^\circ$ K or less). The quantum expressions for p_o and β are:

$$1/p_o = (\Lambda^3 kT)^{-1} \exp[-\epsilon_m(0)/kT] \sum_{j_1} \exp[-\epsilon(j_1)/kT] \quad (4.6)$$

where j_1 is the quantum number for the energy levels of an isolated atom on a site;

$$\beta = N_s - \frac{\sum_{j_2} \exp[-\epsilon(j_2)/kT]}{N_s \left\{ \sum_{j_1} \exp[-\epsilon(j_1)/kT] \right\}^2} \quad (4.7)$$

where j_2 is the quantum number for the eigen states of a pair of interacting atoms.

For helium adsorbed on argon, the values of p_o computed from Equation 4.6 using the theoretical values of the energy states agree very well with the experimental measurements over the range 14° to 20° K (20). The experimental β were found to range from ~ 2 at 14° K to ~ 1 at 20° K; qualitative considerations, using Equation 4.7, lead to the tentative conclusion that these results are indicative of a net repulsive interaction between atoms on nearest neighbor sites. The classical calculation (see Table II) indicates a weak attractive energy; however, the net interaction will most likely be repulsive when the large zero point

motion of the adsorbed atoms is taken into account. Figure 2 shows that displacements of 1 Å. from the site center are reasonably probable; if two helium atoms on neighboring sites are displaced toward each other by 1 Å., their mutual interaction will be repulsive by ~ 1000 cal. per mole. A detailed calculation of the eigen states of a pair of interacting atoms on a surface is now being attempted.

The calculated ground and first excited states shown in Table II for the Ne-Xe, Ar-Xe, and Xe-Xe systems hardly change from one pair to another. This constancy is accidental: As the atomic number of the adsorbate is increased, the increase in mass tends to decrease the spacing of the levels; however, this decrease is cancelled by the increase in spacing due to the larger gradients in potential energy present in the systems with larger atomic numbers. The separation of the energy levels is roughly the same in all three dimensions; this indicates that one must use either the completely quantum equations for p_o and β (Equations 4.6 and 4.7) or the completely classical equations (Equations 2.19 and 3.4). Since monolayer experiments are generally carried out at temperatures higher than the freezing points of the adsorbates, it may be surmised that the quantum equations may be required in the Ne-Xe systems, the classical equations in the Xe-Xe case, and possibly a semiclassical (13) treatment for Ar on Xe.

The Ar-Xe system has been studied experimentally (18). Unfortunately for the purpose of this paper, these measurements are primarily concerned with the multilayer properties. An analysis of the low coverage portion of these data is now being attempted. There is, however, one interesting point of comparison. The experiments show that the heat of adsorption of argon on xenon at zero coverage is about 250 cal. per mole greater than the heat of sublimation of solid argon at 60° K. The theoretically calculated heat of adsorption at 0° K, zero coverage, is $-1862 + 2(59) + 73 = -1671$ cal. per mole. This value is 180 cal. per mole greater than the experimental heat of sublimation of Ar at 0° K (5). Since the enthalpy change of argon between 0° and 60° K would be expected to be about the same for the adsorbed and the solid states, one may conclude that the theoretical and experimental estimates are in good agreement.

Discussion

It is widely accepted that localized adsorption is a result of large variation in potential energy from point to point on the adsorbent surface, and that the lateral interaction in such systems must be affected to some extent by the existence of these variations (3). This paper consists in a more quantitative formulation of these concepts than has been available previously. Furthermore, it is shown that, for adsorption on crystallographically perfect surfaces, a considerable amount of information about the nature of the potential field at the surface of the solid can be obtained from a proper treatment of the experimental data. This approach to the adsorption problem can also be extended to give the formal equations applicable to adsorption on a heterogeneous surface; however, it seems unlikely that much practical use could be made of these equations because of the very large number of unknown parameters which appear.

The calculations of the potential functions for the various rare gas pairs indicate that monolayer adsorption in these systems will be highly localized at temperatures near the boiling points of the adsorbates. From the magnitudes of the values of $-E/\epsilon_m(0)$ shown in Figure 1, it may be surmised that localized adsorption will generally be found if the adsorbate atoms are smaller than the atoms

of the adsorbent. In view of the fact that the numerous "lattice gas" treatments of adsorbed monolayers (2, 6, 10, 14) apply only to localized systems, a knowledge of the degree of localization is of great value in the interpretation of experimental data in terms of these theories. For instance, many investigations of the properties of adsorbed films on graphitized carbon black have been reported (1, 4, 15, 17, 19, 21). These data should be suitable for theoretical interpretation, since the surface of the adsorbent can be made reasonably homogeneous. The lattice spacing of the exposed face of the graphite lattice is small compared to the atomic sizes of most adsorbates, and thus one might suppose that the potential variation from point to point over a carbon surface would be small (except possibly for helium). Calculations show this to be correct for the argon-carbon system (4). The parallel variations should thus be negligible for all adsorbates with molecular sizes larger than argon. If this is the case, one ought to be able to compare the monolayer adsorption data for such systems with the two-dimensional imperfect gas model. Such comparisons would be of particular interest in view of the statements that some adsorbed films made up of molecules larger than argon form localized monolayers on graphitized carbon (15, 19).

Many adsorption systems can be shown to correspond either to a localized adsorption model or to a two-dimensional gas. However, there must also be a large number of adsorbate-adsorbent pairs for which the potential energy functions will have variations intermediate between the extremes required for the limiting models. The formal equations applicable to these systems are included in the theory presented here, and furthermore, it appears to be feasible to carry out specific computations of the isotherms and heats for such systems up to moderate coverages (11, 24).

Literature Cited

- (1) Aston, J. G., Greyson, J., *J. Phys. Chem.* **61**, 613 (1957).
- (2) Bumble, S., Honig, J. M., *J. Chem. Phys.* **33**, 424 (1960).
- (3) Champion, W. M., Halsey, G. D., Jr., *J. Phys. Chem.* **57**, 646 (1953).
- (4) Crowell, A. D., Young, D. M., *Trans. Faraday Soc.* **49**, 1080 (1953).
- (5) Dobbs, E. R., Jones, G. O., *Repts. Progr. Phys.* **20**, 516 (1957).
- (6) Fowler, R., Guggenheim, E. A., "Statistical Thermodynamics," p. 437, Cambridge University Press, Cambridge, England, 1952.
- (7) Freeman, M. P., Halsey, G. D., Jr., *J. Phys. Chem.* **59**, 181 (1955).
- (8) Hill, T. L., *J. Chem. Phys.* **17**, 762 (1949); **14**, 441 (1946).
- (9) Hill, T. L., *J. Phys. Chem.* **63**, 456 (1959).
- (10) Hill, T. L., "Statistical Mechanics," McGraw-Hill, New York, 1956.
- (11) Hill, T. L., Greenschlag, S., *J. Chem. Phys.* **34**, 1538 (1961).
- (12) Hill, T. L., Saito, N., *Ibid.*, **34**, 1543 (1961).
- (13) Hirschfelder, J. O., Curtiss, C. F., Bird, R. B., "Molecular Theory of Gases and Liquids," p. 419, Wiley, New York, 1954.
- (14) Honig, J. M., *ADVANCES IN CHEM. SER.*, No. **33**, 239 (1961).
- (15) Isirikyan, A. A., Kiselev, A. V., *J. Phys. Chem.* **65**, 601 (1961).
- (16) Kiselev, A. V., *Quart. Revs.* **15**, 99 (1961).
- (17) Pace, E. L., Siebert, A. R., *J. Phys. Chem.* **63**, 1398 (1959).
- (18) Prenzlow, C., Halsey, G. D., Jr., *Ibid.*, **61**, 1158 (1957).
- (19) Ross, J. W., Good, R. J., *Ibid.*, **60**, 1167 (1956).
- (20) Ross, M., Steele, W. A., *J. Chem. Phys.* **35**, 0000 (1961).
- (21) Spencer, W. B., Amberg, C. H., Beebe, R. A., *J. Phys. Chem.* **62**, 613 (1957).
- (22) Steele, W. A., Halsey, G. D., Jr., *J. Chem. Phys.* **22**, 979 (1954).
- (23) Steele, W. A., Ross, M., *Ibid.*, **33**, 464 (1960).
- (24) *Ibid.*, in press.

RECEIVED June 12, 1961.

Heats of Immersion in Silica-Water Systems

J. W. WHALEN

Field Research Laboratory, Socony Mobil Oil Co., Inc., Dallas, Tex.

The heats of immersion in water of two quartz samples and three silica gels are compared with reference to surface bound water loss during out-gassing at elevated temperatures. The average heat of rehydration for the silica gel surfaces is 4700 cal. per mole of bound water. One silica gel surface contained, in addition to the normal surface hydroxyl content, bound water molecules which on rehydration exhibit a binding energy of 525 cal. per mole of water. Water vapor adsorption studies and energetic calculations based on immersion heats in water suggest that bound water on quartz is present both in hydroxyl form and as water molecules. Energies associated with bound water molecules range from 2300 to 3600 cal. per mole of water, depending on the degree of surface crystallinity. Loss of bound water in the form of hydroxyl groups is encountered only with the disordered quartz surface.

The surface structure of silica gel is widely accepted as consisting of hydroxyl (silanol) groups and oxide (siloxane) linkages (4). It has been suggested that the surface structure of quartz is analogous (5). In recent years a number of techniques have been employed (7, 19, 20) to characterize silica surface water interactions. Particular emphasis has been placed on the silica-water system, partly in view of the adaptability of the adsorbate to detection by these techniques and partly in view of the number of interaction possibilities, including the conversion of siloxane to silanol surface sites. Unfortunately, these tools, which have provided penetrating insight into adsorbate interactions on the silica surface, are confined to high surface area materials. This leads to the exclusion of crystalline silicas, such as quartz. This paper examines the heats of immersion of several silica materials in water, with emphasis on the utility of the immersion heat method in characterizing the surface structure of quartz by analogy to the behavior of more readily characterized silica gel surfaces. For comparison, silica gel surfaces studied extensively by other techniques are included (1, 8).

Materials and Techniques

Five silica samples were studied. Two were sized quartz particles from finely ground quartz (99.82% SiO₂) provided by the Standard Silica Co., Ottawa, Ill., obtained by sedimentation and elutriation in water, and air-dried at 110°C. Quartz A was the fraction corresponding in sedimentation time to particles smaller than 5 microns. Quartz B consisted of material remaining after exhaustive elutriation designed to remove particles smaller than 20 microns. An upper size limit of 40 microns was assigned to quartz B on the basis of the manufacturer's sieve analysis. The BET surface area obtained from treatment of nitrogen adsorption data on quartz A was 7.5 sq. meters per gram. The Harkins-Jura absolute surface area measurement showed 7.7 sq. meters per gram. The surface area of quartz B was 0.046 sq. meter per gram (a value kindly provided from krypton adsorption data by Norman Hackerman, University of Texas).

Three amorphous silicas were studied: FS, SB, and SL. Silica FS is a chromatographic column silica gel manufactured by Frederick Smith and Co., having a purity of 99.85% SiO₂. The BET (nitrogen) surface area was determined as 746 sq. meters per gram. Silicic acid special luminescent (SL) and silicic acid special bulky (SG), obtained from the Mallinckrodt Chemical Works, St. Louis 7, Mo., are precipitated silica gels of high purity (99.9% SiO₂, exclusive of water content). These silicas are of particular interest in view of previous surface characterization by other techniques (5, 6). From BET treatment of nitrogen adsorption data we obtain a surface area of 353 sq. meters per gram for silica SB and 665 for silica SL. Brunauer, Kantro, and Weise (1) report 382 sq. meters per gram for silica SB and 650 to 710 for silica SL. As noted by these authors, and again in our study, there is some variation in the surface area of silica SL. We assign an uncertainty in surface area of ±10% to the comparison of silica SL samples in the "as received" and dehydrated states.

Water vapor adsorption data for quartz A in the normal surface condition, following 110° C. outgassing, have been reported (15). Adsorption-desorption data reported herein were obtained following outgassing at 110°, 200°, 300°, and 400° C. The samples were maintained at constant (±2° C.) temperature under vacuum until a limiting pressure of 10⁻⁶ mm. of Hg was attained prior to determination of the adsorption isotherms. The data were obtained in a greaseless McBain-Baker quartz spring system using 2.5-gram capacity springs having sensitivities near 20 mg. per mm. spring elongation. The spring length was determined to ±0.01 mm. The system and associated techniques have been described (15).

Weight loss determinations associated with the loss of bound water were obtained in the course of gravimetric adsorption studies of various vapors on these surfaces. Quartz springs of 250-mg. capacity and sensitivities near 1 mg. per mm. were used in the above system. Outgassing in the 300° to 400° C. temperature range required 4 to 9 days to obtain the required low pressure measurement.

Heat evolution during immersion processes involving surface rehydration has been found to occur over a 20- to 40-minute interval, so that high precision methods are required if immersion heats include a contribution due to rehydration. The immersion heat determinations were carried out in a microcalorimeter having a temperature sensitivity of 5 × 10⁻⁶° C., rapid thermal response, and carefully determined heat transfer characteristics. The calorimetric system has a demonstrated capability of handling heat input rates as low as 0.005 joule per second (15). Samples for immersion were contained in very thin-walled bulbs holding

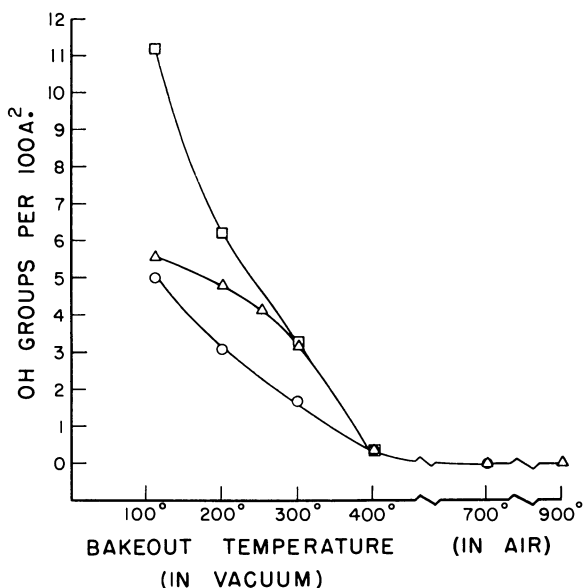


Figure 1. Surface hydroxyl content for selected silica gels

□ Silica SB
 △ Silica FS
 ○ Silica SL

quantities from 0.1 gram of the silica gels to 2.5 grams of quartz. The bulbs were completely shattered to provide rapid and complete dispersion of the solid phase in the wetting fluid. Outgassing conditions for immersion samples were as described for adsorption studies—i.e., constant thermal conditions until a limiting pressure of 10^{-6} mm. of Hg was reached. This treatment has been demonstrated to yield reproducible immersion heat values in our studies.

Results and Discussion

Figure 1 presents bound water loss as a function of thermal pretreatment for the three silica gels studied. All weight loss is assigned to bound water. The gel samples represent surfaces which appear to range from 11.4 to 5 OH groups per 100 sq. A. in the normal surface state after physically adsorbed water is removed at 110° C. Essentially complete siloxane character is reflected by the three gel surfaces following outgassing at 400° C.

Two proposals have been made relative to the maximum number of hydroxyl groups which can be structurally accommodated on the the gel surface (4). The surface structure is regarded by many workers as silanol saturated at 8 OH groups per 100 sq. A., based on analogy of the gel surface to the cristobalite structure. The bound water loss for silica SB is considerably in excess of this value, but not so high as would be required by an alternative proposal (4) involving both hydroxyl groups and bound water molecules (equivalent to 13.8 OH groups per 100 sq. A.) based on analogy of the gel surface to the tridymite structure. Silicas SL and FS exhibit initial hydroxyl content considerably below the accepted surface saturated value. In view of the moderately high activation temperatures to which

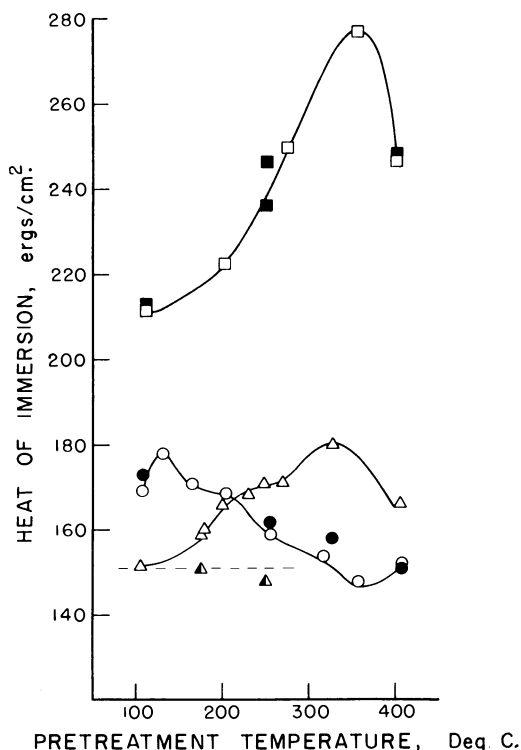


Figure 2. Heat of immersion in water of selected silica gel surfaces as a function of pretreatment temperature

- Silica SB
- Silica SB soaked in water
- Silica SL
- Silica SL soaked in water
- △ Silica FS
- ▲ Silica FS immersed in water

these materials were subjected during manufacture, siloxane character would be anticipated in their surface structure.

The influence of thermal pretreatment on immersion heats in water is shown in Figure 2. Silicas FS and SL exhibit immersion heat values in the 150 erg per sq. cm. range. The general level of immersion heats for silica SB is considerably higher than for most amorphous silica surfaces. Both silicas exhibit immersion heat maxima following thermal pretreatment in the 300° to 400° C. range. Immersion heat maxima in this thermal pretreatment range have been reported (2). Exact correspondence between thermal pretreatment and immersion heat maxima for such systems should not be anticipated, in view of probable surface structure differences arising from differences in outgassing conditions and calorimetric precision with regard to slow heat evolution. Comparison should be attempted only on the basis of established silanol-siloxane structure.

The hazard involved in generalization with regard to thermal pretreatment conditions is further emphasized by the immersion heat characteristics of Silica SL. This material is characterized by a decreasing immersion heat over a very wide range of outgassing conditions. The maximum immersion heat is obtained follow-

ing outgassing at 125° C. There is a slight minimum near 300° C. outgassing temperature conforming to the location of the maximum exhibited by the other gel systems.

The increase in immersion heat values as a function of pretreatment temperature is well established (2, 10) as evidence of rehydration of the siloxane structure on immersion. Maxima, with regard to thermal pretreatment, in the immersion heat curves undoubtedly relate to the increasing stability of the siloxane surface with increasing pretreatment temperature. The absence of strain associated with surface oxide structure in catalyst materials subjected to high temperature treatment has been established (9). The extent to which rehydration occurs has been considered (2, 6). Many of the conclusions relative to the extent of rehydration have been based on vapor adsorption data (6, 17, 18). In general, it would appear that indications of complete rehydration from the vapor phase are valid with regard to immersion processes. Indications of incomplete rehydration are not necessarily valid when applied to immersion processes. It would seem dangerous to extend conclusions regarding the stability of siloxane linkages resulting from the condensation of silanol groups at high temperature to systems in which the condensation occurs at low temperature. Flame-hydrolyzed silicas (8) and fused silica (18) should not be comparable in siloxane stability (17) to surfaces containing siloxane linkages developed below 250° to 300° C.

There is, in addition, a readily recognizable rehydration rate dependence on the surface siloxane content. This is most apparent in the immersion heat data for silica FS, for which the time of slow heat evolution on immersion becomes appreciably longer for sample pretreatment temperatures above 225° C. Consideration of the precision of the calorimetric measurement with regard to slow heat input does not seem to have been afforded adequate attention. Immersion heat calorimeters constructed for the essentially instantaneous wetting heat measurement often do not perform adequately when heat is evolved slowly.

The relationship of immersion heats to silica surface structure has been the subject of considerable discussion (2, 3) relative to the necessity for secondary rehydration of the surface in order to ensure reversible hydration characters. In this study, relative to the gel surfaces, the stability of the original (as received) surface was demonstrated by immersion of the materials in water for periods ranging from 2 hours to weeks. The comparison (Figure 2) of immersion heat data for both silica SB and silica SL before and after soaking for 3 weeks in water is barely outside the precision limits of the immersion heat measurement. Comparable data were obtained for silica FS by immersion of outgassed samples in water for 2 hours, approximately twice the time interval involved in the immersion heat determination, prior to outgassing at 100° C. and calorimetric immersion. Again immersion heat values identical, within the precision of the measurement, to the initial value indicate that rehydration proceeded to the original (stabilized) surface state for samples outgassed below 250° C. On the basis of this study it would appear necessary only to distinguish between siloxane sites obtained at high temperatures (in excess of 250° to 300° C.) and those obtained at lower temperatures. A high temperature silanol condensation has occurred for many commercially available gels during an activation treatment.

At thermal pretreatment temperatures above 110° C., rehydration contributions are significant. The rehydration energy can be obtained from the increase in immersion heat values when the silica surface rehydrates completely to its stable surface state, and the heat of immersion determination is such that the total heat evolved, including that evolved slowly, is included in the measurement.

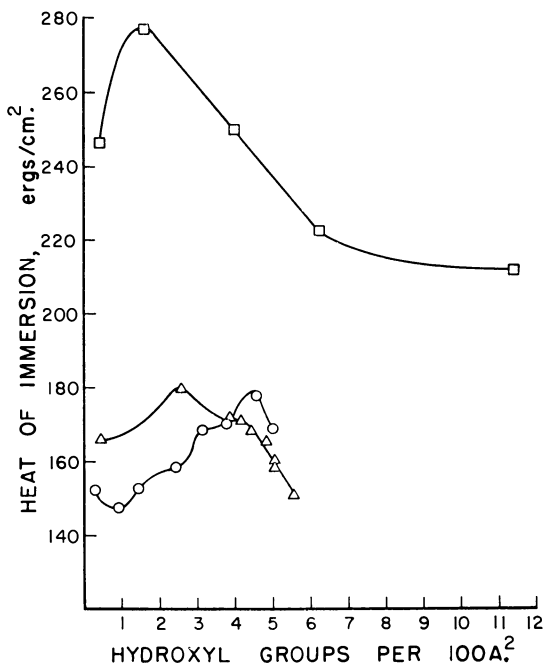


Figure 3. Heat of immersion in water of silica gel surfaces as a function of surface hydroxyl content

□ Silica SB
 △ Silica FS
 ○ Silica SL

The immersion heat curves for the three gel samples are shown as a function of surface hydroxyl content in Figure 3. Silicas SB and FS exhibit a linear relationship between hydroxyl content and immersion heat over segments of the total curve. The rehydration of silica SL is confined to a very limited silanol content. Rehydration energies, obtained from the straight-line portion of the immersion heat curves, are given in Table I.

For silica SB the linear portion of the curve is confined to the surface structure 7 to 1.6 OH groups per 100 sq. A. The portion of the curve below 1.6 OH groups per 100 sq. A is attributed to incomplete rehydration. The portion above 7 OH groups per 100 sq. A. exhibits a calculated average replacement energy of 525 cal. per mole of water. In the light of these data the surface structure of silica SB should be considered as containing, in addition to hydroxyl bound water, water molecules not removed during vacuum pretreatment at temperatures below 200° C. Total bound water would consist of 7 hydroxyl groups and 2.2 water molecules per 100 sq. A.

Table I. Rehydration Energies for Water on Silica Gel

Silica	Silanol Content, OH Groups/100 Sq. A.	Av. Rehydration Energy, Cal./Mole Water
SB	11.4	3430
FS	5.5	4425
SL	5.0	6450

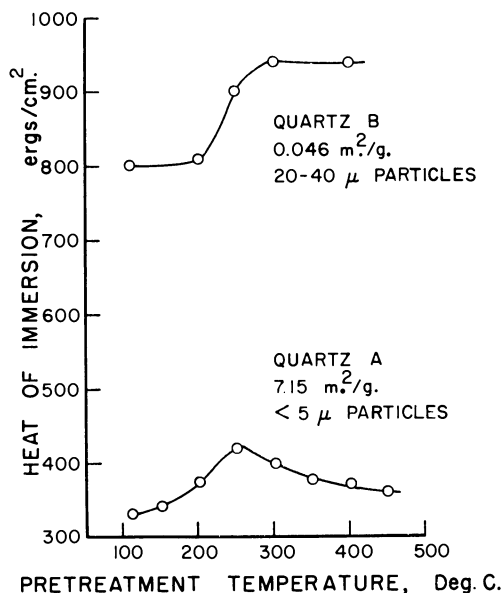


Figure 4. Heat of immersion of quartz in water as a function of pretreatment temperature

Infrared absorption data obtained on silica SB (8) have been interpreted in terms of the completely random association of tetrahedra. This is consistent with the absence of any high temperature treatment for this material. If true, the association of this surface with geometrical considerations based on crystalline materials of comparable density is of doubtful validity. If such association is made, these data indicate that the surface structure is more comparable to tridymite than to cristobalite. The tridymite structure has been shown (4) to accommodate 4.6 hydroxyl groups and 4.6 water molecules per 100 sq. A.

The use of average rehydration energy values should be qualified as to the silanol content of the surface but more particularly with regard to the previous thermal history of the sample. Structural rearrangement of the surface resulting in stable siloxane structure must have appreciable influence on the stability of the remaining silanol structure as indicated by the wide variation in rehydration energies shown in Table I. In utilizing data based on heat of solution measurements, the average value must include the hydration of otherwise stable siloxane sites and may involve considerably different energies than those associated with the reversible rehydration process.

The average rehydration energy value for silica FS, obtained over that portion of the immersion heat curve for which reversible rehydration was demonstrated, is very close to the average value obtained in the Brunauer, Kantero, and Weise (1) investigation of silicas SL and SB. The average value for these two materials from our work is 4990 cal. per mole of water, compared to 4660 reported by those authors. For silica FS the silanol content over which the average rehydration energy is applicable is 5.5 to 4.4 OH groups per 100 sq. A.; for silica SL it is 5.0 to 4.6.

Figure 4 presents the immersion heats of two quartz materials in water as a function of pretreatment temperature. There is no decline in the immersion heat

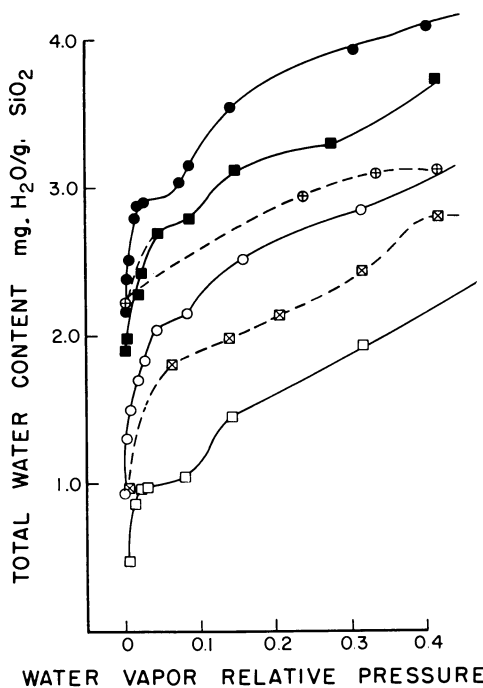


Figure 5. Total water content of quartz A above 400°

- Adsorption-desorption following 110° C. thermal pretreatment
- Adsorption-desorption following 200° C. thermal pretreatment
- Adsorption ⊕ desorption following 300° C. thermal pretreatment
- Adsorption ⊠ desorption following 400° C. thermal pretreatment

curve for quartz B at high outgassing temperatures. The immersion heat curve for quartz A is strikingly similar to that obtained for the completely hydrated silica SB.

The discrepancy in values for the small particle sample (quartz A) as opposed to the large particle sample (quartz B) has been reported (14, 16). This behavior has been explained in terms of the semi-amorphous character of the smallest quartz particles obtained in crushing and grinding operations. While larger particles are believed to be representative of increasing ideality in surface crystalline order, there is, at present, no confirmation for the supposition that the larger (20- to 40-micron) quartz B particles approach the ideal crystal structure. Thermal analysis shows that, relative to the large particles, as much as 48% of the less than 5-micron material may be noncrystalline with respect to the $\alpha - \beta$ quartz transition (16).

Figure 5 summarizes the low pressure end of water vapor adsorption isotherms obtained on quartz A. Bound water loss, above the surface condition resulting from 400° C. outgassing in vacuum, is indicated by displacement of the adsorption origin to reflect total water content (bound water plus adsorbed water) as a function of water vapor relative pressure. Vapor desorption curves show that

Table II. Thermal Dehydration of Quartz A from Adsorption-Desorption Data

Pretreatment Temp., ° C.	H ₂ O Molecules/100 Sq. A.	
	Loss	Replacement
110	—	—
200	1.3	1.3
300	5.5	5.5
400	9.7	4.2

the replacement of bound water lost during thermal pretreatment is complete from the vapor phase for samples outgassed at temperatures up to 300° C. Total replacement of bound water is not complete from the vapor phase for the sample outgassed at 400° C. In view of the extremely low surface area associated with quartz B, similar data could not be obtained.

Bound water loss, in terms of molecules per 100 sq. A. for quartz A (Table II) is far in excess of maximum values which could be assigned to quartz on the basis of condensation of structural hydroxyl groups. In addition, binding energies between silicon and oxygen atoms (11) do not suggest that hydroxyl group condensation should be accomplished by the moderate thermal energies attained in these studies. Since quartz A and quartz B show comparable immersions heat behavior for thermal pretreatment below 300° C., bound water loss in this region cannot be attributed to the condensation of hydroxyl groups occasioned by the semi-amorphous character of quartz A.

On applying to the quartz A immersion heats the set of assumptions previously utilized with some success in evaluating the energy associated with rehydration of the gel surface, we obtain 2350 cal. per mole of bound water for the bound water reversibly lost during thermal pretreatment. This value is approximately half that for the average rehydration energy of the silica gel surface.

Although bound water loss is not known for the quartz B surface, if it is assumed that the basic structural spacing of silicon and oxygen atoms is unchanged, the same bound water content may be tentatively assigned to both quartz A and quartz B, although differences in bonding energy must be anticipated. On this basis we obtain an average energy of 3630 cal. per mole of water for the rehydration of the quartz B surface. Again this value is considerably lower than that obtained for the gel surfaces and suggests that the loss of bound water from the quartz surface does not represent condensation of hydroxyl groups.

The suggestion has been made (3, 16) that adsorbed water molecules constitute the bulk of the "bound" water loss from quartz surfaces. The disposition of silicon and oxygen atoms in ideal crystal planes is well known (13). Table III represents a compilation of the possible numbers of hydroxyl groups and water molecules which could be accommodated on the various faces of the ideal quartz structure. In obtaining these values it is assumed that, while surface silicon atoms terminate the structure in hydroxyl groups, underlying silicon-oxygen linkages accommodate water molecules.

Table III. Accommodation of Bound Water on Ideal Quartz Crystal Faces

Plane	Unit Cell Area, Sq. A.	OH Groups	Water Molecules	Total Possible Water Loss. Molecules/ 100 Sq. A.
0001	20.8	2	1	9.6
1010 (prison)	26.4	2	1	7.6
1120 (prison)	45.6	4	1	6.5
1010 (rhombohedral)	77.2	6	3	8.9
2131 (trapezohedron)	73.0	5	3	6.8

Sufficient water can be accommodated only on the 0001 plane (not a naturally occurring crystal face) to account for the observed water loss. The 1010 crystal plane, which is also the lowest energy plane (12) and thus statistically preferable as a fracture face, shows a reasonably high accommodation for water molecules (4 per 100 sq. A.).

Irreversible bound water loss, encountered for the quartz A surface at pretreatment temperatures in excess of 250° C., may be attributed to the condensation of hydroxyl groups, possible because of the lower surface bond energies associated with the disordered structure. This effect is absent in our study of quartz B and would be predictable on the basis of the approaching ideal order in the larger particles.

Conclusions

Gel structures, stabilized by activation conditions, exhibit reversible behavior with respect to the low temperature condensation and rehydration of surface silanol groups. Rehydration is a slow process, the rate of which depends on the extent of siloxane surface. Significant calorimetric immersion measurements must be capable of resolving low-level, long-term heat effects. Rehydration energies calculated from the immersion heat curves indicate that, while activated gels contain only hydroxyl groups, the high silanol content gel used in this work contains, in addition, bound water molecules which are not removed prior to outgassing at 175° C. The maximum in heat of immersion data for quartz as a function of pretreatment temperature is suggested, on the basis of rehydration energy calculations, to be related to the loss of bound water molecules on the quartz surface.

Acknowledgment

The author expresses appreciation to the Socony Mobil Oil Co., Inc., for permission to publish the results of this study.

Literature Cited

- (1) Brunauer, S., Kanro, D. L., Weise, C. H., *Can. J. Chem.* **34**, 1483 (1956).
- (2) Egorov, M. M., Krasil'nikov, K. G., Sysoev, E. A., *Doklady Akad. Nauk S.S.S.R.* **108**, 103 (1956).
- (3) Hackerman, N., Makrides, A. C., *J. Phys. Chem.* **63**, 594 (1959).
- (4) Iler, R. K., "Colloid Chemistry of Silica and Silicates," Cornell Univ. Press, Ithaca, N. Y., 1955.
- (5) Kiselev, A. V., *Doklady Akad. Nauk S.S.S.R.* **98**, 427 (1954); *Proc. Second Intern. Congr. Surface Activity* **11**, 179 (1957).
- (6) Kohlschutter, H. W., Kampf, G., *Z. anorg. u. allgem. Chem.* **292**, 298 (1957).
- (7) McDonald, R. S., *J. Am. Chem. Soc.* **79**, 850 (1957).
- (8) McDonald, R. S., *J. Phys. Chem.* **62**, 1168 (1958).
- (9) Oblad, A. G., Weller, S. W., Mills, G. A., *Proc. Second Intern. Congr. Surface Activity* **11**, 309 (1957).
- (10) Patrick, W. A., "Colloid Chemistry of Silica and Silicates," p. 240, Cornell Univ. Press, Ithaca, N. Y., 1955.
- (11) Saksena, B. D., *Proc. Indiana Acad. Sci.* **19A**, 357 (1944).
- (12) Saksena, B. D., Pant, J. M., *J. Chem. Phys.* **18**, 1304 (1950).
- (13) Seifert, von H., Buhl, R., Siefert, K. F., *Kolloid Z.* **141**, 146 (1955).
- (14) Wade, W. H., Every, R. L., Hackerman, N., *J. Phys. Chem.* **64**, 355 (1961).
- (15) Whalen, J. W., *Ibid.*, in press.
- (16) Whalen, J. W., Southwest Regional Meeting, ACS, December 1958.
- (17) Young, G., *J. Colloid Sci.* **13**, 67 (1958).
- (18) Zhdanov, S. P., *Doklady Akad. Nauk S.S.S.R.* **100**, 1115 (1955); **155**, 938 (1957).
- (19) Zimmerman, J. R., Brittin, W. E., *J. Phys. Chem.* **61**, 1328 (1957).
- (20) Zimmerman, J. R., Holmes, B. G., Lasater, J. A., *Ibid.*, **60**, 1157 (1956).

RECEIVED May 9, 1961.

Adsorption Studies on Bone Mineral

Heats of Adsorption of Nitrogen and Argon at -195° C.

JAMES M. HOLMES

Carleton University, Ottawa 1, Canada

RALPH A. BEEBE

Amherst College, Amherst, Mass.

We have measured isotherms and calorimetric heats of adsorption of nitrogen and argon adsorbed on bone mineral. The surface of the bone mineral was treated by evacuation at 450° C. and also by covering with approximately a monolayer of methanol or water. The heats of adsorption of nitrogen on the bare surface start at 5.5 kcal. per mole and the values fall off to about 2.0 kcal. at the monolayer. On the chemically treated surfaces considerably lower heats of adsorption were found. These effects are explained on the basis of the attraction of the polarizable nitrogen molecules to a surface of varying polarity, depending on the method of treatment. The data obtained agree well with results reported by Beebe and Emmett on heats of adsorption of nitrogen on bone mineral measured from retention times in chromatography.

Because of the importance of the surface chemistry of bone mineral in physiological systems, we have undertaken a series of gas adsorption studies on hydroxyapatite in the form of anorganic bone. In a recent publication from this laboratory (4) results of calorimetric studies of the adsorption of water and methanol vapors on bone mineral and on synthetic hydroxyapatite were reported. The adsorption potential for nitrogen on dehydrated hydroxyapatite, whether from bone or from synthetic sources, was rather profoundly altered by the addition to the surface of chemisorbed methanol or water prior to the adsorption of nitrogen at -195° C. This effect was reflected in the specific surface areas, in the BET C values, and in the resultant values of $E_1 - E_l$ (net heats of adsorption) as shown in Table I of the above paper.

In the work cited above, as well as in other work (8, 9, 11), the BET V_m values as determined by nitrogen adsorption are diminished by the presence of

chemisorbed layers. As a result, the question arises whether this apparent diminution in surface area should be attributed to blocking of very narrow pores or to a less condensed packing of the nitrogen molecules on the methanol-covered or water-covered surfaces. To improve our understanding of these phenomena and possibly to answer the specific question indicated, we have undertaken a calorimetric study of the heats of adsorption of nitrogen on the bone mineral both in its dehydrated state and in the state resulting from modification by chemisorbed layers of water or methanol and we have measured heats of adsorption of argon on some of these surfaces.

Further interest in the calorimetric data has arisen from a chromatographic study on dehydrated and on water-covered bone mineral surfaces from which heats of adsorption have been derived (3). This appears to be the first report of a comparison of heats of adsorption data by the two methods on the same adsorption system.

Experimental

Materials. BONE MINERAL. Calorimetric measurements have been made on two samples of anorganic bone mineral obtained from Armour and Co. and designated as Ossar Femur Head lot 34 and lot 33-43, the latter being a mixture of two lots. Both samples were 20/40 mesh and had specific surface areas varying from 95 to 105 sq. meters per gram based on the weight of the dehydrated material.

The properties of lot 34 and the preparation of the Ossar samples have been described by Dry and Beebe (4). Lot 33-43 has been used in an investigation, the results of which are to be published later from this laboratory, dealing with pore size distributions as well as the effect of outgassing temperature on weight loss and specific surface area changes. For reasons discussed elsewhere (4) we have adopted a procedure for dehydration which consists of degassing the samples in vacuo for at least 15 hours at 450°.

ADSORBATES. Nitrogen, argon, and helium used for dead space measurements were research grade gases obtained from Matheson Co. and further purified (5). Reagent grade methanol and distilled water were purified and deaerated by bulb to bulb distillation in vacuo. These liquids were stored in flasks equipped with a cold finger so they could be further deaerated before use and both gave constant vapor pressures which agreed with the accepted values.

PREPARATION OF WATER-COVERED AND METHANOL-COVERED SURFACES. In this work we are essentially concerned with three types of bone mineral surface: (1) "bare surface," the Ossar sample which has been dehydrated or outgassed by evacuation at 450° for at least 15 hours; (2) "methanol-covered surface," the bare surface to which has been added approximately a monolayer of chemisorbed methanol, and (3) "water-covered surface," which has approximately a monolayer of water chemisorbed on the bare surface. The latter surface is very close in adsorption potential for nitrogen to the surface obtained by outgassing the Ossar samples at 0°.

Several methods have been used in an attempt to cover the bone mineral surface with a monolayer or more of methanol or water. The most generally used technique consisted of equilibrating the bone mineral in the calorimeter at 0° with saturated vapor of either of the two liquids at this temperature. Then the calorimeter was pumped out at 0° for several hours until no residual pressure could be detected. From the isotherms reported by Dry and Beebe (4) we then determined the relative pressure which would produce 1.2 to 1.4 layers of methanol or water on the bone mineral and added this amount of the adsorbate to the calorimeter. Other techniques involved no addition of methanol after pumping out at 0° and also pumping out only to the required relative pressure.

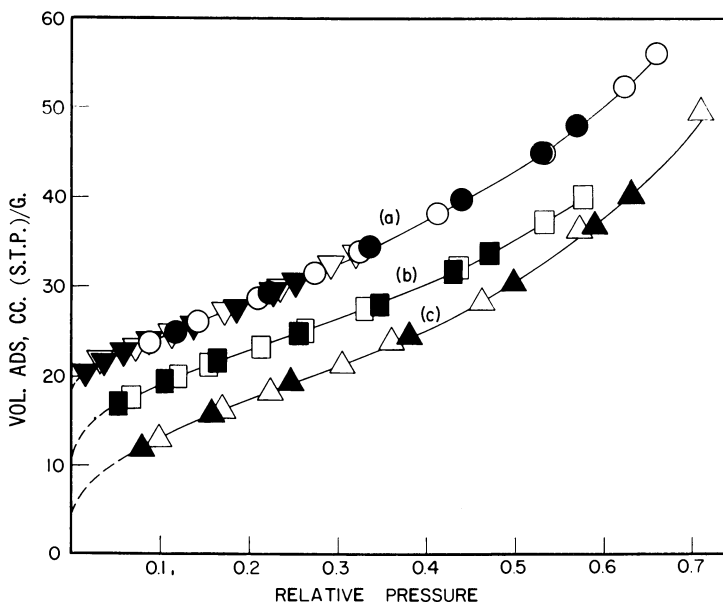


Figure 1. Isotherms of nitrogen on bone mineral at -195°C .

○ Run 1, bare surface
 ◻ Water-covered surface
 ◂ Run 4, bare surface
 ◃ Methanol-covered surface
 ●, ▲, ■ Desorption points

Apparatus. The gas-handling and vacuum systems used were standard volumetric equipment (5). Liquid nitrogen was used as a constant temperature bath around the calorimeter and the pilot sample; its temperature was checked by means of an oxygen vapor pressure thermometer.

The type of calorimeter and the method of calculating the heats of adsorption from the experimental data were essentially the same as described in previous papers (1, 4, 10). Two calorimeters of the same design were used, one employing a filler made of copper as described by Dry and Beebe (4) and the other a filler of aluminum. (A drawing and brief description of this calorimeter will be supplied on request addressed to the authors at Amherst College.) In one run for nitrogen adsorption on the bare surface we employed a liquid nitrogen trap to prevent contamination of the sample in the calorimeter by condensed mercury. Data from all runs on the various calorimeters and samples checked within the accuracy of the experiments.

In all of our experiments a pilot sample was placed in the system very close to the calorimeter, so that it received the same heat treatment as the sample in the calorimeter. This pilot sample was used to obtain more complete isotherms and to establish a final weight of the adsorbent. Weight losses on evacuation at 450° for the samples used averaged 6.1 to 6.3% of the initial weight.

A more detailed investigation of the weight loss on evacuation will be reported in a subsequent publication.

Results and Discussion

Nitrogen Isotherms. Sample isotherms for nitrogen adsorption at -195° for the variously treated bone mineral surfaces are shown in Figure 1. Curves *a*, *b*, and *c* refer to measurements on the bare, water-covered, and methanol-covered surfaces, respectively. These isotherms are plotted from data measured on the pilot sample and the volumes adsorbed are calculated on the basis of the weight of the sample degassed at 450° . This value was obtained by sealing off the pilot

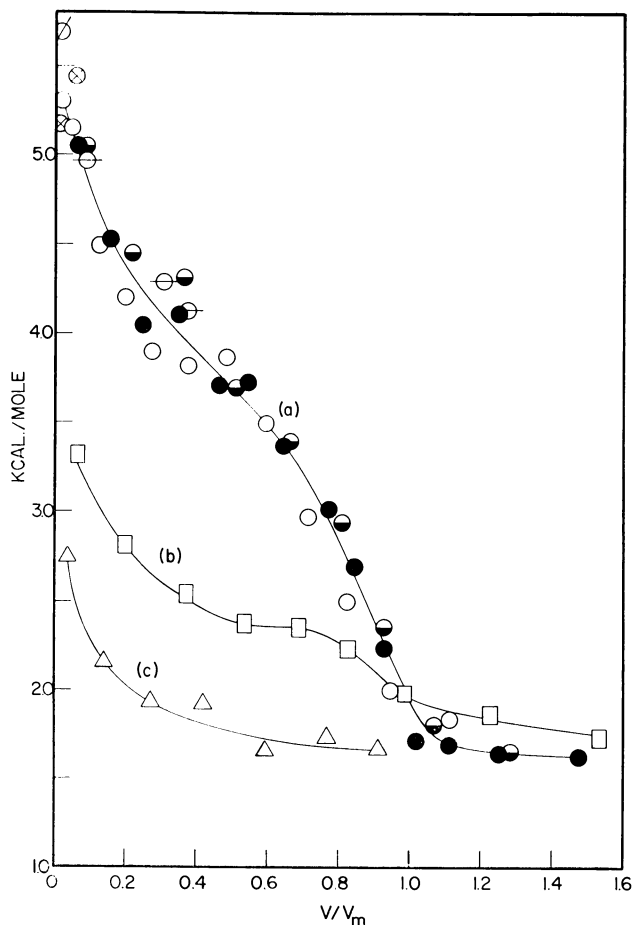


Figure 2. Differential heats of adsorption for nitrogen on bone mineral at -195°C .

$\circ, \bullet, \ominus, \otimes, \otimes$ Bare surface, runs 1 to 6
 \square Water-covered surface \triangle Methanol-covered surface

sample in vacuo after degassing at 450° at the end of the runs, weighing bulb plus sample, removing the sample, and weighing the parts. Small differences between the isotherms obtained in the pilot sample and in the calorimeter are due to more efficient evacuation of pilot sample (~ 0.4 gram) than the larger sample in the calorimeter (~ 4.5 grams). The significance of our calorimetric data is not seriously affected by these differences, since we calculated the fraction of the surface covered by determining the BET monolayer volume from the isotherm measured in the calorimeter.

We show here only one set of isotherm data, in order to show the similarity of these isotherms to those determined by Dry and Beebe (4), although the technique of preparing the modified surface was somewhat different in the two investigations. The methanol-covered sample shown in Figure 1 was prepared by adding more methanol after the sample was pumped at 0° to produce about 1.4 layers. The isotherm data gave good straight-line BET plots. In Table I are listed the

Table I. BET Parameters for Adsorption of N₂ on Bone Mineral at -195°

Sample	No. of Runs	V_m , Cc. S.T.P./G.	Specific Surface, Sq. M./G.	BET C Value	Net Heat of Ads., Cal./Mole.
Bare surface	6	22.5	97.9	236	830
Water-covered	3	19.6	84.0	105	710
Methanol-covered	5	16.55	68.0	23	480

BET parameters for the variously treated samples. Between run 1 and run 4 of Figure 1, the bone mineral sample had been heated to 450° in vacuo 12 times, treated with methanol twice, and with water once. In view of the complex nature of the adsorbent, it seems noteworthy that the isotherms from runs 1 and 4 are so nearly coincident.

Heats of Adsorption of Nitrogen at -195°. The results of the calorimetric work for nitrogen on bone mineral at -195° are represented in Figure 2, where the differential heats as measured for successive small increments are plotted against the coverage expressed as V/V_m . The V_m values were determined as described above by BET treatment of the nitrogen isotherms. Curves *a*, *b*, and *c* of Figure 2 represent, respectively, the heat for the bare, water-covered, and methanol-covered surface.

There is a considerable spread of the experimental points of curve *a*, especially in the regions of lowest (0.01 to 0.03 V/V_m) and intermediate coverage (0.2 to 0.5 V/V_m). Because of our interest in comparing the present results with the chromatographic data discussed below, it was deemed desirable to obtain calorimetric data for the smallest feasible initial increments of nitrogen. This resulted in a higher percentage error in the measurements as reflected in the spread in the heat values for the initial increments of different runs. The differential heat values of Figure 2 for the region $V/V_m = 0.05$ to 0.4, unlike those for coverage $V_m < 0.2$ or $V_m > 0.5$, do not represent equilibrium conditions. The resulting thermal drift, discussed in some detail below, gives rise to an uncertainty in the heat values reflected in the very considerable spread of points in the intermediate region ($V_m = 0.2$ to 0.5). The experimental points shown for curve *a* of Figure 2 are based on the observed heat evolution at the end of 5 minutes after admission of a given increment. This thermal drift was absent for the treated surfaces, and hence all points on curves *b* and *c* represent measurements under equilibrium conditions.

HEAT DATA ON BARE SURFACE. From Figure 2 it is seen that the heats of adsorption for nitrogen fall off from an initially high value of about 5.4 kcal. per mole at the lowest coverage studied to less than 1.7 kcal. at the estimated completion of the monolayer. The initial high values are doubtlessly attributable to the effect of the strongly polarizing ionic surface of the bone mineral upon the easily polarizable nitrogen molecules. Energetic heterogeneity in physical adsorption as related to experimental heat data on chabazite surfaces has been discussed in detail in a recent publication by Kington and Macleod (7). It seems probable that the considerations put forth by Kington and Macleod are pertinent to the present system and that much of the high energy of adsorption is attributable to the quadrupole interaction with the polar or ionic surface.

The heats of adsorption of nitrogen on the bare surface remain above 3 kcal. per mole until about 80% of the surface is covered. The expected drop in the heat curve at the completion of the monolayer is also evident. Although the heat measurements above the monolayer are more difficult and less precise, the heat values remain well above the heat of vaporization as the second layer begins to

fill. We take this as evidence for orientation effects of the polar surface extending into the second adsorbed layer of nitrogen.

HEAT DATA ON TREATED SURFACES. In contrast to the data of curve *a* of Figure 2, the initial differential heat values of curves *b* and *c* are far lower when nitrogen is physisorbed on top of an approximate monolayer of chemisorbed water or methanol. This observation is, of course, consistent with the lower BET *C* values calculated from the isotherms and reported earlier in this paper.

In the case of the water-covered surface, there is evidence for a plateau in curve *b* in the second half of the monolayer of nitrogen. A similar plateau was found in heat values for nitrogen on two other similar but not identical water-covered bone mineral surfaces. In one set of experiments we measured heats of adsorption for nitrogen at -195° on a bone mineral surface subjected to a long outgassing at room temperature but never heated above that temperature. The resulting surface, while probably having essentially a monolayer of chemisorbed water, would probably contain some carbonate and oxalate in higher percentage than would be found in the bone mineral surface after being outgassed at 450° . The differential heat-coverage curve for nitrogen on this material outgassed at room temperature ran some 200 cal. per mole lower than curve *b* of Figure 2, but had the same general form.

In the adsorption of nitrogen on top of the methanol-covered surface we see from curve *c* that the heat values run even lower than in curve *b*. It has been suggested by Dry and Beebe (4) that the chemisorbed monolayer of methanol is probably oriented with the methyl groups away from the surface, thus presenting a paraffin-like surface to the nitrogen adsorbate. It was hoped that the methanol-covered surface might present an energetically homogeneous surface to the nitrogen which might result in virtually constant differential heats for successive increment at low coverage. From curve *c* of Figure 1, it is apparent that this is not the case, since the heat for the initial increment in particular is about 600 cal. per mole higher than that for successive increments. Moreover in experiments not represented in Figure 2, it was found that the initial heat value for nitrogen on the methanol-covered surface was very sensitive to the method of adding the estimated monolayer of methanol. For instance, if the method of Dry and Beebe was followed, the initial heat value for nitrogen was 3.2 kcal. per mole. Thus we were not successful in preparing a truly paraffin-like surface, but there were always "holes" in the methanol layer through which the electrostatic attraction of the underlying bone mineral could make itself felt.

THERMAL DRIFT OR SLOW HEAT EVOLUTION. Evidence for Very Narrow Pores. For the initial increments of curve *a* for nitrogen on the bare surface of bone mineral at -195° ($V/V_m < 0.05$), the observed time-temperature curves were normal, exhibiting no evidence for any slow heat evolution, and the same was true for increments at $V/V_m > 0.4$, as well as for all points represented in curves *b* and *c*. However, for increments of curve *a* in the region $V/V_m = 0.05$ to 0.4, heat continued to be liberated for some time after the initial rapid thermal process. For different nitrogen increments within this range of coverage the heat produced in this slow process was from 5 to 12% in excess of that instantaneously evolved. The slow process was observed over a period of 20 to 30 minutes. In one extreme case it was still not complete after 45 minutes, which was about the maximum practicable period for observation.

A similar phenomenon was reported by Beebe and Dowden (2) for nitrogen and several other gases on chromic oxide and by Kington and Aston (6) for the

nitrogen-titanium dioxide system. In the former publication the observations were discussed in detail and possible mechanisms were suggested. In the experiments of Beebe and Dowden as well as in the present experiments, the slow evolution of heat could not be accounted for on the basis of slow adsorption of nitrogen from the gas phase, since the magnitude of the pressure drop after the first minute following admission of a given increment indicated that only a negligibly small amount of nitrogen was disappearing from the gas phase during the period of slow heat evolution.

From our experimental observations we may conclude that the initial increments of curve *a* of Figure 1 represent adsorption of nitrogen on sites of the bare surface of the bone mineral which are readily accessible and possess a high adsorption potential, resulting in the rapid evolution of high heats of adsorption of the order of 5.0 to 5.5 kcal. per mole. Successive increments of nitrogen may now be instantaneously adsorbed on readily accessible sites of lower adsorption potential, but this nitrogen may then be slowly transferred to less accessible sites of high potential. This transfer may well be due to a slow migration into very narrow pores. After the narrow pores are filled, the thermal drift would disappear and further increments of nitrogen would release the heats of adsorption on the readily accessible but low energy sites corresponding to $V/V_m > 0.4$.

It is especially noteworthy that the thermal drift effect was not observed for nitrogen adsorption on top of a water-covered or methanol-covered surface. From this observation we may conclude that the pores or crevices, present in the bare bone mineral used for curve *a*, are now filled by water or methanol, thus precluding any nitrogen adsorption in these difficultly accessible areas. We may conclude further that these pores are very narrow ones, because they are filled by no more than an approximate monolayer of chemisorbed water or methanol. This would suggest that the pores might be no greater than 8 to 10 Å across or perhaps 2 to 3 molecular diameters. Such pores might be in fact grain boundaries between the submicroscopic crystallites of hydroxyapatite.

In light of the present evidence it would seem that the decreased values for V_m caused by the presence of chemisorbed layers of water or methanol, as initially observed by Dry and Beebe and confirmed by the present work, can best be explained on the basis of the blocking, to nitrogen adsorption, of the very narrow pores by the chemisorbed monolayers rather than by the alternative suggestion of a less condensed packing of the nitrogen molecules adsorbed on top of water or methanol.

In a subsequent paper we intend to present evidence, based on gas adsorption studies, to shed further light on the structure of bone mineral. In constructing a plausible model, we shall make use of this evidence for very narrow pores or grain boundaries as well as of the adsorption-desorption hysteresis to evaluate the pore size distribution in the region of coarser pore structure.

COMPARISON WITH HEATS OF ADSORPTION DETERMINED FROM GAS-SOLID CHROMATOGRAPHY. Beebe and Emmett (3) have recently reported heat values for nitrogen adsorption on bone mineral as determined from the retention times of nitrogen pulses in a helium stream at several temperatures. These authors report 5.6 and 5.8 kcal. per mole for pulses containing, respectively, 2.3 and 0.02 ml. of nitrogen over a bone mineral column of 380-ml. nitrogen monolayer capacity, prepared in such a way as to correspond to the bare surface used for curve *a* of Figure 1 of this work. From a comparison with Figure 1 we note a close agreement between the heat values obtained from gas-solid chromatography and

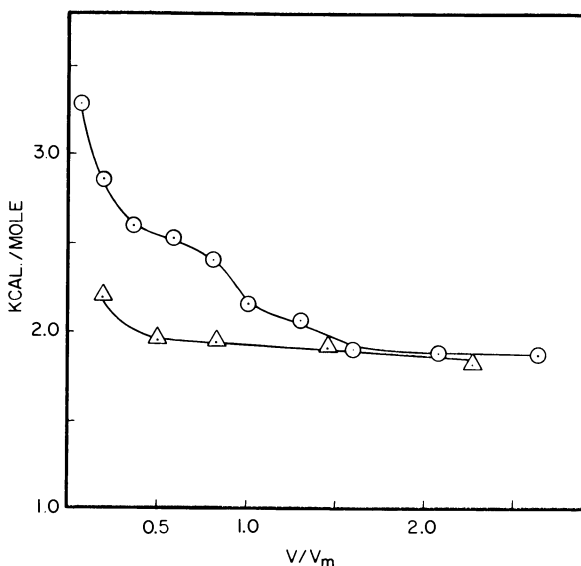


Figure 3. Differential heats of adsorption for argon on bone mineral at -195°C .

○ Bare surface △ Methanol-covered surface

the calorimetric heat values at low coverage. This suggests that the observed chromatographic retention times are related to relatively high energy sites at low coverage. However, quantitative comparison of the data obtained by the two methods might be pushed too far because of possible differences in the surfaces used in the two sets of experiments. Moreover, the chromatographic work was of necessity carried out in the temperature range 0° to -78° , which is far above -195° used in the calorimetric measurements.

Some less carefully executed chromatographic work by Beebe and Emmett (3) on an essentially water-covered surface yielded values in the range 2.5 to 3.0 kcal. per mole, in qualitative agreement with the low coverage calorimetric data for nitrogen on a comparable surface.

Adsorption Data for Argon on Bone Mineral at -195° . In previous sections we have emphasized that the polarizability of the adsorbate on the polar bone mineral surface contributes to high heats of adsorption. For comparison we have made calorimetric measurements of the heat of adsorption of argon at -195° on the bare surface of bone mineral and on a methanol-covered surface. The data for differential heats of adsorption of argon at -195° are shown in Figure 3 and isotherms as measured on the pilot sample are recorded in Figure 4.

In the case of argon adsorption there is again a marked difference between its heat of adsorption on a bare and methanol-covered surface, though as might be expected the magnitude of the effect is less than in the case of nitrogen. On the bare surface the highest value of heat of adsorption measured by us was 3.2 kcal. per mole and the heat values fall off to slightly over 2 kcal. at the monolayer ($V/V_m = 1$). On the methanol-treated surface the highest initial heat value measured was 2.2 kcal. per mole and the heat values dropped rapidly to a value of 1.9 at $V/V_m = 0.3$. In both heat-coverage curves of Figure 3 the heat values approach the heat of vaporization (1.8 kcal. per mole) at the higher coverages.

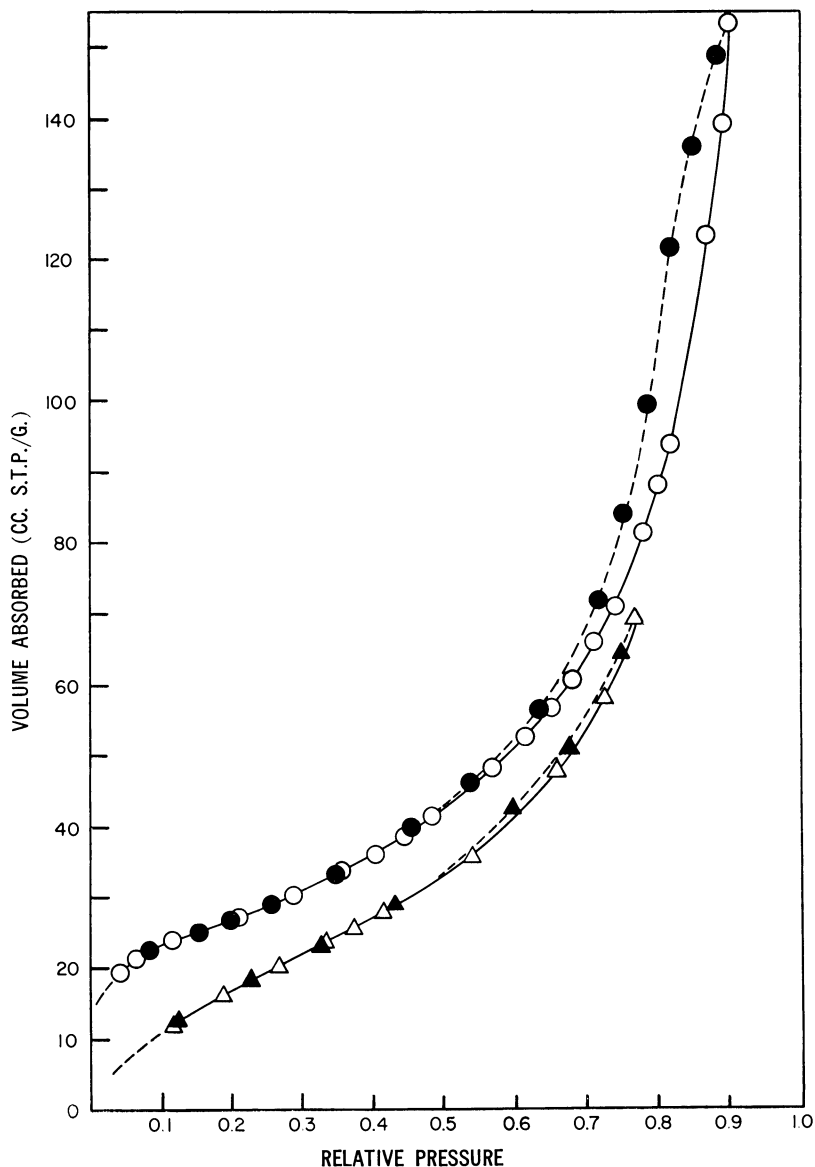


Figure 4. Isotherms for argon on bone mineral at -195°C .

Upper curve. Bare surface
 ○ Adsorption ● Desorption
 Lower curve. Methanol-covered surface
 △ Adsorption ▼ Desorption

The thermal drift, which was observed in the calorimetric work with nitrogen for intermediate coverages on the initially bare bone mineral, was not in evidence at any coverage with argon as the adsorbate.

In Figure 4, isotherms as determined on the pilot sample for the adsorption of argon on bone mineral surfaces are shown for comparison with those of nitrogen. The shapes of the isotherms show the same relative behavior as the nitrogen iso-

therms in Figure 1. A relatively large desorption hysteresis has been found in the case of argon adsorbed on the bare surface. Evidence of desorption hysteresis is also seen on the methanol-covered surface. We did not carry our data to high relative pressures and are thus observing only a portion of a scanning loop here. BET plots from isotherms on bare and treated surfaces in the calorimeter and in the pilot sample gave very good straight lines in the relative pressure range 0.05 to 0.35. The values of V/V_m used in plotting heat data in Figure 3 were calculated using the monolayer volumes as obtained from these BET plots for the argon data on the calorimeter sample.

Literature Cited

- (1) Amberg, C. H., *J. Am. Chem. Soc.* **79**, 3980 (1957).
- (2) Beebe, R. A., Dowden, D. A., *Ibid.*, **60**, 2912 (1938).
- (3) Beebe, R. A., Emmett, P. H., *J. Phys. Chem.* **65**, 184 (1961).
- (4) Dry, M. E., Beebe, R. A., *Ibid.*, **64**, 1300 (1960).
- (5) Holmes, J. M., Beebe, R. A., *Can. J. Chem.* **35**, 1542 (1957).
- (6) Kington, G. L., Aston, J. G., *J. Am. Chem. Soc.* **73**, 1929 (1951).
- (7) Kington, G. L., Macleod, A. C., *Trans Faraday Soc.* **55**, 1799 (1959).
- (8) Kiselev, A. V., Kovaleva, N. V., Korolev, A. Ya., Shcherbakova, K. D., *Compt. rend. Acad. Sci. U.R.S.S. (Doklady Akad. Nauk S.S.S.R.)* **124**, 617 (1959).
- (9) McIver, D. S., Tobin, H. H., *J. Phys. Chem.* **64**, 683 (1960).
- (10) Millard, B., Beebe, R. A., Cynarski, J., *Ibid.*, **58**, 468 (1954).
- (11) Stone, F. S., Tiley, P. F., *Nature* **167**, 654 (1951).

RECEIVED May 29, 1961. Contribution from Department of Chemistry, Amherst College. Research supported by Grant A-2896 from the National Institutes of Health.

On Physical Adsorption

XIII. The Adsorption Potentials and Vibrations of Inert Gases on Graphite

SYDNEY ROSS and JAMES P. OLIVIER

*Department of Chemistry,
Rensselaer Polytechnic Institute, Troy, N. Y.*

The kinetic model assumed in the method of Ross and Olivier for the analysis of heterogeneous surfaces by means of the adsorption isotherms is extended to give a more precise account of the temperature dependence of the isotherm, by allowing for an adsorbate-vibration normal to the surface. A limiting case of the Ross-Olivier method is developed for the treatment of adsorption data in the Henry's law region of the isotherm and applied to the data of Halsey *et al.* for the adsorption of the inert gases by graphite, with the following results: The isosteric heats calculated from kinetic contributions agree with those calculated thermodynamically by the Clausius-Clapeyron equation; and the temperature dependence of the isosteric heat is accounted for by this kinetic hypothesis.

In our previous paper of this series (5), which discussed chiefly adsorption at temperatures below 100° K, it was sufficiently accurate to ascribe the standard differential entropy change, ΔS_s , on adsorption of a monatomic gas as due entirely to the loss of one degree of translational freedom. For polyatomic molecules one ought to consider the possible additional loss of degrees of rotational freedom and, though much less likely to occur on adsorption, the change of modes of internal degrees of freedom. The vibration with respect to the surface of all types of adsorbed molecules is always a factor in the entropy change—a factor that increases in significance at higher temperatures. If this contribution to the entropy, ${}_a S^{\text{vib}}$, is that of a harmonic oscillator in one degree of freedom, for which the frequency does not change with temperature, it is given by

$$\left. \begin{aligned} {}_a S^{\text{vib}} &= \frac{{}_a E^{\text{vib}} - 1/2 N h \nu}{T} - \frac{{}_a F^{\text{vib}} - 1/2 N h \nu}{T} \\ \text{or} \\ {}_a S^{\text{vib}} &= \frac{N h \nu}{(e^{h \nu / k T} - 1) T} - R \ln (1 - e^{-h \nu / k T}) \end{aligned} \right\} \quad (1)$$

where ν is the frequency of the vibration.

The potential energy change on adsorption is defined as

$$U = {}_gP - {}_aE^{\text{vib}} \quad (2)$$

where ${}_gP$ is the potential energy per mole for adsorption of a molecule in the gas phase and ${}_aE^{\text{vib}}$ is the average vibrational energy per mole of a molecule in the adsorbed state. If no vibration normal to the surface exists—i.e., ${}_aS^{\text{vib}} = 0$, then ${}_aE^{\text{vib}} = 0$ and $U = {}_gP$. It is never correct, however, to assume ${}_aS^{\text{vib}} \equiv 0$; for large values of $h\nu/RT$ —e.g., at low temperatures, ${}_aS^{\text{vib}}$ will have, however, a negligible effect on the determination of U ; ΔS_s may then be equated simply to the loss of one degree of translational freedom (for a monatomic gas). This procedure is the one adopted in our previous paper to obtain U (calculated). The approximation is a good one when Δ , defined as $\Delta S_{s\text{-obs}} - \Delta S_{s\text{-model}}$, is less than one entropy unit. We now propose, however, to extend the model to take into account vibrational entropy and so permit the calculation of adsorptive energies at higher temperatures.

The model we are to consider is that of an adsorbed molecule capable of free translation parallel to the surface and vibrating normal to the surface. The average vibrational energy ${}_aE^{\text{vib}}$ is now not equated to zero; we write instead

$${}_aE^{\text{vib}} = \frac{Nh\nu}{e^{h\nu/kT} - 1} + \frac{1}{2}Nh\nu \quad (3)$$

At 0°K , ${}_aE^{\text{vib}} = {}_aE_0^{\text{vib}} = \frac{1}{2}Nh\nu$, and at higher temperatures ${}_aE^{\text{vib}}$ approaches RT .

The relations between U and the more familiar heats of adsorption, q^{diff} (the differential heat of adsorption) and q^{st} (the isosteric heat of adsorption), are as follows:

$$q^{\text{diff}} = U - \Delta E^{\text{tr}} - \Delta E^{\text{rot}} + {}_aP^{\text{ia}} \quad (4)$$

and

$$q^{\text{st}} = q^{\text{diff}} + RT \quad (5)$$

where $\Delta E^{\text{tr}} = {}_aE^{\text{tr}} - {}_gE^{\text{tr}}$; $\Delta E^{\text{rot}} = {}_aE^{\text{rot}} - {}_gE^{\text{rot}}$, and ${}_aP^{\text{ia}}$ is the adsorption potential in the adsorbed film due to lateral interaction. For the adsorption of a monatomic gas, we shall assume that the adsorbed film is mobile; that it can be described by the two-dimensional van der Waals equation of state, Equation 8; and that the molecules can rotate as freely when adsorbed as when in the gaseous state. Expressed mathematically these assumptions appear, respectively, as $\Delta E^{\text{tr}} = -\frac{1}{2}RT$; ${}_aP^{\text{ia}} = 2\alpha\theta/\beta$; and $\Delta E^{\text{rot}} = 0$. Equation 4 thus applied becomes:

$$q^{\text{diff}} = U + \frac{1}{2}RT + 2\alpha\theta/\beta \quad (4A)$$

The differential heat of adsorption, q^{diff} , measures the energy necessary to remove an adsorbed molecule from its average vibrational state and from the attractive forces of its adsorbed neighbors to an infinite distance from the surface, plus energy equivalent to the degrees of freedom of the molecules of the gas in excess of those in the adsorbed state.

The adsorptive energy, U , defined by Equation 2, is temperature-dependent, because of the variation of ${}_aE^{\text{vib}}$ with T . An absolute adsorptive potential that refers to the zero point energy of the adsorbed molecule, for which ${}_aE^{\text{vib}} = \frac{1}{2}Nh\nu$, has the advantage of being temperature-independent. We define this quantity as

$$U_0 = {}_gP - {}_aE_0^{\text{vib}} = {}_gP - \frac{1}{2}Nh\nu \quad (6)$$

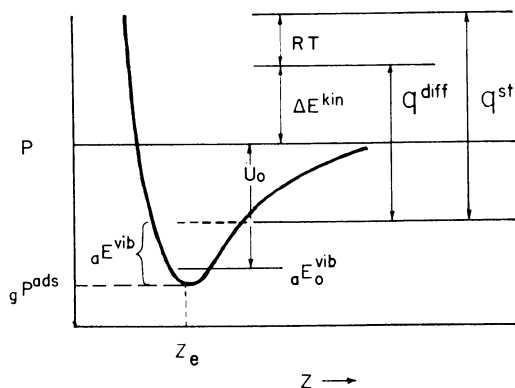


Figure 1. Potential well for adsorption (neglecting lateral interactions) showing relation of various heats of adsorption

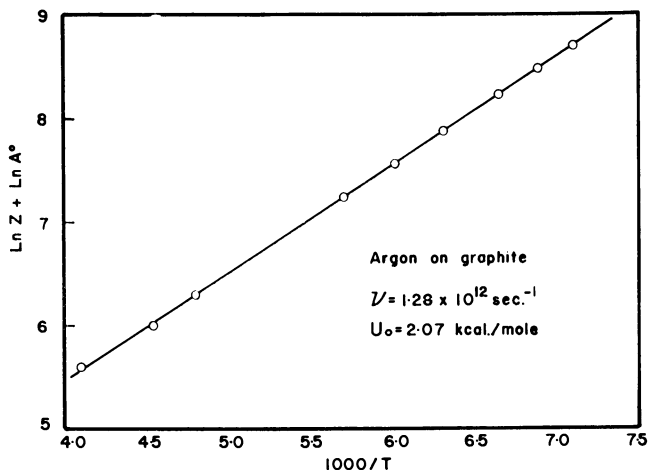


Figure 2. Adsorption data of Halsey *et al.* for argon adsorbed by graphite at various temperatures
Plotted according to Equation 18A, for evaluation of ν and U_o'

Figure 1 shows the connection between the various adsorptive potentials that we have discussed.

The definitions developed above are required for the analysis of adsorption data obtained from experiments at higher temperatures. Suitable data, in the monolayer region of adsorption, have recently been published by Halsey *et al.* (1, 2, 7). These data refer to adsorption of the inert gases on graphitized carbon black [P33(2700°)] at temperatures from 174° to 273° K; the adsorption was measured at such low surface concentrations that the adsorption isotherm has the form of a straight line through the origin, described by the equation $p = K\theta$, which is generally recognized as the two-dimensional analog of Henry's law. The method developed in our previous paper for the analysis of adsorption isotherms in the monolayer region requires data that extend to at least 60% of the saturated monolayer; in order to analyze the Henry's law region of the monolayer we must

develop an alternative treatment, which is actually a limiting case of the original theory.

The most general form of the adsorption isotherm is

$$\theta = \int_e^g \Phi(U_o) \Psi(p, U_o) dU_o \quad (7)$$

where the symbols have the significance previously defined (5). The adsorbed film on each infinitesimal homotactic surface patch is assumed to be a two-dimensional nonideal gas that can be described by a two-dimensional van der Waals equation of state, which gives the isotherm

$$p = K_i \frac{\theta_i}{1 - \theta_i} \exp \left[\frac{\theta_i}{1 - \theta_i} - \frac{2\alpha\theta_i}{RT\beta} \right] \quad (8)$$

where

$$K_i = A_i^0 \exp \left(- \frac{U_{0i}}{RT} \right) \quad (9)$$

Given conditions where θ_i is small for every surface patch at a given pressure, Equation 8 reduces to

$$p = K_i \theta_i \quad (10)$$

The necessary condition for Equation 10 to obtain is that the surface must have only a moderate range of adsorptive energies; otherwise the Henry's law region of the isotherm may occur at too low over-all surface concentrations to be observed.

The distribution of adsorptive potentials of the adsorbent surface is again taken as the Gaussian probability function:

$$\Phi(U_o) dU_o = \frac{1}{n} \exp \left[-\gamma(U_o - U_o')^2 \right] dU_o \quad (11)$$

On combining Equations 8, 9, 10, and 11, the limiting isotherm for the heterogeneous surface is

$$\theta = p \int_e^g \frac{\Phi(U_o) dU_o}{K_i}$$

or

$$\theta = \frac{p}{nA_o^0} \int_e^g \exp \left[-\gamma(U_o - U_o')^2 + \frac{U_o}{RT} \right] dU_o \quad (12)$$

assuming A_i^0 has the same value for every patch ($A_i^0 = A^0$). The evaluation of A^0 (Equation 24) shows that this assumption puts the same vibrational frequency of the adsorbed atom on every surface patch: not strictly true, but not seriously in error save for surfaces of extreme heterogeneity. Let $X = U_o - U_o'$; then

$$\theta = \frac{p \exp \left(\frac{U_o'}{RT} \right)}{nA_o^0} \int_{U_o' - e}^{g - U_o'} \exp \left(-\gamma X^2 + \frac{X}{RT} \right) dX \quad (13)$$

For values of γ greater than about 1, the integrand becomes negligible at $\pm X$ greater than 2.5 kcal. per mole; we can without error, therefore, set the limits of integration as $-\infty$ to $+\infty$; the normalizing factor n then becomes $\sqrt{\frac{\pi}{\gamma}}$. The value of the definite integral is given (4) as

$$\int_{-\infty}^{+\infty} \exp \left(-\gamma X^2 + \frac{X}{RT} \right) dX = \sqrt{\frac{\pi}{\gamma}} \exp \left[\frac{1}{4\gamma(RT)^2} \right] \quad (14)$$

Equation 13 becomes

$$p = K'\theta \exp \left[-\frac{1}{4\gamma(RT)^2} \right] \quad (15)$$

where K' is defined in terms of the average adsorptive energy, U_o' , by

$$K' = A^\circ \exp \left(-\frac{U_o'}{RT} \right) \quad (16)$$

Two different average adsorptive energies have been defined: U refers to the average vibrational state of the adsorbed molecule on any homotattic patch; U' refers to this adsorptive energy on the average (most frequent) homotattic patch of a given heterogeneous surface. U_o is a special value of U —i.e., at 0° K—and U_o' is the value of U_o on the most frequent surface patch.

The adsorption isotherm described by Equation 15 is a straight line through the origin. Let the slope of this line, $(dV/dp)_{T,S}$, equal Z ; then $V = Zp$. From Equation 15 we have

$$\theta = \frac{P}{K'} \exp \left[\frac{1}{4\gamma(RT)^2} \right]$$

Let $\theta = V/V_\beta$, where V_β is the monolayer capacity of the surface when the molecules are compressed to an area defined by the two-dimensional van der Waals constant β in Equation 8: then

$$Z = (V_\beta/K') \exp \left[\frac{1}{4\gamma(RT)^2} \right] \quad (17)$$

hence

$$\ln Z + \ln A^\circ = \frac{U_o'}{RT} + \ln V_\beta + \frac{1}{4\gamma(RT)^2} \quad (18)$$

To evaluate $\ln A^\circ$ we consider the adsorption process between the standard states of the gas and of the adsorbed phase. For the gas the standard state is 1-atm. pressure at the temperature of the experiment; for the adsorbed state we follow de Boer (3) in selecting the condition that the average separation of the molecules is the same in both standard states at 0° C., which gives

$$\theta_s = \frac{\beta}{4.08T}$$

where β , the two-dimensional van der Waals constant, is taken as equal to the effective cross-sectional area of the adsorbate molecule; for argon, $\beta = 13.6$ sq. A. For this process,

$$\Delta F_s = -q^{\text{diff}} - T\Delta S_s \quad (19)$$

We shall consider the most frequent homotattic patch of surface and Equation 8 in the following substitutions:

$$\Delta F_s = RT \ln \frac{p_s}{760}$$

where p_s is related to θ_s by Equation 8; therefore,

$$\Delta F_s = RT \ln K' + RT \ln \frac{\theta_s}{1 - \theta_s} + RT \frac{\theta_s}{1 - \theta_s} - \frac{2\alpha\theta_s}{\beta} - \ln 760 \quad (20)$$

and, from Equations 3, 4A, and 6,

$$q^{\text{diff}} = U_o' - ({}_{\text{vib}}E - \frac{1}{2}Nh\nu) + \frac{1}{2}RT + \frac{2\alpha\theta}{\beta} \quad (21)$$

Combining Equations 16, 19, 20, and 21:

$$\ln A^\circ = -\frac{\Delta S_s}{R} + \frac{{}_aE^{\text{vib}} - \frac{1}{2}Nh\nu}{RT} - \frac{1}{2} - \ln \frac{\theta_s}{1 - \theta_s} - \frac{\theta_s}{1 - \theta_s} + \ln 760 \quad (22)$$

For our present model ΔS_s includes ${}_aS^{\text{vib}}$ as well as the loss of one degree of translational freedom:

$$\Delta S_s = \Delta S_s^{\text{tr}} + {}_aS^{\text{vib}} \quad (23)$$

Making use of Equation 1 for ${}_aS^{\text{vib}}$ gives

$$\ln A^\circ = -\frac{\Delta S_s^{\text{tr}}}{R} + \frac{{}_aF^{\text{vib}} - \frac{1}{2}Nh\nu}{RT} - \frac{1}{2} - \ln \frac{\theta_s}{1 - \theta_s} - \frac{\theta_s}{1 - \theta_s} + \ln 760 \quad (24)$$

We propose to use Equation 18 for the quantitative description of the inert gas-graphite interfaces, using available experimental data. The values of both V_β and γ for the adsorption of argon on this graphite have been determined from the experimental data of Ross and Winkler (6), using the Ross-Olivier method (5) of matched isotherms, and taking into account the polarization of the adsorbate by the surface field of graphite: $V = 3.83$ cc. (STP) g^{-1} and $\gamma = 400$ kcal. $^{-2}$ mole $^{-2}$. The values of γ for the other inert gases on this near-homotropic adsorbent would have the same order of magnitude, and consequently make the last term of Equation 18 negligible compared to the other terms. Thus, for example, by taking into account the term in γ when making the calculations from the data for argon, the value of U_o' is diminished by 0.1% and the value of ν is diminished by 0.2%; these corrections are just about the same magnitude as the precision of the result. But although we may disregard the γ term in the calculation, it must not be inferred that even such a low degree of heterogeneity is without effect on the shape of the isotherm, but only that it is without appreciable effect on the initial slope at low values of θ . The isotherms computed for $\gamma = 400$ and $\gamma = \infty$ at 77.5° K show small but distinct differences.

Equation 18 now reduces to:

$$\ln Z + \ln A^\circ = \frac{U_o'}{RT} + \ln V_\beta \quad (18A)$$

For inert gas adsorbates other than argon, the values of V_β were determined from the argon value by the relation

$$V_\beta = \frac{3.83(13.6)}{\beta} = \frac{52.1}{\beta} \quad (25)$$

in which β (A^2 per molecule) is the two-dimensional van der Waals constant for the gas. At the temperature to which the data (1, 2, 7) refer $\theta \ll 1$; consequently Equation 24 reduces to

$$\ln A^\circ = -\frac{\Delta S_s^{\text{tr}}}{R} + \frac{{}_aF^{\text{vib}} - \frac{1}{2}Nh\nu}{RT} - \frac{1}{2} - \ln \theta_s - \theta_s + \ln 760 \quad (24A)$$

For a monatomic gas (3),

$$-\Delta S_s^{\text{tr}} = {}_aS_s^{\text{tr}} - {}_aS_s^{\text{tr}} = \frac{R}{2} \ln M + \frac{R}{2} \ln T + 2.31 \quad (26)$$

The only unevaluated quantity that prevents our immediate use of Equation 18 is the vibrational frequency, ν , of the adsorbed molecule, which determines (${}_aF^{\text{vib}} - \frac{1}{2}Nh\nu$) by the relation:

$${}_aF^{\text{vib}} - \frac{1}{2}Nh\nu = RT \ln (1 - e^{-h\nu/kT}) \quad (27)$$

A crude determination of ${}_aS^{\text{vib}}$ for argon on P-33 (2700°) at an average temperature of 84° K has been reported (5) as about 1 e.u., which yields $\nu = 3 \times 10^{12}$

Equation 28 is derived from Equations 5 and 21 and the relation:

$${}_aE^{\text{vib}} - \frac{1}{2}Nh\nu = \frac{Nh\nu}{(\rho^{h\nu/kT} - 1)} \quad (29)$$

The isosteric heats of adsorption synthesized in this way by the use of Equation 28 are based directly on the model of a mobile adsorbed film that we have developed; they can be compared with values of q^{st} obtained by the use of the thermodynamic definition, which has no reference to any model—viz.,

$$q^{\text{st}} = RT^2 \left(\frac{\partial \ln p}{\partial T} \right)_\theta$$

at zero coverage this definition becomes

$$\lim_{\theta \rightarrow 0} q^{\text{st}} = RT^2 \frac{d \ln K'}{dT} + \frac{1}{2\gamma RT} \simeq -RT^2 \frac{d \ln Z}{dT} \quad (30)$$

For the adsorbent used in these experiments, which is near-homotropic with a high value of γ , the isosteric heats defined by Equations 28 and 30 should be the same.

The values of q^{st} calculated by Equations 28 and 30 are in excellent agreement for all four adsorbates at the temperatures indicated (Table I, columns 5 and 6) and, although not reported, the same agreement is found at other temperatures within the range of the measurements; thus demonstrating that the consequences of our model of the adsorbed film are quantitatively in agreement with the thermodynamics of the process.

Acknowledgment

The authors gratefully acknowledge a grant in aid of these researches from Esso Research and Engineering Co.

Literature Cited

- (1) Constabaris, G., Halsey, G. D., Jr., *J. Chem. Phys.* **27**, 1433 (1957).
- (2) Constabaris, G., Singleton, J. H., Halsey, G. D., Jr., *J. Phys. Chem.* **63**, 1350 (1959).
- (3) de Boer, J. H., "The Dynamical Character of Adsorption," pp. 114–16, Clarendon Press, Oxford, 1953.
- (4) de Haan, D. B., "Nouvelles Tables d'Integrales Definies," G. E. Stechert and Co., New York, 1939.
- (5) Ross, S., Olivier, J. P., *J. Phys. Chem.* **65**, 608 (1961).
- (6) Ross, S., Winkler, W. W., *J. Colloid Sci.* **10**, 319 (1955).
- (7) Sams, J. R., Jr., Constabaris, G., Halsey, G. D., Jr., *J. Phys. Chem.* **64**, 1689 (1960).

RECEIVED May 9, 1961.

On Physical Adsorption

XIV. The Nature of the Adsorptive Forces between the Inert Gases and a Graphite Surface

SYDNEY ROSS and JAMES P. OLIVIER

*Department of Chemistry,
Rensselaer Polytechnic Institute, Troy, N. Y.*

Calculations of the energies of interaction between a gas and a solid surface have hitherto not been definitively compared with experimental results, because of difficulty in evaluating the contributions that make up the measured heat of adsorption. Methods described in previous papers provide a means of analyzing experimental data in terms of the adsorptive potential of the gas with respect to the most frequent patch of the surface. The adsorptive potential thus obtained is made up of the dispersion interactions plus an energy term due to interaction between the dipole of the adsorbate and the electric field of the substrate. For the inert gases adsorbed by graphite enough information is now available for calculation of the necessary quantities. The results derived from experiment are compared with calculations of the dispersion energies using potential functions of different degrees of approximation. Crowell's approximation of the lattice sum, in which the graphite lattice is treated as a set of planes of continuous structure and uniform density, when applied to a 6-8-10-12 potential function, is found to correspond most closely to the observed values.

Observations of a large number of adsorption systems disclose that the heat evolved during adsorption may be anywhere from a few hundred calories to over a hundred kilocalories per mole adsorbed. Early workers in the field used a value of 20 kcal. per mole to define the upper limit of physical adsorption, believing that heats of adsorption above this value could arise only from a chemical bonding between the adsorbate and the surface. We are now aware that a wide

range of heats of adsorption could arise from any one of four adsorption mechanisms or combinations thereof; and therefore that a knowledge of the heat of adsorption is not enough, save in extreme cases, to distinguish between adsorption mechanisms.

Origins of Adsorptive Potential

Four general types of molecular interaction lead to a potential energy for adsorption:

1. London-type dispersion forces resulting from induced-dipole/induced-dipole and multipolar attractions
2. Induction forces brought about by the operation of a surface electric field on induced or permanent dipoles of resident molecules
3. Charge transfer (6) between the adsorbed molecule and the surface, resulting in a no-bond resonance state
4. Dative bonding resulting from a chemical reaction between the adsorbate and surface atoms

The first two types of interaction are certainly physical adsorption; the fourth is certainly chemisorption; the third, which is a postulated mechanism whose actual occurrence has not yet been adequately demonstrated, exists in a twilight zone that defies classification as either physical or chemical adsorption. Previous papers of this series have not been concerned with the source of the adsorptive potential, but have postulated only that the adsorbed film be mobile; their considerations could apply, therefore, to all adsorption situations other than No. 4. The present paper is devoted to a consideration of the adsorptive potential arising from 1 and 2—that is, physical adsorption properly so called. This general topic has been discussed by de Boer (5) for a number of specific cases; the theory and techniques that we have developed enable us to derive from experimental data a quantity, ρ^{ads} , the depth of the adsorptive potential well, which can also be calculated *a priori* from physical properties of the system. We are therefore able to compare theory and observation and so have an independent test of conclusions reached in previous papers.

Expressions for Dispersion Potential

The Direct Lattice Sum. Dispersion forces between two atoms can be described by a potential function expressed in terms containing inverse powers of the internuclear separations, s . The simplest function of this sort includes a potential energy of attraction proportional to the inverse sixth power of the separation and a repulsion that is zero at distances of separation greater than a particular value s_e and infinite at separations less than s_c . This is the so-called "hard sphere" or van der Waals model. Such an approximate potential function can be improved in two respects. Investigations of the second virial coefficient have revealed that the potential energy of repulsion is best described as proportional to the inverse twelfth power of the separation; and the term in s^{-6} , which accounts for the greater part of the total attraction potential, due to the attraction of mutually induced dipoles, should have added to it the dipole-quadrupole and quadrupole-quadrupole attractions, expressed as terms in s^{-8} and s^{-10} , respectively. The complete potential function for the forces between two atoms is, therefore:

$$P_{ij} = C_1 s_{ij}^{-6} + C_2 s_{ij}^{-8} + C_3 s_{ij}^{-10} - (R s_{ij}^{-12}) \quad (1)$$

where P_{ij} is the potential energy lost by two particles, i and j , on approaching each

other from an infinite separation to a separation s ; C_1 , C_2 , and C_3 are dipole-dipole, dipole-quadrupole, and quadrupole-quadrupole coefficients, respectively; and \mathcal{R} is a repulsion constant. To calculate the potential energy lost by a gas molecule on approaching a surface, the potential difference, P_{ij} , has to be summed for the simultaneous interactions of the gas molecule, i , with each of the atoms of the adsorbent.

$$\sum_j P_{ij} = {}_0P = C_1 \sum_j s_{ij}^{-6} + C_2 \sum_j s_{ij}^{-8} + C_3 \sum_j s_{ij}^{-10} - \mathcal{R} \sum_j s_{ij}^{-12} \quad (2)$$

For a polyatomic adsorbate it may be necessary to sum the interactions over each atom of the adsorbate molecule as well. The various values of s_{ij} in Equation 2 can, for a particular adsorbent of known crystal lattice, be calculated in terms of a single distance, z , which is defined as the distance between the center of an adsorbate atom and the mathematical plane in which lie the centers of the surface atoms of the adsorbent.

The constants C_1 , C_2 , and C_3 in Equation 2 can be evaluated by means of the following approximate quantum mechanical equations (1, 7):

$$C_1 = 6mc^2\xi_i\xi_j \frac{1}{\frac{\xi_i}{\chi_i} + \frac{\xi_j}{\chi_j}} \quad (3)$$

$$C_2 = \frac{45h^2}{32\pi^2m} \xi_i\xi_j \left\{ \frac{1}{2\left[\left(\frac{\xi_j}{\chi_j}/\frac{\xi_i}{\chi_i}\right) + 1\right]} + \frac{1}{2\left[\left(\frac{\xi_i}{\chi_i}/\frac{\xi_j}{\chi_j}\right) + 1\right]} \right\} \quad (4)$$

$$C_3 = \frac{105h^4}{256\pi^4m^2} \xi_i\xi_j \left\{ \frac{\xi_i/\chi_i}{3\left(\frac{\xi_j/\chi_j}{\xi_i/\chi_i}\right) + 1} + \frac{3}{4\left(\frac{\chi_i}{\xi_i} + \frac{\chi_j}{\xi_j}\right)} + \frac{\xi_j/\chi_j}{3\left(\frac{\xi_i/\chi_i}{\xi_j/\chi_j}\right) + 1} \right\} \quad (5)$$

In these equations ξ represents polarizability and χ represents diamagnetic susceptibility; subscripts i and j refer to the adsorbate and the adsorbent, respectively.

No theoretical expression for the repulsion constant, \mathcal{R} , has been developed; it can, however, be evaluated in terms of the equilibrium separation, $z = z_e$, where the potential function has its maximum value. At $z = z_e$, $dP/dz = 0$; hence

$$\mathcal{R} = \frac{C_1 \frac{d}{dz} \sum_j s_{ij}^{-6} + C_2 \frac{d}{dz} \sum_j s_{ij}^{-8} + C_3 \frac{d}{dz} \sum_j s_{ij}^{-10}}{\frac{d}{dz} \sum_j s_{ij}^{-12}} \quad (6)$$

The derivatives in Equation 6 can be obtained in two ways. The summations may be plotted *vs.* z in the range bracketing the equilibrium separation, z_e , and the slopes found graphically; or these plots may be expressed by an empirical equation and the slopes obtained analytically. The latter method is more accurate, as an equation of the form

$$\sum_j s_{ij}^{-n} = az^{-b} \quad (7)$$

has been found to hold (1).

The method described above has been used by Avgul *et al.* (1) to calculate the dispersion interactions between a number of adsorbates and the cleavage surface of graphite. A prime disadvantage of the method of direct lattice sums, apart

from the laborious calculations, is the dependence of the answer on the lattice position above which the adsorbate molecule is situated (see Figure 1). For a mobile adsorbed film the proper procedure would be to find the weighted average interaction of all possible positions on the surface. In practice, only a few principal positions are ever worked out and a straight arithmetic average of the interactions for these positions would not be characteristic of the mobile molecule.

Figure 1 is a schematic diagram of an argon atom on the three principal positions of the basal plane of graphite: on top of a carbon atom, between two carbon atoms, and in the center of a ring. The results calculated by Avgul *et al.* (1) are reported for neon, argon, and krypton in Table I; we do not include a number of other calculations made by the same authors for polyatomic adsorbates, as the writers do not take into account the anisotropies of polarizability and magnetic susceptibility when calculating dispersion interactions for oriented molecules.

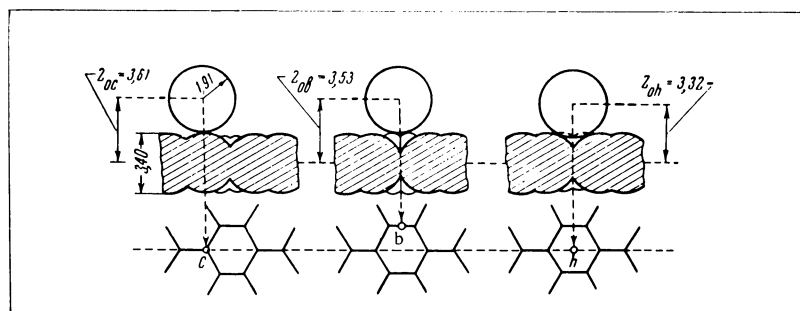


Figure 1. Argon atom in different positions relative to graphite substrate (1)

Drawn to scale

Table I. Calculated Values of ρP^{ads} by Equation 2 for Inert Gas Molecules Situated at Different Parts of Graphite Substrate

Adsorbent	(Kcal./mole)			Av.
	Above C Atom	Between Two C Atoms	Center of Ring	
Neon	0.77	0.84	1.11	0.91
Argon	1.95	2.07	2.64	2.22
Krypton	2.59	2.78	3.47	2.95

Crowell's Expression for Lattice Sum. THE ORIGINAL APPLICATION. Crowell (2) has shown how to evaluate the lattice sums, $\sum_j s_{ij}^{-n}$, for a layer-lattice structure by an analytical method. The lattice is approximated by a set of layer planes, each with a uniform distribution of matter, and separated by the interplanar distance, d . The lattice sum is approximated by integrating over the planes and forming the sum of the resulting terms. Let the adsorbate, at a distance z from the surface, be separated by a distance s_{ij} from any point in the m^{th} plane below the surface. The vertical distance of the adsorbate from this plane is $(z + md)$; let y be the projection of s_{ij} on the m^{th} plane. Then the summation of s_{ij}^{-n} for the m^{th} plane is

$$\sum_{j(m)} s_{ij}^{-n} = 2\pi\rho \int_0^\infty [(z + md)^2 + y^2]^{-n/2} y dy \quad (8)$$

where ρ is the number of atoms per unit area in the m^{th} plane. For the whole lattice the summation becomes

$$\sum_j s_{ij}^{-n} = \sum_{m=0}^{\infty} \sum_{j(m)} s_{ij}^{-n} = 2\pi\rho(n-2)^{-1}d^{2-n} \sum_{m=0}^{\infty} (x+m)^{2-n} \tag{9}$$

where $x = z/d$. The summation of $(x+m)^{2-n}$ is the generalized Riemann zeta function of x and $n-2$. These functions have been tabulated (4) as derivatives of $\Psi(x) = (d/dx)\ln(x!)$. The fundamental expansion of this expression for the k^{th} derivative of $\Psi(x)$ is

$$\Psi^k(x) = (-1)^{k+1} k! \sum_{m=0}^{\infty} (x+m)^{-k-1} \tag{10}$$

Equation 9 can now be written as

$$\sum_j s_{ij}^{-n} = \frac{2\pi\rho(-1)^n}{(n-2)d^{n-2}(n-3)!} \Psi^{n-3}(x) \tag{11}$$

The functions $\Psi^k(x)$ have been tabulated for values of k up to 4. For higher values of k the function must be calculated by Equation 10; fortunately one can neglect all but the first term of the series for $k > 4$, provided $x < 2$, as is commonly the case in adsorption calculations.

The concept, incorporated in this approximation, that matter is distributed continuously in each layer plane, while it might not be permissible for a localized adsorbed film, is actually close to the truth for a mobile adsorbed film, in which the rapid translation of the molecules along the surface prevents their responding to its fine structure. This approximation produces just the sort of average that is desired and is so difficult to obtain from the direct lattice sum.

Crowell (3) has used his lattice sum expression, Equation 11, to calculate the interaction of inert gases with graphite, assuming that the dispersion energy of attraction could be adequately accounted for by the dipole-dipole interaction only—i.e.,

$${}_0P = C_1 \sum_j s_{ij}^{-6} - R \sum_j s_{ij}^{-12} \tag{12}$$

Substituting Equation 11 for the lattice sums gives

$${}_0P = \frac{C_1 \pi \rho}{12d^4} \Psi^3(x) - \frac{R \pi \rho}{5z^{10}} \tag{13}$$

where, by Equation 6,

$$R = - \frac{C_1 d^6 x_e^{11}}{24} \Psi^4(x_e)$$

and

$$x_e = \frac{z_e}{d}; z_e = \frac{d}{2} + r_e$$

where r_e is the crystal radius of the adsorbate. Therefore,

$${}_0P = \frac{C_1 \pi \rho}{12d^4} \left[\Psi^3(x) + \left(\frac{z_e}{z} \right)^{10} \frac{x_e}{10} \Psi^4(x_e) \right] \tag{14}$$

Equation 14 is the analytical description of the potential well for this model; the maximum potential energy loss, or the depth of the well, is that value of ${}_vP$ (which we term ${}_vP^{\text{disp}}$) at which $z = z_e$ —i.e.,

$${}_vP^{\text{disp}} = \frac{C_1\pi\rho}{12d^4} \left[\Psi^3(x_e) + \frac{x_e}{10} \Psi^4(x_e) \right] \quad (15)$$

An advantage of having an analytic expression, such as Equation 14, for the potential well is that it can be used to estimate the vibrational frequency of the adsorbed molecule with respect to the surface. For vibrations of small amplitudes the system behaves as a harmonic oscillator for which the frequency is given by

$$\nu = \frac{1}{2\pi} \sqrt{\frac{\kappa}{m}} \quad (16)$$

where m is the mass of the adsorbate molecule and κ is the force constant defined by

$$\kappa = - \left(\frac{d^2{}_vP}{dz^2} \right)_{z \rightarrow z_e}$$

or

$$\kappa = \frac{1}{d^2} \left(\frac{d^2{}_vP}{dx^2} \right)_{x \rightarrow x_e}$$

Applied to Equation 14,

$$\kappa = - \frac{C_1\pi\rho}{12d^6} \left[\frac{120}{x_e^6} + \frac{11\Psi^4(x_e)}{x_e} \right] \quad (17)$$

A REFINED APPLICATION. Avgul *et al.* (1) have shown that the dipole-quadrupole and quadrupole-quadrupole terms in Equation 2 are not negligible, as was assumed by Crowell; nor are they cancelled by the repulsion term, as has been stated by de Boer (5). A more accurate result could, therefore be obtained by using all the terms in Equation 2 in conjunction with Crowell's expression for the lattice sums, Equation 11. Instead of Equation 13 we would now have:

$${}_vP = \frac{C_1\pi\rho}{12d^4} \Psi^3(x) + \frac{C_2\pi\rho}{3z^6} + \frac{C_3\pi\rho}{4z^8} - \frac{B\pi\rho}{5z^{10}} \quad (18)$$

where

$$B = - \frac{C_1d^6}{24} x_e^{11} \Psi^4(x_e) + C_2z_e^4 + C_3z_e^2$$

hence

$${}_vP = \frac{C_1\pi\rho}{12d^4} \left[\Psi^3(x) + \left(\frac{z_e}{z} \right)^{10} \frac{x_e}{10} \Psi^4(x_e) \right] + \frac{C_2\pi\rho}{z^6} \left[\frac{1}{3} - \frac{1}{5} \left(\frac{z_e}{z} \right)^4 \right] + \frac{C_3\pi\rho}{z^8} \left[\frac{1}{4} - \frac{1}{5} \left(\frac{z_e}{z} \right)^2 \right] \quad (19)$$

The depth of the potential well, ${}_vP^{\text{disp}}$, is given by Equation 19 by putting $z = z_e$; hence

$${}_vP^{\text{disp}} = \frac{C_1\pi\rho}{12d^4} \left[\Psi^3(x_e) + \frac{x_e}{10} \Psi^4(x_e) \right] + \frac{2}{15} \frac{C_2\pi\rho}{z_e^6} + \frac{1}{20} \frac{C_3\pi\rho}{z_e^8}$$

As before, the vibrational frequency of the adsorbed molecule with respect to the surface can be obtained by means of Equation 16. Applied to Equation 19,

$$\kappa = - \frac{C_1\pi\rho}{12d^6} \left[\frac{120}{x_e^6} + \frac{11\Psi^4(x_e)}{x_e} \right] + \frac{7C_2\pi\rho}{z_e^8} + \frac{4C_3\pi\rho}{z_e^{10}} \quad (20)$$

The Lattice Treated as a Continuum

A rough approximation of the lattice sums is made by treating the lattice as a continuum by integrating, rather than summing, the s_{ij}^{-n} terms in Equation 1—i.e., by writing

$${}_oP = \rho_v \iiint P_{ij} dV \quad (21)$$

where the integration is over a semi-infinite volume and ρ_v is the number of adsorbent atoms per cubic centimeter. Using the terms in s_{ij}^{-6} and s_{ij}^{-12} only, since we are already approximating so much, we get

$${}_oP = \frac{C_{1\pi\rho_v}}{6z_e^3} \left[\left(\frac{z_e}{z}\right)^3 - \frac{1}{3} \left(\frac{z_e}{z}\right)^9 \right] \quad (22)$$

which was obtained by evaluating the repulsion coefficient as before from the condition that at $z = z_e$, $dP/dz = 0$. The expression for ${}_oP^{\text{disp}}$ for this model is

$${}_oP^{\text{disp}} = \frac{C_{1\pi\rho_v}}{9z_e^3} \quad (23)$$

For evaluating the vibrational frequency of the adsorbed molecule with respect to the surface, this model yields, by Equation 16

$$\kappa = \frac{3C_{1\pi\rho_v}}{z_e^5}$$

hence

$$\nu = \frac{3\sqrt{3}}{2\pi z_e} \sqrt{\frac{{}_oP^{\text{disp}}}{m}} \quad (24)$$

Calculations of Dispersion Potentials by Various Models for Inert Gases Adsorbed by Graphite

We have developed general expressions in the preceding sections for the calculation of the dispersion potential contribution to the potential energy for adsorption and for the vibrational frequency of the adsorbed molecule, using various expressions for the lattice sums. We now propose to apply these equations, for the purpose of comparison with experiment, to the adsorption of the inert gases by graphite.

In the preceding paper (9) we quoted the observed values of the isosteric heats of adsorption of neon, argon, krypton, and xenon on P33 (2700°) graphite, as well as corresponding values of U_0' and ν obtained from a kinetic-molecular model of the adsorbed film. From these latter quantities we can derive the depth of the adsorption potential well, given by

$${}_oP^{\text{ads}} = U_0' + \frac{1}{2} N h \nu \quad (25)$$

The adsorption potential contains contributions from two sources: dispersion interactions, and a potential that is due to the electrostatic interaction of the induced dipole of the adsorbate molecules with the surface electric field—i.e.,

$${}_oP^{\text{ads}} = {}_oP^{\text{disp}} + {}_oP^{\text{elec}} \quad (26)$$

where

$${}_oP^{\text{elec}} = \frac{1}{2} F^2 \xi \quad (27)$$

F and ξ being the surface of the adsorbent and the polarizability of the adsorbate, respectively. The surface field of graphite is about 1.2×10^5 e.s.u. per

sq. cm. as determined from adsorption isotherms of polar molecules (8) and we use this value in Equation 27 to calculate ${}_gP^{\text{elec}}$ for each of the inert gases. The results are reported in the first line of Table III. The parameters involved in the calculation of the dispersion potentials of the inert gases on graphite are reported in Table II. The observed values of ${}_gP^{\text{disp}}$ and ν , calculated by Equation 26, are compared in Table III with the results calculated using the various expressions for dispersion potentials and frequencies discussed above. The best agreement (and an excellent one) between observation and theory is given by the use of Equations 19 and 20, based on the refined application of Crowell's approximation for the direct lattice sum.

Table II. Parameters Involved in Calculating Dispersion Potentials of Inert Gases on Graphite

	Carbon	Neon	Argon	Krypton	Xenon
r_e , A.	1.70	1.59	1.91	2.01	2.25
z_e , A.	...	3.29	3.61	3.71	3.95
$\chi \times 10^{30}$, cc.	10.5	12.0	32.2	46.5	71.5
$\xi \times 10^{24}$, cc.	0.937	0.398	1.63	2.48	4.00
$C_1 \times 10^{45}$, kcal. mole ⁻¹ cm. ⁶	...	0.214	0.77	1.15	1.82
$C_2 \times 10^{60}$, kcal. mole ⁻¹ cm. ⁸	...	0.026	0.104	0.157	0.252
$C_3 \times 10^{76}$, kcal. mole ⁻¹ cm. ¹⁰	...	0.04	0.17	0.31	0.43

Table III. Observed and Calculated Values of Dispersion Potentials (${}_gP^{\text{disp}}$) and Vibrational Frequencies for Inert Gases Adsorbed by Graphite

	Related Equation No.	Neon	Argon	Krypton	Xenon
${}_gP^{\text{elec}}$, kcal./mole	(27)	0.043	0.180	0.256	0.415
${}_gP^{\text{ads}}$, kcal./mole	Observed	0.737	2.12	2.80	3.69
${}_gP^{\text{disp}}$, kcal./mole	Observed	0.694	1.94	2.54	3.28
$\nu \times 10^{-12}$, sec. ⁻¹	Observed	1.19	1.28	1.00	0.85
${}_gP^{\text{disp}}$	(2)	0.91	2.22	2.95	...
${}_gP^{\text{disp}}$	(15)	0.729	1.84	2.48	3.11
$\nu \times 10^{-12}$	(17)	1.16	1.20	0.93	0.78
${}_gP^{\text{disp}}$	(19)	0.764	1.92	2.59	3.22
$\nu \times 10^{-12}$	(20)	1.20	1.23	0.96	0.80
${}_gP^{\text{disp}}$	(23)	0.23	0.64	0.88	1.2
$\nu \times 10^{-12}$	(24)	0.55	0.60	0.47	0.40

Acknowledgment

The authors gratefully acknowledge a grant in aid of these researches from the Esso Research and Engineering Co.

Literature Cited

- (1) Avgul, N. N., Kiselev, A. V., Lygina, I. A., Poschkus, D. P., *Izvest. Akad. Nauk S.S.S.R., Otdel. Khim. Nauk* **1959**, 1196.
- (2) Crowell, A. D., *J. Chem. Phys.* **22**, 1397 (1954).
- (3) *Ibid.*, **26**, 1407 (1957).
- (4) Davis, H. T., "Tables of Higher Mathematical Functions," Vol. 2, Principia Press, Bloomington, Ind., 1933.
- (5) de Boer, J. H., *Advances in Colloid Sci.* **3**, 1-66 (1950).
- (6) Gundry, P. M., Tompkins, F. C., *Trans. Faraday Soc.* **56**, 846 (1960).
- (7) Lennard-Jones, J. E., Dent, B. M., *Ibid.*, **24**, 92 (1928).
- (8) Ross, S., Machin, W. D., unpublished results.
- (9) Ross, S., Olivier, J. P., *ADVANCES IN CHEM. SER.*, No. 33, 301 (1961).

RECEIVED May 9, 1961.

On Physical Adsorption

XV. Evidence of Marked Asymmetry in the Distribution of Adsorptive Potentials of Certain Solid Surfaces

SYDNEY ROSS, J. P. OLIVIER, and J. J. HINCHEN

*Department of Chemistry,
Rensselaer Polytechnic Institute, Troy, N. Y.*

The interpretation of adsorption isotherms in terms of a surface displaying a symmetrical (Gaussian) distribution of adsorptive potentials to the adsorbate has been successfully applied to a number of systems; but marked exceptions have been found, particularly with crystals that were selected as likely to have completely homotactic surfaces. These exceptional adsorption isotherms are readily interpreted, however, as the result of a sum of two, or occasionally three, distinctly different Gaussian distributions, presumably deriving from the same number of surface constituents. Among these constituents the expected homotactic substrate, which is associated with a particular crystal face, can always be identified.

A previous paper of this series (13) describes the analysis of adsorption isotherms for heterogeneous surfaces in terms of a Gaussian distribution of adsorptive potentials. The distribution of adsorptive potential energies may not, however, have a form that is symmetrical about a mean; it could possess enough asymmetry so that the adsorption isotherm could not be described by a model that assumed a Gaussian distribution.

Imagine, for example, an otherwise uniform surface that is contaminated by a small amount of a nonvolatile impurity of higher adsorptive potential. The adsorption isotherms of a gas on this substrate would show a small "knee" at the low-pressure end of the isotherm, thereby indicating the presence of the impurity. The shape of the isotherm would be the same whether we consider the impurity as a coating on a part of the surface of the major constituent or as a mechanically separate ingredient of the mixture. We could, therefore, account for such an isotherm by assigning separately to each of the surfaces its own values of the adsorption parameters V_β , γ , and K' . By doing so we are actually describing substrates of non-Gaussian adsorptive energy distributions in terms of a sum of Gaussian distributions.

Although not described quite in this way, a number of adsorbents have been reported to be effectively mixtures of two surfaces. The most clear-cut example is a slightly oxidized graphite surface for which the adsorption isotherm of water vapor shows a pronounced knee whose height varies with the degree of oxidation of the surface; reducing the surface with hydrogen eliminates the knee (7, 10). The great dissimilarity of the adsorptive potentials of the two surfaces for the polar water molecule makes it obvious to the eye that two distinct adsorbing surfaces are present. Molybdenum disulfide, most samples of which have a partially oxidized surface, is another example (1, 2). The adsorption isotherms of argon and nitrogen on boron nitride show a similar knee, though to a much less marked extent; it is, in fact, visible only when the low pressure portion is plotted on an expanded scale as was done by Winkler (16). The presence of a trace of boron oxide in the sample was detected by wet analysis; the prominence of the initial concavity of the isotherm to the pressure axis was found to relate to the amount of oxide contaminant in the boron nitride.

The surface of a solid is rarely smooth but is interrupted by cracks, crevices, capillaries, cavities, corners, and edges. Even on a molecular scale roughness is frequently introduced by lattice disorder or spiral dislocations. The utmost effort to obtain completely homotactic substrates has not yet succeeded in avoiding residual inhomogeneities. When graphite has a chemically pure adsorbing surface, the inhomogeneity has the form of a symmetrical distribution about a mean (13); the mean is representative of the basal plane of the graphite lattice. This type of random distribution presumably arises from the factors that disturb the geometrical smoothness of the surface. For oxidized graphite, molybdenum disulfide, and boron nitride the asymmetry of the distribution curve has been traced to the simultaneous presence of two chemically different adsorbing surfaces, each presumably with its own random distribution of adsorptive energies. In general, we may consider each chemically distinct adsorbing surface that is present in a mass of adsorbent to have its individual random distribution of adsorptive energies; this applies whether the chemical difference rises from different surface planes of the

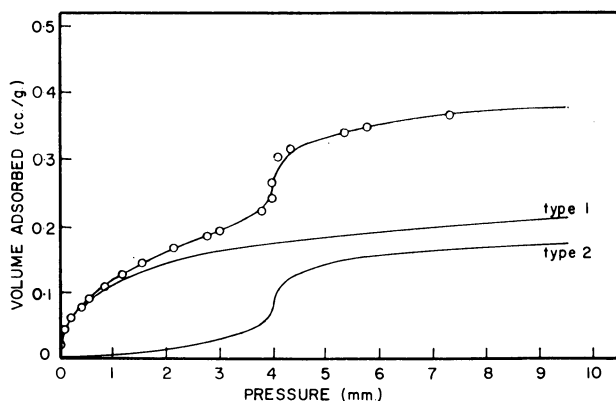


Figure 1. Adsorption isotherm of argon on cadmium bromide at 77.5° K

Two lower curves are theoretical isotherms for two surface constituents

— Sum of two theoretical curves

○ Experimental points

same crystal, surface contamination, oxide, hydroxide, or other surface compounds, or even gross admixture of other chemical substances.

Cadmium Bromide

The adsorption isotherm of argon at 77.5° K on cadmium bromide is shown in Figure 1. This adsorption isotherm shows characteristics that are indicative of

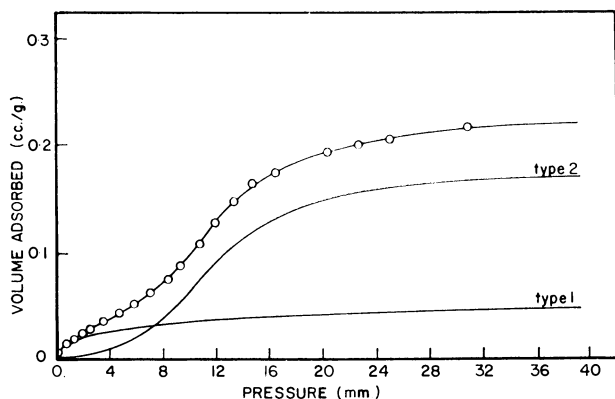


Figure 2. *Adsorption isotherm of argon on sodium bromide at 77.5° K*

Two lower curves are theoretical isotherms for two surface constituents

— Sum of two theoretical curves
 ○ Experimental points

both low and high degrees of heterogeneity. The latter is indicated by the concave shape of the isotherm with respect to the pressure axis and the former by the sigmoidal shape at higher pressures. No one of the model adsorption isotherms, such as those shown in Figure 2 of (13), possesses both those features.

Using the tables of model isotherms (8, 14) and a process of trial and error, the experimental isotherm shown in Figure 1 can be described quantitatively by a dual distribution of adsorptive energies. We have no information concerning the surface electric field of cadmium bromide and therefore used the tables calculated for $2 \alpha^{id}/RT \beta^{id} = 6.5$, where $\alpha^{id}/\beta^{id} = a/2b$, and a and b are the van der Waals constants for argon gas. The two model isotherms ultimately obtained are referred to as type 1 and type 2 in Figure 1; their sum provides a satisfactory match with the experimental points, which are indicated by circles. The adsorption parameters for each of the two surfaces are reported in Table I; the numerical values would be slightly different were the magnitude of the surface field known and taken into account. The two surface constituents are: first, a relatively heterogeneous surface ($\gamma = 3$) with an average adsorptive energy, U' (calculated), of 1.76 kcal. per mole, which is present as 59% of the total surface; second, an essentially homotactic surface with an adsorptive energy, U' (calculated), of 1.65 kcal. per mole, present as 41% of the total surface.

The adsorbent was chosen purposefully as one likely to give a near-homotactic surface, because of the hexagonal layer-lattice structure of the crystal; the surface constituent of low heterogeneity is therefore identified with the basal plane of

cadmium bromide, consisting of close-packed bromine atoms. The cadmium bromide was prepared by dehydration of the tetrahydrate and the second surface constituent could perhaps be cadmium hydroxide, formed by surface hydrolysis. To test this supposition, a sample of finely divided cadmium bromide was prepared under anhydrous conditions, by subliming the material in a stream of dry argon and collecting the particles on a microporous filter. Care was taken to preserve the sample from contact with anything but argon. Detailed information about the method of preparation will be published elsewhere. The adsorption isotherm of argon at 77.5° K on this substrate then showed only the characteristic—i.e., the same value of K' —of the type 2 surface; almost all evidence of type 1 was lacking. This result confirms the truth of our analysis of the surface into two distinct distributions, one of which, the more heterogeneous, is probably the result of surface hydrolysis.

Sodium Bromide

Cube crystals of sodium bromide have the same lattice plane—i.e., $\{100\}$ —on all faces. Such crystals have often been favorite candidates for the preparation of a completely homotactic adsorbent, and the assumption has always been made that the heterogeneity of the resulting surface is negligible. No definite criteria have hitherto been available to check this assumption. In Figure 2 we report the argon adsorption at 77.5° K on a specimen of sodium bromide, prepared according to the directions given by Fisher and McMillan (6). The shape of the isotherm is itself sufficient in the light of the present reasoning to indicate a dual distribution of adsorptive energies. A quantitative description of the isotherm in these terms has been obtained by a process of trial and error using $2\alpha^{\text{id}}/RT \beta^{\text{id}} = 6.5$, and is shown in Figure 2; the adsorption parameters are reported in Table I. The surface has two constituents, one of high and the other of low degree of heterogeneity, as was the case with the cadmium bromide described previously. Of the total surface, 75% consists of a near-homotactic constituent ($\gamma = 200$), which presumably derives from the $\{100\}$ planes of the crystal; this portion of the surface has a relatively low average argon adsorptive energy U' (calculated) of 1.49 kcal. per mole. The remaining 25% of the surface has a wide distribution ($\gamma = 3$) of adsorptive energies, with the average U' (calculated) at 1.59 kcal. per mole. Once again, chemisorbed water may well be the source of the second surface constituent.

Table I. Adsorption Parameters of Argon Adsorbed at 77.5° K.

	V_{β} , Cc./G.	γ	K'	U' (Calcd.), Kcal./Mole
Dual Surface of Cadmium Bromide				
Type 1	0.37	3	20.6	1.76
Type 2	0.26	∞	42.1	1.65
Dual Surface of Sodium Bromide				
Type 1	0.080	3	61.6	1.59
Type 2	0.24	200	120	1.49

A verification of the interpretation of the surface of sodium bromide, when prepared under usual conditions, as a dual distribution is again provided by a new preparation under anhydrous conditions of a sample of the sublimed crystals, which when used as an adsorbent shows evidence of type 2 surface only. The

adsorption of argon at 77.5° K by these crystals is shown in Figure 3. The whole isotherm is described by the same values of K' and γ that are reported in Table I for the type 2 surface of sodium bromide. The surface area of the new preparation is much greater than that of the sample reported in Table I.

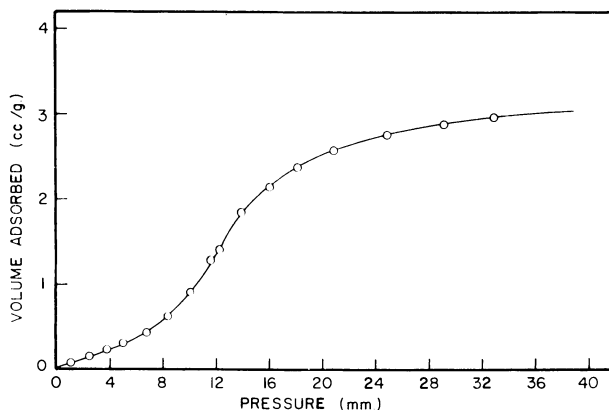


Figure 3. Adsorption isotherm of argon on anhydrous preparation of sodium bromide at 77.5° K

— Theoretical isotherm corresponding exactly to that labeled type 2 in Figure 2
○ Experimental points

Other Examples from Previously Reported Data

The shape of the isotherm in Figure 2 resembles all those reported for the alkali halides as adsorbents, as well as other inorganic salts that were prepared in attempts to procure near-homotactic substrates. Examples are the sodium chloride of Orr (9) and those of Ross and coworkers (11, 12, 15), the potassium chloride of Clark (3), the calcium fluorides of Edelhoeh and Taylor (5) and Ross and Winkler (15), and the sodium bromide of Fisher and McMillan (6). A part of the surface (type 2) of each of the adsorbents was sufficiently homotactic to allow two-dimensional phase transitions to manifest themselves on lowering the temperature of adsorption, as near-discontinuities in the isotherms; if these portions of the surface had any other than a very narrow range of adsorptive potentials, the phase transitions would occur over too wide a range of pressure to be identified as such. On the type 1 part of these surfaces, phase transitions cannot be identified because of the great heterogeneity of this part of the substrate.

Ross and Boyd (11) prepared crystals of sodium chloride in which both the {100} and the {111} surfaces were developed; the adsorption isotherm of ethane at 90.1° K gave evidence of two type 2—i.e., near-homotactic—surfaces, as well as showing the initial knee, which is evidence of a type 1 surface. This isotherm is shown in Figure 4, which also includes for comparison an ethane isotherm measured at the same temperature for a sodium chloride adsorbent that had only {100} faces developed; the pressure characteristic of the phase transition of ethane on the homotactic {100} surface of sodium chloride at 90.1° K shows on both isotherms as the location of a discontinuity at $p = 4.5 \times 10^{-3}$ mm.; the homotactic {111} portion of the surface is responsible for the convex shape (with respect to the pressure axis) of the isotherm beyond the “knee,” though the rise is not suffi-

ciently pronounced to be described as another discontinuity. The evidence is almost enough to determine relative magnitudes of the surface fields and the adsorptive potentials of the $\{111\}$ and $\{100\}$ crystal faces. The absence of a phase change on the $\{111\}$ faces is probably genuine; though enough heterogeneity in the characteristic distribution associated with those faces could, even if a phase change were to occur, dissolve the evidence. Supposing the two crystal faces to have been equally well developed, however, as indeed was indicated by the appearance of the crystals in the microscope, the two-dimensional phase change of ethane on the $\{100\}$ and its absence on the $\{111\}$ faces show that the former substrate has the weaker surface field. Furthermore, the relative pressures at which the two crystal faces make themselves manifest in the adsorption isotherm—i.e., lower pressure for $\{111\}$ than for $\{100\}$ —are evidence of a smaller adsorptive potential for the $\{100\}$ faces.

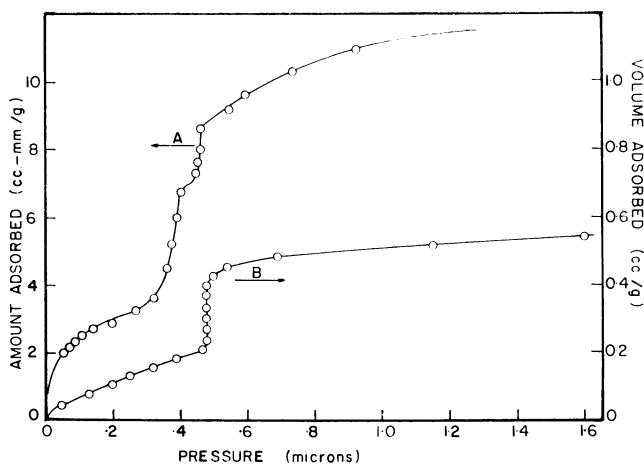


Figure 4. Adsorption isotherm of ethane on sodium chloride at 90.1° K

A. Adsorbent as prepared displayed both $\{100\}$ and $\{111\}$ faces. Data of Ross and Boyd (11)

B. Adsorbent as prepared displayed only $\{100\}$ faces. Data of Ross and Winkler (15)

Surface Electric Field

The surface field of a near-homotactic surface can be estimated from the observed value of the two-dimensional critical temperature ${}_aT_c$. According to de Boer (4),

$$\frac{\alpha}{\alpha^{\text{id}}} = \frac{{}_aT_c}{{}_aT_c^{\text{id}}} \quad (1)$$

where α and ${}_aT_c$ refer to the observed two-dimensional van der Waals interaction constant and the observed two-dimensional critical temperature, respectively; the same symbols with the superscript id refer to the ideal values of these quantities; and

$$\lambda = \alpha - \alpha^{\text{id}} = -\frac{\pi\mu^2}{d} \quad (2)$$

where μ is the dipole induced on the adsorbate by the electric field, F , of the substrate, and d is the diameter of the adsorbed molecule. The induced dipole is related to the surface field by

$$\mu = F\xi \quad (3)$$

where ξ is the polarizability of the adsorbate. Hence

$$F = \frac{1}{\xi} \left[\frac{\alpha^{\text{id}} d}{\pi} \left(1 - \frac{aT_c}{aT_c^{\text{id}}} \right) \right]^{1/2} \quad (4)$$

In spite of the presence of the type 1 part of the surface, one can frequently estimate the two-dimensional critical temperature of the phase transition, provided that the type 2 part of the surface is uniform enough to make the transition manifest. Thus we can use this procedure, for example, with the supra- and sub-critical isotherms of methane, ethane, and xenon adsorbed by the $\{100\}$ face of sodium chloride, published by Ross and Clark (12). Using estimates of aT_c from these data in Equation 4 yields a value for the surface field of $F = 1.5 \pm 0.5 \times 10^5$ e.s.u. per sq. cm.; the poor precision of the result is due to the difficulty of interpolating the temperature of the critical isotherm by eye. The surface field of the $\{100\}$ face of sodium bromide can be estimated in a similar way, using the data of Fisher and McMillan (6) for the adsorption of methane and krypton. The result for the surface field is again between 1 and 2×10^5 e.s.u. per sq. cm.

A better estimate of the surface field of the $\{100\}$ face of sodium bromide can be made from the argon isotherm reported in Figure 2 by assuming that the type 2 part of the surface is actually much closer to homotactic than would be indicated by a γ value of 200; since this value had been assigned on the basis of no surface field, the assumption that it is actually higher is well justified. If we now put $\gamma > 1000$ for the type 2 surface, we find on refitting it to the model isotherms that $2\alpha/RT\beta = 5.7$, rather than the previously assumed ideal ratio of 6.5. Assuming $\beta = \beta^{\text{id}}$ for argon, we calculate the induced dipole to be 0.24 debye and the surface field to be 1.4×10^5 e.s.u. per sq. cm. The same result is derived from the argon adsorption isotherm for the sodium bromide prepared under anhydrous conditions (Figure 3).

For potassium chloride, Clark (3) observed phase transitions to take place at temperatures lower than on a sodium chloride substrate. We deduce that the surface field of potassium chloride is greater than that of sodium chloride or sodium bromide.

The configuration of ionic surfaces at which both positive and negative ions are present does not lead to the concept of a uniform surface field expressible by a single number, but rather to a field fluctuating from point to point along the surface. This varying field induces varying dipoles in the adsorbed molecules and the average component of these dipoles normal to the surface is the quantity that we calculate from the observed lowering of α^{id} or aT_c^{id} . When we use Equation 4 for such a surface, we are calculating the equivalent uniform surface field that, if it were actually present, would cause the observed effects.

Acknowledgment

The authors gratefully acknowledge grants in aid of these researches from Esso Research and Engineering Co., Linden N. J., and the donors of The Petroleum Research Fund, administered by the American Chemical Society.

Literature Cited

- (1) Ballou, E. V., Ross, S., *J. Phys. Chem.* **57**, 653 (1953).
- (2) Cannon, P., *Ibid.*, **64**, 858 (1960).
- (3) Clark, H., Ph.D. thesis, Rensselaer Polytechnic Institute, 1954.
- (4) de Boer, J. H., "The Dynamical Character of Adsorption," p. 155, Clarendon Press, Oxford, 1953.
- (5) Edelhoch, H., Taylor, H. S., *J. Phys. Chem.* **58**, 344 (1954).
- (6) Fisher, B. B., McMillan, W. G., *J. Chem. Phys.* **28**, 549, 555, 563 (1958).
- (7) Millard, B., Caswell, E. G., Leger, E. E., Mills, D. R., *J. Phys. Chem.* **59**, 976 (1955).
- (8) Olivier, J. P., Ph.D. thesis, Rensselaer Polytechnic Institute, 1960.
- (9) Orr, W. J., *Proc. Roy. Soc. (London)* **173A**, 349 (1939).
- (10) Pierce, C., Smith, R. N., Wiley, J. W., Cordes, H., *J. Am. Chem. Soc.* **73**, 4551 (1951).
- (11) Ross, S., Boyd, G. E., U. S. At. Energy Comm., **MDDC864** (1947).
- (12) Ross, S., Clark, H., *J. Am. Chem. Soc.* **76**, 4291, 4297 (1954).
- (13) Ross, S., Olivier, J. P., *J. Phys. Chem.* **65**, 608 (1961).
- (14) Ross, S., Olivier, J. P., "On Physical Adsorption," Interscience, New York, in preparation.
- (15) Ross, S., Winkler, W., *J. Am. Chem. Soc.* **76**, 2637 (1954).
- (16) Winkler, W., Ph.D. thesis, Rensselaer Polytechnic Institute, 1955.

RECEIVED May 9, 1961.

The Effect of Lateral Interaction on Monolayer Adsorption

J. G. ASTON, E. S. J. TOMESKO, and HAKZE CHON

*Cryogenic Laboratory, College of Chemistry and Physics,
The Pennsylvania State University, State College, Pa.*

On a smooth surface rare gas molecules interact laterally according to a two-dimensional van der Waals equation. This equation can be used to calculate the lateral interaction energy on the smooth part of a heterogeneous surface. When the lateral interaction energy is thus taken into account, a reasonable model of a heterogeneous surface can be used to calculate an adsorption isotherm in good agreement with experiment. Partial molal enthalpies (differential heats) of adsorption can be calculated on the same basis. For the first time reasonable agreement with experiment is obtained.

Some time ago it was demonstrated conclusively that high heats of adsorption were due to many-sided sites on the surface of the adsorbant (5). Previously attempts to predict differential heats of adsorption and the detailed nature of the isotherm up to a monolayer had had only indifferent success (2). It was, however, suggested that the real difficulty lay in the inability to treat lateral interaction on a heterogeneous surface (2).

Recently a surprisingly simple method for doing this has become available. As a result, the situation with regard to predicting differential heats of adsorption and isotherms up to a monolayer on the basis of a simple model is now more encouraging. This paper demonstrates to a first approximation what the nature of the lateral interaction energy is, and how to allow for this with a reasonable degree of accuracy.

Lateral Interaction on a Smooth Surface

It can be demonstrated that the molal integral lateral interaction energy on a completely smooth surface is given by the equation

$$\tilde{E}_1 = -\frac{a}{2b}\theta \quad (1)$$

where a and b are the van der Waals constants, θ is the coverage, and \tilde{E}_1 is the molal interaction energy (1). Figure 1 shows graphs of the differential heats of

adsorption of neon, argon, and krypton which have been analyzed previously (1) on graphitized carbon plotted against the coverage. Figure 2 is a graph of the heats of adsorption of argon on a single crystal of zinc (3) plotted against coverage.

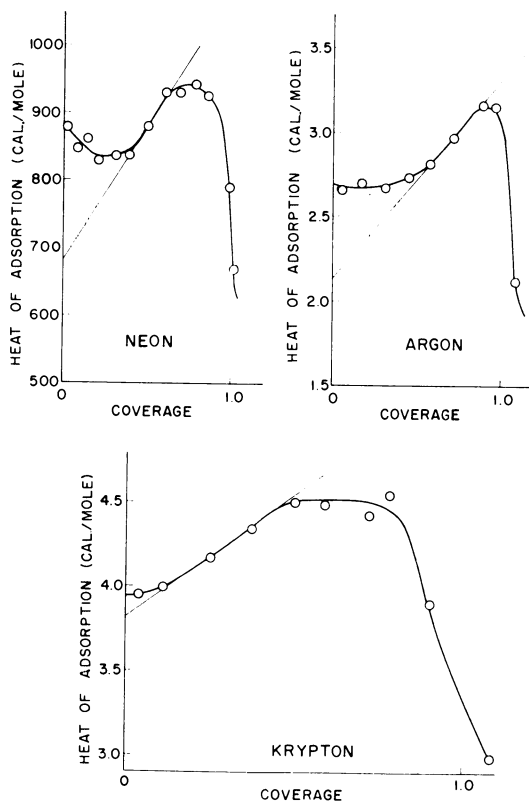


Figure 1. Heats of adsorption of neon, argon, and krypton on graphitized carbon black

The graphs for the three rare gases on graphitized carbon clearly show the effect of a small amount of heterogeneity at low coverages in increasing the differential heats of adsorption. The graph for argon on zinc shows less of this effect, probably since the work was done on a single crystal. An inspection of the graph on zinc indicates that the tangent drawn at the point of inflection has a slope which corresponds to the formula

$$\bar{E} = 1100 \theta \quad (2)$$

for the differential heat of lateral interaction. The value of a/b for argon is $1020 \text{ cal. mole}^{-1} \text{ cm}^{-2}$. The deviation of this graph from a straight line at low coverages is due either to a failure of the formula at low surface concentrations or to some surface effects of the single crystal. Rhodin estimates that about 10% of the surface is rough. In view of this it seems natural to draw similar tangents on graphs of the differential heats of adsorption *vs.* coverage for the rare gases on graphite at the point where the curves have the maximum slope. These tangents are drawn in Figure 1. When this is done, the slopes are very closely equal to

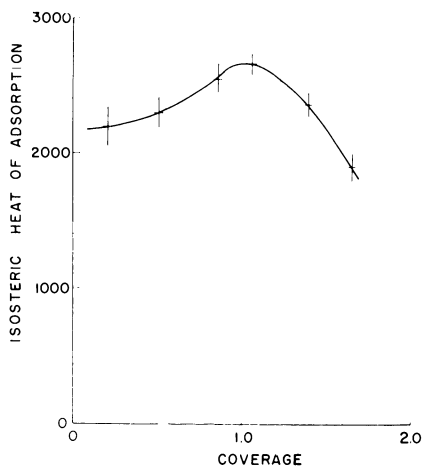


Figure 2. Heats of adsorption of argon on single crystals of zinc

the value of the ratio a/b for all three rare gases, as can be seen from Table I. In all four graphs the differential heats of adsorption fall sharply at the monolayer. Part of this sharp fall is due to a compressive effect of the molecules in the second layer which tend to reduce the lateral interaction. The evidence just given that the energy of lateral interaction on a smooth surface is given by Equation 1 is sufficiently strong to justify the application of this formula to the smooth parts of a heterogeneous surface. The effect of the sites other than on the flat surface is obviously to isolate the molecules and prevent lateral interaction. Thus it is hard to imagine a molecule on a three-sided site having much opportunity to interact with other adsorbed molecules. Thus allowance for the effect of lateral interaction was made in the fraction of molecules located on the one- and two-sided sites. This device has been used in what follows. There is no physical significance whatever to such a procedure and it might be better to neglect entirely the lateral interaction for all molecules not on the flat surface.

Table I. Measured and Theoretical Energy of Lateral Interaction

	$E_1/\theta,$ Max., Cal./Mole	$a/b,$ Cal./Mole
Helium	105 ^a	35
Neon	360	300
Argon	1160	1005
Krypton	1400	1410

^a From data of (7).

Heterogeneous Surfaces

In Figure 3 is presented a graph of the differential heat of adsorption of helium vs. coverage on a titanium dioxide surface which has been covered with various amounts of argon (5). It is evident that at 6/10 of a monolayer of argon the differential heat of adsorption of helium on the surface is essentially constant over the surface. This is because the lateral interaction energy of helium is small, as can be seen from the value of a/b . There is very little doubt on the basis of the

data in this figure that the high heats of adsorption at low coverages are due to many-sided sites. The heat of adsorption of helium on titanium dioxide where no argon has been added is also shown in Figure 3. This graph is a clear indication of the heterogeneity of the bare surface. An attempt has been made to calculate the adsorption isotherm and the curve for differential heat of adsorption against coverage for neon on the surface of the same sample of titanium dioxide (rutile).

The model adopted was essentially that used previously for adsorption on a heterogeneous surface (2), modified by the addition to the energy of the one- and two-sided sites of a term dependent on the coverage of the site which would allow for the lateral interaction energy.

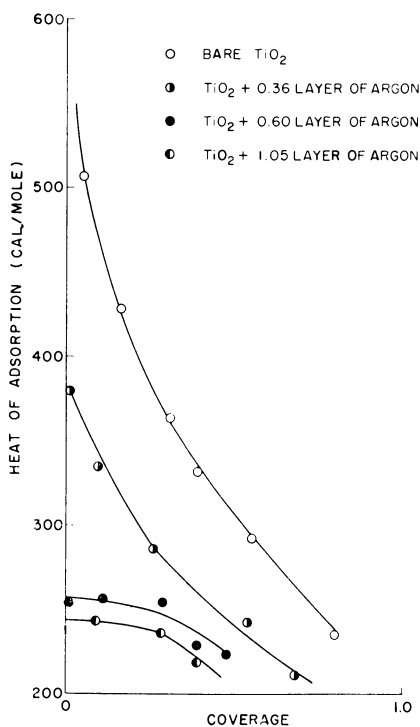


Figure 3. Helium heats of adsorption on titanium dioxide covered with various amounts of argon

The equations used for calculating the isotherms and the differential heats of adsorption were those used previously (2). Only four types of sites were used with energies ϵ_1 , ϵ_2 , ϵ_3 , and ϵ_4 , respectively, because of interaction with the adsorbent alone such that

$$\epsilon_4 = 4\epsilon_1, \epsilon_3 = 3\epsilon_1, \epsilon_2 = 2\epsilon_1, \epsilon_1 = 300 \text{ cal. per mole} \quad (3)$$

These sites correspond roughly to the flat surface and two-, three-, and four-sided sites, respectively. Molecules adsorbed on the flat surfaces and two-sided sites are assumed to have energy due to mutual lateral interaction, in addition to ϵ_1 and ϵ_2 , respectively, given on a molal basis by Equation 1. The value of θ used is the

fraction of the surface covered by the flat surface and the two-sided sites together. On the three- and four-sided sites lateral interaction was neglected. Thus, on a molal basis the energies of adsorption per molecule for one- and two-sided sites, are, respectively, $-(\epsilon_1 + a\theta_i/2b)$ and $-(\epsilon_2 + a\theta_i/2b)$ while for three- and four-sided sites they were simply $-\epsilon_3$ and $-\epsilon_4$, respectively. This choice assumes that the two-sided sites surround flat areas, making a single area in which all molecules interact equivalently.

The equations of Aston, Tykodi, and Steele thus become

$$\theta = F_i\theta_i = \sum_{i=1}^{i=4} F_i/1 + p^{-1}f(T) \exp - (\epsilon_i + g_i\theta_i a/2b)/RT \quad (4)$$

$$\bar{Q} = \sum_{i=1}^{i=4} iZ_i\theta_i(\epsilon_i + g_i\theta_i a/2b + RT) \quad (5)$$

$$q_{st} = \frac{\partial N\bar{Q}}{\partial N} = \bar{Q} + N \frac{\partial \bar{Q}}{\partial N} \quad (6)$$

where N is the total number of moles adsorbed on the surface and \bar{Q} is the total heat content (relative to the vapor phase) of that quantity of surface which contains one mole. The other quantities used in the equations are $g_1 = 1$, $g_2 = 1$, $g_3 = 0$, and $g_4 = 0$, $f(T) = (2\pi mkT)^{3/2} kT/h^3$, Z_i = number of sites of the i th kind, and Z = total number of sites. θ_i is the fraction of the part of the total sites assigned to ϵ_1 and ϵ_2 .

For multilayer adsorption these equations become

$$\bar{Q} = \sum_{i=1}^{i=4} c_i X F_i / (1 + c_i X - X)(1 - X) = \sum_{i=1}^{i=4} F_i \theta_i \quad (7)$$

$$\bar{Q} = -N^{-1} [N_0 \Delta H_0 - \sum_{i=1}^{i=4} i Z_i \theta_i (\epsilon_i + g_i \theta_i a / 2b + RT)] \quad (8)$$

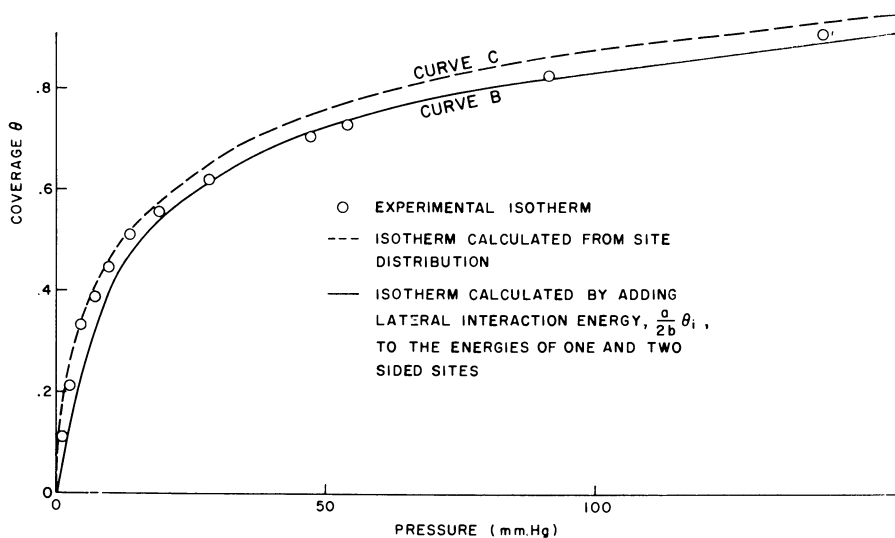


Figure 4. Isotherm for neon on titanium dioxide at 30° K

where $c_i = \exp \epsilon_0 - (\epsilon_i + g_i \theta_i a/2b)$, ΔH_0 is the molar heat of liquefaction of the bulk liquid, N_0 is the number of molecules with energy $-\epsilon_0$, X is the relative pressure p/p_0 , and N_i is the number of molecules with energy $-\epsilon_i$. The isotheric heat is given by Equation 6.

A site distribution assuming no lateral interaction was determined using Steele's method (4) for neon on titanium dioxide. The site energies and distribution are given in Table II (columns 3 and 5). With this site distribution, Equations 2.3 and 3.6 of Aston, Tykodi, and Steele (2) were used to calculate the isotherm and differential heats of adsorption for neon on titanium dioxide which already has been treated by Aston, Tykodi, and Steele. Table II (columns 2 and 4) also gives the site distribution of Aston, Tykodi, and Steele. In Figure 4,

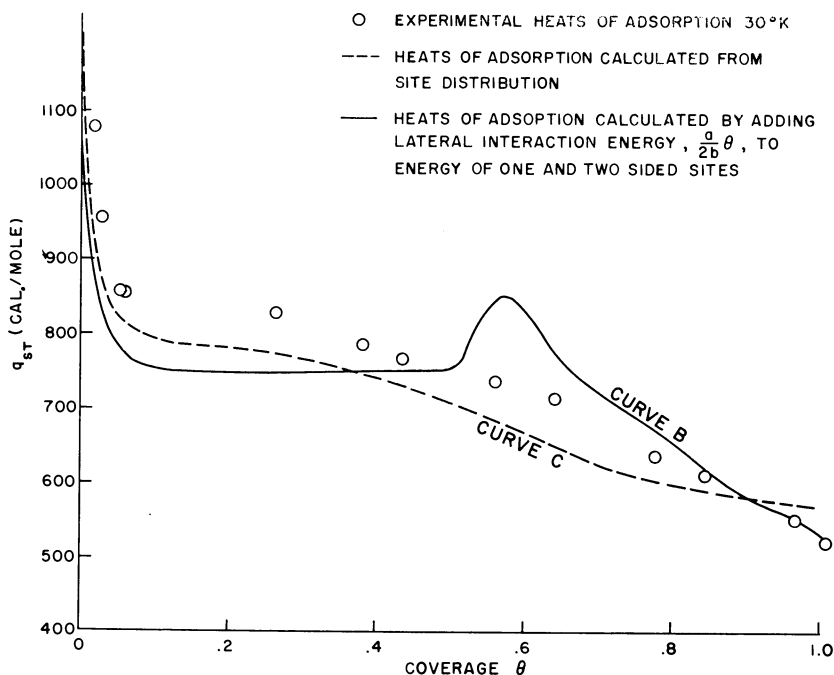


Figure 5. Heat of adsorption for neon on titanium dioxide at 30° K

the isotherm, curve C, was calculated on the basis of the derived site distribution of Table II (column 5) and the energies in Table II (column 3) assuming no lateral interaction energy contribution. The experimental points are circles. In Figure 5, the differential heats of adsorption calculated on the same basis are given as curve c, while the circles represent the experimental values.

Table II. Site Energies and Site Distribution on Titanium Dioxide

Site Index, <i>i</i>	Site Energy, Cal./Mole		Site Distribution, Z_i	
	A.T. and S.	A.T. and C.	A.T. and S.	A.T. and C. cc./g.
1	600	550	$\text{Exp}(-9/4)$	6.15
2	1200	720	$4 \exp(-18/4)$	22.47
3	1800	900	$6 \exp(-27/4)$	0.52
4	2400	1200	$4 \exp(-36/4)$	0.04
5	3000	..	$\exp(-45/4)$	0.00

$V_m = 29.18 \text{ cc./g.}$

Since the site distribution given in columns 3 and 5 of Table II was that deduced to give the best "statistical" fit with the isotherm and the partial molal enthalpies of adsorption, it gives the best curves which can be obtained without varying one or both of these. Such a variation could reasonably be obtained only by lateral interaction. It seems simplest and perhaps most reasonable to consider that the site energy alone varies. It is also reasonable for reasons already given to consider that the sites on the homogeneous part of the surface vary in energy as the fraction of their own coverage, as for a completely homogeneous surface, while the sites on the heterogeneous part of the surface have an energy independent of coverage except in the case of the two-sided sites. The latter were considered part of the smooth surface in computing the value of θ governing the lateral interaction.

In Figure 4, curve *B* represents the isotherm calculated from Equation 7, using the site distribution in Table III, which makes proper allowance for the variation of the lateral interaction energy as a function of coverage. In Figure 5, *B* represents the differential heats of adsorption calculated from Equations 6 and 8, allowing for the lateral interaction energy as a function of coverage. In obtaining curve *B* of both figures the calculation was made by successive approximations.

Table III. Site Distribution on Titanium Dioxide (Rutile)

Site Index	Site Energy, Cal./Mole	Site Distribution, Cc./G.
1	$300 + a \theta_i/2b$	6.15
2	$600 + a \theta_i/2b$	22.47
3	900	0.52
4	1200	0.04

It is evident from Figures 4 and 5 that consideration of lateral interaction energy is necessary to obtain satisfactory isotherms and differential heats of adsorption at high coverages.

In keeping with curve *B* for the differential heats of adsorption, curve *B* in Figure 4 is in at least as good agreement with the experimental isotherm at coverages above 0.6θ as curve *C*. *B* in Figure 5 for the differential heats of adsorption has derivatives very like the experimental values above 0.6θ , while *C* is quite different. A peak in the calculated values of the differential heats of adsorption is evident in curve *B* of Figure 5 at about 0.66θ . Such a maximum does not occur in the experimental data. Evidently the two-sided sites take a part in lateral interaction more complicated than postulated and there are energy sites intermediate between the types imagined here. Many alternative situations for lateral interaction have been examined. All of them are characterized by a maximum somewhere.

Literature Cited

- (1) Aston, J. G., Chon, H., *J. Phys. Chem.* **63**, 1015 (1961).
- (2) Aston, J. G., Tykodi, R. J., Steele, W. A., *Ibid.*, **59**, 1055 (1955).
- (3) Rhodin, T. N., *Ibid.*, **57**, 143 (1953).
- (4) Steele, W. A., *Ibid.*, **61**, 1551 (1957).
- (5) Steele, W. A., Aston, J. G., *J. Am. Chem. Soc.* **79**, 2393 (1957).

RECEIVED July 6, 1961. Contribution 122, Cryogenic Laboratory, Pennsylvania State University.

Density Studies in Clay-Liquid Systems

I. The Density of Water Adsorbed by Expanding Clays

C. T. DEEDS and H. VAN OLPHEN

*Shell Development Co.,
Houston 1, Tex.*

Apparent pycnometric densities of expanding clays in water and in various organic liquids are compared with crystallographic densities. Differences between the various density values are obtained. These differences are interpreted in terms of both abnormal fluid densities in the neighborhood of the clay surfaces and void spaces within particle aggregates which are inaccessible to certain liquids. We concluded that aggregate void space occurs when the clays are immersed in fluids which do not penetrate between the unit layers; the density of the first two monolayers of water or of polar organic fluids which are adsorbed between the unit layers is slightly below normal in most expanding clays; and the density of water adsorbed beyond the first two monolayers of water is normal within the experimental error.

The properties of a liquid are likely to be modified in the neighborhood of a solid surface, partly because of the molecular geometry of the boundary, and partly because of the effect of adsorption forces on the molecules of the liquid. How far from the surface the adsorption forces significantly affect the properties of the liquid is still a matter of controversy. A case in point is the density of water adsorbed by clays. Although water vapor adsorption isotherms indicate that the adsorption energy of successive adsorbed monolayers decays rapidly over a distance of about 10 Å., corresponding with the thickness of four monolayers of water, density anomalies in the water phase at distances of at least 60 Å. are suggested by the results of the very carefully conducted experiments by Anderson and Low (1). These authors compare the volume increments of water squeezed out of a clay paste with the corresponding volume increments of mercury pressed into the paste. In a typical experiment, they find that the water density gradually decreases from the normal value to a value which is about 3% below normal at water contents of the pastes ranging from 5 to 1 gram per gram of clay. This

range corresponds with a minimum distance range of about 60 to 10 Å. from the clay surface.

Pycnometric data reported in the literature give undifferentiated values for the average density of the water phase in clay-water systems (2, 3, 4, 6, 7, 8). Deviations of the water density from normality are generally reported, but in spite of the simplicity of the experiments, there is little agreement about the magnitude or even the sign of the deviations. The reason for the scatter of the results is that in some of the work, certain precautions were not taken which are important when working with clay systems. We have repeated some of the pycnometer work, and have extended our investigations to systems with a known amount of preadsorbed water and to different displacement fluids.

Experimental Procedure

Vacuum-jacketed pycnometers with capillary stoppers and ground-glass caps were used. They were calibrated with water. All weighings were reduced to vacuum. The measurements were carried out at $26.00^\circ \pm 0.01^\circ\text{C}$.

The organic fluids were Baker Analyzed or Spectro grade samples. They were thoroughly dried with Linde 4A Molecular Sieve. Water was triple-distilled and was used freshly boiled.

The clays were occasionally used in their native form, but they were usually converted to a certain ion form by resin exchange and washed and centrifuged to remove coarse nonclay matter or to separate a particle size fraction. The clays were used in powder form, as flakes, or as a freeze-dried voluminous powder. They were dried to a constant weight at 105°C . at 0.1-mm. pressure and transferred to the pycnometers in a dry box. The dry condition of the clay was checked by measurement of the basal spacing by x-ray diffraction.

The expanding clays admit water and certain organic compounds with polar groups between the unit layers of 10-Å. thickness; therefore, a large contact area between the liquid and a crystallographically flat surface is created. Since the contact area is of the order of 800 sq. meters per gram, relatively large bulk effects can be expected if density anomalies near the surface occur. Unfortunately, however, the workable clay concentration is limited to a few per cent, since gelation prohibits adequate vacuum deaeration at higher concentrations. In hydrocarbon liquids, in which the clays do not show interlayer swelling, the contact area is considerably smaller, but larger clay concentrations can be tolerated.

Results and Discussion

The results of the pycnometric determinations are presented in terms of "apparent densities" of the clays in the various displacement fluids. The apparent density of a clay is that density calculated from the data by the assumption that the density of the displacement fluid is normal throughout the liquid phase. When dissimilarities are observed for the apparent densities using different displacement fluids and the apparent densities deviate from the actual density, the possibility of density abnormalities of the liquid in the proximity of the clay surface should be considered. Moreover, consideration must also be given to another possible cause of certain deviations—i.e., the existence of a void space within the clay system which is inaccessible to the liquid.

Clays in Hydrocarbon Liquids ("Nonpenetrating Liquids"). When the dry clays are immersed in dry hydrocarbon liquids, the basal spacing of the clay is

unchanged; therefore, these liquids do not penetrate between the unit layers of the clay.

The apparent density of both native and sodium Wyoming bentonite in a number of nonpenetrating liquids is 2.694 grams per cc. (11 determinations, standard deviation 0.006 gram per cc.).

The actual density of the clays in these systems can be evaluated from the unit cell dimensions determined by x-ray diffraction, and the unit cell weight can be computed from chemical analysis data with the application of the Ross-Hendricks method of calculation. The crystallographic density of the sodium Wyoming bentonite was 2.804 grams per cc., and this value is estimated to be accurate within ± 0.012 gram per cc. Therefore, the apparent density of the clay in hydrocarbon liquids is appreciably smaller than the actual crystallographic density of the clay. Since both the contact area and the adsorption forces between clay and hydrocarbon liquids are relatively small, we propose that the discrepancy between apparent and crystallographic density is entirely due to the presence of void space within the clay phase which is inaccessible for hydrocarbons. The magnitude of this assumed void space is found from the difference between the apparent and the crystallographic specific volumes. Taking the specific data for the sodium clay, we find that the inaccessible void space amounts to $0.3720 - 0.3566 = 0.0154$ cc./g. (± 0.0015 cc./g.), or 4.1% of the specific volume. We further propose that this void space occurs within the clay aggregates between partially overlapping unit layers, as sketched in Figure 1,a (left). Such a void space is accessible only via the channels between touching unit layers, and since hydrocarbon liquids are unable to penetrate between the unit layers, they would indeed be unable to pass through these channels.

Clays in Water (Penetrating Liquid). The apparent densities of the expanding clays in water are higher than those of the same clays in hydrocarbon liquids. For example, the apparent density of sodium Wyoming bentonite in water is 2.793 grams per cc. (four determinations, standard deviation 0.008 gram per cc.).

We have also determined the apparent density of a sodium Wyoming bentonite clay with a small amount of preadsorbed water (approximately 300 mg. per gram of clay), using *n*-decane as the pycnometer fluid. Assuming normal densities for both *n*-decane and the preadsorbed water, we found that the apparent density of the clay in this experiment is identical with the apparent density of the clay when completely immersed in water (2.786 grams per cc.). This particular experiment will be discussed in more detail later.

Within the experimental error, these values are identical with the crystallographic density of the dry clay.

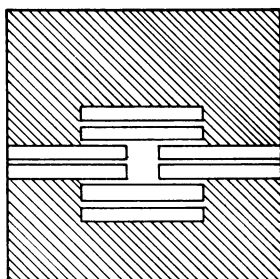
It is tempting to interpret these results simply as follows: The void space within aggregates which is inaccessible to hydrocarbons is accessible to water, and the density of the water phase is normal throughout the system within the experimental error.

However, in order to show precisely which assumptions are made in arriving at any conclusions regarding the density of water in the system, we must give the results a somewhat more sophisticated analysis.

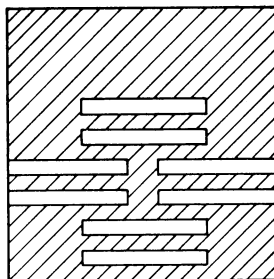
When comparing the density data obtained in hydrocarbons with those obtained in water, we can formally attribute the difference between the corresponding specific volumes to an "apparent" void space inaccessible to hydrocarbons but accessible to water and, at the same time, define that this space is completely filled if the water is assigned a normal density. This apparent void

(a) Apparent behavior of unit layer aggregates.

Distribution of a hydrocarbon fluid. Aggregate void space is empty ("inaccessible voids").

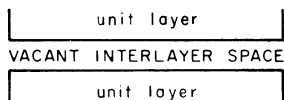


Apparent distribution of water of normal density. Void space is filled ("selectively accessible void space").



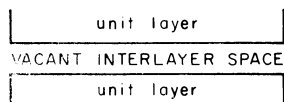
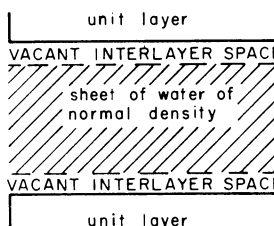
(b) Apparent behavior of water in interlayer space.

Dry clay immersed in a hydrocarbon fluid.



SODIUM BENTONITE AND HECTORITE

Hydrated clay.



SODIUM VERMICULITE

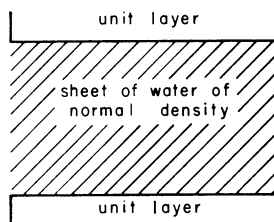


Figure 1. Schematic representation of apparent hydration of expanding lattice clays

space, which will be called the "selectively accessible void space," appears to be identical with the previously defined inaccessible void space. Therefore, we shall assume that both relate to the same real void space within aggregates. It is indeed likely that this void space which is created between partially overlapping unit layers would be accessible via the interlayer channels for penetrating liquids such as water (Figure 1, a, right). Furthermore, we assume that there is no other aggregate void space which is inaccessible for water. This assumption is reasonable, since such a void space must be accessible for hydrocarbon fluids.

When these assumptions are accepted, we see that the identity of the apparent density of the clay in water and the crystallographic density of the dry clay means that the system behaves as if the dry clay expands in water by admitting a sheet

of water of normal density between the unit layers. However, this observation does not imply that the actual density of the water adsorbed between the unit layers is normal, for the following reasons.

Contrary to the situation in the hydrocarbon systems, the crystallographic density of the dry clay is not necessarily the true reference value for the hydrous systems in which the clay occurs in the expanded condition. The c spacing of the dry clay as it exists in the hydrocarbon system is 9.6 Å. Since the thickness of the unit layers proper in van der Waals contact is smaller than 9.6 Å., the unit layers in the bentonite clay are not in contact (see Figure 1,*b*). If the c spacing of the uncharged prototype mineral pyrophyllite (9.14 Å.) is arbitrarily taken as the van der Waals thickness of the unit layers in the clay, the unit layers in the clay will be 0.46 Å. apart. The vacant space between the unit layers in the dry clay is occupied only by the sodium exchange ions. Since these ions are accounted for in the computation of the crystallographic density of the dry clay as it exists in the hydrocarbon systems, a true reference value could be established for these systems. In the expanded hydrous system, on the other hand, water molecules may occupy this originally vacant space in the domain of the oxygen surfaces of the unit layers, which also includes holes within hexagonal rings of oxygen atoms into which the water molecules may sink to some extent. At the same time, the sodium ions which were originally embedded in these holes may diffuse into the water phase. Without knowing exactly how the layers of adsorbed water are embedded in the unit layer surfaces, or where the cations are located in the hydrated clay, we cannot establish an exact crystallographic reference value for the hydrous systems.

For these reasons, we stated that the bulk density measurements only indicate that the clay behaves as if a sheet of water of normal density is admitted between the unit layers (see Figure 1,*b*). In reality, however, the interlayer water may expand in such a fashion that the originally vacant space becomes occupied. Since the bulk density measurements would not be affected by the expansion, no information on this matter can be obtained from such measurements. However, if the expansion occurs, we can make a rough estimate of the average density of the interlayer water, in so far as we can speak about the bulk property of density on the molecular scale of the interlayer space. In the experiment in which the apparent density of the clay with 300 mg. of preadsorbed water per gram of clay was determined in *n*-decane, the c spacing of the clay was 15.4 Å. If the water between the unit layers should expand to touch the unit layers, its volume would be increased roughly in the ratio of $(15.4 - 9.6)$ to $(15.4 - 9.14)$, and the "density" of the interlayer water would be 7.3% below normal. Possibly, a better value for the van der Waals thickness of the unit layers in the clay is 9.3 Å., which we derived by adding twice the radius of an oxygen atom (2×1.35 Å.) to the 0-0 center distance in the unit layers (6.6 Å.). Taking this value and applying the same reasoning, we find that the "density" of the interlayer water would be 5% lower than normal if it expands to touch the unit layers. In these estimates, the effects of a partial sinking of the water molecules into the hexagonal holes, as well as of a diffusion of the cations into the water phase, are neglected, but these corrections would be comparatively small, and they would, moreover, partially cancel.

The above interpretation is probably valid for most expanding montmorillonite clays, of which only sodium hectorite was studied in addition to sodium Wyoming bentonite. An exceptional behavior is shown by sodium vermiculite clay, an expanding clay differing essentially from the other expanding clays in the charge density, which is about twice as high.

Unlike the situation in the bentonite and hectorite clays, the apparent density of the sodium vermiculite clay in water is appreciably higher than the crystallographic density of the clay. The apparent density in water is 3.045 grams per cc. (three determinations, standard deviation 0.012 gram per cc.). The crystallographic density is 2.827 grams per cc. for the dry clay which has a c spacing of 9.82 Å. Only if a c spacing value of 9.12 Å. is used in computing the crystallographic density is there an equality of the crystallographic density and the apparent density of the clay in water; therefore, the system behaves as if water of normal density touches the oxygen surface of the unit layers (see Figure 1, *b*). However, the uncharged prototype mineral for this clay is talc, which has a basal spacing of 9.26 Å. If we take this spacing as the van der Waals thickness of the unit layers in the vermiculite clay, we find that the interlayer water would actually be somewhat compressed. Since the c spacing of the hydrated clay is 14.82 Å., the interlayer water would be compressed in the ratio $(14.82 - 9.12)$ to $(14.82 - 9.26)$, and the "density" of the interlayer water would be 2.5% above normal, when the corrections for sinking in the holes and redistribution of sodium ions are neglected.

The difference between the density behavior of vermiculite and other expanding clays is paralleled by the difference in swelling behavior. In bentonite, the two-layer hydrate has a c spacing of 15.4 Å., which is 5.8 Å. or the thickness of two monolayers of water more than the c spacing of the dry clay. The subtraction of the same thickness from the 14.82-Å. spacing of the hydrated vermiculite gives a reference spacing of 9.02 Å., which is in reasonable agreement with the conclusions drawn from the density determinations.

The compression of the interlayer water between the unit layers of the vermiculite clay is probably a consequence of the large attractive force between the negatively charged unit layers and a densely populated layer of sodium ions midway between the unit layers. This large attractive force also keeps the unit layers from swelling beyond a two-layer complex.

In conclusion, definite information on the density of adsorbed interlayer water cannot be derived from the bulk density measurements. However, such measurements supplement adsorption isotherm data, and both will be helpful in the interpretation of x-ray structure analysis of the configuration of water molecules and exchange cations in the interlayer space.

DRYNESS OF CLAY. The question of the complete dryness of the clay after heating at 105° C. in vacuum remains an uncertain element. When the clays are fired at about 900° C., dehydroxylation takes place. The weight loss due to dehydroxylation can be computed from the chemical formula of the clay. Generally, the actual weight loss, with reference to the weight of the clay dried at 105° C., is approximately 2% higher than the theoretical weight loss. Therefore, there may be some strongly adsorbed water in the clay dried at 105° C. that is lost in the same temperature range in which dehydroxylation occurs. Such strongly adsorbed water may be retained in the holes in the unit layer surface; alternatively, the excess weight loss may be due to strongly held oxygen atoms in these holes. Another interpretation, proposed by McConnell (5), is the assumption that part of the silicon-oxygen tetrahedrons in the clay are replaced by $(\text{OH})_4$ tetrahedrons to such an extent that the excess weight loss corresponds with the dehydroxylation in the tetrahedral part of the unit layers.

A re-evaluation of the analysis of the density data on the basis of either model does not significantly change the estimates for the interlayer water density.

Clays in Polar Organic Liquids (Penetrating Liquids). In general, the apparent densities of clays in organic penetrating liquids are the same as those ob-

tained in water. For example, the apparent density of sodium Wyoming bentonite in ethylene glycol is 2.818 grams per cc. as compared with 2.793 ± 0.008 grams per cc. in water; the apparent density of native Wyoming bentonite in dioxane is 2.843 grams per cc. and in water is 2.835 grams per cc. Therefore, the same packing considerations apply for these liquids as for water. In some systems, however, the apparent density of the clay in the organic liquids is appreciably higher than in water; this indicates that the particular organic is more closely packed in the interlayer space. An example is the pyridine-bentonite system, which will be discussed in another paper. Sometimes, abnormal values can be attributed to chemical changes in the organic liquid which may occur when it is contacted by a clay. For example, the erratic apparent density values obtained for Wyoming bentonite in acetone, which drifted as a function of time, were determined to be due to the partial conversion of acetone by the dry clay to diacetone alcohol.

Density of Water at Larger Distances from the Clay Surface. Since the previously quoted work by Anderson and Low (1) covers density anomalies in the water phase at larger distances from the clay surface, we attempted to check their results pycnometrically by comparing systems of clays with preadsorbed water, using *n*-decane as the displacement fluid and systems of totally immersed clays. As previously mentioned, the apparent densities of the clays in both systems were identical. This result seems to contradict the data of Anderson and Low. If their data were applicable, the apparent density of the clay immersed in water would have been about 20% lower than that of the clay with preadsorbed water immersed in *n*-decane. According to the limits of accuracy of the pycnometer experiments, and with the assumption that no density anomalies occur at the *n*-decane-water interface, the average density of the water in the range of water-clay ratios in which density anomalies were observed by Anderson and Low would not deviate more than 0.02 to 0.03% from the normal value, instead of the approximate 1.5% low average value derived by them.

EXPERIMENTAL DETAILS. A fair comparison between the apparent densities of clays immersed in water and of clays with a certain number of preadsorbed monolayers immersed in *n*-decane requires that each preadsorbed monolayer of water between the unit layers is completed, so that no vacant space within a monolayer exists. The clay should be in the same state of hydration in the entire system. The selectively accessible void space should be completely filled, as well as capillaries in the clay aggregates. The homogeneous distribution of the adsorption water was achieved by slowly equilibrating thin flakes of clay with almost saturated water vapor. After about one month of equilibration, the uniform state of hydration of the clay was shown by the sharpness and order of the x-ray diffraction pattern. The completion of the monolayers was judged from the amount of water taken up by the clay, with the knowledge that about 100 mg. of water is needed per gram of clay for the formation of a monolayer.

A very suitable system for this type of experiment is the sodium vermiculite-water system, in which the clay is hydrated with two monolayers of water. Since the clay does not hydrate beyond this stage, there is no danger of creating an incompletely filled third monolayer between the unit layers. The water uptake was 270 mg. per gram, which leaves an excess of about 70 mg. of water per gram to fill the void space of about 0.013 cc. per gram and to fill the capillaries by capillary condensation. The apparent density of the clay in this condition in *n*-decane was 3.049 grams per cc, which is identical with the apparent density of the clay immersed in water (3.045 ± 0.012 grams per cc.).

Two additional experiments were carried out with very thin flakes of sodium Wyoming bentonite. According to x-ray analysis, two-layer complexes were formed, and the water uptake was 275 and 304 mg. per gram, respectively, and the apparent densities were 2.768 and 2.786, respectively. The higher value

is identical with the apparent density of the clay in water (2.793 ± 0.008 grams per cc.) within the experimental error. The other value is somewhat low; this can be attributed to an insufficient excess of water to fill the capillaries completely.

In their analysis, Anderson and Low assume that the clay dissociates fully into single unit layers which are at the same distance throughout the system. On this basis, the distance of a certain increment of volume of water from the clay surface is derived from the water contents. Although this assumption may be correct for sodium Wyoming bentonite, a complete dissociation of unit layers is not expected to occur in potassium Wyoming bentonite, for which analogous results were obtained. Against the conclusions of our work on sodium Wyoming bentonite, the objection might be raised that the system of the clay with the preadsorbed water in which the unit layers are two monolayers apart is not directly comparable with that in which the clay is immersed in water, if, in the latter system, the unit layers are much farther apart. Since this objection would not apply to the sodium vermiculite system, it would be interesting to study this system with the technique of Anderson and Low.

A possible flaw in the method used by Anderson and Low might be that the development of grain pressure in the clay matrix in the range of high clay concentrations causes local high pressures. Such local pressures may cause small local volume changes of the container, or they may cause some compression of the inter-layer water, which according to our analysis, has a low density of packing. It can be shown that the latter factor alone could be responsible for, at most, about one third of the total effect. This compression factor would not exist for the sodium vermiculite system.

Literature Cited

- (1) Anderson, D. M., Low, P. F., *Proc. Soil Sci. Am.* **22**, 99–103 (1958).
- (2) Bradley, W. F., *Nature* **183**, 1614–15 (1959).
- (3) de Wit, C. P., Arens, P. L., *Trans. IVth Inter. Congr. Soil Sci.* **2**, 59–62 (1950).
Moisture Content and Density of Some Clay Minerals.
- (4) Hauser, E., Le Beau, D. S., *J. Phys. Chem.* **42**, 1031–50 (1938).
- (5) McConnell, D., *Am. Mineralogist* **35**, 166–72 (1950).
- (6) Mackenzie, R. C., *Nature* **181**, 334 (1958).
- (7) Nitzsche, W., *Kolloid Z.*, **93**, 110–15 (1940).
- (8) Tscapek, W., *Z. Pflanzenernähr., Düng. u. Bodenk.* **34**, 265–71 (1934).

RECEIVED June 2, 1961.

Statistical Mechanical Verification of the Gibbs Adsorption Equation

FRANK P. BUFF

Department of Chemistry, University of Rochester, Rochester, N. Y.

The foundations of the Gibbs adsorption equation are examined by both the molecular hydrostatic and statistical mechanical approaches. The former serves to confirm the assumptions inherent in its phenomenological derivation. It yields the work element and provides a proof that surface tension also possesses free energy properties. The statistical mechanical theory employs the exact molecular formula for surface tension as a starting point and involves explicit expressions for locally averaged components of the stress. The dependence of this formula on the uniform thermodynamic variables of the adjacent bulk phases enters through integral equations for the required number density derivatives. Thus, when uniformity of temperature and chemical potentials on a molecular basis are supplemented by the corresponding mechanical equilibrium conditions, the resulting expressions reduce to the familiar adsorption equation. The excess thermodynamic functions appearing in this relation are automatically expressed in statistical mechanical terms. The derivation leads to a relation between density fluctuations and a generalized virial term which underlies the validity of the equation.

This paper confirms the assumptions inherent in the thermodynamic derivation of the Gibbs adsorption equation, and contrasts this mode of deduction with its direct statistical mechanical verification. The adsorption equation, whose validity is now generally accepted, yields the excess thermodynamic functions characterizing the interface in terms of derivatives of the surface tension, γ , with respect to the intensive variables of the fluid bulk phases. Its phenomenological derivation is based on two ideas. The first is the functional form of the additional work element

appearing in the fundamental thermodynamic equation, which properly takes into account the presence of the interface. The second is the recognition that γ possesses the mechanical property of surface tension and may also be identified as an excess surface free energy. These concepts can be confirmed by hydrostatic techniques and under conditions of complete thermodynamic equilibrium lead to the desired adsorption equation.

This hydrostatic approach also yields a formal closed formula for γ in terms of the components of the stress tensor. When the stress tensor is expressed in terms of molecular variables, the resulting statistical mechanical formula for γ provides a direct means for the calculation of surface tension. For example, it may be used directly to compute the surface tension of dilute ionic solutions (6). It also illustrates in molecular detail the iterative subtractive procedures that lead to the excess functions of the familiar phenomenological approach.

This statistical mechanical expression for surface tension depends explicitly on the potentials of intermolecular force and molecular distribution functions. Upon recognition that the two-phase system under consideration is thermodynamically open, it follows that the distribution functions must be represented in the grand canonical ensemble. Thus, the dependence of γ on temperature, T , and chemical potentials, $\{\bar{\mu}_i\}$, enters through the implicit dependence of the distribution functions on these uniform thermodynamic variables. This dependence follows from the definitions of the required distribution functions, the number densities, in the grand ensemble. It may be summarized by means of integral equations which provide recursion formulas for the chemical potential and temperature derivatives of the number densities. Since surface tension has its root in a force relationship, the verification of the adsorption equation must be supplemented by the mechanical equilibrium relations satisfied by the number densities. With use of these expressions, the total differential of the statistical mechanical formula for γ finally reduces to the molecular equivalents in the adsorption equation. The derivation shows in detail the necessity for complete thermal, diffusional, and mechanical equilibrium in the experimental application of this basic equation. It also leads to an interesting relationship that must be obeyed by the excess density fluctuations, which constitutes an extended virial relation.

For multicomponent systems, the expression for γ here employed may be shown equivalent to that involved in the cluster diagram technique (6), which is currently being employed in a variety of problems. The present derivation shows that the starting expressions satisfy the thermodynamic consistency relation embodied by the adsorption isotherm. It is, however, important to observe that any direct application of these alternative rigorous approaches, which is of necessity of an approximate nature, leads to some violation of the complete internal equilibrium conditions. Similarly, calculations of surface tension which employ the adsorption equation as a starting point invariably violate mechanical equilibrium in some order of approximation.

In preparation for our subsequent treatment, we now consider a macroscopic two-phase fluid system with a planar interface of area s separating the bulk phases α and β . For the description of surface phenomena, the concentrations of the various components, $\{\rho_i^{(1)}\}$, and the components of the stress tensor δ must be specified. In the interior of the bulk phases, the concentrations, $\{\rho_i^{(1)}\}$, will be uniform and the tangential component of the stress tensor, σ_T , is equal to its normal component, σ_N . In the interfacial region, with the z -axis perpendicular to the interface, it follows by symmetry that the singlet number density and stress tensor δ vary as follows:

$$\rho_i^{(1)} = \rho_i^{(1)}(z) \quad (1)$$

$$\delta = \sigma_N \mathbf{k}\mathbf{k} + \sigma_T(z)(\mathbf{i}\mathbf{i} + \mathbf{j}\mathbf{j})$$

\mathbf{i} , \mathbf{j} , and \mathbf{k} are the unit vectors of the Cartesian coordinate system. It follows from the hydrostatic relation $\frac{\partial \sigma_N}{\partial z} = 0$, that the normal component of the stress is everywhere constant and that it is related to the bulk pressures, p_α and p_β , by

$$\sigma_N = \sigma_T(\pm \infty) = -p \quad (2)$$

$$p = p_\alpha = p_\beta$$

Although Equations 1 and 2 suffice for the gross hydrostatic description, the statistical mechanical formalism for pairwise intermolecular forces also requires specification of the pair number density $\rho_{ij}^{(2)}$. It is defined by the statement that $\rho_{ij}^{(2)}(I, 2) dv_1 dv_2$ represents the average number of molecular pairs, one member of type i being located in the volume dv_1 surrounding the point \mathbf{R}_1 and the other member of type j is in dv_2 at \mathbf{R}_2 . In the interior of the bulk phases, $\rho_{ij}^{(2)}$ depends only on the distance between the pair, while in the transition zone

$$\rho_{ij}^{(2)} = \rho_{ij}^{(2)}(z_1, \mathbf{R}_{12} \cdot \mathbf{k}, |\mathbf{R}_{12} \times \mathbf{k}|) \quad (3)$$

$$\mathbf{R}_{12} = \mathbf{R}_2 - \mathbf{R}_1$$

The thermodynamic work done by the system, $\delta W^{(2)}$, follows from Equations 1 and 2. For a Gibbs dividing surface, bounded by the closed curve C , which divides the total volume into the volumes v_α and v_β , it is found that (5)

$$\begin{aligned} \delta W^{(2)} - \delta \int \int \int p_\alpha dv_\alpha - \delta \int \int \int p_\beta dv_\beta &= - \int \gamma \mathbf{t} \times \bar{\mathbf{k}} \cdot (\delta \bar{\mathbf{x}} + \delta_b \bar{\mathbf{x}}) \\ &= - \delta \int \int \gamma ds \end{aligned} \quad (4)$$

Here \mathbf{t} is the unit tangent along C and $\mathbf{t} \times \mathbf{k}$ is drawn outward. Two kinds of displacement must be considered: the virtual displacement, $\delta \bar{\mathbf{x}}$, required for the element of virtual work, which is of a mechanical nature, and the actual boundary displacement, $\delta_b \bar{\mathbf{x}}$, which corresponds to the actual increase in area and applies to the free energy relationships. Since the identical parameter γ appears in both types of work, it is demonstrated that γ is simultaneously surface tension and possesses excess surface free energy properties.

The derivation leading to Equation 4 yields the following expression for γ :

$$\begin{aligned} \gamma &= \int_{-\infty}^{\infty} (\sigma_T(z) - \sigma_{\alpha\beta}) dz \quad (5) \\ \sigma_{\alpha\beta} &= -p_\alpha[1 - U(z)] - p_\beta U(z) = -p \\ U(z) &= 0 \quad z \leq 0 \\ &= 1 \quad z > 0 \end{aligned}$$

Even this simple hydrostatic formula clarifies the nature of the surface tension. The concentration variation within the interfacial region leads to a nonuniform stress tensor. The neglect of this nonuniformity gives rise to the conventional description of bulk phases. The iterative subtractive procedure demanded by the convergent expression given by Equation 5 corrects for this oversimplification at the boundary of the phases and yields an asymptotic correction (2) to the free energy of the total system in terms of its geometrical properties.

The last line of Equation 4 then justifies the following expression for the total differential of the energy, E , of the system

$$dE = TdS + \sum_{i=1}^n \mu_i dN_i - p_\alpha dv_\alpha - p_\beta dv_\beta + \gamma ds \tag{6}$$

with the corresponding free energy relationship

$$E = TS + \sum_{i=1}^n \mu_i N_i - p_\alpha v_\alpha - p_\beta v_\beta + \gamma s \tag{7}$$

Here S is the entropy and $\{N_i\}$ is the composition of the system. It is convenient to subtract the corresponding bulk phase equations pertaining to the volumes v_α and v_β from these relations and to introduce intensive excess thermodynamic functions. The familiar result is given by

$$dE_s = TdS_s + \sum_i \mu_i d\Gamma_i \tag{8}$$

and

$$E_s = TS_s + \sum_i \mu_i \Gamma_i + \gamma \tag{9}$$

where $E_s(S_s)$ is the excess energy (entropy) per unit area and Γ_i is the superficial excess density of component i . For example, $\Gamma_i = \frac{N_i - N_i^\alpha - N_i^\beta}{s}$, where

N_i^α and N_i^β are the bulk composition of component i in v_α and v_β which neglect surface effects. Differentiation of Equation 9 and use of Equation 8 then lead to the Gibbs adsorption equation

$$d\gamma = -S_s dT - \sum_i \Gamma_i d\mu_i \tag{10}$$

For comparison with the statistical mechanical theory, it is convenient to transform this equation into the equivalent form

$$d\frac{\gamma}{T} = E_s d\frac{1}{T} - \sum_i \Gamma_i d\frac{\mu_i}{T} \tag{11}$$

It has been assumed throughout this derivation that T and $\{\mu_i\}$ are uniform throughout the system.

The statistical mechanical verification of the adsorption Equation 11 proceeds most conveniently with use of the expression for γ given by Equation 5. An identical starting formula is obtained via the virial theorem or by differentiation of the grand partition function (3). We simplify the presentation, without loss of generality, by restricting ourselves to multicomponent classical systems possessing a potential of intermolecular forces of the form

$$V^{\{N\}} = \frac{1}{2} \sum_{\alpha, \beta=1}^v \sum_{i_\alpha=1}^{N_\alpha} \sum_{i_\beta=1}^{N_\beta} V_{\alpha\beta}(i_\alpha, i_\beta) \tag{12}$$

where $V_{\alpha\beta}(i_\alpha, i_\beta)$ is the spherically symmetric interaction potential between the centers of mass of molecules i_α and i_β of species α and β . For this type of system, the formula for γ in terms of molecular variables has long been available. The most careful derivation for a point function stress tensor is due to Irving and Kirkwood (7). Their result, generalized for multicomponent systems, is

$$\begin{aligned} \mathfrak{d}(\mathbf{R}) &= -kT \sum_i \rho_i^{(1)}(\mathbf{R}) \mathbf{1} + \frac{1}{2} \sum_{ij} \int \frac{\mathbf{R}_{12} \mathbf{R}_{12}}{R_{12}} \frac{dV_{ij}(R_{12})}{dR_{12}} \rho_{ij}^{(2)}(\mathbf{R}, \mathbf{R}_{12}) dv_{12} \tag{13} \\ \bar{\rho} &= \int_0^1 \rho^{(2)}(\mathbf{R} - \alpha \mathbf{R}_{12}, \mathbf{R} - \alpha \mathbf{R}_{12} + \mathbf{R}_{12}) d\alpha \end{aligned}$$

where $\mathbf{1}$ is the unit tensor and k is the Boltzmann constant. Substitution of Equation 13 into Equation 5, with use of Equation 3, yields the desired molecular expression for γ . It may immediately be simplified on the basis of these observations. Since only an averaged stress is required, the integration with respect to α is trivial. To bring out the mechanical nature of γ , it is convenient, by means of symmetry, to rearrange the intermolecular force contribution to the stress tensor. The final result is

$$\beta\gamma = -\sum_i \Gamma_i + \frac{\beta}{2} \sum_{ij} \int \mathbf{r}_i \cdot \nabla_1 V_{ij}(1, 2) \Gamma_{ij}(\mathbf{R}_{12}) dv_{12} \quad (14)$$

where

$$\begin{aligned} \beta &= 1/kT & \mathbf{r}_i &= x_i \mathbf{i} + y_i \mathbf{j} \\ \Gamma_i &= \int_{-\infty}^{\infty} \rho_i^{(1)}(z) dz - \int_{-\infty}^0 \rho_i^{(1)}(z = -\infty) dz - \int_0^{\infty} \rho_i^{(1)}(z = \infty) dz \\ \Gamma_{ij} &= \int_{-\infty}^{\infty} \rho_{ij}^{(2)}(z_1, \mathbf{R}_{12}) dz_1 - \int_{-\infty}^0 \rho_{ij}^{(2)}(z_1 = -\infty, \mathbf{R}_{12}) dz_1 - \int_0^{\infty} \rho_{ij}^{(2)}(z_1 = \infty, \mathbf{R}_{12}) dz_1 \end{aligned}$$

γ is invariant to the dividing surface selected, while the Γ_i , arising from the momentum contribution to the stress tensor, are identical with the phenomenologically defined parameters appearing in the adsorption Equation 11.

The remaining program is as follows. Recognizing the implicit dependence of the ρ 's on T and $\{\mu_i\}$, the total differential of both sides of Equation 14 is taken. This procedure clearly leads to the derivatives of the ρ 's with respect to these thermodynamic variables. These are obtained from their defining equations in the grand canonical ensemble.

We require the generic center of mass number, $\rho_{n_1 \dots n_\nu}^{(n)}(1, \dots, n)$, defined as the average density of sets containing n_1 molecules of species 1, n_2 molecules of species 2, etc., at the points $\mathbf{R}_1, \dots, \mathbf{R}_{n_\nu}$, in a system of total volume V , where

$$n = \sum_{\alpha=1}^{\nu} n_{\alpha}$$

In the semiclassical limit $\rho^{(n)}$ is related to thermodynamic variables and potentials of intermolecular force by

$$\begin{aligned} \rho^{(n)} &= e^{\beta\Omega} \sum_{N_1=n_1}^{\infty} \prod_{\alpha=1}^{\nu} \frac{e^{\beta N_{\alpha} \mu_{\alpha}'}}{(N_{\alpha} - n_{\alpha})!} \int \dots \int e^{-\beta V \{N\}} \prod_{k=n+1}^N dv_k \\ &\quad \dot{N}_{\nu} = n_{\nu} \\ \rho^{(0)} &= 1; \quad N = \sum_{\alpha=1}^{\nu} N_{\alpha} \\ \mu_{\alpha}' &= \mu_{\alpha} - \mu_{\alpha}^*(T) \\ \mu_{\alpha}^* &= \lim_{\{\rho_{\alpha}\} \rightarrow 0}^{(1)} [\mu_{\alpha} - kT \log \rho_{\alpha}] \end{aligned} \quad (15)$$

The required derivatives have been previously exhibited by the author (3, 4). They are obtained by differentiation of both sides of Equation 15 and rearrangement of terms. The results are

$$\begin{aligned} &\left(\frac{\partial \rho_{\{n\}}^{(n)}(1, \dots, n)}{\partial \beta \mu_{\alpha}} \right)_{\beta, \nu, \{\beta \mu\}'} = n_{\alpha} \rho_{\{n\}}^{(n)}(1, \dots, n) \\ &+ \int \{o_{n \dots n_{\alpha} + 1 \dots n_{\nu}}(1, \dots, n+1) - \rho_{\{n\}}^{(n)}(1, \dots, n) \rho_{\alpha}^{(1)}(n+1)\} dv_{n+1} \end{aligned} \quad (16)$$

and

$$\begin{aligned}
 -\left(\frac{\partial \rho^{(n)}}{\partial \beta}\right)_{v, \{\beta \mu'\}} &= V \rho^{(n)}(1, \dots, n) \\
 &+ \frac{1}{2} \sum_{\alpha, \gamma=1}^{\nu} \left\{ 2 \sum_{i\alpha=1}^{n\alpha} \int V_{\alpha\gamma}(i\alpha, n+1) \rho_{n+1 \dots n\alpha+1 \dots n\nu}^{(n+1)}(1, \dots, n+1) dv_{n+1} \right. \\
 &\quad \left. + \iint V_{\alpha\gamma}(n+1, n+2) [\rho_{n+1 \dots n\alpha+1 \dots n\gamma+1 \dots n\nu}^{(n+2)}(1, \dots, n+2) \right. \\
 &\quad \left. - \rho^{(n)}(1, \dots, n) \rho_{\alpha\gamma}(n+1, n+2) \right\} dv_{n+1} dv_{n+2} \quad (17)
 \end{aligned}$$

We now turn in some detail to the chemical potential derivatives. At constant temperature it is found upon application of Equation 16 to Equation 14 that

$$d\beta\gamma = -\sum_i \Gamma_i d\beta\mu_i + \sum_i \epsilon_i d\beta\mu_i \quad (18)$$

$$\epsilon_i = I_i(\text{system}) - I_i(\text{bulk contributions})$$

A typical residual term, I_i , has the form

$$\begin{aligned}
 sI_i(\text{system}) &= \Sigma \iint [\rho_{ij}^{(2)}(1, 2) - \rho_i^{(1)}(1) \rho_j^{(1)}(2)] dv_1 dv_2 \\
 &\quad + \frac{\beta}{2} \sum_j \iint \mathbf{r}_1 \cdot \nabla_1 V_{ij}(1, 2) [\rho_{ij}^{(2)}(1, 2) + \rho_{ji}^{(2)}(1, 2)] dv_1 dv_2 \\
 &\quad + \frac{\beta}{2} \sum_{j,k} \iint \mathbf{r}_1 \cdot \nabla_1 V_{jk}(1, 3) [\rho_{jki}^{(3)}(1, 2, 3) - \rho_{jk}^{(2)}(1, 2) \rho_i^{(1)}(3)] dv_1 dv_2 dv_3 \quad (19)
 \end{aligned}$$

where the analogous bulk contribution serves to provide convergence. The first set of terms on the right-hand side of Equation 19 arises from the momentum contribution to the stress tensor and is by definition of the number densities related to the density fluctuations in the open system (4). The remaining virial terms arise from the intermolecular force contribution to the stress tensor. For the reduction of these terms we recall the mechanical nature of γ and employ the mechanical equilibrium condition among the molecules in the set. This is given by the set of Born and Green equations (1) which follow by taking the gradient of both sides of Equation 15. For the combination required by Equation 19, they take the form

$$\begin{aligned}
 \nabla_1 [\rho_{ji}^{(2)}(1, 2) - \rho_j^{(1)}(1) \rho_i^{(1)}(2)] &= -\beta \nabla_1 V_{ij}(1, 2) \rho_{ji}^{(2)}(1, 2) - \\
 &\quad \beta \sum_k \iint \nabla_1 V_{ik}(1, 3) [\rho_{jik}^{(3)}(1, 2, 3) - \rho_{jk}^{(2)}(1, 3) \rho_i^{(1)}(2)] dv_3 \quad (20)
 \end{aligned}$$

Upon taking the scalar product of $\mathbf{r}_2 - \mathbf{r}_1$ and Equation 20, with summation over the components j and integration over the coordinates 1 and 2, it is found after rearrangement that

$$\begin{aligned}
 \sum_j \iint \mathbf{r}_{12} \cdot \nabla_1 [\rho_{ji}^{(2)}(1, 2) - \rho_j^{(1)}(1) \rho_i^{(1)}(2)] dv_1 dv_2 &= 2 \sum_j \iint \rho_{ij}^{(2)}(1, 2) \\
 - \rho_i^{(1)}(1) \rho_j^{(1)}(2) dv_1 dv_2 &+ \sum_j \iint \nabla_1 \mathbf{r}_{12} [\rho_{ji}^{(2)}(1, 2) - \rho_j^{(1)}(1) \rho_i^{(1)}(2)] dv_1 dv_2 \\
 &= \beta \sum_j \iint \mathbf{r}_1 \cdot \nabla_1 V_{ij}(1, 2) [\rho_{ij}^{(2)}(1, 2) + \rho_{ji}^{(2)}(1, 2)] dv_1 dv_2 \\
 &\quad + \beta \sum_{j,k} \iint \mathbf{r}_1 \cdot \Delta_1 V_{jk}(1, 2) [\rho_{jki}^{(3)}(1, 2, 3) - \rho_{jk}^{(2)}(1, 2) \rho_i^{(1)}(3)] dv_1 dv_2 dv_3 \quad (21)
 \end{aligned}$$

The first set of terms after the last equality sign follow from the relation $\nabla_1 V_{ij} = -\nabla_2 V_{ij}$. The last set of terms follow by pairwise cancellation of the integrand

involving $\mathbf{r}_2 \cdot \nabla_1 V_{jk}$ (I, 3) and relabeling of the coordinates. By comparison of Equation 21 with Equation 19 and use of cylindrical coordinates, it is found that

$$I_i = -\pi \sum_j \int \int \left\{ \lim_{r_{12} \rightarrow \infty} r_{12}^2 [\rho_{ji}^{(2)}(z_1, z_{12}, \mathbf{r}_{12}) - \rho_j^{(1)}(z_1) \rho_i^{(1)}(z_1 + z_{12})] \right\} dz_1 dz_{12} \quad (22)$$

We finally observe that with z_1 and z_2 fixed and \mathbf{R}_1 and \mathbf{R}_2 infinitely far apart, ρ_{ji} approaches $\rho_j^{(1)}(z_1) \rho_i^{(1)}(z_2)$ sufficiently rapidly that by Equation 22 ϵ vanishes. The use of this convergence criterion is thus basic to the confirmation of the adsorption isotherm.

The corresponding temperature variation of γ is obtained with use of Equation 17. Since this recursion formula will lead to number densities for sets of four molecules, we summarize only the analogous reduction. Again with use of the mechanical equilibrium condition, here for both pair and triplet distribution functions, vanishing residual terms are found. The condition, similar to that of Equation 22, is that for fixed \mathbf{R}_1 and \mathbf{R}_2 , with \mathbf{R}_3 at infinity, $\rho^{(3)}(1,2,3)$ approaches $\rho^{(2)}(1,2) \rho^{(1)}(3)$.

The final result is confirmation of the adsorption equation

$$d\beta\gamma = E_s d\beta - \sum_i \Gamma_i d\beta\mu_i \quad (23)$$

which is identical with Equation 11. Γ_i is given in molecular terms by Equation 14 and E_s is given by the statistical mechanical formula

$$E_s = \sum_i \bar{E}_i^*(T) \Gamma_i + \frac{1}{2} \sum_{ij} \int \int V_{ij}(1,2) \Gamma_{ij}(\mathbf{R}_{12}) dv_{12} \quad (24)$$

$$\bar{E}_i^* = \frac{d\beta\mu_i^*}{d\beta}$$

Thus the use of the exact molecular expression for γ in the verification of the adsorption equation automatically yields the molecular formula for E_s .

We finally contrast the preceding derivation with the quasithermodynamic approach initiated by Tolman (8). In his work, the surface tension is assumed to be given by

$$\gamma = \int_{-\infty}^{\infty} [p - p(z)] dz \quad (25)$$

where $p(z)$ is an undefined macroscopic pressure which varies through the interface. It is further postulated that $p(z)$ satisfies a local Gibbs-Duhem equation, which in our notation takes the form

$$d\beta p(z) = -E_v(z) d\beta + \sum_i \rho_i(z) d\beta\mu_i \quad (26)$$

where $E_v(z)$ is a local energy density. p is taken to be the bulk pressure which correctly satisfies the Gibbs-Duhem equation. The total differential of γ as given by Equation 25, supplemented by Equation 26, then immediately leads to the desired adsorption equation. Since our statistical mechanical theory shows that $p(z)$ must be identified as a smoothed tangential stress component, which does not satisfy a local Gibbs-Duhem equation, Tolman's approach only constitutes an internal consistency argument for the quasithermodynamic model.

Literature Cited

- (1) Born, M., Green, H. S., *Proc. Roy. Soc. (London)* **A188**, 10 (1946).
- (2) Buff, F. P., *Discussions Faraday Soc.* **30**, 52 (1960).
- (3) Buff, F. P., *J. Chem. Phys.* **23**, 419 (1955).
- (4) Buff, F. P., Brout, R., *Ibid.*, **23**, 458 (1955).
- (5) Buff, F. P., Saltsburg, H., *Ibid.*, **26**, 23 (1957).
- (6) Buff, F. P., Stillinger, F. H., Jr., *Ibid.*, **25**, 312 (1956).
- (7) Irving, J. M., Kirkwood, J. G., *Ibid.*, **18**, 817 (1950).
- (8) Tolman, R. C., *Ibid.*, **16**, 758 (1948).

RECEIVED June 22, 1961. Work supported by the National Science Foundation under Grant 3056.

**American Chemical Society
Library**

1155 16th St., N.W.

In SOLID SURFACES, Copenhagen, Denmark;
Advances in Chemistry; American Chemical Society, Washington, DC, 1961.

Washington, D.C. 20036

A Thermodynamic Theory of Adsorption

L. E. COPELAND

*Research Department, Portland Cement Association,
Skokie, Ill.*

T. F. YOUNG

*George Herbert Jones Chemical Laboratory,
The University of Chicago, Chicago, Ill.*

The concept of a monodisperse liquid adsorbent has been used in the development of a nearly rigorous thermodynamic theory of adsorption. It is found to be instructive to discuss changes in integral (as well as partial molal) properties of the components of an adsorption system. Changes in the partial molal properties of the adsorbent (associated with changes in surface energies) are significant, and some are large. It is predicted that changes in the escaping tendencies of solid adsorbents will be several times as large as values calculated from adsorption isotherms without an allowance for failure of the solid adsorbent to attain equilibrium with itself.

A finely divided adsorbent is inherently unstable. Very small crystals in a powdered crystalline mass disappear as it ages. Eventually, especially, at high temperatures, a few relatively large crystals or even a single crystal remain. A spray of fine liquid droplets becomes a set of comparatively large drops or may coalesce to a single mass (13, 19).

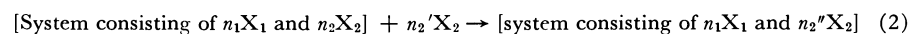
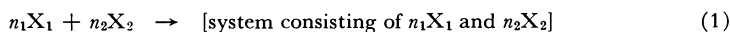
The thermodynamics of finely divided crystals is complicated by the fact that parts of even a single crystal are not, in general, in equilibrium with one another; the rigidity of a crystal may prevent the internal adjustments essential to the equalizing of the escaping tendencies of material in its surface and of material in the interior of the crystal.

The thermodynamics of a drop of liquid is comparatively simple. Surface tension produces a pressure which increases the partial molar free energy at any point within the drop. The escaping tendencies of material within the drop and of material in its surface are thus equalized. Considerations of this equilibrium have been recognized as fundamental in classic discussions of the thermodynamics of surface tension (18) and in investigations of pressures within, and the shapes of, bubbles and drops (2, 22).

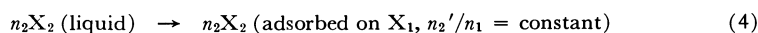
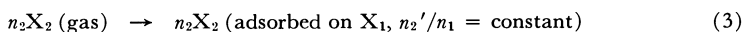
If the adsorbent is known to be a monodisperse liquid (9, 14), the thermodynamics of adsorption is also comparatively simple. It is simplified by the fact that we can conceive of the existence of complete equilibrium of the adsorbent in all parts of an adsorption system and can indulge in thermodynamic reasoning without mental reservations concerning slow exchange of adsorbate or adsorbent between particles of different sizes and shapes.

Thermodynamic Processes

In general, the thermodynamic processes to be considered are of two general types, integral and differential. Two integral processes of frequent occurrence may be written as follows (4, 5, 12, 15):



The differential processes most frequently encountered in adsorption are the following:



The values of n_2 and n_2' of Equations 3 and 4 are not related to the values of n_2 and n_2' of either Process 1 or Process 2, nor are they necessarily equal for Processes 3 and 4.

Equation 3 represents the adsorption of n_2 mole of gaseous X_2 , the adsorbate, on an indefinitely large amount of X_1 which already holds n_2' mole of adsorbate for each n_1 mole of adsorbent. The mole ratio n_2'/n_1 is, of course, unchanged—i.e., increased only infinitesimally. Equation 4 represents a similar differential process: the disappearance of n_2 mole of liquid X_2 and its reappearance in the infinitely large adsorption system. The free energy change for this differential process is important in the discussions that follow. It is readily calculated from the ratio of the fugacities of liquid X_2 and of X_2 in the equilibrated adsorption system. If gaseous X_2 is a nearly perfect gas, the free energy change for the process is:

$$\Delta G (\text{Process 4}) = n_2\Delta\bar{G}_2 = n_2 RT \ln \frac{p}{p^\circ} \quad (5)$$

From a series of adsorption isotherms (vapor pressure *vs.* n_2/n_1) the differential heat of adsorption may be determined for both of the differential processes.

Equation 1 represents the adsorption of n_2 moles of X_2 on a finite amount, n_1 moles, of adsorbent to produce the system containing n_1 moles of X_1 and n_2 moles of X_2 . Equation 2 represents the addition of a specified finite number of moles of adsorbate, n_2' , to a finite system containing n_1 moles of X_1 and n_2 moles of X_2 . Since both n_2' and the system are finite, the composition of the resulting system differs from that of the initial system.

If it were possible to work with monodisperse liquid adsorbent, it would be important and interesting to compare values of thermodynamic properties determined by measurements of different types. Agreement would indicate correctness of the methods and their interpretation.

It is more important to compare values of thermodynamic properties determined in different ways when solid adsorbents are used. Most adsorption experiments are made with adsorbents consisting of small solid particles of varying sizes and shapes. Complete equilibrium in such systems is not possible, but for many

purposes it may be possible to disregard that fact. The most important available test of the possibility of such a departure from exactness is the comparison of results of methods which differ from each other in the essential approximations incorporated within them.

Probably the most significant comparisons which can be made are of values of properties determined from calorimetric measurements with values calculated from adsorption isotherms. Two general methods are available for the comparison of values of enthalpies determined from experiments of the two types. One involves two differentiations: The change in the partial molal enthalpy, $\Delta\bar{H}_2$, of X_2 , for Process 4, is determined from the differentiation with respect to n_2/n_1 of the integral heat of adsorption measured in a series of calorimetric experiments of the type represented by Equation 1. The values of the differential heats of adsorption (heats corresponding to the differential Process 4) are compared with values determined from the temperature variation of $\Delta\bar{G}_2/T$ for a series of values of n_2/n_1 in Process 4. This type of comparison has been made successfully by several groups of authors (3, 5, 10).

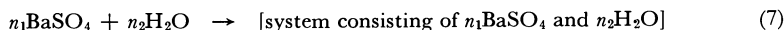
The other method for the comparison of enthalpies depends upon the integration of Equation 5 as indicated by Equation 6 for each of a set of adsorption iso-

$$\Delta G = \int_0^{n_2} \bar{G}_2 dn_2 \quad (6)$$

therms to determine a corresponding set of integral free energy changes for Process 1. For a constant composition, $\Delta G/T$ is then differentiated with respect to temperature to yield an integral ΔH for Process 1. The calculated integral ΔH may then be compared with the integral ΔH measured directly in the calorimeter. This method, apparently, has been used very little, but is used by Wu and Copeland (20).

Changes in Integral Free Energy

There is no general method for the determination of changes in integral free energy for a process such as Process 1. Incidental to a comparison of integral enthalpy changes, a series of integral free energy decreases has been calculated (20) for this process:



The plot of ΔG (Process 7) is shown in Figure 5 (20) for n_2/n_1 varying from 0 to 0.03. The curve was calculated by Equation 6 from an adsorption isotherm from which the free energy change, $n_2\Delta\bar{G}_2$, of Process 4 had been derived. Shown also in Figure 5 is a plot of $n_2\Delta\bar{G}_2$. The large difference between the $n_2\Delta\bar{G}_2$ and the integral free energy change is an indication of large changes in the partial molal properties of the adsorbent.

Partial Molal Properties of Adsorbent

Little has been written about changes in the escaping tendency of adsorbents, and in some treatments of adsorption the effect has been ignored entirely. That changes in escaping tendency must occur during dispersal of a material and during adsorption of another substance on it is a consequence of the self-evident truth that substance X_1 cannot attract substances X_2 unless X_2 also attracts X_1 . This recognition of the existence of changes in escaping tendency does not imply that

there are changes in free energy and other properties which are not part of, or are not associated with, changes in surface free energy. There can be no such changes. It seems that changes in various properties produced by adsorption can be rather large. For example, several authors have reported some surprising volume changes which occur in the adsorption of various gases on porous glass and other materials (1, 17, 21).

Thermodynamics of Small One-Component Particles

The volume of a drop formed by coalescence of two small drops is not exactly the sum of their volumes. The enthalpy, H , is not the sum of the enthalpies of the two small drops. In other words, a sufficiently sensitive measurement would reveal a ΔV and a ΔH associated with the coalescence. We can calculate the ΔH for the process with considerable precision if the drops are very small but large enough to ensure that surface tension is nearly the same as for the liquid in bulk. The calculation involves ΔH per unit area calculated from the temperature coefficient of surface tension (8) and the area which disappears in the process. (The coalescence of two drops of water at 25° C. each 0.01 cm. in diameter produces a temperature rise of $3.5^\circ \times 10^{-4}$ C.)

These facts mean that extensive thermodynamic properties are not truly "homogeneous" (11) in the sense in which that word is used in mathematics and thermodynamics. Experiments with relatively large particles show that thermodynamic functions are homogeneous within the limits of precision ordinarily attained in the laboratory. The fact is simply that we usually do not detect deviations from homogeneity. It is not true that such differences do not exist. Most texts and treatises dismiss the problem so quickly that students are likely to conclude that even the mention of the word "homogeneity" is somewhat pedantic.

The partial molal free energy of a spray of finely dispersed droplets is not so simply related to escaping tendency as it is in systems usually treated by thermodynamic methods. Even the definition of the partial molal free energy is not entirely devoid of difficulty. To discuss equilibrium we wish to think of the transfer of a small amount of adsorbent from each droplet in the spray to another phase—e.g., the gas phase (16). If a little material leaves each droplet, there must be a concomitant decrease in surface area, A , and an increase in specific area, σ (area per mole or per gram). The quantity related to escaping tendency of material is not the derivative of free energy with respect to n , the number of moles in the spray at either constant area or constant specific area. The condition is that the number of droplets, ν , be constant. (This means that area divided by mass to the 2/3 power is nearly invariant.)

The measure of escaping tendency for a monodisperse spray of one component droplet is

$$\bar{G} = \left(\frac{\partial G}{\partial n} \right)_{P, T, \nu} \quad (8)$$

This quantity is, of course, a partial molal free energy. The fact that the extensive free energy depends upon ν means that the free energy of each drop is not proportional to the amount of material in the drop. Hence, when the amount of material per drop is small, the extensive free energy, G , is not equal to $n\bar{G}$.

Constant Specific Surface Area

Another definition of partial molal free energy avoids this particular difficulty. Consider the addition of an increment of substance to the spray of finely

dispersed liquid adsorbent. To keep the drop size constant, the quantity of material in each addition must be equal to that in a whole drop, or a multiple of it. If an amount of material less than that in a single uniform drop were introduced as a smaller drop, the system would be unstable and no single value of the molal or partial molal free energy of the substance could be stated. We shall define a new continuous function of n equal for all integral values of ν to the free energy of the system. A complete new set of thermodynamic functions may be defined in a corresponding manner.

One such function is illustrated in Figure 1. The ordinate might be any extensive property of the system containing a varying number of moles of liquid. The volume has been chosen for illustration. The abscissa of point A is n_A , the number of moles of substance in a single drop of the uniformly dispersed adsorbent; the ordinate is the volume of one drop. Point B represents the number of moles of adsorbent in, and the volume of, two of the drops; point C, the moles in, and volume of, three drops, etc. Curve 1 represents the volume of a single drop of any size as a function of n , the number of moles of adsorbent. The curve represents the volume for both n less than n_A and n greater than n_A . Curve 2 represents the volume of two drops, the size of one being standard, the size of the other variable. Curve 3 represents three drops, two of standard size and the third variable. The straight line connects the series of discrete volumes contained in integral numbers of uniform drops. The volume V^\dagger , indicated by the straight

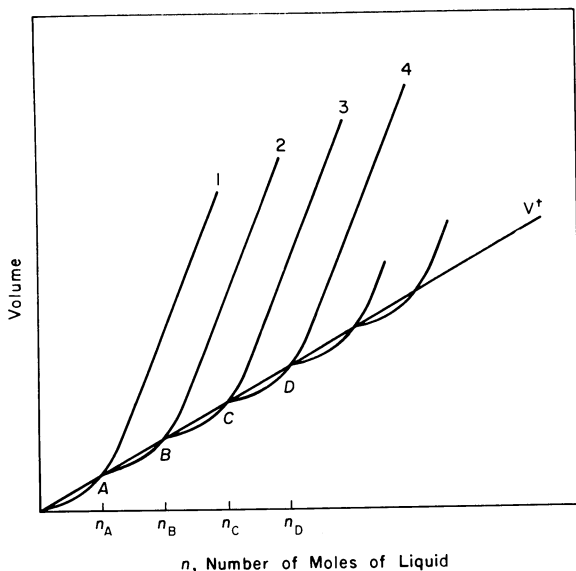


Figure 1. Volume as a function of n for various integral numbers of drops

1. One drop, of varying size
2. One standard drop plus another of variable size
3. Two standard drops plus another of variable size

A, B, C, D. Intersections

V^\dagger . Continuous function which equals actual total volume of any integral number of standard drops

line, is a property which is a continuous¹ and linear homogeneous function of n .

The derivative of each of the curves 1, 2, 3, etc., where it crosses the V^\dagger line is the derivative of the volume with respect to n , at constant ν —i.e., it is the partial molal volume corresponding to \bar{G} of Equation 8. The functions represented by curves 1, 2, and 3 are not homogeneous. The slope of V^\dagger is the derivative of the volume at constant specific area. V^\dagger , of course, was defined so that it is a homogeneous function of n .

A qualitative representation of free energies of varying numbers of moles and varying numbers of drops of adsorbent is similar to Figure 1, but the curves corresponding to 1, 2, and 3 are convex toward the free energy axis. The slope of these curves where each crosses the G^\dagger line is the partial molal free energy of Equation 8. The slope of the G^\dagger line is also partial molal free energy, the derivative of free energy at constant specific area, σ .

$$\bar{G}^\dagger = \left(\frac{\partial G^\dagger}{\partial n} \right)_{P,T,\sigma} \quad (9)$$

Though \bar{G}^\dagger is not an exact measure of escaping tendency, the homogeneity of \bar{G}^\dagger confers upon it a distinct advantage. We offer the postulate that in practice it will prove to be an adequate measure of escaping tendency; we believe that it will also lead to interesting predictions and experiments.

To discuss the addition of adsorbate to a monodisperse adsorbent we shall use a similar device, a function G^\dagger for the system of two components that strictly is equal to the free energy only when the number of moles of adsorbent, n_1 , is a multiple of the number of moles of adsorbent in a single standard droplet. For each value of n_1 , however, $G^\dagger = G$ varies continuously as a function of n_2 . \bar{G}_2 may be defined in the usual manner:

$$\bar{G}_2 = \left(\frac{\partial G}{\partial n_2} \right)_{n_1,P,T,\sigma} = \left(\frac{\partial G^\dagger}{\partial n_2} \right)_{n_1,P,T,\sigma} \quad (10)$$

The subscript, σ , is redundant in both of these derivatives but is included as a reminder that each droplet is to contain an unvarying amount of X_1 . The specific surface area, σ , is defined therefore as the area per unit mass that would be observed if the adsorbate were removed. \bar{G}_1^\dagger is defined as in Equation 9, except that it is now necessary to include the restriction that both n_2 and σ are to be constant.

$$\bar{G}_1^\dagger = \left(\frac{\partial G^\dagger}{\partial n_1} \right)_{n_2,P,T,\sigma} \quad (11)$$

At constant σ and constant n_2/n_1 the free energy, G^\dagger , is proportional to n_1 and hence proportional to n_2 . G^\dagger is therefore a homogeneous function of n_1 and n_2 . Consequently, an equation similar to the Gibbs-Duhem equation is valid.

$$n_1 d\bar{G}_1^\dagger + n_2 d\bar{G}_2 = 0 \quad (12)$$

The change in \bar{G}_1^\dagger may be evaluated by integration of Equation 12. It bears an interesting relation to the difference between the integral free energy change of

¹ This defined extensive property bears a relation to the discrete values of the volumes of uniform drops which is somewhat analogous to the relation of the gamma function of z to the factorials of integral values of z . Chemical thermodynamics, in general, involves an approximation of a similar kind. We think in terms of mathematical operations which are dependent upon the transfer of infinitesimal quantities of material, although we are not quite aware that transfers cannot involve—even in thought—fractions of molecules. We have become so accustomed to this discrepancy between mathematics and realizable processes that we seldom mention it in thermodynamic arguments.

a process such as that represented by Equation 1 or 7 and the free energy change of the differential process represented by Equation 4.

$$n_1 \Delta \bar{G}_1^\dagger = \int_0^{n_2} \Delta \bar{G}_2 dn_2 - n_2 \Delta \bar{G}_2 \quad (13)$$

This equation follows from the integration of Equation 12 and the "formula for integration by parts" (7). An illustration of its use with a solid adsorbent is given by Wu and Copeland (20, Figure 5).

There is also an interesting relation between $\Delta \bar{G}_1^\dagger$ and the surface free energy, γ , defined by Gibbs [cf. Equations 514 and 675 of (6)].

$$\Delta \bar{G}_1^\dagger = A \Delta \gamma \quad (14)$$

Here $\Delta \gamma$ is the change in surface free energy for a process such as Process 1 or 7. Changes in the extent of surface, usually small, are ignored.

Adsorption on Solids

Most adsorbents studied in the laboratory are solids. The thermodynamic treatment of solid particles is more difficult than the treatment of uniformly dispersed liquid droplets. Some interesting conclusions concerning them can be drawn, however. As an approximation divide the solid material into two classes: interior matter and surface matter. In general they are not in equilibrium; the escaping tendency of material in the surface exceeds that of material in the interior. There may be a continuous gradation of escaping tendency over a wide range, but in keeping with our approximation we shall treat the escaping tendency of material in the interior as if it had a single value (the average interior value) and escaping tendency of surface matter as if it had another single (usually larger) value. Moreover, we shall regard the escaping tendency of material in the surface as conditioned merely by the fact that it is in the surface—i.e., differences arising from the shapes of solid particles will be ignored in this approximation.

A discussion of the escaping tendency of material in the interior infers the existence of a (conceptual) process by which material could be added to the interior without a change in amount of adsorbent in the surface. We can imagine removal of part of a surface, addition of substance to the interior, replacement of the surface, and distortion of the particles to restore the extent of surface to its former value. The derivative of the free energy in this thought process with respect to the number of moles in the interior is \bar{G}_1 (interior). Similarly, a substance may be added to the surface with an accompanying distortion to keep constant the quantity of material in the interior. The derivative of free energy with respect to number of moles in the surface is \bar{G}_1 (exterior). These definitions are in harmony with Equation 8—i.e., each of these partial molal free energies is a measure of escaping tendency.

The extensive free energy of a system cannot be observed directly. An attempt to measure partial molal free energies would, therefore, be a problem of a different type. We may conceive of the measurement of vapor pressure, solubility, or the e.m.f. of a cell in which the adsorbent functions as an electrode. A successful measurement of such an intensive property would yield information concerning the escaping tendency or partial molal free energy of material of one class, presumably the exterior kind, of material. A partial molal free energy so obtained would not be an average for both interior and exterior material. Even a measurement only moderately successful could yield a change in partial molal

free energy much closer to the value for the exterior material than to the value for interior material. It might in such a case be several times as large as the "average value." This interesting complication is a consequence of the lack of equilibrium within solid adsorbents. It would not occur if a monodisperse liquid adsorbent could be used.

If the quantity of adsorbent should be increased by the addition of more material in the same state of subdivision, we could measure changes in volume, in heat capacity, and in certain other extensive properties which can be directly observed. We could differentiate any one of these properties with respect to the number of moles of adsorbent (whether the system contains one, two, or more components) to obtain a partial molal property. The partial molal property so obtained would be the weighted average for interior and exterior adsorbent and is in harmony with Equations 9 and 11.

A change in partial molal free energy of the adsorbent calculated from adsorption isotherms is an average for the exterior and interior adsorbent because we have taken the total number of moles of adsorbent as n_1 . This average, multiplied by the total number of moles of adsorbent, is an extensive free energy function. Its temperature variation yields a heat of adsorption which is also extensive. This heat divided by the number of moles of adsorbent is the average heat of adsorption per mole. Fortunately, it is this quantity which is most directly determined in a calorimeter.

In the following paper average heats of adsorption for one system (BaSO_4 and H_2O) are compared with values calculated from adsorption isotherms at three temperatures (20). The satisfactory agreement obtained shows that the prevailing concepts and approximations are adequate for an understanding of these phenomena for this particular system involving a powdered adsorbent. Undoubtedly there are other systems and other types of properties for which it will not prove adequate to ignore the complications inherent in solid adsorbents.

Acknowledgment

We are indebted to Stephen Brunauer, Rulon E. Johnson, Paul Seligmann, and Y. C. Wu for interesting and instructive discussions, suggestions, and penetrating arguments. We do not imply that all of our arguments are in complete agreement with the opinions of each of these scholars.

Literature Cited

- (1) Amberg, C. H., McIntosh, R., *Can. J. Chem.* **30**, 1012 (1952).
- (2) Bashforth, F., Adams, J. C., "An Attempt to Test the Theories of Capillary Action," Cambridge University Press, Cambridge, 1883.
- (3) Brunauer, S., "Adsorption of Gases and Vapors. Vol. I. Physical Adsorption," p. 218, Princeton University Press, Princeton, N. J., 1945.
- (4) Dole, M., McLaren, A. D., *J. Am. Chem. Soc.* **69**, 651 (1947).
- (5) Dunford, H. B., Morrison, J. L., *Can. J. Chem.* **33**, 904 (1954).
- (6) Gibbs, J. W., "Collected Works," Vol. 1, Yale University Press, New Haven, Conn., 1944.
- (7) Granville, W. A., Smith, P. F., Langley, W. R., "Elements of Calculus," p. 283, Ginn, Boston, 1946.
- (8) Harkins, W. D., "Physical Chemistry of Surface Films," pp. 80-3, Reinhold, New York, 1952.
- (9) Johnson, I., LaMer, V. K., *J. Am. Chem. Soc.* **69**, 1184 (1947).
- (10) Kington, G. L., Aston, J. G., *Ibid.*, **73**, 1929 (1951).
- (11) Klotz, I. M., "Chemical Thermodynamics," p. 11, Prentice-Hall, New York, 1950.
- (12) *Ibid.*, p. 211.

- (13) Kolthoff, I. M., Sandell, E. B., "Textbook of Quantitative Analysis," 3rd ed., p. 116, Macmillan, New York, 1952.
- (14) LaMer, V. K., Gruen, R., *Trans. Faraday Soc.* **48**, 410 (1952).
- (15) Lewis, G. N., Randall, M., "Thermodynamics, rev. by K. S. Pitzer, L. Brewer, p. 388, McGraw-Hill, New York, 1961.
- (16) *Ibid.*, p. 482.
- (17) Powers, T. C., *Proc. Am. Concrete Inst.* **43**, 584 (1947).
- (18) Thomson, W., *Phil. Mag.* (4) **42**, 488 (1871).
- (19) Treadwell, F. P., Hall, W. T., "Analytical Chemistry," Vol. II, 9th ed., p. 26, Wiley, New York, 1942.
- (20) Wu, Y. C., Copeland, L. E., *ADVANCES IN CHEM. SER. NO. 33*, 357 (1961).
- (21) Yates, D. J. C., *Advances in Catalysis* **9**, 481 (1957).
- (22) Young, Thomas, *Phil. Trans. Roy. Soc.* **65**, Part I (1805).

RECEIVED September 25, 1961.

Thermodynamics of Adsorption

The Barium Sulfate–Water System

Y. C. WU and L. E. COPELAND

*Research Department, Portland Cement Association,
Skokie, Ill.*

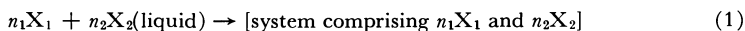
Adsorption isotherms for the system $\text{BaSO}_4\text{-H}_2\text{O}$ at three temperatures have been obtained. Thermodynamic study of these data reveals that part of the free energy decrease in the adsorption process involves changes in the partial molal free energy of the adsorbent. From the three isotherms differential and integral heats of adsorption were derived and compared with new calorimetric determinations of the same thermodynamic functions. In both kinds of measurements exactly the same system and exactly the same materials were used.

The primary purpose of this paper is to demonstrate the significance of the thermodynamic treatment developed in the previous paper (6), with an application to a simple binary adsorption system for which isotherms at three temperatures and calorimetric heats of adsorption have been made available. A free energy function, ΔG^\ddagger , was defined (6) to be equal to the change in free energy in an adsorption process involving a monodisperse adsorbent in which true thermodynamic equilibrium could be achieved. In this paper we use this free energy function, and functions for enthalpy and entropy defined in a similar manner, for the interpretation of data obtained from the adsorption of water on barium sulfate. Although the samples of adsorbent have a constant specific surface, they are not monodisperse and thermodynamic equilibrium within adsorbent particles probably is not maintained. The approximations that must be made to apply the thermodynamic functions to solid adsorbents were discussed in the previous paper. The agreement between enthalpy changes calculated from adsorption isotherms with calorimetrically determined values shown in this paper indicates that the approximations did not introduce significant errors. A change in the partial molal property of each component has been found to be an essential part of the corresponding integral change usually determined. The discussion of adsorption presented is closely parallel to discussions of solutions presented in familiar thermodynamic treatises.

An equation developed in the first paper (6) is identified in this paper by the Roman numeral I, followed by the number of the equation in that paper.

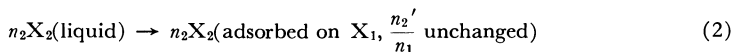
Two kinds of thermodynamic process will be discussed: an integral process, and a differential process.

The integral process may be written



This process represents the adsorption of n_2 moles of X_2 , initially liquid, upon n_1 moles of X_1 . It is equivalent to Process 1 of the preceding paper (6).

The differential process is Process I-4.

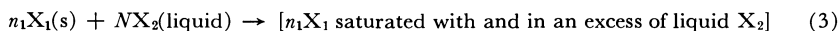


The negative of the enthalpy change for this particular process corresponds to the "net heat" of adsorption, since the process involves the transfer of the adsorbate from its liquid state to the surface of the adsorbent. (The "net heat" of adsorption of liquid adsorbate is in turn the difference between the heat of adsorption of the adsorbate vapor and the heat of condensation of the vapor.)

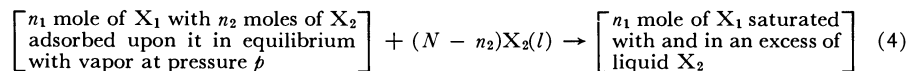
Enthalpy Changes in Adsorption

It has long been realized that the heat of adsorption can be calculated more accurately from determinations of heats of immersion than from equilibrium vapor pressures of adsorbates. Harkins and Boyd (8) and Jura and Harkins (10) have discussed the emersion process and have developed an expression for the enthalpy of desorption that is the negative of the one above. That the immersion process is equivalent to the process we are discussing can readily be shown with the aid of the following two-step process:

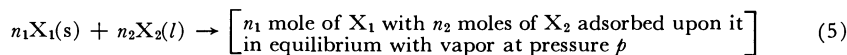
A. Immerse a clean adsorbent from a vacuum into a liquid adsorbate:



B. Immerse the adsorbent from a vapor, wherein n_1 moles of X_1 adsorbed n_2 moles of X_2 in equilibrium with vapor at pressure p , into a large amount of liquid adsorbate.



The difference between these two steps (A - B) gives the integral Process 1 expressed above:



The integral heat of adsorption is the difference between the heat of immersion of the clean adsorbent and the heat of immersion of the adsorbent, with n_2 moles of X_2 adsorbed upon it. This calorimetric heat of adsorption is to be compared with the heat of adsorption calculated from the temperature coefficient of the integral free energy change by Equation 6.

$$\left(\frac{\partial \frac{\Delta G^\dagger}{T}}{\partial \frac{1}{T}} \right)_{n_1, n_2, \sigma} = \Delta H^\dagger \quad (6)$$

The integral free energy is determined from an adsorption isotherm by Equation I-6. In practice it is sometimes simpler to determine the partial molal

free energy of the adsorbent, $\Delta\bar{G}_1^\dagger$, by integration of Equation I-12 (cf. I-4, 6) and then to obtain ΔH^\dagger by Equation 7

$$n_1 \left(\frac{\partial \frac{\Delta\bar{G}_1^\dagger}{T}}{\partial \frac{1}{T}} \right)_{n_1, \bar{G}_2, \sigma} = \Delta H^\dagger \quad (7)$$

Equation I-14 expresses the equality of $\Delta\bar{G}_1^\dagger$ with the surface excess free energy, $\sigma\Delta\gamma$. If, as is customary, the film pressure, π , is used for $-\Delta\gamma$, and the vapor can be considered to be a perfect gas, Equation 7 can be rewritten in its more familiar form

$$-n_1 \left(\frac{\partial \frac{\pi}{T}}{\partial \frac{1}{T}} \right)_{n_1, x, \sigma} = \Delta H^\dagger \quad (7a)$$

where x is the relative pressure of the vapor in equilibrium with the adsorbate.

The differential enthalpies can be deduced either by differentiation of the integral enthalpy with respect to the amount of each component or from the expressions for the corresponding differential free energies. The partial molal enthalpy of the adsorbent is

$$\Delta\bar{H}_1^\dagger = \left(\frac{\partial \frac{\Delta\bar{G}_1^\dagger}{T}}{\partial \frac{1}{T}} \right)_{n_1, n_2, \sigma} \quad (8)$$

This equation is similar to Equation 7, except that n_1 , n_2 , and T are the independent variables rather than n_1 , \bar{G}_2 , and T . Similarly, the partial molal enthalpy of the adsorbate is

$$\Delta\bar{H}_2 = \left(\frac{\partial \frac{\Delta\bar{G}_2}{T}}{\partial \frac{1}{T}} \right)_{n_1, n_2, \sigma} = R \left(\frac{\partial \ln x}{\partial \frac{1}{T}} \right)_{n_1, n_2, \sigma} \quad (9)$$

where x is the relative pressure of vapor in equilibrium with adsorbate. Equation 9 says that the net "isosteric" heat of adsorption is the negative change in partial molal enthalpy of the adsorbate. The "net" integral heat of adsorption could also be obtained by integration of the isosteric heat of adsorption over the range $n_2 = 0$ to n_2 .

Entropy Change in Adsorption

As with enthalpy changes, entropy changes are determined from appropriate temperature coefficients of the corresponding free energy changes. The change in partial molal entropy of the adsorbate is determined directly from the temperature coefficient of the change in free energy of the differential process (Equation 2).

$$\Delta\bar{S}_2 = - \left(\frac{\partial \Delta\bar{G}_2}{\partial T} \right)_{n_1, n_2, \sigma} = \left(\frac{\partial \Delta S^\dagger}{\partial n_2} \right)_{n_1, \sigma, T} \quad (10)$$

The integral change in entropy, ΔS^\dagger , is determined from the temperature coefficient of ΔG^\dagger . The change in differential entropy of the adsorbent, $\Delta\bar{S}_1^\dagger$, can be determined either from the difference between the changes in entropy of the integral

process and the differential Process 2, or from the temperature coefficient of $\Delta\bar{G}_1^\dagger$. These two procedures give precisely the same result, because the Gibbs-Duhem relation is applicable to $\Delta\bar{S}_2$ and $\Delta\bar{S}_1^\dagger$.

Experimental Procedures and Results

The Adsorbent. The barium sulfate used in these experiments was one of the finely divided materials prepared for the adsorption studies made by W. D. Harkins and his coworkers. This material was chosen for this work because we expected the barium sulfate-water system to be a simple system to investigate. That it is not a simple system became evident when the initial area determinations were obtained. Table I contains areas determined by adsorption of water on samples outgassed at 23° and 450° C.; by adsorption of nitrogen on a sample outgassed at 450° C.; and by the heat of immersion of a sample saturated with water. The molecular area of the water molecule was taken to be 11.4 sq. A. In experiment 2, the barium sulfate was outgassed at 450° C. and the area determined by adsorption of water. The sample was then outgassed by evacuation at room temperature and 10⁻⁶ mm. of Hg for 24 hours and the area re-determined (experiment 3). The agreement was poor. The fair agreement between the area calculated from experiment 3 and the area calculated from the heat of immersion (experiment 4) of the saturated sample suggested that barium sulfate might be slightly porous or that some water might be chemisorbed.

Table I. Measurements of Area of BaSO₄

No.	Method	Outgassing Temp., °C.	σ , Sq. M./G.
1	N ₂ adsorption	450	5.0
2	H ₂ O adsorption	450	4.5
3	H ₂ O adsorption	23	2.9
4	Heat of immersion	450	2.7

A vacuum thermogravimetric balance was then used to determine necessary conditions for outgassing. The result is shown in Figure 1. The sample was held at the temperatures indicated until the sample weight appeared to be constant over an interval of at least 4 hours. The results show that the water cannot be removed completely at any temperature below 600° C. Since our adsorption apparatus is not made of quartz, the outgassing temperature could not be as high as 600° C. The results reported here were obtained on samples outgassed in the temperature range 490° to 515° C. for 24 hours at 10⁻⁶ mm. of Hg. It is evident in Figure 1 that even this treatment did not remove all the water.

The area determined from nitrogen adsorption (5 sq. meters per gram) was used to calculate the surface pressure, π . The changes in free energy, enthalpy, and entropy for the processes being discussed are reported for the system containing 1 mole of barium sulfate, so any uncertainty pertaining to the accuracy of the area is not reflected in the results reported here, except for the absolute values of π .

Walton and Walden (15) have explained the behavior of barium sulfate. These authors suggest that the water coprecipitated with barium sulfate is held in pockets in the crystallites, where 3 molecules of water substitute for one BaSO₄ ion pair in the crystal lattice. In some instances, they found that more than 25% (mole basis) of water was held in this manner and could not be removed completely below 500° C. A small but measurable expansion of the lattice results from

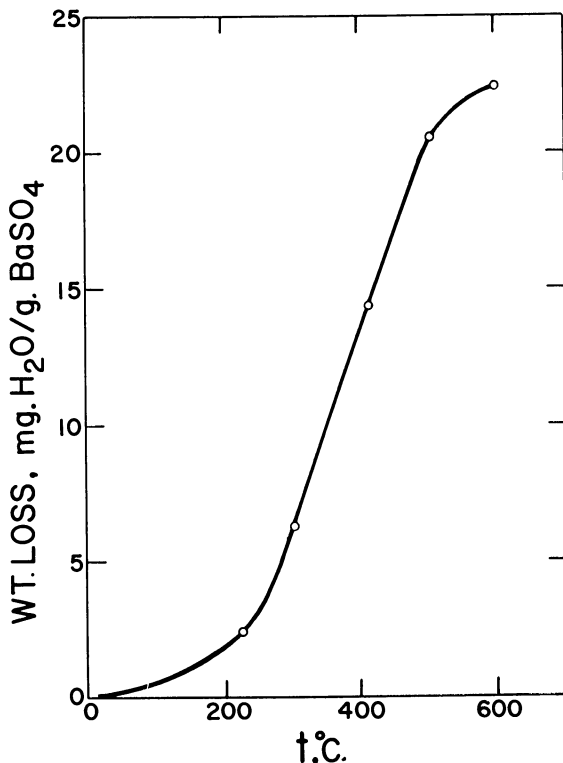


Figure 1. Weight loss of BaSO_4 in outgassing at different temperatures

the substitution. If the surface of barium sulfate contains a proportionate share of these pockets, the results shown in Table I are explainable.

Adsorption Isotherms. Adsorption isotherms (Figure 2) were determined at three different temperatures, 12.3°, 23.5°, and 31.5° C., by two procedures, one volumetric, the other gravimetric.

In the volumetric apparatus, the amount of water distilled from a calibrated capillary tube was determined by measurement of the change in level of the water in the capillary with a slide micrometer. The estimated error is about 1% of the amount adsorbed at low coverages, and less than 0.2% at high coverages.

In the gravimetric apparatus, a fused silica spring with a sensitivity of 2.8 mg. per mm. was used. Elongation of the spring was measured with a slide micrometer. The sample was suspended from the spring in a bucket, weighing 17 mg., formed from borosilicate glass wool. The error in weight of adsorbed water is estimated to be ± 0.01 mg. per gram of sample.

The water was purified by a vacuum distillation from alkaline potassium permanganate solution, followed by repeated vacuum sublimation from ice until the vapor from the water showed no residual permanent gas in a McLeod gage.

Pressure in the volumetric apparatus was measured by a McLeod gage and by a wide-bore (30-mm.) mercury manometer. Pressures measured with the McLeod gage were corrected for capillary depression of the mercury meniscus. Pressure in the gravimetric apparatus was controlled by regulation of the tempera-

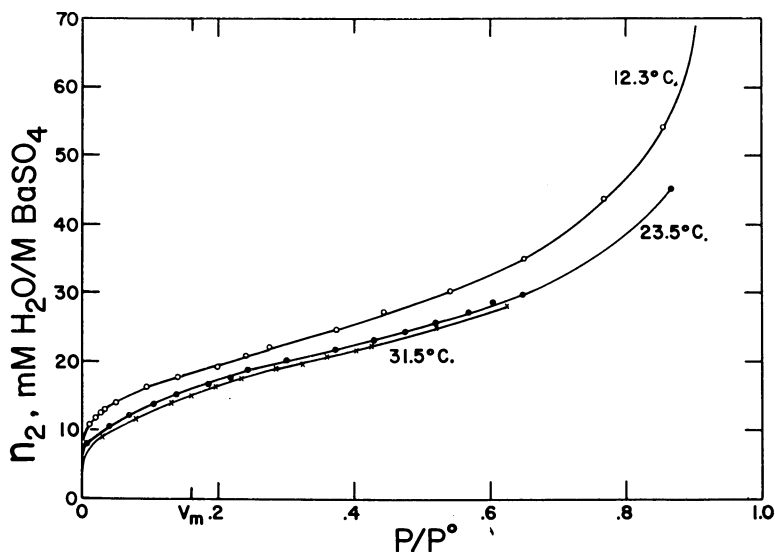


Figure 2. Adsorption isotherms of H_2O on BaSO_4

ture of the water source, except at one pressure (8.5 microns of Hg) where a mixture of magnesium perchlorate dihydrate and tetrahydrate was used (5).

Heat of Immersion. The adiabatic differential calorimeter used was similar in design to the isothermal differential calorimeter used by T. F. Young and somewhat like that used by Lange and Robinson (12). It will be described in detail elsewhere. The calorimeter was submerged in a water bath, the temperature of which was maintained the same as the mean temperature of the calorimeter to within 0.0005°C . The experiments were made at 23.5° to 24°C .

Samples were held in evacuated glass bulbs designed by Pierce (13). The sample bulb in the reference compartment contained water vapor at the same pressure as that in equilibrium with the sample, to compensate for the heat of condensation of water vapor in the sample bulb. Because of the design of the bulbs, no heat of breaking appeared in the calorimeter.

The amount of water adsorbed after the samples were outgassed was controlled by adjustment of the pressure in one of three ways: use of a sensitive Cartesian diver manostat, use of a water source at a controlled temperature, or use of the mixed magnesium perchlorate hydrates mentioned above. The amount of water adsorbed by the sample was measured either by the gain in weight of a companion sample or by interpolation from the isotherm at 23.5°C . The heat of immersion of samples with no water adsorbed was determined with samples sealed off from the vacuum line while they were still in the furnace at 500°C .

There is some evidence that the heat of immersion of the well outgassed samples was liberated during a rather long time. Consequently, the heats of immersion of these samples, and also of some of the samples with small amounts of water adsorbed, were determined by integration of the recorded time-temperature curve from the time the samples were wetted until the temperature of the calorimeter had returned to its steady state. Sixteen hours were required in the case of the freshly outgassed samples instead of the 5 to 6 hours normally required.

The heat of immersion results are plotted in Figure 3. The precision of the measurement depends upon the magnitude of the heat developed, and varies from about $\pm 5\%$ at saturation to about $\pm 2\%$ for the outgassed sample.

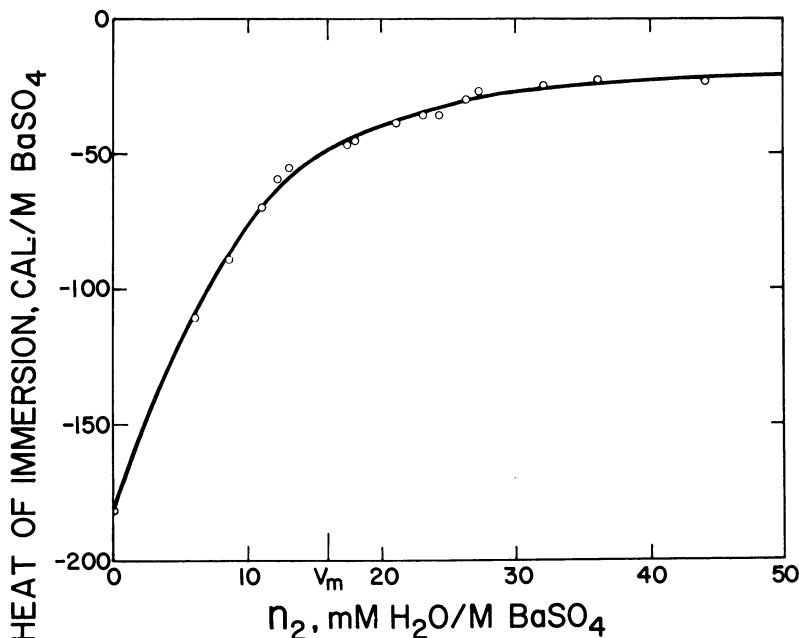


Figure 3. *Enthalpy of immersion*

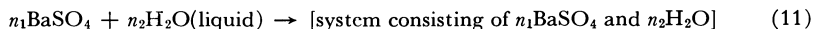
Graph shows change in enthalpy occurring when BaSO₄ with n_2 moles of water adsorbed upon it is immersed in water

Discussion of Results

The results presented here are for 1 mole—e.g., cal. mole⁻¹—except for π , which is reported in the customary units, erg cm⁻². It was also assumed that water vapor is a perfect gas; therefore

$$\Delta\bar{G}_2 = RT \ln x$$

Free Energy Change. The integral free energy change for the process



can be obtained by Equation I-6, although it is frequently more convenient to use the identity expressed in Equation 12.

$$\Delta G^\dagger = \int_0^{n_2} \bar{G}^2 dn_2 \equiv n_2 \bar{G}_2 - \int_0^{n_2} n_2 d\bar{G}_2 \quad (12)$$

The use of this identity is equivalent to the integration of the Gibbs adsorption equation (I-4).

$$\pi = \frac{RT}{\sigma} \int_{x=0}^x \frac{n_2}{n_1} d \ln x \quad (13)$$

Satisfactory integration cannot be performed unless adsorption data are obtained at very low pressures (11). The lowest pressure that could be measured reliably in this series of experiments was 8.5 microns of Hg. An empirical equation fitted to the experimental points at low pressure was used to extrapolate the isotherm to zero pressures. π calculated from each of the isotherms is plotted in Figure 4. Values of the decrease in surface energy, π , range upward to 200 ergs cm^{-2} at room temperature, a value about the same as is found in other solid-vapor adsorption systems and less than ten times as high as is obtained by the spreading of insoluble monolayers on water (7).

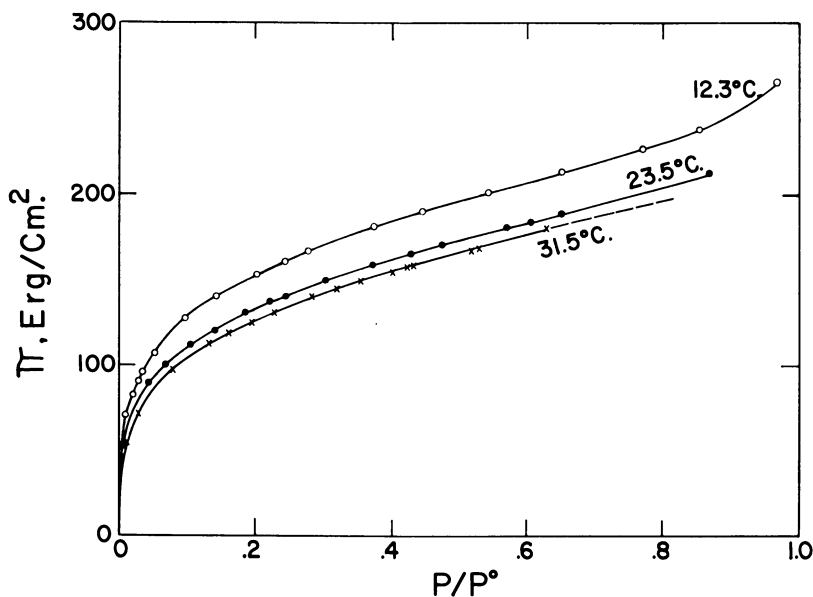


Figure 4. Reduction in surface free energy, π , caused by adsorption of water

The integral change in free energy, ΔG^\ddagger , and the contribution to ΔG^\ddagger by barium sulfate, $n_1\Delta\bar{G}_1^\ddagger$, and by water, $n_2\Delta\bar{G}_2$, are plotted in Figure 5. The dashed lines are extrapolations to zero coverage based upon the empirical equations fitted to the data at low pressures.

The integral change in free energy, ΔG^\ddagger , decreases monotonically with increasing coverage, as it must because the adsorption process is spontaneous for an increase in vapor pressure of the adsorbate. The curve for $n_2\Delta\bar{G}_2$ has a slope of $-\infty$ at zero coverage and decreases with increasing coverage in the low coverage region, but passes through a minimum and increases with increasing coverage in the region where experimental points could be obtained. The difference between these curves gives the curve for $n_1\Delta\bar{G}_1^\ddagger$. This curve decreases monotonically with coverage, and shows that BaSO_4 is not an "inert adsorbent" (9) for water. The behavior of $n_1\Delta\bar{G}_1^\ddagger$ and $n_2\Delta\bar{G}_2$ at low coverages suggests that in systems where Henry's law is obeyed, and perhaps in systems that give a Type III isotherm, the "inert adsorbent" approximation might be satisfactory for some purposes even though $\Delta\bar{G}_1^\ddagger$ is not zero.

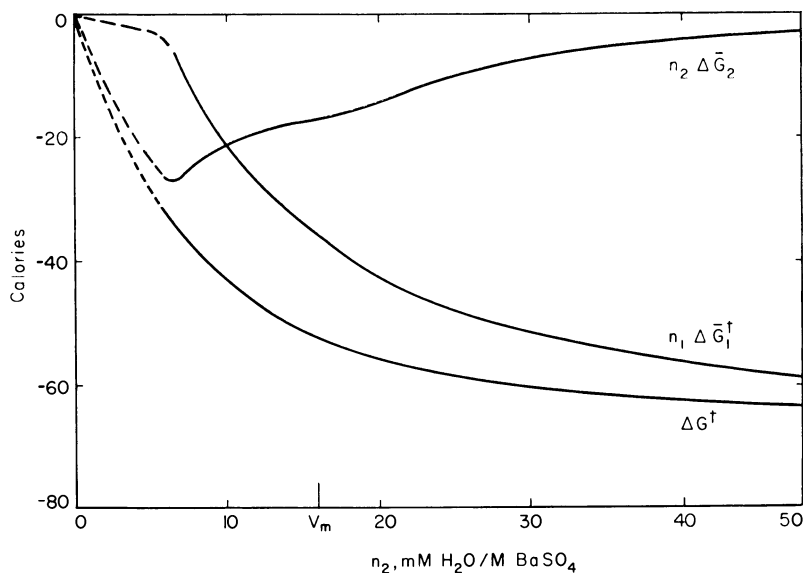


Figure 5. Free energy change of adsorption of water on barium sulfate. Integral change in free energy, ΔG^\ddagger , is for system containing 1 mole of barium sulfate
 - - - Extrapolations

Enthalpy Change. The enthalpy change measured by the heats of immersion (smooth curve) and calculated with Equation 7 (plotted points) is compared in Figure 6. The agreement is satisfactory, since the integration of the Gibbs adsorption equation depends so strongly upon the extrapolation of the adsorption isotherm to $x = 0$.

The differential enthalpies are shown in Figure 7. The line through the chords represents $\Delta\bar{H}_2$ from heats of immersion. The plotted points are calculated from the isotherms with Equation 9, and agree satisfactorily with the curve. The curve for $\Delta\bar{H}_1^\ddagger$ was calculated from $\Delta\bar{H}^\ddagger$ and $\Delta\bar{H}_2$. In general, the changes in partial molal thermodynamic properties of adsorbents are smaller than for adsorbates, because partial molal properties are average properties of the respective component. Figure 7 shows that $\Delta\bar{H}_1^\ddagger$ is smaller than $\Delta\bar{H}_2$; nevertheless, the contribution of barium sulfate to the integral enthalpy change is larger than that of water, except at coverages lower than about a half of a monolayer (Figure 6).

It was pointed out (6) that the partial molal properties of the adsorbent are average properties. The change may not be so large near the center of an individual particle as at its surface. Because the adsorbent is a solid, complete equilibrium of each part of a given particle with other parts of it cannot be assumed. The center of a large particle at a depth to which the effect of adsorbate does not penetrate may sometimes be regarded as entirely inert material—of no more importance to the problem than a phase of an entirely different inert substance. The changes in the partial molal properties of regions near the surface therefore are likely to be somewhat larger than the quantities calculated. The phenomenon therefore is one which must not be ignored in a completely thermodynamic treatment of adsorption. For some purposes, however, the effects may be ignored—and the procedures will be entirely adequate for those purposes.

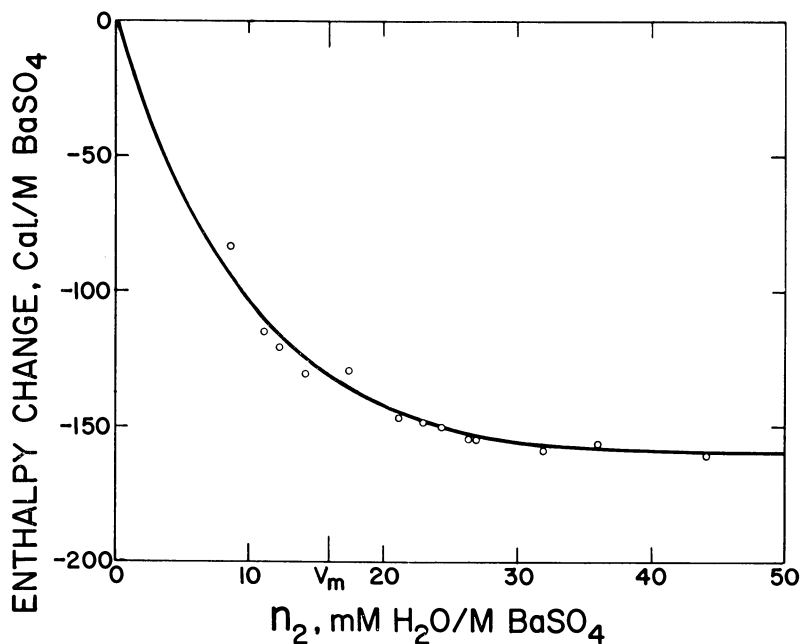


Figure 6. Enthalpy change for adsorption of water (l) on 1 mole of barium sulfate

— Data determined calorimetrically
 ○ Results calculated from temperature coefficient of π

The maximum magnitude of the change in partial molal enthalpy of the adsorbent at its surface may be estimated from the following speculations. We have used n_1 as the number of moles of solid in the system. We know that the contribution to the surface energy from the respective layers in the lattice decreases rapidly as the distance from the surface increases. In fact, a large fraction of the surface energy is contributed by the first layer (14). About 1.6% of the BaSO_4 in this sample is in the first surface layer of ions. If we assume that only this first layer is affected by adsorption, the partial molal change in enthalpy of the adsorbent would be 70 times as great as shown in Figure 7. Several layers can be affected by adsorption, and the value of $\Delta\bar{H}_1^\dagger$ at a monolayer coverage would still be of the same order of magnitude as that of $\Delta\bar{H}_2$.

As pointed out above, ΔH^\dagger for the process studied here is the net heat of adsorption. $\Delta\bar{H}_2$ is then a net differential heat of adsorption. $\Delta\bar{H}_1^\dagger$ is the same as it would be for the adsorption process involving adsorption of vapor instead of liquid.

Entropy Change. The entropy change in the adsorption of water on barium sulfate is shown in Figure 8. The integral entropy, ΔS^\dagger , calculated from ΔG^\dagger and ΔH^\dagger decreases monotonically with increasing amount adsorbed. ΔS^\dagger can also be calculated from the temperature coefficient of π by

$$\Delta S^\dagger = n_1 \sigma \left(\frac{\partial \pi}{\partial T} \right)_{x, n_1, \sigma} - n_2 R \ln x \quad (14)$$

Points calculated by Equation 14 are plotted on the curve for ΔS^\dagger .

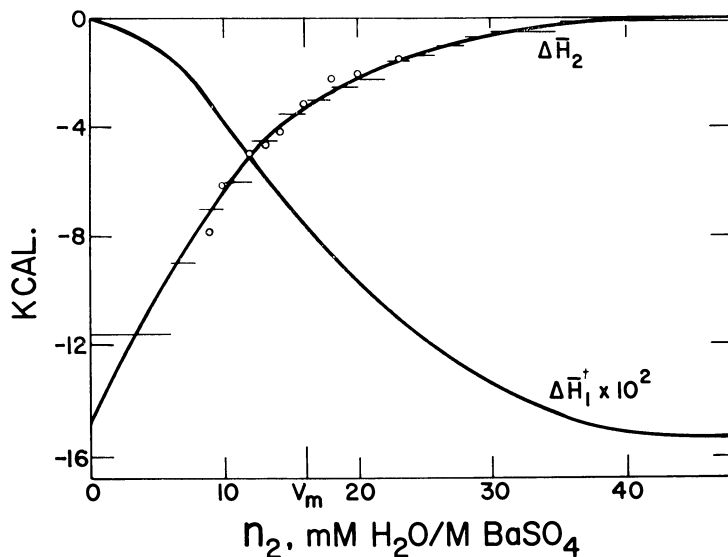


Figure 7. Differential enthalpy changes for adsorption of water (l) on barium sulfate

- $\Delta\bar{H}_2$. Change in partial molal entropy of water
 — Chord plot of calorimetric data
 ○ Results calculated from temperature coefficient of x
 $\Delta\bar{H}_1^\dagger$. Change in partial molal entropy of barium sulfate

The partial molal entropies are calculated from the partial molal free energies and enthalpies. The change in the partial molal entropy of water increases monotonically to a value near zero with increasing amount adsorbed. The partial molal entropy of barium sulfate decreases with increasing amount adsorbed.

Conclusion

Data from two types of experiments have been used to calculate changes in thermodynamic properties of adsorption systems. The agreement is within experimental error and indicates that a complete thermodynamic treatment is as useful for adsorption systems as for solutions.

In the very low coverage region we used an empirical equation to obtain π . The integral heat of adsorption calculated from isotherms is very sensitive to the temperature coefficient of π . Figure 6 shows that agreement between heats of adsorption calculated from the temperature coefficient of π and those measured calorimetrically is good, and Figure 8 shows that ΔS^\dagger calculated from the integral free energy and enthalpy changes agrees within experimental error with ΔS^\dagger calculated from the temperature coefficient of π . The enthalpy change depends upon the temperature coefficient of π , and the free energy change depends upon the magnitude of π . The agreements indicate that the temperature coefficient, as well as the magnitude, of π was estimated satisfactorily.

Much more work on many systems is needed to achieve an adequate understanding of the low coverage region of adsorption systems.

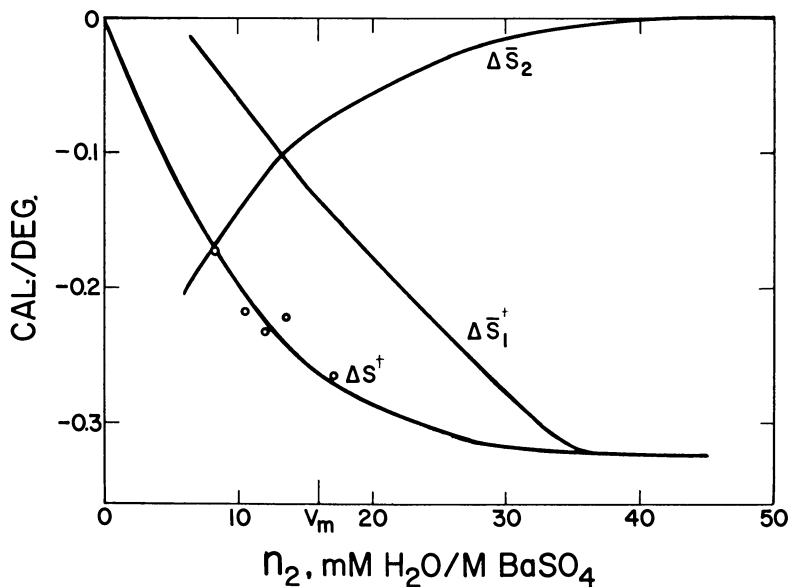


Figure 8. Entropy change for adsorption of water (l) on barium sulfate

— Entropy functions calculated from free energy changes and calorimetrically determined enthalpy changes
 ○ Entropy changes calculated from temperature coefficient of π

Acknowledgment

We express appreciation to T. F. Young and to Stephen Brunauer for many helpful discussions and constructive criticism. We are indebted to Conway Pierce for suggestions improving our experimental techniques, and to Robert Landgren and Fletcher Klouthis for aid in preparing this manuscript.

Literature Cited

- (1) Armbruster, M. H. A., Austin, J. B., *J. Am. Chem. Soc.* **66**, 159 (1944).
- (2) Bangham, D. H., *Trans. Faraday Soc.* **33**, 805 (1937).
- (3) Bangham, D. H., Razouk, R. I., *Proc. Roy. Soc. (London)* **A166**, 572 (1938).
- (4) Bangham, D. H., Razouk, R. I., *Trans. Faraday Soc.* **33**, 1463 (1937).
- (5) Copeland, L. E., Bragg, R. H., *J. Phys. Chem.* **58**, 1075 (1954).
- (6) Copeland, L. E., Young, T. F., *ADVANCES IN CHEM. SER. No. 33*, 348 (1961).
- (7) Harkins, W. D., "Physical Chemistry of Surface Films," Reinhold, New York, 1952.
- (8) Harkins, W. D., Boyd, G. E., *J. Am. Chem. Soc.* **64**, 1195 (1942).
- (9) Hill, T. L., *Advances in Catalysis* **4**, 212 (1952).
- (10) Jura, G., Harkins, W. D., *J. Chem. Phys.* **11**, 561 (1943).
- (11) Jura, G., Hill, T. L., *J. Am. Chem. Soc.* **74**, 1598 (1952).
- (12) Lange, E., Robinson, A. L., *Chem. Revs.* **9**, 89 (1931).
- (13) Pierce, W. C., University of California, Riverside, Calif., private communication.
- (14) Van der Hoff, B. M. E., Benson, G. C., *J. Chem. Phys.* **22**, 475 (1954).
- (15) Walton, G., Walden, G. H., Jr., *J. Am. Chem. Soc.* **68**, 1750 (1946).

RECEIVED October 2, 1961.

A

Activation energy..... 141
 energy for surface diffusion of argon
 and methane..... 180

Adams, A..... 237

Adams, J. C..... 355

Adamson, A. W..... 51, 60, 62, 70

Adsorbate-adsorbent interaction..... 222
 spreading pressure..... 249

Adsorbent self-potentials..... 248

Adsorption. *See also* Argon, Benzene,
 Butane, Chlorodifluoromethane,
 Cyclohexane, Deuterium,
 Dichlorofluoromethane, Do-
 decane, Ethane, Halide ions,
 Hydroxyl ions, Inert gases,
 Iso-octane, Methane, Meth-
 anol, 2-Methylpentane, Neon,
 Neopentane, Nitrogen, Oxy-
 gen, Pinene, Propanol, Sulfur
 hexafluoride, Thermodynam-
 ics, Water vapor, Xenon

Adsorption on. *See* Anatase, Asbestos,
 Bone mineral, Boron nitride,
 Cadmium bromide, Calcium
 chabazite, Carbon black, Cha-
 bazite, Chlorodifluoromethane,
 Chromic oxide, Cobalt
 molybdate, Diamond, Ferric
 hydroxide, Germanium,
 Graphite, Graphon, Halozeo-
 lite, Hydroxyapatite, Metals,
 Mica, Nickel, Octadecane,
n-Octadecylamine, Paraffin,
 Platinum, Quartz, Rutile,
 Saran charcoal, Silica, So-
 dium bromide, Thoria, Ti-
 tanium dioxide, Zinc oxide

on aged surface..... 155

apparatus, automatic..... 133, 134

average heat of..... 7

change with surface pretreatment.. 156

delay in..... 147

free energy of..... 40

-extension. *See* Argon, Ethane,
 Helium, Hydrogen, Krypton,
 Nitrogen, Water vapor

of gases, effect on contact potential. 100

integral entropy of..... 39

isotherms. *See also* Argon, Ben-
 zene, Bone mineral, Bromine,
 Cyclohexane, Methanol,
 Neon, Nitrogen, Quartz

for the square lattice..... 246

knee..... 317

physical..... 13, 317

Adsorption potentials..... 248, 257
 of oxygen and nitrogen on anatase
 224
 rate of, at low surface coverage... 146
vs. thermal history of solid..... 158

sites, change in..... 155

thermodynamics of..... 348, 357

Adsorptive energy..... 302
 forces between inert gases and a
 graphite surface..... 309
 potentials, Gaussian distribution of. 317

Adzumi, H..... 172, 176

Alder, B. J..... 26, 30

Alite, hydration of..... 200

Allen, A. O..... 70

Alumina, low angle x-ray scattering . 23

Aluminosilicate..... 123

Aluminum oxide..... 20

Amberg, C. H..... 182, 280, 300, 355

Amphlett, C. B..... 70

Anatase, adsorption of oxygen and
 nitrogen on..... 224

Anderson, D. M..... 332, 338, 339

Anderson, Elaine..... 219

Anderson, P. J..... 171

Andrews, J. F..... 263

Anomalous solubility of ferric oxide.. 78
 of quartz..... 79

Area of barium sulfate..... 360

Arens, P. L..... 339

Argon
 adsorption..... 126
 on cadmium bromide..... 318
 on calcium chabazite..... 127
 on diamond..... 146
 -extension..... 252
 on graphite..... 146, 303
 on halozeolite..... 127
 isotherm..... 8, 299
 parameters..... 307, 320
 on saran charcoal..... 173
 on silica..... 77
 on sodium bromide..... 319
 differential heats of adsorption...
 298, 326, 327
 dispersion interaction with graph-
 ite..... 312
 heat of adsorption. 127, 128, 131, 175, 291
 instantaneous isotherms..... 157
 rate of adsorption on diamond.....
 153, 155, 156

Armbruster, M. H. A..... 368

Armstrong, E. J..... 41

Arnold, J. R..... 228

Asbestos, ethane adsorption on..... 158
 irradiation of..... 67

Asbestos, surface area of.....	67
Aston, J. G.....	70, 71, 87, 280, 296, 325, 331, 355
Asymmetry in adsorptive potentials on solid surfaces.....	317
Atomic oxygen in lattice structure....	119
Auger ionization.....	70
Austin, J. B.....	368
Avgul, N. N.....	311, 312
Azides.....	79

B

Bailar, J. C., Jr.....	81
Balk, P.....	27, 29
Ballou, E. V.....	133, 139, 324
Bangham, D. H.....	249, 368
Bardeen, J.....	237
Bare surface, heterogeneity of.....	328
Barium sulfate, differential enthalpy for water adsorption.....	367
enthalpy for adsorption of water on	366
entropy for adsorption of water....	368
solubility.....	82
Barium sulfate-water system.....	357
Barium titanate.....	77
Barrer, R. M.....	123, 132, 173, 257, 268
Barrett, E. P.....	134, 135
Barrie, J. A.....	181
Barron, T. K. H.....	263
Bartell, F. E.....	41
Barth, R. T.....	133
Bashforth, F.....	355
Bassett, D. W.....	197
Baudisch, O.....	43
Baynham, J. W.....	132
BDDT theory.....	6, 13
See also BET theory	
Becker, J.....	143, 227
Beebe, Ralph A.....	71, 181, 280, 291, 300
Bemmels, C.....	11, 17
Benard, J.....	99
Benedicks, C.....	76
Benson, G. C.....	26, 33, 34, 257, 263, 368
Benton, D. P.....	169
Bentonite clay.....	336
Benzene, adsorption isotherms on Fe ₂ O ₃ gel.....	11
adsorption on TiO ₂	8
Berard, J.....	87
Berenyi, L.....	52
Berg, W. T.....	263
Berman, R.....	158
Bernal, J. D.....	45
Bernett, M. K.....	101
Beskova, G. S.....	198
BET.....	2, 291
analysis.....	39, 47, 56, 125
apparatus.....	175
method.....	65, 202
model.....	222
plots.....	231
surface area.....	135, 137, 138, 260, 265, 282

BET theory.....	6, 111, 220
Bewig, K. W.....	100
Bieffer, G. J.....	171
Bienes, H.....	181
Bigelow, W. C.....	113
Bird, R. B.....	280
Blake, J. C.....	171
Block, J.....	237
Blue, E. M.....	197
Bockris, J. O'M.....	171
Bohr magneton.....	97
Bone mineral, adsorption on.....	291
Booth, F.....	171
Booth, H. S.....	49
Borelius, G.....	99
Born, M.....	33, 345
Boron nitride, adsorption of argon and nitrogen on.....	318
Boswell, F. W. C.....	74
Boudart, M.....	158, 159
Boyd, G. E.....	8, 9, 41, 321, 322, 358
Bradley, W. F.....	339
Bragg, R. H.....	219, 368
Brattain, W.....	237
Bray, R. I.....	9, 10
Breck, D. W.....	132
Brewer, L.....	356
Bridgman, P. W.....	19, 20
Brittin, W. E.....	290
Britton, J. Doyle.....	98
Brockway, L. O.....	111
Bromine, adsorption isotherms on silica gel.....	10
Brout, R.....	347
Brown, W. L.....	237
Brünig, H.....	87
Brunauer, Stephen.....	2, 5, 17, 43, 47, 49, 55, 70, 73, 113, 125, 146, 199, 219, 221, 222, 223, 227, 263, 282, 287, 355, 368
Buchanan, A. S.....	171
Buessem, W.....	80
Buff, Frank P.....	340, 347
Buhl, R.....	290
Bulk compression in crystals.....	74
Bultitude, F. W.....	132
Bumble, S.....	240, 243, 245, 246, 280
Bunn, C. W.....	85
Bupp, L. P.....	63
Burger, R. M.....	121
Bursh, T. P.....	41
Burwell, R. L., Jr.....	183, 197
Butadiene.....	197
Butane, adsorption on rutile.....	56
from thiophene.....	182
Butene.....	191
Butler, C. C.....	74

C

Cadmium bromide, adsorption of ar- gon on.....	318
Caffrey, J. M., Jr.....	70

- Calcite 78
 Calcium chabazite 127
 fluoride 83
 β -orthosilicate, stabilized 80
 palmitate 101
 silicate hydrate 13
 silicates, surface hydration of 199
 sulfate 83
 Cameron, A. E. 10
 Cannon, Peter 122, 132, 268, 324
 Carbon black, graphitized 63
 irradiation of 67
 surface area 67
 Carbon dioxide, heat of adsorption 131
 Carbon monoxide, heat of adsorption 131
 Carbon surface, interaction with gas
 or liquid 258
 Cardew, M. 197
 Carman, P. C. 173
 Caron, A. 65
 Carpenter, Frank G. 146, 159
 Carruthers, J. C. 171
 Cassie, A. B. D. 11
 Caswell, E. G. 324
 Cawley, C. M. 197
 Chabazite, adsorption on 127
 isosteric heat on 130
 Champion, W. M. 70, 280
 Chandron, G. 87
 Channen, E. W. 263
 Chapman, J. A. 111
 Charge transfer, adsorption energy
 from 310
 Checkel, R. L. 113
 Chemical reactivity of solids 77
 Chemisorption 73, 222
 of oxygen 114
 surface polarization in 225
 Chessick, J. J. 41, 229, 237
 Chlorodifluoromethane adsorption 123, 125
 Chon, Hakze 325
 Choudhury, B. K. 171
 Chromia catalyst 184
 Chromic oxide, adsorption of deu-
 terium 158
 of hydrogen 158
 Clampitt, B. H. 8, 9, 11
 Clark, A. M. 11, 17
 Clark, H. 321, 323
 Clay-liquid systems, density studies
 in 332
 Clay-water systems 333
 Clays, density of water absorbed by 332
 Clelland, D. W. 41
 Clinoenstatite 80
 Cobalt molybdate catalyst, adsorp-
 tion on 188
 reactions on 185
 Coes, L. 78
 Colatitude curves 116
 Cole, H. D. 35
 Collier, D. W. 159
 Complexes, effect on nucleation 83
 Concrete 13
 Constabaris, G. 308
 Contact potential, difference of alu-
 minum and soft steel 103, 106
 of gold and platinum 104, 105
 of platinum and coated platinum 107
 effect of adsorbed solid monolayer
 on 110
 effect of gas adsorption on 100
 effect of humidity on 106, 107
 Conway, J. 22
 Cook, M. A. 220, 228
 Cooling rate of powders 150
 Copeland, L. E. 5, 6, 13, 14, 17,
 200, 213, 219, 348, 356, 357
 Cordes, H. 50, 324
 Corrin, M. L. 70
 Courant, Richard 4
 Cremer, E. 192
 Crowell, A. D. 280, 313, 314
 Crowell's lattice sum 312
 Crystal growth, effect of temperature
 on 83
 pulsating 82
 smooth 83
 Crystallization, hydrates 82
 sodium chloride 82
 Cubicciotti, D. 29
 Culbertson, J. L. 41
 Cupric acetylide 79
 halides, electronic interaction in 79
 Curtis, C. F. 280
 Cushioning particles in crystalliza-
 tion 82
 Cutler, J. B. 228
 Cyclohexane, adsorption on ferric hy-
 droxide 43
 adsorption isotherms of 44, 45
 Cynarski, J. 300
 Czanderna, A. W. 70
- D**
- d*-Band 89
 Dacey, J. R. 172, 181, 249, 251
 Dana, E. S. 49
 Dary, W. 87
 Dasgupta, D. R. 45
 Dative bonding, adsorption energy
 from 310
 Datta, S. K. 51, 62, 70
 Davis, H. M. 80
 Davis, H. T. 316
 Davis, L. 237
 De, P. K. 171
 de Boer, J. H.
 61, 105, 239, 305, 310, 314, 322
 Decalin, adsorption of 170
n-Decane 338
 D'Eustachio, D. 41
 Deeds, C. T. 332

de Haan, D. B.	308
Deitz, V. R.	146, 159
deMars, G. A.	237
Deming, L. S.	11, 17, 113
Deming, W. E.	11, 17, 113
DeMoyer, G.	171
Dempsey, Edward	26
Dempsted, P. B.	41
Dent, B. M.	73, 316
Derjaguin, B. V.	166
De Smet, M.	171
Desorption isotherm	136
Deuterium, adsorption on chromic oxide	158
adsorption on saran charcoal	173
heat of adsorption	175
de Wit, C. P.	339
De Witt, T. W.	9, 10, 181
Diamond, adsorption of argon and nitrogen on	146
cooling rate of	152
heat capacity of	151
β -Dicalcium silicate	13, 14, 199
Dichlorodifluoromethane adsorption	123
Differential energy of adsorption	127
heats of adsorption of rare gases	326, 327
Digital computer and automatic adsorption	133
Dillon, J. A., Jr.	121
Dipole moments of ions in surface layers	32, 34
Direct lattice sum	310
Dispersion potential	310
Displacement of ions in surface layers	31, 34
Distortion correction of surface region	30
Dobbs, E. R.	276
Docosyl alcohol monolayer on electrode	110
Dodecane, adsorption of	170
Dole, M.	355
Dolomite	78
Domb, C.	247
Doolen, O. K.	139
Douglas, B. E.	81
Dowden, D. A.	296, 297
Drain, L. E.	56
Dry, M. E.	292, 293, 294, 296, 297
Dukhin, S. S.	166
Dunford, H. B.	355
Durability of solid monolayer	109
Dusting of solids	80

E

Edelhoch, H.	321
Effluorescence on scratching	80
Egorov, M. M.	41, 290
Ehrlich, G.	142, 223
Einstein, Albert	4
Eischens, R. P.	226

Electrodes, resin-coated, adsorption on	103
Electron diffraction	114
Electronic properties of solids	77
El Gobeily, M. A.	50
Ellis, R.	170
Elongation as a function of pressure	254
Elovich, S. Yu.	226
Elovich-Taylor-Thon equation	226
Elton, G. A. H.	169
Emmett, P. H.	2, 5, 6, 9, 10, 11, 17, 43, 47, 49, 56, 70, 71, 85, 181, 182, 183, 221, 222, 228, 297
Energy change on adsorption, potential	302
Enright, D. P.	76
Enthalpy changes in adsorption	358
partial molal	350
of the sorbed phase	123
Entropy change in adsorption	359
differential, on adsorption	301
Environment, effect on properties of solids	72
Epitaxy	83
Equilibria, effect of environment on	73
Ethane, adsorption on asbestos	158
on sodium chloride	322
adsorption-extension	255
Eucken, A.	75
Evans, U. R.	78
Evdomikov, V. B.	99
Eversole, W. G.	132
Every, R. L.	41, 290
Exchange processes	115
Expansion of silica glass	77
Eyring, E. M.	4, 140, 145, 226

F

Fajans, K.	73, 74, 77, 79
Faraday, Michael	77, 80
Farnsworth, H. E.	114, 121
Feigl, F.	78, 82
FEP Teflon as electrode coating	102
Ferric hydroxide, adsorption of methanol on	43
Ferric oxide, adsorption on	78
apparent solubility	45
Field, E.	61
Fisher, B. B.	320, 321, 323
Flood, E. A.	173, 248, 263
Flow rate of water vapor through micropore carbon	253
Fluorination of silica-alumina catalyst	137
Ford, M. A.	18
Foreign atoms, effect on surface symmetry	77
Forestier, H.	76, 81
Foster, A. G.	49
Foster, E. L.	158
Fowkes, F. M.	112

Fowler-Guggenheim isotherm.....	239
Fowler, R. H....	61, 115, 120, 247, 263, 280
Fox, H. W.....	113
Fractional change in interaction energy.....	274
Frazier, W.....	139
Free energy change.....	363
Freeman, M. P.....	280
Freeman, P. I.....	26
French, R. O.....	228
Frenkel, J.....	53, 60, 73
Freundlich relationship.....	169, 222, 227
Friedrick, H. G.....	159
Frumkin, A.....	171
Fuerstenau, D. W.....	168, 171
Funk, H.....	219

G

Gaines, G. L., Jr.....	132, 264, 268
Galstaun, L. S.....	87
Gamma irradiation.....	67
Gamov, George.....	4
Gard, J. A.....	216
Garner, W. E.....	237
Garret, C. G. B.....	237
Gas flow through charcoal.....	179
Gas lattice structures.....	118
Gatos, H. C.....	158
Gaudin, A. M.....	167, 171
Gaussian distribution of adsorptive potentials.....	317
Gehm, G.....	99
Geith, M. A.....	43
George, T. H.....	121
Gerlick, D.....	237
German, D. E.....	8, 9, 11
Germanium, adsorption of 1-pro- panol on.....	229, 237
Gershinowitz, Harold.....	145
Ghosh, D. N.....	171
Gibb, J. G.....	41
Gibbs adsorption equation.....	340, 363
Gibbs-Duhem equation.....	346
Gibbs, J. W.....	15, 263, 354
Gibbs potential.....	248, 251
Gibson, A. F.....	237
Gilbert, E. C.....	63
Gillespie, J. F.....	98
Gillespie, L. J.....	87, 91, 99
Girgis, B. S.....	42
Glass, E.....	113
Glauberger, A. E.....	33
Goethite.....	43
Gold, lattice parameters in.....	74
Gomer, R.....	12, 85
Good, R. J.....	71, 280
Goodman, J. F.....	42, 46
Gottlieb, M. H.....	112
Gouy, G.....	171
Gouy theory.....	165
Granville, W. A.....	355

Graphite	
adsorption of argon and nitrogen on.....	146
potentials and vibrations of inert gases on.....	301
of water vapor on.....	318
dispersion interaction of inert gases with.....	312
lattice parameter.....	74
surface, adsorptive forces between the inert gases and.....	309
Graphon, adsorption on.....	58
Green, H. S.....	345
Green, M.....	237
Greenberg, S. A.....	215
Greenfield, B. F.....	70
Greenschlag, S.....	280
Greenwald, S.....	41
Gregg, S. J.....	42, 46, 50
Greyson, J.....	70, 280
Griffith, A. A.....	75
Griffith, R. H.....	184
Griffith's flaws.....	75
Grossman, L.....	25
Grove, D. M.....	181
Growth-active impurities.....	83
Grudemo, A.....	213
Gruen, R.....	356
Guggenheim, E. A.....	61, 247, 248, 280
Gundry, P. M.....	316

H

Habgood, H. W.....	192
Hackerman, Norman.....	35, 41, 282, 290
Haines, R. S.....	76, 250
Haissinsky, M.....	70
Halenda, P. P.....	134, 135
Halide ions, adsorption on paraffin...	169
Hall, A. C.....	41
Hall, C. C.....	197
Hall, F. P.....	98
Hall, W. K.....	198
Hall, W. T.....	356
Halozoolite, adsorption of argon on.. surface properties of.....	126
Halsey, G. D., Jr.....	60, 70, 269, 280, 303, 307
Hammar, C. G. B.....	197
Hanlan, J. E.....	197
Hardy, W. B.....	109
Harkins-Jura absolute surface area...	282
Harkins, W. D.....	6, 8, 9, 15, 41, 50, 65, 66, 355, 358, 368
Harrison, L. G.....	34
Hartung, W. H.....	43
Hassis, C. H.....	229
Hathaway, Donn.....	219
Hauser, E.....	339
Haybittle, J. L.....	70
Haydon, D. A.....	165
Hayes, J. C.....	200, 219
Healey, F. H.....	41

Heat	
of adsorption	309
on aluminosilicates	122
constant	12
differential	302
<i>vs.</i> gas polarizability	131
integral	350
isosteric	57, 302
of silica	36
variation with coverage	12
capacity of diamond	151
of emersion	9
of immersion of quartz	38
in silica-water systems	281
of solution of tobermorite	15
transfer	150
of vaporization, bulk liquid	8
thin films	8
Hectorite clay	337
Hedvall, J. A.	81
Heinemann, H.	193
Helium	
adsorption, effect on contact potential	109
-extension for	252
differential heat of adsorption of, <i>vs.</i> coverage on TiO ₂	327
potential energy of interaction with argon	276
Heller, L.	13, 219
Helmholtz, H.	163
Helmholtz-Smoluchowski equation	166
Helper, L. G.	61
Hematite	45
Henry, D. C.	171
Henry's law region	303
Herring, C.	113
Heterogeneous surface, adsorption on	328
Hexafluoropropylene as electrode coating	10
Hexene, effect on thiophene conversion	193
Heyding, R. D.	263
Heymann, E.	171
HFPS. <i>See</i> Hexafluoropropylene	
High pressure isotherms	65
Hijmans, J.	239
Hill, E.	61
Hill, T. L.	11, 12, 36, 39, 223, 280, 368
Hilsenrath, Seymour	247
Hime, William	219
Himmelsturm, D.	87
Hinchen, J. J.	317
Hirschfelder, J. O.	280
Hoare, F. E.	99
Hofmann, U.	74
Holbeche, T. A.	113
Holmes, B. G.	290
Holmes, J. M.	291, 300
Honig, J. M.	
.	52, 56, 65, 70, 239, 247, 280
Howard, F. L.	41
Howison, J. W.	216
Huber, M. E.	263
Hudda, F. G.	223
Hüttig, G. F.	43, 46
Huggins, M. L.	34
Hulburt, H. M.	99
Hund's rule	90
Hydration of expanding lattice clays	335
of incompletely screened surfaces	79
Hydrocarbon liquids, clays in	333
Hydrodesulfurization of thiophene	182
Hydrogen	
adsorption on chromic oxide	158
effect on contact potential	109
-extension for	252
by palladium	86
on saran charcoal	173
heat of adsorption	131, 175
isotherms on palladium	91
-palladium system	87
Hydrogen sulfide, displacement by hydrogen	195
from thiophene decomposition	182, 197
Hydroxyapatite, adsorption on	153
Hydroxyl ions, adsorption by octadecane	170
I	
Idleman, J. A.	198
Iler, R. K.	41, 219, 290
Induction forces, adsorption energy from	310
Inert gases, adsorption potentials and vibrations of, on graphite	301
effect on reactivity of solids	80
Infrared spectra of halozeolite	124
Integral free energy	350
Interaction of adsorbable gas with ideal interface	261
Interaction energy, fractional change in	274
of gas and solid	126
minimum for adsorbed gases	278
Interface, effect on stability of solids	80
Interfacial transition region	260
Inversion of quartz	76
Irving, J. M.	343
Isirikyan, A. A.	280
Iso-octane, adsorption on saran charcoal	173
Isosteric heat of adsorption	126, 130
Isotherm	
Type I	125
Type II	10, 43, 220, 221
Type III	10, 43
Type IV	11, 43
Ivanovskii, F. P.	195
J	
Jarvis, N. L.	113
Jeffery, J. W.	208
Joffe, A. F.	75

Johansen, P. G.	171
John, G. S.	61
Johnson, F. M. G.	15
Johnson, I.	355
Johnson, R. E.	355
Johnson, W. C.	159
Jones, G. O.	276
Jones, T. I.	99
Jordan, D. O.	171
Joyner, L. G.	11, 56, 71, 134, 135
Juhola, A. J.	263
Jura, George	18, 26, 30, 36, 39, 65, 66, 358, 368

K

Kahn, A. H.	29
Kalousek, G. L.	213
Kalvar'skaya, R. S.	198
Kampf, G.	290
Kantro, D. L.	15, 17, 199, 219, 222, 282, 287
Karle, J.	111
Katz, Max.	236
Keary, N. L.	268
Keenan, R. G.	55, 227
Keighton, W. B., Jr.	198
Keith, M. L.	76
Kelsey, C. H.	200, 212, 216
Kendall Award	2
Kingston, R. H.	237
Kington, G. L.	71, 123, 130, 295, 296, 355
Kipling, J. J.	47, 237
Kirkwood, J. G.	4, 130, 343
Kirkwood-Müller expression	129, 130
Kirsch, F. W.	193
Kiselev, A. V.	41, 280, 290, 300, 316
Kisliuk, P.	142, 145
Klement, R.	85
Klotz, I. M.	355
Klouthis, Fletcher	368
Knaggs, E. A.	184
Knudsen flow	172
Knudsen permeability	179
Knudsen's law	174
Kobozev, N. I.	89, 99
Koddermann, E.	85
Kohlschütter, H. W.	75, 76, 290
Kohn, H. W.	71
Kokes, R. J.	197, 198
Kolthoff, I. M.	356
Komarevsky, V. I.	184
Korolev, A. Ya.	300
Korpi, G. K.	164
Kortum, G.	171
Kovaleva, N. V.	300
Krasil'nikov, K. G.	41, 290
Kruger, F.	99
Krypton	
adsorption-extension for	251
on mica	264
parameters on graphite	307

Krypton, differential entropy of ad-	
sorption of	267
heat of adsorption on carbon	
black	326
dispersion interaction with graphite	312
isosteric heat of adsorption on mica	267
Kubicka, H.	99
Kulawic, D.	197
Kumari, Z. I.	198
Kunii, D.	159

L

Lachowicz, S.	198
Lakhanpal, M. L.	263
Lambert, B.	11, 17
LaMer, V. K.	355, 356
Lange, E.	362
Landgren, Robert	368
Langley, W. R.	355
Langmuir-Blodgett multilayer	101
Langmuir equation	68, 222, 227
isotherm	54, 91, 125, 239
mechanism	192
theory	12
Lasater, J. A.	290
Lateral interaction, the effect of, on	
monolayer adsorption	325
Lattice as a continuum	315
-defect sites	114
parameters, change from skin to	
bulk	77
sum, Crowell's	312
sum, direct	310
Law, J. T.	237
LCAO approximation	122
Lead bromide surface	83
chloride, effect on NaCl nucleation	83
perchlorate, effect on BaSO ₄ solu-	
bility	82
Le Beau, D. S.	339
Leger, E. E.	181, 324
Leider, H. R.	63
Lennard-Jones, J. E.	73, 220, 316
Lennard-Jones potential functions	275
Lepidocrocite	43
Levine, O.	109
Lewis, G. N.	356
Ligenza, J. R.	237
Limido, G.	187
Limiting surface area, effect of tem-	
perature on	48
Linde, J. O.	99
Ling, Irene	51, 60, 62, 70
Lipsett, S. G.	15
Lithium aluminum hydride	18
Littlewood, A. B.	197
Local adsorption isotherm	52
Local isotherm functions, non-Lang-	
muirian	59
Localized adsorption	279
Loeb, A. L.	159

London-type dispersion forces, ad- sorption energy from.....	310
Lopez-Gonzalez, J. de D.....	159
Love, A. E. H.....	263
Love, K. S.....	55, 227
Low, P. F.....	332, 338, 339
Lygin, V. I.....	41
Lygina, I. A.....	316

M

Maass, Otto.....	15
McAdams, W. H.....	159
McConnell, D.....	337
McDonald, R. S.....	41, 290
Macfayden, K. A.....	113
Machin, W. D.....	316
McIntosh, R. L.....	76, 249, 251, 263, 355
McIver, D. S.....	300
MacKay, A. L.....	45
McKeehaan, L. W.....	99
McKenna, T. A.....	198
Mackenzie, R. C.....	339
McKinley, J. B.....	182
McKinstry, H. A.....	75
Mackor, E. L.....	171
McLaren, A. D.....	355
Macleod, A. C.....	130, 295
McMillan, W. G.....	320, 321, 323
Madden, H. H.....	114
Madelung, E.....	34
Maghemite from lepidocrocite.....	45
Magnesium oxide, variation of lattice parameter with crystal size... oxide, x-ray study of.....	74 21
Magnetic susceptibility of palladium.....	86
Makishima, S.....	71
Makrides, A. C.....	41, 290
Mallouk, R. S.....	113
Mal'tsev, A. N.....	99
Manganese complex as growth-active impurity..... sulfide, interaction of surface film with HgS.....	83 78
Mann, H. M.....	200
Many, A.....	237
Many-sided sites of adsorption.....	328
Mapes, J. E.....	226
Marboe, E. C.....	72, 74, 76
Marsh, J. D. F.....	184
Martinez, E.....	163
Mason, S. G.....	171
Mathews, J. C.....	99
Maurer, J.....	76
Maxwell, J. C.....	263
Mayer, J. E.....	3, 29, 33, 34
Mayer, Maria.....	3
Mazur, J.....	171
Megaw, D. L.....	200
Megaw, H. D.....	212, 216
Meier, W. M.....	132
Meigs, P. S.....	237
Melting point of KNO ₃	76
Memory effect of solids.....	154
Mercuric sulfide, solubility interaction with MnS.....	78
Metals, adsorption studies on.....	229, 237
Metastable hydrates.....	80
Methane, adsorption on saran char- coal..... heat of adsorption.....	175 175
Methanol, adsorption on ferric hy- droxide..... adsorption isotherm of..... adsorption-resorption isotherms...	43 47 49
2-Methylpentane, adsorption on saran charcoal.....	173
Meyer, D. E.....	35
Mica, adsorption of argon and kryp- ton on.....	264
Microreactor technique.....	182
Mikhail, R. Sh.....	42, 50
Mikos, N. N.....	41
Millard, B.....	300, 324
Milliken, T. H., Jr.....	79
Mills, D. R.....	324
Mills, G. A.....	79, 290
Milton, R. M.....	132
Mitchell, A.....	87
Mitscherlich, E.....	75
Miyabe, H.....	208
Modi, H. J.....	171
Molar integral heat of adsorption...	128
Moldavskii, B. L.....	198
Molecular interaction.....	310
Molybdenum disulfide, dual adsorp- tion surface of.....	318
Monoatomic gases, cubic structures of.....	81
Monodisperse liquid adsorbent.....	348
Monolayer adsorption, the effect of lateral interaction on..... coverage, fit of BET equation in... physical adsorption, theory of....	325 8 269
Montgomery, H.....	237
Montgomery, P. W.....	18, 25
Montmorillite, a layer crystal.....	13
Montmorillonite clays.....	336
Montroll, E. W.....	247
Morrison, J. A.....	34, 56, 257
Morrison, J. L.....	355
Morrison, S. R.....	237
Mortensen, E. M.....	145
Mrozowski, S.....	262
Müller. See Kirkwood-Müller	
Müller, W.....	237
Multimolecular adsorption isotherms.	222
Mutzbauer, G.....	237

N

Nace, D. M.....	87
Nathans, M.....	22
Neale, S. M.....	171

- Neon
 adsorption isotherm on TiO_2 329
 parameters on graphite 307
 on saran charcoal 173
 differential heat of adsorption on
 carbon black 326
 on TiO_2 330
 dispersion interaction with graphite
 heat of adsorption 312
 heat of adsorption 175
- Neopentane, adsorption on saran
 charcoal 173
- Neutron irradiation, effect on sigma
 values 67
- Newell, G. F. 247
- Newling, W. B. S. 184
- Nichols, M. H. 113
- Nickel
 adsorption of deuterium on 158
 of hydrogen on 158
 oxygen chemisorption on 114
 sulfide, effect of polarization on
 solubility 78
- Nicolson, M. M. 74
- Nitric oxide isotherm on palladium 92
- Nitric oxide, sorption of 86
- Nitrogen
 adsorption 6, 9, 55, 58
 on anatase 224
 automatic 133
 on barium sulfate 360
 and desorption 138-9
 on diamond 146, 151
 effect on contact potential 107
 -extension for 252
 on gold 104
 on graphite 146
 isotherm 8, 64
 on platinum 104
 on rutile 56, 68
 on tungsten 142
 heat of adsorption 131
 on bone mineral 291, 294
 instantaneous isotherms of, on
 diamond 157
 isotherms of, on bone mineral 293
- Nitzsche, W. 339
- Niven, W. D. 263
- Noble metal, coated, as reference
 electrode 101
- Nonionogenic surface 165
- Norberg, R. E. 87
- Nucleation catalysts 82
- Nucleation, effect of polarizability on 83
- O**
- Oblad, A. G. 79, 225, 226, 227, 290
- Occam, William 132
- O'Connor, D. J. 171
- Octadecane, adsorption of OH^- ions
 by 170
- n*-Octadecylamine adsorption on
 platinum 107
- n*-Octadecylamine monolayer as elec-
 trode coating 107
- Olivier, J. P. 61, 156, 301, 308, 309, 316, 317
- Optical transparency as criterion of
 theoretical density 19
- Optically clear crystals from growth-
 active impurities 83
- Order-disorder theory in physical
 adsorption 239
- Orr, W. J. 321
- Ottewill, R. H. 171
- Outgassing technique 148
- Overbeek, J. Th. G. 168, 171
- Owens, E. A. 87, 99
- Owens, P. J. 182, 198
- Oxygen
 adsorption on anatase 224
 effect on contact potential 107
 at low temperature 56
 on nickel 116
 on rutile 56
 by silica 77
 chemisorption on nickel 114
 heat of adsorption 131
- P**
- Pace, E. L. 280
- Pace, J. 158
- Pack, D. H. 223, 224, 225
- Palladium, magnetic susceptibility,
 effect of hydrogen adsorption
 on 86
- Pant, J. M. 290
- Paraffin, adsorption of halide ions on 160
 -water interface 160
- Paramagnetism of palladium *vs* ad-
 sorbed hydrogen 95
- Parameter C 7
- Parameter V_m 9
- Parravano, G. 159
- Parreira, H. C. 160, 171
- Parsons, R. 171
- Partition function 127
 free rotational 141
- Partial molal properties of adsorbent 350
- Pass, G. 197
- Patai, I. F. 113
- Patrick, W. A. 290
- Peakall, D. B. 47, 237
- Pease, R. N. 198
- Perrin, J. 169
- Perry, J. H. 99
- Peticolas, W. L. 222
- Phase transformation of HgI_2 76
- Phillips, G. 101
- Phillips, Norman 25
- Photoelectric work function 114, 119
- Physical adsorption 13, 317
- Pierce, Conway 50, 61, 71, 324, 368
- Pierce, W. C. 362, 368

α -Pinene, adsorption on saran charcoal.....	173
Pitt, C. H.....	221, 227, 228
Pitzer, K. S.....	223, 356
Place exchange between nickel and adsorbed oxygen.....	114
Platinized electrodes.....	163
Platinum, adsorption on.....	24
low-angle x-ray scattering.....	24
particles, growth of.....	22
Poiseuille flow.....	172
Polanyi, M.....	248
Polanyi potential model.....	65
Polanyi theory.....	7
Polar organic liquids, clays in.....	337
Polarizability of gas <i>vs.</i> heat of adsorption.....	131
Polarization of anions, effect on equilibria.....	79
effect on reaction rates.....	78
Polley, M. H.....	71
Polytetrafluoroethylene as electrode coating.....	101
Pomerantz, M. A.....	113
Pore area.....	135, 138
radius.....	135
median.....	138
size distribution.....	133, 138
of silica-alumina catalyst.....	136
very narrow.....	297
volume.....	135, 138
Porosity of carbon.....	175
Porous solids, expansion on adsorption.....	76
systems, pore size distribution of.....	133
Portland cement.....	13, 199
Poschkus, D. P.....	316
Potassium chloride, supersolubility of.....	83
Potential energy for adsorption.....	310
Potential well for adsorption.....	303
Powell, R. E.....	22, 23
Powers, T. C.....	200, 356
Powney, J.....	171
Prebus, A. F.....	213
Prenzlów, C.....	280
Pressler, E. E.....	219
Pressure sintering.....	18
Price, W. C.....	18
Primak, W.....	66
Prokopchuk, N.....	198
Propanol adsorption on germanium.....	230, 237
chemisorption on germanium.....	233
Protoenstatite.....	80
Pryor, M. J.....	78
Pulvari, C. F.....	77
Pyrophyllite, crystal density of.....	336

Q

Quadrupole-ion field interaction.....	130
Quartz, adsorption isotherm for fused.....	38

Quartz, adsorptive properties of... particles, preparation of.....	35 282
--	-----------

R

Raal, F. A.....	181
Radiation, effect on surfaces of solids.....	62
Randall, M.....	356
Rate phenomena, effect of adsorbed molecules on.....	73
Razouk, R. I.....	42, 50, 263, 368
Reactivity of freshly formed surfaces.....	79
Reed, T. B.....	132
Reference electrodes, resin-coated.....	101
Relative humidity, effect on contact potential difference.....	105
Repulsion constant in potential function.....	311
Reyerson, L. H.....	9, 17, 56, 65, 86, 99
Rhodin, T. N.....	326, 331
Richardson, E.....	79
Rideal, E. K.....	113
Ritchie, P. D.....	41
Roberts, L. E. J.....	71
Robinson, A. L.....	362
Roginskii, S. Z.....	54
Romanchuck, M. A.....	41
Rose, G. S.....	34
Rosenberg, A. J.....	71
Ross-Hendricks method.....	334
Ross, J. W.....	71, 280
Ross, M.....	280
Ross-Olivier method.....	306
Ross, P.....	139
Ross, Sydney.....	61, 156, 158, 301, 308, 309, 316, 317, 324
Runchagen, O.....	81
Russell, H. W.....	159
Rutgers, A. J.....	162
Rutile, low temperature adsorption of butane.....	56
of nitrogen.....	56
of oxygen.....	56
Rutkowski, C. P.....	268
Rymer, T. B.....	74

S

s-Band.....	90
St. Williams, E.....	87
Saito, N.....	280
Saito, Y.....	71
Saksena, B. D.....	290
Salem, A. S.....	50
Saltsburg, H.....	347
Samoilov, O. Ya.....	171
Sams, J. R., Jr.....	308
Samson, J.....	87
Sandell, E. B.....	356
Saran charcoal, adsorption on.....	173, 174
Saunders, R. D.....	70
Scarborough, J. B.....	34
Schairer, J. F.....	85
Schlier, R. E.....	121

- Schreiber, H. P. 33
 Schreiner, G. D. L. 71
 Schuit, G. C. A. 159
 Schulman, F. 113
 Schulman, J. H. 113, 160
 Schultze, D. 237
 Schulz, E. G. 13, 219
 Schusterius, C. 80
 Schwab, G. -M. 229
 Schweppe, Cynthia 247
 Screened surfaces. 79, 81
 Seifert, von H. 290
 Self-potentials. 257
 Seligmann, Paul. 355
 Selwood, P. W. 87, 95
 Semiconductors, chemisorption on. . . 230
 Shafrin, E. G. 113
 Shalit, H. 198
 Sharpe, J. W. 41
 Shcherbakova, K. D. 41, 300
 Shereshefsky, J. L. 12, 158, 159
 Sherman, Ann. 247
 Shockley, William 29, 90
 Shot reactions. 184
 Siebert, A. R. 280
 Siefert, K. F. 290
 Sievertz, A. 87, 99
 Silanol groups on silica gel. 281
 Silica
 adsorptive properties of. 35
 aerogel. 153
 -alumina catalyst, fluorination of. . 137
 metal impregnation of. 138
 C. 78
 expansion on adsorption. 77
 gel, palladium on. 86
 specific surface. 10
 surface area from V_m 9
 surface hydroxyl content of. 283
 surface structure of. 281
 heat of immersion in water. 281
 irradiation of. 67
 reaction with HF. 78
 surface area. 64
 W. 78
 Silicosis, reactivity of silica in. . . . 79
 Siloxane linkages on silica gel. 281
 Silver-halide electrodes. 163
 Sinanoglu, O. 223
 Singleton, J. H. 308
 Sintering of refractory materials. . . . 18
 Sips, R. 52, 55
 Sitrine, Richard. 236
 Site distribution on TiO_2 330
 Site energy distribution. 51, 53, 54, 62
 differential. 69, 70
 integral. 68, 69
 in rutile. 68
 Site energy on TiO_2 330
 Skin tension in crystals. 74
 Skiva, A. 99
 Slater average electron orbit radii. . . 129
 Slow heat evolution. 296
 Slygin, A. 228
 Small one-component particles, thermodynamics of. 351
 Smekal, A. 84
 Smith, C. S. 12, 85
 Smith, D. P. 87
 Smith, N. 50
 Smith, P. F. 355
 Smith, R. N. 324
 Smith, W. R. 9, 71
 Smoluchowski, R. 71
 Sodium
 bentonite, behavior on hydration. . . 336
 bromide, adsorption of argon on. . . 319
 chloride, adsorption of ethane on. . 322
 hectorite, behavior on hydration. . . 336
 vermiculite clay, apparent density in water. 337
 Sokolova, N. P. 198
 Solbakken, Aage. 86, 99
 Solid-gas interface. 5
 Solid monolayer, durability of. 109
 Solid solutions of alkali halides. . . . 75
 Solid state reactions, correlation with van der Waals forces. 81
 Solid surfaces and the gas-solid interface. 5
 conference on. 12
 Somerjai, G. 22
 Spalaris, C. N. 63
 Specific reaction rate. 140
 Specific surface area, changes in. . . . 62
 constant. 351
 effect of heating on. 46
 of finely divided solids. 13
 Spencer, W. B. 280
 Spheron 6. *See* Carbon black
 Spilners, A. *See* Carbon black. 71
 Spreading pressure, adsorbate. 249
 Spurlock, B. 197
 Square lattice of adsorption sites. . . . 239
 Srinivasan, Ganapathy. 229
 Stahl, P. 85
 Statz, H. 237
 Stearic acid monolayer on electrode. . 110
 Steatite. 80
 Steele, W. A. 269, 280, 329, 330
 Stein, H. N. 216
 Sterling FT. *See* Carbon black
 Stern layer. 165
 Stern theory. 164
 Stevenson, D. H. 193
 Sticking coefficient. 140, 141
 Sticking probability of nitrogen on tungsten. 142
 Stillinger, F. H., Jr. 347
 Stoddart, C. T. H. 197
 Stone, F. S. 300
 Strachan, E. 181
 Streaming potential on paraffin wax. . 160
 Strength of a brittle solid. 75

Stress-corrosion.....	78
Stresses for disorganized carbon.....	257
Stromberg, Harold.....	18
Stuart, W. I.....	123, 268
Stuckardt, K.....	80
Suggitt, R. M.....	41
Suhrmann, R.....	105
Sulfur hexafluoride, adsorption of on saran charcoal.....	173
Sun, C. E.....	145
Sun, S. C.....	167
Supersaturation phenomena.....	158
Surface active agents, effect on streaming potentials.....	162, 164
Surface area from adsorption of cy- clohexane.....	48
from adsorption of methanol.....	48
determination, methods of.....	66
effect of high energy radiation on.....	62
limiting.....	46
specific.....	44
Surface condensation forces.....	220
cracks.....	75
diffusion of gases on charcoal.....	172
distortion of sodium chloride.....	26
effect on stability of solids.....	80
electric field.....	322
Surface energy, amorphous silica....	15
calcium hydroxide.....	15
calcium oxide.....	15
correction.....	30, 33
effect of high energy radiation on..	62
of the hemicrystal.....	28
hydrous amorphous silica.....	15
of sodium chloride.....	30
Surface enthalpies.....	15
Surface film, mechanical tension in..	76
reactivity of, on carriers.....	78
redistribution of electron densities	76
solubility under tension.....	78
Surface flow, efficiency of.....	181
Surface hydration of calcium silicates.	199
Surface hydroxyl content of silica gel..	283
Surface polarization in chemisorp- tion.....	225
Surface polarization from observa- tion of photoelectric work function.....	115
Surface potentials, for disorganized carbon.....	257
Surface as seat of asymmetry.....	73
Surface states of oxide-coated ger- manium.....	230
Surface structure of fused quartz....	40
Surface symmetry, effect of foreign atoms on.....	77
Surface tension <i>vs.</i> unit free surface energy.....	101
Surfaces as lattice vacancies.....	73
Swallow, A. J.....	70
Swensson, B.....	87
Sysoev, E. A.....	41, 290

T

Tabor, D.....	111
Talc.....	337
Tamaru, K.....	194
Tamm, I.....	90
Tamm state.....	90
Taylor, A. J.....	170, 171
Taylor, E. H.....	71
Taylor, H. A.....	226
Taylor, H. F. W.....	13, 200, 216
Taylor-Howison hypothesis.....	215
Taylor, H. S.....	2, 5, 158, 197, 321
Teflon as electrode coating.....	101
Teller, E.....	5, 6, 11, 17, 43, 47, 70, 113, 221
Temkin, A.....	228
Temkin equation.....	55, 56, 227
Temkin isotherm.....	222
Tessman, J. R.....	29
Tetraethylmethane, adsorption on saran charcoal.....	173
Tetrafluoroethylene as electrode coating.....	101
TFE. <i>See</i> Tetrafluoroethylene	
Thermal conductivity of alkali halides.....	75
of argon.....	150
of diamond.....	150
of graphite.....	150
of helium.....	150
Thermal drift.....	296
expansion of quartz.....	75
patch.....	70
Thermodynamic equilibria.....	248
processes.....	358
relations within a liquid-vapor interface.....	259
Thermodynamics of adsorption... 348,	357
Thiophene desulfurization.....	182
Thomas, D. G.....	181
Thomas, T. L.....	132
Thompson, W. B.....	113
Thomson, W.....	356
Thon, N.....	226
Thoria, adsorption of carbon dioxide on.....	228
Thornhill, F. S.....	9, 10
Tiley, P. F.....	300
Titanium dioxide, adsorption of iso- therm of neon on.....	329
differential heat of adsorption of neon on.....	330
irradiation of.....	67
heat of adsorption of helium on... 327	
site energies and distribution on... 330	
surface area.....	66
Tobermorite, crystal structure.....	213
electron micrograph.....	14
specific surface area.....	13, 14
surface area of.....	214
surface energy of.....	15, 16, 199

Tobin, H. H.	197, 198, 300
Tolman, R. C.	346
Tolpin, J. G.	61
Tomezsko, E. S. J.	325
Tomlinson, R. H.	181
Tompkins, F. C.	316
Transition elements, effect on nucle- ation	83
Transmission coefficient	141
Trapnell, B. M. W.	61, 227
Treadwell, F. P.	356
Tricalcium silicate, hydration of	13, 14, 199
Trzebiatowsky, W.	87
Tscapek, W.	339
Tuttle, O. F.	76
Twigg, G. H.	228
Tykodi, R. J.	71, 329, 330

U

Unit free surface energy	101
Universal isotherm	66

V

Vaisnys, J. R.	26, 30
Van der Hoff, B. M. E.	34, 368
van der Waals equation of state	304
self-potentials	256
van der Waals-London dispersion forces	239
Van Looy, H.	187
Van Olphen, H.	332
van Zeggeren, F.	33, 34
Varley, J. H. O.	71
Vermiculite, a layer crystal	13
Verwey, H.	159
Verwey, E. J. W.	32, 105, 171
Vibrational frequencies for inert gases on graphite	316
Volume changes of solids	76
von Neumann, John	4

W

Waddams, J. A.	79
Wade, W. H.	35, 41, 290
Wadsworth, M. E.	221, 226, 227
Walden, G. H., Jr.	360
Walling, F. C.	99
Walton, G.	360
Wanlass, F. M.	140
Warren, R. M.	6
Water, adsorption on barium sulfate	360
enthalpy change for adsorption	366, 367
entropy change for adsorption	368
Water vapor adsorption	103, 318
adsorption-extension, on carbon	250
flow rate through micropore car- bon	253
Weir, C. E.	158
Weise, C. H.	15, 17, 199, 219, 222, 282, 287

Weiser, H. B.	50
Weiss, Al.	78
Weiss, Ar.	78
Weller, S. W.	290
Weyl, W. A.	72, 85
Whalen, J. W.	41, 281, 290
White, P.	27, 29
Whitney, W. R.	171
Wiig, W. A.	251
Wijga, P. W. O.	168
Wiley, J. W.	324
Wilhelm, R. H.	159
Wilkinson, G. R.	18
Williams, G. C.	171
Wilm, D.	74
Winkler, W. W.	158, 306, 318, 321, 322
Wood, F. W.	170
Wood, L. J.	171
Wu, Y. C.	350, 354, 355, 357
Wynkopp, R.	159

X

X-irradiation	67
Xenon, adsorption parameters on graphite	307
adsorption by silica	77
-rare gas interaction, minimum potential energy of	277

Y

Yagi, S.	159
Yamaguchi, G.	208
Yamamoto, T.	83
Yamins, H. G.	113
Yates, D. J. C.	76, 77, 222, 249, 251, 356
Yonoda, Y.	71
Young, D. M.	181, 280
Young, G. F.	41, 290
Young, T. F.	348, 362, 368
Young, Thomas	356
Yu, Y. F.	237

Z

Zeldovich, Y.	228
Zeolite, calcium A	123
Zerfoss, S.	80, 81
Zeta	223
potential for paraffin	168
vs. pH	169
for quartz	167
Zettlemoyer, A. C.	41, 64, 229, 237, 238
Zhdanov, S. P.	290
Zieglaff, C. L.	171
Zimmerman, J. R.	290
Zinc oxide, adsorption of deuterium on	158
of hydrogen on	158
Zisman, W. A.	100, 113
Zubowich, I. A.	99
Zucker, G. L.	163, 164
Zuehlke, Richard	99